JUN 15 1942

VOLUME 95 NUMBER 3

THE ASTROPHYSICAL JOURNAL

AN INTERNATIONAL REVIEW OF SPECTROSCOPY AND ASTRONOMICAL PHYSICS

Founded in 1895 by GEORGE E. HALE *and* JAMES E. KEELER

Edited by

PAUL W. MERRILL
Mount Wilson Observatory of the Carnegie Institution of Washington

HARLOW SHAPLEY
Harvard College Observatory Cambridge, Massachusetts

J. H. MOORE
Lick Observatory University of California

OTTO STRUVE
Yerkes Observatory of the University of Chicago

MAY 1942

THE DYNAMICS OF THE INTERSTELLAR MEDIUM. III - - - - *Lyman Spitzer, Jr.* 329
NOTES ON ECLIPSING VARIABLES - - - - - - - - - - - *Henry Norris Russell* 345
THE SPECTRA OF TEN GASEOUS NEBULAE - - - - - - - - - - *A. B. Wyse* 356
THE SPECTRUM OF BD+11°4673 DURING THE YEARS 1937–1941 - - *Paul W. Merrill* 386
ABSOLUTE DIMENSIONS OF A WOLF-RAYET STAR AND THE EXPANDING-ENVELOPE HYPOTHESIS - - - - - - - - - - - - - - - *O. C. Wilson* 402
THE SPECTROGRAPHIC ORBIT OF THE COMPANION TO RIGEL *Roscoe F. Sanford* 421
THE SPECTROGRAPHIC ORBIT OF 42 CAPRICORNI - - - - - *Roscoe F. Sanford* 425
SPECTRAL STAGES OF NOVAE - - - - - - - - - - - *Dean B. McLaughlin* 428
A REMARK ON METEORS - - - - - - - - - - - - - *Theodore E. Sterne* 437
ON STELLAR ROTATION - - - - - - - - - - - - - *Martin Schwarzschild* 441
ON THE ROTATION OF STARS WITH CONVECTIVE CORE - - - *Gunnar Randers* 454
LUMINOSITIES OF THE M-TYPE VARIABLES OF SMALL RANGE *Philip C. Keenan* 461
SPECTROGRAPHIC OBSERVATIONS OF 17 LEPORIS - - *Burke Smith and Otto Struve* 468
THE STATISTICS OF THE GRAVITATIONAL FIELD ARISING FROM A RANDOM DISTRIBUTION OF STARS. I - - - - - *S. Chandrasekhar and J. von Neumann* 489
TERM ANALYSIS OF THE THIRD SPECTRUM OF IRON (Fe III) *B. Edlén and P. Swings* 532
ON THE CLUSTERING OF NEBULAE. I - - - - - - - - - - *F. Zwicky* 555
ON THE CLUSTERING OF NEBULAE. II - - - *L. Katz and Gerard F. W. Mulders* 565
NOTES
THE CENTRAL DENSITY OF THE STARS - - - - - - - - - - *Zdeněk Kopal* 569
REVIEWS - 571
INDEX - 573

THE UNIVERSITY OF CHICAGO PRESS
CHICAGO, ILLINOIS, U.S.A.

May 1942 Vol. 95, No. 3

THE ASTROPHYSICAL JOURNAL

AN INTERNATIONAL REVIEW OF SPECTROSCOPY AND ASTRONOMICAL PHYSICS

Edited by

PAUL W. MERRILL
Mount Wilson Observatory of the Carnegie Institution of Washington

HARLOW SHAPLEY
Harvard College Observatory
Cambridge, Massachusetts

J. H. MOORE
Lick Observatory
University of California

OTTO STRUVE
Yerkes Observatory of the University of Chicago

With the Collaboration of the American Astronomical Society

Collaborating Editors:

1942
EDWIN HUBBLE
Mount Wilson Observatory
D. B. McLAUGHLIN
University of Michigan
J. A. PEARCE
Dominion Astrophysical Observatory, Victoria

1942-43
S. A. MITCHELL
Leander McCormick Observatory
LYMAN SPITZER, Jr.
Yale University

1942-44
CECILIA H. PAYNE-GAPOSCHKIN
Harvard College Observatory
H. N. RUSSELL
Princeton University
F. H. SEARES
Mount Wilson Observatory

The Astrophysical Journal is published bimonthly by the University of Chicago at the University of Chicago Press, 5750 Ellis Avenue, Chicago, Illinois, during July, September, November, January, March, and May. ¶The subscription price is $10.00 a year; the price of single copies is $2.00. Orders for service of less than a full year will be charged at the single-copy rate. ¶Postage is prepaid by the publishers on all orders from the United States and its possessions, Argentina, Bolivia, Brazil, Chile, Colombia, Costa Rica, Cuba, Dominican Republic, Ecuador, Guatemala, Haiti, Republic of Honduras, Mexico, Morocco (Spanish Zone), Nicaragua, Panama, Paraguay, Peru, Rio de Oro, El Salvador, Spain (including Balearic Islands, Canary Islands, and the Spanish Offices in Northern Africa; Andorra), Spanish Guinea, Uruguay, and Venezuela. ¶Postage is charged extra as follows: for Canada and Newfoundland, 42 cents on annual subscriptions (total $10.42); on single copies, 7 cents (total $2.07); for all other countries in the Postal Union, 96 cents on annual subscriptions (total $10.96), on single copies 16 cents (total $2.16). ¶Patrons are requested to make all remittances payable to The University of Chicago Press, in United States currency or its equivalent by postal or express money orders or bank drafts.

The following are authorized agents:

For the British Empire, except North America, India, and Australasia: The Cambridge University Press, Bentley House, 200 Euston Road, London, N.W. 1, England. Prices of yearly subscriptions and of single copies may be had on application.

Claims for missing numbers should be made within the month following the regular month of publication. The publishers expect to supply missing numbers free only when losses have been sustained in transit, and when the reserve stock will permit.

Business correspondence should be addressed to The University of Chicago Press, Chicago, Illinois.

Communications for the editors and manuscripts should be addressed to: Otto Struve, Editor of THE ASTROPHYSICAL JOURNAL, Yerkes Observatory, Williams Bay, Wisconsin.

Line drawings and photographs should be made by the author, and all marginal notes such as co-ordinates, wave lengths, etc., should be included in the cuts. It will not be possible to set up such material in type.

One copy of the corrected galley proof should be returned as soon as possible to the editor, Yerkes Observatory, Williams Bay, Wisconsin. Authors should take notice that the manuscript will not be sent to them with the proof.

The cable address is "Observatory, Williamsbay, Wisconsin."

The articles in this journal are indexed in the *International Index to Periodicals*, New York, N.Y.

Applications for permission to quote from this journal should be addressed to The University of Chicago Press, and will be freely granted.

Entered as second-class matter, July 31, 1940, at the Post-Office at Chicago, Ill., under the act of March 3, 1879.
Acceptance for mailing at special rate of postage provided for in United States Postal Act of October 3, 1917, Section 1103, amended February 28, 1925.

[PRINTED IN U.S.A.]

THE ASTROPHYSICAL JOURNAL

AN INTERNATIONAL REVIEW OF SPECTROSCOPY AND ASTRONOMICAL PHYSICS

VOLUME 95 MAY 1942 NUMBER 3

THE DYNAMICS OF THE INTERSTELLAR MEDIUM

III. GALACTIC DISTRIBUTION

LYMAN SPITZER, JR.

ABSTRACT

Measurements of the rotational velocity in NGC 3115 show that the random stellar velocities in this elliptical galaxy are of the order of 200 km/sec; other elliptical systems with masses of $\cdot 10^{10}$ M$\odot$ will also contain stars with the same velocity dispersion. The random velocities of interstellar atoms and dust particles in equilibrium, however, are less than 20 km/sec. Analysis of electron captures and free-free transitions, taking into account the variation of the g-factors with energy, shows that atoms of appreciable abundance will, in fact, reach such a low-velocity equilibrium within 10^7–10^8 years; collisions between dust particles will similarly reduce dust velocities within 10^5–10^6 years. Unless interstellar particles are subject to unknown forces, the velocities of these particles in the more massive elliptical and spherical galaxies must be much less than those of the stars.

It follows that any interstellar matter in such stellar systems must be highly concentrated to the center or to the equatorial plane. For a rigorously spherical system the total mass of such matter cannot exceed 4×10^{-4} times the mass of all the stars. In an elliptical system the mass is unrestricted, but if the mass of interstellar matter exceeds that of the stars, then half of such matter must lie within 3 parsecs from the equatorial plane. In any case the light observed from spherical and elliptical systems of large mass must be direct starlight, not diffuse or scattered light.

The equatorial layer of interstellar matter in an elliptical galaxy may in theory contain as much or more matter than the stars in the system. The determination by Oort of the stellar density distribution in the elliptical nebula NGC 3115, and in particular the high-luminosity gradient which he found close to the equatorial plane, suggest that a large fraction of the mass of this system may be in the form of dark matter in the equatorial plane. Matter in so dense a layer would presumably be quite different in its physical state from interstellar matter in our own Galaxy and would perhaps condense into faint stars of low random velocity. Further observations are necessary to decide whether a rotating massive disk of dark matter may play an important part in the structure of some elliptical systems.

The presence of interstellar atoms and dust particles in spiral galaxies is known from direct observation. The question naturally arises as to whether interstellar particles may be present also in elliptical and globular galaxies. The diffuse, nonstellar appearance of most elliptical systems has frequently led to the suggestion that most of the light from such galaxies might consist of diffuse radiation, scattered by small particles.

Direct observations on this point are difficult and by themselves not very conclusive. Fortunately, the equilibrium of interstellar particles in a galactic system is susceptible to rather simple theoretical analysis. Given the forces that act on the particles, it should be possible to demonstrate which equilibrium configurations are possible. It has been shown in the first two papers of this series[1] that the interstellar medium behaves as a

[1] L. Spitzer, Jr., *Ap. J.*, **93**, 369, 1941; **94**, 232, 1941.

perfect gas and that the direct effects of radiation pressure may be neglected for most purposes. The problem is therefore reduced to the equilibrium of a gas in a gravitational field.

The most important quantity in such a problem is the ratio of the random stellar velocities to the velocities of the interstellar particles. Stellar velocities in elliptical galaxies are unfortunately rather uncertain. For one system, NGC 3115, direct measurements of the rotational velocity by Humason[2] are available; the observed values range from 80 km/sec near the center to 450 km/sec farther out. It is clear that since this nebula has a considerable extension perpendicular to its galactic plane, the random stellar velocities must be an appreciable fraction of the rotational velocities and are probably in the neighborhood of 200 km/sec.

For other systems the only relevant data are the random velocities of nebulae in clusters, which indicate a mass of roughly 10^{10} $M\odot$ or more for an elliptical system.[3] Since the radius[4] containing half the mass of an elliptical system is at most 1000 parsecs, the virial theorem gives a mean square stellar velocity of 200 km/sec. Nebular masses are so uncertain, however, that this value for the random stellar velocities cannot be assumed for all elliptical systems.

Nevertheless, it is of considerable interest to investigate the effects associated with such high galactic masses. The following analysis will therefore be developed for galaxies in which the random stellar velocities are assumed to be of the order of 200 km/sec. The results of the analysis may be applied with some certainty to NGC 3115. It is highly probable that they are relevant to many other elliptical and globular galaxies as well. Whether or not most of the elliptical and globular galaxies have such high masses and such high random stellar velocities cannot be decided until more observational data are available.

In contrast to the assumed velocities of 200 km/sec for stars, the equilibrium random velocities of interstellar particles are quite low, some 20 km/sec for protons and electrons at 10,000°, less for other atoms, and negligibly small for dust particles. Since equilibrium will be reached in much less than 10^9 years, we may infer that the root mean square velocity of interstellar particles does not exceed 20 km/sec. It follows that the root mean square stellar velocities in the elliptical galaxies considered here are some ten or more times as great as the velocities of interstellar particles.

A necessary consequence of this large difference in velocities is that any interstellar matter in such a system must be almost entirely concentrated toward the equatorial plane or, in the case of a spherical system, toward the center. A factor of ten in velocities corresponds to a factor of one hundred in kinetic energy per unit mass. Hence a star in the equatorial plane of an elliptical galaxy will have at least one hundred times as much energy per unit mass as any atoms or dust particles in the vicinity and will clearly be able to rise much farther from the equatorial plane before the gravitational attraction of the galaxy pulls it back.

The analysis proceeds in three separate parts in the following sections. First, the rate of dissipation of energy for atoms or dust particles at high velocities must be determined in order to exclude the possibility that the interstellar medium could have remained at a temperature of millions of degrees during 10^9 years. Second, the equilibrium of a gas within a spherical gravitational field is examined, and a maximum total mass is found for the interstellar matter in a spherical galaxy. In the case of a typical globular cluster the situation is quite different, since the mean square stellar velocities are comparable with the atomic ones. It is doubtful, however, whether some of the smaller clusters have a sufficient gravitational force to hold atoms at all.

[2] *Report of the Director, Mt. W. Obs., 1936–37*, p. 31.

[3] S. Smith, *Ap. J.*, **83**, 23, 1936; F. Zwicky, *Ap. J.*, **86**, 217, 1937.

[4] E. Hubble, *The Realm of the Nebulae*, p. 178, Yale University Press, 1936.

In the third and last section the equilibrium of dust and atoms in systems possessing angular momentum is investigated. Here again the relative concentration of the interstellar medium may be evaluated, and as in a spherical system it may be shown that the amount of interstellar matter throughout most of a massive elliptical galaxy must be quite small. The effect which a thin, dense equatorial layer of dark matter can produce on the distribution of stars is also examined. A comparison of the predicted effects with observational data in NGC 3115 suggests that this galaxy may, in fact, possess a large amount of dark matter concentrated to its equatorial plane.

1. DISSIPATION OF ENERGY

In the general case of a gas at high temperature the dissipation of energy will proceed in many ways. To obtain an upper limit for the time required to dissipate large energies, we shall here consider the two types of interstellar media which are the most likely to remain at an initially high temperature—a medium consisting wholly of hydrogen atoms and one composed exclusively of dust particles. In each case the rate of loss of energy will be computed; possible mechanisms for an offsetting increase in energy will be considered later. Since dust and atoms are considered wholly separately, the following results are independent of the equipartition of kinetic energy between dust and atoms which appears when both types of particles are present and which was discussed quantitatively in paper I. It is clear that if both dust and atoms are present together the rate of energy dissipation will be increased from the values found below. This strengthens the conclusion that interstellar particles cannot long remain at high velocities.

A medium composed wholly of hydrogen atoms will be considered first. If the average kinetic energy per atom exceeds the ionization energy E_0, the gas will be largely ionized, since the cross-section for ionization by electronic or atomic impact is much greater than that for electron capture. The resultant assembly of protons and free electrons will come to equipartition of kinetic energy fairly rapidly. It was shown in paper I that for protons and electrons with an assumed density of 1 atom per cm^3 and a kinetic temperature of 10,000°, deviations from equipartition of energy fell to $1/e$ their initial value in 0.48 years. Since this time varies as the cube of the velocity, it is evident that even for velocities of 600 km/sec, corresponding to a temperature of 14,000,000°, the time of equipartition is only 2.7×10^4 years. We may therefore use with confidence the appropriate Maxwellian velocity distributions for both protons and electrons.

A gas of protons and electrons may lose energy by radiation in two ways—electron captures and free-free transitions. Probabilities for these processes are known from wave-mechanical theory. It is frequently assumed in astrophysical investigations that the Gaunt "g-factor" is equal to unity. This is a valid approximation for low energies but may be badly off when the energies are very high. Accurate values of g have been exhaustively determined by Menzel and Pekeris.[5] The equations given by Bethe,[6] based on the analyses of Sommerfeld, Stobbe, and others, are less complete but are in a more convenient form for the present purpose. The rate of loss of energy will be computed from these equations for two processes—recapture of electrons directly in the ground state and radiation of energy in free-free transitions. If other processes are important, they will, of course, increase the rate of energy dissipation.

Let E and v be the energy and velocity, respectively, of an electron, and let E_0 be the ionization energy of hydrogen. The energy radiated in a single recombination into the ground state will be a function of the initial relative velocity V; if V were the same for all encounters, the number of such recombinations per second would be $\pi\sigma_c^2 n_p n_e V$, where $\pi\sigma_c^2$, a function of V, is the cross-section for the capture process, and n_p and n_e are the numbers of protons and electrons per cm^3, respectively. Since the protons have a root

[5] *M.N.*, **96**, 77, 1935.

[6] *Handb. d. Phys.*, **24**, Part I, 488, 1933.

mean square velocity only 1/43 as great as the electrons, we may without serious error replace the relative velocity V by the electron velocity v; with this approximation the energy radiated in a single encounter becomes $E+E_0$. To find the rate of change of $\bar{E}$, the mean energy of protons and electrons, the energy loss per unit time must be averaged over all values of v and divided by $n_p + n_e$, or $2n_e$. This yields the equation

$$\frac{d\bar{E}}{dt} = -\frac{3}{2}\left(\frac{3}{\pi}\right)^{1/2}\frac{n_p}{m^{1/2}\bar{E}^{3/2}}\int_0^\infty E\,(E+E_0)\; e^{-3E/2\bar{E}}\pi\sigma_c^2 dE\,, \tag{1}$$

where m is the mass of the electron.

The capture cross-section $\pi\sigma_c^2$ for the lowest quantum state may be written as

$$\pi\sigma_c^2 = A\frac{E_0^{5/2}}{(E+E_0)\,E^{3/2}}\vartheta_1\left(\frac{E_0}{E}\right), \tag{2}$$

where

$$A = \frac{2^6 e^2 h}{3m^2c^3} = 1.44\times 10^{-21}\text{cm}^2\,. \tag{3}$$

If we let k^2 equal E_0/E, then $\vartheta_1(E_0/E)$ in equation (2) may be written in the form

$$\vartheta_1(k^2) = \frac{2\pi k}{1+k^2}\,\frac{\exp(-4k\cot^{-1}k)}{1-\exp(-2\pi k)}\,. \tag{4}$$

When k is very large or very small we have the expansions

$$\vartheta_1(k^2) = \frac{2\pi e^{-4}}{k}\left(1+\frac{1}{3k^2},\ldots.\right), \tag{5}$$

$$\vartheta_1(k^2) = 1-\pi k\ldots\ldots \tag{6}$$

Since the Gaunt g-factor is given by

$$g = 4\,(3)^{1/2}\left(\frac{E_0}{E}\right)^{1/2}\vartheta_1\left(\frac{E_0}{E}\right), \tag{7}$$

it is evident that when E_0/E is large, g is equal to its familiar value, $8\pi 3^{\frac{1}{2}}e^{-4}$, or 0.797. When E_0/E is small and ϑ_1 is unity, the value of g is very much less than unity. Values of $\vartheta_1(E_0/E)$ are given in Table 1.

TABLE 1

CORRECTION FACTOR ϑ_1

E/E_0	ϑ_1	E/E_0	ϑ_1	E/E_0	ϑ_1
0.01	0.012	1.0	0.14	100	0.74
.02	.016	2.0	.20	200	.81
.04	.023	4.0	.29	400	.86
.06	.029	6.0	.34	600	.88
.08	.034	8.0	.39	800	.89
.10	.038	10.0	.42	1,000	.90
.20	.054	20.0	.52	4,000	.95
.40	.080	40.0	.63	10,000	.97
.60	.102	60.0	.68	40,000	.98
0.80	0.120	80.0	0.72	100,000	0.99

Equations (2) and (4) may be substituted into equation (1) to give an integral formula for $d\bar{E}/dt$. Since this integral can apparently not be evaluated in a simple analytical form, we may approximate by taking $\vartheta_1(E_0/E)$ outside the integral sign with its value for some appropriate value of E. This obviously gives asymptotically correct results as $\bar{E}$ approaches infinity and $\vartheta_1(k^2)$ becomes equal to unity. If this procedure is also to give correct results when $E_0/\bar{E}$ is large, and $\vartheta_2(k^2)$ is approximately given by equation (5), then it is readily shown that the appropriate value of E is $2\bar{E}/3\pi$. This value is relatively small, since, when $E_0/\bar{E}$ is not large, most of the energy losses come from the recapture of low-velocity electrons. With this approximation, then, $d\bar{E}/dt$ becomes

$$\frac{d\bar{E}}{dt} = -\frac{3\,A\,n_p E_0^{5/2}}{2^{1/2} m^{1/2} \bar{E}^2} \vartheta_1\left(\frac{3\pi E_0}{2\bar{E}}\right). \tag{8}$$

This method of procedure, although correct when $\bar{E}$ is very large or very small, is not very accurate when $E_0/\bar{E}$ is near unity; the resultant error in equation (8) should be less than some 20 per cent at the most, however, which is as accurate as we shall need here. Since E_0 varies as the square of the ionic charge, it is evident that a few highly ionized elements will very greatly increase the rate of radiation.

To visualize conveniently the order of magnitude of the effects involved, one may define a time of dissipation T_d by the relationship

$$T_d = \frac{\bar{E}}{\left|\dfrac{d\bar{E}}{dt}\right|}. \tag{9}$$

The quantity T_d so defined is the length of time required for the complete dissipation of energy by radiation if the rate of dissipation remained constant as $\bar{E}$ decreased. Since actually $|d\bar{E}/dt|$ increases as $\bar{E}$ decreases, the actual time required for the cooling of a gas at high temperature is somewhat less than T_d. If we insert numerical values into equation (8) and substitute into equation (9), we have for the time of dissipation arising from recombinations in the ground state

$$T_d\,(\text{rec}) = \frac{6.6\times 10^4}{n_p \vartheta_1\,(4.7E_0/\bar{E})}\left(\frac{\bar{E}}{E_0}\right)^2 \text{ years}. \tag{10}$$

Values of T_d(rec) for n_p equal to unity and for various root mean square proton velocities are given in Table 2.

TABLE 2

VALUES OF THE TIME OF DISSIPATION

v Km/Sec	100	200	400	600	1000
$\bar{E}/E_0$	3.82	15.3	61	137	382
T_d(rec)	8.0×10^6	6.0×10^7	5.3×10^8	2.6×10^9	1.4×10^{10}
T_d(f-f)	5.3×10^6	1.1×10^7	2.1×10^7	3.2×10^7	5.3×10^7
T_d(dust)	1.1×10^6	5.5×10^5	2.8×10^5	1.8×10^5	1.1×10^5

NOTE

Values of T_d give the time in years required to dissipate the entire kinetic energy of the assembly if the rate of dissipation remained constant and if no other process were acting.

The free-free transitions may be similarly treated, except that here we must integrate over all possible transitions as well as over all velocities. The exact equations become

very complicated, and it will suffice to take the asymptotic form for small $E_0/\bar{E}$, which becomes

$$\frac{d\bar{E}}{dt} = \frac{3}{8\pi}\left(\frac{3}{\pi}\right)^{1/2} \frac{A n_p E_0}{m^{1/2}\bar{E}^{3/2}} \int_0^\infty E e^{-3E/2\bar{E}} \vartheta_2\left(\frac{E_0}{E}\right) dE\,, \tag{11}$$

where the various symbols have the same meanings as before. If we again let k^2 equal E_0/E, we have

$$\vartheta_2(k^2) = 2\pi k \int_1^\infty \frac{1}{1-\exp(-2\pi u k)} \log\frac{u+1}{u-1}\,\frac{du}{u^2}\,. \tag{12}$$

These results may be derived either from the formula given by Bethe, which is valid only for large electron energies, or from the asymptotic result given by Menzel and Pekeris,[7]

$$g = \frac{2\cdot 3^{1/2} l}{1-\exp(-2\pi l)} \log\frac{l+k}{l-k}\,, \tag{13}$$

where k^2 equals E_0/E as usual and l equals E_0/E'; E and E' are the initial and final energies of the electron, respectively. The quantity u in equation (12) is the ratio of l to k.

When E is large, $2\pi(E_0/E)^{\frac{1}{2}}$ is small, and for most of the relevant range of integration in equation (12) the denominator may be replaced by $2\pi uk$. The resultant integral may then be evaluated exactly, and we find that ϑ_2 is unity. Equation (11) can then be integrated, and we have

$$\frac{d\bar{E}}{dt} = -\frac{A n_p E_0 \bar{E}^{1/2}}{2\pi(3\pi)^{1/2} m^{1/2}}\,. \tag{14}$$

This is equivalent to a formula given by Menzel,[8] provided that $\bar{g}$ is set equal to $2\cdot 3^{\frac{1}{2}}/\pi$, or 1.10. Thus we see that the average value of g is very nearly unity, despite the fact that g varies from a small quantity to infinity over the range of integration. When $\bar{E}$ is small, g may be set equal to unity, as may be seen from the series expansions given by Menzel and Pekeris.[5] We may therefore assume that equation (14) is valid for intermediate velocities as well as for high velocities.

If we define T_d as in equation (9), the time of dissipation arising from free-free transitions becomes

$$T_d(f\text{-}f) = 2.7\times 10^6 \frac{1}{n_p}\left(\frac{\bar{E}}{E_0}\right)^{1/2} \text{years}\,. \tag{15}$$

Values of $T_d(f\text{-}f)$ are shown in Table 2 for various values of the root mean square proton velocity; the number of protons per cm^3 is again set equal to unity. It is evident from this table that, for most velocities, recaptures in the ground state are of negligible importance in the dissipation of energy. This is presumably true for recaptures in other lower states as well. The condition for continuity at the series limit indicates that recaptures in the higher quantum states will behave in the same way as the free-free transitions. Such recaptures will, of course, decrease the time of dissipation even further from the values given in Table 2.

Lastly, the dissipation of energy by direct encounters between dust particles must be computed. Let us consider an encounter between two particles of equal mass, m_d, such that the center of gravity of the two particles is at rest and their original relative velocity is V_1. Let the perpendicular distance between the original paths be equal to p_1. Then the total initial energy and angular momentum of the two particles is $\frac{1}{4}m_d V_1^2$ and $\frac{1}{2}p_1 m_d V_1$.

[7] Ref. 5, eqs. (1.47) and (1.49).

[8] *Ap. J.*, **85**, 330, 1937, eq. (30); a factor K/h has been omitted from this equation.

If V_2 is the relative velocity of separation and p_2 the value of p after collision, the energy loss per particle becomes

$$\Delta E = \frac{1}{8} m_d \left(V_1^2 - V_2^2 \right) \tag{16}$$

while the conservation of angular momentum yields

$$p_1 V_1 = p_2 V_2 . \tag{17}$$

The elimination of V_2 from equations (16) and (17) gives

$$\Delta E = \frac{1}{8} m_d V_1^2 \left(1 - \frac{p_1^2}{p_2^2} \right) . \tag{18}$$

It is obvious that the total loss of energy must be the same if the center of gravity is not at rest, and we may therefore use equation (18) for the energy loss in every collision.

The maximum loss of energy occurs when p_2 is a maximum. Since p_2 can scarcely exceed 2σ, the geometrical diameter of each particle, we may replace p_2 by 2σ in equation (18) and multiply the resultant expression by ζ, the ratio of the actual energy loss to the maximum loss possible. To find the rate of decrease of the mean kinetic energy $\bar{E}$, we must multiply ΔE by $2\pi p_1 dp_1 V_1 n_d$, where n_d is the number of dust particles per cm^3, and then integrate over p_1 from zero to 2σ. This yields

$$\frac{d\bar{E}}{dt} = -\frac{\pi}{4} \bar{\zeta} \sigma^2 m_d V_1^3 n_d , \tag{19}$$

where a mean value of ζ has been taken.

Finally, we must determine the mean value of the factor V_1^3 in equation (19). If the distribution of dust-particle velocities is assumed to have spherical symmetry, then

$$\overline{V_1^2} = 2\overline{v_d^2} , \tag{20}$$

where $\overline{v_d^2}$ is the mean square velocity of the individual particles. If the distribution of dust velocities were Maxwellian, we should have

$$\overline{V_1^3} = \frac{2^{7/2}}{3^{3/2}\pi^{1/2}} \left(\overline{V^2} \right)^{3/2} . \tag{21}$$

Although there is apparently no reason why the velocities of very rapidly moving dust particles should obey the Maxwellian distribution, equation (21) should provide an adequate approximation to the true state of affairs, particularly since the numerical factor in equation (21) should not differ much from unity in any case. If we let m_d equal $4\pi\sigma^3 d/3$, where d is the density of matter within the particle, and let n_d equal ρ_d/m_d, where ρ_d is the density of dust in grams/cm^3, we may combine equations (19), (20), and (21) to find

$$\frac{1}{\bar{E}} \frac{d\bar{E}}{dt} = -\frac{4}{(3\pi)^{1/2}} \frac{\rho_d \bar{\zeta}}{\sigma d} \left(\overline{v_d^2} \right)^{1/2} \tag{22}$$

where now $\bar{\zeta}$ denotes an average over V_1 as well as over p_1. With the same definition of T_d as before, we find that if σ equals 10^{-5}cm, d equals 7.8, and ρ_d is 1.7×10^{-24}, equation (22) gives

$$T_d \,(\text{dust}) = \frac{1.1 \times 10^{12}}{\bar{\zeta} \left(\overline{v_d^2} \right)^{1/2}} \text{ years} . \tag{23}$$

The quantity $\bar{\zeta}$ is not likely to be very small when $\overline{v_d^2}$ is large. For the rapid collisions we are concerned with here, the energy of impact is very much greater than the binding energy of the particles, which is normally the source of the elastic forces. Hence such rapid collisions will probably be completely inelastic, and two such particles will in all likelihood vaporize when their velocity of impact is several hundred kilometers per second. To find a lower limit on T_d, however, $\bar{\zeta}$ has been set equal to 0.1 in the computation of the values in Table 2.

It is evident from Table 2 that interstellar matter of appreciable density will have lost its high energy in 10^7 years or less. There is no evidence for any mechanism which can avert this loss of kinetic energy. Ionization by radiation provides at most an energy comparable to E_0 for each such recombination; ionization by electron impact is likely to be more frequent, and this involves no net change in $\bar{E}$. Interaction with stars will be small, particularly at such high velocities. For a particle to be deflected 90° by a star of solar mass, moving with a relative velocity of 200 km/sec, the undisturbed path of the particle must come within 4 solar radii of the sun's surface. Even though this distance may be considerably increased by radiation pressure from the brighter stars, such close encounters are rare and may be neglected.

The role of cosmic rays is somewhat more obscure, since little is known about the numbers of low-energy particles, which would be of importance in this connection. Particles of the energy and abundance observed terrestrially may be shown to be unimportant. The number of particles entering the earth's atmosphere per cm^2 per sec is[9] 0.09. Since the cross-section of a light nucleus for cosmic-ray impact is roughly $10^{-25} cm^2$, the mean life between encounters is 10^{18} years. Since the mean energy acquired per encounter is at most 10^{10} e.v., this corresponds to a gain of 1 e.v. per particle in 10^8 years, which is insufficient to offset a loss of several hundred e.v. per particle in 10^7 years.

If the mass of interstellar matter in a galaxy is comparable with that of the stars, it is difficult to find any mechanism which will maintain the particles of the medium in a state of high kinetic energy. An energy loss of 400 e.v. in 10^7 years, corresponding to an initial proton velocity of roughly 300 km/sec, is a loss of 1 erg per gram per second; and to maintain this in a medium of appreciable mass requires an energy source comparable to that of all the stars. There is no evidence whatever for such an additional source of energy. We may conclude that, on the basis of present theory, the mean square velocity of interstellar particles cannot possibly be as high as 100 km/sec if the density of such matter is appreciable; in all probability interstellar matter is in kinetic equilibrium with a velocity temperature between 5,000° and 20,000°, and with velocities of not more than 20 km/sec.

This analysis refers, of course, to purely random velocities. These results, therefore, do not exclude the possibility that the interstellar medium could be supported by large-scale currents with velocities much greater than the microscopic random velocities of the individual particles. If such currents are assumed to be irregular, as in the case of turbulent stellar atmospheres, the energy of macroscopic motion would soon be dissipated in all probability. When two such currents, with velocities far exceeding the velocity of pressure waves in the medium, encountered each other, the directed macroscopic velocities would tend to be converted into random microscopic motions. The only current system which could apparently be stable in 10^9 years or more would be a simple rotation of the medium about the center of the system—a case which is, of course, relevant in an elliptical galaxy. With this exception one may assume that large-scale currents play no direct part in the equilibrium of the interstellar medium.

2. SPHERICAL SYSTEMS

The equilibrium of interstellar matter in a spherical galaxy is simplified when the mean square velocity of the interstellar particles is much less than that of the stars. As

[9] I. S. Bowen, R. A. Millikan, and H. V. Neher, *Phys. Rev.*, **53**, 217, 1938.

we shall see below, the total mass of the interstellar medium in such a case must be much less than that of the stars and will therefore not affect appreciably the structure of the stellar system. The problem therefore reduces to the equilibrium of a gas in a potential field which arises partly from a known distribution of stars, partly from the gas itself.

The specific analysis is complicated by two factors. In the first place, the structure of the spherical galaxies is not well known. Second, the mass of the medium complicates the equations. General limits will therefore be discussed for the most part. Where effects produced by the precise structure of a galaxy are of interest, the Emden polytrope for $n = 5$ will be used. This is known to give a good approximation for globular clusters, and even for galaxies it should give some indication of the general effects to be expected when the mass of the system is highly concentrated toward the center.

First, let us derive the form of the virial theorem which will be useful. The equation of motion in the x-direction for a particle of mass m_p may be written

$$m_p \frac{d^2x}{dt^2} = F_x \,. \tag{24}$$

A subscript p will be used throughout to denote interstellar particles, either dust or atoms. If we multiply equation (24) by x, we find

$$\frac{1}{2} m_p \frac{d^2x^2}{dt^2} - m_p \left(\frac{dx}{dt}\right)^2 = xF_x \,. \tag{25}$$

If it is assumed that the system comprises a large number of identical particles in a steady state, we may average over all the particles, in which case the second derivative in equation (25) vanishes. The contribution of the atomic interaction forces to xF_x may be neglected, on the average, compared to the external and gravitational forces. If we assume also that both the distribution of velocities and the potential field possess spherical symmetry, then equation (25) becomes

$$\overline{v_p^2} = -\overline{rF_r}/m_p \,, \tag{26}$$

where F_r is the radial force, and $\overline{v_p^2}$ is the mean square velocity of the particles in question.

For a gas of small mass in a cluster of uniform stellar density ρ_{s0} the radial force is given by

$$\frac{F_r}{m_p} = -\frac{4\pi G \rho_{s0}}{3} r \,. \tag{27}$$

The assumption that ρ_{s0} is constant is legitimate when the medium is concentrated toward the core of the system. From equation (26) we have in this case

$$\overline{v_p^2} = \frac{4\pi G \rho_{s0}}{3} \overline{r_p^2} \,, \tag{28}$$

where a subscript p is used to indicate that r^2 as well as v^2 is averaged over all the particles (atoms or dust) in the medium.

For the stars the force per unit mass is less than that given by equation (27), since the density decreases outward. From equation (28) and the corresponding inequality for $\overline{v_s^2}$, we have, therefore, the inequality

$$\frac{\overline{r_p^2}}{\overline{r_s^2}} < \frac{\overline{v_p^2}}{\overline{v_s^2}} \,. \tag{29}$$

When we come to extend this result to a specific stellar structure, such as the Emden polytrope $n = 5$, we find that $\overline{r_s^2}$ is infinite. The analysis is therefore best given in terms of $r_{s\frac{1}{2}}$ and $r_{p\frac{1}{2}}$, the radii containing half the stellar mass and half the mass of the medium, respectively. The analysis involves a determination of the mean potential energy of the polytrope.[10] The final result is

$$\frac{r_{p1/2}}{r_{s1/2}} = 0.414 \left(\frac{\overline{v_p^2}}{\overline{v_s^2}} \right)^{1/2} . \tag{30}$$

We may infer that the ratio of the size of the interstellar system to that of the stellar one is in general somewhat less than the ratio of the root mean square velocities.

The neglect of the total mass M_p of the interstellar particles is valid, provided that the density of the medium is everywhere less than that of the stars. When this is not the case, when ρ_p is greater than ρ_{s0}, it is evident that the gravitational attraction of the medium on itself will be greater than that of the stars on the medium. We may replace equation (28) by the more general formula

$$\overline{v_p^2} = \frac{4\pi G \rho_{s0}}{3} \overline{r_p^2} + \beta \frac{GM_p}{(\overline{r_p^2})^{1/2}} , \tag{31}$$

where β is a constant of unit order of magnitude. The second term in equation (31) is the one which usually appears in applications of the virial theorem and is equal but opposite in sign to the potential energy per unit mass of a sphere of gas in its own gravitational field.

It is evident from equation (31) that if M_p is fixed there is a value of $\overline{r_p^2}$ such that $\overline{v_p^2}$ is a minimum. Similarly, if $\overline{v_p^2}$ is fixed, there is a value of $\overline{r_p^2}$ at which M_p is a maximum. This maximum value of M_p is given by

$$\{M_p(\max)\}^2 = \frac{1}{9\pi\beta^2\rho_{s0}} \left(\frac{\overline{v_p^2}}{G} \right)^3 , \tag{32}$$

which may be written as

$$\left\{ \frac{M_p(\max)}{M_s} \right\}^2 = \frac{4}{27\beta^2} \left(\frac{\overline{v_p^2} r_{s1/2}}{GM_s} \right) \frac{3M_s}{4\pi r_{s1/2}^3 \rho_{s0}} . \tag{33}$$

It is clear that $3M_s/4\pi r_{s\frac{1}{2}}^3$ is twice the mean stellar density interior to $r_{s\frac{1}{2}}$; this will be less, as a rule, than the central density ρ_{s0}. Since $GM_s/r_{s\frac{1}{2}}$ is roughly equal to $\overline{v_s^2}$ and β is approximately unity, we have

$$\frac{M_p(\max)}{M_s} \lesssim 0.38 \left(\frac{\overline{v_p^2}}{\overline{v_s^2}} \right)^{3/2} . \tag{34}$$

If we turn again to the polytrope $n = 5$, we find that in this special case $3M_s/4\pi r_{s\frac{1}{2}}^3$ is equal to 0.447 ρ_{s0}, while $GM_s/r_{s\frac{1}{2}}$ is equal to 2.60 $\overline{v_s^2}$. These two factors reduce the constant in equation (34) from 0.38 to 0.060. This indicates that equation (34) gives a generous upper limit on M_p. If, in accordance with the results of section 1, we assume that the ratio of root mean square velocities for stars and particles is roughly equal to ten, it

[10] It is sometimes stated that the potential energy of the polytrope $n=5$ is infinite, since a factor $n-5$ appears in the usual formula for the total potential energy. But the radius R of the system is also infinite in this case; the energy is, in fact, finite, and may be determined by a direct integration.

follows from equation (34) that the maximum possible mass of interstellar matter in a spherical galaxy is at most 4×10^{-4} of the stellar mass and that any such matter must be highly concentrated toward the center of the galaxy.

The existence of a maximum mass for the medium may be explained simply. Let us consider an assemblage of interstellar particles whose mean square velocity is fixed and whose distribution in the cluster satisfies the equations of equilibrium; let us examine the sequence of configurations which is obtained as the total mass M_p is gradually increased. When M_p is zero the value of $\overline{r_p^2}$ will satisfy equation (28). As the mass of the medium is gradually increased, the self-attraction of the medium begins to become important. At first this may be offset by a contraction in the medium, reducing the attraction of the stars on the interstellar matter. Eventually, however, a point is reached at which a further contraction increases the self-attraction exactly as much as it decreases the attraction of the stars. At this point no increase in M_p is possible without also increasing $\overline{v_p^2}$—this is the point of maximum mass for a fixed mean square velocity. When M_p has a value less than this critical one, equation (31) will have two relevant roots for $\overline{r_p^2}$, one corresponding to a diffuse configuration in which the gravitational attraction of the stars is predominant, the other, a dense system subject primarily to its own self-attraction.

The relevance of this maximum mass is restricted by the fact that the analysis holds only for systems possessing no angular momentum whatever. Most spherical galaxies probably have some angular momentum, and in such a case interstellar matter could contract to the equatorial plane, forming a flattened, rapidly rotating disk of dark matter of the type discussed in the next section. The total mass of such matter could not be very great, however, since the gravitational attraction of a very massive layer of dark matter would impart some ellipticity to the observable stellar distribution. In any case we may conclude that interstellar dust and atoms play a wholly subordinate role in the constitution of spherical stellar systems of large mass and large random stellar velocity.

In systems of small mass, such as globular clusters, the random stellar velocities are of the same order as the velocities of the particles. In such systems the total mass of dust particles present could in theory be very large, provided that not more than a small number of atoms was present. An appreciable number of atoms would slow down the dust particles as is shown in paper I and lead eventually to a collapse of the medium, unless the mass of atoms present exceeded sufficiently the mass of dust to support the dust particles.

For a primarily gaseous medium, on the other hand, a new restriction appears. If the mean square atomic velocities were slightly greater than those of the stars and M_s were assumed to be much greater than M_p, the atoms would apparently leave the system entirely. According to equation (26), the average value of $r\mathrm{F}_r$ must vary directly with the mean square velocity. While it is easy to find a distribution of matter for which this average will be very much decreased, given the gravitational field of a particular stellar system, there is a limit to the amount this quantity can be increased. Since most of the stars are near the region in which rF_r is a maximum, the average value of this quantity for any distribution of matter will not much exceed its average value for the stars. For the polytrope $n=5$, for instance, the maximum value of rF_r is only 1.31 times its average value for the entire polytrope. It follows that interstellar particles with a mean square velocity some 20 or 30 per cent greater than the velocity of the stars and a total mass considerably less than that of the stars cannot possibly be in equilibrium within a cluster.

A disequilibrium of this sort would not lead to an immediate escape of the medium, provided that the mean square particle velocities were less than the mean square velocity of escape. In fact, the medium would expand adiabatically to reach a new equilibrium with lower mean square velocities of the particles. But in the case of atoms the

kinetic temperature is presumably determined essentially by the color temperature of the ionizing radiation and other factors; if these various factors tended always to give the atoms a mean square velocity appreciably greater than that of the stars and if the gravitational attraction of the medium upon itself were unimportant, such an atomic medium would gradually expand and leave the cluster. If the mass of the interstellar atoms exceeded that of the stars, this difficulty would not arise. In such a case the medium would hold itself together under its own attraction, and the observed stellar system would be imbedded in a globular atomic cluster of much greater mass.

3. ELLIPTICAL SYSTEMS

The analysis of the preceding section must be modified for systems which possess angular momentum and axial symmetry. In such a case the interstellar medium will be confined to the equatorial plane, forming a highly flattened disk imbedded in the more extended elliptical aggregation of stars. If the initial distribution of the medium is assumed to be the same as that of the stars, then, as the random velocities of the interstellar particles decreased, there would be some contraction toward the galactic center as well as toward the equatorial plane. The constancy of angular momentum during such a contraction would lead to an increase of the centrifugal force, which would remain proportional to the inverse cube of the distance from the axis of rotation. A new equilibrium would therefore be reached in which the increased centrifugal force just balanced the attraction toward the galactic center; the medium would, of course, be revolving about the galactic center more rapidly at any point than the stars in the immediate neighborhood.

The relative contraction necessary to attain such an equilibrium may be computed on various assumptions; the ratio of the equilibrium and initial distances from the axis of rotation for a given element of matter is roughly equal to the ellipticity of the nebula or of the fourth root of the ellipticity, depending on whether the potential is that of a point mass or of a homogeneous spheroid. This subject is intimately connected with the uncertain problem of the origin of the galaxies. We shall therefore not consider the problem of the density distribution of interstellar matter with increasing distance along the equatorial plane but rather the distribution in directions perpendicular to this plane. Such an analysis rests on firm ground, since it depends only on the conditions of equilibrium and not on any assumed initial properties.

In the following analysis, distance from the equatorial plane will be denoted by z; the distance of a point from the axis of rotation will be denoted by R. As before, subscripts p and s will be used to distinguish quantities pertaining to the interstellar particles—dust or atoms—from those pertaining to the stars. Regions near the center of elliptical systems will not be discussed here, since these will be closely analogous to spherical galaxies; we shall consider, rather, the structure of the galaxy when R is relatively large.

The analysis depends on whether F_z, the gravitational force in the z-direction, arises primarily from the central mass of the system or from the neighboring matter in the equatorial plane. If the former is the case, then both particles and stars will move in the same external potential field, which for small values of z/R varies as z^2. It is clear that in such a case.

$$\frac{\overline{z_p^2}}{\overline{z_s^2}} = \frac{\overline{v_p^2}}{\overline{v_s^2}} . \tag{35}$$

The total mass of the interstellar medium per unit area of the equatorial plane, as well as the total stellar mass per unit area, is quite unrestricted in such a case, provided only that the total density is always less than the central mass of the galaxy, M_c, divided by

$4\pi R^3$; this is the usual condition that the attraction of the central mass be greater than the attraction of the local matter.

When the total density of stars and medium is greater than $M_c/4\pi R^3$, however, we may neglect the rest of the galaxy and as a first approximation consider only the one-dimensional problem, in which the gravitational potential Φ is determined by the equation

$$\frac{d^2\Phi}{dz^2} = 4\pi G(\rho_s + \rho_p), \tag{36}$$

while the condition of equilibrium gives

$$\frac{d}{dz}\left(\frac{1}{3}\rho_s \overline{v_s^2}\right) = -\frac{d\Phi}{dz}\rho_s, \tag{37}$$

together with an equation for the interstellar particles, identical with equation (37) except that a subscript p replaces the subscript s. One may assume that $\overline{v_s^2}$ and $\overline{v_p^2}$ are not functions of z. This neglects primarily the dispersion in stellar masses, since the chief effect of such a dispersion is to increase $\overline{v_s^2}$ with z.

The solution of these equations depends on ρ_{p0} and ρ_{s0}, the densities of particles and stars when $z=0$. Let us assume first that ρ_{p0} is much less than ρ_{s0}. Then we may neglect ρ_p in equation (36); if we divide equation (37) by ρ_s, then differentiate with respect to z, and use equation (36) to eliminate $d^2\Phi/dz^2$, we have

$$\frac{d}{dz}\left(\frac{1}{\rho_s}\frac{d\rho_s}{dz}\right) = -\frac{12\pi G}{\overline{v_s^2}}\rho_s. \tag{38}$$

If we make the substitutions

$$\rho_s = \rho_{s0}\Lambda(\xi), \tag{39}$$

$$z = \xi\left(\frac{\overline{v_s^2}}{12\pi G\rho_{s0}}\right)^{1/2} \tag{40}$$

the equation assumes a dimensionless form. With the boundary conditions that $\Lambda(0)=1$ and that $\Lambda'(0)=0$, the solution of equation (38) becomes

$$\Lambda(\xi) = \operatorname{sech}^2(2^{-1/2}\xi). \tag{41}$$

The mass $M_s(\xi)$ per unit area between $-\xi$ and $+\xi$ is

$$M_s(\xi) = \left(\frac{2\overline{v_s^2}\rho_{s0}}{3\pi G}\right)^{1/2} \tanh(2^{-1/2}\xi). \tag{42}$$

From equations (40) and (42) it follows that $z_{s\frac{1}{2}}$, the value of z such that half the stellar mass per unit area lies between $z_{s\frac{1}{2}}$ and $-z_{s\frac{1}{2}}$, is given by

$$z_{s1/2} = 0.274\frac{M_s}{\rho_{s0}} \tag{43}$$

where M_s equals $M_s(\infty)$ and is simply the total stellar mass above and below a unit area of the equatorial plane. Since $\tanh(\infty)=1$, equation (42) gives M_s in terms of $\overline{v_s^2}$ and ρ_{s0}

For the interstellar particles, on the other hand, we may neglect the change in ρ_s and set $d\Phi/dz$ equal to $4\pi G\rho_{s0}z$. The equation of hydrostatic equilibrium for the particles then yields

$$\log\frac{\rho_p}{\rho_{p0}} = -\frac{6\pi G\rho_{s0}}{\overline{v_p^2}}z^2 . \tag{44}$$

The mass per unit area leads to the usual error function; if we determine the value of $z_{p\frac{1}{2}}$ by integrating equation (44) and if we take $z_{s\frac{1}{2}}$ from equation (43), substituting from equation (42) for M_s, we have

$$\frac{z_{p\frac{1}{2}}}{z_{s\frac{1}{2}}} = 0.87\left(\frac{\overline{v_p^2}}{\overline{v_s^2}}\right)^{1/2} . \tag{45}$$

Here, as in equation (35) and in the globular galaxies, the ratio of the dimensions of the two systems is roughly equal to the ratio of the root mean square velocities.

The chief difference between the elliptical and the globular systems is the absence of any maximum mass for the interstellar medium. No matter how great the mass of interstellar matter, it is always possible to make $z_{p\frac{1}{2}}$ so small that the mean square velocity is arbitrarily small. If ρ_{p0} should exceed ρ_{s0}, however, equation (44) is no longer applicable. To find the distribution of the medium in this case, a new solution of the equations of equilibrium must be found. If ρ_{p0} is considerably greater than ρ_{s0}, then ρ_p will exceed ρ_s in most of the region in which the density of interstellar matter is appreciable. One may in such a case assume that the distribution of the medium is independent of the presence of stars and set ρ_s equal to zero in equation (36) for the gravitational potential Φ. The resultant equations for ρ_p are identical with equations (38)–(43)—derived for ρ_s on the assumption that ρ_p could be neglected—provided that a subscript p is substituted for the subscript s throughout.

When the equilibrium of the stars is considered in this case, however, the neglect of ρ_s in the determination of Φ will not yield an adequate approximation, if M_s exceeds M_p. In the general case a new solution of equation (38) must be found for ρ_s such that $\Lambda'(0)$ equals a finite value, determined by the gravitational attraction of the thin layer of interstellar dust and atoms. In the limiting case in which M_p is greater than M_s, we may, in fact, neglect ρ_s in the determination of Φ. For all values of z this gives $d\Phi/dz = 2\pi GM_p$. In such a case we have for the stars the usual isothermal distribution in a constant-force field, which gives

$$\log\frac{\rho_s}{\rho_{s0}} = -\frac{6\pi GM_p}{\overline{v_s^2}}z . \tag{46}$$

The value of $z_{s\frac{1}{2}}$ in this case may be found by a simple integration of equation (46).

To compare the results for interstellar matter and for stars in the case when M_p exceeds M_s, we take the value of $z_{p\frac{1}{2}}$ found when equations (42) and (43) are applied to dust and atoms rather than to stars and divide this by the value of $z_{s\frac{1}{2}}$ found from equation (46) above. The resultant ratio is

$$\frac{z_{p\frac{1}{2}}}{z_{s\frac{1}{2}}} = 1.57\frac{\overline{v_p^2}}{\overline{v_s^2}} . \tag{47}$$

We see that when the mass of interstellar matter exceeds that of the stars, the relative concentration varies as the energy rather than as the velocity. It is obvious that for intermediate cases, in which ρ_{p0} exceeds ρ_{s0} but M_p is less than M_s, the ratio of $z_{p\frac{1}{2}}$ to $z_{s\frac{1}{2}}$ will follow a relationship intermediate between equations (45) and (47).

Numerical values for $z_{p\frac{1}{2}}$ may be computed from these results. If the ratio of root mean square velocities is set equal to ten as before and if $z_{s\frac{1}{2}}$ equals 200 parsecs, the value of $z_{p\frac{1}{2}}$ equals 18 parsecs when ρ_{p0} is less than ρ_{s0}, and 3.1 parsecs when the total mass of interstellar matter is greater than that of the stars. If the mass of interstellar matter is an appreciable fraction of the mass of the system, $z_{p\frac{1}{2}}$ will clearly not exceed a few parsecs.

The density of the medium in this latter case would be at least 10^{-20} gm/cm^3, and possibly very much greater. With so great a density it is doubtful whether the electron temperature could remain as high as 10,000°, and it is likely that the root mean square velocity would fall, increasing the density even further. Such a medium would probably be unstable and would perhaps condense into stars, meteorites, or large dark bodies. But these processes of condensation would not increase $\overline{v_p^2}$, and the thin massive layer of matter, surrounded by a vastly more extended stellar envelope, would still remain. The probable state of matter in the equatorial plane will not be discussed in detail here.

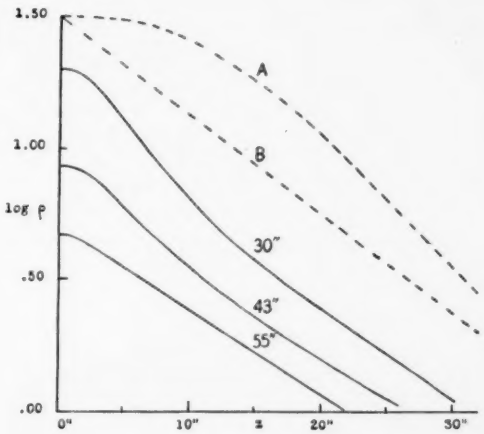

FIG. 1.—Stellar density distribution in NGC 3115. The logarithm of the observed luminosity density, ρ, is plotted against z, the perpendicular distance from the equatorial plane in seconds of arc. The two dashed curves are the theoretical results if ρ is a function of z only, for the two cases: A. A uniform isothermal gas under its own gravitational attraction. B. The same gas under the attraction of a massive equatorial layer of dark matter.

It should be pointed out that such a dark layer is equivalent in its effect to a distribution of very faint dwarf stars with small peculiar motions. In fact, the hypothetical equatorial layer of interstellar matter discussed here might quite possibly condense into stars of absolute magnitude +15 or fainter. The random velocities of stars formed in this way would obviously be small. From an observational standpoint it would be very difficult to distinguish a layer of such stars from a layer containing bodies roughly the size of meteorites; the phrase "dark matter" will be used to denote all such possibilities.

If a massive equatorial layer of this type should exist within an elliptical galaxy, it would lead to directly observable results. The mass deduced from the rotational velocities of the stars would be greater than the mass derived from the luminosity of the system. More important, the distribution of stars on each side of the equatorial plane would follow equation (46) rather than the quite different density function in equation (41). The former distribution is striking in its finite derivative at the equatorial plane. Unfortunately, this effect would be observable only if the plane of the galaxy were parallel to the line of sight from the earth.

These characteristics are remarkably close to the description of NGC 3115, analyzed

in detail by Oort.[11] The luminosity distribution in this elliptical system of class E7 is completely in disaccord with the mass distribution as deduced from the observed constant angular velocity.[2] Furthermore, the logarithmic gradients of luminosity density in the z-direction have a nearly constant slope very near to the equatorial plane. The values of log ρ as a function of z for various values of R are shown in Figure 1. These were taken from Figure 7 in Oort's paper; R and z are expressed in seconds of arc. The curved dashed line A shows the distribution to be expected from equation (41), when the stars themselves are primarily responsible for the gravitational attraction. The straight dashed line B represents the distribution given by equation (46), when the equatorial layer of dark matter is responsible for most of the gravitational force on the stars.

It will be noted that the observed curves in Figure 1 correspond to case B more closely than to case A. The observed logarithmic gradients depart from linearity for very small values of z, but a slight inclination of the equatorial plane to the line of sight would account for this effect. The curvature evident for larger values of z could be explained partly by a dispersion in stellar velocities and partly by the deviation of the potential field from the one-dimensional case discussed here. It seems difficult to account for the observational values of log ρ when z is moderately small, if only luminous stars are assumed to be present. The evidence for an equatorial layer of dark matter in NGC 3115 is suggestive but not conclusive. Further examination of elliptical galaxies, and particularly of the density gradients near the equatorial plane, would be necessary to decide the issue.

The central conclusion of the present paper, however, does not concern the possible existence of such a dark layer. The chief result is that, in NGC 3115 and probably in most of the elliptical and globular galaxies as well, the amount of interstellar matter throughout most of the volume of these systems—in the regions surrounding most of the stars—must be negligible. Unless there are unsuspected forces acting on interstellar particles, the light which comes from elliptical and globular systems of large mass must be almost entirely direct starlight, not diffuse or scattered light.

This view is supported by the failure to find space reddening or interstellar absorption lines in these objects. The lack of interstellar emission lines in elliptical objects.[12] is also consistent with this view, although the absence of early-type stars provides an alternative explanation for these observations. The chief support for these conclusions, however, is the essentially theoretical argument presented here. Better determinations of nebular masses would decide to what extent these results may be applied to all elliptical and globular galaxies.

YALE UNIVERSITY
January 1942

[11] *Ap. J.*, **91**, 273, 1940.

[12] N. U. Mayall, *Pub. A.S.P.*, **51**, 282, 1939.

NOTES ON ECLIPSING VARIABLES

HENRY NORRIS RUSSELL

ABSTRACT

Preliminary elements of an eclipsing variable should represent the whole light-curve and include ellipticity (with similar components), reflection, orbital eccentricity(if present), and limb darkening corresponding to the spectral type.

Corrections for difference in shape and gravity effect may then be made by tables in preparation by Kopal, resulting in improved elements. Only after this is a solution by least squares advisable.

Kopal's preliminary methods are laborious. That for partial eclipses is sometimes divergent, which can be avoided by a simple modification. For partial eclipses of uniform disks, the ratio of the radii is indeterminate for a certain value of the relative brightness.

A *nomogram* for the solution of partial eclipses of uniform disks is given, which illustrates also the cause of indeterminacy.

The tables for "completely darkened" circular disks are exactly applicable to eclipses of similar ellipsoids, upon which the coefficient of darkening is 1 and that of the gravity effect ¼. For actual ellipsoidal stars corrections for nonuniform distribution of brightness over the surface are necessary in accurate work.

The problem of determining the elements of an eclipsing variable from photometric data falls in the same general class as that of finding the orbit of a visual or spectroscopic binary. The percentage precision of the observations is low; and to obtain satisfactory results their number must greatly exceed that of the unknowns—and they must be well distributed over the whole period.[1] The solution is made from a curve (light-curve, velocity-curve, etc.) drawn empirically to follow the course of the observations; but it should never be forgotten that the computer's purpose is to represent the observations and not the curve.

It is therefore highly desirable that the method of solution should lead initially to parameters defining the curve, from which a theoretical curve can at once be computed and compared with the observations. When a satisfactory curve has been obtained, the conventional elements may then be derived from its parameters.

This primary solution is peculiar to the type of problem—visual, spectroscopic, and eclipsing binaries, being handled by radically different analytical methods. When a fairly good first solution has been obtained, it may be improved by general methods common to all the problems. Prerequisite to a second approximation is a precise method for calculating the curve from a given set of parameters. If these parameters have been found by the application of a definite, but in some respects approximate, method to the observed curve, the old "method of false position" may be used. Let O be the observed curve, C that computed from the parameters. Construct a new curve N, which is at every point as far below O as C is above it. From this curve, with the same method of solution, derive new parameters, and from these a new computed curve C'. The latter should be much closer to O than C was. Repetition of this process, if necessary, should result in a good fit—if one can be obtained at all. There is no general guaranty of the convergence of these approximations; but, if they fail, there is little or no hope that the far more laborious adjustment by least squares would give significant results.

Only after a really good fit has thus been obtained is it justifiable to attempt the latter —remembering that the test of a good preliminary job is that the least-square corrections should be of the same order of magnitude as their probable errors.

The principal differences between the eclipse problem and other binary star studies are: (1) The principles on which the theory is based are primarily geometrical, and not

[1] Or most of it, in the case of a visual binary.

dynamical. (2) The relations between the light-curve and the parameters which define it are complicated. (3) The number of parameters necessary for a complete specification of the system is large.

The principal complications are as follows: (*a*) The star disks appear darkened toward the limb. (*b*) The components will be distorted by tidal and centrifugal forces. (*c*) The intrinsic brightness of their surfaces will vary from point to point with the "local" gravity, (*d*) and also on account of the heating of each component by the radiation of the other. (*e*) The orbit may be eccentric.

Clear evidence of each one of these influences has been found in well-observed light-curves, and all but the last are usually present, though sometimes insensible.

I. DETERMINATION OF THE ELEMENTS

A satisfactory first approximation should give a good representation of the whole course of the light-curve, in eclipse and outside. Hence ellipticity and "reflection" must be taken into account. Fortunately, this can be done with very little extra work. Orbital eccentricity makes more trouble but must obviously also be included when sensible.

The degree of limb darkening has important effects on the deduced *elements;* but the *light-curves* derived on different assumptions usually differ very little. In deriving intermediary elements it appears best to assume a value—preferably depending on the spectral class of the star.[2] Corrections to this assumption and allowance for difference in shapes of the components and for uneven distribution of brightness over their surfaces belong to the later adjustment.

Tables for calculating the corrections just mentioned are being prepared by Dr. Kopal.[3] If corrections are calculated from the intermediary elements, the resulting light-curve will agree *worse* with the observations than will the uncorrected curve, because the intermediary adjustment must take up a large part of the influence of the neglected factors. The corrections themselves should be well determined; and, if the observations are corrected for them and a new intermediary solution made, a good set of elements should result.

It appears to the writer that it is only after such corrected elements are available that the application of least squares is justifiable. The intermediary elements must be good enough to permit the accurate calculation of the corrections; but they need not give the best possible fit that can be obtained if the corrections are ignored.[4]

In the intermediary solutions freehand light-curves are very useful. The determination of the elements is often rather a delicate matter, and no really good solution can be made unless the whole course of the variation—during eclipses and outside them—is closely fixed by a plot of the observations. Under these conditions the reading from a freehand light-curve at any phase should be more accurate than any individual observed point near by. By reading the curve for equidistant values of the light-loss (α or n), the calculations may be greatly simplified, with no loss of accuracy.

The methods of solution developed thirty years ago by Shapley and the writer[5] were based on this principle. The number of eclipsing variables was already great; hence numerous tables were prepared to save time for the computer. Increased precision in these tables is now important, and the fundamental tables have been recomputed by Zessewitsch.[6] A comprehensive set of tables, for several degrees of darkening, is in preparation by Dr. John E. Merrill.

[2] Kopal, *Pub. A.A.S.*, **10**, 134, 1941 (observed data); Pannekoek, *M.N.*, **95**, 733, 1935 (theory).

[3] Personal communication.

[4] Compare the correction of a comet's orbit for perturbations.

[5] Russell, *Ap. J.*, **35**, 315, and **36**, 54, 1912; Russell and Shapley, *Ap. J.*, **36**, 239 and 385, 1912.

[6] *Bull. Inst. Astr. Leningrad*, No. 45, 1939, and No. 50, 1940.

The methods recently suggested by Dr. Kopal[7] appear to the writer to be needlessly laborious. For total eclipses his method is based on the same principle as the writer's; but his function F must be calculated anew for each trial, while ψ in the older paper was tabulated to save the computer such labor.

For partial eclipses both methods rest on the fundamental equations[8]

$$\sin^2 \theta(n) = C_1(p - p_0) + C_2(p^2 - p_0^2) , \tag{1}$$

$$a_0 = 1 - \lambda_1 + \frac{1 - \lambda_2}{Q(k,a_0)} . \tag{2}$$

Here

$$p = p(k, na_0) , \qquad p_0 = p(k, a_0) ,$$

$$C_1 = r_1 r_2 \csc^2 i , \qquad C_2 = r_2^2 \csc^2 i = kC_1 .$$

The older method combines equations (1) and (2) to get

$$\frac{\sin^2 \theta(n)}{\sin^2 \theta(\frac{1}{2})} = \chi(k, a_0, n) . \tag{3}$$

When χ and Q have been tabulated—and also $p(k, a)$—the solution of equations (1) and (3) may be found without computation by the nomogram described in section II. Otherwise, values of either k or a_0 may be assumed, those of the other parameter determined from either equation (2) or equation (3) and the resulting pairs substituted in the other equation.

Values for which the functions are tabulated may always be "assumed," and only simple interpolation in the double-entry tables is required, so that the method is fairly rapid. It has the great advantage of showing the range of uncertainty of the solution, which is often great.

Kopal starts also with an assumed value of k, and gets a_0 from equation (2). He then computes n for each observation, finds $p(k, na_0)$ from the table, sets up the system of equations (1) and solves for C_1 and C_2. Then C_2/C_1 gives a new value of k, with which the process is repeated, until the initial and final values of k agree.

This laborious iteration may be avoided. If an assumed value k_1 leads to $C_2/C_1 = k_1'$, and k_2 to k_2', then $k_1 + x(k_2 - k_1)$ should lead to $k_1' + x(k_2' - k_1')$, if second-order variations are negligible. Equating these,

$$k = k_1 + xk_2 = \frac{k_1 k_2' - k_1' k_2}{k_2' - k_2 - k_1' + k_1} . \tag{4}$$

Even so, the formation and solution of two sets of equations involves much more labor than the other method.

The older paper gave values of χ only for $n = 0$, $\frac{1}{4}$, and $\frac{3}{4}$, which are hardly sufficient to define the light-curve. Dr. Merrill's tables give χ for $n = 0.0$, 0.1, 0.2, 0.25, 0.4, 0.6, 0.8, 0.9, and 0.95, which should suffice in any case. The final test of any solution is, of course, to compute the light-curve and plot it against the observations. With these tables this will be simple. Otherwise the light-curve may be computed accurately from the orbital elements and the ψ table.[9]

[7] *Ap. J.*, **94**, 145, 1941.

[8] For the notation see the papers just cited.

[9] Russell, *Ap. J.*, **35**, 331–332, 1912.

To discuss the process of approximation by Kopal's method, suppose that a set of points on an exact light-curve are to be represented. If the initially assumed value of k happens to be correct, equation (1) will give the true values of C_1, C_2, at once. Otherwise they will not (as Dr. Kopal has stated), since the values of p and p_0 corresponding to the assumed and true values of k will differ.

The exact equations of variation, to the first order, are easily found to be

$$d(\sin^2\theta) = P_1 dC_1 + P_2 dC_2 ,$$

when

$$P_1 = 2\left\{ p - p_0 - k(1 + kp)\frac{dp}{dk} + k(1 + kp_0)\frac{dp_0}{dk} \right\} ,$$

$$P_2 = p^2 - p_0^2 + 2(1 + kp)\frac{dp}{dk} - 2(1 + kp_0)\frac{dp_0}{dk} .$$

The analysis may be simplified by setting

$$dC_2 = k dC_1 + C_1 dk .$$

Then

$$d(\sin^2\theta) = P_0 dC_1 + P_2 C_1 dk , \tag{5}$$

when

$$P_0 = 2(p - p_0) + k(p^2 - p_0^2) . \tag{6}$$

The same transformation reduces Kopal's equation to

$$d(\sin^2\theta) = P_0 dC_1 + (p^2 - p_0^2) C_1 dk . \tag{7}$$

It suffices to discuss the case of uniform disks (where the analysis is simpler). Here equation (2) becomes

$$a_0 = 1 - \lambda_1 + \frac{1 - \lambda_2}{k^2} \qquad (a = na_0) .$$

We have also[10]

$$p = \cos\varphi_2 - \frac{1}{k}(1 - \cos\varphi_1) ,$$

$$\pi a = \varphi_2 - \sin\varphi_2 \cos\varphi_2 + \frac{1}{k^2}(\varphi_1 - \sin\varphi_1 \cos\varphi_1) ,$$

$$\sin\varphi_1 = k \sin\varphi_2 .$$

It follows that

$$\frac{dp}{dk} = -\frac{1}{k^2}(1 - \varphi_1 \csc\varphi_1 + \pi n(1 - \lambda_2)\csc\varphi_1) .$$

If L_1 is the light of the larger star, $1 - \lambda_2 = k^2 a_0 L_1$, and

$$\frac{dp}{dk} = \frac{1}{k^2}(1 - \varphi_1 \csc\varphi_1) + \pi a L_1 \csc\varphi_1 . \tag{8}$$

[10] Russell, *Ap. J.*, **90**, 665, 1939.

These equations must be discussed numerically (except for eclipses too shallow to be observable). The case $k = 0.8$, $p_0 = 0$, has been computed, with the results shown in Table 1. For any given value of p, P_2 is a linear function of L_1. It suffices to compute it for $L_1 = 0$ and $L_1 = 1$.

TABLE 1

PARTIAL ECLIPSE (k=0.8, p_0=0)

p	+0.000	+0.151	+0.310	+0.476	+0.646	+0.821	+0.911	+1.000
a	+0.414	+0.328	+0.243	+ .163	+0.091	+0.034	+0.012	+0.000
$\frac{1}{k^2}(1-\varphi_1 \csc \varphi_1)$	−0.194	−0.164	−0.133	− .100	−0.067	−0.034	−0.018	+0.000
$\pi a \csc \varphi_1$	+1.771	+1.489	+1.194	+ .898	+0.598	+0.300	+0.149	+0.000
P_2 if L_1=0.00	+0.000	+0.043	+0.152	+ .338	+0.603	+0.942	+1.158	+1.388
P_2 if L_1=1.00	+0.000	−0.156	−0.410	−0.730	−1.132	−1.599	−1.866	−2.156

It was found that in both cases (and hence in all intermediate ones), P_2 was representable by the expression $a_1(p - p_0) + a_2(p^2 - p_0^2)$, with an average residual of ±0.004 —almost within the error of the slide-rule calculations.

When

$$L_1 = 0\,, \qquad a_1 = +0.098\,, \qquad a_2 = +1.290\,.$$

When

$$L_1 = 1\,, \qquad a_1 = -0.985\,, \qquad a_2 = -1.171\,.$$

With sufficient accuracy, then, we may set (since $p_0 = 0$)

$$P_2 = (0.098 - 1.083\,L_1)p + (1.290 - 2.461\,L_1)p^2\,.$$

Now

$$P_0 = 2p + 0.8p^2\,;$$

hence

$$P_2 = AP_0 + Bp^2\,,$$

where

$$A = 0.049 - 0.542\,L_1\,, \qquad B = 1.251 - 2.027\,L_1\,.$$

If x and y are the values of dC_1C_1dk resulting from the application of Kopal's equation (7) to the data, we have by equation (5)

$$P_0x + p^2y = P_0dC_1 + P_2C_1dk = P_0(dC_1 + AC_1dk) + Bp^2C_1dk = d(\sin^2\theta)\,. \qquad (9)$$

Hence

$$x = dC_1 + AC_1dk\,, \qquad y = BC_1dk\,. \qquad (9a)$$

The depths of minima are $1 - \lambda_1 = 0.414(1 - L_1)$ (occultation), and $1 - \lambda_2 = 0.265\,L_1$ (transit). We then have (Table 2).

TABLE 2

L_1	0.000	0.091	0.124	0.200	0.400	0.618	0.800	1.000
$1-\lambda_1$	0.414	0.386	0.362	0.331	0.248	0.154	0.083	0.000
$1-\lambda_2$	0.000	0.024	0.033	0.053	0.106	0.164	0.212	0.265
A	0.049	0.000	−0.018	−0.059	−0.168	−0.286	−0.385	−0.493
B	1.251	1.068	+1.000	+0.846	+0.440	+0.000	−0.371	−0.776

When L_1 is small (large star faint), the first approximation by Kopal's method is tolerably good and becomes very close if L is near 0.11. But when L_1 is large, it gives the wrong sign for dk and diverges when iterated.

The interpolation method still works. If k_0 is the true value, and $k_1 = k_0 + z_1 \ldots$, equation (9*a*) gives

$$k_1' = k_1 - (1 - B)z_1 .$$

Hence

$$k_1k_2' - k_2k_1' = Bk_0(z_1 - z_2) ,$$

$$k_2' - k_2 - k_1' + k_1 = B(z_1 - z_2) .$$

Hence k is given by equation (4) as the ratio of two quantities, each derived from the difference of much larger computed quantities, and of the order of B. When B is small, k is therefore badly determined, and when $B = 0$ it is indeterminate.

A least-squares solution of equation (9) with weights, w, corresponding to mean error, ϵ_0, gives the normals

$$Dx + Ey = \ldots ,$$

$$Ex + Fy = \ldots ,$$

where

$$D = \Sigma wP_0^2 , \qquad E = \Sigma wP_0p^2 , \qquad F = \Sigma wp^4 \ldots .$$

The values of D, E, F depend only on the distribution and weights of the observations. With equal weights and with p distributed uniformly between its limits 0 and 1, they are proportional to 0.661, 0.340, 0.200.

If we substitute $x' = x + Ey/D$ in the equations of condition, the new normals are

$$Dx' = \ldots , \qquad F'y = \ldots , \qquad F' = F - E^2/D .$$

Hence x' and y are independently determined, and the mean error of $Gx' + Hy$ is given by

$$\epsilon^2 = \left(\frac{G^2}{D} + \frac{H^2}{F'}\right)\epsilon_0^2 .$$

With the assumed typical distribution, $D' = 26\,F'$, and x' is much more accurately determined than y; also

$$x' = x + 0.51y = dC_1 + (A + 0.51B)C_1dk = (1 - 0.80A - 0.41B)dC_1 + (A + 0.51B)dC_2 .$$

The quantity which may be most accurately determined from the light-curve thus ranges from $0.45dC_1 + 0.69dC_2$ when $L_1 = 0$ to $1.71dC_1 - 0.89dC_2$ when $L_1 = 1$, and it equals dC_1 when $x = 0.44$ (in the example here discussed). When the minima are very unequal, the determinations of k, C_1, and C_2 have considerable weight; but, when they are nearly equal, all these become very uncertain. This uncertainty is independent of, and supplementary to, the uncertainty which arises when both eclipses are shallow.

II. A NOMOGRAM FOR THE SOLUTION OF PARTIAL ECLIPSES

The preliminary solution for partial eclipses may be made very simply with the aid of a nomogram. The equations to be solved are

$$\chi(k, a_0, n) = \frac{\sin^2 \theta(n)}{\sin^2 \theta(\frac{1}{2})}, \tag{10}$$

$$a_0 = 1 - \lambda_1 + \frac{1 - \lambda_2}{Q(k, a_0)}. \tag{11}$$

Here the functions χ depend on the degree of darkening of the eclipsed star, and Q upon that of the other component also. For specified values of the darkening they are fully defined numerically, though different for occultation and transit, except for uniform disks.

If we take as rectangular co-ordinates

$$x = a_0, \qquad y = \frac{1}{Q(k, a_0)},$$

then equation (11) represents a straight line. The contours in this plane corresponding to $\chi(k, a_0, n_1) = \text{const}$ may then be plotted for any value n_1 for which the function has been tabulated, first finding corresponding pairs of values k, a_0, from this table and then using the table of Q. The intersection of the straight line

$$x = 1 - \lambda_1 + (1 - \lambda_2)y \tag{12}$$

and the contour $\chi = \text{const}$ then determine directly the values of a_0 and $1/Q$. The contours $k = \text{const}$ may also be drawn in this plane, so that a_0 and k may be read directly.

For uniform disks, $Q = 1/k^2$, and the construction is simplified. In this case it is known that, if $\chi(k, a_0, n_1)$ is constant, $\chi(k, a_0, n_2)$ will be nearly so, for any other n_2, and any one value of χ practically fixes the whole curve.

The value $n = \frac{1}{4}$ was used in 1912; but it now appears that one corresponding to the lower portion of the light-curve, which is more accurately observable, would be preferable, hence $\chi(k, a_0, 0.8)$ has been used in Figure 1 (prepared by Mr. Alfred K. Blackadar, of the class of 1942, and drawn by Miss D. N. Davis). The co-ordinates are $x = a_0$, $y = 1/k^2$. If a thread is stretched across it so as to pass over the points $y = 1$, $x = 1 - \lambda_1 + 1 - \lambda_2$, and $y = a$, $x = 1 - \lambda_1 + a(1 - \lambda_2)$, its intersection with the curve $\chi = \sin^2 \theta(0.8)/\sin^2 \theta(0.5)$ immediately gives the values of a_0 and k.

With the aid of Merrill's new tables an accurate light-curve for the whole eclipse can then be quickly plotted. Inspection of this curve will show what changes in $\sin^2 \theta(0.5)$ and the χ's would improve the fit, while the more complicated changes resulting from an alteration of $\chi(k, a_0, 0.8)$ and, if necessary, of $1 - \lambda_1$, $1 - \lambda_2$, can be found from the nomogram.

The nomogram illustrates very clearly the degree of determinateness of the solution. The observational uncertainties of $1 - \lambda_1$, $1 - \lambda_2$, and χ can be estimated directly from the light-curve, and their effects on the solution become apparent.

Between $y = 1$ and $y = 1.5$, the χ-contours are almost perfectly straight, and the solution (whether graphical or analytical) is indeterminate to a high degree, for a certain slope of the intersecting line. This happens when the minima are of equal depth. The function χ has no singularity at $k = 1$. With the radius of the smaller star as unit, exactly the same geometrical figures and values of χ are obtained for $a_0' = k^2 a_0$, $k' = 1/k$, as

ordinarily for a_0 and k. On our nomogram, $x' = xy$, $y' = 1/y$, $(x - x')/(y - y') = xy/(1 + y)$. If $y - y'$ goes to zero, $y = 1$, and $dx/dy = \frac{1}{2}x$. The line $x = 1 - \lambda_1 + (1 - \lambda_2)y$ will touch the contour if $1 - \lambda_2 = \frac{1}{2}x = 1 - \lambda_1$. The appearance of the diagram suggests that the tangency is of a higher order. For any other values of a_0 and y,

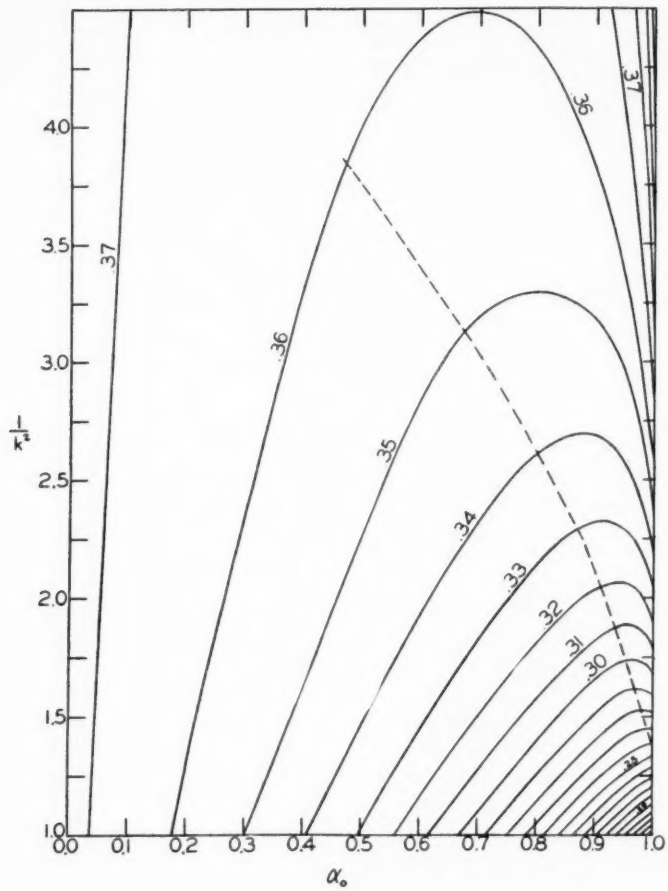

FIG. 1

their solution will be indeterminate if the tangent to the curve cuts the line $y = 1$ at a positive value of a_0. It is evident that, in all such cases, $1 - \lambda_1 < 1 - \lambda_2$; that is, the solution is always determinate when the hotter star is the smaller. Beyond the dashed curve on the nomogram, the solution is also determinate.

III. ELLIPTICITY, DARKENING, AND GRAVITY EFFECT

Let the equation of an ellipsoid E be

$$\frac{x^2}{A^2} + \frac{y^2}{B^2} + \frac{z^2}{C^2} = 1 . \tag{13}$$

This is converted into the sphere S',

$$x'^2 + y'^2 + z'^2 = R^2 , \tag{14}$$

by the transformation

$$x = A'x' , \qquad y = B'y' , \qquad z = C'z' , \tag{15}$$

when

$$A' = \frac{A}{R} , \qquad B' = \frac{B}{R} , \qquad C' = \frac{C}{R} . \tag{16}$$

A line with direction cosines lmn is transformed into one with direction cosines $l'm'n'$, where

$$l = hA'l' \qquad m = hB'm' , \qquad n = hC'n' , \tag{17}$$

when

$$\frac{1}{h^2} = A'^2L'^2 + B'^2M'^2 + C'^2N'^2 . \tag{18}$$

The plane $Lx + My + Nz = 0$ transforms into

$$L'x' + M'y' + N'z' = 0 ,$$

when LMN and $L'M'N'$ are direction cosines and

$$L = \frac{HL'}{A} , \qquad M = \frac{HM'}{B} , \qquad N = \frac{HN'}{C} , \tag{19}$$

$$\frac{1}{H^2} = \frac{L'^2}{A'^2} + \frac{M'^2}{B'^2} + \frac{N'^2}{C'^2} . \tag{20}$$

The angle γ between the line and the normal to the plane transforms into γ' where,

$$\cos \gamma = lL + mM + nN = Hh \cos \gamma' . \tag{21}$$

An element of surface $d\sigma$ with direction cosines LMN transforms into $d\sigma'$. The ratio of their projections on $x' = 0$ is

$$\frac{Ld\sigma}{L'd\sigma'} = \frac{dydz}{dy'dz'} = BC .$$

Hence

$$\frac{d\sigma}{d\sigma'} = \frac{A'B'C'}{H} . \tag{22}$$

By equation (21)

$$\frac{\cos \gamma d\sigma}{\cos \gamma' d\sigma'} = A'B'C'h . \tag{23}$$

These equations are exact.

Now let

$$3R = A + B + C\,, \qquad A' = 1 + a\,, \qquad B' = 1 + b\,, \qquad C' = 1 + c\,.$$

Then

$$a + b + c = 0\,, \qquad A'B'C' = 1 + ab + bc + ca + \ldots\,,$$

and, to the first order in a, b, c,

$$h = 1 - (al'^2 + bm'^2 + cn'^2) = 1 - q\,, \tag{24}$$

$$H = 1 + aL'^2 + bM'^2 + cN'^2 = 1 + Q\,, \tag{25}$$

$$d\sigma = (1 - Q)d\sigma'\,, \quad \cos\gamma d\sigma = (1 - q)\cos\gamma' d\sigma'\,, \quad \cos\gamma = (1 - q + Q)\cos\gamma'\,. \tag{26}$$

Let P be a point on E, with direction cosines LMN of the normal, and let lmn be those of the observer, O. After transformation, the direction cosines of O' are $l'm'n'$, and those of the normal to S' at P' are $L'M'N'$.

Let the surface brightness of E be $J = J_0(1 - g + yg/g_0)$, where g is the local and g_0 the mean value of gravity. By Clairaut's theorem,[11] to the first order, $g/g_0 - 1 = K(r/R - 1)$, where $K = -4$ for the Roche model and -1 for a homogeneous ellipsoid. (In general, $K = (2k - 4)/(2k + 1)$, where k is the constant which appears in the formula for the dynamical ellipticity.) The co-ordinates of P' are $x' = L'R$, etc.; those of P, $x = A'L'R$, etc. Hence

$$r = R[1 + (aL'^2 + bM'^2 + cN'^2) + \ldots.] = R(1 + Q)\,,$$

and

$$J = J_0(1 + KyQ)\,. \tag{27}$$

If limb darkening is present, the apparent surface brightness of E at P, as seen from O, will be

$$J_a = (1 - x + x\cos\gamma)J = J_0\{(1 - x)(1 + KyQ) + x\cos\gamma'(1 - q + [1 + Ky]Q)\}. \tag{28}$$

The surface brightness of S' at P', as seen from O', will be

$$J'_a = J_a\cos\gamma' d\sigma'/\cos\gamma d\sigma = (1 - q)J_a\,.$$

The expression (28) becomes simple in two cases:

$$(a) \quad x = y = 0\,; \qquad J_a = J_0\,,$$

$$(b) \quad x = 1\,, \qquad y = -1/K\,; \qquad J_a = (1 - q)J_0\cos\gamma'\,.$$

The first gives uniform disks. For the second, the apparent brightness distribution on S' corresponds to "complete darkening," and that on E may be derived from this by "stretching" all the contours so that circles are changed into ellipses similar to the limb

[11] T. E. Sterne, *Proc. Nat. Acad. Sci.*, **27**, 99, 1941.

and concentric with it. This is exactly the distribution which was assumed in 1912[12] for "darkened" ellipsoids. It was then recognized that this hypothesis did not correspond to darkening with the factor cos γ; but the conditions in which it is actually true have not apparently been previously specified.

For the Roche model the "darkened" tables correspond to $x = 1$, $y = \frac{1}{4}$. It is this condition, and not limb darkening without gravity effect, which has tacitly been assumed in the application of the ordinary "darkened" tables to ellipsoidal stars; and this may be regarded as the standard "darkened" state, upon which the remainder of the gravity effect, *plus* reflection, is to be superposed in the determination of a definitive light-curve.

The only effect of this change on the solution is that the photometric ellipticity effect upon the light sent in different directions is $2q$, while for $x = 1$, $y = 0$, it is $\frac{8}{5}q$. The values of the geometrical ellipticity derived in existing "darkened" solutions should therefore be multiplied by 0.8. New solutions are desirable in refined work.

For ordinary light the theoretical values of x and y are 0 and $\frac{1}{4}$ for infinitely hot stars and greater for all others. The new auxiliary tables will therefore be required for the precise calculation of any actual light-curve, superposing

$$\Delta J = \{(1 - x)Ky + x \cos \gamma'(1 + Ky)\}J_0Q$$

upon the standard brightness assumed in calculating the tables for partial darkening.

Hearty thanks are due to Mr. Blackadar and Miss Davis for the preparation of the nomogram.

PRINCETON UNIVERSITY OBSERVATORY
January 1942

[12] Russell and Shapley, *op. cit.*, p. 400.

THE SPECTRA OF TEN GASEOUS NEBULAE*

A. B. WYSE

ABSTRACT

Observations of faint nebular lines, previously published in collaboration with Dr. I. S. Bowen, have been extended to include nine planetaries and the Orion nebula. Wave lengths, estimated intensities, and probable identifications are tabulated. Aside from lines that are merely suspected in a single object, the table includes, in the region between 3700 and 6750 A, about 270 spectral lines, of which approximately 60 per cent are identified.

Additional evidence is found for the existence of metallic elements in the nebulae—[*Fe* II] and [*Fe* III], for instance, are well represented in the Orion nebula. All the objects observed appear to be very closely similar in chemical composition. The differences in spectral line intensities from one object to another are ascribable mainly, if not entirely, to differences in physical conditions. The present observations tend to confirm earlier conclusions by Bowen and the writer concerning the relative abundance of the chemical elements in the gaseous nebulae.

The desirability of extending observations of gaseous nebulae to fainter spectral lines has been emphasized by two circumstances: first, recent laboratory analyses of the spectra of certain elements, particularly those of the first long period, have permitted the prediction of numerous forbidden lines, hitherto unobserved; and, second, the development, during the past few years, of more sensitive photographic emulsions has greatly extended the limit of what can be photographed, in this as in other fields of astronomical photography. With these considerations in view, an investigation of the spectra of three of the brightest planetaries—NGC 6572, 7027, and 7662—was undertaken in 1938 in collaboration with Dr. I. S. Bowen. A report of the observational data and a discussion of the relative abundance of the chemical elements in NGC 7027 were published the following year.[1]

The principal result of the investigation was the demonstration that the "gaseous" nebulae consist not only of elements that assume the gaseous state under terrestrial conditions but also of ions of metallic elements, such as magnesium, potassium, calcium, and iron. In fact, the chemical composition of NGC 7027, according to the analysis which was necessarily only a first approximation, was found to be entirely similar to the chemical composition of the solar atmosphere, as determined by Russell.[2]

The present paper is a continuation of the earlier investigation. It attempts to answer such questions as the following: (*a*) Is NGC 7027 typical of the planetary nebulae in respect to chemical composition? (*b*) Are there two sequences of nebulae, carbon and nitrogen, as in the Wolf-Rayet stars? (*c*) Do important differences of chemical composition exist between the planetaries and the diffuse nebulae? (*d*) What new lines, not appearing in the three nebulae previously observed, can be found in other bright objects? Some of the data from the earlier investigation, though by no means all, are incorporated into the present paper. For a complete account of the study it would be necessary to consider the two papers together.

All the spectrograms were made with instruments attached to the 36-inch refractor. For the nine planetaries the ordinary spectrograph slit was replaced by an image-slicer,[3]

* *Contributions from the Lick Observatory, University of California*, Ser. II, No. 4.

[1] I. S. Bowen and A. B. Wyse, *Lick Obs. Bull.*, **19**, 1, 1939.

[2] Russell, Dugan, and Stewart, *Astronomy*, p. 503; rev. ed., 1938. There is some evidence that the abundance ratio, metals to hydrogen, in the solar atmosphere, is somewhat smaller than Russell's value (Pannekoek, *Pub. Astron. Inst. Univ. Amsterdam*, No. 4, p. 10, 1935; Menzel, *P.A.* **47**, 136, 1939).

[3] Bowen, *Ap. J.*, **88**, 113, 1938.

which was specially constructed at the California Institute of Technology and which was lent to the Lick Observatory for the present investigation. The trapezium region of the Orion nebula is so large that a wide spectrum is obtained without the use of the image-slicer.

The spectrograph employed for the visual and infrared[4] regions ($\lambda > 4800$ A) consists of a visually corrected collimator of 37-mm aperture and 722-mm focal length; three $63\frac{1}{2}°$ prisms of Jena No. 102 glass; and a Dallmeyer motion-picture camera lens of focal length about 75 mm and of focal ratio f/1.9. The dispersion at the D lines is 200 A/mm.

In the ordinary photographic region the 1938 plates taken with a two-prism spectrograph demonstrated the desirability of increasing the resolving-power and suppressing the continuous spectrum by means of an additional prism. Consequently, the spectrograph was rearranged to accommodate three prisms for the photographic region, and all ten nebulae were observed with the instrument in this form. The collimator, corrected for the photographic region, is of 37-mm aperture and 722-mm focal length; the three 60° prisms are of light flint glass; and the camera is a Dallmeyer motion-picture lens of focal length about 90 mm and focal ratio f/1.9. The dispersion at $H\gamma$ is 90 A/mm.

In addition to the above, an exposure of the Orion nebula was made in the photographic region with a camera of approximately 150-mm focus substituted for that of 90-mm focus; the resulting dispersion at $H\gamma$ is 53 A/mm. The use of a narrower slit for the latter spectrogram served to weaken the continuous spectrum with respect to the emission lines, so that several additional faint lines were recorded.

Table 1 contains a list of the observed objects, arranged in order of increasing right ascension, together with certain details of the observations. The normal two-night exposures were generally supplemented by exposures of about one hour, and of five or ten minutes, in order to aid in the estimates of line intensities. All the photographs in the visual region were made on Agfa Superpan Press film, hypersensitized in ammonia. For the ordinary photographic region, Imperial (H & D 1200) plates were generally used; during the last months of observing, mercury-vapor hypersensitization of these plates was applied to advantage for the long exposures, at the suggestion of I. S. Bowen and L. T. Clark.[5] In this connection it may also be mentioned that the optical parts of the spectrograph employed for the photographic region were coated with nonreflecting films in November, 1940, by Dr. John Strong, of the California Institute of Technology. The consequent doubling in speed[6] was very beneficial in the case of the later plates.

The spectrograms were measured in the ordinary way. Wave lengths were determined with the aid of a Hartmann interpolation formula, calculated separately for each plate. Empirical corrections to the interpolation formulae were derived from known wave lengths of nebular lines, which were satisfactory for the purpose. It is estimated that the mean error in wave length of a single line of average quality is about 0.3 A in the photographic region, and 0.4 A in the visual region. Faint, doubtful, and overexposed lines, however, and lines of wave length greater than 6500 A are subject to considerably greater uncertainty. The above figures apply to a single nebula; and the wave lengths listed in Table 2, when they represent the average for several objects, should be more accurate.

In general, lines that appeared to be of somewhat doubtful reality were measured along with the others. These have been included in the final table, with warning question marks. It is seen that a large percentage of the suspected lines either have convincing identifications or appear in more than one object and are therefore probably real. Of the remainder, it seems likely that, although many must be spurious, an appreciable number are real. It is therefore considered better to include these suspected lines, noting them as

[4] Infrared exposures were made on the brightest objects with hypersensitized Eastman I-N plates; they were made simultaneously with those of the visual region. No nebular lines were recorded.

[5] *J. Opt. Soc. Amer.*, **30**, 508, 1940.

[6] N. U. Mayall and A. B. Wyse, *Pub. A.S.P.*, **53**, 120, 1941.

TABLE 1

RECORD OF OBSERVATIONS OF GASEOUS NEBULAE

Date	Exposure	Emulsion	Extent of Continuous Spectrum (Angstrom Units)	Remarks
	IC 418: 5^h22^m8; $-12°46'$			
1940, Nov. 27	4^h56^m	Agfa Hyp.	4830–6730	Effective exposure, $3^h5\pm$
1940, Nov. 28, 30	5 10	1200 Hyp.	3830–5050	Effective exposure, $4^h5\pm$
1940, Nov. 30	0 20	1200	.....	
1940, Nov. 30	0 5	1200	.....	
1940, Dec. 1	0 40	Agfa Hyp.	.....	
1940, Dec. 1	0 5	Agfa Hyp.	.....	
	Orion Nebula: 5^h30^m4; $-5°27'$			
1939, Nov. 11, 14	15 55	Agfa Hyp.	4830–6730	
1940, Feb. 18	1 0	Agfa Hyp.	.....	
1940, Feb. 18	0 10	Agfa Hyp.	.....	
1940, Oct. 30, 31	9 27	1200 Hyp.	3900–5000	
1940, Nov. 30	0 40	1200	.....	
1940, Nov. 30	0 6	1200	.....	
1941, Nov. 18, 19	16 13	Ilford Hyp.	3900–5000	3-prism, 6-inch camera
	IC 2165: 6^h17^m1; $-12°56'$			
1938, Dec. 22, 23	16 5	Agfa Hyp.	None	Effective exposure, $15^h5\pm$
1940, Feb. 18	1 0	Agfa Hyp.	.....	
1940, Feb. 18	0 10	Agfa Hyp.	.....	
1940, Nov. 30	1 0	1200	.....	
1940, Nov. 30	0 6	1200	.....	
1940, Dec. 1, 2	14 0	1200 Hyp.	4100–4800	
	NGC 2440: 7^h37^m5; $-17°58'$			
1938, Nov. 19, 20, 21	16 18	Agfa Hyp.	5700–6730	Effective exposure, $16^h0\pm$
1939, Feb. 17	1 0	Agfa Hyp.	.....	3-prism, 6-inch camera
1939, Feb. 17	0 35	Agfa Hyp.	.....	3-prism, 6-inch camera
1940, Feb. 18	1 0	Agfa Hyp.	.....	
1940, Feb. 18	0 6	Agfa Hyp.	.....	
1940, Nov. 30	1 0	1200	.....	
1940, Nov. 30	0 5	1200	.....	
1941, Jan. 26	6 22	1200 Hyp.	None	
1941, Jan. 27, 28	14 28	1200 Hyp.	4050–4800	
	NGC 6572: 18^h7^m2; $+6°50'$			
1938, July 27, 28	13 30	Agfa Hyp.	4830–6730	
1939, Aug. 15	1 0	Agfa Hyp.	.....	
1939, Aug. 15	0 5	Agfa Hyp.	.....	
1940, June 2, 3	13 45	1200	3870–5050	
1940, Aug. 2	1 0	1200	.....	
1940, Aug. 2	0 5	1200	.....	

TABLE 1—*Continued*

Date	Exposure	Emulsion	Extent of Continuous Spectrum (Angstrom Units)	Remarks
	NGC 6741: 18^h57^m5; $-0°35'$			
1939, July 17, 18	13^h56^m	Agfa Hyp.	None	
1939, Aug. 15	1 0	Agfa Hyp.	.....	
1940, July 3, 4	13 29	1200	None	
1940, Aug. 2	1 0	1200	.....	
	NGC 7009: 20^h58^m7; $-11°46'$			
1939, Aug. 13, 14	15 33	Agfa Hyp.	4830–6730	
1939, Aug. 15	1 0	Agfa Hyp.	.....	
1939, Aug. 15	0 10	Agfa Hyp.	.....	
1940, July 31, Aug. 1	15 16	1200	3870–5000	
1940, Aug. 2	1 0	1200	.....	
1940, Aug. 2	0 10	1200	.....	
	NGC 7027: 21^h3^m3; $+41°50'$			
1938, July 25, 26	11 58	Agfa Hyp.	4830–6730	‡
1938, Aug. 22, 23	16 37	Agfa Hyp.	4830–6730	
1938, Aug. 24, 25	16 43	850	3900–5050	2-prism, 3½-inch camera
1939, Aug. 15	1 0	Agfa Hyp.	.....	
1939, Aug. 15	0 6	Agfa Hyp.	.....	
1940, June 6, 7	13 22	1200	4100–5000	Effective exposure, $13^h0\pm$
1940, Oct. 1	1 0	1200	.....	
1940, Oct. 1	0 5	1200	.....	
	IC 5217: 22^h19^m9; $+50°28'$			
1939, Aug. 15	1 0	Agfa Hyp.	.....	
1939, Aug. 15	0 10	Agfa Hyp.	.....	
1939, Oct. 8, 9	18 40	Agfa Hyp.	None	
1940, Sept. 29, 30	18 39	1200 Hyp.	4100–4850	
1940, Oct. 1	1 0	1200	.....	
1940, Oct. 1	0 10	1200	.....	
	NGC 7662: 23^h21^m1; $+41°59'$			
1938, Sept. 19, 20	18 50	Agfa Hyp.	4830–6730	
1938, Sept. 21, 22	19 20	*	3870–5000	2-prism, 3½-inch camera
1939, Aug. 15	1 0	Agfa Hyp.	.....	
1939, Aug. 15	0 10	Agfa Hyp.	.....	
1939, Aug. 15	0 5	Agfa Hyp.	.....	
1939, Sept. 10, 11, 12	13 27	†	5000–6500	Effective exposure, $11^h\pm$
1939, Sept. 17	9 30	†	5000–6500	
1940, Aug. 28, 29	15 20	1200	3900–5000	Effective exposure, $15^h0\pm$
1940, Oct. 1	1 0	1200	.....	
1940, Oct. 1	0 10	1200	.....	

* Agfa Spektralblau ultrarapid.

† Eastman Superpanchro Press, hypersensitized.

‡ The film was damaged in handling, in the green region of the spectrum.

merely suspected, than to omit them all or to tabulate them separately. One exception to the above treatment occurs in NGC 7662, where three spectrograms of about equal quality between 4850 and 6400 A are available. In this case only those lines which were measured on at least two of the three spectrograms were included in the final table. It should be emphasized that the measurements were made as objective as possible by avoiding reference to other plates and to expected lines, during measurement. While it is impossible to eliminate the subjective element in all cases, a definite effort has been made to minimize it.

The accurate determination of the relative intensities of faint lines in the gaseous nebulae is exceedingly difficult. Several factors render the spectrograms unsuitable for making microphotometer tracings. Some of these factors are evident from Plates XII–XIII, such as the narrowness of the individual strips of spectrum from the image-slicer and the effects of chromatic aberration in the telescope objective; and the others scarcely require to be enumerated. Alternative methods of observation, while they remove some of the difficulties of spectrophotometry of faint lines, introduce others; so that a thorough investigation of the line intensities lies beyond the scope of this study. It was found that the best way to utilize the present spectrograms was to estimate the line intensities with the aid of specially prepared scale plates and to correct these observed intensities as well as practicable for such systematic errors as instrumental absorption, etc., in order to convert them into the true energies of the spectral lines. It is hoped that the results, which are given in Table 2, may be of some value, even though they must certainly not be considered to be very accurate.

The scale plates were made by taking a series of photographs of the helium lines, 4471 and 5875 A, with the spectrographs and emulsions employed for the nebular observations. The illumination from the helium discharge tube was varied by known amounts between successive exposures by means of an iris diaphragm. Some of the scale plates were made with the helium spectrum superposed upon a faint continuous spectrum of fixed intensity, from a tungsten lamp, in order to simulate the appearance of the nebular lines when the nebular continuous spectrum was visible. The "contrast" of the emulsions for the nebular spectra was assumed to be equal to that for the scale plates in the visual and photographic regions, respectively, and was assumed to be independent of wave length throughout each region. (It is to be noted that the "contrast" for emission lines is not the ordinary relation between surface brightness of source and density of photographic image.) The nebular line intensities were estimated on all spectrograms, ranging in exposure from five minutes to two or three nights, and the individual plates of each object were connected by means of lines that appeared in measurable strength on more than one plate. When the nebular continuous spectrum was not visible, the effect of its contribution to the strength of the emission lines was taken into account.

The estimated intensities for NGC 7027 were compared with Plaskett's values for the visual region[7] and with Aller's values for the photographic region,[8] in order to evaluate the systematic errors introduced by the variations with wave length of plate sensitivity, instrumental absorption, and atmospheric extinction. The systematic corrections so derived were then applied to all the nebulae observed: information as to the variation of atmospheric extinction from one object to another is so fragmentary that it is not considered worth while to attempt further refinements of this kind, especially in view of the inexact nature of the results.

The intensity unit for each nebula has been adjusted in Table 2 so as to make the intensity of $H\beta$ equal to 100. It will be noted that, in consequence, the intensity of the faintest observable lines varies considerably from one object to another, for a given spectral region. This fact should be kept in mind in judging of the reality of faint lines or in comparing the existence of faint lines in various nebulae. For each object, in any spec-

[7] *Pub. Dom. Ap. Obs., Victoria*, **4**, 187, 1928. [8] *Ap. J.*, **93**, 236, 1941.

PLATE XII

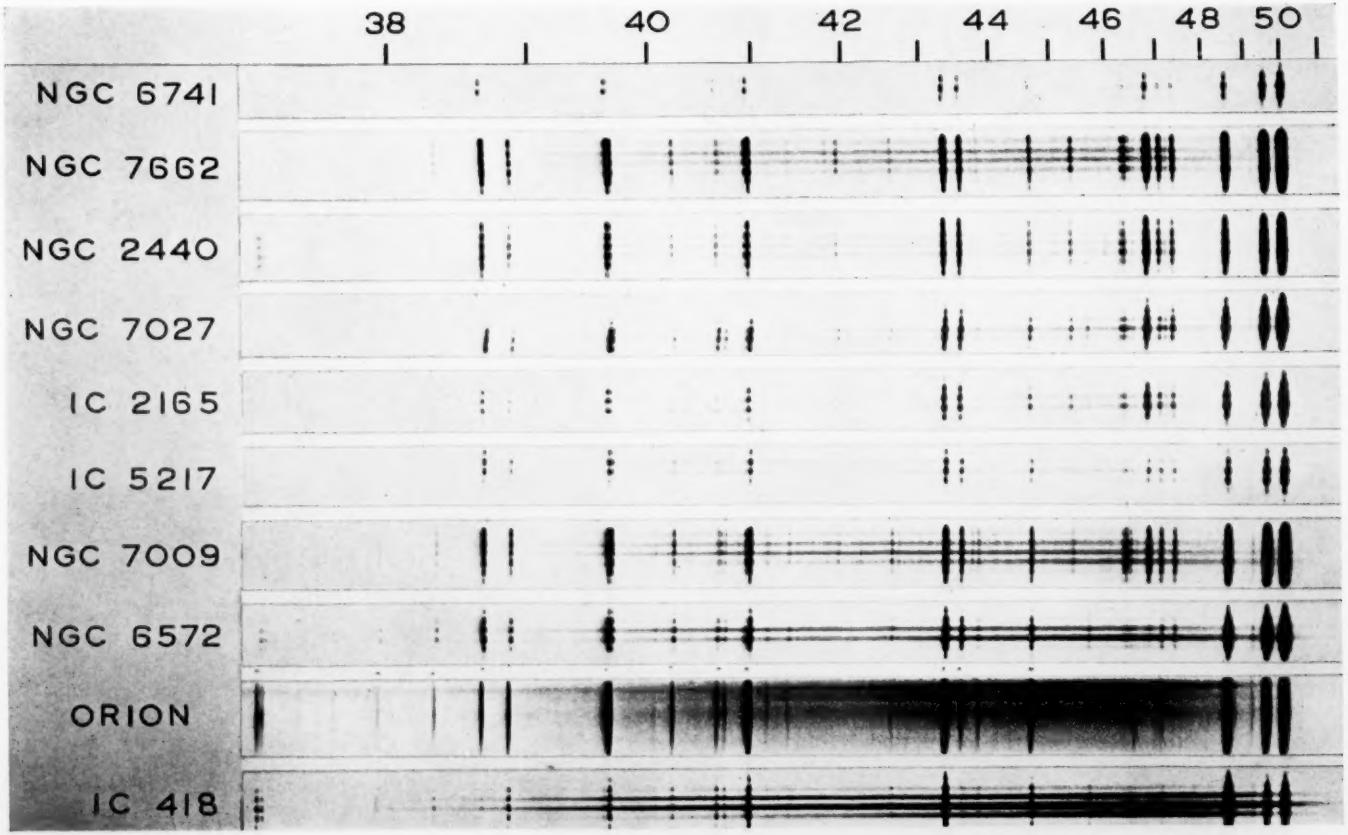

SPECTROGRAMS OF GASEOUS NEBULAE IN THE PHOTOGRAPHIC REGION

PLATE XIII

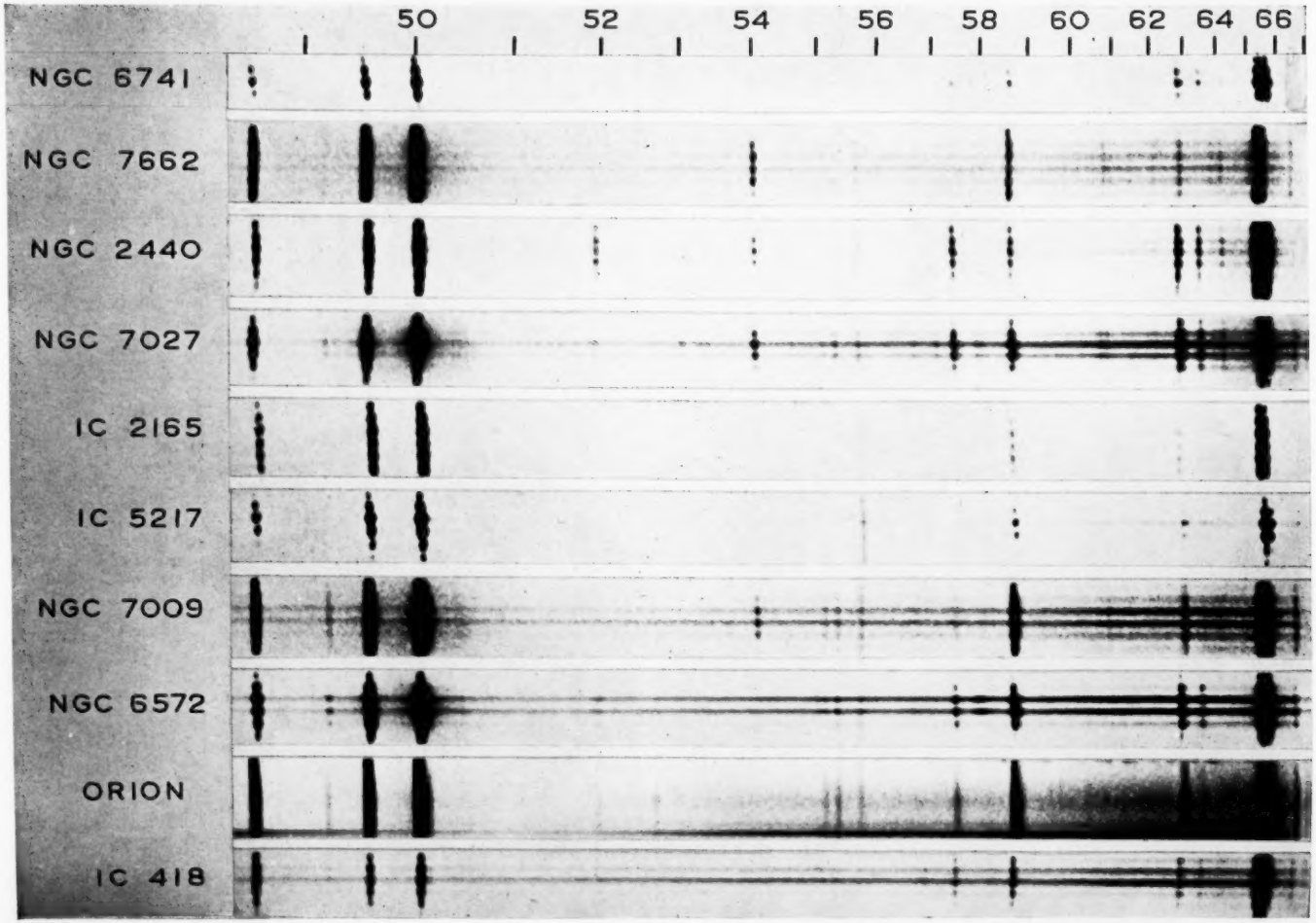

SPECTROGRAMS OF GASEOUS NEBULAE IN THE VISUAL REGION

tral region, the faintest lines visible on the plates can easily be recognized from Table 2, since the question marks are usually associated with lines just at the limit of visibility.

Some idea of the distribution of line intensities throughout the nebulae can be gained from the spectrograms in favorable cases. In general, however, the present plates are not well suited to such studies, because of the small scale. Therefore all the lines observed, whether nebular or nuclear, have been grouped into the one table without differentiation. For information on the distribution of light in the monochromatic images, the reader should consult other sources.[9]

A few remarks on the possibility of future observations of still fainter lines in the ten nebulae studied may be of interest. In the fourth column of Table 1 are given the wave-length limits between which the continuous spectrum has an appreciable strength on the long exposures. In some objects this continuous spectrum originates primarily in the nucleus, while in others it comes principally from the nebula. In either case it is evident that, once the continuous spectrum is reached, one cannot hope to find much fainter lines with the present spectrographs—not, at least, unless fine-grain, contrasty plates of high speed should become available. A simple increase of speed of future emulsions, however, without increased contrast or fineness of grain, would make it practicable to suppress the continuous spectrum still further and therefore to extend the observations to fainter lines by either of two methods: (1) increasing the angular dispersion with the use of more prisms or with the use of a grating in the orange-red region, without changing the camera lens; (2) employing a longer-focus camera lens and a narrower slit. The first method would be the more efficient. It is evident that in the ultraviolet region, the limit of faintness of the present observations is set by instrumental absorption, especially in the telescope objective, and that a reflector would be more effective in that part of the spectrum. Otherwise the efficiency is more or less independent of the telescope characteristics, such as aperture and focal ratio, since the nebulae in question appear as extended objects in large or medium-sized telescopes. In fact, a larger telescope might work to a disadvantage on the nebular lines of such objects as IC 418, because it would strengthen the spectrum of the stellar nucleus relative to the nebular lines.

The mean wave lengths of the spectral lines and the individual estimated intensities, reduced as nearly as possible to a true energy scale, are listed in Table 2 for the ten nebulae observed, together with the probable identifications. The nebulae are arranged in the order of decreasing excitation energy, according to Bowen's[10] classification. Lines of doubtful reality have usually been given half-weight in forming mean wave lengths. The abbreviations are explained at the end of the table. The last three columns of the table contain the predicted or laboratory wave length, the ion, and the classification of the transition responsible for each emission line.[11] The identifications are restricted, in general, to ions that are believed to be appreciable contributors to the observed lines. Dashes in the "identification" columns indicate that the major contributor to a blend is of unknown origin. In certain cases a line may be principally due to one element in objects of high excitation and to a different element in those of low excitation. An attempt has been made to specify such details concisely. For example, in the line at 4026.1 A, "*He* II^{H}" signifies that *He* II is the major contributor in objects of high excitation (generally the first four nebulae of the table); whereas "*He* I^{L}" indicates that *He* I is the principal contributor in objects of low excitation (generally the last two or four nebulae).

[9] Especially Wright, *Lick Obs. Pub.*, **13**, 193, 1918.

[10] *Ap. J.*, **67**, 1, Table II, 1928.

[11] Most of the data in these last three columns have been taken either from Miss Moore's *Multiplet Table of Astrophysical Interest* or from the paper by Bowen and Wyse (*loc. cit.*). The classification of some lines, including those of *O* II, is taken from Edlén ("Wellenlängen und Termsysteme . . . . ," *Nova acta reg. Soc. scient. Upsal.*, Ser. IV, Vol. **9**, No. 6, 1934). I am indebted to Dr. P. Swings for unpublished data on the term values of *Fe* III and also for a list of predicted forbidden lines of *Co* VII and *Ni* VIII based on term values of Anderson and Mack (*Phys. Rev.*, **59**, 717, 1941).

TABLE 2

OBSERVED WAVE LENGTHS, ESTIMATED INTENSITIES, AND IDENTIFICATIONS OF NEBULAR LINES

λ_{obs}	NGC 6741	NGC 7662	NGC 2440	NGC 7027	IC 2165	IC 5217	NGC 7009	NGC 6572	Orion Nebula	IC 418	λ	Ion	Classification
3704.8	.....	.....	.....	.....	.....	.....	.....	.....	6n	.....	03.9 05.0	*H* I *He* I	$2\ ^2S, P-16\ ^2S, P, D$ $2p^3P-7d^3D$
3711.9	.....	3?	.....	.....	.....	.....	.....	.....	6n	.....	12.0	*H* I	$2\ ^2S, P-15\ ^2S, P, D$
3722.1	.....	5	.....	2	.....	.....	.....	4?	7n	.....	21.9	*H* I	$2\ ^2S, P-14\ ^2S, P, D$
3723	.....	.....	.....	.....	.....	.....	.....	.....	4?	.....			
3726.1	.....	8	50	8	.....	.....	8	12	50	50	26.2	[*O* II]	$2p^3\ ^4S-2p^3\ ^2D_{1½}$
3728.8	.....	5	30	4	.....	.....	.....	6	30	20	29.1	[*O* II]	$2p^3\ ^4S-2p^3\ ^2D_{2½}$
3734.2	.....	4	.....	.....	.....	.....	.....	2?	6	.....	34.4	*H* I	$2\ ^2S, P-13\ ^2S, P, D$
3741	.....	3?	.....	.....	.....	.....	.....	.....	.....	.....	40.2	[*Fe* VI]	$3d^3\ ^4F_{4½}-3d^3\ ^2H_{4½}$
3750.3	.....	4	.....	2?	.....	.....	7	3	6	.....	50.2	*H* I	$2\ ^2S, P-12\ ^2S, P, D$
3755.6	.....	2	.....	.....	.....	.....	.....	.....	.....	.....			
3759.8	.....	5	.....	2	.....	.....	.....	.....	.....	.....	59.9 59.9	*O* III [*Fe* VII]	$3s^3P_2-3p^3D_3$ $3d^2\ ^3F_4-3d^2\ ^1G$
3762	.....	.....	.....	.....	.....	.....	.....	.....	4?	.....			
3765.7	.....	.....	.....	.....	.....	.....	.....	.....	4?	.....			
3770.6	.....	5	.....	1.5	.....	.....	.....	3	6	4	70.6	*H* I	$2\ ^2S, P-11\ ^2S, P, D$
3775.7	.....	.....	.....	.....	.....	.....	.....	.....	4?	.....	.....		
3792	.....	.....	.....	.....	.....	.....	.....	.....	3?irr	.....			
3797.9	.....	8	.....	2	.....	.....	7	5	10	4	97.9	*H* I	$2\ ^2S, P-10\ ^2S, P, D$
3819.8	.....	.....	.....	.....	.....	.....	.....	1.5	3	.....	19.6	*He* I	$2p^3P_1-6d^3D$
3825	.....	.....	.....	.....	.....	.....	.....	.....	2?	.....			

? = Line only suspected at time of measurement. n = Nebulous or diffuse. irr = Irregular.

TABLE 2—*Continued*

? = Line only suspected at time of measurement. n = Nebulous or diffuse. irr = Irregular.

TABLE 2—*Continued*

λ_{obs}	NGC 6741	NGC 7662	NGC 2440	NGC 7027	IC 2165	IC 5217	NGC 7009	NGC 6572	Orion Nebula	IC 418	λ	Ion	Classification
3835.4	.....	10	10	3	.....	7	8	6	12	6	35.4	*H* I	$2\ ^2S, P-9\ ^2S, P, D$
3855.8	.....	.....	.....	.....	.....	.....	.....	.....	2n	.....	56.0	*Si* II	$sp^2\ ^2D_{2\frac{1}{2}}-4p^2P_{1\frac{1}{2}}$
3859	.....	1	.....	.....	.....	.....	.....	.....	.....	.....	58.1	*He* II	$4\ ^2S, P, D, F-17\ ^2S, P, D, F, G$
3862.4	.....	.....	.....	.....	.....	.....	.....	.....	2n	.....	62.6	*Si* II	$sp^2\ ^2D_{1\frac{1}{2}}-4p^2P_{\frac{1}{2}}$
3865	.....	2	.....	.....	.....	.....	.....	.....	1?	.....	63	[*Ni* VIII]?^{H}	$3d^3\ ^4F_{3\frac{1}{2}}-3d^3\ ^2G_{4\frac{1}{2}}$
											—	—^{L}	
3868.7	60	60	60	40	50	70	50	50	20	3	3900±	[*Ne* III]	$2p^4\ ^3P_2-2p^4\ ^1D$
3872	.....	.....	.....	.....	.....	.....	.....	.....	1?	.....			
3888.8	12	25	20	7	10	25	12	15	15	15	89.1	*H* I	$2\ ^2S, P-8\ ^2S, P, D$
											88.6	*He* I	$2s^3S-3p^3P$
3907	.....	.....	.....	.....	.....	.....	.....	.....	1?d?	.....			
3913	.....	.....	.....	.....	.....	.....	.....	.....	0.5?irr	.....			
3919.4	.....	.....	.....	.....	.....	.....	.....	0.6	0.5	0.5	19.0	*C* II	$3p^2P_{\frac{1}{2}}-4s^2S$
3920.8	.....	.....	.....	.....	.....	.....	.....		0.6		20.0	*C* II	$3p^2P_{1\frac{1}{2}}-4s^2S$
3923.8	.....	1.5	.....	0.8	.....	.....	.....	.....	.....	.....	23.5	*He* II	$4\ ^2S, P, D, F-15\ ^2S, P, D, F, G$
3926.5	.....	.....	.....	.....	.....	.....	.....	0.5	0.7	.....	26.5	*He* I	$2p^1P-8d^1D$
3929	.....	.....	.....	.....	.....	.....	.....	.....	0.4?	.....			
3937	.....	.....	.....	.....	.....	.....	0.7	0.4?	.....	.....	35.9	*He* I	$2p^1P-8s^1S$
3944.5±	5?	.....	.....	.....	.....	.....	.....	0.3?	.....	.....	45.1	*O* II^L	$2p^2(^3P)3s^2P_{\frac{1}{2}}-2p^2(^3P)3p^2P_{1\frac{1}{2}}$
3958	.....	.....	.....	.....	.....	.....	.....	.....	0.4	.....			
3965.0	.....	.....	.....	.....	.....	.....	.....	.....	1	1.5	64.7	*He* I	$2s^1S-4p^1P$

^{H} Assignment applies predominantly or entirely to high-excitation nebulae, i.e., to those in the left-hand part of the table.
^{L} Assignment applies predominantly or entirely to low-excitation nebulae. d = Double.

TABLE 2—*Continued*

λ_{obs}	NGC 6741	NGC 7662	NGC 2440	NGC 7027	IC 2165	IC 5217	NGC 7009	NGC 6572	Orion Nebula	IC 418	λ	Ion	Classification
3967.4	30	25	30	15	25	30	20	25	7	0.6?	4000±	[*Ne* III]	$2p^4\ ^3P_1-2p^4\ ^1D$
3970.1	12	20	15	8	15	20	10	15	20	15	70.1	*H* I	$2\ ^2S, P-7\ ^2S, P, D$
3976.5±	.....	.....	.....	.....	.....	.....	.....	.....	0.4?	0.4?	76.3	[*Fe* III]?	$3d^6\ ^5D_4-3d^6\ ^3G_3$
3988	.....	.....	.....	.....	.....	.....	.....	0.3?	.....	.....			
3994	.....	.....	.....	.....	.....	.....	.....	.....	0.2?	.....			
3998	.....	0.5?	.....	.....	.....	.....	.....	0.3?	.....	.....	96.3	[*F* IV]	$2p^2\ ^3P_1-2p^2\ ^1D$
											98.7	*N* III?	$4d^2D_2-5f^2F_3$
4000	.....	.....	.....	.....	.....	.....	.....	.....	0.4	...			
4005	.....	.....	.....	.....	.....	.....	.....	0.3?	.....	0.4?			
4009.6	.....	0.9	.....	.....	.....	.....	0.6	0.6	0.6	0.4?	09.3	*He* I	$2p^1P-7d^1D$
4019	.....	.....	1?	.....	.....	.....	.....	.....	.....	.....			
4021.0	.....	.....	1	.....	.....	.....	0.4?	0.3	.....	.....			
4026.1	.....	5	5	2	3	6	4	4	3	3	25.6	*He* II^H	$4\ ^2S, P, D, F-13\ ^2S, P, D, F, G$
											26.2	*He* I^L	$2p^3P-5d^3D$
4030.9	.....	0.7	.....	.....	.....	.....	.....	.....	.....	.....	32	[*Ni* VIII]?	$3d^3\ ^4F_{3½}-3d^3\ ^2G_{3½}$
4032	.....	.....	.....	.....	.....	.....	.....	.....	0.3?irr	.....			
4037	.....	0.5?	.....	.....	.....	.....	.....	0.3?	.....	.....			
4043	.....	.....	.....	.....	.....	.....	0.4irr	.....	.....	.....			
4048	.....	0.5?	.....	.....	.....	.....	.....	.....	.....	.....			
4051	.....	.....	.....	.....	.....	.....	.....	.....	0.3b	.....			
4056	.....	.....	.....	.....	.....	.....	.....	.....	0.3?irr	.....			

b = Broad.

TABLE 2—*Continued*

4056													

b = Broad.

TABLE 2—*Continued*

λ_{obs}	NGC 6741	NGC 7662	NGC 2440	NGC 7027	IC 2165	IC 5217	NGC 7009	NGC 6572	Orion Nebula	IC 418	λ	Ion	Classification
4059.4		0.7									59.3	[*F* IV]	$2p^2\ ^3P_2-2p^2\ ^1D$
4062.6							0.4						
4068.9	6	2	6	5	3	4	1.5	3	2	4	68.5	[*S* II]	$3p^3\ ^4S-3p^3\ ^2P_{1½}$
											69.2	*C* III^H	$4f^3F-5g^3G$
4072.3					1?		0.7	0.3?	0.3		72.2	*O* II	$2p^2(^3P)3p^4D_{2½}-2p^2(^3P)3d^4F_{3½}$
4076.3	3	0.7	2	2		1.5	1	1.5	1	1.5	76.5	[*S* II]	$3p^3\ ^4S-3p^3\ ^2P_{½}$
											75.9	*O* II	$2p^2(^3P)3p^4D_{3½}-2p^2(^3P)3d^4F_{4½}$
4084.7		0.6?					0.4		P*		85.1	*O* II	$2p^2(^3P)3p^4D_{2½}-2p^2(^3P)3d^4F_{2½}$
											83.9	*O* II	$2p^2(^3P)3d^4F_{2½}-2p^2(^3P)4f^2G_{3½}$
4089.6							0.4		0.2		92.9	*O* II	$2p^2(^3P)3p^4D_{3½}-2p^2(^3P)3d^4F_{3½}$
											89.3	*O* II	$2p^2(^3P)3d^4F_{4½}-2p^2(^3P)4f^4G_{5½}$
4096.3	3			1?									
4097.6	3	3±	5	2	2	3	3±	1±?	0.2?		97.3	*N* III	$3s^2S-3p^2P_{1½}$
4101.7	25	25	30	12	25	25	20	30	20	20	01.8	*H* I	$2\ ^2S,\ P-6\ ^2S,\ P,\ D$
											03.4	*N* III	$3s^2S-3p^2P_{½}$
4109			0.7?				0.3?		P†				
											—	—	
4112.1		0.6?	0.7?	0.3?		1?	0.3?		P†		12.0	*O* II	$2p^2(^3P)3p^4P_{2½}-2p^2(^3P)3d^2F_{2½}$
											10.8	*O* II	$2p^2(^3P)3p^4P_{1½}-2p^2(^3P)3d^4D_{½}$
4120.8		0.7	0.8	0.4		1n	0.6	0.9	0.6	0.6	20.9	*He* I	$2p^3P-5s^3S$
											19.5	*O* II	$2p^2(^3P)3p^4P_{2½}-2p^2(^3P)3d^4D_{3½,\ 1½}$
											21.5	*O* II	$2p^2(^3P)3p^4P_{½}-2p^2(^3P)3d^4P_{½}$
											20±	[*K* V]^H?	$3p^3\ ^4S-3p^3\ ^2D_{2½}$
4129		0.6?	0.7?b	0.4?					0.2?n		29.6	*Si* II?	$3d^2D-4f^2F$
4132.2±							0.3		0.3	0.4?	32.8	*O* II	$2p^2(^3P)3p^4P_{½}-2p^2(^3P)3d^4P_{1½}$

* Faint unresolved emission suspected, extending between the lines 4076.3 and 4089.6 A; P = Present.

† Faint unresolved emission from about 4108 to 4114 A.

TABLE 2—*Continued*

λ_{obs}	NGC 6741	NGC 7662	NGC 2440	NGC 7027	IC 2165	IC 5217	NGC 7009	NGC 6572	Orion Nebula	IC 418	λ	Ion	Classification
4135.5±	.....	0.6	.....	0.4?	.....	.....	0.3?	.....	.....	0.4?			
4140.5±	.....	.....	.....	.....	.....	1?	0.3?	.....	.....	.....			
4143.8	.....	0.8	1	0.4	.....	1.5	0.7	1	0.7	0.6	43.8	*He* I	$2p^1D-6d^1D$
4147	.....	.....	0.7?n	.....	.....	.....	.....	.....	0.2?	.....			
4153.3	.....	0.6?	.....	0.4?	.....	1	0.4	0.4	0.4	.....	53.3	*O* II	$2p^2(^3P)3p^4P_{1½}-2p^2(^3P)3d^4P_{2½}$
4156.8	.....		.....		.....	.....	0.3	.....	0.4	.....	56.5	*O* II	$2p^2(^3P)3p^4P_{2½}-2p^2(^3P)3d^4P_{1½}$
4163.5	.....	0.6	.....	0.4	.....	.....	.....	.....	0.2?	.....	60±	$[K\ V]^{2H}_{\ \ L}$	$3p^3\ ^4S-3p^3\ ^2D_{1½}$
											—		
4170	.....	0.5?	.....	0.3?	.....	.....	0.3irr	0.4	0.4	.....	69.0	*He* I	$2p^1P-6s^1S$
											69.2	*O* II	$2p^2(^3P)3p^4P_{2½}-2p^2(^3P)3d^4P_{2½}$
4177	.....	0.5?	0.7?	0.3?	.....	.....	.....	.....	0.2?	.....	—	$^{\ \ H}_{L}$	
											77.2	$[Fe\ II]^{L}$	$a^4F_{4½}-a^4G_{4½}$
4185	.....	.....	.....	.....	0.6n	.....	0.3?	.....	0.2?	.....	85.5	*O* II	$2p^2(^1D)3p^2F_{2½}-2p^2(^1D)3d^2G_{3½}$
4187.0	.....	0.9	1.d?	0.4	.....	.....	.....	.....	.....	.....	87.0	*C* III	$4f^1F-5g^1G$
4190	.....	.....	.....	.....	.....	.....	0.3	.....	0.2?	.....	89.8	*O* II	$2p^2(^1D)3p^2F_{3½}-2p^2(^1D)3d^2G_{4½}$
4194.9	.....	.....	0.8	.....	.....	.....	.....	.....	.....	.....	95.7	*N* III	$2s2p(^3P)3s^2P_1-2s2p(^3P)3p^2D_2$
4197	.....	.....	.....	0.3?	.....	.....	.....	.....	.....	0.5?			
4199.9	.....	3	1.5	1	2	.....	0.6	.....	.....	.....	99.9	*He* II	$4\ ^2S, P, D, F-11\ ^2S, P, D, F, G$
											00.0	*N* III	$2s2p(^3P)3s^2P_2-2s2p(^3P)3p^2D_3$
4207.5±	.....	0.5?	.....	0.3?	.....	.....	.....	.....	.....	.....			
4219	.....	.....	0.6?	0.3?	.....	.....	0.3?b	.....	.....	.....			
4227.8	.....	0.6	0.9	0.3?n	.....	.....	0.5	.....	.....	.....			
4232	.....	.....	.....	.....	.....	.....	.....	.....	.....	0.5?			

TABLE 2—*Continued*

TABLE 2—*Continued*

λ_{obs}	NGC 6741	NGC 7662	NGC 2440	NGC 7027	IC 2165	IC 5217	NGC 7009	NGC 6572	Orion Nebula	IC 418	λ	Ion	Classification
4237.5			0.7										
4243.6				0.3?		1?			0.4n		44.0	$[Fe\ II]^L$	$a^4F_{4½}-a^4G_{5½}$
											—	—	
4248.4									0.2n				
4250			0.6?										
4253.3									0.2n				
4255.6			0.7				0.3?n		0.4?	0.6	—	—	
											53.9	*O* II	$2p^2(^1D)3d^2G-2p^2(^1D)4f^2H$
4262							0.3?		0.4n	0.5?			
4267.2		1.5	1	0.9	1.5n	1?	2	1.5	0.7	1.5	67.2	*C* II	$3d^2D-4f^2F$
4276		0.5	0.6?	0.4	0.6?		0.5	0.4	0.5n		76.0	*O* II	$2p^2(^3P)3d^4D_{3½}-2p^2(^3P)4f^4F_{4½,\ 3½}$
											76.9	$[Fe\ II]^L$	$a^4F_{3½}-a^4G_{4½}$
4284.5				0.3?			0.3				85.7	*O* II	$2p^2(^3P)3d^2F_{2½}-2p^2(^3P)4f^4F_{3½}$
											83.8	*O* II	$2p^2(^3P)3d^4D_{1½}-2p^2(^3P)4f^4F_{1½}$
4287.6			0.6?n						0.5		87.4	$[Fe\ II]^L$	$a^6D_{4½}-a^6S_{2½}$
											—	$—^H$	
4292							0.3?				91.2	*O* II	$2p^2(^3P)3d^4P_{2½}-2p^2(^3P)4f^4G_{3½}$
											92.2	*O* II	$2p^2(^3P)3d^2F_{2½}-2p^2(^3P)4f^4F_{2½}$
4294.9							0.3				94.8	*O* II	$2p^2(^3P)3d^4P_{1½}-2p^2(^3P)4f^4D_{1½}$
4304.1		0.5	0.6?	0.4			0.4	0.4, d?	0.3irr		03.8	*O* II	$2p^2(^3P)3d^4P_{2½}-2p^2(^3P)4f^4D_{3½}$
4311				0.3?									
4318.1		0.5			0.5?		0.4n	0.4n	0.3n		18.4	*O* II	$2p^2(^3P)3s^4P_{½,\ 1½}-2p^2(^3P)3p^4P_{1½,\ 2½}$
4328			0.8			1?		0.4?	0.3		27.5	$O\ II^L$	$2p^2(^1D)3p^2D_{2½}-2p^2(^1D)3d^2D_{2½}$
											28.6	$O\ II^L$	$2p^2(^1D)3p^2P_{1½}-2p^2(^1D)3d^2S$
											28.2	$N\ III^H$	$2s2p(^3P)3p^4D_{1½}-2s2p(^3P)3d^4D_{1½}$

TABLE 2—*Continued*

λ_{obs}	NGC 6741	NGC 7662	NGC 2440	NGC 7027	IC 2165	IC 5217	NGC 7009	NGC 6572	Orion Nebula	IC 418	λ	Ion	Classification
4332.8	.....	.....	.....	.....	.....	.....	.....	.....	0.3	.....			
4340.4	35	40	30	20	40	50	25	35	35	25	40.5	*H* I	2 ^{2}S, P−5 ^{2}S, P, D
4349.1	.....	.....	.....	.....	.....	.....	.....	.....	0.3	.....	47.4	*O* II	$2p^2(^1D)3s^2D_{1½}-2p^2(^1D)3p^2D_{1½}$
											49.4	*O* II	$2p^2(^3P)3s^4P_{2½}-2p^2(^3P)3p^4P_{2½}$
				0.3?		1?	0.5	0.4			48.4	*N* III?^{H}	$2s2p(^3P)3p^4D_{3½}-2s2p(^3P)3d^4D_{3½}$
4352	.....	.....	.....	.....	.....	.....	.....	.....	0.3?	.....	51.3	*O* II	$2p^2(^1D)3s^2D_{2½}-2p^2(^1D)3p^2D_{2½}$
											52.8	[*Fe* II]^L	$a^4F_{2½}-a^4G_{4½}$
4359	.....	.....	.....	.....	.....	.....	0.3?	.....	0.5	0.5?	59.3	[*Fe* II]	$a^6D_{3½}-a^6S_{2½}$
											58.4	[*Fe* II]	$a^4F_{1½}-a^4G_{2½}$
4363.2	15	15	20	10	10	15	7	10	3	1.5	63.2	[*O* III]	$2p^2\ ^1D-2p^2\ ^1S$
4368.3	.....	.....	.....	.....	.....	.....	.....	.....	0.5	0.6	66.9	*O* II	$2p^2(^3P)3s^4P_{2½}-2p^2(^3P)3p^4P_{1½}$
											69.3	*O* II	$2p^2(^3P)3p^2D_{1½}-2p^2(^3P)3d^2D_{1½}$
4372.5±	.....	.....	.....	.....	.....	.....	.....	.....	0.3?	.....	72.4	[*Fe* II]	$a^4F_{1½}-a^4G_{3½}$
4375	.....	0.5?	.....	.....	.....	.....	.....	.....	.....	.....			
4379.3	.....	0.7	1	0.4	.....	1	0.9	0.3?	0.4?d?	0.5?	79.1	*N* III	$4f^2F-5g^2G$
4387.9	.....	0.9	1	0.8	0.9	2	1	1.5	1.5	1.5	87.9	*He* I	$2p^1P-5d^1D$
4393	.....	.....	.....	.....	0.6?	.....	.....	.....	.....	.....			
				0.3?									
4397.4	.....	.....	.....	.....	.....	.....	0.3	.....	.....	.....	96.0	*O* II	$2p^2(^3P)3p^2D_{2½}-2p^2(^3P)3d^2D_{2½}$
4402	.....	0.5?	.....	.....	0.6?	.....	.....	.....	.....	.....			
4410.7	.....	.....	.....	.....	.....	.....	0.3n	.....	.....	0.5?	11.4	*C* II	$3d'\ ^2D-4f'\ ^2F$
				0.3?									
4415.6	.....	0.5n	0.6?	.....	.....	.....	0.4n	.....	0.6n	.....	15.8	*O* II	$2p^2(^3P)3s^2P_{½,\ 1½}-2p^2(^3P)3p^2D_{1½,\ 2½}$
											13.8	[*Fe* II]^L	$a^6D_{2½}-a^6S_{2½}$
											16.3	[*Fe* II]^L	$a^6D_{4½}-b^4F_{4½}$
4426.1	.....	.....	.....	.....	.....	.....	.....	.....	0.3n	.....			

TABLE 2—*Continued*

4426.1									0.3n				

TABLE 2—*Continued*

λ_{obs}	NGC 6741	NGC 7662	NGC 2440	NGC 7027	IC 2165	IC 5217	NGC 7009	NGC 6572	Orion Nebula	IC 418	λ	Ion	Classification
4432.7							0.3n		0.3				
4437.1		0.5			0.6?n	1?	0.3?n	0.4	0.6	0.6	37.5	*He* I	$2p^1P-5s^1S$
4446						1?							
4453		0.5?					0.3		0.4		52.4 52.1	*O* II? [*Fe* II]^L	$2p^2(^3P)3s^2P_{1½}-2p^2(^3P)3p^2D_{1½}$ $a^6D_{1½}-a^6S_{2½}$
4457								0.4?					
4458.1									0.4		58.0	[*Fe* II]	$a^6D_{3½}-b^4F_{3½}$
4461				0.3?									
4464.5±						1			0.3?				
4471.6	3	5	5	5	5	8	5	10	6	4	71.5	*He* I	$2p^3P-4d^3D$
4480					0.6?						81.2	*Mg* II?	$3d^2D-4f^2F$
4486										0.5?			
4490.0							0.3		0.3n		90.0 88.8	*O* II [*Fe* II]^L	$2p^2(^3P)3d^2P_{½,\ 1½}-2p^2(^3P)4f^2D_{1½?,\ 2½}$ $a^6D_{2½}-b^4F_{2½}$
4495		0.5?											
4499							0.3?						
4511.2		0.5	1	0.3?			0.4				10.9	*N* III	$2s2p(^3P)3s^4P_{½,\ 1½}-2s2p(^3P)3p^4D_{1½,\ 2½}$
4518.5			0.8?				0.3?				16.0	*N* III	$2s2p(^3P)3s^4P_{2½,\ ½}-2s2p(^3P)3p^4D_{3½,\ ½}$
4524				0.3?							23.6	*N* III	$2s2p(^3P)3s^4P_{1½}-2s2p(^3P)3p^4D_{1½}$
4531				0.3?						0.5?			
4541.6	2	3	4	1.5	3		1				41.6	*He* II	$4\ ^2S,\ P,\ D,\ F-9\ ^2S,\ P,\ D,\ F,\ G$
4546								0.4?		0.5?			

TABLE 2—*Continued*

λ_{obs}	NGC 6741	NGC 7662	NGC 2440	NGC 7027	IC 2165	IC 5217	NGC 7009	NGC 6572	Orion Nebula	IC 418	λ	Ion	Classification
4552	.....	0.5?	.....	0.3?	.....	.....	.....	.....	.....	0.5?	52.6	*Si* III?	$4s^3S-4p^3P_2$
4557	.....		.....	0.3?	.....	.....	.....	.....	.....				
4563	.....	.....	0.7?	.....	.....	.....	.....	.....	.....	.....			
4571.2	1.5?	0.6	0.8	1	0.6b	1?	.....	1	0.3n	1	71.1 73.9	*Mg* I? $[Fe\ III]^L$?	$3s^2\ ^1S-3s3p^3P_1$ $3d^6\ ^5D_4-3d^6\ ^3F_2$
4579	.....	.....	.....	0.3?	.....	.....	.....	.....	.....	.....			
4584	.....	.....	.....	.....	.....	.....	.....	0.4?	.....	0.6?			
4590	.....	0.5	.....	0.3	.....	.....	0.3n	.....	.....	.....	91.0	*O* II	$2p^2(^1D)3s^2D_{2\frac{1}{2}}-2p^2(^1D)3p^2F_{3\frac{1}{2}}$
4598	.....	.....	.....	.....	.....	.....	0.3?	0.4?	.....	0.7	96.2	*O* II	$2p^2(^1D)3s^2D_{1\frac{1}{2}}-2p^2(^1D)3p^2F_{2\frac{1}{2}}$
4603	.....	.....	.....	.....	.....	.....	.....	0.4?	0.3?		01.5	*N* II	$3s^3P_1-3p^3P_2$
4606.3	.....	0.5	1.5n	0.4	.....	.....	.....	.....	0.5	.....	03.2 07.0	*N* V?^{H} $[Fe\ III]^L$	$3s^2S-3p^2P_2$ $3d^6\ ^5D_4-3d^6\ ^3F_3$
4609.5	.....		.....	.....	0.7	.....	0.4	.....	.....	.....	09.4 10.1	*O* II *O* II	$2p^2(^3P)3d^2D_{2\frac{1}{2}}-2p^2(^3P)4f^2F_{3\frac{1}{2}}$ $2p^2(^3P)3d^2D_{1\frac{1}{2}}-2p^2(^3P)4f^4F_{2\frac{1}{2}}$
4615	.....	.....	.....	.....	.....	.....	.....	0.4?	.....	.....	13.9	*N* II	$3s^3P_1-3p^3P_1$
4621	.....	0.6?	.....	.....	.....	.....	.....	0.4irr	.....	.....	21.4	*N* II	$3s^3P_1-3p^3P_0$
4628.8	.....	.....	.....	.....	.....	.....	.....	.....	0.3	.....			
4632.4	.....	.....	.....	.....	.....	.....	.....	.....	.....	0.7			
4634.4	2	2	3	1	2	1.5	2	0.7	.....	.....	34.2	*N* III	$3p^2P_{1\frac{1}{2}}-3d^2D_{1\frac{1}{2}}$
4640.9	4	4	5	3	4	3	5	1	0.6n‡	0.6?	40.9 40.6	*N* III *O* II	$3p^2P_{1\frac{1}{2}}-3d^2D_{1\frac{1}{2}},\ 2\frac{1}{2}$ $2p^2(^3P)3s^4P_{\frac{1}{2}},\ 1\frac{1}{2}-2p^2(^3P)3p^4D_{1\frac{1}{2}},\ 2\frac{1}{2}$
4649.1	.....	1	1	0.8n	1	1.5	1.5	0.8	0.6	0.8	49.5 49.8	*C* III^H *O* II^L	$3s^3S-3p^3P$ $2p^2(^3P)3s^4P_{\frac{1}{2}},\ 2\frac{1}{2}-2p^2(^3P)3p^4D_{\frac{1}{2}},\ 3\frac{1}{2}$

‡ Shaded violetward; the measured wave length for the Orion nebula is 4641.9 A.

TABLE 2—*Continued*

‡ Shaded violetward; the measured wave length for the Orion nebula is 4641.9 A.

TABLE 2—*Continued*

λ_{obs}	NGC 6741	NGC 7662	NGC 2440	NGC 7027	IC 2165	IC 5217	NGC 7009	NGC 6572	Orion Nebula	IC 418	λ	Ion	Classification
4658.6	1.5?irr	1	2	0.9	1	1.5	0.5n	0.7	1.5	0.7	58.6 58.2	*C* IV^{H} [*Fe* III]^{L}	$5g^2G-6h^2H$ $3d^6\ ^5D_4-3d^6\ ^3F_4$
4665									0.4		67.1	[*Fe* III]	$3d^6\ ^5D_3-3d^6\ ^3F_2$
4668		0.8						0.4?					
4676.2								0.6	0.6b		75.4 —	*O* II —	$2p^2(^3P)3s^4P_{1½,\ 2½}-2p^2(^3P)3p^4D_{½,\ 2½}$
4683.7										0.8			
4686.0	35	60	40b	40	40	10	15	1			85.8	*He* II	$3\ ^2S,\ P,\ D-4\ ^2S,\ P,\ D,\ F$
4695								0.5?	0.5?				
4701.0									0.8	0.8	01.5 00.4	[*Fe* III] *O* II	$3d^6\ ^5D_3-3d^6\ ^3F_3$ $2p^2(^1D)3p^2D_{2½,\ 1½}-2p^2(^1D)3d^2F_{3½,\ 2½}$
4705									0.4?		05.4	*O* II	$2p^2(^3P)3p^2D_{2½}-2p^2(^3P)3d^2F_{3½}$
4711.9	8	15	15	3	8	8	4	4	2	1	11.4 13.2	[*A* IV]^{H} *He* I^{L}	$3p^3\ ^4S-3p^3\ ^2D_{2½}$ $2p^3P-4s^3S$
4724.7		2	3	1.5	2		0.4?irr		0.4?				
4733.3									0.6		33.8	[*Fe* III]	$3d^6\ ^5D_2-3d^6\ ^3F_2$
4740.0	10	12	12	7	8	7	4	3	0.6		40.3	[*A* IV]	$3p^3\ ^4S-3p^3\ ^2D_{1½}$
4750		1?					0.5?				51 —	*N* V?^{H} —^{L}	$6p^2P-7d^2D$
4754.8				0.4?					0.9	0.9n	54.9	[*Fe* III]	$3d^6\ ^5D_3-3d^6\ ^3F_4$
4759							0.5?						
4768.2									0.8		69.3	[*Fe* III]	$3d^6\ ^5D_2-3d^6\ ^3F_3$
4769.5		1									72	[*Ni* VIII]?	$3d^3\ ^4F_{4½}-3d^3\ ^4P_{2½}$

TABLE 2—*Continued*

λ_{obs}	NGC 6741	NGC 7662	NGC 2440	NGC 7027	IC 2165	IC 5217	NGC 7009	NGC 6572	Orion Nebula	IC 418	λ	Ion	Classification
4777.7									0.7		77.7	[*Fe* III]	$3d^6\ ^5D_1-3d^6\ ^3F_2$
4789				0.5?n							89.5	[*F* II]	$2p^4\ ^3P_2-2p^4\ ^1D$
4804			2?n					0.6?			07.5 —	[*Fe* VI]^H_L	$3d^3\ ^4F_{2\frac{1}{2}}-3d^3\ ^2G_{4\frac{1}{2}}$
4815.2									0.8		13.8 14.6	[*Fe* III] [*Fe* II]	$3d^6\ ^5D_1-3d^6\ ^3F_2$ $a^4F_{4\frac{1}{2}}-b^4F_{4\frac{1}{2}}$
4821							0.7?n	0.6?		1?	24.1	[*Fe* III]	$3d^6\ ^5D_2-3d^6\ ^3F_4$
4830.5±								0.7?		1?			
4848			4?						0.5?	1			
4851.0		1	3?	0.6							50.9	[*Fe* VI]	$3d^3\ ^4F_{1\frac{1}{2}}-3d^3\ ^2G_{3\frac{1}{2}}$
4854.5±			4?										
4861.3	100	100	100	100	100	100	100	100	100	100	61.3	*H* I	$2\ ^2S,\ P-4\ ^2S,\ P,\ D$
4873							1				71.6	*O* II	$2p^2(^1D)3p^2P_{1\frac{1}{2}}-2p^2(^1D)3d^2D_{2\frac{1}{2}}$
4882±									0.7	2?n	84.0 81.0	[*Fe* III] [*Fe* III]	$3d^6\ ^5D_2-3d^6\ ^3P_0$ $3d^6\ ^5D_4-3d^6\ ^3H_4$
4888.5±								0.9?		2?	90.9	*O* II?	$2p^2(^3P)3p^4S-2p^2(^3P)3d^4P_{\frac{1}{2}}$
4896				0.7?			1.5?		0.4		93.9 —	[*Fe* VII]^H_L	$3d^2\ ^3F_2-3d^2\ ^3P_1$
4904				0.7?			1.5	1?		2?			
4910			4?							2?			
4915							1.5?						
4922.0		3	4?n	3	4?	6?	3	4	3	3	21.9	*He* I	$2p^1P-4d^1D$
4924±									P?§		24.7	[*Fe* III]	$3d^6\ ^5D_4-3d^6\ ^3H_5$

§ This suspected line is evidenced as a faint wing on the redward side of λ 4922.0 A.

TABLE 2—*Continued*

§ This suspected line is evidenced as a faint wing on the redward side of λ 4922.0 A.

TABLE 2—*Continued*

λ_{obs}	NGC 6741	NGC 7662	NGC 2440	NGC 7027	IC 2165	IC 5217	NGC 7009	NGC 6572	Orion Nebula	IC 418	λ	Ion	Classification
4931.5	.....	2	.....	1.5	.....	.....	2	0.9	0.5?	2	31.8	[O III]‖	$2p^2\ ^3P_0-2p^2\ ^1D$
											30.7	[Fe III]‖	$3d^6\ ^5D_1-3d^6\ ^3P_0$
4937	.....	.....	.....	.....	.....	.....	1.5	0.6		....	36.2	[Fe III]	$3d^6\ ^5D_3-3d^6\ ^3P_1$
4943	.....	.....	4?	0.7?	.....	.....	.....	0.5?	.....	2?	42.3	$[Fe\ VII]^H$	$3d^2\ ^3F_3-3d^2\ ^3P_2$
											42.2	$O\ II^L$	$2p^2(^3P)3p^2P_{1/2,\ 1/2}-2p^2(^3P)3d^2D_{1/2,\ 2/2}$
4949	.....	.....	.....	.....	.....	.....	1.5?irr	0.5?	.....	3?			
4959.0	540	360	370	430	420	410	430	310	120	50	59.5	[O III]	$2p^2\ ^3P_1-2p^2\ ^1D$
4969	.....	.....	.....	.....	.....	.....	.....	.....	.....	3?			
4986	.....	.....	.....	.....	.....	.....	1.5?	.....	0.7?irr	.....	86	[Fe III]	$3d^6\ ^5D_{4,\ 3}-3d^6\ ^3H_{6,\ 4}$
											87.4	N II	$3p^3S-3d^3P_0$
4994	.....	.....	4?	0.8?	.....	.....	1.5	.....	0.6?irr	.....	89.4	$[Fe\ VII]^H$	$3d^2\ ^3F_2-3d^2\ ^3P_0$
											94.4	$N\ II^L$	$3p^3S-3d^3P_1$
													$3s^5P_2-3p^5P_3$
5006.7	1620	1200	1170	1190	1360	1330	1480	1070	430	230	07.6	[O III]	$2p^2\ ^3P_2-2p^2\ ^1D$
5015.5±	.....	.....	.....	P	.....	7±?	4±	7±	3±	7	15.7	He I	$2s^1S-3p^1P$
5026	.....	.....	.....	.....	.....	.....	.....	0.6?	.....	.....	25.7	N II	$3p^3D_3-3d^3F_3$
5032.7	.....	.....	.....	.....	.....	.....	2	0.6?	0.6?	.....	32.9	[Fe III]	$3d^6\ ^5D_3-3d^6\ ^3H_5$
5040.6	.....	.....	.....	1	.....	.....	.....	0.7	0.6?	3?	—	—	
											41.1	Si II?	$4p^2P_{1/2}-4d^2D_{1\,1/2}$
5048.0	.....	.....	5?d	1	.....	.....	.....	1	0.7	3?	47.7	He I	$2p^1P-4s^1S$
5056.9	.....	.....	.....	.....	.....	.....	.....	.....	0.8	.....	60.1	[Fe III]	$3d^6\ ^5D_1-3d^6\ ^3P_1$
											56.2	Si II?	$4p^2P_{1\,1/2}-4d^2D$
5065	.....	1.5	.....	.....	.....	.....	.....	.....	.....	.....	67	N V?	$6d^2D-7p^2P$
5074	.....	.....	4?	.....	.....	.....	1.5	.....	.....	.....	73.6	N II?	$3s^1P_1-3p^3S$

‖ The line is due to [Fe III] in the Orion nebula and IC 418; [Fe III] may also be an appreciable contributor in NGC 7009, but not in the other three objects.

TABLE 2—*Continued*

λ_{obs}	NGC 6741	NGC 7662	NGC 2440	NGC 7027	IC 2165	IC 5217	NGC 7009	NGC 6572	Orion Nebula	IC 418	λ	Ion	Classification
5090				0.9?			1.5?						
5112				0.9					0.6?	3?n			
5121.5		1.5		0.9									
5125										3?			
5133			4?	2									
5146				2					0.6?		46.8	$[Fe\ VI]^{H}_{L}$	$3d^3\ {}^4F_{3\frac{1}{2}} - 3d^3\ {}^2G_{3\frac{1}{2}}$
5153			4										
5159.6				2					0.7		58.3	$[Fe\ VII]^{H}$	$3d^2\ {}^3F_3 - 3d^2\ {}^3P_1$
											58.3	$[Fe\ II]^{L}$	$a^4F_{3\frac{1}{2}} - b^4P_{1\frac{1}{2}}$
5168			4?										$a^4F_{4\frac{1}{2}} - a^4H_{6\frac{1}{2}}$
5178		1.5	5± ¶	2							77.0	[Fe VI]	$3d^3\ {}^4F_{4\frac{1}{2}} - 3d^3\ {}^4G_{4\frac{1}{2}}$
5181							1.5?				79.5	N II?	$3p^5D_4 - 3d^5F_5$
5186.2		1.5	5± ¶										
5192.0		1.5	5± ¶	2				1	0.7				
5199.1	9± **		30	3				2	0.9	3	99.2	[N I]	$2p^3\ {}^4S - 2p^3\ {}^2D$
5207.2		1.5	3?										
5212			3?						0.6	3?			
5216				0.8?									
5221									0.6?				
5232.7		1.5	3	1							36.6	[Fe VI]	$3d^3\ {}^4F_{2\frac{1}{2}} - 3d^3\ {}^4P_{2\frac{1}{2}}$

¶ Unresolved.

** In NGC 6741 the intensities of these faint lines seem probably to have been estimated too large.

TABLE 2—*Continued*

¶ Unresolved.

** In NGC 6741 the intensities of these faint lines seem probably to have been estimated too large.

TABLE 2—*Continued*

λ_{obs}	NGC 6741	NGC 7662	NGC 2440	NGC 7027	IC 2165	IC 5217	NGC 7009	NGC 6572	Orion Nebula	IC 418	λ	Ion	Classification
5236									0 6irr				
5243.6									0 6				
5252			3?										
5262.1				1±¶					0 6		61.6	[*Fe* II]	$a^4F_{3\frac{1}{2}} - a^4H_{5\frac{1}{2}}$
5271.3				1±¶				0 9?	1		70.3 71	[*Fe* III] [*Fe* II]	$3d^6\ ^5D_3 - 3d^6\ ^3P_2$ $a^4F_{4\frac{1}{2}, 2\frac{1}{2}} - b^4P_{2\frac{1}{2}, 1\frac{1}{2}}$
5278.6			3	1.5±¶							79.2 76.1	[*Fe* VI] [*Fe* VII]	$3d^3\ ^4F_{1\frac{1}{2}} - 3d^3\ ^4P_{1\frac{1}{2}}$ $3d^2\ ^3F_4 - 3d^2\ ^3P_2$
5286.2			3										
5296				0.9?									
5303.5±		1?	2?										
5308.5				4							08.9	[*Ca* V]	$3p^4\ ^3P_2 - 3p^4\ ^1D$
5314						3?							
5323		1.5		1?			1?				22.2	[*Cl* IV]	$3p^2\ ^1D - 3p^2\ ^1S$
5334.6		1.5		1.5							36.4	[*Fe* VI]	$3d^3\ ^4F_{1\frac{1}{2}} - 3d^3\ ^4P_{\frac{1}{2}}$
5345.8				1.5			1.5						
5366										3?			
5387			1?		4?								
5397										3?			
5402	10±**				4?		1?						
5411.5	15	12	25	12	5	3?	8	0.8?			11.6	*He* II	4 ^{2}S, P, D, F—7 ^{2}S, P, D, F, G
5418.5±								0.7?		3?			

TABLE 2—*Continued*

λ_{obs}	NGC 6741	NGC 7662	NGC 2440	NGC 7027	IC 2165	IC 5217	NGC 7009	NGC 6572	Orion Nebula	IC 418	λ	Ion	Classification
5426	.....	1	4	1	.....	.....	.....	.....	.....	.....	27	[*Fe* VI]	$3d^3\ {}^4F_{2\frac{1}{2}, 3\frac{1}{2}} - 3d^3\ {}^4P_{1\frac{1}{2}, 2\frac{1}{2}}$
5435.4	.....	.....	.....	1.5	.....	.....	.....	.....	.....	.....			
5454	.....	.....	.....	.....	.....	.....	.....	.....	.....	3?irr			
5468	.....	.....	.....	1?	.....	.....	.....	.....	.....	.....			
5488	.....	.....	.....	.....	.....	.....	1?	.....	.....	.....			
5505	.....	.....	.....	.....	.....	3?	.....	.....	.....	.....			
5518.2	10± **	1.5n	4n	1.5	.....	.....	2	1.5	1.5	.....	17.2	[*Cl* III]	$3p^3\ {}^4S - 3p^3\ {}^2D_{2\frac{1}{2}}$
5530	.....	.....	.....	.....	.....	.....	1.5	.....	.....	3?	30.3	*N* II	$3s^5P_2 - 3p^5D_3$
5538.2	10± **	1.5n	4n	5	.....	.....	3	3	2	3	37.7	[*Cl* III]	$3p^3\ {}^4S - 3p^3\ {}^2D_{1\frac{1}{2}}$
5557	.....	.....	.....	.....	.....	.....	.....	.....	0.7d, irr	.....			
5563.2	.....	.....	4?	.....	.....	.....	1.5	.....	.....	.....			
5577.3	10± **	2	6	3	10	15	3	2	1.5	3	77.3	[*O* I]††	$2p^4\ {}^1D - 2p^4\ {}^1S$
5592.4	.....	1.5	5	1.5	.....	.....	.....	.....	.....	.....	92.4	*O* III	$3s^1P - 3p^1P$
5604.5±	.....	.....	4?b	1?	.....	.....	.....	.....	.....	.....	03	[*K* VI]	$3p^2\ {}^3P_1 - 3p^2\ {}^1D$
5616	.....	.....	.....	.....	.....	.....	.....	.....	0.7?n	.....			
5634	.....	.....	5, d?	.....	.....	.....	1.5	.....	.....	.....	31.6	$[Fe\ VI]^H_L$	$3d^3\ {}^4F_{3\frac{1}{2}} - 3d^3\ {}^4P_{1\frac{1}{2}}$
5658	.....	.....	.....	.....	.....	.....	.....	.....	.....	3?			
5677.4	.....	.....	.....	1.5	.....	.....	1.5?b	.....	0.7?irr	3	78.2	*N* II‡‡	$3s^3P_{0, 2} - 3p^3D_{1, 3}$
5692	.....	.....	.....	.....	.....	.....	.....	.....	0.7?	.....			
5695.9	.....	.....	.....	.....	.....	.....	1.5?	.....	.....	4			

†† Mainly night-sky radiation.

‡‡ This line in NGC 7027 is probably due in part to the [*Fe* VI] transition $3d^3\ {}^4F_{3\frac{1}{2}} - 3d^3\ {}^4P_{2\frac{1}{2}}$ at 5678.0 A.

TABLE 2—*Continued*

†† Mainly night-sky radiation.

‡‡ This line in NGC 7027 is probably due in part to the [*Fe* VI] transition $3d^3\ {}^4F_{3/2} - 3d^3\ {}^4P_{3/2}$ at 5678.0 A.

TABLE 2—*Continued*

λ_{obs}	NGC 6741	NGC 7662	NGC 2440	NGC 7027	IC 2165	IC 5217	NGC 7009	NGC 6572	Orion Nebula	IC 418	λ	Ion	Classification
5702			4?										
5720.0				4							20.9	[*Fe* VII]	$3d^2\ {}^3F_2 - 3d^2\ {}^1D$
5734.8			4				1.5						
5754.9	30	1.5	50	20			1.5	12	4	12	55.0	[*N* II]	$2p^2\ {}^1D - 2p^2\ {}^1S$
5765.5±				1.5?					0.9	3?			
5776									0.8?				
5800±		1		3			1.5?b	7n			01.5	*C* IV	$3s^2S - 3p^2P_{1½}$
5813±		1.5		2		3	1.5?	6n			12.1	*C* IV	$3s^2S - 3p^2P_{½}$
5829.0	8±**												
5839				1.5?									
5847									0.9?				
5875.6	70	15	30	35	20	40	35	60	30	20	75.6	*He* I	$2p^3P - 3d^3D$
5885±			4±?	10±			P	3±	3±n				
5894			4?irr										
5954.4								2	1				
5970.7	5?						1.5						
5978.4				2?					1.5		— 79.0	— *Si* II?	$4p^2P_{½} - 5s^2S$
6003.0				2?					0.9				
6018.0					3								
6035		1n					1		0.8?	2?			
6041			3?	2?									

TABLE 2—*Continued*

λ_{obs}	NGC 6741	NGC 7662	NGC 2440	NGC 7027	IC 2165	IC 5217	NGC 7009	NGC 6572	Orion Nebula	IC 418	λ	Ion	Classification
6049						3?			1	2			
6063		0.8?		2?									
6066.8						3?	0.9?		1				
6073.0		1		3?									
6078	4?						0.9?						
6084									0.8?				
6085.9				5							85.5 85.9	[*Fe* VII] [*Ca* V]	$3d^2\ ^3F_3-3d^2\ ^1D$ $3p^4\ ^3P_1-3p^4\ ^1D$
6097							1		0.8?irr				
6101.8		1.5	3?	5							01.1	[*K* IV]	$3p^4\ ^3P_2-3p^4\ ^1D$
6111										2?			
6118.0		0.8?		2					0.8?				
6130.4	3?									2			
6136.0									0.8				
6141							0.8?						
6155							0.8?n						
6161.3					2?			1.5	0.8				
6170.0	2?	1n	3										
6178.5					2								
6185.2									0.9				
6188		0.8											

TABLE 2—*Continued*

TABLE 2—*Continued*

λ_{obs}	NGC 6741	NGC 7662	NGC 2440	NGC 7027	IC 2165	IC 5217	NGC 7009	NGC 6572	Orion Nebula	IC 418	λ	Ion	Classification
6194	2?					2?							
6200									0.8?				
6211										2?			
6232.6		1	2?	3							29	[*K* VI]	$3p^2\ ^3P_2-3p^2\ ^1D$
6243								1.5?			42.5	*N* II	$3d^1F-4p^1D$
6253							0.9			2?			
6259.4			3										
6267									1 irr				
6300.1	50	0.9††	70§§	40§§	7§§	8§§	2	15§§	4	8	00.2	[*O* I]	$2p^4\ ^3P_2-2p^4\ ^1D$
6311.3	20	4	12	15	5	6	3	6	5	4	10.2	[*S* III]	$3p^2\ ^1D-3p^2\ ^1S$
6331.2			3					1.5?		2n			
6346.8±	2	0.8		2?		3		1.5?	1	2	— 47.1	— *Si* II?	$4s^2S-4p^2P_{1½}$
6363.8	30		30	20§§	4	4	1	8§§	1.5	5	63.9	[*O* I]	$2p^4\ ^3P_1-2p^4\ ^1D$
6386										2?			
6403.7±		1.5	3?b	2			0.9?		1?				
6423							1			2?n			
6435.0	5	1.5	10	8							32	[*A* V]	$3p^2\ ^3P_1-3p^2\ ^1D$
6461		1						2?					
6483		0.9?											
6493						3?							

§§ Night-sky radiation present, but relatively unimportant.

TABLE 2—*Continued*

λ_{obs}	NGC 6741	NGC 7662	NGC 2440	NGC 7027	IC 2165	IC 5217	NGC 7009	NGC 6572	Orion Nebula	IC 418	λ	Ion	Classification
6501	.....	.....	3	.....	.....	.....	.....	.....	1	.....			
6529	.....	1	.....	.....	.....	.....	.....	.....	.....	.....			
6548	260	P	230	90	50	P	P	40±	40±	110	48.4	[*N* II]	$2p^2\ ^3P_1-2p^2\ ^1D$
6563	470	360	270	420	470	380	470	230±	350±	410	62.8	*H* I	$2\ ^2S,\ P-3\ ^2S,\ P,\ D$
6584	580	12±	810	190	100	60	30	110	70	240	83.9	[*N* II]	$2p^2\ ^3P_2-2p^2\ ^1D$
6614±	.....	2?	6	3?	.....	.....	1.5?	.....	.....	.....			
6621±	.....	.....	.....	.....	.....	4?	.....	2?	1	.....			
6638±	.....	.....	.....	3?	.....	.....	.....	2	1	4			
6644±	.....	1.5?	.....	.....	.....	5?	.....	2?	.....	.....			
6660±	.....	.....	.....	3?	.....	.....	.....	.....	.....	.....			
6678.0	P	4	8	20	.....	20	15	20	12	12	78.1	*He* I	$2p^1P-3d^1D$
6716	.....	4	12	8	.....	.....	6d	2	6	10	17.3	[*S* II]	$3p^3\ ^4S-3p^3\ ^2D_{2½}$
6730	.....			15	.....	.....		3	8	12	31.5	[*S* II]	$3p^3\ ^4S-3p^3\ ^2D_{1½}$
6755	.....	.....	.....	.....	.....	.....	.....	.....	.....	12?			

Aside from the lines that are only suspected in a single object, Table 2 contains approximately two hundred and seventy nebular (or nuclear) lines. About one-third of these, including all the strong ones, were known prior to the beginning of this investigation in 1938. While the unidentified lines contain less than 5 per cent of the energy of all the lines in question, they number about 40 per cent of the total, so that a good deal of work remains to be done on the identifications. In the earlier paper,[1] specific comments were made on the identification of certain elements in the nebulae. The few modifications and additions resulting from the present study are now given.

F II.—The strongest forbidden line of *F* II, λ 4789, is suspected in NGC 7027. While the evidence for *F* II is very meager and uncertain, its existence in the nebulae would not be surprising in view of the presence of *F* IV in NGC 7662.

Mg II.—The line λ 4481 would be expected to be fainter than the limit of the present observations. A single suspected line in IC 2165 is the only evidence for *Mg* II, and the identification must be considered extremely doubtful.

Si II.—The coincidence of λ 3855.8 and λ 3862.4 in the Orion nebula with the two strong members of an important *Si* II multiplet is very probably significant, and it confirms earlier, less conclusive, evidence for the existence of *Si* II in the nebulae.

Fe II, *Fe* III, *Fe* V.—The occurrence of the dozen strongest lines of [*Fe* II] in the Orion nebula, as well as all but the faintest [*Fe* III] lines, confirms the existence of iron in the gaseous nebulae. Some of these lines are also probably present in other nebulae of low excitation, but the evidence is not so convincing as in the Orion nebula.

There are numerous additional predicted forbidden lines of *Fe* III arising from relatively high metastable levels. While these high-level lines show several coincidences with observed lines in the Orion Nebula, calculations indicate that the number of coincidences is no larger than would be expected from chance alone;[12] whereas the coincidences with forbidden lines arising from low metastable levels and listed in Table 2 are much too frequent to be attributed to chance.

Since the structures of *Fe* III and *Fe* V are similar, the observations of [*Fe* III] in RY Scuti by Swings and Struve[13] provide an approximate prediction of the relative intensities to be expected in [*Fe* V]. The three strongest predicted lines of the latter are unfavorably located on the short-wave-length side of 3900 A, and, in addition, one of them would be masked by *Hζ*. Even after making allowance for these facts, however, one finds that the coincidences between nebular lines and [*Fe* V] lines do not agree with the predicted intensities. Furthermore, one of these nebular lines, λ 4227.8, is also observed in the Wolf-Rayet star BD+30°3639 and therefore presumably traces its origin, at least in part, to a transition that is not forbidden. On the whole, the evidence is against the assignment of [*Fe* V] to lines thus far observed in the nebulae.

Ni VIII.—The structures of *Co* VII and *Ni* VIII are similar to that of *Fe* VI, so that the theoretical[14] and observational data for the latter are of some help in judging of the former. The coincidences between predicted lines of *Co* VII and nebular lines appear definitely to result from chance alone, since they occur primarily in objects of low excitation and since they do not agree with the expected relative intensities. There is fair, though not conclusive, evidence for *Ni* VIII in NGC 7662: the three lines assigned in Table 2 to [*Ni* VIII]?, together with another predicted line at 4106 A, which would be masked by *Hδ*, are expected to be the strongest lines of this ion; a few other lines, however, which should be only slightly fainter, are not observed.

It is perhaps worthy of mention that the following unidentified lines in the spectra of the nebulae are also found, without satisfactory identifications, in BD+30°3639 and

[12] Cf. Russell and Bowen, *Ap. J.*, **69**, 201, 1929.

[13] *Ap. J.*, **91**, 581, 1940.

[14] Pasternack, *Ap. J.*, **92**, 129, 1940.

occasionally in other Wolf-Rayet stars. The wave lengths are taken from Table 2: 4227.8, 4237.5, 4457, 5090, 5133, 5303.5, 5468, 6461 A. A more thorough comparison between the spectra of the nebulae and those of novae and other peculiar stars would undoubtedly disclose additional similarities, which might be of some aid in the eventual line identifications.

When one combines the new classifications with those previously accepted, it appears that the following ions are represented in the spectra of one or more of the nebulae observed: *H* I, *He* I, *He* II, *C* II, *C* III, *C* IV, *N* I, *N* II, *N* III, *N* V?, *O* I, *O* II, *O* III, *F* II?, *F* IV, *Ne* III, *Ne* V, *Mg* I?, *Si* II, *Si* III?, *S* II, *S* III, *Cl* III, *Cl* IV, *A* III, *A* IV, *A* V, *K* IV, *K* V?, *K* VI, *Ca* V, *Fe* II, *Fe* III, *Fe* VI, *Fe* VII, *Ni* VIII?. The more recent observations confirm the principal conclusion of the earlier paper, as it was summarized in the following statement: "In finding definite evidence for the presence of several of the commoner metals in the nebulae, these observations remove the chief outstanding qualitative difference in chemical composition between these objects and the stars."

The relative abundance of the chemical elements in NGC 7027 has been re-examined on the basis of the revised line intensities. Only minor changes are indicated in the relative population among the various stages of ionization and in log (a/b) of Table 3 of the earlier paper and in the logarithm of the total abundance; the greatest change in the latter is 0.3, which is equivalent to the addition of a + or − sign in that table. In view of the approximate nature of the discussion, it is not considered worth while to publish the revised results for NGC 7027.

In order to examine the possible variations in chemical composition among the nebulae, it is not necessary to repeat for each nebula the calculations already made for NGC 7027, because the other objects can be compared with NGC 7027 differentially. It is necessary, however, to make allowance first for differences in physical conditions among the various objects. I shall outline the general procedure and the trend of the results, without going into details. The first step in the comparison is to tabulate, for each nebula, the line-intensity ratios, I_{neb}/I_{7027}, for the strongest lines of all the ions observed and to take the mean for each ion; lines that are seriously affected by blending are not included. In order to estimate the relative population in the various stages of ionization (in terms of NGC 7027, for which this datum has already been estimated), the second step is to plot the mean intensity ratios, I_{neb}/I_{7027}, for each nebula against the ionization potential of the ion responsible for the lines.[15]

The plots of intensity ratio against ionization potential give a fair indication of the degree of excitation in each nebula, as compared with NGC 7027, and make it possible to estimate the percentage of ions of a given element in a given stage of ionization. It is true that the individual points show considerable scattering. But this is no greater than would be expected when one considers not only the uncertainties of the intensity estimates but especially the neglect of differences in density among the nebulae, as well as the variations in density and temperature throughout a single nebula. The relative degree of excitation among the different objects, as indicated by these plots, is fairly consistent with that deduced by Bowen[10] from the intensities of N_1 and N_2 as compared with $H\beta$. It was noted in the previous paper that NGC 7027 has a remarkable range in excitation energy, in that ions from the first to the seventh stage of ionization are represented in considerable strength. NGC 2440 is a similar case, though somewhat less extreme.

[15] In making such a plot, one should remember that the intensity of the *forbidden O* II lines, for example, is a measure of the abundance of *O* II; whereas the intensity of the *permitted O* II lines, since these are essentially recombination lines, is a measure of the abundance of *O* III. Inasmuch as we are seeking to determine the distribution among the different stages of ionization, we must therefore plot the intensity ratios for permitted lines against the ionization potential of the *next higher* stage of ionization, if they are to be comparable with the intensity ratios for the forbidden lines. The abscissae for *H* I and *He* II are somewhat arbitrary, because the ionization potentials of *H* II and *He* III have meaning only as a kind of average effect.

In NGC 7662, however, lines arising from ions in very low or very high stages of ionization are definitely suppressed relative to NGC 7027. NGC 6741 is rather similar to NGC 7662 in excitation, although because of its faintness there are not many lines to judge by. The other six nebulae give a consistent picture of decreasing excitation, approximately in the order in which they are arranged in Table 2; and here the high stages of ionization are not found. These few remarks may be useful in the future assignment of line identifications.

It is now possible, for each nebula, to estimate the relative abundance, in terms of NGC 7027, of any ion observed, and by summing over all stages of ionization to arrive at the total relative abundance for each element. The results disclose no significant differences in chemical composition among the ten nebulae observed. More definitely, it may be said that no variations by as much as a factor 5 were noted.

In a few of the nebulae the plots of line intensity against ionization potential show an unusually large amount of scattering of the individual points; and in NGC 2440, in particular, the scatter is so large that one hesitates to proceed directly to a determination of the ionization distribution and thence to the chemical composition. For example, most ions with ionization potentials up to 35 e.v. have line-intensity ratios $I_{2440}/I_{7027} \sim 1$; but in the 3727 A doublet of [*O* II] the ratio is $(50 + 30)/(8 + 4) = 6.7$, and in the 5199 A doublet of [*N* I] the ratio is $30/3 = 10$. These lines are the most strongly forbidden, i.e., they have the lowest transition probabilities, of all the nebular lines observed. They would therefore be expected to be enhanced relative to the other forbidden lines, at extremely low densities. These considerations suggest the plotting of the intensity ratios, I_{2440}/I_{7027}, for the forbidden lines, against the corresponding transition probabilities. I have made such a plot, using a logarithmic scale for both co-ordinates, having first allowed for the distribution among the various stages of ionization in each object. The plotted points indicate very nearly a straight-line relationship, in the sense that forbidden lines of very low transition probability are stronger in NGC 2440 than in NGC 7027, whereas those of relatively high transition probability are weaker. The scatter of the individual points is surprisingly small, in view of the several unknown variable factors that have been neglected. A more refined investigation would require detailed knowledge of the variation of electron temperature and density and of ionization temperature throughout the two nebulae. Altogether, the comparison bears out the conclusion previously stated, namely, that the variations in line intensities, among the nebulae observed, arise primarily from differences in physical conditions rather than from differences in chemical composition.

The similarity in chemical composition between the Orion nebula and the planetaries is interesting. While little is known of the origin of the planetary nebulae, it seems likely that they consist of matter that has been thrown off from the central stars. The diffuse nebulae, on the other hand, as typified by the Great Nebula in Orion, have presumably never been in the form of stars. One might therefore expect to find significant differences in chemical composition between the two kinds of objects, especially so in the light of Bethe's[16] studies of the sources of energy in stellar interiors. If the foregoing assumptions are all taken at their face-value, the similarity in chemical composition indicated by the present investigation would appear to imply that the material constituting the planetary nebulae has been affected only slightly, if at all, by the transmutation of elements in the deep interior of the central stars. Such a conclusion is, of course, only tentative, and further study of the problem would be desirable.

Menzel and Aller[17] have recently published some conclusions about the relative abundance of *O* III and *H* II in several planetary nebulae. They find, for NGC 7027, an abun-

[16] *Phys. Rev.*, **55**, 434, 1939.

[17] *Ap. J.*, **94**, 30, 1941.

dance ratio for *O* III/*H* II which is smaller by a factor of 50 than the ratio found for the same object by Bowen and Wyse, using other methods. Hagihara has also made an analysis (unpublished) of Aller's spectrophotometric observations of NGC 7027, by a method similar to that of Menzel and Aller. He, too, derives an abundance ratio that is smaller than ours by the order of 10^{-2}. While it has already been emphasized that our determination may be affected by systematic errors incident to the comparison of very strong and very faint nebular lines and also that it involves several simplifying assumptions, nevertheless, a discrepancy of the order of 100 is deserving of inquiry.

It may be recalled that the determination by Bowen and Wyse of the relative abundance of *O* III and *H* II in NGC 7027 hinged largely on a single line, 4379 A of *N* III. Naturally, if the line attributed to *N* III were actually a blend with some unknown line and the effect of blending were not allowed for, the resulting relative abundance of *H* II and *O* III would be in error. It is therefore of importance that in one planetary nebula, NGC 7009, more than twenty lines or blends of *O* II have been observed, free of blending with lines of other elements.[18] There are good grounds for the assumption, previously made, that these lines originate in electron captures by *O* III ions, just as the Balmer lines originate in electron captures by *H* II ions, and that therefore the relative intensities of the oxygen and hydrogen lines give a measure of the rates of recombination, and therefore of the relative abundance, of the two kinds of ions (the difference in electric charge must, of course, be taken into account). The important thing is that for this nebula a sufficient number of oxygen lines has been observed to eliminate all doubt of the correctness of their identification, even though they are very faint; and also that they permit the direct estimation of the relative abundance of *H* II and *O* III ions, without resort to nitrogen as a connecting link, by a method that is relatively independent of assumptions regarding electron density and velocity distribution or their variations throughout the nebula. Thus it is found from the permitted lines of *O* II and *H* I in NGC 7009 that $\Delta \log_{10}$ abundance (O III $-$ H II) $= -2.1$, averaged over the whole nebula, as compared with Menzel and Aller's value of -4.7 for the same object. Parenthetically, it may be noted that when all stages of ionization are taken into account, I find $\Delta \log_{10}$ abundance ($O - H$) $= -1.8$ for NGC 7009, which agrees closely with the value previously found for NGC 7027, namely, -1.7 ("2−").

The discrepancy, then, between the relative abundance found by Menzel and Aller, on the one hand, and from the recombination spectra, on the other, is of the order of 50 for NGC 7027 and of 500 for NGC 7009. In view of the uncertainties of the two methods, it is perhaps gratifying that the difference is not even larger! It appears that the principal sources of error, aside from observational uncertainties, are likely to be (1) the assumption by Menzel and Aller that the electron density is constant throughout the nebula and (2) the assumption by Bowen and Wyse that *O* II is hydrogenic, as far as the *observed* lines are concerned, and the further assumption that the rate of electron capture is proportional to the square of the net electric charge of the ion. A further possible source of error has been privately suggested by Hagihara, namely, the neglect, in his analysis and in Menzel's, "of other atomic mechanisms in which slow electrons are concerned (slower than those corresponding to χ_{PD} or χ_{DS} of *O* III)."

It appears to the writer that the most accurate solution of the relative abundance of *H* II and *O* III would be one based upon the determination, by quantum-mechanical methods, of the oscillator strengths of the observed *O* II lines (since those of the *H* I lines are already known) and of the relative rates of electron capture by *O* III and *H* II ions. While such calculations would be laborious, they would not be prohibitive; and by leading to greater accuracy in estimates of the relative abundance of these ions, they would aid toward a better understanding of the physical conditions in the nebulae. In order to

[18] The higher-dispersion plate of the Orion nebula, taken after this discussion was written, likewise shows a large number of *O* II lines. The argument could therefore be applied also to the Orion nebula.

take full advantage of such calculations, a more accurate determination of the relative intensities of the *H* I and *O* II lines in NGC 7009 would be desirable.

The principal conclusions of the present paper may be summarized as answers to the questions raised on page 356: (*a*) NGC 7027 is typical of the planetary nebulae in respect to chemical composition; the relative abundances previously published for NGC 7027 are representative of all the objects observed. (*b*) The nebulae are not divided into two sequences, carbon and nitrogen, like the Wolf-Rayet stars, if the ten observed objects are a fair sample (this remark is not intended to apply to the planetary *nuclei*, which are beyond the scope of the investigation). (*c*) No important differences of chemical composition are found between the planetaries and the diffuse nebulae, as typified by the trapezium region of the Orion nebula. (*d*) Numerous new lines have been observed, including those of [*Fe* II] and [*Fe* III] in the Orion nebula. About 40 per cent of the observed nebular lines remain unidentified.

LICK OBSERVATORY
MOUNT HAMILTON, CALIFORNIA
January 23, 1942

THE SPECTRUM OF BD+11°4673 DURING THE YEARS 1937–1941*

PAUL W. MERRILL

ABSTRACT

This article is the fourth in a series giving detailed data concerning numerous lines in the complex spectrum of the peculiar emission-line star BD+11°4673. A résumé of changes since 1915 is included.

The *bright lines* of *H* have been wider and more intense than formerly. The 800-day cycle in the displacements has continued with little change of phase, but the amplitude has diminished, and the mean velocity has become algebraically smaller. The amplitude apparently had reached a maximum in 1928. The chief lines of *He* I have remained prominent. Singlets and triplets behave differently. The negative displacements of the dark components are now greater than at any other time. A feature of special interest is the increasing intensity of the bright line λ 4686 *He* II. Other lines studied include those of *Fe* II, [*Fe* III], *N* II, *N* III, *Si* I, *Si* II, *Si* III, *Si* IV, *Mg* I, and a few of unidentified origin.

The *dark bands* of *TiO* have gradually grown stronger, until in 1940 and 1941 their intensities were approximately equal to those in class M1. Thus BD+11°4673 enters the group of stars with combination spectra and may assist in the interpretation of these anomalous objects.

An *intercomparison of lines* shows many differences in behavior, summarized in Tables 10 and 11.

Progressive changes since 1915, illustrated in Figures 1, 6, and 7 (see Tables 2, 4, 6, and 7), include strengthening and widening of bright lines of *H* and *He* I; increasing negative displacements of dark lines; a general increase in the ionization of the atmosphere, evidenced by the behavior of lines of *He*, *Fe*, *N*, and *Si*.

The hypothesis of an *expanding atmosphere* is briefly discussed. Certain facts suggest that the velocities of atoms increase as they travel outward and that the degree of ionization also increases.

This article is the fourth detailed report by the writer on the spectrum of BD+11°4673.[1] The first one[2] described the spectrum as it was in 1915. The second[3] reported the emergence of helium emission in 1919–1920 and gave an account of the remarkable periodic behavior of the lines of various elements during the years 1919–1928. The third article[4] recorded an intensive investigation of the cycle of the 800-day period which occurred in the years 1929–1931. The present contribution gives data for the interval 1937–1941 and includes a résumé of changes since 1915. A brief note calling attention to certain recent changes of special interest has already been printed.[5]

A valuable description of the spectrum in 1939 has been published by Swings and Struve.[6]

Spectrograms of the new series are listed in Table 1. The V plates were taken with a three-prism spectrograph, 10-inch camera, attached to the 60-inch telescope; the γ plates with a one-prism instrument, 18-inch camera, attached to the 60-inch; and the C plates with another one-prism spectrograph, 18-inch camera, attached to the 100-inch. The dispersion of all plates is about 35 A/mm at $H\gamma$. The slit was usually narrow, the spectrum widened. The emulsion regularly employed was Cramer Hi-speed Special. The portion of the spectrum below $H\delta$ is more satisfactorily shown on recent plates, especially

* *Contributions from the Mount Wilson Observatory, Carnegie Institution of Washington*, No. 659.

[1] AG Pegasi, HD 207757; R.A., 21^h46^m2; Declination +12°9′; mag. about 7.6; spectrum Bep.

[2] "A Spectrum of the P Cygni Type," *Pub. Obs. Univ. Michigan*, **2**, 71, 1916.

[3] "The Spectrum of BD+11°4673," *Mt. W. Contr.*, No. 381; *Ap. J.*, **69**, 330, 1929.

[4] "The Spectrum of BD+11°4673 during the Years 1929–1931," *Mt. W. Contr.*, No. 450; *Ap. J.*, **75**, 413, 1932.

[5] *Pub. A.S.P.*, **53**, 124, 1941.

[6] *Ap. J.*, **91**, 546, 1940.

TABLE 1

JOURNAL OF OBSERVATIONS AND VELOCITIES FROM BRIGHT LINES (KM/SEC)

PLATE	DATE	JD 242	*H*	*He* I		*He* II	*Fe* II	*N* II	*N* III		*Si* I	*Si* II	*Si* III	*Si* IV	NOTES
				Sing.	Trip.				λ4097	Sev.					
V 1980	1937 Aug. 23	8769	− 9	− 2	+ 4	.....	−15	−15	+30	−14	−17	−17	.....	+10	
Vic 27239	Sept. 12	8789	− 9	0	+ 1	.....	.....	−31	.....	.....	.....	.....	.....	.....	1
V 2254	1938 May 17	9036	+ 7	(+18)	+20	+10	.....	+12	+35	+ 3	.....	.....	+23	(+26)	
2307	June 16	9066	0	+ 3	+15	.....	.....	− 8	(+ 8)	.....	.....	.....	+ 6	(+17)	
2311	June 17	9067	+ 2	+ 6	+19	.....	.....	− 6	+37	0	.....	.....	(+ 6)	+20	
2343	July 16	9096	− 1	− 2	+14	− 6	.....	− 6	+38	− 4	.....	.....	− 7	− 4	
2356	July 29	9109	+ 2	0	+17	− 9	.....	− 4	+19	−10	.....	.....	− 7	(+ 8)	
2358	Aug. 6	9117	(− 4)	(−11)	+ 6	.....	.....	− 6	+ 9	.....	.....	.....	.....	(+ 5)	2
2360	Aug. 7	9118	+ 4	− 6	+13	−14	.....	−17	+18	−16	.....	.....	− 2	+10	
2392	Aug. 19	9130	+ 3	+ 5	+13	−10	.....	0	+28	−10	.....	.....	− 4	(+20)	
2393	Sept. 2	9144	− 6	−11	+ 3	−18	.....	−18	+15	−11	.....	.....	+ 1	(+11)	
2404	Sept. 19	9161	− 1	− 8	+ 3	−25	.....	−17	+14	− 8	.....	.....	(+ 5)	− 3	
C 7220	Oct. 12	9184	− 2	+ 7	+12	− 7	.....	−15	+27	+ 2	.....	.....	− 3	+13	
7221	Nov. 5	9208	(− 2)	.....	.....	.....	.....	.....	.....	.....	.....	.....	.....	.....	3
γ 21536	Nov. 8	9211	− 7	− 2	+ 3	−13	.....	−11	− 5	− 8	.....	.....	− 9	(− 5)	
21541	Nov. 9	9212	− 9	− 4	+ 7	(−30)	.....	−17	+ 6	(−24)	.....	.....	−12	(+ 4)	
21564	Nov. 30	9233	− 6	−12	− 4	−20	.....	−20	+ 8	−17	.....	.....	−16	(− 7)	
C 7315	1939 June 7	9422	−19	−18	− 7	−29	− 9	−21	+10	−21	−11	.....	−24	−18	
7336	July 4	9449	−16	−16	− 8	−25	−12	−29	+ 6	−27	−17	.....	−24	(− 9)	
7354	July 29	9474	.....	.....	.....	.....	.....	.....	.....	.....	.....	.....	.....	.....	4
7358	July 30	9475	−14	−15	− 7	−32	−14	−15	− 1	−20	−12	−15	−35	−20	
7367	Aug. 31	9507	(−14)	(−15)	(+ 2)	−34	−11	0	(− 4)	(−30)	.....	.....	− 8	(−19)	
7396	Oct. 4	9541	−14	− 6	+ 1	− 5	− 8	−12	+ 5	− 9	− 7	(− 1)	−16	−12	
γ 22299	Dec. 3	9601	−12	−18	− 6	.....	−13	−19	(+28)	.....	−18	−17	.....	−13	5
C 7424	Dec. 21	9619	−10	− 8	+ 4	− 1	−14	−18	+ 4	− 9	−16	(−24)	−14	− 8	

TABLE 1—*Continued*

Plate	Date	JD 242	*H*	*He* I		*He* II	*Fe* II	*N* II	*N* III		*Si* I	*Si* II	*Si* III	*Si* IV	Notes
				Sing.	Trip.				λ4097	Sev.					
C 7497	1940 May 20	9770	+ 7	+15	+21	− 5	−16	− 4	+24	+ 2	−20	(−14)	(+10)	+12	
7533	July 19	9830	+ 4	0	+12	−10	−18	− 7	+17	+ 2	−23	−19	−12	+ 7	
7582	Sept. 17	9890	+ 6	+ 4	+12	.....	(−23)	+ 4	+17	+ 4	−25	−16	.....	+ 7	
7585	Sept. 18	9891	+11	+ 6	+24	− 8	(− 6)	+ 6	+28	+ 7	.....	.....	+ 4	+11	
7607	Oct. 19	9922	+ 6	− 1	+ 9	−16	−15	+ 3	+ 9	− 4	− 6	(−19)	(− 6)	+ 4	
7614	Oct. 20	9923	(0)	(− 8)	(+13)	− 2	(−24)	− 6	+16	+ 2	.....	(−23)	− 6	+ 5	6
7615	Oct. 20	9923	(− 5)	.....	.....	.....	.....	.....	.....	.....	.....	.....	.....	.....	3
7616	Oct. 20	9923	(+ 5)	.....	.....	+ 1	.....	.....	(+23)	0	.....	.....	(0)	.....	6
7622	Nov. 19	9953	− 2	− 5	+13	− 2	(−26)	−19	+13	0	.....	−15	− 7	+ 1	
C 7681	1941 May 16	0131	−15	−38	− 6	−18	−10	−13	+ 7	−21	−11	.....	−29	(− 5)	7
7685	July 14	0190	−13	−19	− 2	(−25)	− 7	−21	− 1	−17	− 3	(− 6)	(−26)	−21	
Mean	.....	.....	− 4.0	− 5.1	+ 6.9	−13.0	−13.5	−12.2	+15.4	− 7.6	−14.3	−15.9	− 8.3	+ 1.0	

NOTES TO TABLE 1

1. I am indebted to Dr. C. S. Beals for the opportunity of measuring this spectrogram taken by him at Victoria.
2. Wrong tilt. Out of focus from *Hδ* toward the red.
3. Very weak exposure.
4. Definition poor.
5. Overexposed from *Hε* toward the red.
6. Includes visual portion of the spectrum. Emulsion 103E.
7. JD 2430131.

those taken since 1938, than on those obtained in previous series. The tabulated data on wave lengths and displacements are the means of measurements by Miss Cora G. Burwell and the writer.

HYDROGEN LINES

The bright hydrogen lines have been decidedly wider and more intense than formerly (see Fig. 1). If their intensity in the years 1915, 1919, and 1920 be arbitrarily called 1, it was about 2 from 1921 to 1931, and about 5 from 1937 to 1941. During the years 1937–

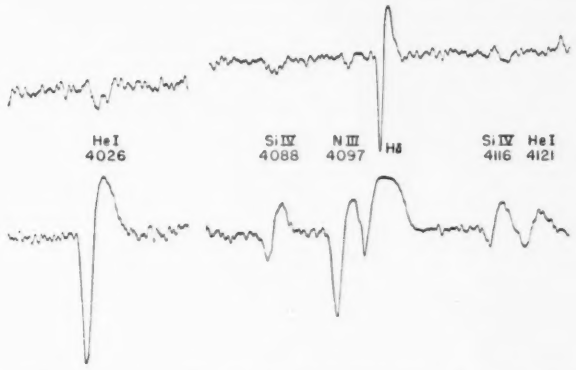

FIG. 1.—Tracings of the region near *Hδ*. Above, September 5, 1919; below, November 19, 1940

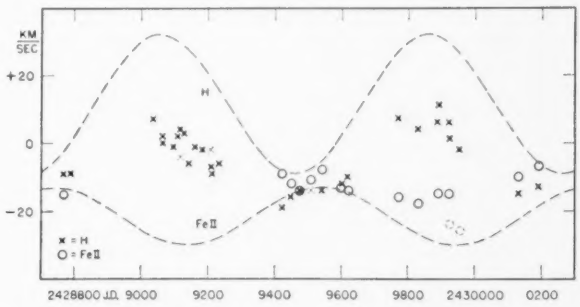

FIG. 2.—Velocities from emission lines of hydrogen and iron. Dotted symbols indicate low weight. The sine-curves (dashed lines) represent the variations about 1926. Note the changes indicated by the recent observations.

1941, little variation in intensity could be detected. The 800-day cycle, which was so prominent from 1921 to 1930, although still exhibited by the displacements (see Fig. 2), was no longer evident in the intensities.

The narrow absorption borders on the violet edges of the bright lines have been weak; in fact, on most of the plates they were not definitely present. When measured (1939), they yielded relatively large negative displacements. In $H\gamma$, for example, the distance between the effective centers of bright and dark components was about 2.8 A, compared with 1.0 A in 1919–1920, and 1.8 A in 1929–1930. Since the dark lines are narrow, these measured separations are but slightly greater than the apparent half-widths of the emission lines.

The measured displacements of the bright hydrogen lines in Table 1 depend on the

lines $H\beta$, $H\gamma$, $H\delta$, $H\epsilon$, and $H\eta$, the line $H\zeta$ being omitted because of blending with He λ 3889. The velocities from individual lines, including those of shorter wave length than $H\eta$, usually agree well, although on certain plates the lines from $H\eta$ to the ultraviolet yield positive residuals. On plate γ 22299[7] the series was measured as far as $H32$, λ 3660.

The plot of the velocities (Fig. 2) shows that the 800-day cycle has continued with little if any change of phase. The amplitude, however, has diminished, and the mean velocity has become algebraically smaller. The record[8] indicates that the amplitude increased from 1921 to 1929, but has since decreased. Data for certain years are in Table 2. The general course of the displacement-curve is indicated in Figure 6. The development and decline, within a few decades, of an 800-day pulsation in a stellar atmosphere is of considerable interest.

The intensities of the bright lines have shown an inverse correlation with their displacements, and also with the intensities of the dark lines, both in the 800-day cycle[9] and in the general behavior over a term of years. That is to say, when the dark borders are weak, the bright lines are strong, and their centers have algebraically small displacements. Thus, when dark borders are strong, it might appear that they weaken the bright components and displace them slightly to the red by clipping off their violet edges.

TABLE 2

DATA CONCERNING HYDROGEN LINES

Year	Intensity		Displ.	Velocity from Em. Lines (Km/Sec)			
	Em.	Abs.	Em.-Abs.	Max.	Min.	Semiamp.	Mean Velocity (V_0)
1915.....	6	3	1.6 A	.....	.....	?	(+16)
1920.....	5	6	1.0	+23	0	12	+12
1928.....	12	2	1.7	+35	−15	25	+10
1939.....	30	1	2.8	+ 8	−16	12	− 4

Among bright lines of various elements, moreover, it is true in general that those with strong borders exhibit positive displacements with respect to lines without borders. The relationship is not a simple one, however, as certain data, notably for the helium lines, make it clear that intensity of the dark border is not the only factor which affects the position of a bright line.

HELIUM LINES

The chief lines of neutral helium have remained prominent features of the spectrum. Since the singlets and triplets behave differently, they must be discussed separately. Classifications are given in Table 3.

The bright components of the triplet lines are now somewhat stronger than formerly, the dark borders much stronger (see Table 4). In 1937 the dark lines were about as strong as from 1921 to 1931, but in 1938 they became much stronger. The singlet series $^1P - {}^1D$ behaved differently; the emission was nearly constant in intensity from 1921 to 1941 (no observations were obtained in the years 1932–1936), while the dark borders were strong from 1921 to 1937, then became decidedly weaker from 1938 to 1941. The

[7] See illustration in *Mt. W. Contr.*, No. 642; *Ap. J.*, **93**, 40, 1941.

[8] *Mt. W. Contr.*, No. 381; *Ap. J.*, **69**, 330, 1929, Fig. 4; and *Mt. W. Contr.*, No. 450; *Ap. J.*, **75**, 413, 1932, Fig. 2.

[9] See Fig. 6, and *Mt. W. Contr.*, No. 381; *Ap. J.*, **69**, 330, 1929, Fig. 1.

line λ 3965, $^1S - {}^1P$, on the other hand, has changed but little since 1921, the dark component remaining conspicuous.

The displacements of the bright helium lines (Table 1) exhibit the 800-day period with about the same amplitude as before (see Fig. 3). The maxima and minima, however, are now in phase with those of hydrogen, whereas they formerly preceded them by about 160 days.

TABLE 3

CLASSIFICATION OF LINES OF *He* I*

Triplet System	
$^3S-{}^3P$	10830, 3889, 3188
$^3P-{}^3S$	7065, **4713, 4120,** 3867
$^3P-{}^3D$	5876, **4471, 4026, 3820,** 3705
Singlet System	
$^1S-{}^1P$	20582, 5016, **3965,** 3614
$^1P-{}^1S$	7281, 5048, 4438
$^1P-{}^1D$	6678, 4922, **4388, 4143, 4009,** 3926

* Lines in boldface type are those best observed in BD+11°4673.

TABLE 4

INTENSITIES OF LINES OF HELIUM*

YEAR	$^3P-{}^3D$ λ 4471		$^1S-{}^1P$ λ 3965		$^1P-{}^1D$ λ 4388		*He* II λ 4686E / *He* I λ 4712E
	E	A	E	A	E	A	
1915	.....	1	.....	.....	.....	1	0
1919	.....	1	.....	.....	.....	2	0
1920	1	.....	?	?	.....	1	0
1921–1931	8	5	4	4	1	5	0
1937	10	4	4	4	4	5	0.3
1938	8	8	4	4	4	3	0.5
1939	10	8	4	5	4	2	0.9
1940	10	8	4	4	4	1	1.3
1941	10	9	4	5	4	1	1.5

* The dark border of λ 3888, $^3S - {}^3P$, was very strong from 1937 to 1941, and there is evidence that the bright component, blended with $H\zeta$, also was strong.

The velocity-curve based on measurements of the singlets resembles that from the hydrogen lines, while that based on the triplets is displaced about 10 km/sec toward algebraically greater values. As far as the $^1P - {}^1D$ series is concerned, this displacement might conceivably have some connection with the relative weakness of the dark borders, but the negative displacement of λ 3965, $^1S - {}^1P$, which has a conspicuous dark border, is as great as that of the lines of $^1P - {}^1D$, which have extremely weak dark borders. An idea of the relative displacements of lines in various series may be gained from Table 5. The displacements seem to be more closely dependent on the series classification than on the presence or absence of dark components. The lines λ 4026 and λ 3965, for example,

do not differ very greatly in structure or intensity; nevertheless, the average relative displacement is 10.8 km/sec.

The negative displacements of the dark components of the helium lines have been greater from 1937 to 1941 than at any other time since 1915. This is true of the relative displacements, emission *minus* absorption (Table 6) as well as of the actual displacements (Table 7). In fact, since 1915 the dark lines have shown a remarkable progressive tend-

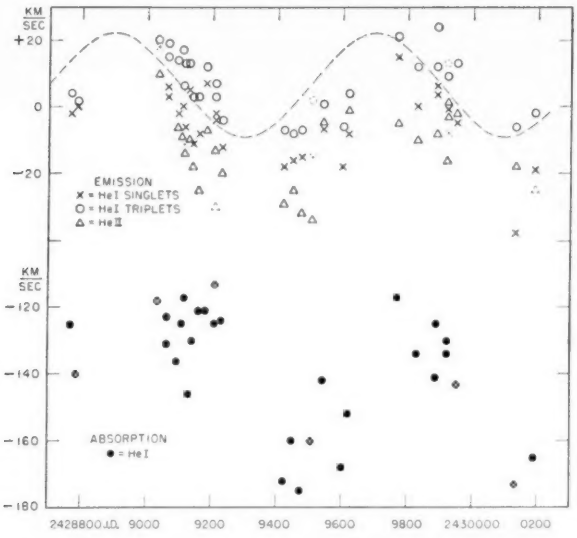

FIG. 3.—Velocities from helium lines. Dotted symbols indicate low weight. The sine-curve (dashed line) represents the variations of lines of neutral helium about 1926.

TABLE 5

RELATIVE DISPLACEMENTS OF BRIGHT LINES OF *He* I (1938–1941)

Lines in the same series.....	Singlets	λλ 4388–4143	+ 1.0±1.2 km/sec
	Triplets	λλ 4471–4026	+ 3.8 0.7
Singlets in different series.....		λλ 4388–3965	+ 0.8 1.4
Neighboring pairs, triplet *minus* singlet.....		λλ 4471–4388	+13.7 1.0
		λλ 4026–3965	+10.8 1.2

ency toward increased displacements (see Fig. 7). The singlet lines exhibited their largest values in 1939, with little or no general increase from 1937 to 1941. In this connection their decrease in intensity should be considered. The triplet lines on the whole indicate a continued progression toward the violet. Although the scatter is considerable, the displacements of the dark lines (Fig. 3) appear to oscillate in phase with those of the bright lines, probably with a larger amplitude.

A feature of special interest is the increasing intensity of the bright line λ 4686 of ionized helium. Prior to 1931 it had not been seen at all; in 1931 a barely visible trace was present; in 1937 it was considerably stronger, its intensity relative to λ 4712 *He* I being

0.3, which increased to 1.5 in 1941 (see Table 4). This is clear evidence of a recent increase in the ionization of the emitting atmosphere. The elements *Fe*, *N*, and *Si* also indicate increased ionization.

TABLE 6

RELATIVE DISPLACEMENTS OF BRIGHT AND DARK COMPONENTS

(Angstrom Units)

Year	Emission *minus* Absorption										
	He I								*N* III	*Si* IV	
	$^1S-{}^1P$	$^1P-{}^1D$			$^3P-{}^3S$		$^3P-{}^3D$				
	λ 3965	λ 4009	λ 4143	λ 4388	λ 4120	λ 4713	λ 4026	λ 4471	λ 4097	λ 4088	λ 4116
1921–1928	1.1	1.0	1.1	1.4	0.9	1.6	1.1	1.6	.....	.....	.....
1929–1931	1.2	1.1	1.2	1.4	1.1	1.8	1.3	1.7	.....	.....	.....
1937	1.8	1.7	1.7	1.9	1.5	1.7	1.7	2.1	1.5	1.2	1.1
1938	1.7	1.6	1.6	1.8	1.7	2.2	1.7	2.1	1.5	1.3	1.3
1939	1.9	2.0	2.0	1.9	1.9	2.4	2.1	2.4	1.6	1.3	1.4
1940	1.7	1.6	1.7	1.8	1.7	2.2	1.9	2.4	1.6	1.4	1.4
1941	1.8	.....	1.8	1.8	1.6	2.4	2.0	2.5	1.9	1.6	1.8

TABLE 7

DISPLACEMENTS OF DARK LINES (KM/SEC)*

Year	*He* I	*N* II	*N* III	*Si* III	*Si* IV
1915	− 11	+ 4	.....	−13	(+ 5)
1919–1920	− 45	−37	.....	−19	− 30
1921–1928	− 85	−66	.....	−69	− 40
1929	− 90	−80	.....	−74	− 50
1930	−104	−97	.....	−93	− 39
1931	− 79	−63	.....	−66	− 30
1937	−132	.....	− 83	.....	− 74
1938	−125	.....	− 90	.....	− 83
1939	−161	.....	−116	.....	−111
1940	−132	.....	−101	.....	− 96
1941	−169	.....	−138	.....	−132

* The lines upon which the above data are chiefly based are: *He* I, λλ 3965, 4026, 4471; *N* II, λ 3995; *N* III, λ 4097; *Si* III, λ 4552, λ 4567; *Si* IV, λ 4088, λ 4116.

The displacements of λ 4686 are algebraically smaller than those of *H* or of *He* I. The mean velocity is about −13 km/sec, nearly the same as that for other sets of lines without dark borders (see Table 10).

IRON LINES

The laboratory lines of singly ionized iron, *Fe* II, present in emission only, showed marked variations in intensity; in 1937 and again in 1939 they were fairly strong, but in 1938 they were absent or extremely weak. On the arbitrary scale previously used[10] the

[10] *Mt. W. Contr.*, No. 381; *Ap. J.*, **69**, 330, 1929, Table III; *Mt. W. Contr.*, No. 450; *Ap. J.*, **75**, 413, 1932, Table I.

average intensities for the years 1937–1941 were, respectively, 6, 0, 6, 2, 2. The lines are narrow and sharp without dark components, thus differing decidedly in appearance from most of the other emission lines. The measured displacements (Table 1) do not show a large range, although there may be a flat minimum (at about −19 km/sec) near JD 2429800, nearly in phase with the displacement-curve for previous years. The mean value, -13.4 ± 0.7 km/sec, is algebraically greater by 8 km/sec than that in previous years; in fact, it is about the same as the maximum, −13.0 km/sec, of the sine-curve used to represent the earlier velocities. Thus the curve has apparently flattened and moved up to the previous position of the maxima. The forbidden lines, [*Fe* II], have not been seen at all from 1937 to 1941.

The line λ 4658 [*Fe* III] recently identified by Edlén and Swings[11] with a forbidden transition of doubly ionized iron, has, on the other hand, been somewhat stronger than before. It remains, however, a relatively inconspicuous feature. The mean velocity, derived from fairly reliable measures on twenty-six plates, is -14.3 ± 2.5 km/sec.

NITROGEN LINES

The intensities of various nitrogen lines have changed in an interesting way. Lines in the triplet system of *N* II have become weaker than before. The bright components of the

TABLE 8

CHIEF LINES OF *N* III

I.A.	Intensity	Classification	I.A.	Intensity	Classification
3934.41	3	$^2P-^2D$	4379.09	10n	$^2F-^2G$
3938.52	4				
			4510.92	6	$^4P-^4D$
3998.69	3n	$^2D-^2F$	4514.89	7	
4003.64	4n				
			4634.16	8	$^2P-^2D$
4097.31	10	$^2S-^2P$	4640.64	10	
4103.37	9		4641.90	3	
4195.70	5	$^2P-^2D$			
4200.02	6				

singlet lines, λ 3995, λ 4447, have become stronger, the dark borders weaker; this behavior resembles that of the singlet lines of *He* I, e.g., λ 4388. The dark borders of the *N* II lines, in fact, have been scarcely visible during the interval 1937–1941.

The measured displacements of the bright lines, λ 3995, λ 4447, are scattering, and evidence of periodicity is not now strong. The mean value, −12.2 km/sec, is 18 km/sec below the earlier value of V_0, +6.0 km/sec.

From 1915 to 1931, the lines of doubly ionized nitrogen, *N* III, were absent or so weak that their presence was doubtful. In 1937, however, they were decidedly stronger, and their intensities continued gradually to increase during the next four years. Thus nitrogen along with helium and iron affords evidence of increasing ionization. With the exception of λ 4103, which is blended with the very strong *Hδ* line, all the lines in Table 8 have been found in the star. The first four lines have very low intensities. The last two lines—λ 4640.64 and λ 4641.90—were measured as a blend whose effective wave length in 1939 was λ 4641.6, indicating that a third line, perhaps λ 4643.11 *N* II, was involved. As the

[11] *Observatory*, **62**, 234, 1939.

N III lines became stronger, the measured wave length of this feature decreased, until in 1941 it was λ 4640.9, probably a reasonable value for the blend of the two *N* III lines.

The only line of *N* III to exhibit a well-marked dark border is λ 4097, whose general appearance resembles that of the helium lines λ 3965 and λ 4026. Dark borders to the other doublet lines are absent or extremely weak, while those to the quartet lines λ 4511, λ 4515 are narrow and inconspicuous. The relatively strong dark component of λ 4097 may occur because the excitation potential of the lower term of this line is considerably less than the corresponding potentials of the other lines.

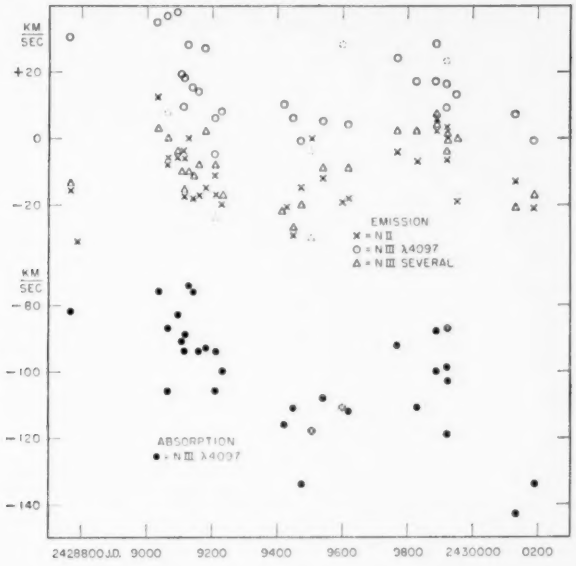

FIG. 4.—Velocities from nitrogen lines. Dotted symbols indicate low weight

The radial velocities from the bright component of λ 4097 average 23 km/sec greater than those from other bright lines of *N* III. For both groups of lines there is evidence of the 800-day period (see Fig. 4).

SILICON LINES

Silicon is represented in the spectrum by lines of the neutral atom as well as those of the first three stages of ionization. Of the two chief neutral lines in the region observed—λ 3905.53 and λ 4101.95—only λ 3905 is available for study because the other is hopelessly blended with *Hδ*. It occurs as a sharp bright line of moderate intensity whose appearance strongly resembles that of the lines of *Fe* II. Moreover, it exhibits variations in intensity which parallel those of the iron lines. Since there happens to be a line of *Fe* II with nearly the same wave length, the identification may be questioned. Regarded as a line of *Si* I λ 3905.53, the mean displacement is -14.3 ± 1.3 km/sec (probable error computed on the assumption of constant velocity), which agrees with the displacement of other lines without dark borders, in particular with that of the certainly identified lines of *Fe* II. For the line of *Fe* II λ 3906.04, however, the mean displacement would be −53.7 km/sec, a value so different from that for any other group of bright lines that identification with *Fe* II must be rejected. The range of velocities yielded by λ 3905 is not large, but there is indication of a minimum near JD 2429850. The conclusion is that the line is

due to *Si* I, although in its appearance and general behavior it strongly resembles lines of *Fe* II.

The bright lines of *Si* II, λ 3855 and λ 3862, are of low intensity but, like λ 3905 of *Si* I, are sharp. They have been measured on most of the spectrograms having reasonable density in their region. The mean displacement is -15.9 ± 1.0 km/sec; the amplitude of the 800-day fluctuation is quite small, probably less than that for *Si* I. The *Si* II lines λ 4128, λ 4130 are absent or extremely weak. Their unexpectedly low intensities in several bright-line spectra have frequently been commented upon.

From 1915 to 1931 the blue triplet of *Si* III, λλ 4552, 4567, 4574, was represented by dark lines with occasional bright fringes on their red sides. From 1937 to 1941, on the other hand, the bright lines were well developed, while the absorption was inconspicuous.

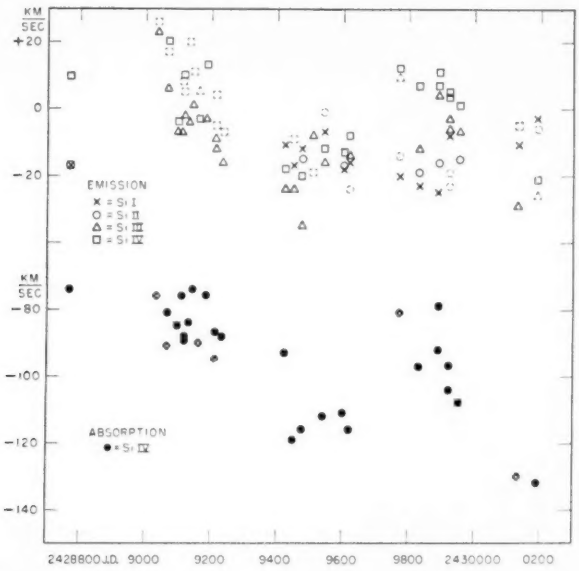

FIG. 5.—Velocities from silicon lines. Dotted symbols indicate low weight

The bright lines are fairly narrow but not so sharp as the lines of *Fe* II or as λ 3905 *Si* I. The displacements exhibit systematic fluctuations with a minimum near JD 2429420 and a maximum (poorly defined) hear JD 2429800 (see Fig. 5). The curve, although incomplete, indicates that this maximum was lower than the preceding one.

The lines of *Si* IV λ 4088, λ 4116 formerly observed in absorption (1915–1931) are now well-marked bright lines with weak dark borders on their violet edges. The fluctuations in velocity are well marked, resembling those of lines of *Si* III, although the times of maxima may be slightly later. The progression in the march of the dark lines toward the violet is shown by Tables 6 and 7 and Figure 7.

The lines of *Si* I and *Si* II are sharp and narrow, while those of *Si* III and *Si* IV are broadened and slightly diffuse, resembling lines of *He* and *N*. The lines of *Si* III and *Si* IV exhibit decidedly greater fluctuations in velocity than do those of *Si* I and *Si* II. The curve for *Si* I, although not well marked, appears to differ in phase by nearly half a cycle from the curves for *Si* III and *Si* IV (see Fig. 5).

MISCELLANEOUS LINES

A faint, somewhat diffuse emission line, measured on fifteen plates, yielded a mean wave length reduced to sun[12] of 4227.23 A, which differs by more than ten times the probable error of measurement from the position of the line of *Ca* I, λ 4226.73. The identification with the calcium line is therefore improbable. Another persistent, slightly widened bright line of low intensity has been measured at λ 4503.7 (reduced to sun). A trace of emission is present near K of *Ca* II, but lines of other elements are probably involved. A very narrow dark line at K, measured on six or eight plates, yields the velocity −5 km/sec. Since this line appears to vary slightly in intensity, it may possibly be circumstellar rather than interstellar.

On most plates there is a sharp bright line near λ 3938.1 (reduced to sun). Like other sharp lines, it varies in intensity with the lines of *Fe* II; but, although the normal wave length must be about 3938.3 A, identification with the faint *Fe* II line λ 3938.29 seems improbable. Identification with the stronger *Fe* II line λ 3938.97 is ruled out by the difference of wave length. The observed line is too sharp and of too short wave length to be *N* III λ 3938.52. The nitrogen line, however, is believed to be present as a weak, slightly widened line, on which the sharp line is usually superposed. If the normal wave length

TABLE 9

ADDITIONAL BRIGHT LINES MEASURED ON PLATE γ 22299

3736.92*	*Ca* II?	3930.32	
83.28	*Fe* II?	33.26	*Ca* II?
3900.48	*Ti* II?	34.16	
13.42	*Ti* II?	45.20	

* Wave lengths reduced for probable velocity.

of the sharp line is λ 3938.29 as measured on the early plates,[3] the mean displacement in the present series is −13 ± 1 km/sec.

An unusual number of faint, sharp bright lines in the region λλ 3700–4000 were measured on plate γ 22299,[7] taken on December 3, 1939, not only because the density in this region was greater than on most plates, but also because the sharp lines were especially prominent at that time. Of considerable interest are three low-excitation lines of *Mg* I, λλ 3829, 3832, 3838 (observed also by Swings and Struve[6] in October, 1939), which yield the velocity −14 km/sec, in agreement with that from the sharp lines of *Fe* II, *Si* I, and *Si* II on the same plate. The *Mg* I triplet certainly varies in intensity, being much weaker on several other recent plates on which this spectral region is well shown. A few additional well-defined emission lines measured on this plate are listed in Table 9.

TITANIUM OXIDE BANDS

The presence of absorption bands of *TiO* in a high-excitation spectrum is a feature of special interest. These bands (notably λ 4955), absent in 1919, gradually grew stronger until they became unmistakable, their intensities in 1940 and 1941 being approximately equal to those in spectra of class M1. Although traces of the bands can be detected on most of the spectrograms taken since 1921, the development has been somewhat irregular. The bands cannot be seen, for example, on plates taken in 1930, although they are present in low intensity on numerous plates taken in 1929 and 1931.

[12] Because no dark component was observed, the appropriate mean velocity of the bright line is probably less than zero, perhaps −14 km/sec, for which value the corresponding wave length would be 4227.42 A.

Thus, through the presence of the *TiO* bands, BD+11°4673 takes its place in the group of stars with "combination" spectra, and the observed behavior of its spectral lines may have a useful bearing on the interpretation of these remarkable "symbiotic" objects.

INTERCOMPARISON OF LINES

Most of the bright lines, while fairly well defined, are appreciably widened, but those of *Fe* II, *Si* I, *Si* II, and *Mg* I appear narrow and sharp. These lines yield mean displace-

TABLE 10

DATA CONCERNING DISPLACEMENTS OF LINES,* 1937–1941

(Km/Sec)

Element	Semi-amplitude	Mean Velocity (V_0)	Element	Semi-amplitude	Mean Velocity (V_0)
H	12	− 4	*N* III λ 4097	(15)	+ 15
He I sing.	13	− 5	*N* III others	14	− 8
He I trip.	14	+ 7	*N* III λ 4097 abs.	(20)	−101
He I abs.†	(23)	−138	*Si* I	(7)	− 14
He II	15	− 13	*Si* II	(4)	− 16
Fe II	5	− 14	*Si* III	(12)	− 8
[*Fe* III]	?	− 14	*Si* IV	18	+ 1
N II	14	− 12	*Si* IV abs.	(20)	− 94
			Mg I	?	(− 14)

* Emission unless noted.

† Mean of λλ 3965, 4026, 4471.

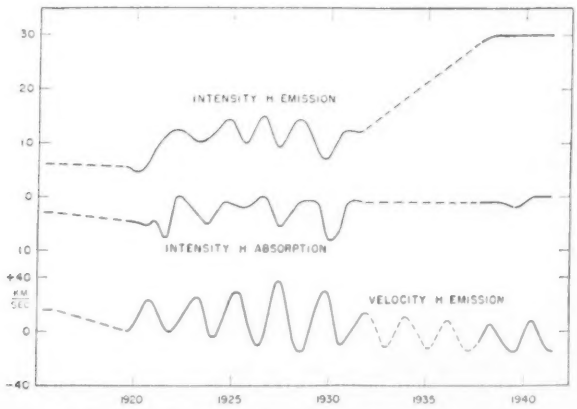

FIG. 6.—Behavior of hydrogen lines since 1915

ments of −14 km/sec. Other lines which yield about the same values are those of *He* II, [*Fe* III], and *N* II. It is significant that none of these lines have dark borders. The line λ 4097 *N* III, in which the dark component is relatively strong, yields the mean displacement +15 km/sec, indicating that the effective center of the bright portion is shifted farther toward the red than that of any other line. The displacements of *H*, *He* I, *Si* III, *Si* IV, and most of the lines of *N* III are intermediate (see Table 10).

The semiamplitudes exhibited by the oscillations of the sharp lines are about 5 km/sec, while those of most other bright lines are about 14 km/sec. That from *Si* IV is probably

larger, +18 km/sec, while the apparent semiamplitudes from the dark lines are 20–23 km/sec.

Previous observations brought out the fact that the 800-day velocity-oscillations of lines of various elements exhibited remarkable differences not only in amplitude and mean velocity but also in phase. In the present series of observations the hydrogen lines yield a minimum (Fig. 2) at JD 2429460, which agrees with the time computed from the sine formula previously derived. The time of minimum velocity yielded by the sharp

TABLE 11

GROUPING OF LINES ACCORDING TO STRUCTURE AND BEHAVIOR

Group	Semi-amplitude (Km/Sec)	Mean Velocity (Km/Sec)
I. Emission sharp; no dark borders. *Fe* II, *Si* I, *Si* II, (*Mg* I)	5	−14
II. Emission broad; dark borders weak or absent. *H*, *He* I sing.,* *He* II, [*Fe* III], *N* II, *N* III,† *Si* III	13	−14 to − 4
III. Emission broad; strong dark borders. *He* I trip., *N* III λ 4097, *Si* IV	16	+ 1 to +15

* Dark border of λ 3965 is strong.

† Except λ 4097.

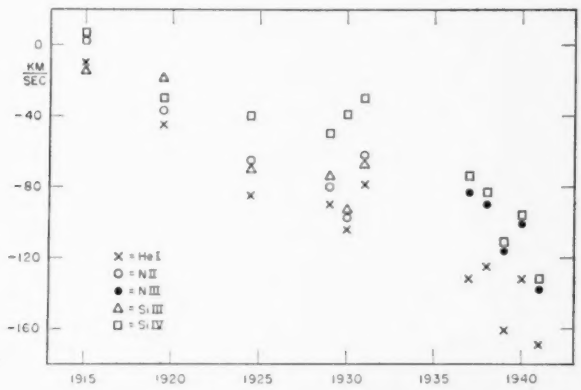

FIG. 7.—Mean velocities of absorption lines since 1915

lines of *Fe* II, *Si* I, and *Si* II is JD 2429830, but this is unreliable because of meager data and the small amplitude of the curve. The time derived from other groups of bright lines is JD 2429400, that from the absorption lines of *He* I, *N* III, and *Si* IV, JD 2429440; these times are not very accurate, and it is not quite certain that the relatively small departures from the hydrogen minimum are significant. With the exception of the sharp lines, the phase differences between various curves appear smaller than in previous years.

The relationship of the structure of the lines to their mean positions and to the amplitude of their oscillations is shown in Table 11. The sharp lines have the smallest amplitudes and large negative displacements. The broad lines exhibit larger amplitudes, while the mean velocity, on the whole, increases algebraically with intensity of the dark border.

The helium singlet line λ 3965 offers an exception to this rule; although it has a strong dark border, its displacement resembles that of other singlet lines of *He* I with weak borders.

PROGRESSIVE CHANGES

Continual changes in the intensity, structure, and displacement of the lines make the spectrum of BD+11°4673 a fascinating one for investigation. Observed changes are both periodic and progressive. Minor unclassified modifications, possibly irregular, also occur. The periodic variations, in cycles of 800 days, have been extensively discussed in the present *Contribution* as well as in preceding ones.[3, 4]

Among the progressive changes since 1915, partially illustrated in Figures 1, 6, and 7 (see also Tables 2, 4, 6, and 7), are the strengthening and widening of lines of *H* and *He* I. The dark borders accompanying these and other lines have shown increasing negative displacements. Should the widening of the bright lines and the trend of the dark lines toward the violet continue at the same average rate as in the last twenty years, it would not be many decades before the widths and displacements become comparable with those in certain novae. A cessation or reversal of the present trend may, of course, occur at any time.

A noteworthy feature is a general increase in the ionization of the atmosphere evidenced by the appearance or increased intensity of bright lines of *He* II, [*Fe* III], *N* III, *Si* III, and *Si* IV.

HYPOTHESIS OF AN EXPANDING ATMOSPHERE

The hypothesis of one or more expanding shells at some distance above the photosphere is now generally accepted as the explanation of many typical features in the spectra of novae and of stars like P Cygni. Of the two general forms which this hypothesis may take—(*a*) the nearly instantaneous expulsion from the body of the star of atoms which travel outward as a shell of ever increasing radius and (*b*) the continuous emission of atoms which produce a particular spectrum line only in a certain stratum at a nearly fixed distance above the photosphere—(*a*) is generally adopted for novae, (*b*) for stabilized stars with lines of the P Cygni type.

Hypothesis (*b*) explains the general relationship of the bright and dark lines in the spectrum of BD+11°4673, as well as some of the details of the observed displacements. For example, the relative displacements of broad bright lines with and without dark borders (groups II and III, Table 11) can be accounted for fairly well by the geometrical consideration that absorption of the continuous spectrum takes place only in that portion of the shell seen by the observer to be projected against the photosphere, while the emission lines receive contributions from all portions of the shell except that directly behind the star. But certain details, particularly the negative displacements of the sharp lines, cannot readily be explained in this manner without assuming that atoms responsible for various lines have different outward velocities. While such an assumption impairs the attractive simplicity of the original shell hypothesis, it should probably cause the modification rather than the rejection of this hypothesis.

Another possible complication is that ejected atoms may be appreciably accelerated before they pass through the zone of observation. A number of facts may, indeed, be explained on the assumption that the velocities increase from the photosphere outward. On this assumption the origin of lines in group I, Table 11, would be localized in the zone nearest the photosphere, where the velocities are relatively small and where the occultation effect[13] causes a small negative shift of the effective line centers. In and near this zone the effects of absorption are negligible, the permitted lines of *He* II, *Fe* II, *N* II, *Si* I, *Si* II (and *Mg* I?) yielding the same mean displacements as forbidden lines of [*Fe* III]. In zones farther from the photosphere the outward velocities are greater and the effects of absorption more prominent (groups II and III, Table 11). Lines of *N* III and of *Si* IV

[13] I.e., the hiding of the rear part of the shell by the body of the star.

would be assigned to an upper zone.[14] Perhaps the effective zones for absorption lie partially outside those for emission.

In the scheme outlined in the preceding paragraph the amplitudes of the 800-day velocity-oscillations appear to increase from the photosphere outward. The whole atmosphere seems to be in a condition far removed from the normal thermodynamic equilibrium with the photosphere.

Sharp lines, corresponding to low velocities, arise from fairly heavy atoms, which are either neutral or lack one electron, while broader lines arise either from light atoms or from heavier ones which lack two or three electrons. These circumstances suggest some atomic effect in which both mass and charge play a role.

Recent changes in the spectrum hint that the future may supply data more valuable than any we now have for the detailed study of the hypothesis of an outflowing atmosphere. At present the following conclusions appear to be justified.

1. Observed outward velocities are not the same for all atoms.
2. The velocities of many, but not of all, atoms have undergone a considerable general increase since 1915.
3. Observed velocities and therefore probably the velocities of ejection fluctuate in a period of 800 days.
4. Amplitudes in the 800-day cycle are not the same for all bright lines. Sharp lines have smaller amplitudes than broad ones. Dark lines have relatively large amplitudes.
5. The amplitude of the hydrogen oscillations increased from 1919 to 1929 and has since decreased.
6. Certain facts suggest that velocities of atoms increase as they travel outward from the photosphere and that the degree of ionization also increases.

COMPARISON WITH OTHER OBJECTS

The lines in the spectrum of BD+11°4673 in 1941 present a general correspondence to those of a nova during the intermediate period between the α Cygni stage and that characterized by nebular lines. A more profitable comparison, however, is perhaps that with the so-called combination or "symbiotic" spectra, such as those of the stars Z Andromedae and RW Hydrae. The resemblance of BD+11°4673 to such objects has been gradually increasing since 1915. The parallel development of high-excitation lines—e.g., *He* II 4686—and of *TiO* bands is a most remarkable circumstance which seems strongly to confirm the previous indication from other objects that these spectral features are related in some curious interdependent (symbiotic) manner. Here again the future promises to bring forth important facts. The constancy of the magnitude of BD+11°4673 within recent years[15] is not favorable to the hypothesis that the features arise in independent stars.

It is too early to discuss in detail the correspondence between BD+11°4673 and other stars with combination spectra. It would be important to know whether these other stars undergo complicated changes in line-displacements something like those in BD+11°4673. Meager data for Z Andromedae,[16] RW Hydrae,[17] and BF Cygni[17] suggest that they may. It will be a laborious task to gather extensive data for these and similar stars, but one which will obviously have to be accomplished before we can gain an adequate understanding of this mysterious group of objects.

CARNEGIE INSTITUTION OF WASHINGTON
MOUNT WILSON OBSERVATORY
January 1942

[14] O. Struve concluded that in P Cygni the velocity increases with height above the photosphere while the ionization decreases (*Ap. J.*, **81**, 66, 1935). In an adequate comparison of various stars more than one parameter would doubtless be involved.

[15] K. Himpel, *A.N.*, **270**, 184, 1940.

[16] H. H. Plaskett, *Pub. Dom. Ap. Obs.*, **4**, 119, 1928: Swings and Struve, *Ap. J.*, **91**, 608, 1940; **93**, 356, 1941.

[17] Unpublished measurements by the writer.

ABSOLUTE DIMENSIONS OF A WOLF-RAYET STAR AND THE EXPANDING-ENVELOPE HYPOTHESIS*

O. C. WILSON

ABSTRACT

Measures of the equivalent width of the $H\gamma$ absorption line of the B-type component of HD 193576 have been made during and outside of eclipse. These data, combined with a preliminary unpublished light-curve by G. E. Kron and the spectrographic orbit by the writer, permit the derivation of the absolute dimensions of the system with fair accuracy. It is found that the Wolf-Rayet star is the larger and brighter of the pair, although it has the smaller mass, and Gaposchkin has shown it to have the smaller surface brightness.

The hypothesis that the Wolf-Rayet emission bands are formed in an expanding envelope surrounding the star is discussed critically. Arguments based upon observations, although not decisive, tend to throw doubt on the validity of the hypothesis.

The binary character of HD 193576 offers a means of deciding whether or not the emission bands of the Wolf-Rayet component are produced in an expanding envelope. In view of the facts that the band width corresponds to an ejection velocity of 2000 km/sec and that the character of the Wolf-Rayet spectrum is not seriously modified by the presence of the companion, it is assumed that the ejected particles follow linear trajectories. As a consequence of this assumption, the radial velocity measured by the displacement of the emission band must differ from the true radial velocity of the star. The chief consequence of this transit-time effect is a difference between the observed times of eclipse and the times predicted by the spectrographic orbit. Formulae are derived from the transit-time effect and computations of its magnitude are made for three velocity distributions and for a variety of inner and outer radii of the envelope, with the aid of the absolute dimensions of the system derived in section I. Similar computations are made of the magnitude of the violet shift of the bands due to occultation. The existing observations limit the difference between the observed and the computed times of eclipse to $0.01P$, which requires that the supposed envelope be so small as to lead to violet shifts of some hundreds of km/sec. Since such shifts are not observed, it is concluded that the emission bands are probably not formed in an expanding envelope.

The measured intensities of the λ 4686 band of *He* II are investigated as a function of phase. The intensity is very nearly the same at phases 0.25, 0.50, and 0.75, but the band is about 19 per cent weaker at primary minimum. Perhaps there is a "reflection effect," which causes the Wolf-Rayet star to radiate more strongly in the λ 4686 band from the hemisphere facing the companion.

A few tentative remarks are made concerning possible alternatives to the expanding-envelope hypothesis, although no satisfactory solution is found. A zone of turbulence might be invoked to account for the great widths of the emission bands. This explanation, however, leads to difficulties with the displaced absorption components sometimes observed in Wolf-Rayet spectra. Moreover, it leaves unexplained the red shift of the bands in HD 193576 and their periodic changes in shape.

I. ABSOLUTE DIMENSIONS OF THE SYSTEM HD 193576

Since the publication[1] of the spectrographic orbit of HD 193576, S. Gaposchkin has shown that this binary star is also an eclipsing variable.[2] He has published his light-curve, together with several solutions for the absolute dimensions of the system. As he states in his paper, however, "the results which can be derived from a light curve with such shallow minima are rather indeterminate." The absolute dimensions derived by Gaposchkin cannot, therefore, be considered as definitive. Nevertheless, his work definitely establishes two important points of permanent value. The first is that the radius of the Wolf-Rayet star is very much greater than that required to account for the observed red shift of the emission bands as a relativistic gravitational displacement. The second point is that the surface brightness of the Wolf-Rayet star is less than that of the B-type component and that it corresponds to a surface temperature of the order of 13,000°.

* *Contributions from the Mount Wilson Observatory, Carnegie Institution of Washington*, No. 660.

[1] *Mt. W. Contr.*, No. 623; *Ap. J.*, **91**, 379, 1940.

[2] *Ap. J.*, **93**, 202, 1941.

The present work has a dual purpose: first, to derive more accurate values of the absolute dimensions of the system by utilizing new observational data and, second, to employ these dimensions in an attempt to answer the question: Where do the emission bands of the Wolf-Rayet star originate?

The system of HD 193576 is composed of a star of early type (spectrum about B1) and a Wolf-Rayet star of type WN5 revolving in circular orbits about their mutual center of gravity in a period of 4.212 days. Although the $H\gamma$ absorption line of the B-type component is quite weak, both its displacement and its intensity are measurable with fair accuracy. Comparison of the equivalent width of this line near primary and secondary minimum with the width outside of eclipse should provide sufficient additional data to eliminate much of the indeterminacy in the solutions based solely on the light-curve. The method of combining the measures of equivalent width with the photometric material is as follows.

Let L_W and L_B represent, respectively, the light of the Wolf-Rayet and the B-type component in the wave-length region covered by the photometric observations, and let $q = L_W/L_B$. Then the amplitude of primary minimum is given by

$$A_p = \frac{L_W + L_B}{L_W + (1 - \alpha_0)L_B} = \frac{q+1}{q + (1-\alpha_0)}, \tag{1}$$

where α_0 is the fraction of the disk of the B-type star which is obscured at mid-eclipse. Similarly, the amplitude of secondary minimum is

$$A_s = \frac{q+1}{(1 - k^2\alpha_0)\, q + 1} \tag{2}$$

where $k = R_B/R_W$ is the ratio of the radii of the two stars.

At some point, λ, within the $H\gamma$ absorption line of the B-type star the intensity divided by that of the continuous spectrum is

$$r_B = \frac{I_\lambda}{I_B}. \tag{3}$$

Then, outside of eclipse, the corresponding ratio in the combined spectrum is

$$r_0 = \frac{I_\lambda + I_W}{I_B + I_W} = \frac{r_B + q}{1+q}, \tag{4}$$

since, to a close approximation, $I_W/I_B = L_W/L_B$. In similar fashion, at the bottom of primary minimum we have

$$r_p = \frac{(1-\alpha_0)\, r_B + q}{(1-\alpha_0) + q}, \tag{5}$$

while at the bottom of secondary minimum the ratio is

$$r_s = \frac{r_B + (1 - k^2\alpha_0)q}{1 + (1 - k^2\alpha_0)q}. \tag{6}$$

Since the equivalent width of a line, W, is defined as $W = \int (1-r)d\lambda$, equations (4), (5), and (6) reduce to

$$W_0 = \frac{W_B}{1+q}, \tag{7}$$

$$W_p = \frac{(1-\alpha_0)W_B}{(1-\alpha_0) + q} \tag{8}$$

and

$$W_s = \frac{W_B}{1+(1-k^2a_0)q}, \tag{9}$$

respectively, the notation being obvious. The foregoing derivations are, of course, based upon the assumptions of circular disks and no limb darkening.

Equations (2) and (9) are not independent, by virtue of equation (7), and there are thus four equations from which to solve for the four unknowns, q, a_0, k, and W_B. From equations (1), (7), and (8) we find

$$q = \frac{1-\frac{W_p}{W_0}}{A_p-1}, \tag{10}$$

$$1-a_0 = \frac{1}{A_p}\frac{W_p}{W_0}, \tag{11}$$

and

$$W_B = \frac{W_0}{A_p-1}\left(A_p-\frac{W_p}{W_0}\right). \tag{12}$$

The value of k may be found from either equation (2) or equation (9).

During the summer of 1941, 44 spectrograms of the star were obtained covering the phases near 0.0, 0.25, 0.50, and 0.75 as thoroughly as permitted by the available observ-

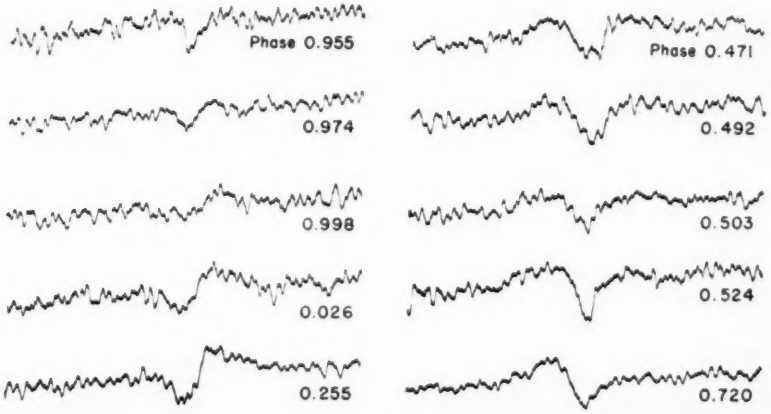

FIG. 1.—Microphotometer tracings of the $H\gamma$ region of the spectrum of HD 193576

ing time. These spectrograms, unlike those used for the orbit determination, were intended primarily for spectrophotometry. The star was accordingly trailed along the slit during the exposures, to provide widened spectra, and efforts were made to adjust the exposure times to yield densities suitable for photometry both at $H\gamma$ and over the *He* II emission band at λ 4686. The latter was overexposed on a few of the plates, but on the whole the results were satisfactory. Only two spectrograms taken prior to last summer were included.

Really accurate determinations of the equivalent width of $H\gamma$ from single plates are impossible, owing to the weakness of the line itself, but results based upon a number of spectrograms should be fairly reliable. The measurement of $H\gamma$ is rendered additionally difficult because the absorption line is accompanied by a very weak emission component,

not previously noted. The latter is not part of the normal Wolf-Rayet emission spectrum, since it appears on opposite sides of the absorption line at phases 0.0 and 0.5. Perhaps it originates in or near the B-type star. The appearance of the $H\gamma$ region is illustrated by the microphotometer tracings in Figure 1; and the measured equivalent widths of $H\gamma$, in arbitrary units, are listed in Table 1, as a function of phase. The phases have been computed from the formula

$$JD = 2428771.357 + 4^d.21238E,$$

which resulted from the orbit determination.[1]

In Figure 2 the values of W measured near primary and secondary minimum are plotted against phase. The results near phases 0.25 and 0.75 are not shown in detail, the mean value of W_0, 0.74, being indicated by the horizontal line. The curve in Figure 2 will be referred to later. It is evident that the plotted points are too few and too scatter-

TABLE 1

MEASURED EQUIVALENT WIDTHS OF $H\gamma$ (ARBITRARY UNITS)

Phase	E.W.	Phase	E.W.	Phase	E.W.
0.942	0.43	0.026	0.60	0.461	0.82
.948	.63	.032	0.45	.471	0.75
.955	.56	.224	0.63	.481	0.94
.957	.68	.234	0.85	.483	0.92
.966	.52	.239	0.78	.484	0.75
.968	.60	.247	0.46	.492	0.38
.974	.50	.255	0.63	.493	0.81
.978	.35	.277	0.64	.499	0.70
.980	.48	.707	0.72	.503	0.77
.986	.30	.713	0.65	.503	1.00
.993	.27	.717	1.04	.512	1.04
.998	.49	.717	0.90	.515	0.95
.001	.44	.720	0.82	.524	1.00
.009	.42	.727	0.80	0.549	0.80
.017	.25	.730	0.65		
0.018	0.75	0.767	0.80		

ing to justify an attempt at a solution of high accuracy. It is clear, however, that W_p is considerably less than W_0, while W_s definitely exceeds the latter. Thus, to obtain an approximate solution we simply estimate from Figure 2 that $W_p = 0.35$ and $W_s = 0.89$. These values, combined with the photometric data in the manner outlined above, should give results which are reasonably close to the truth.

Gaposchkin's determinations of A_p and A_s could be used in the solution. However, Dr. G. E. Kron has supplied me with a preliminary light-curve for λ 4500 based upon his observations with the photoelectric photometer of the Lick Observatory during the summer of 1940 and has generously given me permission to make use of it. Kron's curve, although preliminary and incomplete, is considerably more accurate than Gaposchkin's and differs from the latter in several important details. The only difference that need be mentioned here is that the width of primary minimum appears definitely to be considerably greater than that of secondary minimum, and greater also than the width shown in Gaposchkin's published light-curve. The depths of the two minima are nearly the same in both curves, but for consistency I shall adopt Kron's values. From his curve I estimate the half-width of primary minimum, from first contact to minimum light, to be $0.127P$ and the depths of the minima, measured from the mean light at phases 0.25 and

0.75, to be $\Delta m_p = 0.345$ and $\Delta m_s = 0.145$. From the latter quantities it follows that $A_p = 1.37$ and $A_s = 1.14$.

With the preceding values of W_p, W_0, A_p, and A_s, equations (10), (11), and (12) yield the results

$$q = \frac{L_W}{L_B} = 1.42 ,$$

$$1 - \alpha_0 = 0.346 ; \quad \alpha_0 = 0.654 ,$$

$$W_B = 1.79 .$$

From equation (2), $k = 0.567$, while from equation (9), $k = 0.656$. We adopt $k = 0.6$ in round numbers. With the half-width of primary minimum given above, the usual methods lead to $i = 67°.6$ and $R_W = 0.477\ (a_1 + a_2)$, and the introduction of the spectroscopic data gives the following absolute dimensions of the system:

$$\begin{aligned} i &= 67°.6 , \\ \mu_W &= 12.4\odot , \\ \mu_B &= 31.8\odot , \\ a_1 + a_2 &= 2.69 \times 10^7 \text{ km} = 38.7 R\odot , \\ R_W &= 1.28 \times 10^7 \text{ km} = 18.5 R\odot , \\ R_B &= 0.77 \times 10^7 \text{ km} = 11.1 R\odot , \\ \left.\begin{aligned} L_W &= 0.586 \\ L_B &= 0.414 \end{aligned}\right\} & \lambda \sim 4500 . \end{aligned}$$

The system is drawn to scale in Figure 3.

The present results differ essentially from Gaposchkin's as to the relative luminosities and radii of the two stars. Whereas he preferred a solution which makes the Wolf-Rayet

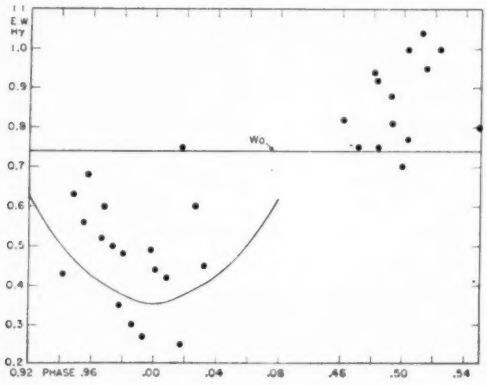

FIG. 2.—Equivalent widths (in arbitrary units) of $H\gamma$ as a function of phase. The mean equivalent width for phases near 0.25 and 0.75 is represented by the horizontal line.

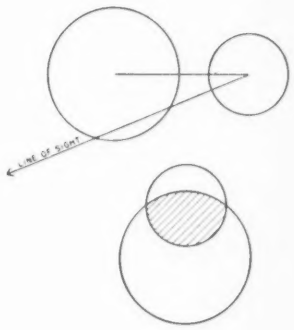

FIG. 3.—The system of HD 193576. The Wolf-Rayet component is the larger.

star fainter than the B star by more than two magnitudes, we now find that the Wolf-Rayet is slightly the more luminous; and whereas he considered the radius of the Wolf-Rayet to be considerably smaller than that of the B, we now come to the opposite conclusion. As to the relative luminosities, I believe that simple inspection of the spectro-

grams lends support to the present solution, for the emission bands do not have the appearance of being overlaid by a continuous spectrum (from the B-type star) more than five times as intense as that with which they should normally be associated. Even the weak bands of *N* v are easily visible. If it be granted that the relative luminosities derived in this paper are essentially correct, the larger radius for the Wolf-Rayet follows at once, since Gaposchkin's own work has shown the latter to possess the smaller surface brightness. Another fact which may point toward the incorrectness of Gaposchkin's solution is that the absolute magnitude of HD 193576 derived from the strength of the interstellar *Ca* II lines in its spectrum is -1.7 compared to a mean of -2.1 for 12 WN stars.[3] If the system were actually as he proposed, its absolute brightness would probably be more than two magnitudes in excess of the mean for other WN stars. Such a magnitude is scarcely allowed by the interstellar-line intensities. However, since the star lies just on the edge of a heavily obscured region in Cygnus, it is perhaps unfair to lay much stress upon absolute-magnitude determinations, in which accurate account of the obscuration cannot be taken. Finally, the present solution gives values of the mass and radius of the B-type component, which are in excellent agreement with the mass-radius relationship based upon observational data collected by G. P. Kuiper;[4] but in this respect Gaposchkin's results are equally acceptable.

From equations (1), (7), and (8) it follows that the course of W through primary minimum is given as a function of phase by

$$W = (1 - \alpha)\, AW_0 . \tag{13}$$

Taking A as a function of phase from Kron's light-curve and computing corresponding values of α from the present solution, we find the predicted variation of W with phase shown by the curve in Figure 2. The agreement is perhaps as good as might be expected in view of the considerable scatter of the observations and the rather limited range of phase covered by them. Possibly a slightly larger value of W_p would have yielded better general agreement. In any event, there seems no reason to suppose that the absolute dimensions quoted above are not reasonably close approximations.

II. FORMATION OF THE EMISSION BANDS

In any study of the physical nature of Wolf-Rayet stars, it is of vital importance to know the correct answer to the question: Where are the emission bands formed? The current views on this subject are due chiefly to Beals,[5] who suggested that the emission bands are produced in an expanding envelope surrounding the star and that the band widths are, therefore, simply a manifestation of Doppler effect. An immediate explanation is thus provided for the observational fact that the widths of bands belonging to series of atomic transitions are found to vary according to the relationsip $\Delta\lambda \propto \lambda$. Moreover, the Wolf-Rayet emission bands are sometimes accompanied on their violet edges by absorption components similar in appearance and position to those which are observed on the violet edges of bands in the spectra of novae during the earlier stages. Since the matter ejected from certain novae has, in the course of time, become directly observable, the idea of ejection to account for the Wolf-Rayet bands thus received support. This general picture was, therefore, quite attractive and has justifiably gained wide acceptance.

Following the earlier work on the subject, B. P. Gerasimovič,[6] S. Chandrasekhar,[7]

[3] Sanford and Wilson, *Mt. W. Contr.*, No. 613; *Ap. J.*, **90**, 235, 1939.

[4] *Ap. J.*, **88**, 472, 1938; see Fig. 2.

[5] *Pub. Dom. Ap. Obs.*, **4**, 271, 1930, and several later papers.

[6] *Zs. f. Ap.*, **7**, 335, 1933.

[7] *M.N.*, **94**, 522, 1934.

and the writer[8] approached the matter from somewhat different standpoints. Gerasimovič suggested that the rounded contours of the bands were due to radial-velocity gradients within the envelopes, and the writer gave simplified methods of computation for this case. Chandrasekhar adopted the same idea and, in addition, called attention to the important consequences of an occultation of a portion of the envelope by the opaque body of the star. Unless the radii of the regions effective in the production of the bands are fairly large compared to the radius of the star, the emission bands should be asymmetrical in the sense that their red halves would be weakened, and the center of gravity of the entire band accordingly displaced toward the violet. All the foregoing investigations included the assumption that the envelope is transparent to its own radiation as well as to that of the central star.

Since no very critical examination of the expanding-envelope hypothesis seems yet to have been made, the following considerations are necessary as a background to the remainder of the present work. As far as I am aware, no published material has revealed evidence of either the asymmetrical contours or the violet displacements of the Wolf-Rayet bands to be anticipated as consequences of the occultation effect. In fact, the available data point rather to a shift of the bands toward the red.[9] It is legitimate, therefore, to ask why there is no observable evidence for the occultation effect.

The most obvious reply to this query is simply that the envelope is large with respect to the star. The actual relative dimensions of the envelope and star which are necessary to reduce the effects of occultation below the observable limit will depend, of course, upon the accuracy with which the observations can be made and upon the assumed mechanism of ejection and excitation of the emitting atoms. Under nearly any reasonable circumstances, however, as will be shown later, the outer radius of the envelope must be at least three or four times that of the photosphere in order to reduce the predicted violet shift to a fairly small value. Taken by itself, this requirement as to the size of the envelope presents no difficulties, although some doubts are raised by the following observational considerations:

1. The absorption components sometimes found on the violet edges of certain Wolf-Rayet emission bands have appreciable widths which can be directly measured with fair accuracy. If it be assumed that these widths are due entirely to the spread of the radial velocities of the outward-moving atoms projected upon the stellar disk, the radius of the latter relative to that of the envelope may be estimated by comparison of the widths of the absorption lines with those of the corresponding emission bands. Measures by the writer on several Wolf-Rayet spectra indicated that the radii of the envelopes were only about twice those of the central stars.[10] Thus rather large occultation effects would be anticipated; but, since the widths of the absorption components might conceivably be due, at least in part, to turbulent motions or velocity gradients within the envelope, the results of the measures cannot be accepted as entirely conclusive.

2. No evidence available from the spectra indicates any great dilution of radiation. For instance, although λ 3889 of *He* I is usually the strongest absorption line in the photographic region, it is generally, if not always, accompanied by other *He* I absorption lines such as λ 4471. Since λ 3889 arises from the metastable 2^3S level, while most of the other lines originate in ordinary levels of short lifetime, it is clear that the prevailing physical conditions are much closer to those in ordinary stellar atmospheres than to those in the gaseous nebulae. Pending an investigation of the absorption lines in Wolf-Rayet spectra, which might be expected to yield valuable results concerning the actual dilution factors, it may simply be stated that the observed lines rule out the possibility of a large envelope surrounding a relatively small star.

3. A third point, of less weight for present purposes than the other two, is that no emissions resulting from forbidden transitions have been found in Wolf-Rayet spectra.

[8] *Mt. W. Contr.*, No. 500; *Ap. J.*, **80**, 259, 1934.

[9] *Mt. W. Contr.*, No. 624; *Ap. J.*, **91**, 394, 1940. The data, except the writer's measures of HD 193576, are due to Beals.

[10] *Mt. W. Contr.*, No. 624; *Ap. J.*, **91**, 394, 1940. Using a similar method, P. Swings derived even smaller relative radii for Wolf-Rayet envelopes (*Ap. J.*, **95**, 112, 1942).

The second possible way of accounting for the lack of observable occultation effects is to suppose that, although such effects do, in fact, exist, they are masked because absorption within the envelope, either of its own radiation or that of the photosphere or both, acts to depress and modify the violet halves of the bands in just the right manner to compensate for the effects of occultation upon the red halves, the net result being symmetrical undisplaced bands. Such absorption effects have been invoked by Struve and Sherman to explain the redward displacement of the emission lines in the spectrum of 29 Canis Majoris[11] and are apparently favored by them for HD 193576, although the latter shows no P Cygni type absorption lines. The application of this type of explanation to the Wolf-Rayet stars in general seems improbable because of the stringent conditions which must be imposed upon the hypothetical absorptions. Detailed objections follow.

1. In spectra in which some of the bands show well-marked absorption components, other bands, some more intense and some less so, exhibit no trace of absorption. It seems reasonable to suppose that the "compensation" of bands without accompanying absorptions should be much less complete than that of bands which have absorption. While it must be conceded that further data are required to settle this question, it is true that no gross effects have as yet been reported which would indicate systematic differences in displacement between bands with or without accompanying absorptions.

2. The bands present in Wolf-Rayet spectra represent a rather large range in required excitation, and this fact is generally interpreted to mean that the envelope is so stratified that bands needing various amounts of excitation originate in shells of different radii. The occultation effect, however, varies quite rapidly with distance from the photosphere, until this distance becomes three or four times the stellar radius. Hence, unless all the bands are formed at some distance from the star, the absorbing properties of the various shells would have to be so arranged as to compensate for an occultation effect varying considerably from band to band. Moreover, consideration of the relative velocities of the particles within an envelope shows that the absorption of continuous radiation from the central star is much more likely than the absorption by the envelope of its own radiation. Thus, consider the case of a strong band, a portion of which is removed by occultation at a wave length where, without occultation, the intensity of the band alone would exceed that of the underlying continuous spectrum. If, at the corresponding wave length on the violet side of the band, the compensating absorption is effective only upon the continuous stellar radiation, the latter can, at most, be removed entirely. In this case, however, it is evident that the compensation of the occultation effect cannot be complete. The difficulty would be even greater if the supposed absorption were required not merely to compensate for the occultation but to overwhelm it and produce a net shift of the band toward the red. In connection with these arguments it may be recalled that in the star HD 193576, where the measures are numerous enough to deserve considerable weight, the weak bands of *N* v, requiring a total excitation of about 221 volts, have the same red shift as the very strong λ 4686 band of *He* II, whose total required excitation is only 72 volts.

Last, it is possible that no occultation effects are found simply because the bands are not produced in an expanding envelope.

III. TEST OF THE EXPANDING-ENVELOPE HYPOTHESIS PROVIDED BY HD 193576

In the case of a Wolf-Rayet star moving in a straight line through space, the particles ejected from its surface during the interval *dt* will, at any later time *t*, form a spherical shell concentric with the star. The Wolf-Rayet component of HD 193576 is, however, subject to a large acceleration which constrains it to move in a circular orbit, and the preceding statement cannot apply. Lacking any sound theoretical means of procedure, we appeal to two facts of observation. The first is that the half-width of the λ 4686 band corresponds to an extreme ejection velocity of 2000 km/sec—fully three times the velocity of escape from the star. With such enormous velocities, however acquired, it seems reasonable to suppose that the great majority of the particles will move out, not only from the Wolf-Rayet star itself, but from the system of both stars, in essentially

[11] *Ap. J.*, **93**, 84, 1941.

linear trajectories. Only the paths of those particles which are directed close to the companion would be expected to suffer very great distortion. Even these distortions could well be minimized or even nullified, since the companion is a hot star of early type whose gravitational attraction for the passing atoms might easily be overcome by the outward pressure of its intense radiation.

The second observational fact is that the spectrum of the Wolf-Rayet star is modified to only a minor degree by the presence of the companion. Certain cyclical changes in the appearance of the bands are known to occur[10] and will be referred to in more detail later. But, as far as first-order effects are concerned, the spectrum is quite normal. The conclusion is that the processes responsible for the formation of the Wolf-Rayet spectrum are largely unaffected by the presence of the B-type star. In the following investigation of the expanding-envelope hypothesis we shall, therefore, assume that the ejected particles move linearly outward from the surface of the Wolf-Rayet star, and we shall neglect those which impinge directly upon the surface of the companion. Thus the matter leaving the surface between times t and $t + dt$ will form, at any later time, a spherical distribution whose center moves with the orbital velocity along the tangent to the orbit at the point occupied by the star at time t. At any instant the radial velocity of such a spherical shell will not be equal to that of the star, owing to the change in phase angle of the latter during the time interval since the shell was ejected. We are thus led to the consideration of what may briefly be designated as "transit-time effects." It is clear that these will be small for small envelopes, whereas the occultation effect will be minimized for large envelopes; and it must now be investigated whether, in the case of HD 193576, the expanding-shell hypothesis is capable of providing bands for which both effects are sufficiently small to be in agreement with the observations.

Let us assume that we are dealing with a recombination spectrum; hence the emission per unit volume is proportional to ρ^2, where ρ is the density of the matter. Then a thin spherical shell of radii R and $R + dR$, whose outward velocity is v, will produce an elementary rectangular contour, the height of which is given by[12]

$$dI(u) = 2\pi k R^2 \rho^2 v^{-1} dR . \tag{14}$$

The total emission from the entire thin spherical shell is then

$$dE = 2\pi k R^2 \rho^2 v^{-1} dR (u_1 - u_2) , \tag{15}$$

where u_1 and u_2 are the radial velocities of the two extremities of the elementary contour. For no occultation, $u_1 = v$ and $u_2 = -v$, and an envelope composed of a continuous series of such shells extending between the radii R_1 and R_2 will emit the energy

$$E = 4\pi k \int_{R_1}^{R_2} R^2 \rho^2 dR . \tag{16}$$

This expression could have been written down at once by first principles.

If the shell is concentric with an opaque spherical body of radius r, it follows by simple geometry that the elementary contour extends from $-v$ on the violet to $v\sqrt{1 - r^2/R^2}$ on the red. Hence in this case

$$u_1 - u_2 = v\left(1 + \sqrt{1 - \frac{r^2}{R^2}}\right), \tag{17}$$

and the total emission of the envelope is given by

$$E = \int dE = 2\pi k \int_{R_1}^{R_2} R^2 \rho^2 \left(1 + \sqrt{1 - \frac{r^2}{R^2}}\right) dR . \tag{18}$$

[12] *Mt. W. Contr.*, No. 500; *Ap. J.*, **80**, 425, 1934, equation (4) with $\beta = 0$.

The radial velocity of the shell, $\bar{u}$, is given simply by the mid-point of the elementary contour produced by it. Hence

$$\bar{u} = \frac{u_1 + u_2}{2} = -\frac{v}{2}\left(1 - \sqrt{1 - \frac{r^2}{R^2}}\right). \tag{19}$$

The whole band may be thought of as the superposition of all the elementary contours formed by the successive thin shells into which the envelope may be divided. Let $\bar{U}$ be the displacement of effective center of the band which, by definition, corresponds to its radial velocity. Then clearly

$$\bar{U} = \frac{\int \bar{u}\, dE}{\int dE}, \tag{20}$$

where the integrations are to be extended throughout the envelope. Thus, designating by $\bar{U}_2$ the apparent radial velocity caused by the occultation effect, we have by equations (18), (19), and (20),

$$\bar{U}_2 = -\frac{r^2}{2}\,\frac{\int_{R_1}^{R_2} \rho^2 v\, dR}{\int_{R_1}^{R_2} R^2 \rho^2 \left(1 + \sqrt{1 - \frac{r^2}{R^2}}\right) dR}. \tag{21}$$

The equation of continuity requires that

$$\rho(R) = \frac{\text{const.}}{R^2 v(R)}. \tag{22}$$

Some assumption regarding the velocity distribution being necessary at this stage, I have adopted the form

$$v(R) = v_0 \left(\frac{R}{r}\right)^n, \tag{23}$$

where n may be positive, negative, or zero, as sufficiently general for all practical purposes. Inserting equations (22) and (23) into equation (21), we find

$$\bar{U}_2 = -\tfrac{1}{2} v_0 r^{-n+2}\,\frac{\int_{R_1}^{R_2} R^{-(n+4)}\, dR}{\int_{R_1}^{R_2} R^{-2(n+1)} \left(1 + \sqrt{1 - \frac{r^2}{R^2}}\right) dR}, \tag{24}$$

an expression which gives the radial velocity of the band in so far as the latter depends upon occultation.

The calculation of the dependence of the radial velocity upon the transit-time must now be considered. If V_0 is the orbital velocity of the Wolf-Rayet star, its radial velocity may be written as

$$u_W = V_0 \sin \vartheta, \tag{25}$$

where ϑ is the phase angle in the orbit. At a time t when the phase angle of the star is ϑ, a given elementary shell will have the radial velocity $u_W(\vartheta - \Delta\vartheta)$, where $\Delta\vartheta$ is the increment in phase angle of the star during the elapsed time Δt since the ejection of the particular shell. Evidently

$$u_W(\vartheta - \Delta\vartheta) = V_0 \sin(\vartheta - \Delta\vartheta). \tag{26}$$

For values of $\Delta\vartheta$ which are not too large, we may approximate in equation (26) by writing

$$u_W(\vartheta - \Delta\vartheta) = V_0(\sin\vartheta - \Delta\vartheta\cos\vartheta)\,. \tag{27}$$

We have

$$\Delta\vartheta = \frac{2\pi}{P}\Delta t\,, \tag{28}$$

where P is the period of orbital motion, and

$$\Delta t = \int_r^R \frac{dR}{v(R)}\,. \tag{29}$$

Hence,

$$u_W(\vartheta - \Delta\vartheta) = V_0\sin\vartheta - \frac{2\pi}{P}V_0\cos\vartheta\int_r^R\frac{dR}{v(R)}\,. \tag{30}$$

The first term on the right-hand side of equation (30) is simply the radial velocity of the star at phase angle ϑ and is the same for all the elementary shells composing the envelope. The second term is the transit-time correction for the shell of radius R and must be integrated through the envelope to obtain the correction for the band as a whole. Designating the latter by $\bar{U}_3$, we find, from equations (20), (23), and (30),

$$\bar{U}_3 = -\cos\vartheta\,\frac{2\pi}{P}\,\frac{V_0}{v_0}\,\frac{r^n}{-n+1}\,\frac{\int_{R_1}^{R_2}R^{-2(n+1)}(R^{-n+1}-r^{-n+1})\left(1+\sqrt{1-\frac{r^2}{R^2}}\right)dR}{\int_{R_1}^{R_2}R^{-2(n+1)}\left(1+\sqrt{1-\frac{r^2}{R^2}}\right)dR}\,. \tag{31}$$

Thus, subject to the assumptions, the radial velocity given by the Wolf-Rayet emission bands consists of the sum of three terms:

$$U = U_1 + \bar{U}_2 + \bar{U}_3\,. \tag{32}$$

The first term is simply the radial velocity of the star itself, $V_0\sin\vartheta$, by equation (30); the second is a constant violet shift (equation [24]) due to the effects of occultation; the third is the result of the finite velocity of the ejected particles and is a periodic term out of phase with the orbital motion by a quarter-period. It should be noted that the derivation of $\bar{U}_2$ implies that the centers of the star and the envelope are coincident, while the existence of $\bar{U}_3$ depends upon the fact that they are not. Hence calculations based upon equation (24) cannot be strictly accurate. However, since the effects of occultation are greatest for those shells nearest the star, whose centers deviate least from that of the star, the error is probably of the second order and will be neglected. We are not striving for high accuracy but only for the correct order of magnitude.

The influence of occultation upon the radial velocities diminishes as the size of the envelope is increased, while the opposite is true of the transit-time effect. The next step, therefore, is to make computations of the two effects, based upon the known dimensions and properties of HD 193576, and to find what conclusions may be drawn from a comparison of the results with the existing radial-velocity and photometric data. Three different velocity distributions in the envelope have been considered, as well as a number of effective inner and outer radii, in order to illustrate the consequences of varying these parameters. The velocity distributions investigated are those with $n = 0, +2$, and -2 in equation (23), which correspond to constant outward velocity, accelerated motion, and decelerated motion, respectively. As will appear from the general similarity of the results in these three cases, it is not likely that other velocity distributions would essentially change the conclusions arrived at. All the computations have been made in such a manner as to be readily comparable with the observations. Thus in every instance the

value of v_0, eq. (23), has been so chosen, in conjunction with R_1 and R_2, as to yield a band whose total width is equal to the 4000 km/sec observed for λ 4686. The detailed results follow.

CASE I. CONSTANT OUTWARD VELOCITY; $n = 0$

The violet edges of all the elementary contours coincide, and the extension of the band toward the red is determined by the outermost shell. If v_0 is the constant outward velocity, simple geometry shows that the band width, ΔU, is

$$\Delta U = v_0\left(1+\sqrt{1-\frac{r^2}{R^2}}\right),$$

which determines v_0 as a function of the outer radius, R_2, for a given ΔU. For the specified band width, $\Delta U = 4000$ km/sec, the corresponding values of v_0 and R_2 are listed in Table 2.

TABLE 2

v_0 AS FUNCTION OF R_2 FOR $\Delta U = 4000$ KM/SEC AND $n=0$

R_2/r	v_0	R_2/r	v_0
1.43	2340 km/sec	5.00	2010 km/sec
2.00	2140	∞	2000
3.00	2060		

TABLE 3

CALCULATED VALUES OF $-\bar{U}_2$ AND $(-\bar{U}_3/\cos\vartheta)\sin i$ FOR CONSTANT VELOCITY; $n=0$

R_1/r	R_2/r				
	1.43	2.00	3.00	5.00	∞
1.00	571 6	388 13	292 23	241 38	188 .....
1.43	.....	215 22	154 34	121 50	84 .....
2.00	.....	.....	97 46	68 70	44 .....
3.00	.....	.....	.....	36 99	18 .....
5.00	.....	.....	.....	.....	8 .....

The numerical constants required for the computations are: orbital velocity, $V_0 = 335$ km/sec; period, $P = 4.212$ days $= 3.64 \times 10^5$ sec.; radius of Wolf-Rayet star, $r = 1.28 \times 10^7$ km. The integrations in equations (24) and (31) have been performed (only simple trigonometrical transformations are required) and the numerical data have been used to determine the component of the radial velocity due to occultation, $\bar{U}_2$, and the amplitude of the transit-time effect, $\bar{U}_3/\cos\vartheta$, in km/sec. These amplitudes have been

multiplied by sin i to make them strictly comparable with the observations. The results are given in km/sec in Table 3, where the uppermost of each pair of entries is $-\bar{U}_2$ and the lower one is $(-\bar{U}_3/\cos\vartheta)\sin i$.

CASE II. ACCELERATED MOTION; $n = +2$

Both the violet and the red edges of the band are determined by the outer boundary, and the value of v_0 required to yield a specified band width is given by

$$v_0 = \frac{\Delta U}{\left(\frac{R_2}{r}\right)^2\left(1+\sqrt{1-\frac{r^2}{R_2^2}}\right)}.$$

Corresponding values of v_0 and R_2 necessary to produce a band 4000 km wide are listed in Table 4. The results of the computations are in Table 5, which is arranged in the same manner as Table 3.

TABLE 4

v_0 AS FUNCTION OF R_2 FOR $\Delta U = 4000$ KM/SEC AND $n = +2$

R_2/r	v_0	R_2/r	v_0
1.43	1142 km/sec	3.00	228 km/sec
2.00	536	5.00	81

TABLE 5

CALCULATED VALUES OF $-\bar{U}_2$ AND $(-\bar{U}_3/\cos\vartheta)\sin i$ FOR ACCELERATED MOTION; $n = +2$

R_1/r	R_2/r				
	1.43	2.00	3.00	5.00	∞
1.00	400 7	181 22	77 52	27 153	0 . . . . .
1.43	. . . . .	150 47	63 127	23 352	0 . . . . .
2.00	. . . . .	. . . . .	62 156	23 445	0 . . . . .
3.00	. . . . .	. . . . .	. . . . .	19 665	0 . . . . .
5.00	. . . . .	. . . . .	. . . . .	. . . . .	0 . . . . .

CASE III. DECELERATED MOTION; $n = -2$

The matter at the inner boundary of the envelope, R_1, is moving most rapidly and thus determines the position of the violet edge of the band. Investigation shows that the position of the red edge of the band is set by whichever boundary is closest to $r\sqrt{3/2} =$

$1.225r$. For all the pairs of radii in which we are interested, therefore, the value of v_0 is a function of R_1 only, and the relationship between the two quantities is shown in Table 6.

The results for decelerated motion are shown in Table 7 in km/sec as before.

Inspection of Tables 3, 5, and 7 shows that some of the entries for the transit-time effect exceed the orbital velocity. These large values are, of course, meaningless except in so far as they indicate the circumstances under which the effects of finite velocity of

TABLE 6

v_0 AS FUNCTION OF R_1 FOR $\Delta U = 4000$ KM/SEC AND $n = -2$

R_1/r	v_0	R_1/r	v_0
1.00	2890 km/sec	3.00	18900 km/sec
1.43	4760	5.00	50600
2.00	8570		

TABLE 7

CALCULATED VALUES OF $-\bar{U}_2$ AND $(-\bar{U}_3/\cos\vartheta)\sin i$ FOR DECELERATED MOTION; $n = -2$

R_1/r	R_2/r				
	1.43	2.00	3.00	5.00	∞
1.00	430 8	179 29	58 105	14 499	0 .....
1.43	.....	152 22	57 68	14 307	0 .....
2.00	.....	.....	60 45	17 177	0 .....
3.00	.....	.....	.....	19 90	0 .....
5.00	.....	.....	.....	.....	0 .....

ejection become great and the assumption of small $\Delta\vartheta$ in equation (27) becomes invalid. For given pairs of radii the smaller values of the effect all agree in general order of magnitude, regardless of the value of n, and all occur in conjunction with values of the occultation effect which are far from negligible. Thus, although it appears unlikely that the expanding-envelope hypothesis is capable of meeting the requirements of observation in the case of HD 193576, we turn to a closer investigation of the consequences of a finite velocity of ejection.

In equation (32) neglect the constant term $\bar{U}_2$ and consider the periodic terms U_1 and $\bar{U}_3$. Apart from the common factor $\sin i$, we have

$$U_1 = V_0 \sin\vartheta \quad \text{and} \quad \bar{U}_3 = V_3 \cos\vartheta$$

where V_3 is used to designate the factor of cos ϑ in equation (31). The sum of the periodic terms is

$$U_1 + \bar{U}_3 = V_0 \sin \vartheta + V_3 \cos \vartheta = V_0 \left(\sin \vartheta + \frac{V_3}{V_0} \cos \vartheta \right). \qquad (33)$$

If it is permissible to represent the net result of the transit-time effect as a simple phase shift, we should have

$$U_1 + \bar{U}_3 = V' \sin (\vartheta + \Delta\vartheta) = V' (\sin \vartheta + \Delta\vartheta \cos \vartheta) . \qquad (34)$$

Comparison of the coefficients of equations (33) and (34) gives

$$\left. \begin{aligned} V' &= V_0 \\ \Delta\vartheta &= \frac{V_3}{V_0} \end{aligned} \right\} . \qquad (35)$$

Thus to a first approximation the introduction of a transit-time effect of relatively small amplitude leaves the form and amplitude of the radial-velocity-curve essentially unchanged and causes only a phase shift of amount $\Delta\vartheta = V_3/V_0$. The observational consequence of the latter should evidently be a constant difference between the observed times of eclipse and the predicted times based upon the spectrographic orbit. Figure 4 illustrates the transit-time effect. Curve A has the amplitude of the observed radial-velocity-curve of the Wolf-Rayet component of HD 193576. Curve B represents a transit-time effect with an amplitude of 50 km/sec. Curve C is the resultant of A and B, and it is evident that the only change of observational importance is the phase shift, which amounts, in the case illustrated, to 0.027 P. Figure 4 shows also in which sense the observed times of eclipse would be expected to differ from the calculated times. Curve A is the "true" radial-velocity-curve of the opaque body of the star, while C is the "observed" curve. Evidently the eclipses should occur earlier than predicted by the amount

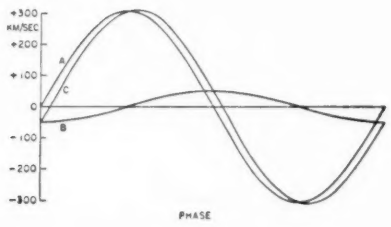

FIG. 4.—Radial-velocity-curves illustrating the phase shift produced by the finite velocity of the ejected matter.

$$\Delta P = \frac{P}{2\pi} \Delta\vartheta .$$

The phases used by Kron for his light-curve were computed from the formula derived from the spectrographic observations by the writer; and, although his curve is incomplete, the portions near both minima are covered fairly well. It is difficult to be precise in such a case, but I believe that Kron's results definitely rule out the possibility of any phase differences between the observed and the computed times of minimum light amounting to as much as 0.01 period. The amplitude of the transit-time effect must, therefore, be less than 20 km/sec, and inspection of Tables 3, 5, and 7 shows that the

simple expanding-envelope hypothesis would require a corresponding violet shift of some hundreds of km/sec due to occultation. No such displacement is observed; in fact, there is almost certainly a red shift of about 90 km/sec. Apparently the only way of preserving the expanding-envelope idea is to postulate very great absorption effects acting upon the violet portions of the bands. However, in view of the objections to this procedure pointed out in section II above, the present investigation raises grave doubts concerning the current hypothesis that the emission bands of Wolf-Rayet stars are actually formed in expanding envelopes.

IV. INTENSITIES AND CONTOURS OF THE λ 4686 *He* II BAND

Inspection of Figure 1 of Gaposchkin's paper[2] shows that, according to his solution, a considerable portion of any envelope surrounding the Wolf-Rayet star should be eclipsed at secondary minimum, unless the envelopes were quite large compared to the star itself. If such an eclipse effect were detectable by measurement of the total intensity of the λ 4686 band, it is possible that the relative dimensions of the star and envelope could be determined. This was one of the original aims of the present work. Although we have now seen that Gaposchkin's solution is probably incorrect and have been unable to produce any evidence to support the expanding-envelope hypothesis, the measures of shape and intensity of the band remain of interest in themselves and will be of value in future discussions of the structure of the Wolf-Rayet star.

The total energy, E, emitted in the band is given by

$$E \propto I_c \int (r' - 1)\, d\lambda = I_c \cdot A \ , \tag{36}$$

where I_c is the intensity of the continuous spectrum under the band and r' is the ratio of the intensity at any point in the band to that of the continuous background. In the case of HD 193576, the intensity of the continuous spectrum varies with phase in a known manner and equation (36) may be used to investigate variations in the emission of the band by writing

$$\frac{E}{E_0} = \frac{I_c \cdot A}{I_{c0} \cdot A_0} \ , \tag{37}$$

where E_0, I_{c0}, and A_0 are the values of the quantities at some phase chosen as standard.

The contours of λ 4686 were measured in the usual way. One source of error which

TABLE 8

PHASE INTERVALS AND NUMBERS OF PLATES

ΔΦ	No.	ΔΦ	No.
0.930–0.975	5	0.224–0.277	13
0.975– .025	9	0.707– .730	
0.025–0.050	3	0.461–0.549	12

has doubtless contributed to the scatter of the results is the fact that the apparent maximum intensity in the continuous spectrum fell very close to the center of the band, thus producing a rather sharply curved background beneath it. To eliminate some of the resulting purely accidental error, the mean central intensities were formed for certain groups of plates, and the ordinates of each band were multiplied by the factor required to make its central intensity equal to the mean for its group. The phase intervals covered by these groups and the numbers of plates they contain are shown in Table 8.

The reduced contours were then plotted, and the area $A = \int (r' - 1) d\lambda$ under each was measured with a planimeter. The values of A are given in Table 9.

Running means of A were formed for the phases near the minima, with groups of five values and overlaps of two. These mean values (Table 10) are plotted in Figure 5. The plotted points clearly show the influence of primary eclipse by rising to a maximum

TABLE 9

MEASURES OF λ 4686, *He* II: ARBITRARY UNITS

Phase	A	Phase	A	Phase	A
0.936	106	0.026	106	0.727	104
.948	105	.032	108	.730	114
.957	108	.047	106	.461	129
.968	102	.224	117	.471	133
.974	112	.234	110	.481	125
.980	120	.239	123	.483	124
.986	126	.247	118	.484	130
.988	132	.255	107	.492	134
.991	118	.277	118	.493	128
.993	118	.707	105	.499	116
.998	124	.713	113	.503	131
.001	120	.717	105	.503	129
.017	135	.717	108	.515	136
0.018	120	0.720	116	0.549	118

TABLE 10

RUNNING MEAN VALUES OF A; λ 4686

Phase	A	Phase	A
0.955	107	0.028	115
.979	118	.476	128
.994	124	.490	126
0.005	123	0.510	126

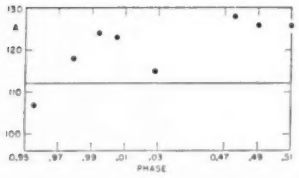

FIG. 5.—Running mean values of A for λ 4686 plotted against phase.

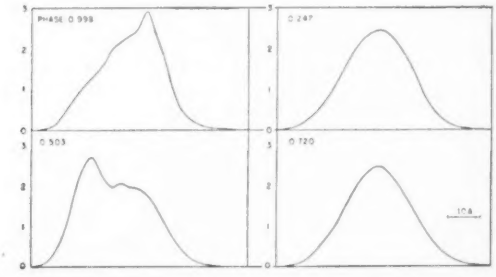

FIG. 6.—Typical contours of λ 4686, *He* II. Ordinates and abscissae are $r' - 1$ and wave lengths, respectively.

as the continuous spectrum falls to its minimum, but no effect of secondary eclipse is visible. The mean value of A for phases near 0.25 and 0.75 is 112, and we estimate from Figure 5 that A is approximately equal to 125 and 126 at phases 0.0 and 0.5, respectively. In equation (37) let $E_0 = 1$, and $I_{e0} = 1$ when $A = 112$. Then at phase 0.0, $I_e = 0.73$

from the amplitude of primary minimum, and equation (37) gives $E_{0.0} = 0.81\,E_0$. Similarly, at secondary minimum, $I_c = 0.88$ and equation (37) gives $E_{0.5} = 0.99E_0$. Thus the emission in the band appears to be essentially constant at phases 0.25, 0.50, and 0.75, but is diminished by about 19 per cent at primary minimum. There is no measurable eclipse effect when the Wolf-Rayet star lies behind its companion. There must, of course, be such an effect, but it is either too small to be observable with the available accuracy, or it is compensated by another effect which causes the Wolf-Rayet star to radiate most strongly in λ 4686 from the hemisphere facing the companion. The latter explanation would imply a kind of "reflection effect" and is not unreasonable in view of the fact that the emission in the band is observed to be reduced when the hemisphere of the Wolf-Rayet star facing the companion is turned away from the observer. A more detailed and complete coverage of all phases will be of interest in deriving the "light-curve" for the band.

The appearance of the λ 4686 band at various phases is illustrated by the typical contours reproduced in Figure 6.

V. SUMMARY AND CONCLUSIONS

The absolute dimensions of the stars which form the system of HD 193576 have been determined by combining Kron's photometric data with measures of the equivalent width of the $H\gamma$ absorption line of the B-type star inside and outside of eclipse. The results are that the Wolf-Rayet component is the larger and brighter, although it has the smaller surface brightness. Arguments for and against the hypothesis that the emission bands of the Wolf-Rayet stars are formed in expanding envelopes are presented in section II, and it is found that certain important, though not decisive, observational objections may be raised against it.

A more conclusive test of the expanding-envelope hypothesis is provided by HD 193576, on the fundamental assumption that the trajectories of the ejected particles are essentially unaffected by the presence of the B-type component. This assumption is rendered reasonable by the large velocities of the particles (2000 km/sec) and by the observational fact that only minor modifications of the spectrum of the Wolf-Rayet star result from its membership in a binary system. The assumption of linear trajectories leads to the conclusion that the radial velocity shown by the bands will differ from the true radial velocity of the star owing to the finite velocities of the ejected particles. Formulae are derived for the transit-time effect as well as for the displacement of the bands due to occultation and are applied to HD 193576. The transit-time effect is shown to consist chiefly of a shift in phase between the times of eclipse as observed photometrically and as predicted from the spectrographic orbit. The maximum amount of such a shift estimated as permissible from the existing data is so small as to require an envelope which is quite close to the photosphere. This requirement leads in turn to the prediction that the occultation effect should displace the center of gravity of the band toward the violet by some hundreds of km/sec—a prediction which is, of course, entirely unfulfilled by the observations.

Thus, unless some very serious error has crept into the derivation of the absolute dimensions of the stars or unless the assumption of linear trajectories of the ejected particles is completely wrong, one seems forced to doubt that the emission bands are formed in an expanding envelope surrounding the star. In fact, the very close agreement between the predicted and observed times of eclipse suggests strongly that the portion of the Wolf-Rayet star wherein the bands originate is very intimately connected with the opaque body of the star responsible for the periodic eclipses of the other component. In ordinary eclipsing binaries the photometric phases agree perfectly with those computed from the radial velocities. The same statement applies to HD 193576, where the radial velocities depend on the emission bands. It is possible that the postulation of appropriate

absorption effects on the violet portions of the bands might save the situation for the expanding-envelope hypothesis. In view of the discussion in section II, however, it seems fair to require that this question be given a more thorough physical treatment than heretofore.

In conclusion, a few remarks looking toward possible alternatives to expanding envelopes may not be amiss. For a variety of reasons the interpretation of the large band widths in terms of Doppler effect will probably be retained. If this be so and if the observable hemisphere of the star be required to provide the velocities of both signs necessary for the production of symmetrical bands, some form of large-scale turbulence must probably be demanded. In principle, very rapid rotation of the star might suffice, but the necessary rotational velocities seem too large to permit the existence of the star. Moreover, the lines of sight to various stars should make different angles with the axes of rotation and thus produce a greater range in band width among the Wolf-Rayet stars than is observed.

The exact location of the supposed zone of turbulence is uncertain. If it is on the outside of the star, in a position analogous to that of the reversing layers or chromospheres of ordinary stars, matter must be continually ejected, since the turbulent velocities exceed the velocity of escape. It must be supposed, in this case, that the ejected material very quickly becomes inactive in contributing to the emission bands, for otherwise the model would soon approximate to an expanding envelope. It is questionable, also, whether matter at the surface could acquire the large downward velocities needed to account for the red halves of the bands. Perhaps the zone of turbulence lies somewhat beneath the outermost regions at an optical depth which is not too great to prevent the visibility of the bands. If so, only a few of the most rapidly moving atoms might escape to form the absorption components sometimes observed on the violet edges of the bands. If the conditions of escape were critical, they might afford a means of explaining why some Wolf-Rayet stars possess absorption components, while others whose emission spectra are very similar, if not identical, do not. The shapes of the Wolf-Rayet emission bands are not too discouraging to the turbulence explanation. The majority of the bands seem to have a peaked or rounded form such as might result from random velocities, bands with flat-topped contours being rather rare. It must be admitted that the preceding discussion appears to be barren of any suggestion to account for the fact that the Wolf-Rayet bands are displaced to the red.

It is a pleasure to express my gratitude to Dr. Kron for permission to use his photometric results and to thank Miss L. Ware for making the necessary microphotometer tracings.

CARNEGIE INSTITUTION OF WASHINGTON
MOUNT WILSON OBSERVATORY
January 1942

THE SPECTROGRAPHIC ORBIT OF THE COMPANION TO RIGEL*

ROSCOE F. SANFORD

ABSTRACT

The orbit of the companion of Rigel has been determined from eighteen spectrograms with a dispersion of 10 A/mm. This orbit differs little from a circle. The period is 9.860 days; the ratio of the masses of the two components, $m_2/m_1 = 0.767$; $(a_1 + a_2) \sin i = 7.771 \times 10^6$ km; and the center of mass velocity, $\gamma = +19.1$ km/sec.

No satisfactory reconciliation of the double-star observations with the spectrographic orbit seems possible at present.

The difference between the systemic velocity of the companion and the velocity of Rigel itself cannot be precisely stated but probably does not exceed 4 km/sec.

The system of Rigel is composed of star A and a companion (here called B) distant 9".5, in position angle 201°. Their visual magnitudes are 0.34 and 6.67, respectively. No certain change in relative position has been observed in one hundred years. This fact, together with the appreciable proper motion of Rigel, is considered by S. W. Burnham[1] as evidence that Rigel and companion form a physical system.

Spectrograms of B taken in 1912, 1913, and 1934–1936 at Mount Wilson (dispersion 35 A/mm at $H\gamma$) indicated a variable radial velocity, but no satisfactory period could be obtained.

The reason for this became apparent when, in 1937, spectrograms were obtained with the coudé grating-spectrograph (second order) and 32-inch Schmidt camera. The higher dispersion—10 A/mm—clearly showed that lines from the spectra of two components are present. The difficulty with the low-dispersion plates had, therefore, been that the component lines were almost always blended. Altogether, eighteen coudé spectrograms (Table 1) have been obtained, eleven of which show satisfactory lines of the components, both of which are of spectral class B9. Although fast and relatively coarse-grained plates had to be used, numerous lines of *H*, *He* I, *Mg* II, *Si* II, *C* II, and *Ca* II were measurable in the primary spectrum. The secondary spectrum, although only slightly fainter than the primary, showed fewer lines, λ 4481 being by far the best for measurement.

These velocities, when brought to one epoch with a period of 9.860 days, are about equally divided between the two phase-intervals during which component velocities can be measured and are fairly well distributed over these intervals. More velocities would, of course, be desirable, but another observing season, at least, would be required to add a significant number. It has therefore been decided to publish an orbit based on the data in Table 1.

The period of 9.860 days is considered to be substantially correct, since it satisfactorily assembles the velocities over an interval of four years or during more than one hundred and fifty orbital revolutions. The other elements of the primary have been obtained by comparing the plotted observations with typical velocity-curves. The elements e, ω, and T are not well determined because there are too few velocities, the probable errors are fairly large, and, when the velocities are near the γ-axis, the lines of the component stars blend and do not furnish separate velocities. A circular orbit may perhaps serve as well as the orbit whose elements appear in Table 2.

The velocities of Table 1 are plotted in Figure 1 together with the velocity-curve of the primary. The velocities of the two components, measured upon eleven of the spectro-

* *Contributions from the Mount Wilson Observatory, Carnegie Institution of Washington*, No. 661.

[1] *General Catalogue of Double Stars*, 2, 411, 1906.

grams, yield another determination of the systemic velocity and also the ratio of the masses of the two components. The graphical method suggested by Olin C. Wilson[2] gives

TABLE 1

VELOCITIES OF RIGEL B

PLATE	JD*	PHASE	VELOCITY (KM/SEC)	
			Prim.	Sec.
Coudé 1535	2428829.994	5d318	+ 0.4	+56.2
1804	9181.035	1.399	+29.0	
1806	81.942	2.306	+23.2	
2211	9626.733	3.397	+ 2.2	+44.3
2216	27.814	4.478	− 2.5	+48.3
2221	28.756	5.420	− 1.1	+51.3
2232	48.635	5.579	− 2.4	+55.5
2237	48.844	5.788	− 1.8	+44.1
2249	57.694	4.778	− 2.5	+55.0
2297	9713.642	1.566	+28.7	
2430	9916.011	6.735	+16.9	
2436	17.012	7.736	+27.0	
2442	18.986	9.710	+52.9	−16.9
2446	20.008	0.872	+39.3	− 3.7
2502	2430036.743	9.147	+43.0	.....
2613	244.006	9.350	+48.0	.....
2617	274.992	0.896	+37.8	− 5.3
2691	333.823	0.567	+40.9	− 8.2

* The decimal is reckoned from noon G.M.T.

TABLE 2

ELEMENTS OF RIGEL B

Period	P	9d860
Periastron passage	T	JD 2429633.196 G.M.T.
Angle of periastron	ω	10°
Eccentricity	e	0.1
Semiamplitudes of velocity variation	K_1	25.0 km/sec
	K_2	32.6 km/sec
Systemic velocity	γ	+19.1 km/sec
	$a_1 \sin i$	3.373×10^6 km
	$a_2 \sin i$	4.398×10^6 km
	$m_1 \sin^3 i$	$0.1134 \odot$
	$m_2 \sin^3 i$	$0.0837 \odot$
	$\frac{m_2}{m_1}$	0.767

$\gamma = +20.5$ km/sec and $m_2/m_1 = 0.767$. This value of γ is 1.4 km/sec larger than that in Table 2. $K_2 = 32.6$ km/sec follows from the above mass ratio and K_1 of Table 2.

The mean distance and mass functions are in Table 2. The smallest value of the distance of the centers, $a_1 + a_2$ (for $i = 90°$) is 7.771×10^6 km. There seems to be no evi-

[2] *Mt. W. Contr.*, No. 640; *Ap. J.*, **93**, 29, 1941.

dence of variability in the light of B, and hence it may be concluded that i is not close to 90°. Although the mass-luminosity relation might be assumed and i derived thereby, this is mere speculation; it would be much more to the point to be able to derive independently a value for i and thus contribute new evidence on the mass-luminosity relation.

Burnham[1] has made the following interesting comments about the companion of Rigel, which he calls BC:

> In 1889 and 1890 it [the companion of Rigel] was certainly single with the 36-inch, with the highest powers under the very best conditions. If the distance had been as much as 0".05, it would have been noticed on some of these occasions with the large refractor. At this time it seemed at least possible that the observed elongation was not real and that it was not double after all. Later the duplicity was fully confirmed by Aitken and Hussey with the 36-inch refractor at Mount Hamilton. Since that time these observers, at my special request, have examined this star at frequent intervals. The distance is probably always under 0".2 and apparently this lasts but a short time. The components are so nearly equal that the quadrants

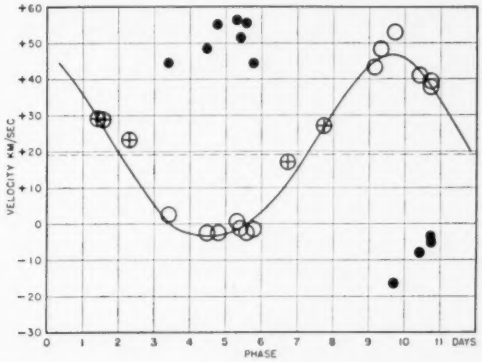

FIG. 1.—Radial velocities of the companion to Rigel (Table 1). Circles indicate the primary; dots, the secondary. The velocity-curve of the primary is that given by the elements of Table 2. The velocity of the system is shown by the broken horizontal line. Phases are reckoned from periastron.

> given by the different observers have no significance and all are subject to a correction of 180°. That this pair is in very rapid motion cannot be doubted and the period may be shorter than that of any known pair.

To this statement may be added these remarks by R. G. Aitken: "I have no hesitation in stating that the star was certainly double in 1898–99 and in 1911. The measures in January, 1903, I think are also reliable."[3] His measures range from a separation of 0".18–0".12 in 1898–1899 to 0".09–0".05 in 1903.

These observations naturally raise the question whether the visual pair and the spectroscopic binary are identical. This seems quite untenable, for a separation of the two components of the visual double even as large as 0".1 and a reasonable parallax of Rigel cannot be reconciled with the values of $a_1 \sin i$ and $a_2 \sin i$ without making i exceedingly small and, therefore, m_1 and m_2 far larger than can possibly be admitted.

Of course, it is possible to assume that Rigel's companion is triple, composed of the spectroscopic binary and another star. This, however, would require that the third star be considerably fainter than either component of the spectroscopic binary. This is contrary to the evidence of the double-star observers who have found the two visual components to be equal. Furthermore, the value of γ for the spectroscopic binary would then be expected to undergo changes as the binary and the third star revolved around

[3] *Pub. Lick Obs.*, **12**, 39, 1914.

their common center of mass. If Burnham's conclusion concerning a very short period is correct, this change in γ should manifest itself in the time covered by our observations. But neither the coudé velocities nor the earlier low-dispersion velocities show any certain variation in γ. The double-star and spectroscopic observations of Rigel's companion are still to be reconciled.

As has been stated, Burnham considered the relative fixity of A and B, together with the proper motion of A, as evidence that the stars form a physical system. It would be of interest to know how the systemic velocity of B and the velocity of A compare.

The velocity of Rigel according to the catalogue of radial velocities by J. H. Moore[4] is +23.6 km/sec—a value 4.5 km/sec larger than the systemic velocity of the companion, B. Other comparisons are afforded by twenty-two spectrograms photographed at Mount Wilson with a dispersion of 2.9 A/mm on Cramer Contrast plates. The following mean velocities have been obtained:

Lines	Km/Sec
H	+22.9
He	+20.0
Si II, *C* II, *Fe* II, *Mg* II	+17.0

The mean for *H* is in good agreement with the catalogue value. But O. Struve[5] found the absorption *Hα* line to be accompanied by emission and shifted about an angstrom to the violet. Mount Wilson observations show that the emission varies and that the absorption line *Hα* is displaced through a considerable range on various plates. Although emission has not been detected with other *H* lines, it is conceivable that their positions may be affected. Hence these lines may not furnish the true radial velocity of Rigel.

The mean for *He* rests upon measures of the wide and shallow *He* lines, which, however, are measurable with fair precision on these high-dispersion plates.

Since the lines of the ionized elements are relatively sharp, they probably yield the most reliable value for the radial velocity.

The systemic velocity of B is within 2 km/sec of the mean velocity of Rigel, whether derived from the lines of *He* or from those of the ionized elements. Thus Burnham's conclusion that A and B form a physical pair is confirmed.

CARNEGIE INSTITUTION OF WASHINGTON
MOUNT WILSON OBSERVATORY
February 1942

[4] *Pub. Lick Obs.*, **18**, 41, 1932.

[5] *Ap. J.*, **77**, 67, 226, 1933.

THE SPECTROGRAPHIC ORBIT OF 42 CAPRICORNI*

ROSCOE F. SANFORD

ABSTRACT

Twenty-nine additional velocities, together with fifty-nine already published, furnish a new set of mean elements of 42 Capricorni. Fourteen of the velocities were obtained from thirteen to eighteen years later than the velocities upon which previous sets of elements have been based.

The new elements are in good agreement with those of H. Spencer Jones. The mean residuals seem to bear out his conclusion that the velocity of the system varies, perhaps in a period as long as thirty years.

Joseph Lunt[1] has published two papers on the orbit of the spectroscopic binary 42 Capricorni (HD 206301; α 21^h 36^m.1, δ −14° 29′, Sp. G5, Mag. 5.3). In addition, H. Spencer Jones[2] has based a paper upon fifty-four observations from 1917 to 1923, sufficient

TABLE 1

RADIAL VELOCITIES OF 42 CAPRICORNI

Plate*	JD†	Velocity	Plate*	JD†	Velocity
		km/sec			km/sec
γ 6173	2421475.812	−26.0	C 6714	2427970.985	−25.1
8359	2150.985	− 5.3	6721	71.994	−15.8
8439	59.955	−14.7	V 920	72.980	−13.8
.....	2524.94	+18.7	1031	8028.827	+12.7
.....	2618.69	+10.2	1040	30.803	+16.6
γ 9644	21.637	−24.3	1102	62.802	−30.1
10288	2889.933	+ 5.9	1111	63.732	−30.8
10298	91.922	+13.2	1118	64.684	−23.7
.....	2961.72	+ 4.3	γ 21459	9182.742	−31.3
.....	98.57	+18.4	21466	83.791	−29.4
γ 10623	3006.613	−11.3	21473	84.626	−17.2
.....	08.56	+ 3.8	21508	2429205.634	+ 9.0
γ 12092	3664.826	−17.5	23471	2430157.985	−30.8
12174	96.683	+18.2	23475	58.988	−25.2
C 2498	3715.684	−24.1			

* Plate numbers refer to Mount Wilson observations. These have not been previously published. The five observations without plate number are taken from *Pub. Lick Obs.*, **16**, 316, 1928.

† The decimals are reckoned from noon G.M.T.

for an independent determination of the elements for each of the years 1917, 1920, and 1923. He concluded that there is a progressive change in the value of the systemic velocity, γ, but found no certain changes in other elements, such as were earlier suspected by Lunt. W. J. Luyten[3] rediscussed the orbit on the basis of the data in Lunt's papers and concluded that they did not prove that even the systemic velocity varies. All the observations seemed to him to be well satisfied by one set of elements.

Twenty-four velocities obtained at the Mount Wilson Observatory and five obtained at the Lick Observatory have not as yet been used in a discussion of the orbit of this

* *Contributions from the Mount Wilson Observatory, Carnegie Institution of Washington*, No. 662.

[1] *Ap. J.*, **47**, 134, 1918; *Cape Ann.*, **10**, Part 6, 3F, 1921.

[2] *Cape Ann.*, **10**, Part 8, 1928.

[3] *Pub. Obs. Univ. Minnesota*, **2**, 17, 1934.

star (see Table 1). The Lick plates were obtained in 1920–1921. Of the Mount Wilson plates, ten were obtained in 1917–1922, fourteen in 1935–1941.

The earliest and latest observations of 42 Capricorni are separated by so many orbital revolutions that the period derived from them may safely be assumed as definitive. The

TABLE 2

ELEMENTS FOR 42 CAPRICORNI

ELEMENT	SANFORD, 1917–1941			JONES, 1917–1923
	Preliminary	Corrections	Final	Mean Elements
P			$13^d.173584$	$13^d.17275$
T	JD 2422069.107	$+0^d.148$	2069.255 ± 0.244	2069.176 ± 0.085
ω	120°.5	+4°.92	175°.42 ±5°.72	172°.48 ±2°.65
e	0.17	−0.0125	0.158 ± 0.016	0.195 ± 0.008
K	24.0	−1.0	23.0 ±0.4	23.32 ±0.21 km/sec
γ	−1.5	−0.3	−1.8	−1.45 km/sec
$a_1 \sin i$			4.103×10^6	4.130×10^6 km
$m_2 \sin^3 i$ / $(m_1+m_2)^2$			$0.0159\odot$	

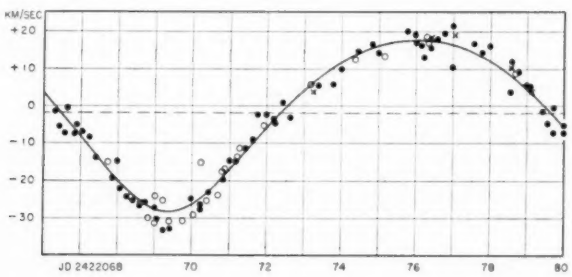

FIG. 1.—Radial velocities of 42 Capricorni. Dots, circles, and crosses represent observations from the Cape, Mount Wilson, and Lick Observatory, respectively. The curve is derived from the elements of column 4, Table 2. The broken horizontal line represents the velocity of the system. Phases are reckoned from periastron.

TABLE 3

MEAN RESIDUALS

Interval	No.	Mean Residual	Interval	No.	Mean Residual
1917–1918	23	−2.3 km/sec	1935	8	+0.4 km/sec
1919–1921	26	+0.4	1938–1941	6	−1.3
1922–1923	25	+1.7			

other five elements were approximated by Russell's method, using thirteen normal places based upon all eighty-eight velocities. Corrections were then obtained by a least-squares solution. Table 2 contains these preliminary elements, the corrections, the final elements, and Jones's mean elements.

Individual velocities are plotted in Figure 1, where the velocity-curve is defined by the elements of the fourth column in Table 2. Residuals were scaled from the figure, and these furnish the probable errors accompanying the elements. The probable error of a single velocity is ± 3.2 km/sec. The mean values of these residuals are given in Table 3 for time intervals in which the number of velocities is large enough to make such means fairly reliable.

Although the eighty-eight velocities are well distributed about the velocity-curve in Figure 1, there are several reasons for suspecting that the systemic velocity varies. First of all, the probable error obtained for a velocity of unit weight, ± 3.2 km/sec, is too high for the G5 spectrum of 42 Capricorni. In the second place, the probable errors of the elements do not seem to become less when the number of velocities and the observed interval increase. In the third place, the mean residuals in Table 3 show a progression consistent with a variation of the systemic velocity in a period of thirty years or more. Unfortunately, no observations were obtained during 1923–1935, a critical interval for a determination of the maximum positive mean residual. Observations during the next few years will be needed to confirm and evaluate the maximum negative mean residual. Nevertheless, Jones's conclusion that the systemic velocity varies is probably correct. The new elements (Table 2) are in good agreement with those of Jones, except that the eccentricity is somewhat smaller.

CARNEGIE INSTITUTION OF WASHINGTON
MOUNT WILSON OBSERVATORY
February 1942

SPECTRAL STAGES OF NOVAE

DEAN B. MCLAUGHLIN

ABSTRACT

Systems of absorption and emission lines in the spectrum of a typical nova are briefly enumerated and described. Criteria for assignment of a nova spectrum to stages of development are defined in terms of (1) emergence, maximum strength, and disappearance of each absorption system and (2) intensity ratios of certain pairs of emission bands.

Spectra of seven bright novae have been examined in detail. Dates and differences of magnitude from maximum light are tabulated for each of twenty-six spectral stages, and these are combined into a table of chronology of a typical nova spectrum. Some deviations of individual objects from the average and some differences between rapid and slow novae are discussed briefly.

INTRODUCTION

A few years ago the writer[1] published dates and magnitudes at which six bright novae passed certain stages of spectral development. That work was based mainly upon Ann Arbor spectrograms of five stars and upon what could be gleaned from the literature on Nova Pictoris. Since then, through the courtesy of the directors of several observatories, it has been the writer's privilege to examine a great number of additional spectrograms and to fill in the gaps which existed in the Ann Arbor series. In particular, a study of Lick and Yerkes plates of Nova Persei and of published reproductions of its spectrum has made it possible to add that star to the list of those which furnish a detailed record. In the course of this work it has also been possible to define several spectroscopic stages in addition to those which were listed in the earlier paper.

It is expected that a more detailed discussion of the typical nova spectrum will be published at a later date. In the following sections we give a brief summary of the absorption and emission systems and definitions of the spectroscopic stages.

ABSORPTION SYSTEMS

1. The *pre-maximum absorption* lasts from the earliest date at which any nova has been observed on the rise until at least a day or two after maximum light (longer in a few cases).

2. The *principal absorption spectrum* becomes dominant within the first few days after maximum. Its displacement is greater than that of the pre-maximum spectrum.[2] It usually resembles the spectrum of a class A or F supergiant.

3. The *diffuse enhanced absorption* is a set of very strong and diffuse lines of hydrogen and ionized metals, with a displacement roughly double that of the principal spectrum. Its lines tend to sharpen and become multiple in its later stages.

4. The *Orion absorption*, a set of strong diffuse lines of *He* I, *O* II, and *N* II (sometimes with and sometimes without hydrogen), emerges later, with a velocity sometimes nearly equal to that of the diffuse enhanced spectrum but in some cases very different from the latter.

5. The strong absorption lines *N* III 4097, 4103 belong to the Orion spectrum, but they persist after the remainder of that system has disappeared.

The sequence of events will be evident from a study of the tables of dates of appearance and disappearance of these groups of lines (Tables 2, 3, and 4).

[1] *Ap. J.*, **85**, 362, 1937.

[2] The principal and pre-maximum absorptions coexist for a time shortly after maximum.

EMISSION SYSTEMS

1. In Nova Herculis an emission spectrum was associated with the pre-maximum absorption, and in some other novae there has been evidence of a faint *pre-maximum emission.*

2. The *principal emission spectrum* appears after maximum light and is clearly associated with the principal absorption. The redward edges of its bands have displacements roughly equal and opposite to those of the lines of the principal absorption.

3. A *diffuse enhanced emission* spectrum is associated with the corresponding absorption, but it is commonly seen only in the lines of hydrogen and the strongest lines of *Fe* II, and at H and K of *Ca* II. Its redward edges have displacements about equal and opposite to those of the diffuse enhanced absorption lines.

4. *Orion emission* is associated with the Orion absorption. The bands are for the most part very vague and wide, and their centers are undisplaced.[3]

5. The diffuse "4640" *emission* and that at *N* III 4097, 4103 are part of the Orion emission spectrum, but they persist after that group as a whole has disappeared. It is especially emphasized that these lines also have members in the principal emission spectrum after the diffuse bands have disappeared.

6. The "*nebular*" *emission* spectrum is simply a continuation of the principal emission spectrum under altered physical conditions. The velocities and band structures leave no doubt on this point. The body of gas which gives rise to this set of bands eventually appears as a visible nebula expanding about the nova.

7. After the expanding nebulosity has faded, a *post-nova stellar emission* spectrum is visible on the continuous spectrum of the nuclear star. Its bright lines are much narrower than were the bands which constituted the spectrum of the expanding shell.

CRITERIA OF SPECTROSCOPIC STAGES

The first emergence, maximum strength, and disappearance of each absorption and emission system should obviously furnish a recognizable stage of development. In practice it is not possible to use the pre-maximum spectrum in this manner, but one stage is marked by its change from class B to class A. The maximum strength of *N* III absorption is poorly defined and not usable. The greatest intensity of the principal absorption follows so closely after its emergence that it is not sufficiently independent. With these exceptions, however, the absorption spectra define a number of stages.

The emergence and disappearance of the principal, diffuse enhanced, and Orion emissions are so closely bound up with the absorptions that they contribute no additional information. However, the emergence and disappearance of the "4640" band (its diffuse member in the Orion spectrum) are two usable stages.

Other criteria depend on relative intensities of lines in the principal emission spectrum. Changing conditions of excitation and density are reflected in the alteration from a set of bright lines of hydrogen, *Fe* II, and a few other elements, to a typically nebular spectrum. The following stages appear very well marked in those novae for which the record is sufficiently detailed.

1. *The "[O I] flash."*—A quick passage of the [*O* I] emissions from less conspicuous to more conspicuous than neighboring lines of *Fe* II is fairly well defined. The criteria are approximately

$$\frac{[O\,\text{I}]\ 5577}{Fe\ \text{II}\ 5534} = 1.2\ ; \qquad \frac{[O\,\text{I}]\ 6300}{Fe\ \text{II}\ 6248} = 1.6\ ; \qquad \frac{[O\,\text{I}]\ 6363}{Fe\ \text{II}\ 6248} = 1.0\ .$$

[3] The term "Orion emission" is strictly limited to these *diffuse* bands. Well-defined bands of *He* I, *O* II, *N* II, etc., with the same widths and structures as those of hydrogen, are referred to the principal spectrum.

2. *The "[N II] flash."*—A rapid increase of [*N* II] 5755 relatively to the permitted line *N* II 5680 and to the auroral [*O* I] line occurs shortly after the [*O* I] flash. The criteria are approximately

$$\frac{[N\,\text{II}]\ 5755}{N\,\text{II}\ 5680} = 1.3\ ; \qquad \frac{[N\,\text{II}]\ 5755}{[O\,\text{I}]\ 5577} = 1.8\ .$$

3. *The "helium flash."*—A rather quick replacement of the D emission lines of *Na* I by the D_3 line of *He* I is well marked. As the *He* I line increases, the *Na* I emission fades rapidly. The criterion is

$$\frac{He\ \text{I}\ 5876}{Na\ \text{I}\ 5890\text{–}5896} = 1.0\ .$$

4. In the ordinary photographic region, shortly after the helium flash, the line *C* II 4267 becomes stronger than *Fe* II 4233, and almost simultaneously *He* I 4472 surpasses *Fe* II 4515. A recognizable stage is given by the criteria

$$\frac{C\,\text{II}\ 4267}{Fe\,\text{II}\ 4233} = 1.0\ ; \qquad \frac{He\,\text{I}\ 4472}{Fe\,\text{II}\ 4515} = 1.0\ .$$

5. *Additional stages.*—These are determined by the intensities of the nebular lines of [*O* III] relative to the emissions of hydrogen and *Fe* II. Thus, each of the following criteria defines a point in the normal development:

First trace of [*O* III] 5007 ; $\qquad \dfrac{[O\,\text{III}]\ 5007}{Fe\,\text{II}\ 4924} = 1.0\ ;$

$$\frac{[O\,\text{III}]\ 4959}{Fe\,\text{II}\ 4924} = 1.0\ ; \qquad \frac{[O\,\text{III}]\ 4363}{H\gamma} = 1.0\ ;$$

$$\frac{[O\,\text{III}]\ 5007}{H\beta} = 1.0\ ; \qquad \frac{[O\,\text{III}]\ 4959}{H\beta} = 1.0\ ;$$

$$\frac{[O\,\text{III}]\ 4959}{H\beta} = 1.5\ ; \qquad \frac{[O\,\text{III}]\ 4959}{H\beta} = 2.0\ .$$

6. *Departures from uniformity.*—In the further history of the spectrum there are large departures from uniformity. Although some novae have shown the ratio [*O* III] 4959/$H\beta$ as great as 5 or even 10, others for which the record is clear do not show it exceeding 2. Indeed, Nova Pictoris never had [*O* III] lines as strong as those of hydrogen, and in its record the corresponding stages were nonexistent. The maximum relative strength and the disappearance of the [*O* III] emissions likewise occur at very different parts of the decline in different novae, though there is rough agreement for Nova Aquilae, Nova Persei, and Nova Cygni.

It is important that in every case the determination of a stage from the criteria should be based on interpolation from several observations rather than upon a single datum. Allowance must be made for oscillatory changes in the line ratios which accompany fluctuations of light.

SPECTROSCOPIC STAGES OF SEVEN BRIGHT NOVAE

Most of the stages which have been mentioned can be recognized in the spectra of the seven bright novae of this century. The writer has made a detailed examination of most of the available spectrograms of these stars, with the exception of pure duplications. Curves have been drawn for each line ratio, and the stages have been interpolated from them. For each stage two quantities may be tabulated: (1) the time interval from

TABLE 1

Nova	Light Maximum		Differences between True and Smoothed Light-Curves	
	Date	Magnitude	Early Decline	Transition
Lac 1936....	June 20.4*	+2.1	$0^m.0$	$+0^m.5$
Aql 1918....	June 10.0†	−1.1	0.0	+0.7 to −0.4
Per 1901....	Feb. 23.5†	+0.2	0.0	+0.8 to −0.8
Cyg 1920....	Aug. 24.0†	+2.0	0.0	+1.4
Gem 1912....	Mar. 14.5†	+3.5	−1.0 to +0.5	+0.4 to −0.5
Her 1934....	Dec. 22.5*	+1.4	−0.9 to +0.9	+7:(min.)
Pic 1925....	June 8*	+1.2	−1.3 to +1.1	+0.5

* U.T.
† G.M.T. (old style).

TABLE 2

DIFFERENCE OF MAGNITUDE FROM LIGHT-MAXIMUM TO EACH SPECTROSCOPIC STAGE FOR SEVEN NOVAE

Spectroscopic Stage	Nova Lac	Nova Aql	Nova Per	Nova Cyg	Nova Gem	Nova Her	Nova Pic	Adjusted Mean Δm
Change from B to A (pre-maximum absorption)	0^m6	$>1^m7$	0^m6	$>0^m6$	$>0^m6$	1^m8	$>1^m1$	1^m5:
Maximum light	0.0	0.0	0.0	0.0	0.0	0.0	0.0	0.0
Emergence of principal absorption spectrum	0.2	1.0:	0.3	0.2	1.4	0.8	0.2	0.6
Emergence of diffuse enhanced absorption	0.8	1.3	0.6	1.4	1.6	1.3	1.8	1.2
Maximum of diffuse enhanced absorption	1.6	1.7	2.0:	2.5	2.1	1.6	2.2	2.0
Emergence of Orion absorption	1.3	1.9	.....	2.2	1.7	2.3	3.0	2.1
[O I] flash	3.2	3.4	2.0:	2.7	2.1	1.6	.....	2.6
Multiple hydrogen absorption	1.9	2.3	3.6	3.5	2.4	3.0	2.3	2.7
Appearance of *N* III absorption	3.2	2.5	2.0	3.1	2.3	.....	3.4	2.7:
Maximum of Orion absorption	2.1	2.9	2.3:	2.7	2.4	3.1	3.3	2.7
Disappearance of diffuse enhanced absorption	2.5	2.9	3.0	4.1	2.6	3.1	3.1	3.0
Appearance of diffuse "4640" emission	3.2	3.4	3.5	3.2	2.2	2.4	3.3	3.0
[N II] flash	3.4	3.7	4.3:	4.3	2.5	2.2	[3.5]	3.3
Disappearance of Orion absorption	3.5	3.6	.....	3.5	2.6	3.2	3.5	3.3
Helium flash	4.0	4.0	3.6	4.3	2.6	[3.4]	.....	3.6
[O III] emission first traced	4.0	3.7	4.3:	4.5	2.7	[3.5]	3.4	3.7
λ 4267 = λ 4233; λ 4472 = λ 4515 (principal emission)	4.0	4.2	.....	4.8	2.7	[3.5]	3.4	3.8
λ 5007 = λ 4924	4.2	4.1	.....	5.1	2.7	3.6	3.8	3.9
Disappearance of principal absorption	3.9	5.0	4.1	4.8	3.2	3.2:	3.7	4.1
λ 4959 = λ 4924	4.3	5.0	4.3	5.6	3.5	[3.9]	3.9	4.4
Disappearance of *N* III absorption	4.1	5.0	.....	4.8	.....	.....	3.6	4.4:
Disappearance of diffuse "4640" emission	4.6	5.6	4.8:	5.4	5.5	3.2	3.8	4.7
λ 4363 = $H\gamma$	5.3	5.1	5.1	6.2	[3.9]	[4.0]	never	4.9
λ 5007 = $H\beta$	5.6	6.0	5.9	6.4	4.4	[4.3]	never	5.4
λ 4959 = $H\beta$	6.1	6.5	6.2	7.0	4.7	4.6	.....	5.8
λ 4959/$H\beta$ = 1.5	6.5	[7.0]	[6.8]	7.5	5.4	5.5	.....	6.4
λ 4959/$H\beta$ = 2.0	6.8	7.3	[7.1]	7.7	[5.7]	5.6	.....	6.7
λ 4959/$H\beta$ = 5	8.8	8.1	never	8.5	never	.....	.....	(8.5:)
[O III] maximum intensity	.....	9.6	10.8	8.9	6.3	.....	.....	(9.5:)
Disappearance of [O III]	.....	11.3:	11.1:	13:	8.3:	.....	.....	(11:)

maximum of light to the stage concerned and (2) the difference between the magnitudes at maximum and at the stage in question. In what follows we shall refer to these as Δt and Δm, respectively.

The determination of Δt would require no comment, were it not for the oscillatory changes of spectrum which accompany fluctuations of light. Where line ratios are concerned, smoothing of the curves has been resorted to as the only possible expedient. A joint study of the light and spectral variations has been made in each individual case.

The measurement of Δm also is rendered difficult by the irregular variations of light. Smoothed light-curves have been adopted for this purpose. Points which departed far from the smoothed curves were regarded as abnormal, and the spectrum was likewise considered abnormal at such times. By interpolation, however, it is believed that correlated smoothed spectral stages and smoothed magnitudes have been obtained. The adopted form of curve was one with continuous upward concavity, so drawn as to average the secondary fluctuations. In the transition stages, however, large deviations occurred in the direction of relative faintness of the true magnitude. Nova Herculis furnishes the most conspicuous example of such departure.

Table 1 gives dates and magnitudes of maxima and minima of the seven novae and shows the amount of deviation of the true light-curve from the smoothed one for two divisions of the decline—the "early decline" and the "transition."[4]

In Table 2 the first column contains the designation of each spectroscopic stage, and the next seven give the values of Δm for each of the seven novae. The figures in brackets are "hypothetical" values, which depend on the use of the normal sequence of stages as a function of Δm for interpolating the positions of unobserved stages between well-observed ones. In the formation of the bracketed values, at least two stages preceding and two following the stage were used wherever possible. A couple of short-range extrapolations have been made, but no *fictitious* stages have been introduced; for example, the last few stages which involve strong nebular lines were never reached by Nova Pictoris and hence the corresponding spaces in the table are blank.

The last column of Table 2 contains the "adjusted mean" value of Δm for each stage, based on all seven novae. In its formation the bracketed values have been included with full weight. In only one case does this differ from the mean of the observed values (bracketed figures omitted) by more than $0^m.2$.

The last three lines of the table, which are set apart from the rest, give data for the discordant late stages of the spectrum. They are included for completeness of the record and have not been used in any way which would influence the other results.

Table 3 gives in similar form the values of Δt in days after maximum light for all the stages of the seven novae. The figures in brackets are the intervals corresponding to the bracketed values of Δm in Table 2. At the foot of each column is given the time required to decline through 3.0 mag. from maximum, as measured on the smoothed light-curve. This interval is adopted as a unit for the time scale of each nova.

The last column of Table 3 contains the "mean relative Δt" based on all seven novae. It is the logarithmic mean of the seven values of Δt when expressed in terms of the unit just defined, the time required to decline through 3.0 mag.

CHRONOLOGY OF A TYPICAL NOVA

When the logarithm of "mean relative Δt" from Table 3 is plotted against the mean Δm from Table 2, all the points after light-maximum, with the exception of the first two, lie very close to a straight line. This line was used to form smoothed values of Δt, simply by reading off the logarithm corresponding to the mean Δm. Table 4 is the resulting chronology of a typical nova. The spectroscopic stage is named in the first column, Δm is given in the second, and the smoothed relative Δt (in units of the interval for a

[4] These terms are defined in the writer's study of light-curves of novae (*Pop. Astr.*, **47**, 418, 1939).

TABLE 3

TIME INTERVAL IN DAYS FROM LIGHT-MAXIMUM TO EACH SPECTROSCOPIC STAGE FOR SEVEN NOVAE

Spectroscopic Stage	Nova Lac	Nova Aql	Nova Per	Nova Cyg	Nova Gem	Nova Her	Nova Pic	Mean Relative Δt
Change from B to A	− 1^{d}0	−(>1^{d}2)	− 0^{d}9	−(>1^{d}3)	− (>1^{d}5)	− 8^{d}5	−(>14^d)	− 0.1
Maximum light	0.0	0.0	0.0	0.0	0.0	0.0	0	0.0
Emergence of principal absorption	+ 0.4	+ 0.2	+ 0.7	+ 1.	+ 3.5	+ 2.5	+ 2	+ 0.04
Emergence of diffuse enhanced absorption	+ 1.4	+ 0.5	+ 1.5	+ 4.5	+ 4.5	+ 13.5	+ 50	+ 0.16
Maximum of diffuse enhanced absorption	+ 3.3	+ 2.0	+ 7:	+ 10.5	+ 10	+ 32	+ 78	+ 0.42
Emergence of Orion absorption	+ 2.6	+ 2.6	.....	+ 8	+ 6.5	+ 70	+ 150	+ 0.46
[*O* I] flash	+ 10:	+ 10	+ 7:	+ 13	+ 10.5	+ 31	.....	+ 0.7
Multiple hydrogen absorption	+ 4:	+ 4.6	+ 20	+ 21	+ 16	+ 93	+ 87	+ 0.8
Appearance of *N* III absorption	+ 10.6	+ 5:	+ 7	+ 16	+ 15	.....	+ 193	+ 0.8
Maximum of Orion absorption	+ 4.8	+ 6	+ 9	+ 13	+ 16	+ 96	+ 178	+ 0.8
Disappearance of diffuse enhanced absorption	+ 6.3	+ 6	+ 13	+ 28	+ 22	+ 96	+ 157	+ 1.0
Appearance of diffuse "4640" emission	+ 10:	+ 9	+ 18	+ 17	+ 11.5	+ 77	+ 179	+ 1.0
[*N* II] flash	+ 13:	+ 12	+ 36	+ 32	+ 19	+ 64	+[215]	+ 1.35
Disappearance of Orion absorption	+ 15:	+ 11	.....	+ 21	+ 22	+ 103	+ 224	+ 1.25
Helium flash	+ 20	+ 14	+ 20:	+ 32	+ 22	+[113]	.....	+ 1.5
[*O* III] emission first traced	+ 20	+ 12	+ 33	+ 35	+ 23	+[118]	+ 247	+ 1.6
λ 4267 = λ 4233; λ 4472 = λ 4515	+ 20:	+ 16	.....	+ 40	+ 23	+[118]	+ 195	+ 1.6
λ 5007 = λ 4924	+ 25	+ 15	.....	+ 45	+ 23	+ 123	+ 266	+ 1.7
Disappearance of principal absorption	+ 18	+ 38	+ 30	+ 41	+ 39	+ 103	+ 252	+ 2.0
λ 4959 = λ 4924	+ 30:	+ 37	+ 36:	+ 57	+ 51	+[141]	+ 285	+ 2.6
Disappearance of *N* III absorption	+ 23	+ 38	.....	+ 40	.....	.....	+ 236	+ 2.8
Disappearance of diffuse "4640" emission	+ 42	+ 68	+ 54:	+ 50:	+ 271	+ 103	+ 267	+ 3.7
λ 4363 = *Hγ*	+ 51	+ 40	+ 67	+ 80	+[65]	+[147]	never	+ 3.7
λ 5007 = *Hβ*	+ 59	+ 92	+ 128	+ 89	+ 200	+[166]	never	+ 6.2
λ 4959 = *Hβ*	+ 92	+ 163	+ 189	+ 161	+ 307	+ 197	.....	+ 9
λ 4959/*Hβ* = 1.5	+107:	+[230]	+[300]	+ 250	+ 408	+ 324	.....	+ 14
λ 4959/*Hβ* = 2.0	+134:	+ 263	+[330]	+ 342	.....	+ 410:	.....	+ 17
λ 4959/*Hβ* = 5	+420	+ 450	never	+ 750	never	.....	.....	+(50:)*
[*O* III] maximum intensity	.....	+ 750	+ 900	+1000:	+ 540	.....	.....	+(70:)*
Disappearance of [*O* III] emission	.....	+ 2000	+ 1600	+5300:	+ 1050	.....	.....	+(200:)*
3.0 mag. below maximum	+ 8.5	+ 7.0	+ 13	+ 15	+ 35	+ 93	+ 150	+ 1.00

* The last three values of "mean relative Δt" are merely intended to indicate the order of magnitude of the time interval. Individual novae differ widely in these last stages.

3.0-mag. decline) in the third. Considering the very large amount of observational material that has been incorporated in this study, it seems unlikely that any appreciable revision of this table will be possible until additional data are supplied by *future* novae.

Table 4 gives not only the spectroscopic history but the typical light-curve as well. A plot of Δm against Δt gives a smooth curve which may be regarded as the typical form for a nonfluctuating nova. The individual characteristics of the seven light-curves have been averaged out.[5]

TABLE 4

CHRONOLOGY OF A TYPICAL NOVA

Spectroscopic Stage	Mean Δm	Smoothed Relative Δt
	0	
Change from B to A (pre-maximum absorption)	(1^m.5)	(− 0.1)
Maximum light	0.0	0.0
Emergence of principal absorption spectrum	0.6	+ 0.04
Emergence of diffuse enhanced absorption	1.2	+ 0.16
Maximum of diffuse enhanced absorption	2.0	+ 0.42
Emergence of Orion absorption	2.1	+ 0.46
[*O* I] flash	2.6	+ 0.7
Multiple hydrogen absorption	2.7	+ 0.8
Appearance of *N* III absorption	2.7:	+ 0.8
Maximum of Orion absorption	2.7	+ 0.8
Disappearance of diffuse enhanced absorption	3.0	+ 1.0
Appearance of diffuse "4640" emission	3.0	+ 1.0
[*N* II] flash	3.3	+ 1.25
Disappearance of Orion absorption	3.3	+ 1.25
Helium flash	3.6	+ 1.5
[*O* III] first traced	3.7	+ 1.6
λ 4267 = λ 4233; λ 4472 = λ 4515	3.8	+ 1.7
λ 5007 = λ 4924	3.9	+ 1.9
Disappearance of principal absorption	4.1	+ 2.2
λ4959 = λ 4924	4.4	+ 2.7
Disappearance of *N* III absorption	4.4:	+ 2.7
Disappearance of diffuse "4640" emission	4.7	+ 3.5
λ 4363 = $H\gamma$	4.9	+ 4.2
λ 5007 = $H\beta$	5.4	+ 6.2
λ 4959 = $H\beta$	5.8	+ 9
λ 4959/$H\beta$ = 1.5	6.4	+ 14
λ 4959/$H\beta$ = 2.0	6.7	+ 17
λ 4959/$H\beta$ = 5	(8.5:)*	+(50:)*
[*O* III] maximum intensity	(9.5:)*	+ 70:)*
Disappearance of [*O* III] emission	(11:)*	+(200:)*

* The last three entries are merely intended to give a rough indication of the difference of magnitude and the time interval from maximum for these stages. Individual novae are extremely discordant in these final stages.

DISCUSSION

Inspection of Tables 2 and 3 will show that no individual nova conforms precisely to the average pattern. We therefore investigate briefly the deviations of individuals from the average. In Figure 1 the data are plotted for the four most rapid of the seven stars: Nova Lacertae, Nova Aquilae, Nova Persei, and Nova Cygni. The four plots in the upper half of the figure have the mean log Δt as abscissa and log Δt of the individual nova

[5] In an earlier tabulation (McLaughlin, *op. cit.*, p. 367) the values of Δt were expressed in days, corresponding to Δm on the light-curve of Nova Lacertae 1936. The present tabulation is free from the objection of dependence upon the light-curve of a single object.

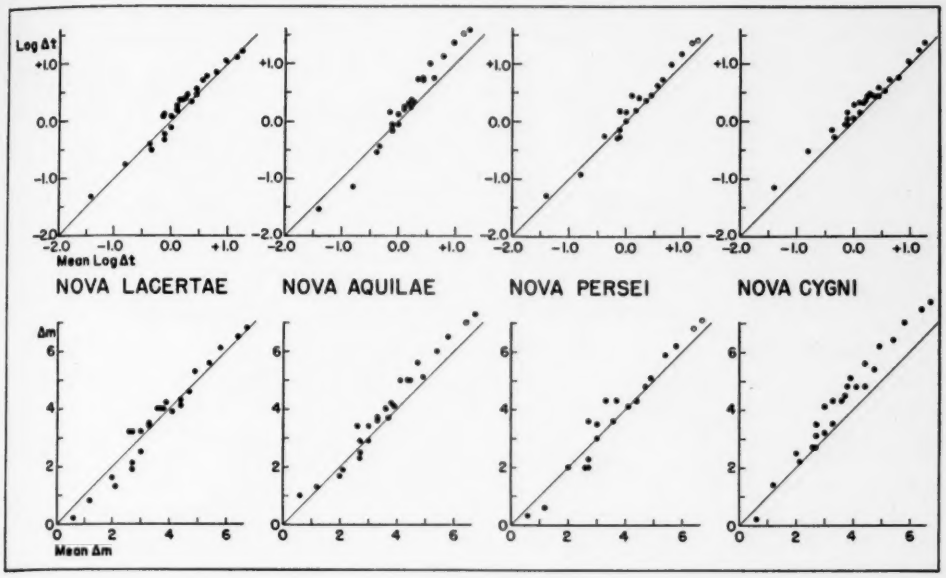

FIG. 1.—Individual comparisons of four rapid novae with the average spectroscopic behavior of seven novae. *Upper row:* Logarithms of relative time intervals from maximum to each spectral stage (unit is time required to decline 3.0 mag. from maximum). *Lower row:* Differences of magnitude from maximum at each stage. In each plot, the abscissa refers to the mean of seven novae; the ordinate refers to the individual object.

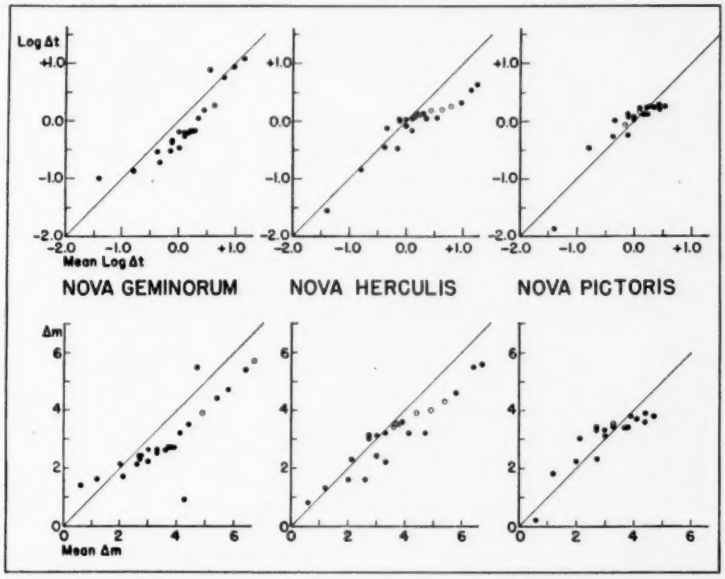

FIG. 2.—Individual comparisons of Nova Geminorum and two slow novae with the average spectroscopic behavior of seven objects. Arrangement of plots is similar to that of Fig. 1.

as ordinate. The four lower diagrams show the relations of Δm in the same form. Figure 2 is arranged in the same way for the other three novae, which declined more slowly.

Although some of the deviations are conspicuous, they are mainly systematic, and actual scatter is not great. The largest systematic differences in Δm are just $1^m.0$ in opposite directions for Nova Cygni and Nova Geminorum. The former would have departed even farther if the observed light-curve, instead of a smoothed one, had been used.

The departures of log Δt for the most part exhibit the same general form as those of Δm. Nova Cygni is an exception; in spite of the large deviation of Δm for the later stages, the values of log Δt lie almost on the 45° line. This is true also of Nova Geminorum. The differences in log Δt show that Nova Aquilae took 2.5 times as long to reach the later stages as one might have expected from the rapidity of its decline through the first 3 mag., while Nova Herculis took only one-fourth as long as expected. These are extreme cases; in general the accordance is much closer.

Another relation that can be seen in these diagrams is the relative rapidity of development in the later stages of the two slowly changing stars, Nova Herculis and Nova Pictoris. Both reached their later stages at a brighter magnitude than the average, and Nova Geminorum showed similar behavior. Likewise, the spectra of the two slow novae changed more rapidly in their later stages, as compared with their earlier ones.[6]

Finally, we mention another marked difference between rapid and slow novae. The two slow ones had strong forbidden lines of *Fe* II in the "transition" stage. These have never been found in rapid novae. The [*Fe* II] emissions also appeared in great strength in the slowly changing star DO Aquilae, in the still slower RT Serpentis, and in the very slow nova-like object η Carinae, in whose spectrum they are still strong. Apparently they are typical of the spectra of slow novae but are somehow inhibited by the physical conditions in the rapidly changing objects. On the other hand, a common feature of the spectra of rapid novae is poorly developed in the slow ones. The well-known absorption lines *N* III 4097, 4103 were not recorded at all in Nova Herculis and were very weak in Nova Pictoris. They were occasionally present in Nova Geminorum, but they had no continuous existence in great strength.

From the foregoing remarks it will be evident that Nova Geminorum had some of the characteristics of a slow nova, although its rate of decline was within the range of the rapid ones. Another point of difference between Nova Geminorum and other fast novae was the irregular nature of its early decline, which is strongly suggestive of the secondary maxima of Nova Pictoris.

The author is greatly indebted to the directors of several observatories for placing spectrograms at his disposal. Dr. Walter S. Adams, director of the Mount Wilson Observatory, and Dr. W. H. Wright, director of the Lick Observatory, made available a large number of spectrograms of many novae, both bright and faint. Dr. Otto Struve, director of the Yerkes Observatory, kindly loaned series of spectrograms of Nova Geminorum and Nova Persei. Other excellent series of Nova Geminorum were loaned by Dr. V. M. Slipher, director of the Lowell Observatory, and by the late Dr. F. C. Jordan, director of the Allegheny Observatory. To all of these the writer records his sincere thanks. The investigation was materially aided by a grant from the research funds of the Horace H. Rackham School of Graduate Studies of the University of Michigan, which is gratefully acknowledged.

THE OBSERVATORY
UNIVERSITY OF MICHIGAN
February 1942

[6] In this respect Nova Geminorum appears to differ from the two slow novae, but this may arise from the fact that the later criteria depend on [*O* III], which was weaker in Nova Geminorum than in Nova Herculis. It was still weaker in Nova Pictoris, so that no corresponding points appear in Fig. 2.

A REMARK ON METEORS

THEODORE E. STERNE[1]

ABSTRACT

Shock waves must play an important physical part when meteors traverse the earth's atmosphere. Preliminary estimates of 2,000,000° for the highest temperature reached in a meteor moving at 60 km/sec through air initially at 180° absolute and of 70,000° after the air's subsequent expansion are excessive because of the lowering by dissociation and ionization of the effective ratio of specific heats. The actual temperatures, however, that arise from the shock wave must be very high.

A projectile moving through air is accompanied by a "shock wave" whenever the velocity of the projectile exceeds the speed of sound. Such shock waves have been photographed many times[2] under experimental conditions and must accompany all meteors with their much higher velocities.

Shock waves, associated with projectiles, have the following characteristics. They move through the undisturbed air with velocities in excess of the speed of sound; they involve discontinuities (or near-discontinuities) in the pressure, density, and temperature; and they are associated with a degradation of energy such that if, after their passage, the air is allowed to expand adiabatically to its undisturbed pressure, then the resulting density will be lower and the resulting temperature higher than the undisturbed density and temperature. The velocity of the shock wave, measured in the direction of motion of the projectile, is, in general, equal to that of the projectile. The air behind the shock wave has a component of velocity normal to the wave surface and relative to the undisturbed air in front of it, whose amount can be computed from the conservation of mass. The changes in density, pressure, and temperature, while not strictly discontinuous, occur in so short a distance (probably some microns at most) that for practical purposes they can be regarded as discontinuous; and the change in the state of the air upon passage of the shock wave is not adiabatic and involves a greater rise in temperature than would occur for an adiabatic transition from the initial to the subsequent pressure. The maintenance of the shock wave requires the projectile to lose kinetic energy, which accounts for much of the resistance to its motion; and the details of the loss of kinetic energy involve the high pressure between the shock wave and the projectile.

Such are some of the main features of shock waves of the type which accompany projectiles with supersonic velocities. For the modern hydrodynamical theory, and for further details, the reader is referred to Lord Rayleigh,[3] who gave approximate formulae for a flat-headed projectile accompanied by a plane shock wave, and to Taylor and Maccoll[4] and Maccoll,[5] who solved exactly the equations applicable to a moving cone—the first three-dimensional problem to yield a rigorous solution. The experiments which the latter authors performed were in good agreement with their theory. Both the Rayleigh and the Taylor-Maccoll treatments lead to pressures and temperatures of the same order of magnitude.

[1] Captain, Ordnance Department, U.S.A.

[2] See, for instance, n. 5.

[3] *Scientific Papers*, **5**, § 346, p. 573, Cambridge University Press, 1912.

[4] *Proc. R. Soc.*, **139**, 278, 1932.

[5] *Proc. R. Soc.*, **159**, 459, 1937.

The shock wave accompanying a meteor need not touch the meteorite itself, for the meteorite is probably surrounded by an envelope of liberated gas. Presumably, the effect of this gas is to increase the size of the "projectile," and the latter, consisting of the meteorite with its surrounding layer of liberated gas, is probably very nearly touched by the shock wave at its most forward point. The behavior[5] of experimental projectiles suggests that behind the meteor, sufficiently far away, the shock wave must approximate to a cone.

One can estimate the pressure and temperature reached by the compressed air, behind the shock wave, at the air's stagnation point just in front of a flat-headed projectile, from the equations given by Rayleigh.[3] Denote by P_0, ρ_0, T_0, and U the pressure, density, and absolute temperature in front of the shock wave and the velocity of the shock wave in the direction of motion. Denote by P_1, ρ_1, T_1, the pressure, density, and temperature just behind the shock wave and by γ the ratio of specific heats of the air. Denote by P_s, ρ_s, T_s, the pressure, density, and temperature at the stagnation point; and by a the velocity of sound in the undisturbed air. Then, from Rayleigh's equations,[6] it follows that, when $U > a$,

$$\frac{\rho_0}{\rho_1} = \frac{\gamma - 1}{\gamma + 1} + \frac{2}{\gamma + 1}\frac{a^2}{U^2}, \tag{1}$$

while

$$\frac{\rho_s}{\rho_1} = \left(\frac{P_s}{P_1}\right)^{1/\gamma}, \tag{2}$$

since the further compression between the shock wave and the stagnation point is adiabatic. Hence

$$\begin{aligned}\frac{T_s}{T_0} &= \frac{P_s}{P_0}\frac{\rho_0}{\rho_1}\left(\frac{P_1}{P_s}\right)^{1/\gamma} \\ &= \left(\frac{P_s}{P_1}\right)^{(\gamma-1)/\gamma}\frac{P_1}{P_0}\frac{\rho_0}{\rho_1} \\ &= \left[\frac{(\gamma+1)^2}{4\gamma}\frac{P_1}{P_0} + \frac{\gamma^2 - 1}{4\gamma}\right]\frac{\rho_0}{\rho_1}\end{aligned} \tag{3}$$

from Rayleigh's formulae. Using the equation

$$\frac{P_1}{P_0} = \frac{2\gamma}{\gamma + 1}\frac{U^2}{a^2} - \frac{\gamma - 1}{\gamma + 1} \tag{4}$$

(Rayleigh's equation 135) and equations (1) and (3), one finds finally that

$$\frac{T_s}{T_0} = \frac{\gamma - 1}{2}\frac{U^2}{a^2} + 1. \tag{5}$$

T_s is the highest temperature reached in front of the meteor. After the meteor's passage, the air expands adiabatically to the undisturbed pressure P_0 and cools to the temperature T at density ρ. Hence

$$\frac{\rho}{\rho_1} = \left(\frac{P_0}{P_1}\right)^{1/\gamma}$$

[6] *Op. cit.*, p. 608.

or

$$\frac{\rho}{\rho_0} = \frac{\rho_1}{\rho_0}\left(\frac{P_0}{P_1}\right)^{1/\gamma},$$

and hence

$$\frac{T}{T_0} = \frac{\rho_0}{\rho_1}\left(\frac{P_1}{P_0}\right)^{1/\gamma}$$

$$= \left(\frac{\gamma-1}{\gamma+1} + \frac{2}{\gamma+1}\frac{a^2}{U^2}\right)\left(\frac{2\gamma}{\gamma+1}\frac{U^2}{a^2} - \frac{\gamma-1}{\gamma+1}\right)^{1/\gamma} \qquad (6)$$

by (1) and (4).

The speed of sound, a, depends only on the undisturbed temperature of the air and upon γ: $a^2 = \gamma P_0/\rho_0$, or $a^2 = \text{const.} \times \gamma T_0$. Taking $\gamma = 1.405$, $T_0 = 180°$ K, and[7] $a = 2.7 \times 10^4$ cm/sec, one finds the following values from equations (5) and (6):

U (km/sec)	T_s (°K)	T (°K)
1	680	290
20	2×10^5	1.5×10^4
60	1.8×10^6	7.4×10^4

I have computed from the exact theory of Taylor and Maccoll what T_s (the temperature at the cone's surface) would be for a conical projectile of semi-apical angle 55° moving at 60 km/sec through air at $T_0 = 180°$ K with $\gamma = 1.405$. I have obtained the temperature 1.5×10^6 degrees K, in substantial agreement with the corresponding temperature yielded by Rayleigh's approximate theory.

Mention should be made here of the work of Epstein,[8] who generalized an exact result obtained by Meyer[9] for the two-dimensional problem of a long wedge moving at right angles to its axis, so as to render it applicable to a long prism moving perpendicularly to its axis. Epstein's formulae yield pressures and temperatures[10] of the same orders of magnitude as those yielded by the Rayleigh and Taylor-Maccoll treatments. Using Epstein's formula (16), for a wedge of semi-angle 45°, with T_0 equal to 180° K as before and with $U = 20$ km/sec, I find for the temperature just behind the shock wave the value 1.6×10^5 degrees K—again in substantial agreement with the value 2×10^5 yielded by the simple Rayleigh treatment.

The preceding estimates of T_s and T cannot be taken at their face values as the temperatures at the stagnation point and in the train after the meteor's passage, respectively. Ionization and dissociation must lower the value of γ and therefore the values of the

[7] This value of T_0 corresponds to a height of 80 km (see F. W. Whipple, *Proc. Amer. Acad. Sci.*, **79**, 499, 1938).

[8] *Proc. Nat. Acad Sci.*, **17**, 532, 1931.

[9] *Mitt. Forscharb. Ingenieurw. V.D.I*, No. 62, 1908.

[10] The temperatures are computed by me from Epstein's formula (16). Epstein himself gives very much lower values for the temperatures computed, according to his own statement on page 544, from the same formula. For example, for a velocity of 19 km/sec Epstein gives a temperature of but 15,600° C; whereas I find from his formula (16), which I have verified, the value 150,000° K when I use his γ and the values $T_0 = 300°$ K, $\omega = 45°$. Unable to duplicate his small values, I am forced to conclude that Epstein must have made a numerical mistake. Epstein does not appear to have been aware of the work of Rankine, Hugoniot, and Rayleigh. The "law" expressed by Epstein's equation (15) was obtained long before by Rankine (*Phil. Trans.*, **160**, 277, 1870. See n. 1, p. 590, eq. 69), was rediscovered by Hugoniot (*Ec. Polyt., Paris*, **57–59**, 1, 1887–1889), and does not express a law so much as a shock-wave condition.

temperature that will actually be reached. Nevertheless, these crude estimates are so enormous as strongly to indicate that the actual temperatures, during and after the meteor's passage, must still be very high.

It is believed that shock waves accompany meteors, that they must play essential physical parts in the associated phenomena, and that any correct treatment of the passage of meteors through the atmosphere must take shock waves into consideration. Here I have merely sketched one particular aspect of the whole problem in a very preliminary way. The problem deserves more extensive and more detailed analysis, which I regret that circumstances prevent me from carrying out. I hope that others may develop the physical consequences further.

It is a pleasure to express my indebtedness to Mr. R. H. Kent, Aberdeen Proving Ground, who pointed out to me that shock waves must be considered in the treatment of meteors, who supplied me with references, and who persuaded me to carry out this preliminary study.

BALLISTIC RESEARCH LABORATORY
ABERDEEN PROVING GROUND, MARYLAND
January 12, 1942

NOTE ADDED IN PROOF

I have just received from Dr. Struve a copy of the *Journal des observateurs*, Vol. **24**, No. 10, October, 1941, containing a very interesting paper by Henri Muraour on the role of shock waves in meteors and other natural phenomena. Muraour computes the temperature just behind the shock wave, ignoring the further compression between the shock wave and the projectile. Despite this cruder treatment, his T_2 agrees as to order of magnitude with the author's T_s under similar conditions. Muraour's Table A is based on an undisturbed temperature of 273° K. He further suggests that there may be shock waves in the sun.

April 12, 1942

ON STELLAR ROTATION

MARTIN SCHWARZSCHILD

ABSTRACT

In section I the general problem of stellar rotation is discussed, and a special formulation, taking account of the viscous forces in a restricted form, is given. The corresponding equations are set down in section II, and the first-order perturbation method for their solution is discussed in section III. For the special case of the standard model in slow rotation the equations are given in section IV and solved in sections V and VI. The solution is found to be unique and to correspond to a solid-body rotation.

I. INTRODUCTION

The problem of stellar rotation might be formulated as follows: To find the equilibrium state of a star which possesses a nonvanishing total angular momentum. As a first trial for the solution of this problem one might assume that because of the viscosity of the material in the star no differential motion exists and, therefore, that the star rotates like a solid body. Von Zeipel[1] has shown that the equilibrium state of a rotating star in radiative equilibrium can correspond to a strict solid-body rotation only in the case where the energy sources of the star fulfil a certain condition. Since the actual energy sources of stars are not likely to fulfil this special condition, one cannot expect stars to rotate strictly like solid bodies.

As a second trial for the solution of the problem of stellar rotation one might neglect the viscous forces altogether and correspondingly permit differential rotational motion. The angular velocity W at a given point in the star may then be taken to be a function $W(z, s)$ depending both on the distance from the equatorial plane z and on the distance from the axis s. Rosseland[2] has shown that the equilibrium equations for a star do not determine $W(z, s)$ uniquely but that one may choose, for example, the angular velocity in the equatorial plane $W(0, s)$ as a function of s at will; the equilibrium equations can then be fulfilled by choosing $W(z, s)$ appropriate for the rest of the star.

As a third trial to find a unique solution of the problem of stellar rotation one might consider the viscous forces arising from differential rotational motion throughout the star. These forces produce large-scale meridional convection currents. Assuming that large-scale convection currents can exist in a permanent state of a star only if they are stationary, the problem would be to find a dependence of the rotational velocity $W(z, s)$ on z and s which not only satisfies the normal equilibrium equations but in addition gives rise to such viscous forces as to produce convection currents which are stationary. Randers[3] has shown that a $W(z, s)$ satisfying these conditions does not exist, except perhaps under special circumstances not likely to prevail for stars in general.

As a fourth trial to find a unique solution of the problem of stellar rotation one might consider the viscous forces in a restricted form. A star like the sun may be taken as consisting of three zones: the convective core, the main part of the star in radiative equilibrium, and the hydrogen convection zone. In the core the turbulence produces adiabatic equilibrium for which von Zeipel's theorem does not hold; indeed, a solid-body rotation is a possible and (because of the high turbulent viscosity) the most likely solution for the

[1] *Festschrift für H. von Seeliger*, p. 144, 1924.

[2] *Astroph. Norvegica*, **2**, 173, 1936, and 249, 1937.

[3] *Ap. J.*, **94**, 122, 1941.

convection core. In the nonturbulent main part of the star the viscous forces are so small that it seems justifiable to neglect them altogether.[4] In the hydrogen convection zone (because of the low temperature) the turbulence is not sufficiently effective to disturb the radiative equilibrium; hence von Zeipel's theorem applies and strict solid-body rotation is not a possible solution for this zone. On the other hand, if differential rotational motions exist, the turbulence will produce appreciable viscous forces; these forces will appear in two forms: (1) forces at the surfaces of the star and (2) differential stresses throughout the hydrogen convection zone. It is possible to eliminate the viscous surface forces by introducing a special surface condition for $W(z, s)$ (the introduction of this surface condition should have the consequence of removing the indeterminateness in the solution for $W[z, s]$, which is encountered if the viscous forces are neglected altogether). It does not seem possible in general to eliminate the differential stresses throughout the hydrogen convection zone; but even if these stresses should produce nonstationary currents, one might expect the consequent disturbances not to be too serious, because of the shallowness of the hydrogen convection zone.

The fourth trial to find a unique solution of the problem of stellar rotation, therefore, consists of the derivation of a dependence of the rotational velocity $W(z, s)$ on z and s, which, on the one hand, is a solution of the equilibrium equations for a rotating star, neglecting the viscous forces, and which, on the other hand, takes account of the viscous forces in a restricted form in that it gives a solid-body rotation to the convective core and that it fulfils the surface condition corresponding to a vanishing viscous surface force. It is the aim of this paper to set down the equations for this fourth trial and to derive the solution for the special case of the standard model.

The above formulation of the fourth trial for the solution of the problem of stellar rotation was instigated by most clarifying discussions with Randers at the Yerkes Observatory.

II. FUNDAMENTAL EQUATIONS

The symbols used will be P for the pressure, T the temperature, ρ the density, Φ the gravitational potential, F the radiation flux per unit area, W the angular velocity, s the distance from the axis of rotation, G the constant of gravitation, k Boltzmann's constant, m the mean molecular weight, κ the absorption coefficient per gram, and ϵ the energy production per gram.

The equilibrium equations for a rotating star, neglecting viscous forces, are as follows:

Law of motion
$$W^2 \vec{s} = \frac{1}{\rho} \operatorname{grad} P + \operatorname{grad} \Phi , \tag{1}$$

Poisson equation
$$\nabla^2 \Phi = 4\pi G\rho , \tag{2}$$

Radiation transfer
$$\operatorname{grad} T = -\frac{3\kappa\rho}{4acT^3} \vec{F} , \tag{3}$$

Conservation of energy
$$\operatorname{div} \vec{F} = \epsilon\rho . \tag{4}$$

Equation of state
$$P = \frac{k}{m} \rho T . \tag{5}$$

[4] *Ibid.*, p. 119.

In the last equation the radiation pressure has been neglected. In the convective core, equations (3) and (4) have to be replaced by the adiabatic relation. In addition to the above equations the usual surface condition has to be fulfilled:

$$T = 0 \quad \text{at the surface } (\rho = 0) . \tag{6}$$

To take account of the viscous forces in the restricted form discussed in the introduction, two further conditions have to be fulfilled by the solution. First, the rotation in the convective core should correspond to a solid-body rotation. Hence,

$$W = \text{constant in the convective core} . \tag{7}$$

Second, the viscous surface force should vanish. This can be secured by letting the normal component of the gradient of the angular velocity vanish at the surface.[5] Hence,

$$(\text{grad } W)_{\text{normal}} = 0 \qquad \text{at the surface} . \tag{8}$$

Equations (1)–(8) represent the mathematical formulation of the problem stated at the end of the introduction.

In preparation for the solution of the above equations, a co-ordinate system has to be chosen, and the equations have to be transformed to these co-ordinates. Introducing as independent variables the distance from the center r and the sin of the latitude μ (the longitude as the third independent variable does not appear explicitly because of the rotational symmetry of the problem), one obtains for the differential equations (1)–(4):

$$+W^2 r (1-\mu^2) = +\frac{1}{\rho}\frac{\partial P}{\partial r} + \frac{\partial \Phi}{\partial r} , \tag{9}$$

$$-W^2 r^2 = +\frac{1}{\rho}\frac{1}{\mu}\frac{\partial P}{\partial \mu} + \frac{1}{\mu}\frac{\partial \Phi}{\partial \mu} , \tag{10}$$

$$\frac{\partial^2 \Phi}{\partial r^2} + \frac{2}{r}\frac{\partial \Phi}{\partial r} + \frac{1}{r^2}\frac{\partial}{\partial \mu}\left[(1-\mu^2)\frac{\partial \Phi}{\partial \mu}\right] = +4\pi G\rho , \tag{11}$$

$$\frac{\partial T}{\partial r} = -\frac{3\kappa\rho}{4acT^3} F_r , \tag{12}$$

$$\frac{\partial T}{\partial \mu}\frac{\sqrt{1-\mu^2}}{r} = -\frac{3\kappa\rho}{4acT^3} F_\mu , \tag{13}$$

$$\frac{\partial F_r}{\partial r} + \frac{2}{r}F_r + \frac{1}{r}\frac{\partial}{\partial \mu}\left(\sqrt{1-\mu^2}\, F_\mu\right) = +\epsilon\rho . \tag{14}$$

Here, F_r and F_μ are the radial and the latitudinal components of the radiation flux.

Another form of the law of motion is obtained by introducing the distance from the center r and the distance from the axis s as independent variables:

$$0 = +\frac{1}{\rho}\frac{\partial P}{\partial r} + \frac{\partial \Phi}{\partial r} , \tag{15}$$

$$+W^2 s = +\frac{1}{\rho}\frac{\partial P}{\partial s} + \frac{\partial \Phi}{\partial s} . \tag{16}$$

Equations (15) and (16) may be used instead of equations (9) and (10).

[5] *Ibid.*, p. 115.

III. APPROXIMATION FOR SLOW ROTATION

A strict solution of the problem set down in the previous paragraph seems mathematically difficult. An appreciable simplification is obtained by using the first-order perturbation method, previously applied to rotating polytropes by Chandrasekhar.[6] The method consists of comparing a rotating star with a nonrotating star by setting

$$\left.\begin{aligned} P &= P_u + P_d\,, & \Phi &= \Phi_u + \Phi_d\,, & & \\ \rho &= \rho_u + \rho_d\,, & F_r &= F_{ru} + F_{rd}\,, & W^2 &= V_d\,, \\ T &= T_u + T_d\,, & F_\mu &= F_{\mu d}\,, & & \end{aligned}\right\} \tag{17}$$

where the quantities without indices refer to the rotating star, the quantities with the index u refer to the nonrotating star, and the quantities with the index d are the perturbations. The mathematical simplification is obtained by considering the rotation to be so slow as to produce only small perturbations, so that terms of second or higher order in these perturbations may be neglected.

A discussion justifying the neglect of the terms of second and higher order even at the surface is given in appendix A.

To derive an estimate of the maximum velocity of rotation for which the first-order perturbation method may still yield results of sufficient accuracy, one might compare the centripetal acceleration produced by the rotation at the equator with the gravitational acceleration. If at the equator the angular velocity is W_e and the linear velocity of rotation is v_e and if the mass of the star is M and its radius is R, one gets for the ratio of centripetal acceleration to gravitational acceleration

$$w = \frac{W_e^2 R}{\dfrac{GM}{R^2}} = \frac{W_e^2 R^3}{GM} = \frac{3}{4}\,\frac{W_e^2}{\pi G\bar{\rho}} = \frac{v_e^2 R}{GM}\,. \tag{18}$$

For the sun with $v_e = 2$km/sec one finds $w = 2\cdot 10^{-5}$; for an early-type, main-sequence star (like μ_1 Scorpii) with $v_e = 100$ km/sec, one would find $w = 2\cdot 10^{-2}$. Hence, one should expect the results obtained with the first-order perturbation method to be exceedingly accurate for the sun and to be sufficiently accurate even for moderately fast rotating B stars, as long as the equatorial velocity of rotation does not exceed 100 km/sec.

IV. THE PERTURBATION EQUATIONS FOR THE STANDARD MODEL

Even though the standard model does not represent actual stars too closely, it seems worth while to integrate the slow-rotation equations first for the standard model before the corresponding much more laborious integration for a more precise model is undertaken, especially since the integration for the standard model should give an insight into the consequences of the viscosity surface condition (8).

The standard model does not contain a convective core. Hence condition (7) is not applicable, and equations (12), (13), and (14) have to be fulfilled throughout the star. The standard model is obtained by assuming the energy generation and the conductivity to be constant. Hence,

$$\epsilon = \text{constant}\,, \qquad K = \frac{4\,a\,c\,T^3}{3\,\kappa\,\rho} = \text{constant}\,. \tag{19}$$

Here, it will be assumed not only that both ϵ and K are constant throughout the rotating star but also that their respective values are identical with their values in the nonrotating star used as unperturbed standard in the first-order perturbation method. To make the

[6] *M.N.*, **93**, 390, 1933.

latter assumption physically reasonable, the nonrotating star should be chosen so as to have the same central temperature and central density as the rotating star. Hence, corresponding to equation (17),

$$T_d = 0\ , \qquad \rho_d = 0\ , \qquad \text{at the center}\ . \tag{20}$$

Having introduced the assumptions (19) and the developments (17) into the fundamental equations of section II, one may (neglecting all terms of second or higher order in the perturbations) split each equation into two, the unperturbed equation containing all zero-order terms and the perturbation equation containing all first-order terms.

The unperturbed equations one finds to be identical with the normal equations for the standard model. Hence the solution is given by

$$r = \frac{R}{\xi_R} \cdot \xi\ , \qquad T_u = T_c \cdot \theta\ , \qquad \rho_u = \rho_c \cdot \theta^3\ , \qquad P_u = P_c \cdot \theta^4\ , \tag{21}$$

where θ as function of ξ is the Lane-Emden function of index 3. Between the constants the following relations exist:

$$\epsilon = \frac{m}{k}\,\pi G K\ , \qquad P_c = \frac{k}{m}\,\rho_c T_c\ , \qquad \rho_c = \frac{k}{m}\,\frac{T_c}{\pi G}\left(\frac{\xi_R}{R}\right)^2 . \tag{22}$$

The perturbation equations (corresponding to the fundamental equations [15] and [16], [11]–[14], and finally [5]) are found to be

$$0 = +\frac{1}{\rho_u}\frac{\partial P_d}{\partial r} - \frac{1}{\rho_u}\frac{dP_u}{dr}\frac{\rho_d}{\rho_u} + \frac{\partial \Phi_d}{\partial r}\ , \tag{23}$$

$$+ V_d s = +\frac{1}{\rho_u}\frac{\partial P_d}{\partial s} + \frac{\partial \Phi_d}{\partial s}\ , \tag{24}$$

$$\frac{\partial^2 \Phi_d}{\partial r^2} + \frac{2}{r}\frac{\partial \Phi_d}{\partial r} + \frac{1}{r^2}\frac{\partial}{\partial \mu}\left[(1-\mu^2)\,\frac{\partial \Phi_d}{\partial \mu}\right] = +4\pi G \rho_d\ , \tag{25}$$

$$F_{rd} = -K\,\frac{\partial T_d}{\partial r}\ , \tag{26}$$

$$F_{\mu d} = -K\,\frac{\partial T_d}{\partial \mu}\,\frac{\sqrt{1-\mu^2}}{r}\ , \tag{27}$$

$$\frac{\partial F_{rd}}{\partial r} + \frac{2}{r}F_{rd} + \frac{1}{r}\frac{\partial}{\partial \mu}\left(\sqrt{1-\mu^2}\,F_{\mu d}\right) = +\epsilon \rho_d\ , \tag{28}$$

$$\frac{P_d}{P_u} = \frac{\rho_d}{\rho_u} + \frac{T_d}{T_u}\ . \tag{29}$$

In the first two of these seven equations r and s are used as independent variables, whereas in the last five r and μ are the independent variables.

The above perturbation equations may be simplified by using equation (29) to eliminate P_d from equations (23) and (24), by using equations (26) and (27) to eliminate F_{rd} and $F_{\mu d}$ from equation (28), and, finally, by using a new quantity A_d, defined by

$$A_d = 4T_d + \frac{m}{k}\,\Phi_d\ , \tag{30}$$

to eliminate Φ_d from equations (23), (24), and (25). Thus one gets

$$0 = +T_u \frac{\partial}{\partial r}\left(\frac{\rho_d}{\rho_u} - 3\frac{T_d}{T_u}\right) + \frac{\partial A_d}{\partial r}, \tag{31}$$

$$+\frac{m}{k} V_d s = +T_u \frac{\partial}{\partial s}\left(\frac{\rho_d}{\rho_u} - 3\frac{T_d}{T_u}\right) + \frac{\partial A_d}{\partial s}, \tag{32}$$

$$\frac{\partial^2 A_d}{\partial r^2} + \frac{2}{r}\frac{\partial A_d}{\partial r} + \frac{1}{r^2}\frac{\partial}{\partial \mu}\left[(1-\mu^2)\frac{\partial A_d}{\partial \mu}\right] = 0, \tag{33}$$

$$\frac{\partial^2 T_d}{\partial r^2} + \frac{2}{r}\frac{\partial T_d}{\partial r} + \frac{1}{r^2}\frac{\partial}{\partial \mu}\left[(1-\mu^2)\frac{\partial T_d}{\partial \mu}\right] = -\frac{\epsilon}{K}\rho_d. \tag{34}$$

The first-order perturbation method has, further, to be applied to simplify the two surface conditions. Equation (6) may be brought into an appropriate form in the following way: If in the nonrotating reference star the density reaches a certain value at a distance from the center r_u and if in the rotating star at a certain latitude the density reaches the same value at a distance from the center $r = r_u + \Delta_\rho$, one obtains the relation

$$\rho(r, \mu) = \rho_u(r_u) = \rho_u(r - \Delta_\rho) = \rho_u - \Delta_\rho \frac{d\rho_u}{dr},$$

or, with $\rho = \rho_u + \rho_d$,

$$\Delta_\rho = -\frac{\rho_d}{\frac{d\rho_u}{dr}}. \tag{35}$$

If, correspondingly, for the temperature, Δ_T is defined so that $T(r, \mu) = T_u(r - \Delta_T)$, one obtains:

$$\Delta_T = -\frac{T_d}{\frac{dT_u}{dr}}. \tag{36}$$

Since in the nonrotating star the surface with $\rho_u = 0$ coincides with the surface with $T_u = 0$ and since in the rotating star corresponding to equation (6) the surface with $\rho = 0$ coincides with the surface with $T = 0$, the two displacements Δ_ρ and Δ_T must be equal at the surface of the star. Hence, equation (6) becomes

$$\Delta_\rho = \Delta_T \qquad \text{at the surface } (r = R). \tag{37}$$

The second surface condition (8) may be brought into an appropriate form in the following way: Assuming that W does not vanish at the surface, a condition equivalent to equation (8) is $d(W^2)/dn = 0$, where d/dn is the derivative in the direction normal to the surface of the star. Since $W^2 = V_d$ is of the first order, the operator d/dn is needed here only in the zero-order approximation and can therefore be replaced by $\partial/\partial r|_{\mu=\text{const}}$. Hence, equation (8) becomes

$$\left.\frac{\partial V_d}{\partial r}\right|_{\mu=\text{const}} = 0 \qquad \text{at the surface } (r = R). \tag{38}$$

The problem of the standard model in slow rotation consists in its present form of the four differential equations (31)–(34), the surface conditions (37) and (38), and the center conditions (20). The solution of this problem will be derived in sections V and VI.

V. THE ROTATIONAL VELOCITIES IN THE STANDARD MODEL

The solving of the problem stated in the previous section may be started most easily with equation (33), since this equation contains only one unknown function. Equation (33) is Laplace's equation in polar co-ordinates for the case of axial symmetry. The most general solution (regular throughout the star) is

$$A_d = \sum_0^\infty a_n r^n P_n(\mu) , \tag{39}$$

where the P_n are Legendre's polynomials. Because of the symmetry of a rotating star with respect to its equatorial plane all odd a_n have to vanish.

To determine the values of the even a_n, a relation between A_d and V_d has to be derived so that eventually the surface condition (38) may be applied. Such a relation can be obtained from equations (31) and (32) in the following way: Differentiating equation (31) with respect to s and equation (32) with respect to r and taking the difference gives

$$+\frac{m}{k}\, s\, \frac{\partial V_d}{\partial r} = +\frac{dT_u}{dr}\, \frac{\partial}{\partial s}\left(\frac{\rho_d}{\rho_u} - 3\,\frac{T_d}{T_u}\right).$$

Further, differentiating equation (31) with respect to s, dividing by T_u, and integrating over r, along a line of constant s, gives

$$-\frac{\partial}{\partial s}\left(\frac{\rho_d}{\rho_u} - 3\,\frac{T_d}{T_u}\right) = +\int_{r=s}^{r} \frac{1}{T_u}\,\frac{\partial^2 A_d}{\partial r\,\partial s}\, dr + \sigma(s) ,$$

where $\sigma(s)$ is an arbitrary function of s only. Substituting the left side of the last equation into the right side of the equation just above, one gets

$$+\frac{m}{k}\, s\, \frac{\partial V_d}{\partial r} = -\frac{dT_u}{dr}\left[\int_{r=s}^{r} \frac{1}{T_u}\,\frac{\partial^2 A_d}{\partial r\,\partial s}\, dr + \sigma(s)\right].$$

On approaching the surface, dT_u/dr does not vanish, whereas T_u becomes zero. Hence, if $\partial^2 A_d/\partial r\partial s$ does not vanish at the surface, the above equation (because of $V_d = W^2$) gives an infinite gradient of the angular velocity at the surface. Introducing the condition that the gradient of the angular velocity should not be infinite at the surface—a much milder condition than the strict viscous surface condition (38)—gives, therefore,

$$\frac{\partial^2 A_d}{\partial r\,\partial s} = 0 \qquad \text{at the surface } (r = R) . \tag{40}$$

In appendix B it is shown that the condition (40) can be fulfilled by the general solution (39) only if $a_n = 0$ for $n > 2$. The remaining terms of equation (39) are

$$A_d = a_0 + a_2 r^2 P_2(\mu) = a_0 + a_2 r^2 \tfrac{1}{2}(3\mu^2 - 1) = a_0 + a_2 r^2 - a_2 \tfrac{3}{2} s^2 . \tag{41}$$

The first use of this solution for A_d will be in checking the surface condition (37). For this purpose equation (41) is introduced into equation (31), then the latter equation is divided by T_u and integrated over r. So one gets

$$\frac{\rho_d}{\rho_u} - 3\,\frac{T_d}{T_u} = -a_2 \int_0^r \frac{2r}{T_u}\, dr + \tau(s) , \tag{42}$$

where $\tau(s)$ is an arbitrary function of s only. With the help of equation (21) one may transform equation (42) to

$$\frac{\rho_d}{\frac{d\rho_u}{dr}} - \frac{T_d}{\frac{dT_u}{dr}} = \frac{1}{\frac{dT_u}{dr}} \frac{1}{3}\left[- a_2 T_u \cdot \int_0^r \frac{2r}{T_u}\, dr + T_u \cdot \tau(s) \right].$$

Since, on approaching the surface, T_u vanishes and the integral diverges only logarithmically, the whole right side vanishes on the surface. Hence the surface condition (37) is automatically fulfilled.

The second use of the solution (41) for A_d will be in deriving a solution for V_d. Introducing, for this purpose, equations (41) and (42) into equation (32) gives[7]

$$V_d = W^2 = +\frac{k}{m} T_u \cdot \frac{1}{s} \frac{d\tau(s)}{ds} - 3\frac{k}{m} \cdot a_2 . \tag{43}$$

The first term on the right side represents a rotation vanishing on the surface, increasing inward as T_u increases and involving a so far undetermined function of s as a factor. The second term on the right side is a constant and therefore represents a solid-body rotation.

Now, finally, the viscosity surface condition (38) can be applied. Because of $s = r\sqrt{1-\mu^2}$ one gets from equation (43)

$$\left.\frac{\partial V_d}{\partial r}\right|_{\mu=\text{const}} = \left.\frac{\partial V_d}{\partial r}\right|_{s=\text{const}} + \sqrt{1-\mu^2} \cdot \left.\frac{\partial V_d}{\partial s}\right|_{r=\text{const}}$$

$$= +\frac{k}{m}\frac{dT_u}{dr}\frac{1}{s}\frac{d\tau}{ds} + \sqrt{1-\mu^2}\,\frac{k}{m} T_u \frac{d}{ds}\left(\frac{1}{s}\frac{d\tau}{ds}\right).$$

Putting this into equation (38) gives (because of vanishing T_u, but nonvanishing dT_u/dr at $r = R$) $d\tau/ds = 0$ for all values of s. Hence, equation (43) becomes

$$V_d = W^2 = -3\frac{k}{m} \cdot a_2 = \text{const} . \tag{44}$$

The result, therefore, is that the only solution for the standard model, fulfilling both the normal equilibrium equations for a rotating star and the special viscosity surface condition, is (in first-order approximation) a solid-body rotation.[8]

In appendix C it is shown that this result is not in discordance with von Zeipel's theorem, since this theorem does not aply to the standard model, if W^2 is constant only in the first-order approximation.

VI. THE ROTATIONAL PERTURBATIONS OF THE STANDARD MODEL

The temperature perturbation T_d may now be determined from the last perturbation equation (34) after ρ_d has been eliminated with the help of equation (42). The last term in the latter equation can be determined by applying this equation to the center where the condition (20) has to be fulfilled. Thus one gets $\tau(0) = 0$. Since, on the other hand,

[7] That a rotation of the type of equation (43) is a possible solution for the standard model in slow rotation has previously been shown by Rosseland (*op. cit.*, p. 258, eq. [24], 1937).

[8] The remainder of this paper will be, of course, very similar to the corresponding parts of the investigations of Milne (*M.N.*, **83**, 118, 1923), von Zeipel (*M.N.*, **84**, 684, 1924), and Chandrasekhar (*loc. cit.*), who have considered certain slowly rotating models under the assumption of constant angular velocity throughout the star.

it was found in the preceding section that $d\tau/ds$ is zero for all values of s, one gets $\tau(s) = 0$ for all values of s. Correspondingly, equation (42) becomes (a_2 being replaced by W^2 in accordance with equation [44])

$$\frac{\rho_d}{\rho_u} = 3\frac{T_d}{T_u} + \frac{W^2}{3}\frac{m}{k}\int_0^r \frac{2r}{T_u}\,dr\,. \tag{45}$$

Introducing this into equation (34) gives

$$\frac{\partial^2 T_d}{\partial r^2} + \frac{2}{r}\frac{\partial T_d}{\partial r} + \frac{1}{r^2}\frac{\partial}{\partial \mu}\left[(1-\mu^2)\frac{\partial T_d}{\partial \mu}\right] + 3\frac{\epsilon}{K}\frac{\rho_u}{T_u}T_d = -\frac{\epsilon}{K}\frac{W^2}{3}\frac{m}{k}\rho_u\int_0^r \frac{2r}{T_u}\,dr\,. \tag{46}$$

This is a linear, nonhomogenous, partial differential equation for T_d.

The solution may be developed with the help of Legendre's polynomials $P_n(\mu)$ as follows:

$$T_d = w \cdot T_c \cdot \sum_0^\infty \eta_n(r) \cdot P_n(\mu)\,, \tag{47}$$

where T_c is the temperature at the center and w the ratio of the centripetal acceleration to the gravitational acceleration at the equator as defined by equation (18). Because of the symmetry of a rotating star with respect to its equatorial plane all odd $\eta_n(r)$ have to vanish. Introducing the development (47) into the differential equation (46) and separating the terms according to Legendre's polynomials gives (with the help of the relations [21] and [22] for the unperturbed values)

$$\frac{d^2\eta_0}{d\xi^2} + \frac{2}{\xi}\frac{d\eta_0}{d\xi} + 3\theta^2\eta_0 = -\frac{4}{9}\frac{\bar{\rho}_u}{\rho_{uc}}\cdot\theta^3\int_0^\xi \frac{2\xi}{\theta}\,d\xi\,, \tag{48}$$

$$\frac{d^2\eta_2}{d\xi^2} + \frac{2}{\xi}\frac{d\eta_2}{d\xi} - \frac{6}{\xi^2}\eta_2 + 3\theta^2\eta_2 = 0\,, \tag{49}$$

$$\frac{d^2\eta_n}{d\xi^2} + \frac{2}{\xi}\frac{d\eta_n}{d\xi} - \frac{n(n+1)}{\xi^2}\eta_n + 3\theta^2\eta_n = 0 \qquad (\text{for } n > 2)\,. \tag{50}$$

In addition to these differential equations, the following boundary conditions have to be fulfilled.

At the center the first of the two conditions (20) is a boundary condition for T_d. Introducing the development (47) into this condition and using $\eta_n(0) = 0$ for $n > 0$ (which is automatically fulfilled by all the solutions of equations [49] and [50] which are nonsingular at the center) one gets

$$\eta_0 = 0 \qquad \text{at the center } (\xi = 0)\,. \tag{51}$$

At the surface a boundary condition for T_d is implicitly contained in equation (25); namely, the Poisson equation has to be fulfilled not only inside but also outside the star, the potential and its normal derivative have to be continuous at the surface, and the potential has to vanish for large distances. Outside the star ($\rho_d = 0$) the most general solution of the Poisson equation which vanishes for large distances is

$$\Phi_d = \sum_0^\infty \Phi_n r^{-(n+1)} P_n(\mu)\,. \tag{52}$$

Inside the star the potential is given by equation (30), if A_d is eliminated with the help of equation (41) and T_d with the help of equation (47) (using equation [44] to eliminate a_2):

$$\Phi_d = a_0 \frac{k}{m} - \tfrac{1}{3} W^2 r^2 P_2(\mu) - 4 \frac{k}{m} T_c w \sum_0^\infty \eta_n(r) P_n(\mu) \ . \tag{53}$$

At the surface of the star the two expressions (52) and (53) have to be equal, and also their normal derivatives have to be equal. Since the corresponding equations are needed only in the first-order approximation, it is sufficient here to take the surface to be given by $r = R$ and the normal derivative to be given by $\partial/\partial r$. Thus one obtains, after separating the terms according to Legendre's polynomials, for $r = R$

$$\Phi_0 R^{-1} = +a_0 \frac{k}{m} - 4 \frac{k}{m} T_c w \eta_0 \ , \qquad \Phi_0 R^{-2} = 4 \frac{k}{m} T_c w \frac{d\eta_0}{dr} \ , \tag{54}$$

$$\Phi_2 R^{-3} = -\tfrac{1}{3} W^2 R^2 - 4 \frac{k}{m} T_c w \eta_2 \ , \qquad 3\Phi_2 R^{-4} = \tfrac{2}{3} W^2 R + 4 \frac{k}{m} T_c w \frac{d\eta_2}{dr} \ , \tag{55}$$

$$\Phi_n R^{-(n+1)} = -4 \frac{k}{m} T_c w \eta_n \ , \qquad (n+1)\Phi_n R^{-(n+2)} = 4 \frac{k}{m} T_c w \frac{d\eta_n}{dr} \quad \text{for } n > 2 \ . \tag{56}$$

The two equations (54) involve the two (otherwise undetermined) constants Φ_0 and a_0. Hence equation (54) does not give a surface condition for η_0. From equations (55) and (56) (eliminating Φ_2 and Φ_n, respectively, and using the relation between W^2 and w given by equation [18]) the following conditions are obtained:

$$3\eta_2 + \xi_R \cdot \frac{d\eta_2}{d\xi} = -\tfrac{5}{9} \xi_R^2 \frac{\bar{\rho}_u}{\rho_{uc}} \ , \tag{57}$$

$$(n+1)\eta_n + \xi_R \cdot \frac{d\eta_n}{d\xi} = 0 \quad \text{for} \quad n > 2 \ , \tag{58}$$

} at the surface ($r = R$) .

This far the problem of determining the temperature perturbation has been reduced to the problem of solving the differential equations (48), (49), and (50) under the boundary conditions (51), (57), and (58).

$\eta_0(\xi)$ is (because of the singularity in equation [48] at the center) completely determined by equations (48) and (51). Since the solution of the homogenous part of equation (48) can be expressed in terms of the Lane-Emden function of index 3 (it is, namely, $\theta + \xi \cdot [d\theta/d\xi]$), η_0 can be computed by numerical quadratures. η_0 is given in Table 1.

$\eta_2(\xi)$ is (because of the singularity in equation [49] at the center) completely determined by equations (49) and (57). Chandrasekhar[9] has derived a solution of equation (49) by numerical integration. By multiplying his solution by an appropriate factor, so as to fulfil equation (57), η_2 can be obtained. η_2 is given in Table 1.

In appendix D it is shown that the only solution fulfilling equations (50) and (58) is

$$\eta_n(\xi) = 0 \qquad \text{for} \qquad n > 2 \ .$$

With these solutions for the coefficients, equation (47) gives as final result for the temperature perturbation

$$T_d = w \cdot T_c [\, \eta_0(r) + \eta_2(r) \cdot (\tfrac{3}{2}\mu^2 - \tfrac{1}{2}) \,] \ , \tag{59}$$

[9] *Op. cit.*, p. 404, Table IV.

where w is the ratio of the centripetal acceleration to the gravitational acceleration at the equator, T_c is the temperature at the center, r is the distance from the center, μ is the sin of the latitude, and η_0 and η_2 are functions, tabulated in Table 1.

With this solution for T_d, the perturbation in the density is uniquely determined by equation (45), the perturbation in the pressure by equation (29), and the perturbation in the potential by equations (53) and (54).

VII. SUMMARY

In the last two sections the solution of the problem of stellar rotation (in the form described at the end of the introduction) has been given for the special case of the standard model in slow rotation. The solution was found to be unique.

The solution obtained may be compared with the observed angular velocities on the surface of the sun. The solution found corresponds to a solid-body rotation, hence does

TABLE 1

ξ	η_0	η_2	ξ	η_0	η_2
0.0	−0.00000	−0.0000	3.6	−0.01026	−0.0373
0.2	.00000	.0004	3.8	.01121	.0398
0.4	.00001	.0014	4.0	.01213	.0424
0.6	.00005	.0030	4.2	.01303	.0452
0.8	.00015	.0050	4.4	.01390	.0481
1.0	.00032	.0073	4.6	.01474	.0512
1.2	.00060	.0098	4.8	.01554	.0545
1.4	.00100	.0123	5.0	.01630	.0579
1.6	.00151	.0148	5.2	.01702	.0615
1.8	.00213	.0172	5.4	.01771	.0654
2.0	.00285	.0195	5.6	.01836	.0694
2.2	.00365	.0218	5.8	.01897	.0736
2.4	.00451	.0240	6.0	.01955	.0780
2.6	.00543	.0261	6.2	.02009	.0827
2.8	.00638	.0283	6.4	.02060	.0875
3.0	.00734	.0304	6.6	.02108	.0925
3.2	.00832	.0326	6.8	.02153	.0977
3.4	−0.00930	−0.0349	7.0	−0.02196	−0.1031

$$\text{At } \xi_R = 6.897 \begin{cases} \eta_0 = -0.02174, & d\eta_0/d\xi = -0.002129, \\ \eta_2 = -0.1004, & d\eta_2/d\xi = -0.02706. \end{cases}$$

not show an equatorial acceleration and, therefore, disagrees with the observations. This discordance does not, however, seem surprising, since the solution for the standard model which was chosen for its mathematical simplicity, should be expected to be of a mathematically simpler form than the solution for the actual sun.

As a next step, therefore, in the attempt to interpret the equatorial acceleration observed on the sun, it would seem necessary to derive the solution of the problem of stellar rotation (as formulated by the equations of sec. II) for a model more closely representing the internal structure of the sun.

APPENDIX A

It is to be shown that the use of the first-order perturbation equations is justified even at the surface.

The usual procedure for the derivation of the perturbation equations is based on the assumption that the quantities P_d/P_u, ρ_d/ρ_u, and T_d/T_u are small. This assumption is not justified near the surface, since the above quantities approach infinity where T_u approaches zero.

This difficulty is circumvented in the following way. The dependent variables appearing in

the fundamental equations are taken as depending not only on the space co-ordinates but also on a parameter (characterizing the total rotational momentum of the star) for which, for example, w as defined by equation (18) might be chosen. Instead of defining the perturbations by equation (17), they may now be defined by

$$f_d = w \cdot \left[\frac{\partial f}{\partial w}\right]_{w=0},$$

where for f each dependent variable should be substituted. With these definitions, which in first-order approximation are identical with those of equation (17), the perturbation equations may be derived (without difficulties at the surface) by differentiating the fundamental equations with respect to w.

APPENDIX B

It is to be shown that the surface condition (40),

$$\frac{\partial^2 A_d}{\partial r \partial s} = 0 \qquad \text{at} \qquad r = R,$$

can be fulfilled by the general solution (39),

$$A_d = \sum_0^\infty a_n r^n P_n(\mu) \qquad (a_n = 0 \text{ for odd } n),$$

only if $a_n = 0$ for $n > 2$.

Replacing the distance from the axis of rotation s by the sin of the latitude $\mu = \sqrt{r^2 - s^2}/r$, one finds for the surface condition [after dividing by $-\sqrt{1-\mu^2}/(\mu r^2)$]

$$r\frac{\partial^2 A_d}{\partial r \partial \mu} + \frac{1-\mu^2}{\mu}\frac{\partial^2 A_d}{\partial \mu^2} - \frac{1+\mu^2}{\mu^2}\frac{\partial A_d}{\partial \mu} = 0 \quad \text{at} \quad r = R.$$

Introducing here the general solution for A_d gives

$$0 = \sum_2^\infty a_n R^n \left(n\frac{dP_n}{d\mu} + \frac{1-\mu^2}{\mu}\frac{d^2P_n}{d\mu^2} - \frac{1+\mu^2}{\mu^2}\frac{dP_n}{d\mu}\right),$$

where the zero-order term is left out because $dP_0/d\mu = 0$. With the help of the differential equation of Legendre's polynomials,

$$(1-\mu^2)\frac{d^2P_n}{d\mu^2} - 2\mu\frac{dP_n}{d\mu} + n(n+1)P_n = 0,$$

and the following interrelations:

$$P_n = \mu P_{n-1} - \frac{1-\mu^2}{n}\frac{dP_{n-1}}{d\mu}, \qquad \frac{dP_n}{d\mu} = nP_{n-1} + \mu\frac{dP_{n-1}}{d\mu},$$

the above form of the surface condition can be transformed into the final form

$$0 = \sum_4^\infty n a_n R^n \cdot \frac{d}{d\mu}\left(\frac{1}{\mu}P_{n-1}\right),$$

where the second-order term is left out because $d(P_1/\mu)/d\mu = 0$. The remaining coefficients $d(P_{n-1}/\mu)/d\mu$ are independent functions of μ. Hence, from the last equation it follows that

$$a_n = 0 \qquad \text{for} \qquad n > 2.$$

APPENDIX C

It is to be shown that in first-order approximation a solid-body rotation for the standard model is not in discordance with von Zeipel's theorem.

Following Eddington's notation[10] in the derivation of von Zeipel's theorem, one gets for the standard model according to his equation (198.41) in zero-order approximation

$$f_u = \frac{\epsilon}{4\pi G} = \text{constant} .$$

Hence, in equation (198.7) $f'(\phi)$ does not contain a zero-order term. Therefore, in the first-order approximation of equation (198.7) the factor $d\phi/dn$ appears only in zero-order approximation. In this approximation $d\phi/dn$ is constant over a level surface; and hence the conclusions drawn from equation (198.7), leading to von Zeipel's theorem, are not valid in the first-order approximation for the standard model in rotation.

APPENDIX D

It is to be shown (for $n > 2$) that the only solution of the differential equation (50),

$$\frac{d^2\eta_n}{d\xi^2} + \frac{2}{\xi}\frac{d\eta_n}{d\xi} = \left[\frac{n(n+1)}{\xi^2} - 3\theta^2\right] \cdot \eta_n ,$$

which fulfils the surface condition (58),

$$+(n+1) \cdot \eta_n + \xi \cdot \frac{d\eta_n}{d\xi} = 0 \qquad \text{for} \qquad \xi = \xi_R ,$$

is the trivial solution $\eta_n = 0$.

Multiplying the above differential equation by ξ^2, integrating over ξ, and finally dividing by ξ^2 gives

$$\frac{d\eta_n}{d\xi} = \xi^{-2}\int_0^{\xi} [\, n(n+1) - 3\theta^2\xi^2 \,]\, \eta_n d\xi .$$

If η_n were neither identically zero nor had for all values of ξ the same sign, there would have to be a smallest ξ_z (>0) with $\eta_n(\xi_z) = 0$. Hence, η_n would have the same sign for $0 < \xi < \xi_z$. Since $n(n+1) > 3\theta^2\xi^2$ for $n > 2$, it would follow from the last equation that $d\eta_n/d\xi$ at $\xi = \xi_z$ would have the same sign as η_n for $\xi < \xi_z$, in contradiction with the definition of ξ_z. Therefore, η_n must be either identically zero or must have the same sign for all values of ξ. If η_n were not identically zero but had the same sign for all values of ξ, it would follow from the last equation that at $\xi = \xi_R$ the derivative $d\eta_n/d\xi$ would not vanish and would have the same sign as η_n, in contradiction with the above surface condition. Therefore, η_n must be identically zero.

I should like to express my gratitude to Dr. S. Chandrasekhar for much helpful advice and to Mr. G. Randers for the discussions which instigated this investigation.

RUTHERFURD OBSERVATORY
COLUMBIA UNIVERSITY
February 1942

[10] *The Internal Constitution of the Stars*, pp. 282–283, 1930.

ON THE ROTATION OF STARS WITH CONVECTIVE CORE

GUNNAR RANDERS

ABSTRACT

The convection in the central core of a rotating star is investigated. It is shown that even an extremely slow rotation has the effect of making the turbulent convective motion take place preferentially in a direction parallel to the axis of rotation. As a consequence, the energy from the central sources is being transported through the convective core mainly toward the poles. The resulting polar heating in the main body of the star leads necessarily to an increase of the rotational velocity toward the equatorial plane.

I. INTRODUCTION AND CONCLUSIONS

It is known that the stellar energy sources are strongly concentrated toward the center of a star. The effect of this concentration is to increase the temperature gradient of the radiative equilibrium to such an extent that in the central regions it exceeds the adiabatic temperature gradient. Under such circumstances convection currents are set up. The convection probably takes the form of turbulent intermixing of adjacent layers. The outward transport of energy will, for the main part, be taken over by the convection. However, a very slightly superadiabatic temperature gradient is already sufficient to take care of the necessary energy transport. One must, therefore, expect a practically adiabatic temperature gradient in the central, convective core of a star.

Thus far we have tacitly assumed the star to be nonrotating. It is important to know what effect rotation will have on the conditions discussed. The problem is, then, to investigate the conditions for stability against convection when the star is rotating. We shall assume the rotation to be that of a rigid body, first, because this is the most reasonable assumption for the central core and, second, because the effect of an outward or inward increase in angular velocity is easily discussed.

In a general way the stabilizing effect of the rotation is not difficult to understand. It is the effect of material ascending from lower levels lacking in angular momentum, compared to the angular momentum of the material in equilibrium at higher levels. This lack of angular momentum means a lack in centrifugal force and a resulting deceleration of the outward motion. Similarly, the excess of angular momentum of material moving inward tends to drive the material out again, thereby stopping the inward motion. The effect will depend, of course, on the direction of the motion relative to the axis of rotation. Before any definite conclusions can be drawn, we must study quantitatively the conditions for stability, in order to see the relative importance of the unstabilizing effect of the steep temperature gradient and the stabilizing effect of the rotation. This is done in section II, using the method of hydrodynamic line-integrals. The result is rather surprising at first. Even with an angular velocity as small as that of the surface of the sun ($W \sim 2 \cdot 10^{-6}$ sec^{-1}), the dynamic stability due to rotation is sufficient to check the thermal instability in directions perpendicular to the axis of rotation. If the direction considered is parallel to the direction of the axis, the stabilizing effect of the rotation disappears, and instability sets in. If the rotational velocity is higher than that of the sun's surface, which according to all available evidence it must be in the central regions, the stabilizing effect is, of course, even stronger.

Physically, the meaning of our result is that the turbulent convection in the central core occurs in "cells of motion," which extend mainly in the direction along the axis, motion in the perpendicular direction being negligible. Considering the extremely small centrifugal force arising from a rotation of the order of 10^{-6} sec^{-1}, it seems at first incredi-

ble that the rotation should be able to affect the thermal instability. The explanation is the fact, previously mentioned, that the superadiabatic gradient set up in the convective core is so extremely close to the adiabatic gradient that the resulting thermal instability is also vanishingly small. If any appreciably superadiabatic gradient were set up, the energy transport outward from the central regions due to the turbulent convection would very soon greatly exceed the observed energy output.

We can now see what will happen in the convective core of a rotating star. As the temperature gradient reaches the value of the adiabatic gradient, convection will set in but will be limited to cells in the direction of the axis of rotation. This "axial" convection will take care of the necessary energy transport, so that the temperature gradient will not increase further. Consequently, the stability limit in directions perpendicular to the axis will not be reached. The heat from the central energy sources will now be transported mainly toward the poles by the axial convection. In the perpendicular direction radiative transport, which is less important, is the only possibility.

The immediate consequence of the transport of energy toward the poles of the convective core is, of course, a higher temperature in the polar regions than in the equatorial regions of a star. How much of the polar excess of temperature will be left at the surface of the star depends upon two things: first, upon how large a part of the star the convective core represents and, second, upon how strong the preference for axial convection is—which again depends upon the velocity of rotation. It is probable that outside the convective core all energy transport is by radiation. From the surface of the core outward, the heat is therefore transported along the temperature gradient. The lower temperature of the equatorial regions will then be partly evened out before we reach the surface. Some difference must remain, however, even if it is extremely small.

The next question to answer is: What is the effect of the polar excess of heat on the rotational velocity in the main body of the star? This question has a simple answer. The angular velocity must be higher in the equatorial regions than in the polar regions (sec. III). Qualitatively, this effect is easily realized. The heating of the polar regions will tend to start an ascending current along the axis of rotation. If there were nothing to stop it, this upward current would be constantly accelerated by the heat, new and colder material moving in from the equatorial regions to replace the warm material ascending along the axis. The only effect which can stop a steadily increasing circulation is a surplus of centrifugal force in the equatorial region. Such a centrifugal force will act against the circulation set up by the polar heat, and equilibrium is possible. This is also the only possible state of equilibrium. An excess of angular velocity in the equatorial regions is, therefore, a necessary consequence of the polar heating. But the polar heating is a direct consequence of the rotation of the convective core. The conclusion is that a rotating star must necessarily have higher angular velocity near the equatorial plane than near the poles. Since the result is thus far dependent upon the assumption that the convective core rotates as a rigid body, it is important to see whether this assumption is essential for the final conclusion. Suppose, first, that the angular velocity increases outward from the axis. In this case the defect in angular momentum of material moving outward is even more pronounced than in the case of rigid-body rotation. The stabilizing effect is therefore stronger, and we have the axial direction of the convection cells as before. Now consider the case when the angular velocity decreases outward. We know that, as long as the product (angular velocity) $\times$ (distance from axis)^2 increases outward the effect of the rotation is stabilizing. When this product remains constant, the rotation has no effect on the stability; when it decreases, the effect is unstabilizing. In the last two cases, therefore, there is either no preference for axial orientation of the convection cells, or there is a preference for the perpendicular, radial orientation. However, as soon as the convective turbulence sets in with an appreciable radial motion, a strong interchange of momentum also sets in, or, in other words, a strong eddy-viscosity arises, which will force a solid-body rotation upon the convective core. Consequently, a rota-

tion with unstabilizing effect leads through an unsteady state back to our original assumption of solid-body rotation. The conclusion reached earlier, that a rotating star with convective core must rotate faster near the equatorial plane than near the poles is therefore generally valid without any assumptions about the rotation in the convective core itself.

Finally, the question should be asked: Does the present analysis enable us to explain the observed rotation on the surface of the sun? This question does not have a simple answer. It is true that from the above we expect the angular velocity to increase toward the equatorial plane. However, before a law of rotation at the surface can be given quantitatively, it is necessary to consider not only the equations of motion, as was done here, but also the equation of energy transfer and the Poisson equation. The latitude distribution of flux and temperature at the surface of the convective core must be found. Then an integration from the convective core to the outer surface must be carried through. Such integrations are not attempted on this paper.

II. CONVECTIVE STABILITY OF A ROTATING STAR

The usual method of studying the stability of a gaseous equilibrium configuration is the well-known "parcel" method. A small individual parcel of gas is imagined to be moved from its equilibrium position to a neighboring position. Adapting itself to the pressure of the new surroundings, the parcel changes its temperature and density adiabatically. If the new temperature and density are such that the net force on the parcel after the displacement is in the direction of the initial displacement, then the configuration is unstable at this point. The displacement of an individual parcel to new surroundings is, of course, not a good picture of what happens in reality. New material will take the place of the removed parcel, and material is being displaced by the parcel in the new surroundings. Actually, what should be studied is a small continuous displacement of the whole region. Then the question of stability would depend upon whether this entire motion tends to decrease or increase after the initial displacement has taken place. The "line-integral" method[1] considers conditions closer to reality than the parcel method, and we shall use it here. Actually, both methods give identical results. In the line-integral method we consider a small closed curve through the neighborhood which we are studying. When a small disturbance is applied to the gas, oscillations are set up. Considering the total acceleration along our closed curve, we study the frequency of the oscillations and thereby the stability. The equation of motion of a rotating gas is, in vector form,

$$W^2R\nabla R - \nabla\Phi - \frac{1}{\rho}\nabla p = 0\,, \tag{1}$$

where W is the angular velocity, R the distance from the axis of rotation, Φ the gravitational potential, ρ the density, and p the pressure. This equation is valid for pure rotation without any component of motion in a meridional section.

Introducing

$$p = \frac{k}{m}\rho T\,, \tag{2}$$

we write equation (1) in the form

$$W^2R\nabla R - \nabla\Phi - \frac{k}{m}T\nabla \log p = 0\,. \tag{3}$$

To study the stability of the rotational motion we apply a small, axially symmetrical disturbance. The motion will now have a small meridional component, and the local val-

[1] V. Bjerknes, *Astroph. Norvegica*, **2**, 263, 1937; E. Höiland, *Arch. f. Mathematik og Naturvidenskap*, **42**, No. 5, 1939.

ues of temperature and gravitational potential, etc., may have undergone small variations ΔT, $\Delta\phi$, etc., from the above equilibrium values. The equation of motion becomes

$$\frac{\partial V}{\partial t} = \{W^2R + \Delta(W^2R)\}\nabla R - \nabla(\phi + \Delta\phi) - \frac{k}{m}(T + \Delta T)\nabla \log p\,, \tag{4}$$

where V is the small perturbation in the velocity. The pressure field is, as usual, supposed to remain undisturbed by the perturbation, the material adjusting itself to the local pressure. By means of the equilibrium equation (3), we can write

$$\frac{\partial V}{\partial t} = \Delta(W^2R)\nabla R - \nabla(\Delta\phi) - \frac{k}{m}\Delta T\nabla \log p\,. \tag{5}$$

Now, multiply equation (5) by a line element δs and integrate along a small closed circuit:

$$\oint \frac{\partial V}{\partial t}\cdot \delta s = \oint \left\{\Delta(W^2R)\nabla R - \nabla(\Delta\phi) - \frac{k}{m}\Delta T\nabla \log p\right\}\cdot \delta s\,. \tag{6}$$

The middle term in the integral on the right-hand side vanishes by integration around a closed circuit, so it may be left out. For the small displacement due to the perturbation we write

$$\rho = \rho_0 e^{i\sigma t}\,. \tag{7}$$

Then

$$\frac{\partial V}{\partial t} = \frac{\partial^2 \rho}{\partial t_2} = -\sigma^2\rho\,, \tag{8}$$

and equation (6) becomes

$$-\sigma^2 \oint \rho\cdot \delta s = \oint \left\{\Delta(W^2R)\nabla R - \frac{k}{m}\Delta T\nabla \log p\right\}\cdot \delta s$$

or

$$\sigma^2 = -\frac{\oint \left\{\Delta(W^2R)\nabla R - \frac{k}{m}\Delta T\nabla \log p\right\}\cdot \delta s}{\oint \rho\cdot \delta s}\,. \tag{9}$$

To study the stability, we have to investigate the frequency of the oscillation resulting from a given perturbation. If, for a certain perturbation, σ^2 becomes negative, then we have instability for such perturbations. We shall choose our path of integration along the closed streamline of the perturbed motion. This means that the product $\rho\cdot\delta s$ is always positive. Hence the denominator in equation (9) is always positive. The condition for instability is, then, that the integral in the numerator is positive. The value of the integral depends obviously upon the path of integration, i.e., upon the streamlines of the perturbation. At a given point the integrand

$$\left\{\Delta(W^2R)\nabla R - \frac{k}{m}\Delta T\nabla \log p\right\}\cdot \delta s$$

is a function of the direction of δs (and ρ). If a direction can be found for which

$$\left\{\Delta(W^2R)\nabla R - \frac{k}{m}\Delta T\nabla \log p\right\}\cdot \delta s > 0\,,$$

then, by choosing a perturbation with streamlines extending mainly in this direction, the integral over these streamlines can also be made positive. (When δs changes sign, the variations ΔT, etc., also change signs, so that integrating back and forth in parallel directions gives contributions of same sign.) Hence the condition for unstable perturbation cells extending in a certain direction is that

$$\left\{\Delta(W^2R)\,\nabla R - \frac{k}{m}\,\Delta T \nabla \log p\right\} \cdot \delta s > 0 \tag{10}$$

in the direction in question. The expression (10) may be simplified. Since we consider perturbations symmetrical about the axis, a ring of material around the axis remains a ring after the perturbation. The "circulation" of such a ring is the simple expression $2\pi WR^2$ and is known from a familiar theorem to remain constant during the motion. This means that for an individual particle

$$W^2 = \text{const} \cdot \frac{1}{R^4}. \tag{11}$$

The local change $\Delta(W^2R)$ of the centrifugal force corresponding to a displacement with component δR away from the axis is, therefore,

$$\Delta(W^2R) = R\Delta W^2 = -R \cdot \frac{4}{R} W^2 \delta R = -4W^2 \delta R\,. \tag{12}$$

The local change ΔT in temperature is the difference between the temperature of the material arriving at the point in question after the perturbation and the original temperature at that point. The temperature of the material arriving at the point considered after the adiabatic displacement $\boldsymbol{\rho}$ is

$$T' = T - \boldsymbol{\rho} \cdot \nabla T + \delta_a T\,. \tag{13}$$

Here ∇T refers to the original temperature field, while $\delta_a T$ is the adiabatic change of temperature as the material is displaced along $\boldsymbol{\rho}$. For $\delta_a T$ we have the equation

$$\frac{\delta_a T}{T} = \frac{\Gamma - 1}{\Gamma}\,\frac{\delta p}{p}, \tag{14}$$

where Γ is the effective adiabatic exponent. By equations (13) and (14),

$$\Delta T = T' - T = T\left(\frac{\Gamma - 1}{\Gamma}\,\frac{\nabla p}{p} - \frac{\nabla T}{T}\right) \cdot \boldsymbol{\rho}\,. \tag{15}$$

Introducing equations (12) and (15) into equation (10), we get the condition for instability

$$\left\{-4W^2R\,\delta R \nabla R - \frac{k}{m}\,T\left(\left[\frac{\Gamma - 1}{\Gamma}\,\frac{\nabla p}{p} - \frac{\nabla T}{T}\right] \cdot \boldsymbol{\rho}\right) \nabla \log p\right\} \cdot \delta s > 0\,. \tag{16}$$

By means of equation (16) we can investigate the stability for convection cells in any direction. In our case we are interested in convection as a means of energy transport from the center of the star outward. It is, therefore, of importance to study the stability of cells extending radially from the center of the star. This means that $\boldsymbol{\rho}$ and δs are both radial displacements ($\propto \delta r$). Since δR is now $|\boldsymbol{\rho}| \cdot \sin\theta$, where θ is the co-latitude, equation (16) may be written

$$\frac{k}{m}\,T\left(\frac{1}{T}\,\frac{\partial T}{\partial r} - \frac{\Gamma - 1}{\Gamma}\,\frac{1}{p}\,\frac{\partial p}{\partial r}\right)\frac{\partial \log p}{\partial r} - 4W^2 \sin^2\theta > 0\,. \tag{17}$$

It is seen that in the direction toward the pole ($\theta = 0°$) the condition reduces to

$$\frac{\Gamma - 1}{\Gamma} \frac{1}{p} \frac{\partial p}{\partial r} - \frac{1}{T} \frac{\partial T}{\partial r} > 0 \tag{18}$$

($\partial \log p / \partial r$ is negative). The rotational term disappears, and the conditon for instability is the usual one. When we consider lower latitudes, the rotational term, which acts against instability, enters the condition with increasing importance as we approach the equator ($\theta = 90°$). Let us consider the stability of the radial convection cells in the equatorial plane. Then $\theta = 90°$, and we have the condition for instability,

$$\frac{k}{m} T \left(\frac{1}{T} \frac{\partial T}{\partial r} - \frac{\Gamma - 1}{\Gamma} \frac{1}{p} \frac{\partial p}{\partial r} \right) \frac{\partial \log p}{\partial r} - 4W^2 > 0 . \tag{19}$$

We must now obtain an estimate of the order of magnitude of the two terms. To take the case of the sun, we may put $W \geqslant 2 \cdot 10^{-6}\ \mathrm{sec}^{-1}$, which gives for the rotational term

$$4W^2 \geqslant 1.6 \cdot 10^{-11}\ \mathrm{sec}^{-1} . \tag{20}$$

The first term of the inequity (19) can also be estimated roughly without making use of special models or integrations. This is because the term is a direct measure of the energy transported by the turbulent convection per unit time. This amount is known by observation of the solar output of energy. Cowling[2] has made such an estimate, with the result that

$$\frac{k}{m} T \left(\frac{1}{T} \frac{\partial T}{\partial r} - \frac{\Gamma - 1}{\Gamma} \frac{1}{p} \frac{\partial p}{\partial r} \right) \frac{\partial \log p}{\partial r} < 4 \cdot 10^{-12}\ \mathrm{sec}^{-1} . \tag{21}$$

From equations (20) and (21) it is seen that the rotational term is the larger, even for an angular velocity as low as that of the sun's surface. Consequently, there will be no convection in radially extending cells in the equatorial plane. The fact that Cowling's estimate of the above quantity was made by assuming convection in all directions from the center may change the value by a factor 2 or so but cannot affect the order of magnitude.

According to our calculations convective transport of energy will set in at a certain latitude, where the factor $\sin^2 \theta$ has reduced the rotational term sufficiently. Roughly speaking, therefore, the energy produced at the center is being transported outward mainly inside of two opposite cones described around the rotational axis. The width of the cones is determined by the angular velocity.

III. ANGULAR VELOCITY IN A STAR WITH POLAR HEATING

The equations of motion (3) may be written

$$W^2 R = \frac{\partial \Phi}{\partial R} + \frac{k}{m} T \frac{\partial \log p}{\partial R} , \tag{22}$$

$$0 = \frac{\partial \Phi}{\partial z} + \frac{k}{m} T \frac{\partial \log p}{\partial z} , \tag{23}$$

[2] *M.N.*, **96**, 52, 1935. When we follow Cowling's way of estimating we must in the case of a rotating star replace quantities like the flux, the temperature, etc., by their mean values over isobaric surfaces of the star. The expression in the parentheses in (19) cannot change much along an isobar since isothermals and isobars coincide in the case of uniform rotation [eq. (24)].

where z is the height above the equatorial plane. Differentiating equation (22) with respect to z, equation (23) with respect to R, and subtracting gives

$$R\frac{\partial W^2}{\partial z}=\frac{1}{p}\frac{k}{m}\left[\frac{\partial T}{\partial z}\frac{\partial p}{\partial R}-\frac{\partial T}{\partial R}\frac{\partial p}{\partial z}\right]. \tag{24}$$

Consider for a moment the upper, right-hand quadrant of a meridional section of the star. The expression in brackets is then the projection of ∇T on the left-hand normal of ∇p. Now ∇p points inward into the star. The left-hand normal of ∇p is, therefore, along an isobar in a direction *away* from the pole. But, since the temperature increases along an isobar *toward* the pole, the projection of ∇T on the isobar must also be directed *toward* the pole. Consequently, the expression (24) is negative. It follows immediately, then, that the angular velocity decreases with height above the equatorial plane.

I am indebted to Dr. S. Chandrasekhar for useful discussions of these problems.

UNIVERSITY OF CHICAGO
March 1942

LUMINOSITIES OF THE M-TYPE VARIABLES OF SMALL RANGE*

PHILIP C. KEENAN

ABSTRACT

Spectroscopic luminosity classes and absolute magnitudes have been determined for 67 semiregular or irregular variable stars of types K and M. These are stars for which the amplitude of the light-variation is less than 2 mag.

The visual absolute magnitudes range from zero (normal giants) to −5 or −6, but the stars are not uniformly distributed over this interval. Thirteen are brilliant supergiants of types K5–M3, while the remainder are of markedly lower luminosity and chiefly of types M3–M6. Irregular variability appears to be uncommon among early M-type giants.

The supergiant variables not only are concentrated near the galactic plane but also show a pronounced grouping in longitude. Five of them are members of the double cluster, h and χ Persei.

Several of the supergiants recognized in this survey are among the most luminous stars known. One of them, RW Cep, is probably brighter than μ Cep.

The red variable stars can be divided into two groups on the basis of the amplitude of their visual light-variation. The stars with a range greater than 2 mag. include nearly all the long-period variables, while those of smaller range are essentially the semiregular and irregular variables. These latter stars, in which the light fluctuates by a comparatively small amount, have always been difficult to classify with respect to the nature of their light-curves, and many of them have been shuttled back and forth between such rather indefinite groups as μ Cephei stars, UU Herculis stars, RV Tauri stars, etc.[1] Consequently, it is now evident that further direct data on the physical properties of such variables must be collected before much progress can be made toward a definitive classification.

We consider, first, the spectral types of the stars with $\Delta m \leq 2^m$. They are distributed roughly as follows:[2]

M	59 per cent	R	2 per cent
K	15	S	1
N	22	Peculiar	1

The stars of types K and M, constituting more than two-thirds of the whole group, are especially well suited to the determination of spectroscopic luminosities, since their spectra are relatively free from the emission lines characteristic of the long-period variables and the spectral changes shown by a given star are usually not great. The special value of spectroscopic parallaxes lies in the fact that they can be found for individual stars, thus making it possible to estimate the degree of homogeneity of the group with respect to the two important physical parameters—luminosity and temperature.

In order to investigate the range of luminosities present in a fair sample of the variables of small range, spectra of 67 stars were obtained during the months of November and December, 1941, with the Cassegrain spectrograph of the McDonald reflector. The combination of glass prisms and f/2 Schmidt camera gave a scale of 66 A/mm at λ 4200. The observed stars are listed in Table 1, followed by the Julian dates of observation, the visual range (except for those values printed in italics, which are photographic magni-

* *Contributions from the McDonald Observatory, University of Texas*, No. 48.

[1] Cf. the discussion by Payne-Gaposchkin and Gaposchkin, *Variable Stars*, chaps. v and vi, 1938.

[2] Taken for the most part from Schneller, *Katalog und Ephemeriden veränderlicher Sterne*, 1941.

TABLE 1

TYPES AND LUMINOSITIES OF K AND M VARIABLES

($\Delta m \leqslant 2.0$)

Star	JD 2430000+	m_v	l	b	Period	Type	Luminosity
SS And	345	8.9– 9.9	76°	− 7°	160^d:	M6	II
UX And	343,346	8.4– 9.9	103	−13	393:	M6	III
TU Aur	346	7.7– 9.1	136	+16	75	M4:	III
TW Aur	345,356	8.0– 8.9	135	+11	.....	M4:	III
UX Aur	342	8.4– 9.2	128	+ 7	90	M4	II
UZ Aur	356	7.7– 9.3	136	+ 2	66	M3	III
RS Cam	357	8.1– 9.5	102	+34	166	M4	III
RV Cam	346	7.9– 9.0	115	+ 7	107	M4	II–III
RY Cam	331	7.6– 9.3	112	+12	135	M3	III
Z Cnc	345	8.5– 9.8	177	+29	80	M6	III
RS Cnc	352,357	5.3– 6.8	163	+43	239	M6	I*b*–II
RT Cnc	341	7.3– 8.6	185	+33	100	M4	III
TZ Cas	352,356	9.1– 9.7	84	− 1	.....	M2	I*a*–I*b*
μ Cep	330	4.0– 4.8	68	+ 4	750	M2	I*a*
RU Cep	342	8.3– 9.3	93	+23	117	M0	III
RW Cep	331,350	6.8– 7.5	71	− 1	.....	M0:	I*a*–0
SS Cep	330,342	6.7– 7.8	104	+10	100	M5	III
ST Cep	346	7.7– 8.9	72	− 1	.....	M0	I*b*
VV Cep	329,330	4.9– 5.6	72	+ 7	7430:	M1p	0
AR Cep	342	7.1– 7.8	87	+23	116:	M4	III
T Cet	359	5.2– 6.0	45	−78	159	M5	II
RW Cyg	338,344	7.6– 9.4	46	0	631:	M3	I*a*
AB Cyg	356	8.3– 9.3	50	−15	529	M4:	III
AZ Cyg	345	8.1– 9.4	55	0	.....	M2:	I*a*
U Del	342	5.6– 7.5	30	−16	.....	M5	II–III
V Eri	345	8.3– 9.4	177	−42	.....	M6	II
Z Eri	345	6.4– 7.8	160	−57	74,1200	M4	III
RR Eri	353	7.2– 8.5	154	−53	.....	M5	III
SU Eri	356	*9.5–10.1*	158	−37	.....	M4:	III
η Gem	350	3.2– 4.2	157	+ 4	236	M2	III
SW Gem	359	9.2–10.6	158	+15	680	M5	III
TV Gem	355	7.0– 7.8	157	+ 3	.....	M1:	I*a*
TW Gem	329,346	7.7– 9.3	161	+15	.....	M0	III
BK Gem	342	8.0– 8.3	166	+ 3	.....	K5	III
RV Hya	346,351	7.6– 8.3	203	+20	.....	M5	II
SU Hya	352	*9.4–10.4*	226	+27	.....	M4	III:
AK Hya	348,351	*7.1– 8.0*	209	+16	.....	M4	III
Z Leo	351	8.6–10.0	170	+50	57	M3	III–IV
V Lyn	345	8.6– 9.8	120	+23	87	M5	III–IV
Y Lyn	338,345	6.9– 7.4	140	+26	.....	M5	I*b*–II
RT Mon	330,331	8.1– 9.3	199	+13	115	M3	III
SW Mon	356	9.1–10.6	173	− 3	110	M4	III
α Ori	344,355	0.1– 1.2	168	− 8	2070	M2	I*b*
BQ Ori	355	6.9– 8.9	155	+ 1	130	M5	III
CI Ori	340	*5.1– 6.8*	171	−17	.....	K5:	III
CK Ori	352	*6.7– 7.3*	167	+14	.....	K2	III
AF Peg	350	8.9– 9.9	55	−36	52	M5	II–III
ρ Per	355	3.2– 4.1	117	−16	910:	M3	III
T Per	331,346	8.0– 9.0	102	− 1	.....	M0	I*a*–I*b*
RS Per	329,330	8.0– 9.4	103	− 3	.....	M3	I*a*–I*b*
SU Per	338	7.0– 8.5	103	− 4	477	M3	I*a*–I*b*
SW Per	350,346	8.2– 9.8	125	− 7	84	M5	III
TT Per	359	8.0– 9.2	100	− 7	92	M5	III
UZ Per	350	7.8– 9.5	124	−20	90	M5	II–III
YZ Per	355,359	7.6– 8.3	105	− 2	.....	M1	I*a*–I*b*

TABLE 1—*Continued*

Star	JD 2430000+	m_v	l	b	Period	Type	Luminosity
AD Per	329,339	7.7– 8.4	103°	− 3°	.....	M1	I*a*–I*b*
TV Psc	346,352	*6.9– 7.3*	84	−44	.....	M3	III
W Tri	350,352	8.2– 9.0	115	−22	148	M4	II
U UMa	351,357	6.1– 6.8	117	+49	.....	M0	III
Y UMa	357	7.7– 9.3	91	+61	.....	M7	II–III:
Z UMa	357	*8.4–10.2*	104	+57	198	M5	III
RY UMa	351	7.2– 8.3	95	+56	311	M3:	III
ST UMa	357	6.5– 7.3	128	+66	81	M4	III
SV UMa	357	8.8–10.0	120	+55	76	K3p:	I*a*:*
TT UMa	357	8.9– 9.5	122	+41	.....	M6	III
TV UMa	351,357	*8.2– 9.0*	142	+75	.....	M4	III
RW Vir	375	7.0– 8.2	250	+58	.....	M5	III

* SV UMa; the line ratios suggest high luminosity, but all lines in the spectrum are so weak that the application of luminosity criteria is uncertain. There is some similarity to the spectra of V Vul and R Sct. If the luminosity criteria are accepted at face value, SV UMa must be situated several thousand parsecs above the galactic plane.

tudes), galactic co-ordinates, and periods.[3] The spectral types given in the seventh column were estimated on the Mount Wilson system[4] on the basis of the strength of the *TiO* bands on the blue side of λ 5500, the limiting wave length in the yellow reached by the Agfa Super Plenachrome Press films on which the spectra were taken.

In relying entirely upon the bands of a single molecule for the assignment of spectral classes, the assumption is made that the relative abundance of the elements composing the molecule is constant in the group of stars considered and that the fraction of the material which will be in the molecular form does not pass through a maximum in the range of temperatures considered. If these conditions are fulfilled, the classification defines a temperature sequence. In the case of the variables photographed at McDonald Observatory it was possible to test the consistency of the classification through the fact that for many of them rather heavily exposed spectra were available, showing the region around λ 4000, where the atomic lines are not seriously weakened by overlying band absorption. Several ratios of resonance lines of elements of low ionization potential to excited lines of iron were selected as independent indicators of temperature. Those most useful were *Ti* 3982, 3989, 3999, 4009/*Fe* 4005, *Ca* 4226/*Fe* 4143, and *Cr* 4254/*Fe* 4250, 4260. Their behavior in the spectral sequence of giants is shown in Plate XIV, in which both variable and nonvariable stars are included. The progression in the ratios for all the stars examined is in agreement with the descriptions given by Merrill[5] and leaves little doubt that the subdivisions of type M giants represent a smoothly decreasing sequence of temperatures. For the supergiants also the scale is probably consistent, but it must be kept in mind that the temperature corresponding to a given spectral type will presumably be a function of luminosity.

The investigation of the luminosities can be carried out most conveniently in two steps: first, the setting-up of a series of standard stars in which known luminosity criteria change progressively and, afterward, the calibration of this scale in terms of absolute magnitudes. The stars used as standards defining the luminosity classes for types M0–M3 are given in Table 2.

The notation is designed to be consistent with that in use for the earlier spectral types.[6] The most sensitive line ratios are 4077/4045, 4172–5/4143, 4216/4226, and 4376,

[3] Taken mostly from Table V, I, of Payne-Gaposchkin and Gaposchkin, *op. cit.*

[4] *Trans. I.A.U.*, **2**, 119, 1925.

[5] *Ap. J.*, **63**, 13, 1926; *Mt. W. Contr.*, No. 306.

[6] Morgan, *Ap. J.*, **87**, 460, 1938; Keenan, *Ap. J.*, **91**, 506, 1940.

4389/4383. In each case the ratio increases as the luminosity becomes greater, and the changes are sufficiently pronounced to be followed easily in Plate XV, *a*, from which VV Cep has been omitted because of the peculiar weakness of all the lines in its composite spectrum, which is not closely matched by any of the other variables observed. The stars of high luminosity are so red that the region to the violet of λ 4200 is usually too far underexposed to be used, but the remaining lines are sensitive enough to make it easy to interpolate between the main classes. The lines at λ 4376 and λ 4389 belong to one of the two multiplets of iron, originating at the normal level of the atom, which Adams and Joy[7] were the first to use as criteria of absolute magnitude.

TABLE 2

Luminosity Class	Stars	Luminosity Class	Stars
0	VV Cep	II	5 Lac, π Aur
Ia	μ Cep	II–III	β Peg
Ib	α Ori, α Sco, 119 Tau	III	β And, χ Peg, η Gem

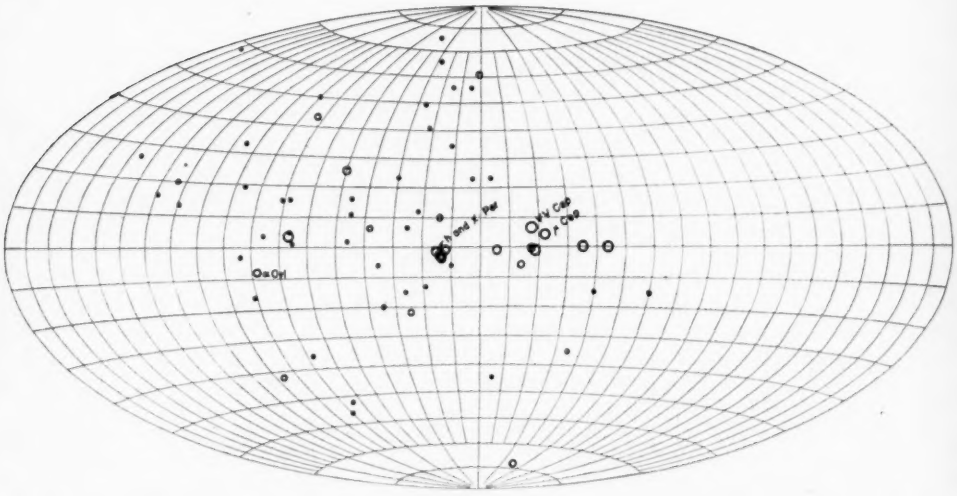

FIG. 1.—Galactic co-ordinates of the variable stars observed. Center of the diagram is at $b = 0°$, $l = 90°$. Size of circle indicates luminosity of each star, the supergiants being largest.

The application of these criteria to the variable stars is illustrated in Plate XV, *b*, *c*, for types M0 and M3. In the spectrum of RW Cep all lines are stronger than normal, and the enhancement of the lines sensitive to luminosity is so great as to make it appear probable that this star has the greatest absolute brightness of any of those studied here, with the exception of VV Cep. It is of interest that these two stars and μ Cep are situated in the same part of the Milky Way, within a few degrees of one another.

SU Per is one of 5 stars in the list which appear to be members of the double cluster, h and χ Persei. Three of them—AD, SU, and RS Per—were assigned to the cluster by Adams, Joy, and Humason[8] on the basis of their radial velocities and proper motions. For

[7] *Pub. A.S.P.*, **35**, 328, 1923.

[8] *Ap. J.*, **64**, 225, 1926; *Mt. W. Contr.*, No. 319.

PLATE XIV

SPECTRAL SEQUENCE

Types assigned from bands in the green region are given at the right. Lines which become stronger with later type are marked at the top.

PLATE XV

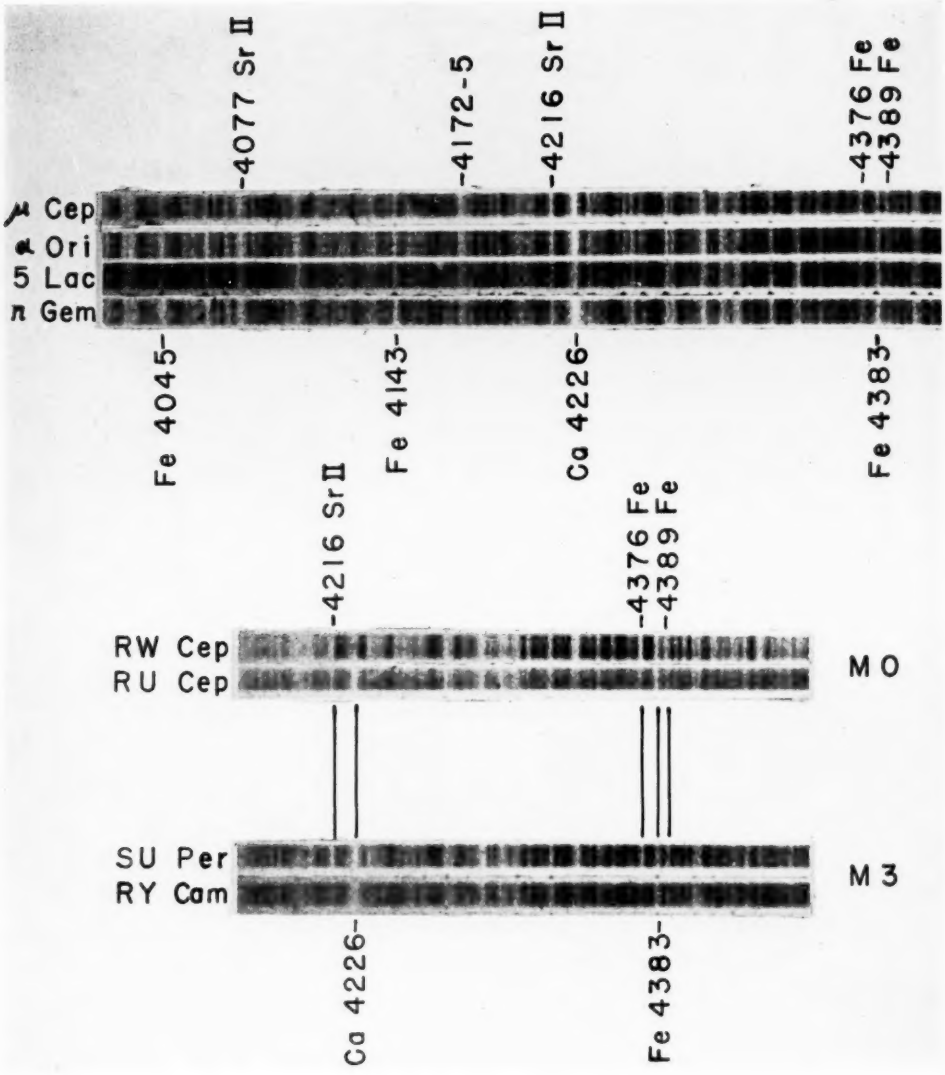

a) Luminosity Sequence for Types M0–M3

As the luminosity increases the lines marked at the top become relatively stronger in comparison to those indicated below the spectra.

b, c) Luminosity Effects in Variable Stars.

Supergiants (RW Cep and SU Per) are shown above giants (RU Cep and RY Cam) of similar spectral type.

the other 2 the proper motions only are available, but they are consistent with membership in the cluster. These stars are all supergiants intermediate in luminosity between α Ori and μ Cep. Further confirmation of their membership in the cluster is found in the distribution over the sky of the observed variables (Fig. 1). Since the material is reasonably complete down to the ninth apparent magnitude within the range of galactic coordinates accessible in winter, the absence of other supergiants within a radius of more than 10° from the cluster emphasizes the physical association of the 5 stars.

The distance of h and χ Persei can now be used to find the mean absolute magnitude of these stars. From a discussion of Oosterhoff's magnitudes and the magnitudes and spectral types given by Trumpler, W. P. Bidelman has derived an apparent modulus of $12^m.5$, taking the photographic absolute magnitude of the main sequence at B9 as $-0^m.3$.[9] The distance obtained in this way is to be preferred to that determined from the radial velocities, since the latter method involves the uncertain assumption that the whole motion of the cluster is to be ascribed to galactic rotation. The modulus of $12^m.5$ leads to the following median visual absolute magnitudes for the variables in the cluster:

T Per	$-4^m.0$	RS Per	$-3^m.8$
AD Per	-4.5	YZ Per	-4.5
SU Per	-4.7		

The mean is $M_v = -4^m.4$ at luminosity class I*a*–I*b*.

Another calibration point, of rather low weight, is furnished by α Sco (type I*b*). If it is assumed to be a member of the Scorpius cluster, its absolute magnitude is in the neighborhood of -4.0.

TABLE 3

CALIBRATION OF LUMINOSITY SCALE

Luminosity Class	M_v	Luminosity Class	M_v
I*a*	-5.2	II	-2.0
I*b*	-3.8	III	-0.2

For the ordinary giants of class III trigonometric parallaxes can be used. The numerous published means for M-type giants might be expected to differ systematically from the proper value for class III, since they generally include some admixture of stars of higher luminosity but none less bright, as no subgiants of type M are known. For this reason a mean was computed from 10 of the brightest class III stars of types M0–M3; the value found was $\bar{M}_v = -0^m.2$.

Finally, the star VV Cep is of some value in estimating the upper end of the scale, where it was placed because λ 4383 is definitely weaker than λ 4376 and is roughly equal to λ 4389 in its spectrum. By combining the spectroscopic and photometric observations of the eclipsing pair, Goedicke,[10] following Gaposchkin, obtained two solutions for the parallax. These correspond, for the M2 component, to $M_v = -6.8$ if there is a sharp photosphere, and to $M_v = -5.0$ if there is a diffuse photosphere extending to 3 per cent of the radius. Probably a simple mean of the two values is the most reasonable estimate to adopt.

From a plot of these calibration points, Table 3 was constructed to allow the reduction of luminosity classes to absolute magnitudes.

[9] This is a provisional value, which Mr. Bidelman has kindly furnished in advance of the publication of his study of the cluster.

[10] *Pub. Univ. Michigan Obs.*, **8**, 1, 1939.

With the help of Table 3 the absolute magnitudes of the observed variable stars can be easily found. However, only the luminosity classes have been entered in the eighth column of Table 1, because the calibration can be improved when a sufficient number of stars of each luminosity class are known to provide reliable mean absolute magnitudes computed from the motions. Then, too, the reduction table applies strictly only to types M3 and earlier. For the later types the luminosity classes themselves are less definite because the atomic line intensities are disturbed by the increasing band absorption, and no good standards of absolute magnitude are known. Thus λ 4045 is badly blended with λ 4044 and λ 4047 of potassium, and *Ca* 4226 is too strong to serve as a good reference line. Consequently, *Fe* 4063 and *Cr* 4254 are used in their stead. With this modification the extension of the criteria to the late M-type stars is reasonable, and real differences in absolute

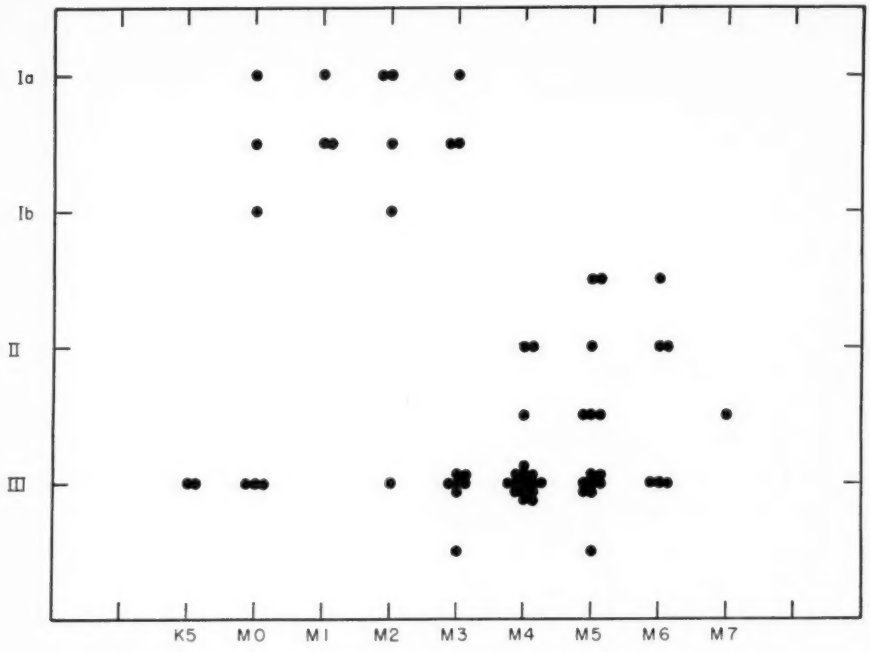

FIG. 2.—Luminosity-spectrum diagram for the variable stars observed

brightness appear to exist, as between Y Lyn and BQ Ori, which are reproduced in Plate XVI.

The distribution of the observed variables in luminosity and spectral type is shown in Figure 2. Most striking is the concentration of supergiants between types M0 and M3 in contrast to the excess of normal giants in the more advanced types. This feature has been suspected before, from the fact that the known red supergiants have only moderately strong bands.[11]

Our knowledge of the nonvariable early M-type stars is sufficient to indicate that their distribution in luminosity is just the reverse of that of the variables, for relatively few supergiants are known among them. Thus the known comparative freedom from variability of the K-giants continues as far as type M3.[12]

[11] Cf. McLeod, *Pop. Astr.*, **45**, 155, 1937; Joy, *Pub. A.A.S.*, **10**, 115, 1941.

[12] This is in agreement with the conclusions reached by Stebbins (*Pub. Washburn Obs.*, **15**, 139, 1934).

PLATE XVI

LUMINOSITY EFFECTS IN GIANTS AT TYPE M5
The lower spectrum is that of an ordinary giant

UNIV. OF MICH.

The apparent preference of the supergiant variables for the early subdivisions of type M may be influenced by the uncertainties in the spectral classification for the stars of high luminosity and in the luminosity sequence for the stars of late type, as well as by the increasing bolometric corrections at low temperatures.[13] However, it is doubtful that these factors are sufficient to produce the discontinuity in the upper right-hand part of Figure 2. Rather, it appears likely that *this region is the domain of stars of type S*, which are known to combine low temperature and high luminosity. In other words, if a star has the absolute magnitude and temperature corresponding to this region, it will presumably develop the bands of *ZrO* and no longer be classed as of type M.

This view is supported by the fact that the *ZrO* band at λ 4619 can be seen faintly in the low-dispersion spectra of several of the late-type variables classed as moderately luminous (Y Lyn; see Pl. XVI) but is not perceptible in the ordinary giants. However, further spectroscopic observations must be made on the few S-type variables of small range before it will be possible to fit them into the diagram, and this will offer some difficulty because of their extreme redness.

It is a pleasure to acknowledge the value of discussions of this problem with Dr. Morgan and the co-operation of the McDonald staff in the observational work.

McDonald Observatory and
Yerkes Observatory
February 1942

[13] This last point was suggested by Dr. Kuiper.

SPECTROGRAPHIC OBSERVATIONS OF 17 LEPORIS

BURKE SMITH AND OTTO STRUVE

ABSTRACT

Spectrographic observations numbering 142 were secured at the Yerkes Observatory from 1928 to 1942. During this interval of 14 years, 9 violent outbursts of nova-like character have been observed in the spectrum. In addition, there have been a number of minor disturbances. Each disturbance is characterized by the appearance of violet components to the normal absorption lines, which themselves show velocities of expansion corresponding to between about 60 and 30 km/sec. The outbursts repeat themselves at intervals of approximately 150 days, but the phenomenon is not periodic, and the intervals between successive outbursts vary between approximately 130 days and 175 days. In a few cases outbursts have been observed at even shorter intervals. The lines of *Mg* II and *Si* II show radial velocities averaging approximately +20 km/sec. The strongest metallic lines frequently have a tendency to show weak emission borders on their red sides. There are marked variations in the intensities and widths of the absorption lines during the normal stage of the star.

The star 17 Leporis is a very remarkable representative of a small group of A-type stars in which $H\alpha$ and sometimes $H\beta$ are bright and in which the sharp metallic lines show a large violet displacement, corresponding to a velocity of expansion of between about −40 km/sec and −140 km/sec. This expanding shell of variable velocity, although giving rise to strong sharp lines of *H*, *Fe* II, *Ti* II, *Fe* I, *Sr* II, *Ca* I, *Ca* II, *Cr* II, *Sc* II, and perhaps a few other atoms characteristic of type A, does not completely hide from view the lines of the reversing layer, consisting of hydrogen wings broadened by Stark effect, of *Mg* II 4481 and of *Si* II. These lines give a radial velocity of around +20 km/sec. The expanding shell contains little *Mg* II 4481—a phenomenon which is believed to be due to the dilution of the exciting radiation.

The lines of the shell undergo large variations in structure and in intensity. Sometimes they become double, evidently as a result of the formation of a new shell which has a larger velocity of expansion. In the earlier work the suggestion was made that the outbursts occur at intervals of about 155 days, but the material was not sufficient to determine whether the phenomena are periodic.

The relative intensities of the lines of separate multiplets are such as to suggest large turbulence in the expanding shell. The square root of the mean value of the squares of the radial velocity components of the turbulent motions is 67 km/sec. This is the largest turbulence known in any stellar atmosphere.

Regular observations of 17 Leporis were begun at the Yerkes Observatory in 1928, and a discussion of the spectral changes during a typical outburst[1] and results of measurements of the first 45 spectrograms[2] were published by Struve in 1930 and 1932. A total of 97 additional spectrograms, taken with the Bruce spectrograph attached to the 40-inch refractor, have been obtained since 1932. This discussion is based on measurements of the entire series of 142 plates.

During the period 1930–1941 a number of outbursts were observed, some of which were minor and did not last more than a week, while others were severe and persisted for over a month before the lines became normal. Table 1 shows the time of beginning of outbursts which were best determined. A typical outburst proceeds about as follows: The absorption lines of the metals, which in 17 Leporis consist principally of lines of *Fe* II and *Ti* II, begin to show broadening, with diffuse wings, and the fainter lines become weakened. Some lines then begin to shade to the violet, indicating that they are about to split into two components. This feature usually occurs first in *Fe* II lines, while *Ti* II lines follow soon after and *Sc* II last. Next, certain of the lines appear double,

[1] *Ap. J.*, **72**, 343, 1930. [2] *Ibid.*, **76**, 85, 1932.

with weak violet components and sharp, narrow red components with sharp edges on the red side. The violet components increase in intensity, while the red components tend to decrease, so that soon the violet components equal or exceed the red components in intensity. Finally, the two lines coalesce into a broadened line. The broadening gradually lessens until the line is normal again. On some plates a faint emission border on the red edge of a few of the stronger lines was observed during outbursts. The spectral changes are sometimes, but not always, accompanied by a decrease in the average radial velocity of the metallic lines from around -30 or -40 km/sec at the beginning to about -60 or -70 km/sec at the end of the outburst. The radial velocity of the violet components during an outburst decreases very rapidly and may reach -170 km/sec, but these high velocities do not persist for more than a few days. It is probable that the

TABLE 1

TIME OF BEGINNING OF OBSERVED OUTBURSTS AS DETERMINED FROM OBSERVATIONS AT OR NEAR THE DATE WHEN DOUBLING OF LINES FIRST APPEARED

TIME OF BEGINNING		INTERVAL, IN DAYS, TO NEXT OBSERVED OUTBURST	NOTES
JD 242+	Date		
6265.....	1930, Oct. 14	3×156	First plate (Oct. 19) shows outburst had begun; Oct. 20 plate shows many double lines
6733.....	1932, Jan. 25	2×166	Jan. 20, *Fe* II lines shade to violet; Jan. 25, doubling beginning
7065.....	1932, Dec. 22	2×139.5	Dec. 22 plate shows doubling; on Dec. 26 several lines were double
7344.....	1933, Sept. 27	5×156	First plate (Sept. 29) shows several double lines
8124.....	1935, Nov. 16	5×143	Only one plate available, taken on Nov. 23; shows outburst well under way
8840.....	1937, Nov. 1	5×156	On Oct. 31 lines were broad and weak; on Nov. 2 doubling had begun
9622.....	1939, Dec. 25	2×136.5	One plate, taken at McDonald Observatory on Jan. 1, 1940, showed outburst well under way; no other plates available
9895.....	1940, Sept. 21	145	Sept. 23 plate shows four double lines; no earlier plates available
10040.....	1941, Feb. 13	2×169	On Feb. 10 many lines showed broadening; on Feb. 15, outburst was under way with many double lines
10379.....	1942, Jan. 18		On Jan. 13 a few lines shade to violet; Jan. 23 plate shows several doubles and lines broadened and weakened

doubling stage represents the throwing-off of a new shell or layer at a high negative velocity, while the radial velocity observed during the normal stage is the normal outward velocity of the shell. The radial velocity of the reversing layer is around $+20$ km/sec.

The duration of a typical outburst varies from 20 to 40 days from the beginning of doubling to the return of the lines to normal intensity and breadth. The duration of the period of doubled lines is usually from 1 to 3 weeks.

THE PERIOD

It is difficult to determine the exact time of beginning of an outburst, but for the purpose of this discussion it is assumed to be the date on which a definite splitting of the lines into two components begins, having been preceded by broadening and shading toward the violet. We were able to fix this date rather definitely in the case of the 10 outbursts shown in Table 1, although there was an uncertainty of several days. From

these results it appears that the period for the 10 outbursts varied between a minimum of 136 days and a maximum of 169 days. The actual variation must have been greater than this, because the beginning of all outbursts could not be determined and the period was computed in all but one case by averaging over two or more cycles. Thus, if it is assumed that there was an intermediate outburst in the interval between January 25, 1932, and December 22, 1932, it is extremely unlikely that it would have occurred exactly at the mean of 166 days. It is, of course, not certain that there was an intermediate outburst.

We next consider whether the dates of expected outbursts, based on Table 1, are consistent with the observations. The dates on which additional outbursts might be expected, as far as there are any observations available, are shown in Table 2. We con-

TABLE 2

TIME OF BEGINNING OF EXPECTED OUTBURSTS

BEGINNING OF EXPECTED OUTBURST ON BASIS OF TABLE 1		OBSERVATIONS
JD 242+	Date	
6421	1931, Mar. 19	One weak plate on JD 6405 shows some indication of doubling, and the next plate on JD 6433, which is also weak, shows some double lines; no additional plates are available; an outburst may have occurred on about JD 6421
6577	1931, Aug. 23	There are no plates from JD 6433 (Mar. 31) to JD 6592 (Sept. 6); the latter plate shows no evidence of an outburst 15 days earlier, but a weak outburst may have occurred at that date
7500	1934, Mar. 2	There was no definite outburst at this time, although some indication toward doubling was present on Feb. 9 and 10, 1934; if this is to be considered as an outburst, it was exceedingly weak
9308	1939, Feb. 13	Two plates are available, at JD 9321 and JD 9322; these plates show no doubling, although some lines are slightly broadened and diffuse. If there was an outburst it may have occurred a few days earlier than JD 9308, say, at JD 9300

clude that in view of the irregularity in the occurrence of observed outbursts, showing that the phenomenon is not strictly periodic, there is no disagreement between times of expected outbursts and the actual occurrence of outbursts.

It is clear that the outbursts are not strictly periodic. In October, 1932 (JD 2427000), the lines were clearly double. This is 65 days before the outburst on December 22, 1932 (JD 2427065), and contradicts the results from other cycles. We have no observations between October 20 and December 22. It is possible that the state of disturbance lasted throughout this long interval. But, if so, the outburst was entirely different from the normal. The presence of only a weak indication of an outburst near JD 2427500 is also in contradiction to the average period of about 150 days.

All we can say is that major outbursts occur at irregular intervals spaced roughly 150 days apart. But the outbursts are not similar in intensity or in duration. Small disturbances, shown only by a violet shading of the stronger *Fe* II lines, occur frequently and may last for weeks or months, while at other times the lines remain sharp and symmetrical for long intervals.

TABLE 3

Radial Velocities of 17 Leporis *

Date (U.T.)	Qual	H	Ti II	Fe II	Fe I	Sr II	Ca II	Ca I	Cr II	Sc II	Mg II	Si II
1932 Sept. 23.42	p	- 76 (2) 107 β	- 39 (14) 117 (4)	- 48 (13) 121 (1)					- 67 (2)	- 41 (2)	-26 (1)	
1932 Oct. 12.43	f	64 (3) 82 β	40 (16) 119 (3)	51 (14) 121 (2)					49 (3)	62 (1)	+13 (1)	
1932 Oct. 17.41	f	71 (3) 72 β	39 (16) 106 (1)	42 (16) 165 (1)					48 (2)	22 (3)	+13 (1)	
1932 Oct. 20.38	p	83 (3) 109 β	33 (11) 117 (5)	40 (10) 136 (3)					40 (2)	16 (1) 73 (1)	+30 (1)	
1932 Dec. 22.24	p	152 (1) 152 β	67 (8) 172 (1)	73 (8)					43 (1)			
1932 Dec. 26.24	f	112 (2) 118 β	67 (16) 124 (1)	59 (14) 141 (2)	- 35 (1)				70 (1)	50 (1)	+11 (1)	
1933 Jan. 1.23	g	88 (3) 52 β	50 (22) 126 (3)	63 (17) 128 (1)	36 (1)		-129 (1)		36 (1)	47 (1)	+18 (1)	
1933 Jan. 4.22	p	128 (2) 113 β	50 (2) 147 (1)	48 (7) 136 (4)						73 (2)	+12 (1)	
1933 Jan. 7.23	f	72 (2)	46 (16) 159 (8)	65 (9) 182 (5)	64 (2)				54 (2) 195 (1)	46 (1)	+28 (1)	
1933 Jan. 12.20	f	80 (2)	60 (19) 129 (4)	67 (17) 156 (13)	32 (2)				75 (3)	51 (3)	+28 (1)	
1933 Jan. 24.23	g	111 (2)	59 (21)	65 (16)	85 (5)				58 (6)	52 (3)	+12 (1)	
1933 Feb. 3.13	f	69 (3) 84 β	50 (20)	48 (15)	69 (3)				52 (2)	26 (2)	+ 5 (1)	
1933 Feb. 9.12	g	68 (3) 80 β	55 (29)	50 (17)	62 (7)	- 50 (1)	- 75 (2)	-51 (1)	33 (7)	40 (3)	+15 (1)	
1933 Feb. 15.11	f	86 (3) 90 β	58 (21)	57 (15)	- 63 (3)			-61 (1)	57 (3)	43 (3)	+17 (1)	
1933 Feb. 23.12	f	110 (3) -110 β	- 52 (18)	- 52 (17)					- 62 (2)	- 42 (4)	+ 5 (1)	

TABLE 3 -- Continued

Date (U.T.)	Qual	H	Ti II	Fe II	Fe I	Sr II	Ca II	Ca I	Cr II	Sc II	Mg II	Si II
1933 Sept. 29.44	g	- 90 (3) 113 β	- 56 (19) 135 (7)	- 76 (19)	- 47 (2)		-109 (2)	-86 (1)	- 48 (2)	- 39 (2)	+11 (1)	
1933 Oct. 11.44	g	88 (3) 98 β	55 (20) 138 (3)	59 (14) 145 (2)	85 (7)	-65 (1)	116 (2)		43 (3)	38 (3)	+15 (1)	
1933 Oct. 14.42	f	125 (1) 125 β	50 (12) 152 (2)	66 (10) 152 (2)					62 (3)	53 (2)	- 9 (1)	
1933 Oct. 17.36	f	133 (3) 123 β	73 (9) 150 (4)	63 (13) 146 (5)					66 (2)	33 (1)	+ 8 (1)	
1933 Oct. 18.36	g	120 (2) 133 β	72 (16) 127 (2)	86 (11)	23 (1)				79 (1)	85 (1)	+35 (1)	+37 (1)
1933 Oct. 25.35	f	116 (3) 116 β	52 (17) 121 (6)	61 (15) 138 (3)		73 (1)			57 (2)	46 (2)	+18 (1)	
1933 Oct. 25.44	g	106 (3) 101 β	60 (17) 155 (2)	62 (17) 141 (4)	10 (2)	24 (1)			38 (2)	57 (2)	+31 (1)	
1933 Oct. 31.35	p	93 (2) 110 β	49 (12) 102 (3)	63 (12)					72 (3)	53 (3)	+ 5 (1)	
1933 Nov. 28.33	g	81 (3) 101 β	50 (24)	55 (19)	58 (3)		97 (1)	55 (1)	51 (6)	49 (5)	+19 (1)	
1933 Nov. 30.39	p	94 (1) 94 β	45 (20)	54 (14)				40 (1)	41 (2)	53 (1)	+20 (1)	
1933 Dec. 18.34	p	63 (3) 83 β	43 (18)	49 (15)				53 (1)	49 (2)	40 (2)	+43 (1)	
1933 Dec. 25.28	f	63 (3) 74 β	41 (29)	44 (18)	48 (3)		37 (2)	39 (1)	34 (3)	38 (2)	+13 (1)	
1934 Jan. 16.24	g	51 (3) 60 β	36 (26)	34 (16)	43 (2)		122 (1)	17 (1)	39 (4)	20 (4)	+20 (1)	
1934 Jan. 21.19	g	52 (3) 62 β	26 (24)	28 (16)	20 (6)	-23 (1)				27 (5)	+24 (1)	85 (1)
1934 Jan. 26.16	f	36 (3) 56 β	27 (21)	26 (14)	50 (2)		37 (1)	35 (2)	35 (3)	15 (3)	+39 (1)	+36 (1)
1934 Jan. 30.19	g	57 (3) - 73 β	- 38 (21)	37 (16) - 90 (1)	- 67 (3)		- 49 (2)	-17 (1)	- 37 (4)	- 43 (4)	+41 (1)	

TABLE 3 -- Continued

Date (U.T.)	Qual.	H	Ti II	Fe II	Fe I	Sr II	Ca II	Ca I	Cr II	Sc II	Mg II	Si II
1934 Feb. 9.15	g	- 65 (3) 63 β	- 37 (21) 128 (1)	- 36 (17) 102 (3)	- 29 (1)		- 53 (2)	-14 (1)	- 32 (4)	- 23 (2) 101 (1)	+14 (1)	
1934 Feb. 10.17	f	67 (3) 73 β	29 (21) 80 (2)	40 (16) 97 (2)	65 (2)		41 (2)	42 (2)	45 (3)	27 (3)	+ 6 (1)	
1934 Feb. 13.13	g	60 (3) 65 β	29 (20)	33 (13)	38 (4)	-32 (2)	68 (1)	4 (1)	37 (2)	15 (2)	+ 1 (1)	
1934 Feb. 15.09	g	69 (3) 87 β	45 (19)	51 (12)	45 (2)	68 (1)	71 (2)	25 (1)	72 (4)	34 (4)	- 5 (1)	+23 (1) 95 (1)
1934 Feb. 18.15	p	34 (1) 34 β	43 (9)	42 (5)							+29 (1)	
1934 Feb. 19.08	f	86 (3) 66 β	43 (19) 116 (2)	55 (16)	47 (2)		67 (2)	40 (1)	42 (3)	38 (4)	-20 (1)	29 (1)
1934 Feb. 23.15	g	78 (3) 87 β	56 (20)	57 (11)	70 (7)		93 (1)	55 (1)	53 (3)	53 (3)	+ 9 (1)	
1934 Feb. 24.09	g	69 (3) 79 β	52 (21)	55 (13)	47 (3)		62 (2)	49 (1)	57 (1)	42 (3)	+13 (1)	
1934 Feb. 27.08	g	62 (3) 56 β	50 (21)	47 (14)	44 (4)	43 (1)		40 (1)	70 (3)	37 (2)	-28 (1)	
1934 Mar. 1.06	f	57 (3) 61 β	42 (20) 151 (1)	50 (16)	53 (2)				32 (2)	40 (3)	+ 8 (1)	
1934 Mar. 5.13	p	70 (3) 79 β	57 (17)	64 (12)					51 (2)	47 (3)	-35 (1)	
1934 Mar. 9.06	p	101 (1) 101 β	47 (7)	62 (7)					70 (2)		+40 (1)	
1934 Sept. 26.41	p		33 (9)	53 (2)					33 (1)			
1934 Oct. 2.45	p	46 (3) 49 β	24 (20)	32 (14)	33 (4)	38 (1)		34 (1)	31 (2)	25 (5)	+28 (1)	95 (1)
1934 Oct. 7.40	g	39 (3) 59 β	25 (26)	27 (17)	25 (5)		63 (1)	15 (1)	23 (4)	27 (3)	+ 3 (1)	+31 (1)
1934 Oct. 8.46	g	36 (3) 96 β	26 (22)	28 (15)	31 (3)			2 (1)	20 (3)	28 (2)	0 (1)	
1934 Oct. 12.38	g	77 (3) -107 β	- 31 (22)	- 42 (14)	- 25 (3)	-19 (1)	- 61 (2)	-37 (1)	- 37 (3)	- 18 (3)	+ 4 (1)	

TABLE 3 -- Continued

Date (U.T.)	Qual	H	Ti II	Fe II	Fe I	Sr II	Ca II	Ca I	Cr II	Sc II	Mg II	Si II
1934 Oct. 13.40	g	- 81 (3) 98 β	- 34 (19)	- 40 (16)	- 13 (3)			-27 (1)	- 39 (2)	- 16 (4)	+17 (1)	
1934 Oct. 30.34	g	70 (3) 74 β	31 (20)	33 (15)	28 (3)		- 83 (2)	15 (1)	31 (2)	18 (3)	-10 (1)	+44 (1)
1934 Nov. 15.35	f	122 (2)	50 (14) 81 (2)	49 (17)			+ 8 (1)	25 (1)	44 (3)	35 (2)	- 7 (1)	18 (1)
1935 Feb. 27.10	g	85 (3) 93 β	56 (20)	58 (15)	66 (2)		- 79 (2)	43 (1)	64 (2)	39 (5)	+25 (1)	
1935 Oct. 15.45	g	98 (3) 102 β	68 (18)	71 (13)				80 (1)	67 (2)	56 (3)	+14 (1)	51 (1)
1935 Oct. 20.43	f	82 (3) 75 β	65 (17)	69 (14)			68 (2)		77 (2)	54 (1)	+10 (1)	+67 (1)
1935 Nov. 23.32	f	123 (3) 121 β	67 (10) 119 (1)	79 (12) 122 (1)			116 (2)			44 (2)	+33 (1)	
1937 Sept. 7.43	p	74 (1) 74 β	46 (5)	45 (2)	20 (1)			84 (1)	37 (1)		-24 (1)	
1937 Sept. 13.43	p	104 (2) 80 β	47 (15) 132 (1)	50 (11)	12 (1)				42 (1)	26 (2)	+24 (1)	
1937 Sept. 21.41	p		34 (8)	34 (8)					53 (1)	45 (2)		
1937 Sept. 22.44	p	134 (1)	28 (13) 104 (1)	29 (7) 108 (1)	7 (1)					27 (1)		
1937 Sept. 26.45	p	74 (2) 123 β	32 (13)	40 (9)	32 (1)				47 (5)	20 (2)	+20 (1)	
1937 Sept. 27.44	f	54 (3) 78 β	39 (18)	37 (14)	31 (3)		99 (2)	30 (1)	32 (4)	18 (5)	- 2 (1)	
1937 Oct. 15.45	p	106 (1) 106 β	46 (10)	43 (13)				48 (1)	50 (2)	24 (1)	+39 (1)	
1937 Oct. 31.36	f	103 (3) 137 β	25 (18)	36 (11)	- 42 (1)		40 (1)	80 (1)	90 (1)	54 (2)	-13 (1)	
1937 Nov. 2.38	f	97 (3) 89 β	26 (17) 109 (1)	30 (13) 91 (1)			62 (1)	-15 (1)	22 (1)	19 (1)	-35 (1)	
1937 Nov. 21.33	p	120 (2) -134 β	- 60 (15)	- 85 (10)			-125 (1)		- 72 (4)	- 74 (2)	+ 3 (1)	

TABLE 3 -- Continued

Date (U.T.)	Qual	H	Ti II	Fe II	Fe I	Sr II	Ca II	Ca I	Cr II	Sc II	Mg II	Si II
1937 Nov. 26.34	p	-124 (3) 111 β	- 58 (14)	- 65 (11)				-53 (1)	- 71 (2)	-121 (1)	-20 (1)	
1939 Feb. 25.06	f	71 (3) 70 β	38 (16)	54 (12)				45 (1)	50 (2)	40 (4)	-20 (1)	
1939 Feb. 26.05	g	80 (3) 93 β	53 (19)	61 (11)	- 41 (1)		- 54 (1)		25 (1)	34 (1)	- 6 (1)	
1940 Sept. 20.42	p	165 (1) 165 β	77 (11)	64 (9)							- 6 (1)	
1940 Sept. 23.42	p	88 (3) 32 β	56 (17) 147 (1)	61 (15) 147 (2)	63 (2) 144 (1)				42 (3)	52 (3)	+44 (1)	
1940 Oct. 2.44	p	76 (3) 120 β	37 (12) 157 (3)	53 (13) 126 (1)					28 (2)	30 (2)	+20 (1)	
1940 Oct. 23.41	f	105 (3) 121 β	79 (17)	77 (15) 111 (2)	79 (2)			77 (1)	83 (3)	61 (2)	+34 (1)	
1940 Nov. 3.39	f	95 (3) 138 β	66 (15)	76 (15)	74 (2)		134 (2)		78 (4)	72 (1)	+22 (1)	
1940 Nov. 25.32	p	103 (3) 140 β	68 (18)	70 (14)	54 (3) 131 (1)		134 (2)		57 (1)	52 (3)	- 2 (1)	+ 1 (1)
1940 Dec. 3.38	g	143 (2) 131 β	53 (12)	63 (14)	65 (2)				68 (2)	48 (2)	+26 (1)	
1941 Feb. 10.13	g	97 (3) 99 β	29 (23)	35 (16)	30 (1)	-23 (1)		19 (1)	26 (4)	24 (2)	+13 (1)	30 (2)
1941 Feb. 15.08	g	39 (3) 87 β	19 (22) 150 (9)	28 (13) 138 (5)	24 (4)			13 (1)	21 (1)	20 (3) 166 (1)	+21 (1)	
1941 Feb. 16.08	f	92 (3) 128 β	27 (26) 134 (6)	29 (15) 139 (7)	47 (5)	29 (1)	92 (2)	22 (1)	40 (4)	29 (3)	+15 (1)	+ 6 (1)
1941 Feb. 16.12	f	107 (3) 103 β	28 (21) 132 (4)	37 (15) 139 (4)	29 (5)		- 83 (2)	8 (1)	21 (3)	38 (3)	+24 (1)	
1941 Feb. 26.02	f	82 (3) 80 β	40 (15) 96 (3)	50 (15) 97 (2)	43 (3)			21 (1)	48 (5)	25 (2) 77 (1)	+18 (1)	-35 (1)
1941 Feb. 26.07	f	88 (1) 88 β	39 (17) 125 (4)	49 (11) 94 (2)	- 23 (1)			- 3 (1)	58 (4)	18 (3)	+ 6 (1)	
1941 Feb. 28.05	p	82 (2) - 92 β	45 (17) -161 (1)	- 50 (14)		-28 (1)			- 38 (5)	- 38 (1)	+46 (1)	

TABLE 3 -- Continued

Date (U.T.)	Qual	H	Ti II	Fe II	Fe I	Sr II	Ca II	Ca I	Cr II	Sc II	Mg II	Si II
1941 Mar. 1.04	g	- 73 (3) 75 β	- 52 (22)	- 52 (19) 87 (2)	- 30 (4)		- 64 (1)	-37 (1)	- 52 (3)	- 45 (2)	+16 (1)	
1941 Mar. 13.07	g	56 (3) 65 β	40 (26)	42 (19) 144 (1)	36 (2)			58 (1)	39 (6)	27 (3)	+24 (1)	
1941 Mar. 23.07	p	93 (1) 93 β	53 (16)	54 (11)				56 (1)	47 (4)	38 (2)	+19 (1)	
1941 Mar. 25.07	g	87 (3) 88 β	43 (26) 72 (1)	52 (22)	54 (4) 78 (1)	- 35 (1)	- 89 (1)	29 (1)	51 (6)	44 (5)	+10 (1)	
1941 Nov. 18.35	f	55 (2) 71 β	45 (13)	56 (10) 119 (1)					30 (3)	55 (1)	+31 (1)	
1941 Dec. 6.36	g	43 (2) 53 β	47 (16)	48 (14)	87 (1)			36 (1)	42 (2)	26 (5)	+11 (1)	
1941 Dec. 11.21	g	62 (2) 63 β	46 (16)	56 (13)				55 (1)	36 (5)	39 (6)	+ 4 (1)	
1941 Dec. 14.24	g	71 (3) 57 β	42 (18)	41 (16)	50 (1)			32 (1)	30 (3)	43 (4)	+ 6 (1)	
1941 Dec. 20.30	f	66 (1) 66 β	47 (16)	54 (14)				26 (1)	55 (3)	25 (3)	-17 (1)	
1942 Jan. 4.20	g	92 (2) 117 β	43 (15)		41 (1)				45 (3)	38 (2)	+26 (1)	
1942 Jan. 5.22	g	72 (2) 113 β	47 (18) 120 (1)	57 (10)	- 5 (1)				52 (2)	34 (2)	+19 (1)	+21 (1)
1942 Jan. 6.18	g	88 (3) 111 β	29 (13) 140 (1)	33 (15) 88 (1)				-43 (1)	31 (1)	49 (3)	+21 (1)	
1942 Jan. 13.17	g	111 (3) 104 β	47 (20) 118 (2)	54 (14)					54 (3)	32 (3)	+21 (1)	
1942 Jan. 23.13	g	83 (3) 74 β	55 (14) 107 (7)	63 (12)					33 (2) 85 (1)	49 (3)	+ 4 (1)	
1942 Jan. 24.25	f	60 (3) - 74 β	47 (14) - 88 (3)	- 58 (15)					- 43 (3)	28 (2) - 81 (1)	+21 (1)	

* The radial velocities are in km/sec, with reference to the sun. The numbers of lines measured for each atom are shown in parentheses. For hydrogen the value obtained from Hβ is given in the second entry for each plate. For other atoms the second entry gives the velocity obtained from the violet components of double lines.

NOTES TO TABLE 3

Description of the spectra, as compared to the spectrum of January 2, 1929 considered as normal. The descriptions refer to Fe II and Ti II absorption lines unless otherwise stated.

1932 Sept. 23 - Lines broadened; some shading toward violet and some doubling. Mg II 4481 broadened.

1932 Oct. 12 - Lines greatly broadened. Several doubles. Red emission borders at several strong Fe II lines.

1932 Oct. 17 - Lines broadened and somewhat hazy with fairly sharp red edges. Two doubles.

1932 Oct. 20 - Poor plate. Lines still broadened, but symmetrical. Several doubles.

1932 Dec. 22 - Poor plate. Doubling beginning.

1932 Dec. 26 - Poor plate. Abnormal stage has begun with some lines shading to the violet and several double lines.

1933 Jan. 1 - Strong outburst under way. Lines which are not double are much broadened. Red component of double lines very sharp and narrow.

1933 Jan. 4 - Poor plate. Many lines appear diffuse. Five doubles.

1933 Jan. 7 - Poor plate. Fainter lines are weakened. Many lines double.

1933 Jan. 12 - Outburst continues. Many doubles. Violet components are equal in intensity to red components, except in the case of Sc II 4246. Mg II 4481 broad. A few of the stronger Ti II and Fe II lines show faint emission borders on the red edge.

1933 Jan. 24 - Lines broad and symmetrical. Mg II 4481 broad.

1933 Feb. 3 - Normal stage. Lines symmetrical. Hβ rather narrow.

1933 Feb. 9 - Normal.

1933 Feb. 15 - All lines narrow.

1933 Feb. 23 - Weak plate. Some lines show shading toward the violet: some lines are broadened.

1933 Sept. 29 - Strong outburst. Doubling has begun. Fainter lines are weakened. H lines sharp on red and shade to violet. Hδ very broad. A few of the stronger Fe II and Ti II lines show faint emission borders on the red side.

1933 Oct. 11 - Red components of double lines are strong and narrow. Violet components still weak. Hδ very strong.

1933 Oct. 14 - The stronger lines which are not double show some shading to violet. Red components are sharp.

1933 Oct. 17 - Doubling continues, but violet and red components are about equal. Hδ appears double.

1933 Oct. 18 - Violet components are strengthened.

1933 Oct. 25 - Lines broad and symmetrical with diffuse wings. Many red and violet components have coalesced.

1933 Oct. 31 - Lines not quite so broad. Mostly symmetrical.

1933 Nov. 28 - Normal.

1933 Nov. 30 - Normal. H lines are diffuse.

NOTES TO TABLE 3 -- Continued

1933 Dec. 18 - Normal.

1933 Dec. 25 - Normal.

1934 Jan. 16 - Normal.

1934 Jan. 21 - Normal.

1934 Jan. 26 - Lines mostly narrow. Some show slight shading to violet.

1934 Jan. 30 - Same.

1934 Feb. 9 - Several lines are slightly double; but not much fading. Hδ looks double.

1934 Feb. 10 - Ca II 3933 has faint central emission. Hδ looks double with red component stronger than violet.

1934 Feb. 13 - Lines normal except for some slight shading toward the violet. Mg II 4481 narrow.

1934 Feb. 15 - Lines slightly broadened. H strong. Mg II 4481 broad.

1934 Feb. 18 - Poor plate.

1934 Feb. 19 - Lines distinctly broadened.

1934 Feb. 23 - Many lines broadened.

1934 Feb. 24 - Normal.

1934 Feb. 27 - Several lines slightly broadened.

1934 Mar. 1 - Lines slightly broadened but no apparent shading to violet. Mg II 4481 broad.

1934 Mar. 5 - Normal.

1934 Mar. 9 - Poor plate.

1934 Sept. 26 - Poor plate.

1934 Oct. 2 - Normal.

1934 Oct. 7 - Mg II 4481 narrow and sharp.

1934 Oct. 8 - Mg II 4481 diffuse.

1934 Oct. 12 - Normal. H strong.

1934 Oct. 13 - Lines slightly weakened.

1934 Oct. 30 - The stronger lines of Ti II and Sc II are sharp and narrow. Some lines shade to violet slightly. H strong. Mg II 4481 broadened.

1934 Nov. 15 - All lines are broadened, but are mostly symmetrical. A few lines shade to violet. Mg II 4481 broad and well defined.

1935 Feb. 27 - Normal.

1935 Oct. 15 - Normal.

1935 Oct. 20 - Normal.

1935 Nov. 23 - All lines are broadened, and the fainter lines are weakened. Fe II 4233 and Ti II 4468 double and may show faint emission borders on red edge. Fe II shows stronger violet components than Ti II. Sc II 4246 shades towards the violet.

1937 Sept. 7 - Poor plate.

1937 Sept. 13 - Poor plate.

NOTES TO TABLE 3 -- Continued

1937 Sept. 21 - Poor plate.

1937 Sept. 22 - Poor plate.

1937 Sept. 26 - Poor Plate.

1937 Sept. 27 - Normal.

1937 Oct. 15 - Poor Plate.

1937 Oct. 31 - Several lines broadened and weakened with some shading of Fe II lines to violet. H strong.

1937 Nov. 2 - Shading to violet more pronounced with diffuse wings. Two doubles. Abnormal stage beginning.

1937 Nov. 21 - Normal.

1937 Nov. 26 - Normal.

1939 Feb. 25 - Normal.

1939 Feb. 26 - Normal.

1940 Sept. 20 - Poor plate.

1940 Sept. 23 - Poor plate. Outburst beginning. Broad weak lines with four doubles and others shading toward the violet. Fe II lines show doubling most distinctly. H strong.

1940 Oct. 2 - Most lines broadened. Red component of some lines sharp and narrow. Fe II 4233, Fe II 4584 and Fe II 4549 show slight emission borders on red edge.

1940 Oct. 23 - Lines broadened, but mostly symmetrical. Mg II 4481 appears double.

1940 Nov. 3 - Lines broadened, but symmetrical. Mg II 4481 narrow. Hβ strong.

1940 Nov. 25 - Lines narrow.

1940 Dec. 3 - All lines narrow. Some Fe II lines shade toward violet. Hβ very strong.

1941 Feb. 10 - Most lines narrow. Fe II 4233 about to split. Sc II 4246 also shows signs of doubling. H strong.

1941 Feb. 15 - Strong outburst, many doubles. Red components are very sharp. Hβ strong. Hγ and Hδ may have central emission. Ti II 4468 and Fe II 4584 give indications of faint emission on the red edge.

1941 Feb. 16 - Same.

1941 Feb. 26 - Violet components have increased in intensity and equal red components. Outburst continues. Hβ shows a faint emission border on red edge. Fe II 4584 is double with a faint emission border on red component. Ti II 4395 and Fe II 4549 show faint emission borders.

1941 Feb. 28 - Weak plate. Most lines appear single but somewhat diffuse.

1941 Mar. 1 - Lines normal. Hβ shows emission border on red edge.

1941 Mar. 13 - One double line, otherwise normal.

1941 Mar. 23 - Normal.

1941 Mar. 25 - Slight shading of some lines toward violet with sharp edge on red side.

1941 Nov. 18 - Normal.

1941 Dec. 6 - Some lines slightly broadened.

1941 Dec. 11 - Normal.

NOTES TO TABLE 3 -- Continued

1941 Dec. 14 - H lines strong and diffuse.

1941 Dec. 20 - Some metallic lines weakened and broadened.

1942 Jan. 4 - Many lines shade to violet. H very strong.

1942 Jan. 5 - Same.

1942 Jan. 6 - Shading to violet not so pronounced. H still very strong. Mg II 4481 broadened.

1942 Jan. 13 - Most lines normal. A few lines shade to the violet. H strong.

1942 Jan. 23 - Lines generally weakened and broadened. Double lines show violet component slightly stronger than red component. H strong.

1942 Jan. 24 - Lines still weakened and broadened. Doubling is about over. H normal.

RADIAL VELOCITIES

Table 3 gives a summary of the measurements of radial velocities of all plates taken since March, 1932. This table is similar to Table 2 of the previous paper by Struve[2] and covers the period from September, 1932, to February, 1942. The radial velocities are given in km/sec with reference to the sun. The numbers of lines measured for each atom are shown in parentheses, and the radial velocity shown is the mean of all lines measured per atom. The lines are often double, but in a few cases the duplicities recorded in Table 3 may not be real. The radial velocity of $H\beta$ is given, as well as that for the mean of $H\beta$, $H\gamma$, and $H\delta$. On some plates one or more of the H lines appeared to be double, but no measurements were made of the two components. The *Ca* II lines H and K are very broad and diffuse and occasionally appear to be double. In the few cases where certain lines appeared to have faint emission borders no measurements of the radial velocity of the emissions were attempted.

Measurements of radial velocities of *Si* II 4128 and *Si* II 4131 are of interest, because it is probable that these lines originate mainly in the reversing layer in a manner similar to the line *Mg* II 4481. The *Si* II lines, however, are very faint and diffuse, and *Si* II 4128 is blended with *Fe* II. These lines are visible on only a few plates. For this reason the measurements shown for *Si* II are subject to greater error than those of *Mg* II 4481, but they agree fairly well, within the limits of error, with the measurements of the *Mg* II line. The mean velocity from *Si* II is about +30 km/sec. There are small, but real, changes in the velocity, intensity, and contour of *Mg* II 4481. The radial velocity is, on the average, about +20 km/sec.

It is possible that absorption lines of a few additional elements, such as *Y* II, *V* II, *Mn* II, and perhaps *He* I are visible on a few plates, but the identifications are doubtful.[3] The notes to Table 3 give a description of the spectrum, with special regard to the character of the lines.

CYCLES

Although there is no true periodicity, there is a certain similarity in the manner in which the radial velocities change during and after a conspicuous outburst. Figure 1 shows a composite plot of the outbursts listed in Table 1, with the addition of a weak outburst, which may have started on February 5, 1934 (JD 2427475). The beginning epoch of each cycle was taken as in Table 1, and the observations were then plotted according to the time elapsed from the beginning of each cycle.

It will be noted that the radial velocities of *Fe* II and *Ti* II follow a fairly well-defined trend during the normal stage of about 100 days from the end of one outburst to the beginning of the next. Starting at −60 or −70 km/sec at the end of an outburst, the radial velocity increases at a fairly uniform rate, until just before the end of the cycle it is about −30 or −40 km/sec. It then begins to decrease, and the next succeeding outburst follows soon thereafter. It must be remembered that most of the lines of *Ti* II and *Fe* II were always measured single. These lines, therefore, displayed in some measure a tendency to widen unsymmetrically toward the violet, without actually splitting into two components. The violet components usually last only a short time. When they first appear they are weak. As they increase in intensity, they at first appear far toward the violet from the normal lines and then rapidly approach the latter, coalescing with them some 2 or 3 weeks after the beginning of the outburst.

Taking into account the general trend shown by the single lines of *Ti* II and *Fe* II and on the assumption that the interval between outbursts is somewhere near that shown in Table 1, additional epochs were fixed. Too much dependence should not be placed on these dates, and, in view of the contradictory evidence at JD 2427000 and JD 2427500, almost certainly some of the cycles are not correct. Nevertheless, it is use-

[3] For identifications in the ultraviolet region see *Ap. J.*, **90**, 727, 1939.

ful to divide the observations somewhat arbitrarily into a number of cycles, as shown in Table 4. Those listed in Table 1 are I, IV, VI, VIII, XIII, XVIII, XXIII, XXV, XXVI and XXVIII. The period, based on these epochs, varied from a minimum of 131 days to a maximum of 175 days.

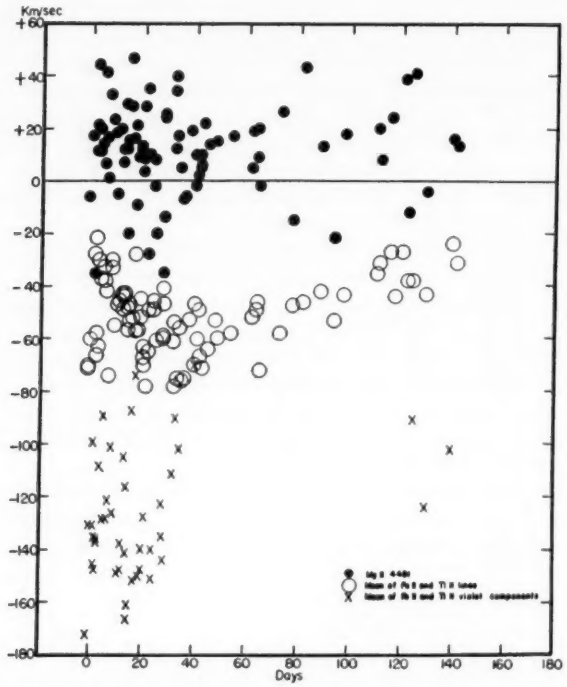

FIG. 1.—Radial velocities of *Fe* II, *Ti* II, and *Mg* II for cycles I, IV, VI, VIII, IX, XIII, XVIII, XX, and XXVI.

TABLE 4

Cycle	I	II	III	IV	V	VI	VIII	IX	X	
Epoch: JD 242+.....	6265	6421	6570	6733	6890	7065	7344	7475	7620	.....

Cycle	XI	XII	XIII	XVII	XVIII	XXI	XXIII	XXV	XXVI	XXVIII
Epoch: JD 242+.....	7790	7950	8124	8690	8840	9300	9622	9895	10040	10379

The epochs are all based on measurements of radial velocities of *Fe* II and *Ti* II lines without regard to the radial velocities of *Mg* II 4481. There is little or no correlation between the radial velocity of the *Mg* II line and that of *Fe* II and *Ti* II. The average radial velocity of *Mg* II is about +10 or +20 km/sec. Not all the scatter of the *Mg* II

points can be due to difficulty of measurement, and the radial velocity of the line undoubtedly varies, although no period has been determined.

The outbursts varied rather widely, both in radial velocities and in spectral changes. Some showed many absorption lines having violet components and others only a few. Some were of much longer duration than others, and in some the acceleration and velocity of expansion of the shell of material which was thrown off was greater than in others.

During the abnormal stage the *H* lines are strong and broad, and occasionally appear to be double. At times $H\beta$ shows a faint emission border on the red edge. On some

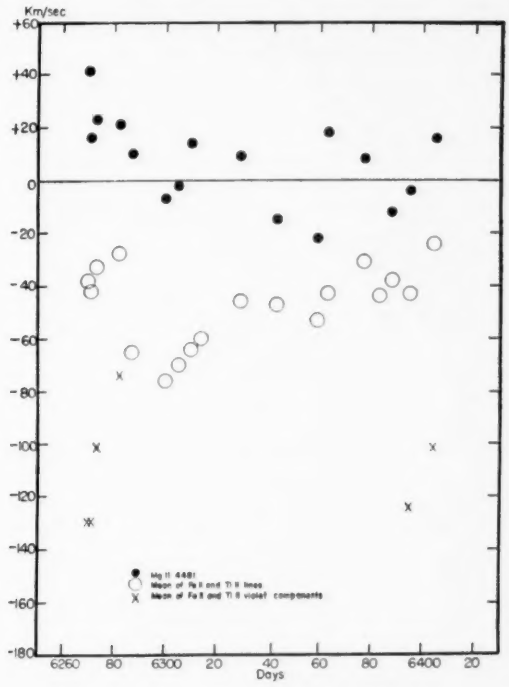

FIG. 2.—Radial velocities of 17 Leporis

plates during the abnormal stage there is an indication of an emission border on the red edge of some of the stronger metallic lines. In such cases the red border is darker than the continuum, and the red edge of the absorption line is sharp. In the case of a few strong lines, such as *Ti* II 4444, *Ti* II 4468, *Fe* II 4233, and *Fe* II 4584, an emission border has been observed on the red component during the double stage. This feature has also been observed in the ultraviolet region by Struve[4] on the spectrogram of 17 Leporis taken on January 1, 1940, at the McDonald Observatory. It is known[5] that P Cygni occasionally shows two absorption components with an emission component on the red side, and there is every reason to believe that these phenomena are of similar origin in the two stars.

[4] *Ap. J.*, **93** 504, 1941.

[5] O. C. Wilson, *Ap. J.*, **84**, 296, 1936.

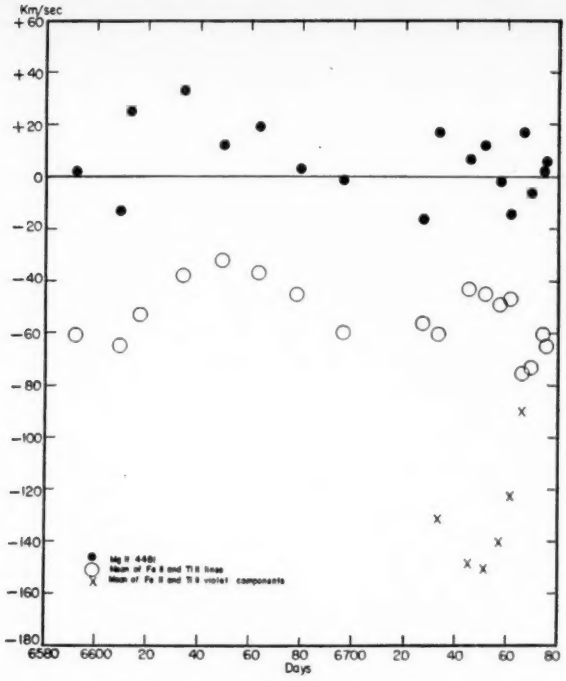

FIG. 3.—Radial velocities of 17 Leporis

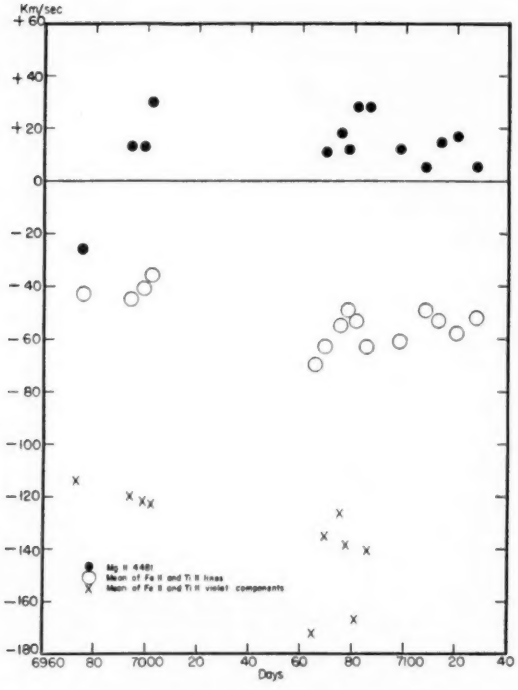

FIG. 4.—Radial velocities of 17 Leporis

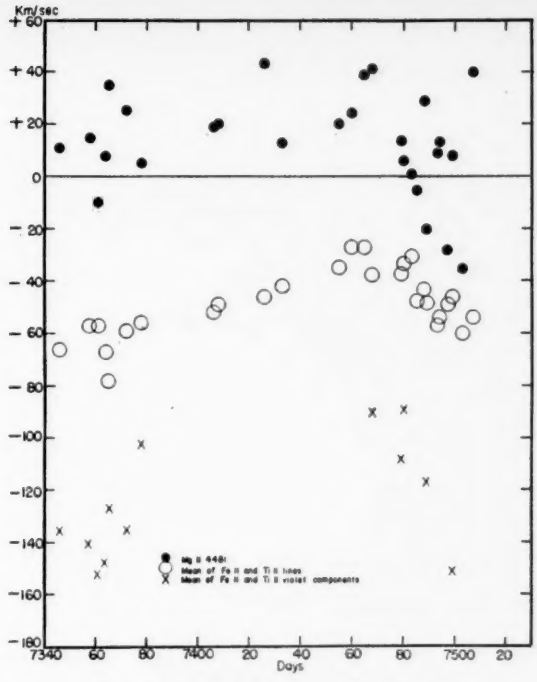

FIG. 5.—Radial velocities of 17 Leporis

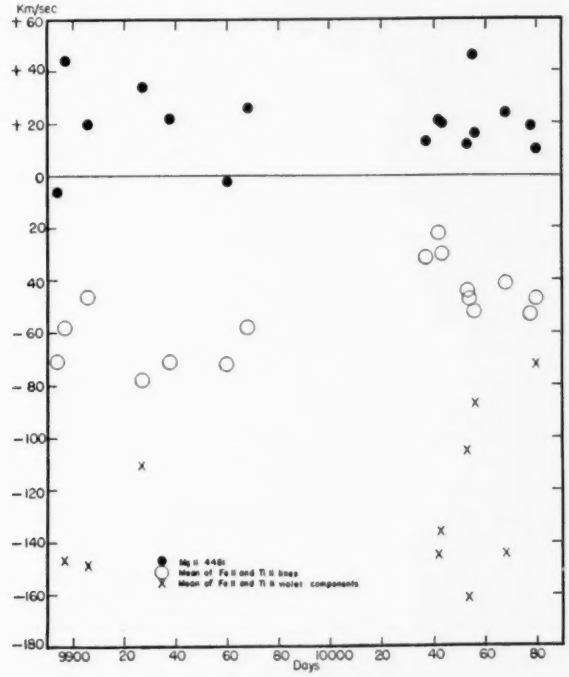

FIG. 6.—Radial velocities of 17 Leporis

SUMMARY OF OBSERVATIONS AND INTERPRETATION

1. The radial velocities of the single metallic lines of the shell undergo a slow variation within the 150-day cycle. Immediately after each outburst they give on the average -60 km/sec. The velocity then slowly increases until it reaches about -40 km/sec. Very soon after maximum velocity is reached, many lines become double, the violet components giving a velocity of about -150 km/sec. These violet components at first rapidly gain in intensity; they then decrease in intensity, and their velocity increases to about -100 to -120 km/sec, at which stage they either disappear or coalesce with the red components. The variation in velocity of the red components—identified with the single lines—may to some extent be influenced by blending.

2. The maximum intensity of the violet components in some outbursts surpassed the intensity of the remaining red components in the case of *Fe* II. In other outbursts the violet components always remained weaker than the red components. In some outbursts the separation of the components was complete, while in others the lines only became broad and diffuse. We conclude that the outbursts are not all of similar violence.

3. A remarkable feature of all typical outbursts is the fact that the splitting of the lines is always best shown by *Fe* II 4233, 4351 and by other weaker *Fe* II lines. *Ti* II shows the phenomenon less conspicuously, the violet components always being relatively weak. *Sc* II 4247 rarely shows the violet component, although in a few outbursts this component was more prominent than in others. Recalling that the ionization potentials are 16.5 volts for *Fe* II, 13.6 volts for *Ti* II, and 12.8 volts for *Sc* II, we conclude that the phenomenon may be due to increased ionization of the violet components.

4. Whenever a violet component is formed, the corresponding red component becomes weaker and sharper. This is most conspicuous for *Sc* II 4247, but the phenomenon is also present in *Ti* II and to some extent in *Fe* II. It is clear that an outburst does not consist of a new mass of gas hurled into the existing shell as an explosion from the stationary reversing layer. Rather must we think of the outburst as a sudden acceleration of a part of the existing shell, accompanied by an appreciable increase in ionization.

5. The fainter metallic lines at the time of an outburst become broader, shallower, and weaker. On the other hand, the strongest lines of *Fe* II, 4924, etc., remain at least as strong during the outburst as prior to it. The explanation is obvious: we can interpret the doubling of the lines as an increase in turbulence. A weak line, which already was on the linear portion of the curve of growth, remains on it; the total intensity remains the same, but broadening makes it appear fainter, and increased ionization may even reduce its equivalent width. A very strong line which previously was on the flat part of the curve of growth is now thrown onto the linear portion. Hence, with the same number of atoms its equivalent width must be increased.

6. The same interpretation holds in the case of *H*, which becomes very strong and broad during the outburst. In the case of *Ca* II, which is normally very strong, the increase in equivalent width is probably checked by increased ionization.

7. The fact that the central intensities of the broad, strong lines of *H* and *Ca* II remain near zero during the entire outburst suggests, rather conclusively, that the outburst does not merely affect certain areas over the disk of the star—for example, hot spots like faculae or granules on the sun—for then the continuous spectrum of the normal regions should raise the bottoms of the violet components and the continuous spectrum of the hot spots should raise the bottoms of the red components. The conclusion is that an entire layer of the shell is suddenly accelerated and at the same time subjected to increased ionization.

8. The question arises whether this layer is at the bottom or at the top of the expanding shell. The only clue to an answer is found in the fact that strong absorption lines always show larger velocities of expansion than weak lines. For example, *H*, whose lines

are very strong, shows velocities of the order of 30 or 40 km/sec more negative than *Fe* II and *Ti* II. The two strong lines of *Ca* II give velocities which are about 20 or 30 km/sec more negative than the lines of *Fe* II, *Ti* II, etc. Even within the Balmer series $H\beta$ gives a greater velocity of expansion than the mean of $H\delta$, $H\gamma$, and $H\beta$. From the new measures the difference is 8 km/sec. It is probable, but not certain, that the greater violet displacement of the stronger lines signifies an outward acceleration. If this is the case, we should be inclined to attribute the accelerated layer during the outbursts to the upper strata of the shell.

9. As far as we can tell, all elements are affected simultaneously by the acceleration, as well as by the increased ionization. Certainly this is true for *Fe* II, *Ti* II, *Sc* II, *Ca* I, and probably other elements contributing to the lines of moderate intensities. The *H* lines are so strong that the visible effects of the outburst are relatively insignificant. It is, therefore, difficult to state whether *H* is affected earlier than the other elements. The doubling takes place in an interval of a few days: on February 10, 1941, the lines were single; on February 15, they were double.

10. The outbursts are not accompanied by any conspicuous changes in the total light of the star. Yet, if the increase in ionization were to be interpreted in terms of temperature of the reversing layer, the change should be noticeable. Roughly speaking, the change in the ionization corresponds to a change in spectral class from about A5 to A0, or from $T = 10{,}000$ to $T = 13{,}000$. This would correspond to a change in bolometric brightness of 1 mag. Any actual change that may have escaped detection probably is less than 0.1 mag.

11. There are small, but real, changes in the velocity, intensity, and contour of *Mg* II 4481. The radial velocity varies between +40 and −10 km/sec. These changes take place in short intervals of a few days, but no period has been found. The line occasionally looks double. More often it is diffuse, suggesting a moderate velocity of axial rotation of perhaps 75 km/sec. Occasionally it is fairly sharp. It is probable that at least a part of the line originates in the shell; but, if so, this presumably inner layer of the shell must be almost stationary with respect to the reversing layer.

12. *Fe* II 4233 and occasionally some of the other metallic lines of the shell show faint violet extensions of the usual absorption lines. These lines are identical in character with the violet components during the outbursts. Their existence shows that even when the star fails to produce a violent outburst there is a tendency for it to shed part of the material by acceleration.

13. During the normal stage, lasting more than 100 days, the spectrum does not change much in character. Certainly, there is no marked change in ionization or in dilution effects. During an interval of 100 days the shell, having an average velocity of 50 km/sec, would have receded to a distance of 4×10^{13} cm. Assuming that the star belongs to the main sequence, as is suggested by the broad *H* lines, its radius must be of the order of 10^{11} or 10^{12} cm. Hence the dilution, as well as the ionization, would change greatly if we were dealing with a single shell expanding from the star. We must conclude that the atoms continually pass through the shell, being rendered invisible at the top through increased ionization and being replenished from the bottom by an unknown mechanism (which may resemble prominence action).

14. There are slow changes in the normal spectrum, which become apparent when we compare plates taken in different years during the normal single-line stage. Sometimes the metallic lines of the shell are very strong, while at other times they are relatively weak. These changes apparently have no effect upon the outbursts. We suspect that there are also slow changes in the intensities of the *H* absorption lines of the shell.

15. The lines of *Si* II 4128, 4131 are difficult to measure. The velocity agrees, however, with that shown by *Mg* II 4481. Hence these lines do not originate in the expand-

ing shell but come from a stationary layer below. The agreement between *Si* II and *Mg* II confirms the hypothesis of dilution: The lines of these two elements come from normal excited levels which connect with lower levels. They are reduced in intensity by dilution. All other lines measured on the Yerkes plates come from metastable levels.

16. It is difficult to explain how a single layer of the expanding shell can be suddenly accelerated and at the same time subjected to increased ionization, while other layers of the shell remain unaffected. This leads to the fundamental problem of P Cygni stars and outer shells—a subject which has been discussed elsewhere.[6]

YERKES OBSERVATORY
February 1942

[6] O. Struve, *Ap. J.*, **95**, 134, 1942.

THE STATISTICS OF THE GRAVITATIONAL FIELD ARISING FROM A RANDOM DISTRIBUTION OF STARS

I. THE SPEED OF FLUCTUATIONS

S. CHANDRASEKHAR AND J. VON NEUMANN

ABSTRACT

This paper is devoted principally to a statistical analysis of the *speed of the fluctuations* in the gravitational field acting at some fixed point in a system containing a random distribution of mass centers (stars) in motion. The solution to the problem depends on the evaluation of the moment $\overline{|f|^2}_F$ of a certain bivariate distribution $W(F, f)$ giving the probability of a force F per unit mass acting at a point and a simultaneous rate of change of F of amount f. This moment $\overline{|f|^2}_F$ is related to the *mean life* T of the state F according to the formula

$$T = \frac{|F|}{\sqrt{\overline{|f|^2}_F}} . \tag{i}$$

The statistical problem has been solved on the assumptions of a spherical distribution of the velocities v and a random spatial distribution. No other restrictions have been introduced; in particular, proper allowance has been made for a distribution over different masses, M.

It is found that if we measure $|F|$ and T in the units

$$|F| = Q_H \beta ; \qquad Q_H = 2.603\, G[\overline{M^{3/2}}]^{2/3} n^{2/3} , \tag{ii}$$

and

$$T = t_0 \tau ; \qquad t_0 = \frac{0.3201}{n^{1/3}} \frac{[\overline{M^{3/2}}]^{1/6}}{[\overline{M^{1/2}|v|^2}]^{1/2}} , \tag{iii}$$

(where G is the constant of gravitation and n is the number of stars per unit volume) we can write

$$\tau = \sqrt{\frac{\beta^{3/2} H(\beta)}{G(\beta)}} , \tag{iv}$$

where $G(\beta)$ and $H(\beta)$ are certain functions of β which have been tabulated. It is further found that, according to equation (iv),

$$\tau \to \beta \qquad (\beta \to 0) ; \qquad \tau \to \sqrt{\frac{15}{8}} \beta^{-1/2} \qquad (\beta \to \infty) . \tag{v}$$

The entire dependence of τ on β has also been tabulated and graphically illustrated.

Certain other related statistical problems have also been considered. Thus, expressions for $\overline{f_\parallel^2}$ and $\overline{f_\perp^2}$ have been derived where $f_\parallel$ and $f_\perp$ are the rates of change of F parallel to and perpendicular to the direction of F, respectively. Further, the probability distribution of f has been considered and the root mean square value of F to be expected for an assigned value of the rate of change f evaluated. Finally, the problem of the accelerations in F to be expected has also been briefly examined.

1. *Introduction.*—A general analysis of the statistical aspects of the fluctuating gravitational field arising from a random distribution of mass centers may be expected to provide the necessary basis for several problems of stellar dynamics. Thus the notion of the time of relaxation of a stellar system is intimately connected with the influence of such fluctuations in the gravitational field on the motions of stars. Also it appears that the dynamical problems presented by star clusters[1] can be treated satisfactorily only in terms of such an analysis. The common characteristic of all these problems is that individual stars are subject to the changing influence of a varying local stellar distribution.

[1] And presumably also clusters of nebulae.

Consequently, it is apparent that the most suitable method for analyzing such situations is a statistical one. More specifically, we may formulate the fundamental problem in the following terms.

The force $\boldsymbol{F}$ acting on a star, per unit mass, is given by

$$\boldsymbol{F} = -G\Sigma\frac{M_i}{|\boldsymbol{r}_i|^3}\boldsymbol{r}_i\,. \tag{1}$$

where M_i denotes the mass of a typical field star and $\boldsymbol{r}_i$ its position vector relative to the star under consideration. Further, the summation in equation (1) is extended over all the neighboring stars. The actual value of $\boldsymbol{F}$ at any particular instant will depend on the instantaneous positions of all the other stars and is, in consequence, subject to fluctuations. It would not therefore be feasible to predict the exact dependence of $\boldsymbol{F}$ on the position and/or the time for any individual case. But the same circumstances would permit us to inquire into the statistical aspects of $\boldsymbol{F}$. Thus one of the questions we can ask is the probability of occurrence,

$$W(\boldsymbol{F})\,dF_x dF_y dF_z = W(\boldsymbol{F})\,d\boldsymbol{F}\,, \tag{2}$$

of $\boldsymbol{F}$ in the range $\boldsymbol{F}$ and $\boldsymbol{F} + d\boldsymbol{F}$. In evaluating this probability we can (consistent with the physical situations we have in view) suppose that fluctuations subject only to the restriction of a constant average density occur. This problem is clearly equivalent to finding the probability of a given *electric* field strength at a point in a gas composed of simple ions. This latter problem has been considered by Holtsmark;[2] and Holtsmark's results can be readily adapted to the gravitational case.[3] However, the specification of the Holtsmark distribution $W(\boldsymbol{F})$ does not characterize all the essential features of the fluctuating field. An equally important aspect of the problem is the *speed of the fluctuations* (*Schwankungsgeschwindigkeit*)[4] and the related questions concerning the *probability after-effects* (*Wahrscheinlichkeitsnachwirkung*).[4] These latter problems are essentially more difficult than the establishment of the stationary distribution. For, according to equation (1),

$$f = \frac{d\boldsymbol{F}}{dt} = -G\Sigma M_i\left(\frac{\boldsymbol{v}_i}{|\boldsymbol{r}_i|^3} - 3\frac{\boldsymbol{r}_i[\boldsymbol{r}_i\cdot\boldsymbol{v}_i]}{|\boldsymbol{r}_i|^5}\right), \tag{3}$$

where $\boldsymbol{v}_i$ denotes the velocity of the typical field star. It is now clear that the speed of the fluctuations can be specified in terms of the distribution

$$W(\boldsymbol{F}, f)\,, \tag{4}$$

which gives the simultaneous probability of a given field strength $\boldsymbol{F}$ and an associated rate of change f. It is seen that this bivariate distribution of $\boldsymbol{F}$ and f will depend on the assignment of a priori probability in the phase space in contrast to the distribution of $\boldsymbol{F}$, which depends only on a similar assignment in the configuration space.

In this paper we shall derive a general formula for $W(\boldsymbol{F}, f)$ and obtain explicit expressions for the moments

$$\overline{|f|^2_{\boldsymbol{F}}} \quad \text{and} \quad \overline{|\boldsymbol{F}|^2_f} \tag{5}$$

[2] *Ann. d. Phys.*, **58**, 577, 1919; *Phys. Zs.*, **20**, 162, 1919, and **25**, 73, 1924. See also R. Gans, *Ann. d. Phys.*, **66**, 396, 1921.

[3] See S. Chandrasekhar, *Ap. J.*, **94**, 511, 1941, where a first attempt at a statistical theory has already been made.

[4] In M. von Smoluchowski's terminology (cf. *Phys. Zs.*, **17**, 557, 585, 1916; see particularly pp. 560–567).

for prescribed values of $\boldsymbol{F}$ and $\boldsymbol{f}$, respectively. These moments have, as we shall see, important applications to problems involving the speed of the fluctuations in the gravitational field. In a later paper we shall study the nature of the correlations in the field at two different points.

2. *The general formula for* $\mathrm{W}(\boldsymbol{F}, \boldsymbol{f})$.—We require the stationary distribution of $\boldsymbol{F}$ and its simultaneous rate of change $\boldsymbol{f}$ at any given point. Without loss of generality we can suppose that the point under consideration is at the origin O of our system of co-ordinates. About O describe a sphere of radius R and containing N stars. In the first instance we shall suppose that

$$\boldsymbol{F} = -G\sum_{i=1}^{N}\frac{M_i}{|\boldsymbol{r}_i|^3}\boldsymbol{r}_i = \sum_{i=1}^{N}\boldsymbol{F}_i \tag{6}$$

and

$$\boldsymbol{f} = -G\sum_{i=1}^{N}M_i\left(\frac{\boldsymbol{v}_i}{|\boldsymbol{r}_i|^3} - 3\frac{\boldsymbol{r}_i[\boldsymbol{r}_i\cdot\boldsymbol{v}_i]}{|\boldsymbol{r}_i|^5}\right) = \sum_{i=1}^{N}\boldsymbol{f}_i\,; \tag{7}$$

but we shall later let R and N tend to infinity simultaneously in such a way that

$$\frac{4}{3}\pi R^3 n = N \qquad \begin{pmatrix} R\to\infty, \\ N\to\infty, \\ n\to\text{constant.}\end{pmatrix} \tag{8}$$

Considering first the distribution $w(\boldsymbol{F}, \boldsymbol{f})$ at the center of the finite sphere of radius R and containing N stars distributed in a random fashion, we seek the probability that

$$\boldsymbol{F}_0 \leqslant \boldsymbol{F} \leqslant \boldsymbol{F}_0 + d\boldsymbol{F}_0; \qquad \boldsymbol{f}_0 \leqslant \boldsymbol{f} \leqslant \boldsymbol{f}_0 + d\boldsymbol{f}_0, \tag{9}$$

where $\boldsymbol{F}$ and $\boldsymbol{f}$ are defined according to equations (6) and (7).

Now the vectors $\boldsymbol{F}_i$ and $\boldsymbol{f}_i$ depend on the position vector $\boldsymbol{r}_i$ and the velocity $\boldsymbol{v}_i$ of the ith star. Accordingly, $\boldsymbol{F}$ and $\boldsymbol{f}$ together depend on the $6N$ variables included in $(\boldsymbol{r}_1, \boldsymbol{v}_1; \boldsymbol{r}_2, \boldsymbol{v}_2; \ldots; \boldsymbol{r}_i, \boldsymbol{v}_i; \ldots; \boldsymbol{r}_N, \boldsymbol{v}_N)$. Let

$$\tau_i(\boldsymbol{r}_i, \boldsymbol{v}_i)\, d\boldsymbol{r}_i d\boldsymbol{v}_i \tag{10}$$

denote the probability that the position and the velocity of the ith star are found in the ranges $(\boldsymbol{r}_i, \boldsymbol{r}_i + d\boldsymbol{r}_i)$ and $(\boldsymbol{v}_i, \boldsymbol{v}_i + d\boldsymbol{v}_i)$. The probability of a definite configuration of the N stars in the phase space is therefore

$$\prod_{i=1}^{N}\tau_i(\boldsymbol{r}_i, \boldsymbol{v}_i)\, d\boldsymbol{r}_i d\boldsymbol{v}_i = \mathrm{T}d\Omega\,(\text{say})\,. \tag{11}$$

It is clear that the specification of the co-ordinates and the velocities of the N stars uniquely determines the values of $\boldsymbol{F}$ and $\boldsymbol{f}$. Consequently the inequalities (9) will be satisfied only in a definite part of the phase space. Accordingly,

$$w(\boldsymbol{F}_0, \boldsymbol{f}_0)\, d\boldsymbol{F}_0 d\boldsymbol{f}_0 = \frac{1}{V^N}\int \mathrm{T}d\Omega\,, \tag{12}$$

where the integration is to be extended only over that part of the phase space in which the inequalities (9) are satisfied. Now, following a procedure due to A. A. Markoff,[5] we introduce under the integral sign in equation (12) an appropriate *Dirichlet* factor

[5] *Wahrscheinlichkeitsrechnung*, §§ 16 and 33, Leipzig, 1912. See also M. von Laue, *Ann. d. Phys.*, **47**, 853, 1915.

which has the value 1 whenever equation (9) is satisfied and the value zero whenever it is not. It is readily found that the required *Dirichlet* factor is

$$\left.\begin{aligned}\frac{1}{\pi^6}\int\int\int_{-\infty}^{+\infty}\int\int\int e^{i[\boldsymbol{\rho}\cdot(\Sigma \boldsymbol{F}_i-\boldsymbol{F}_0)+\boldsymbol{\sigma}\cdot(\Sigma f_i-f_0)]}\frac{d\rho_1 d\rho_2 d\rho_3 d\sigma_1 d\sigma_2 d\sigma_3}{\rho_1\rho_2\rho_3\sigma_1\sigma_2\sigma_3}\\ \times \sin\left(\tfrac{1}{2}\rho_1 F_{x,0}\right)\sin\left(\tfrac{1}{2}\rho_2 F_{y,0}\right)\sin\left(\tfrac{1}{2}\rho_3 F_{z,0}\right)\\ \times \sin\left(\tfrac{1}{2}\sigma_1 f_{x,0}\right)\sin\left(\tfrac{1}{2}\sigma_2 f_{y,0}\right)\sin\left(\tfrac{1}{2}\sigma_3 f_{z,0}\right),\end{aligned}\right\} \tag{13}$$

where

$$\boldsymbol{\rho} = (\rho_1, \rho_2, \rho_3); \qquad \boldsymbol{\sigma} = (\sigma_1, \sigma_2, \sigma_3) \tag{14}$$

are two auxiliary vectors. Introducing the foregoing factor under the integral sign in equation (12), we find

$$w(\boldsymbol{F}_0, f_0)\, d\boldsymbol{F}_0 df_0 = \frac{d\boldsymbol{F}_0 df_0}{64\pi^6}\int\int e^{-i(\boldsymbol{\rho}\cdot\boldsymbol{F}_0+\boldsymbol{\sigma}\cdot f_0)} A_N(\boldsymbol{\rho}, \boldsymbol{\sigma})\, d\boldsymbol{\rho} d\boldsymbol{\sigma}, \tag{15}$$

where we have written

$$A_N(\boldsymbol{\rho}, \boldsymbol{\sigma}) = \frac{1}{V^N}\int_{(6N)}\ldots\int \tau_1\tau_2\ldots\tau_N e^{i(\boldsymbol{\rho}\cdot\Sigma \boldsymbol{F}_i+\boldsymbol{\sigma}\cdot\Sigma f_i)} d\boldsymbol{r}_1 d\boldsymbol{v}_1, \ldots, d\boldsymbol{r}_N d\boldsymbol{v}_N. \tag{16}$$

According to our fundamental assumption, τ_i depends only on the co-ordinates and velocity of the ith star. Hence,

$$A_N(\boldsymbol{\rho}, \boldsymbol{\sigma}) = \left[\frac{1}{V}\int_{|\boldsymbol{r}|<R}\int_{|\boldsymbol{v}|=0}^{|\boldsymbol{v}|=\infty} \tau\, e^{i(\boldsymbol{\rho}\cdot\boldsymbol{F}+\boldsymbol{\sigma}\cdot f)} d\boldsymbol{r} d\boldsymbol{v}\right]^N. \tag{17}$$

We now let R and N tend to infinity according to equation (8); then, $w \to W$, and we have

$$W(\boldsymbol{F}, f) = \frac{1}{64\pi^6}\int_{|\boldsymbol{\rho}|=0}^{\infty}\int_{|\boldsymbol{\sigma}|=0}^{\infty} e^{-i(\boldsymbol{\rho}\cdot\boldsymbol{F}+\boldsymbol{\sigma}\cdot f)} A(\boldsymbol{\rho}, \boldsymbol{\sigma})\, d\boldsymbol{\rho} d\boldsymbol{\sigma}, \tag{18}$$

where

$$A(\boldsymbol{\rho}, \boldsymbol{\sigma}) = \begin{matrix}\text{limit}\\ N\to\infty\\ R\to\infty\end{matrix}\left[\frac{3}{4\pi R^3}\int_{|\boldsymbol{r}|<R}\int_{|\boldsymbol{v}|<\infty} e^{i(\boldsymbol{\rho}\cdot\boldsymbol{\phi}+\boldsymbol{\sigma}\cdot\boldsymbol{\psi})}\tau\, d\boldsymbol{r} d\boldsymbol{v}\right]^N, \tag{19}$$

where we have further written

$$\boldsymbol{\phi} = GM\frac{\boldsymbol{r}}{|\boldsymbol{r}|^3}; \qquad \boldsymbol{\psi} = GM\left(\frac{\boldsymbol{v}}{|\boldsymbol{r}|^3} - 3\frac{\boldsymbol{r}[\boldsymbol{r}\cdot\boldsymbol{v}]}{|\boldsymbol{r}|^5}\right). \tag{20}$$

Finally, we shall suppose that

$$\tau = \frac{j^3}{\pi^{3/2}} e^{-j^2 v^2}; \tag{21}$$

in other words, we assume that all positions are equally likely for a star and that the distribution of the velocities is Maxwellian. We should, however, remark at this point that all the subsequent work will remain valid for *any spherical* distribution of the velocities. We shall indicate at a later stage (§ 12) the modifications necessary to go

from a Maxwellian distribution to a general spherical distribution. Similarly, we shall suppose in the first instance that all the stars have the same mass and later show how the results can be generalized for a distribution over different masses (§ 13).

Finally, we may note that, according to equation (18), $W(\boldsymbol{F}, f)$ is simply the six-dimensional Fourier transform of the function $A(\boldsymbol{\rho}, \boldsymbol{\sigma})$.

3. *The evaluation of* $A(\boldsymbol{\rho}, \boldsymbol{\sigma})$.—In our expression (19) for $A(\boldsymbol{\rho}, \boldsymbol{\sigma})$ we shall introduce $\boldsymbol{\phi}$ and $\boldsymbol{\psi}$ themselves as the variables of integration instead of $\boldsymbol{r}$ and $\boldsymbol{v}$. The corresponding Jacobian of the transformation is seen to be

$$\frac{\partial(\boldsymbol{\phi}, \boldsymbol{\psi})}{\partial(\boldsymbol{r}\ \boldsymbol{v})} = G^6M^6 \begin{vmatrix} \frac{1}{|\boldsymbol{r}|^3} - 3\frac{x^2}{|\boldsymbol{r}|^5} & -3\frac{xy}{|\boldsymbol{r}|^5} & -3\frac{zx}{|\boldsymbol{r}|^5} \\ -3\frac{xy}{|\boldsymbol{r}|^5} & \frac{1}{|\boldsymbol{r}|^3} - 3\frac{y^2}{|\boldsymbol{r}|^5} & -3\frac{yz}{|\boldsymbol{r}|^5} \\ -3\frac{zx}{|\boldsymbol{r}|^5} & -3\frac{yz}{|\boldsymbol{r}|^5} & \frac{1}{|\boldsymbol{r}|^3} - 3\frac{z^2}{|\boldsymbol{r}|^5} \end{vmatrix}^2 \tag{22}$$

or, as may be readily verified,[6]

$$\frac{\partial(\boldsymbol{\phi}, \boldsymbol{\psi})}{\partial(\boldsymbol{r}, \boldsymbol{v})} = 4\frac{G^6M^6}{|\boldsymbol{r}|^{18}} = \frac{4}{G^3M^3}|\boldsymbol{\phi}|^9. \tag{23}$$

Hence,

$$\left.\begin{aligned} d\boldsymbol{r}d\boldsymbol{v} &= \left(\frac{\partial[\boldsymbol{\phi}, \boldsymbol{\psi}]}{\partial[\boldsymbol{r}, \boldsymbol{v}]}\right)^{-1} d\boldsymbol{\phi}d\boldsymbol{\psi} \\ &= \frac{G^3M^3}{4}|\boldsymbol{\phi}|^{-9}d\boldsymbol{\phi}d\boldsymbol{\psi}. \end{aligned}\right\} \tag{24}$$

We have next to express $|\boldsymbol{v}|^2$ in terms of our new variables $\boldsymbol{\phi}$ and $\boldsymbol{\psi}$. According to equations (20), we have

$$\boldsymbol{\phi}\cdot\boldsymbol{\psi} = -2\frac{G^2M^2}{|\boldsymbol{r}|^6}\boldsymbol{r}\cdot\boldsymbol{v}\,; \qquad \boldsymbol{\phi}\times\boldsymbol{\psi} = \frac{G^2M^2}{|\boldsymbol{r}|^6}\boldsymbol{r}\times\boldsymbol{v}. \tag{25}$$

Hence,

$$\left.\begin{aligned} (\boldsymbol{\phi}\cdot\boldsymbol{\psi})^2 + 4(\boldsymbol{\phi}\times\boldsymbol{\psi})^2 &= 4\frac{G^4M^4}{|\boldsymbol{r}|^{12}}[(\boldsymbol{r}\cdot\boldsymbol{v})^2 + (\boldsymbol{r}\times\boldsymbol{v})^2] \\ &= 4\frac{G^4M^4}{|\boldsymbol{r}|^{10}}|\boldsymbol{v}|^2, \end{aligned}\right\} \tag{26}$$

[6] The determinant to be evaluated is

$$\mathrm{Det}\left|\frac{1}{|\boldsymbol{r}|^3}\mathbf{1} - 3\frac{\boldsymbol{r}\otimes\boldsymbol{r}}{|\boldsymbol{r}|^5}\right| = \frac{1}{|\boldsymbol{r}|^{15}}\mathrm{Det}\left||\boldsymbol{r}|^2\mathbf{1} - 3\boldsymbol{r}\otimes\boldsymbol{r}\right|$$

where $\mathbf{1}$ stands for the unit matrix and

$$\boldsymbol{r}\otimes\boldsymbol{r} = \begin{vmatrix} x^2 & xy & xz \\ yx & y^2 & yz \\ zx & zy & z^2 \end{vmatrix},$$

which is thus a matrix of rank 1 and trace $|\boldsymbol{r}|^2$. The characteristic roots of $\boldsymbol{r}\otimes\boldsymbol{r}$ are therefore $|\boldsymbol{r}|^2$, 0, and 0; hence those of $|\boldsymbol{r}|^2\mathbf{1} - 3\boldsymbol{r}\otimes\boldsymbol{r}$ are $|\boldsymbol{r}|^2 - 3|\boldsymbol{r}|^2$, $|\boldsymbol{r}|^2$, $|\boldsymbol{r}|^2$ or $-2|\boldsymbol{r}|^2$, $|\boldsymbol{r}|^2$, $|\boldsymbol{r}|^2$. Consequently,

$$\mathrm{Det}\,||\boldsymbol{r}|^2\mathbf{1} - 3\boldsymbol{r}\otimes\boldsymbol{r}| = -2|\boldsymbol{r}|^6.$$

Equation (23) now follows at once.

or, alternatively,

$$\left.\begin{aligned} |\boldsymbol{v}|^2 &= \frac{|\boldsymbol{r}|^{10}}{G^4M^4}\left[(\boldsymbol{\phi}\times\boldsymbol{\psi})^2+\frac{1}{4}(\boldsymbol{\phi}\cdot\boldsymbol{\psi})^2\right] \\ &= GM|\boldsymbol{\phi}|^{-5}\left[(\boldsymbol{\phi}\times\boldsymbol{\psi})^2+\frac{1}{4}(\boldsymbol{\phi}\cdot\boldsymbol{\psi})^2\right] \\ &= GM|\boldsymbol{\phi}|^{-3}\left[|\boldsymbol{\psi}|^2-\frac{3}{4}|\boldsymbol{\phi}|^{-2}(\boldsymbol{\phi}\cdot\boldsymbol{\psi})^2\right]. \end{aligned}\right\} \tag{27}$$

Finally, it is to be noted that, since the integral over $\boldsymbol{r}$ is restricted by the condition $|\boldsymbol{r}| < R$, we should now require that

$$|\boldsymbol{\phi}| > \frac{GM}{R^2} = \epsilon\,(\text{say})\,. \tag{28}$$

Thus, in these new variables the expression for $A(\boldsymbol{\rho}, \boldsymbol{\sigma})$ becomes

$$A(\boldsymbol{\rho},\boldsymbol{\sigma}) = \lim_{\epsilon\to 0}\left[\frac{3}{4\pi}\left(\frac{\epsilon}{GM}\right)^{3/2}\int_{|\boldsymbol{\phi}|>\epsilon}\int_{|\boldsymbol{\psi}|<\infty} e^{i(\boldsymbol{\rho}\cdot\boldsymbol{\phi}+\boldsymbol{\sigma}\cdot\boldsymbol{\psi})}\tau\frac{G^3M^3}{4}|\boldsymbol{\phi}|^{-9}d\boldsymbol{\phi}d\boldsymbol{\psi}\right]^{\frac{4\pi}{3}\left(\frac{GM}{\epsilon}\right)^{3/2}}, \tag{29}$$

or, substituting for τ according to equations (21) and (27), we have

$$\left.\begin{aligned} A(\boldsymbol{\rho},\boldsymbol{\sigma}) = \lim_{\epsilon\to 0}\Bigg[&\frac{3j^3(GM)^{3/2}}{16\pi^{5/2}}\epsilon^{3/2}\int_{|\boldsymbol{\phi}|>\epsilon}\int_{|\boldsymbol{\psi}|<\infty} e^{i(\boldsymbol{\rho}\cdot\boldsymbol{\phi}+\boldsymbol{\sigma}\cdot\boldsymbol{\psi})} \\ &\times e^{-j^2GM|\boldsymbol{\phi}|^{-3}(|\boldsymbol{\psi}|^2-\frac{3}{4}|\boldsymbol{\phi}|^{-2}[\boldsymbol{\phi}\cdot\boldsymbol{\psi}]^2)}|\boldsymbol{\phi}|^{-9}d\boldsymbol{\phi}d\boldsymbol{\psi}\Bigg]^{\frac{4\pi}{3}\left(\frac{GM}{\epsilon}\right)^{3/2}}. \end{aligned}\right\} \tag{30}$$

Consider the integral with respect to $\boldsymbol{\psi}$ which occurs in equation (30). We have

$$\int_{|\boldsymbol{\psi}|<\infty} e^{i\boldsymbol{\sigma}\cdot\boldsymbol{\psi}-j^2GM|\boldsymbol{\phi}|^{-3}(|\boldsymbol{\psi}|^2-\frac{3}{4}|\boldsymbol{\phi}|^{-2}[\boldsymbol{\phi}\cdot\boldsymbol{\psi}]^2)}d\boldsymbol{\psi}\,. \tag{31}$$

Put

$$\boldsymbol{\psi}_1 = j(GM)^{1/2}\boldsymbol{\psi}\,, \tag{32}$$

and

$$\boldsymbol{\sigma}_1 = \frac{1}{j(GM)^{1/2}}\boldsymbol{\sigma}\,. \tag{33}$$

The integral (31) becomes

$$\frac{1}{j^3(GM)^{3/2}}\int_{|\boldsymbol{\psi}_1|<\infty} e^{i\boldsymbol{\sigma}_1\cdot\boldsymbol{\psi}_1-|\boldsymbol{\phi}|^{-3}(|\boldsymbol{\psi}_1|^2-\frac{3}{4}|\boldsymbol{\phi}|^{-2}[\boldsymbol{\phi}\cdot\boldsymbol{\psi}_1]^2)}d\boldsymbol{\psi}_1\,. \tag{34}$$

To evaluate this integral we shall choose a frame of reference (ξ, η, ζ) such that the ξ-axis is along the $\boldsymbol{\phi}$-direction. Then

$$\phi_\xi = |\boldsymbol{\phi}|\,; \qquad \phi_\eta = \phi_\zeta = 0\,. \tag{35}$$

The integral (34) now becomes

$$\left.\begin{aligned}
&\frac{1}{j^3(GM)^{3/2}}\int_{-\infty}^{+\infty}\int_{-\infty}^{+\infty}\int_{-\infty}^{+\infty} e^{i(\sigma_{1\xi}\psi_{1\xi}+\sigma_{1\eta}\psi_{1\eta}+\sigma_{1\zeta}\psi_{1\zeta})-|\boldsymbol{\phi}|^{-3}(\frac{1}{4}\psi_{1\xi}^2+\psi_{1\eta}^2+\psi_{1\zeta}^2)}d\psi_{1\xi}d\psi_{1\eta}d\psi_{1\zeta}\\
&=\frac{1}{j^3(GM)^{3/2}}\int_{-\infty}^{+\infty} e^{i\sigma_{1\xi}\psi_{1\xi}-\frac{1}{4}|\boldsymbol{\phi}|^{-3}\psi_{1\xi}^2}d\psi_{1\xi}\cdot\int_{-\infty}^{+\infty} e^{i\sigma_{1\eta}\psi_{1\eta}-|\boldsymbol{\phi}|^{-3}\psi_{1\eta}^2}d\psi_{1\eta}\cdot\int_{-\infty}^{+\infty} e^{i\sigma_{1\zeta}\psi_{1\zeta}-|\boldsymbol{\phi}|^{-3}\psi_{1\zeta}^2}d\psi_{1\zeta}\\
&=\frac{2\pi^{3/2}}{j^3(GM)^{3/2}}|\boldsymbol{\phi}|^{9/2}e^{-|\boldsymbol{\phi}|^3(\sigma_{1\xi}^2+\frac{1}{4}\sigma_{1\eta}^2+\frac{1}{4}\sigma_{1\zeta}^2)}\\
&=\frac{2\pi^{3/2}}{j^3(GM)^{3/2}}|\boldsymbol{\phi}|^{9/2}e^{-\frac{1}{4}|\boldsymbol{\phi}|^3(|\boldsymbol{\sigma}_1|^2+\frac{3}{4}|\boldsymbol{\phi}|^{-2}[\boldsymbol{\phi}\cdot\boldsymbol{\sigma}_1]^2)}
\end{aligned}\right\}\quad(36)$$

Accordingly, our expression (30) for $A(\rho,\sigma)$ reduces to

$$A(\boldsymbol{\rho},\boldsymbol{\sigma})=\lim_{\epsilon\to 0}\left[\frac{3}{8\pi}\epsilon^{3/2}\int_{|\boldsymbol{\phi}|>\epsilon} e^{i\boldsymbol{\rho}\cdot\boldsymbol{\phi}-\frac{1}{4}|\boldsymbol{\phi}|^3|\boldsymbol{\sigma}_1|^2(1+3\cos^2\beta)}|\boldsymbol{\phi}|^{-9/2}d\boldsymbol{\phi}\right]^{\frac{4\pi}{3}(\frac{GM}{\epsilon})^{3/2}n},\quad(37)$$

where we have denoted the angle between the vectors $\boldsymbol{\phi}$ and $\boldsymbol{\sigma}_1$ by β:

$$\beta=\sphericalangle(\boldsymbol{\phi},\boldsymbol{\sigma}_1)=\sphericalangle(\boldsymbol{\phi},\boldsymbol{\sigma}).\quad(38)$$

We readily verify that

$$\frac{3}{8\pi}\epsilon^{3/2}\int_{|\boldsymbol{\phi}|>\epsilon}|\boldsymbol{\phi}|^{-9/2}d\boldsymbol{\phi}=1.\quad(39)$$

Hence we can re-write equation (37) in the form

$$A(\boldsymbol{\rho},\boldsymbol{\sigma})=\lim_{\epsilon\to 0}\left[1-\frac{3}{8\pi}\epsilon^{3/2}\int_{|\boldsymbol{\phi}|>\epsilon}\{1-e^{i\boldsymbol{\rho}\cdot\boldsymbol{\phi}-\frac{1}{4}|\boldsymbol{\phi}|^3|\boldsymbol{\sigma}_1|^2(1+3\cos^2\beta)}\}|\boldsymbol{\phi}|^{-9/2}d\boldsymbol{\phi}\right]^{\frac{4\pi}{3}(\frac{GM}{\epsilon})^{3/2}n}.\quad(40)$$

Without altering its value, we can clearly replace $\boldsymbol{\phi}$ by $-\boldsymbol{\phi}$ in the foregoing expression. But this replacement changes

$$e^{i\boldsymbol{\rho}\cdot\boldsymbol{\phi}}\quad\text{into}\quad e^{-i\boldsymbol{\rho}\cdot\boldsymbol{\phi}}\quad(41)$$

under the integral sign; taking the arithmetic mean of the two resulting integrands, we obtain

$$A(\boldsymbol{\rho},\boldsymbol{\sigma})=\lim_{\epsilon\to 0}\left[1-\frac{3}{8\pi}\epsilon^{3/2}\int_{|\boldsymbol{\phi}|>\epsilon}\{1-\cos(\boldsymbol{\rho}\cdot\boldsymbol{\phi})\,e^{-|\boldsymbol{\phi}|^3|\boldsymbol{\sigma}_1|^2(1+3\cos^2\beta)/4}\}|\boldsymbol{\phi}|^{-9/2}d\boldsymbol{\phi}\right]^{\frac{4\pi}{3}(\frac{GM}{\epsilon})^{3/2}n}.\quad(42)$$

Now the integral over $\boldsymbol{\phi}$ which occurs in equation (40) is seen to be absolutely convergent, even when extended over all $\boldsymbol{\phi}$, i.e., also for $\epsilon\to 0$. Hence we can write

$$A(\boldsymbol{\rho},\boldsymbol{\sigma})=\lim_{\epsilon\to 0}\left[1-\frac{3}{8\pi}\epsilon^{3/2}\int_{0<|\boldsymbol{\phi}|<\infty}\{1-\cos(\boldsymbol{\rho}\cdot\boldsymbol{\phi})\,e^{-|\boldsymbol{\phi}|^3|\boldsymbol{\sigma}_1|^2(1+3\cos^2\beta)/4}\}|\boldsymbol{\phi}|^{-9/2}d\boldsymbol{\phi}\right]^{\frac{4\pi}{3}(\frac{GM}{\epsilon})^{3/2}n}\quad(43)$$

or

$$A(\boldsymbol{\rho},\boldsymbol{\sigma})=e^{-\frac{1}{2}n(GM)^3/2C(\boldsymbol{\rho},\boldsymbol{\sigma}_1)}\qquad\left(\boldsymbol{\sigma}_1=\frac{\boldsymbol{\sigma}}{j(GM)^{1/2}}\right),\quad(44)$$

where we have written

$$C(\boldsymbol{\rho}, \boldsymbol{\sigma}_1) = \int\limits_{0<|\boldsymbol{\phi}|<\infty} \{1 - \cos(\boldsymbol{\rho}\cdot\boldsymbol{\phi})\, e^{-|\boldsymbol{\phi}|^2|\boldsymbol{\sigma}_1|^2(1+3\cos^2\beta)/4}\} \frac{d\boldsymbol{\phi}}{|\boldsymbol{\phi}|^{9/2}}. \tag{45}$$

4. *Alternative forms for* $C(\boldsymbol{\rho}, \boldsymbol{\sigma}_1)$.—A more convenient form for $C(\boldsymbol{\rho}, \boldsymbol{\sigma}_1)$ is obtained by choosing a particular orientation of our co-ordinate axes. Let $\boldsymbol{\rho}$ be along one of the axes

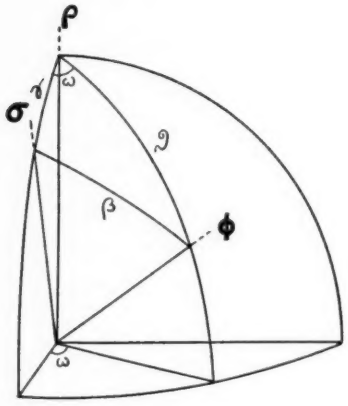

FIG. 1

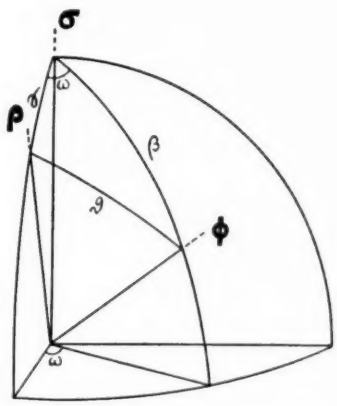

FIG. 2

and $\boldsymbol{\sigma}_1$ lie in one of the principal planes (see Fig. 1). Using polar co-ordinates as indicated in Figure 1 we obtain from the spherical triangle $(\boldsymbol{\rho}, \boldsymbol{\sigma}_1, \boldsymbol{\phi})$

$$\cos\beta = \cos\measuredangle(\boldsymbol{\phi}, \boldsymbol{\sigma}_1) = \cos\gamma\cos\vartheta + \sin\gamma\sin\vartheta\cos\omega\,, \tag{46}$$

where γ is the angle between $\boldsymbol{\rho}$ and $\boldsymbol{\sigma}_1$ (or $\boldsymbol{\sigma}$). Equation (45) accordingly becomes

$$C(\boldsymbol{\rho}, \boldsymbol{\sigma}_1) = \int_0^\infty\int_0^\pi\int_0^{2\pi} \{1 - \cos(|\boldsymbol{\rho}|\,|\boldsymbol{\phi}|\cos\vartheta)\, e^{-|\boldsymbol{\phi}|^2|\boldsymbol{\sigma}_1|^2(1+3\cos^2\beta)/4}\} |\boldsymbol{\phi}|^{-5/2}\sin\vartheta\, d\omega\, d\vartheta\, d|\boldsymbol{\phi}|\,, \tag{47}$$

or, putting

$$\cos\vartheta = t\,, \tag{48}$$

we have

$$C(\boldsymbol{\rho}, \boldsymbol{\sigma}_1) = \int_0^\infty\int_{-1}^{1}\int_0^{2\pi} \{1 - \cos(|\boldsymbol{\rho}|\,|\boldsymbol{\phi}|\,t)\, e^{-|\boldsymbol{\phi}|^2|\boldsymbol{\sigma}_1|^2(1+3\cos^2\beta)/4}\} |\boldsymbol{\phi}|^{-5/2} d\omega\, dt\, d|\boldsymbol{\phi}|\,. \tag{49}$$

Finally, letting

$$z = |\boldsymbol{\phi}|\,|\boldsymbol{\rho}|\,, \tag{50}$$

we obtain

$$C(\boldsymbol{\rho}, \boldsymbol{\sigma}_1) = |\boldsymbol{\rho}|^{3/2} D\left(\frac{|\boldsymbol{\sigma}_1|^2}{|\boldsymbol{\rho}|^3}\right), \tag{51}$$

where

$$D(p) = \int_0^\infty \int_{-1}^{1} \int_0^{2\pi} \{1 - \cos(zt)\, e^{-pz^3(1+3[t\cos\gamma + \sqrt{1-t^2}\sin\gamma\cos\omega]^2)/4}\}\, z^{-5/2} d\omega dt dz\,. \quad (52)$$

An alternative, but equivalent, form for $D(p)$ is obtained if we choose our co-ordinate axes in such a way that $\boldsymbol{\sigma}_1$ is along one of the principal axes and $\boldsymbol{\rho}$ lies in one of the principal planes (see Fig. 2).

$$D(p) = \int_0^\infty \int_{-1}^{1} \int_0^{2\pi} \{1 - \cos(z[t\cos\gamma + \sqrt{1-t^2}\sin\gamma\cos\omega])\, e^{-pz^3(1+3t^2)/4}\}\, z^{-5/2} d\omega dt dz\,. \quad (53)$$

5. *The behavior of* D(p) *for* $p \to 0$.—Our principal interest in the bivariate distribution $W(\boldsymbol{F}, \boldsymbol{f})$ is to determine the different moments of $\boldsymbol{f}$ for a given $\boldsymbol{F}$ and of $\boldsymbol{F}$ for a given $\boldsymbol{f}$ and naturally also in the separate distributions of $\boldsymbol{F}$ and $\boldsymbol{f}$. It is an elementary consequence of equation (18) that these moments depend only on the behavior of $A(\boldsymbol{\rho}, \boldsymbol{\sigma})$ for $|\boldsymbol{\sigma}| \to 0$ and $|\boldsymbol{\rho}| \to 0$, respectively, or, according to equations (44) and (51), on the behavior of $D(p)$ for $p \to 0$ and $p \to \infty$. We shall first examine the behavior of $D(p)$ for $p \to 0$.

According to equation (52), we have

$$D(p) = D(0) + F(p) \quad (54)$$

where

$$D(0) = \int_0^\infty \int_{-1}^{1} \int_0^{2\pi} (1 - \cos[zt])\, z^{-5/2} d\omega dt dz \quad (55)$$

and

$$F(p) = \int_0^\infty \int_{-1}^{1} \int_0^{2\pi} \cos(zt)\, \{1 - e^{-pz^3(1+3[t\cos\gamma + \sqrt{1-t^2}\sin\gamma\cos\omega]^2)/4}\}\, z^{-5/2} d\omega dt dz\,. \quad (56)$$

$D(0)$ is readily evaluated. For, after performing the integrations over ω and t, we obtain

$$D(0) = 4\pi \int_0^\infty (z - \sin z)\, z^{-7/2} dz \quad (57)$$

or, after several integrations by parts,

$$D(0) = \frac{32}{15}\pi \int_0^\infty z^{-1/2} \cos z\, dz = \frac{8}{15}(2\pi)^{3/2}. \quad (58)$$

Returning to the consideration of $F(p)$, it is seen that $F(0) = 0$. We shall therefore examine the behavior of $F'(p)$ for $p \gtrsim 0$. For $p > 0$, differentiation under the integral sign gives

$$\left.\begin{aligned} F'(p) = {} & \int_0^\infty \int_{-1}^{1} \int_0^{2\pi} \cos(zt)\, e^{-pz^3(1+3[t\cos\gamma + \sqrt{1-t^2}\sin\gamma\cos\omega]^2)/4} \\ & \times \frac{1}{4}(1 + 3[t\cos\gamma + \sqrt{1-t^2}\sin\gamma\cos\omega]^2)\, z^{1/2} d\omega dt dz\,. \end{aligned}\right\} \quad (59)$$

The foregoing integral for $F'(p)$ is uniformly and absolutely convergent for $p \geq p_0$ for any fixed $p_0 > 0$; hence, it determines $F'(p)$ for all $p > 0$. On the other hand, the absolute convergence of the integral defining $F'(p)$ is not uniform for $p \gtrsim 0$. Consequently, we cannot be certain of the continuity of $F'(p)$ for $p \gtrsim 0$; and, even if it is continuous,

its limit may well be different from the integral (59) for $p = 0$.[7] However, if we write equation (58) in the form

$$\left.\begin{aligned} F'(p) &= \mathcal{R}\int_0^\infty\int_{-1}^{1}\int_0^{2\pi} e^{izt-\frac{1}{4}pz^3(1+3[t\cos\gamma+\sqrt{1-t^2}\sin\gamma\cos\omega]^2)} \\ &\times\frac{1}{4}(1+3[t\cos\gamma+\sqrt{1-t^2}\sin\gamma\cos\omega]^2)\, z^{1/2}d\omega dt dz \end{aligned}\right\} \quad (61)[8]$$

and regard z and t as complex variables, it is possible to choose paths of integration in such a way that the integral is absolutely and uniformly convergent for all $p \geq 0$ (see the appendix to this paper). We shall not go here into the details of how this can be done except to remark that in the t-plane the path of integration can be any simple continuous curve from -1 to $+1$ lying in the half-plane $\mathcal{I}t > 0$ (for further details see the appendix). Under these circumstances we can expand

$$e^{-pz^3(1+3[t\cos\gamma+\sqrt{1-t^2}\sin\gamma\cos\omega]^2)/4} \quad (62)$$

as a power series in p under the integral sign in equation (61) and evaluate the integral term by term. We thus obtain

$$\left.\begin{aligned} &\frac{1}{4}\int_0^\infty\int_{-1}^{1}\int_0^{2\pi} e^{izt-\frac{1}{4}pz^3(1+3[t\cos\gamma+\sqrt{1-t^2}\sin\gamma\cos\omega]^2)} \\ &\times(1+3[t\cos\gamma+\sqrt{1-t^2}\sin\gamma\cos\omega]^2)\, z^{1/2}d\omega dt dz \\ &= \sum_{n=0}^{\infty} I_n\,, \end{aligned}\right\} \quad (63)$$

where we have written

$$I_n = (-1)^n\frac{p^n}{n!}\int_0^\infty\int_{-1}^{1}\int_0^{2\pi} e^{izt}\left(\frac{1}{4}z^3[1+3(t\cos\gamma+\sqrt{1-t^2}\sin\gamma\cos\omega)^2]\right)^{n+1} z^{-5/2}d\omega dt dz\,. \quad (64)$$

The evaluation of the integral I_n for general values of n will be found in the appendix. For our present purposes it is sufficient to evaluate I_0. We have

$$I_0 = \frac{1}{4}\int_0^\infty\int_{-1}^{1}\int_0^{2\pi} e^{izt}[1+3(t\cos\gamma+\sqrt{1-t^2}\sin\gamma\cos\omega)^2]\, z^{1/2}d\omega dt dz\,. \quad (65)$$

The integration over ω is immediate, and we have

$$I_0 = \frac{1}{2}\pi\int_0^\infty\int_{-1}^{1} e^{izt}\left\{1+3\left[t^2\cos^2\gamma+\frac{1}{2}(1-t^2)\sin^2\gamma\right]\right\} z^{1/2}dt dz\,. \quad (66)$$

[7] The relevance of these remarks becomes apparent when it is noted that the integral on the right-hand side of equation (59) for $p = 0$, namely,

$$\frac{1}{4}\int_0^\infty\int_{-1}^{1}\int_0^{2\pi}\cos(zt)[1+3(t\cos\gamma+\sqrt{1-t^2}\sin\gamma\cos\omega)^2]z^{1/2}d\omega dt dz\,, \quad (60)$$

is neither unconditionally nor absolutely convergent.

[8] We shall use $\mathcal{R}$ and $\mathcal{I}$ to denote the real and imaginary parts of a complex quantity.

Again the integration over z can be carried out. We obtain (cf. appendix)

$$I_0 = \frac{1}{2}\pi\Gamma\left(\frac{3}{2}\right)\int_{-1}^{+1}\left\{1+3\left[t^2\cos^2\gamma+\frac{1}{2}(1-t^2)\sin^2\gamma\right]\right\}(-it)^{-3/2}dt. \quad (67)$$

Remembering that $i = \exp(i\pi/2)$, we have

$$(-i)^{-3/2} = (e^{-i\pi/2})^{-3/2} = e^{+3i\pi/4} = -e^{-i\pi/4}. \quad (68)$$

The expression for I_0 can therefore be re-written in the form

$$I_0 = -\frac{\pi}{2}\Gamma\left(\frac{3}{2}\right)e^{-i\pi/4}\left\{3\left(\cos^2\gamma-\frac{1}{2}\sin^2\gamma\right)\int_{-1}^{+1}t^{1/2}dt+\left(1+\frac{3}{2}\sin^2\gamma\right)\int_{-1}^{+1}t^{-3/2}dt\right\}. \quad (69)$$

The integrals over t occurring in the foregoing equation are, of course, complex integrals. Writing

$$t = e^{i\theta}, \quad (70)$$

we find

$$\int_{-1}^{+1}t^{1/2}dt = i\int_{\pi}^{0}e^{3i\theta/2}d\theta = \frac{2}{3}[\,e^{3i\theta/2}\,]_{\pi}^{0} = \frac{2}{3}(1+i), \quad (71)$$

and

$$\int_{-1}^{+1}t^{-3/2}dt = i\int_{\pi}^{0}e^{-i\theta/2}d\theta = -2[\,e^{-i\theta/2}\,]_{\pi}^{0} = -2(1+i). \quad (72)$$

Substituting from equations (71) and (72) in equation (69), we obtain

$$\left.\begin{aligned} I_0 &= -\frac{\pi}{2}\Gamma\left(\frac{3}{2}\right)e^{-i\pi/4}(1+i)\left\{2\left(\cos^2\gamma-\frac{1}{2}\sin^2\gamma\right)-2\left(1+\frac{3}{2}\sin^2\gamma\right)\right\}, \\ &= 3\pi\Gamma\left(\frac{3}{2}\right)e^{-i\pi/4}(1+i)\sin^2\gamma. \end{aligned}\right\} \quad (73)$$

Hence, according to equations (61), (63) and (73),

$$\left.\begin{aligned} F'(0) &= 3\pi\Gamma\left(\frac{3}{2}\right)\sin^2\gamma\,\mathcal{R}\,e^{-i\pi/4}(1+i) \\ &= 3\pi\Gamma\left(\frac{3}{2}\right)2^{1/2}\sin^2\gamma \\ &= \frac{3}{4}(2\pi)^{3/2}\sin^2\gamma. \end{aligned}\right\} \quad (74)$$

Combining equations (54), (58), and (74), we now have

$$D(p) = \frac{8}{15}(2\pi)^{3/2}+\frac{3}{4}(2\pi)^{3/2}p\sin^2\gamma+O(p^2), \quad (75)$$

or, according to equation (51),

$$C(\boldsymbol{\rho},\boldsymbol{\sigma}_1) = \frac{8}{15}(2\pi)^{3/2}|\boldsymbol{\rho}|^{3/2}+\frac{3}{4}(2\pi)^{3/2}\frac{|\boldsymbol{\sigma}_1|^2}{|\boldsymbol{\rho}|^{3/2}}\sin^2\gamma+O(|\boldsymbol{\sigma}_1|^4). \quad (76)$$

Reverting to our original variable σ (cf. eq. [33]), we have

$$C(\rho, \sigma) = \frac{8}{15}(2\pi)^{3/2}|\rho|^{3/2} + \frac{3(2\pi)^{3/2}}{4j^2GM}\frac{|\sigma|^2}{|\rho|^{3/2}}\sin^2\gamma + O(|\sigma|^4) . \quad (77)$$

Finally, substituting the foregoing expression for $C(\rho, \sigma)$ in equation (44), we obtain

$$A(\rho, \sigma) = e^{-a|\rho|^{3/2} - b|\sigma|^2|\rho|^{-3/2}\sin^2\gamma + O(|\sigma|^4)} , \quad (78)$$

where we have written

$$\left.\begin{aligned} a &= \frac{4}{15}(2\pi GM)^{3/2}n , \\ b &= \frac{3}{8}(2\pi)^{3/2}(GM)^{1/2}j^{-2}n . \end{aligned}\right\} \quad (79)$$

6. *The behavior of* D(p) *for* p $\rightarrow \infty$.—To study the behavior of $D(p)$ for $p \rightarrow \infty$ we shall start from equation (53). Setting

$$z = p^{-1/3}y \quad (80)$$

in this equation, we find that we can express $D(p)$ in the form

$$D(p) = p^{1/2}J(p) \quad (81)$$

where

$$J(p) = \int_0^\infty\int_{-1}^1\int_0^{2\pi} \{1 - \cos(p^{-1/3}[t\cos\gamma + \sqrt{1-t^2}\sin\gamma\cos\omega]y)\, e^{-y^3(1+3t^2)/4}\}\, y^{-5/2}d\omega dt dy . \quad (82)$$

To determine the behavior of $J(p)$ for $p \rightarrow \infty$, we re-write it in the form

$$J(p) = J(\infty) + K(p) \quad (83)$$

where

$$J(\infty) = \int_0^\infty\int_{-1}^1\int_0^{2\pi} [1 - e^{-y^3(1+3t^2)/4}]\, y^{-5/2}d\omega dt dy \quad (84)$$

and

$$K(p) = \int_0^\infty\int_{-1}^1\int_0^{2\pi} e^{-y^3(1+3t^2)/4}[1 - \cos(p^{-1/3}[[t\cos\gamma + \sqrt{1-t^2}\sin\gamma\cos\omega]]y]\, y^{-5/2}d\omega dt dy . \quad (85)$$

$J(\infty)$ is readily evaluated. After performing the integration with respect to ω, we have

$$J(\infty) = 4\pi\int_0^\infty\int_0^1 (1 - e^{-y^3(1+3t^2)/4})\, y^{-5/2}dt dy . \quad (86)$$

Integrating by parts with respect to y, we obtain

$$J(\infty) = \frac{2\pi}{3}\int_0^1\int_0^\infty e^{-y^3(1+3t^2)/4}(1+3t^2)\, y^{-3/2}d(y^3)\, dt . \quad (87)$$

The integrations over y and t can now be carried out and lead to the following result:

$$J(\infty) = \frac{4}{3}\pi\Gamma\left(\frac{1}{2}\right)\int_0^1 \sqrt{1+3t^2}\,dt = \frac{4}{3}\pi^{3/2}Q_0 , \tag{88}$$

where

$$Q_0 = \int_0^1 \sqrt{1+3t^2}\,dt = 1 + \frac{1}{2\sqrt{3}}\log(2+\sqrt{3}) = 1.38017 . \tag{89}$$

Returning to the discussion of $K(p)$, it is clear that, since we are interested only in its behavior as $p \to \infty$, we can expand the term

$$1 - \cos\left(p^{-1/3}[t\cos\gamma + \sqrt{1-t^2}\sin\gamma\cos\omega]\,y\right) , \tag{90}$$

which occurs under the integral sign in equation (85) in a power series and integrate term by term. In this manner we obtain

$$K(p) = \sum_{n=1}^{\infty} K_n(p) \tag{91}$$

where we have written

$$\left.\begin{aligned} K_n(p) = (-1)^{n+1}\frac{p^{-2n/3}}{2n!}\int_0^{\infty}\int_{-1}^{1}\int_0^{2\pi} \\ \times e^{-y^3(1+3t^2)/4}[t\cos\gamma + \sqrt{1-t^2}\sin\gamma\cos\omega]^{2n} y^{(4n-5)/2}\,d\omega\,dt\,dy . \end{aligned}\right\} \tag{92}$$

Performing, first, the integration with respect to y, we find

$$\left.\begin{aligned} K_n(p) = (-1)^{n+1}\frac{p^{-2n/3}}{2n!}\frac{1}{3}\Gamma\left(\frac{2n}{3}-\frac{1}{2}\right)2^{(4n-3)/} \\ \times\int_{-1}^{1}\int_0^{2\pi}\frac{[t\cos\gamma + \sqrt{1-t^2}\sin\gamma\cos\omega]^{2n}}{(1+3t^2)^{(4n-3)/6}}\,dt\,d\omega . \end{aligned}\right\} \tag{93}$$

For our purposes it appears that it is sufficient to evaluate only the term K_1. We have

$$K_1 = \frac{2^{1/3}}{6}\Gamma\left(\frac{1}{6}\right)p^{-2/3}\int_{-1}^{1}\int_0^{2\pi}\frac{[t\cos\gamma + \sqrt{1-t^2}\sin\gamma\cos\omega]^2}{(1+3t^2)^{1/6}}\,dt\,d\omega . \tag{94}$$

After performing the integration with respect to ω, we obtain

$$\left.\begin{aligned} K_1 &= \frac{2^{4/3}\Gamma(\frac{1}{6})\pi}{3}p^{-2/3}\int_0^1 \frac{t^2\cos^2\gamma + \frac{1}{2}(1-t^2)\sin^2\gamma}{(1+3t^2)^{1/6}}\,dt \\ &= \frac{2^{1/3}\Gamma(\frac{1}{6})\pi}{3}p^{-2/3}\left[\cos^2\gamma\int_0^1\frac{3t^2-1}{(1+3t^2)^{1/6}}\,dt + \int_0^1\frac{1-t^2}{(1+3t^2)^{1/6}}\,dt\right] . \end{aligned}\right\} \tag{95}$$

Let

$$\left.\begin{aligned} 2\lambda &= \frac{2^{1/3}\Gamma(\frac{1}{6})\pi}{3}\int_0^1\frac{3t^2-1}{(1+3t^2)^{1/6}}\,dt , \\ 2\mu &= \frac{2^{1/3}\Gamma(\frac{1}{6})\pi}{3}\int_0^1\frac{1-t^2}{(1+3t^2)^{1/6}}\,dt . \end{aligned}\right\} \tag{96}$$

Then

$$K_1 = 2(\lambda\cos^2\gamma + \mu)\,p^{-2/3} . \tag{97}$$

Combining equations (83), (88), (91), (92), and (97), we now have

$$J(p) = \frac{4}{3}\pi^{3/2}Q_0 + 2(\lambda\cos^2\gamma + \mu)\,p^{-2/3} + O(p^{-4/3})\,, \tag{98}$$

or, according to equation (81),

$$D(p) = \frac{4}{3}\pi^{3/2}Q_0 p^{1/2} + 2(\lambda\cos^2\gamma + \mu)\,p^{-1/6} + O(p^{-5/6})\,. \tag{99}$$

Substituting the foregoing form for $D(p)$ in equation (51) we find

$$C(\boldsymbol{\rho}, \boldsymbol{\sigma}_1) = \frac{4}{3}\pi^{3/2}Q_0\,|\boldsymbol{\sigma}_1| + 2(\lambda\cos^2\gamma + \mu)\frac{|\boldsymbol{\rho}|^2}{|\boldsymbol{\sigma}_1|^{1/3}} + O(|\boldsymbol{\rho}|^4)\,, \tag{100}$$

or, finally, according to equations (44) and (100), we have

$$A(\boldsymbol{\rho}, \boldsymbol{\sigma}) = e^{-c|\boldsymbol{\sigma}| - d(\lambda\cos^2\gamma+\mu)|\boldsymbol{\rho}|^2|\boldsymbol{\sigma}|^{-1/3} + O(|\boldsymbol{\rho}|^4)}\,, \tag{101}$$

where we have written

$$\left.\begin{aligned} c &= \tfrac{2}{3}\pi^{3/2}Q_0 GM\, j^{-1}n\,, \\ d &= (GM)^{5/3} j^{1/3} n\,. \end{aligned}\right\} \tag{102}$$

7. *The Holtsmark distribution for* $\boldsymbol{F}$.—According to equation (18) we clearly have

$$W(\boldsymbol{F}) = \frac{1}{64\pi^6}\int_{|\boldsymbol{\rho}|=0}^{\infty}\int_{|\boldsymbol{\sigma}|=0}^{\infty}\int_{|f|=0}^{\infty} e^{-i(\boldsymbol{\rho}\cdot\boldsymbol{F} + \boldsymbol{\sigma}\cdot f)}\,A(\boldsymbol{\rho}, \boldsymbol{\sigma})\,d\boldsymbol{\rho}\,d\boldsymbol{\sigma}\,df\,. \tag{103}$$

But

$$\frac{1}{8\pi^3}\int_{|f|=0}^{\infty} e^{-i\boldsymbol{\sigma}\cdot f}df = \delta(\sigma_1)\,\delta(\sigma_2)\,\delta(\sigma_3)\,, \tag{104}$$

where the δ's are Dirac's δ-functions. Consequently, equation (103) reduces to

$$W(\boldsymbol{F}) = \frac{1}{8\pi^3}\int_{|\boldsymbol{\rho}|=0}^{\infty} e^{-i\boldsymbol{\rho}\cdot\boldsymbol{F}}\,[\,A(\boldsymbol{\rho}, \boldsymbol{\sigma})\,]_{|\boldsymbol{\sigma}|=0}\,d\boldsymbol{\rho}\,, \tag{105}$$

or, using equation (78), we have

$$W(\boldsymbol{F}) = \frac{1}{8\pi^3}\int_{|\boldsymbol{\rho}|=0}^{\infty} e^{-i\boldsymbol{\rho}\cdot\boldsymbol{F}}\,e^{-a|\boldsymbol{\rho}|^{3/2}}\,d\boldsymbol{\rho}\,. \tag{106}$$

Using a frame of reference in which one of the principal axes is in the direction of $\boldsymbol{F}$ and changing to polar co-ordinates, the foregoing formula for $W(\boldsymbol{F})$ can be reduced to

$$W(\boldsymbol{F}) = \frac{1}{4\pi^2}\int_0^{\infty}\int_0^{\pi} e^{-i|\boldsymbol{\rho}||\boldsymbol{F}|\cos\vartheta - a|\boldsymbol{\rho}|^{3/2}}\,|\boldsymbol{\rho}|^2\sin\vartheta\,d\vartheta\,d|\boldsymbol{\rho}|\,. \tag{107}$$

The integration over ϑ is readily effected, and we obtain

$$W(\boldsymbol{F}) = \frac{1}{2\pi^2|\boldsymbol{F}|}\int_0^{\infty} e^{-a|\boldsymbol{\rho}|^{3/2}}\,|\boldsymbol{\rho}|\,\sin(|\boldsymbol{\rho}|\,|\boldsymbol{F}|)\,d|\boldsymbol{\rho}|\,. \tag{108}$$

If we put

$$x = |\boldsymbol{\rho}|\,|\boldsymbol{F}|\,, \tag{109}$$

equation (108) becomes

$$W(\boldsymbol{F}) = \frac{1}{2\pi^2|\boldsymbol{F}|^3}\int_0^\infty e^{-ax^{3/2}/|\boldsymbol{F}|^{3/2}} x \sin x\,dx\,. \tag{110}$$

Since

$$W(|\boldsymbol{F}|) = 4\pi|\boldsymbol{F}|^2 W(\boldsymbol{F})\,, \tag{111}$$

we obtain for the distribution of $|\boldsymbol{F}|$ the formula

$$W(|\boldsymbol{F}|) = \frac{2}{\pi|\boldsymbol{F}|}\int_0^\infty e^{-ax^{3/2}/|\boldsymbol{F}|^{3/2}} x \sin x\,dx\,, \tag{112}$$

which is Holtsmark's result.[9]

We can re-write the foregoing formulae for $W(\boldsymbol{F})$ and $W(|\boldsymbol{F}|)$ more conveniently if we introduce the "normal" field, Q_H, defined by (cf. eq. [79])

$$Q_H = a^{2/3} = \left(\frac{4}{15}\right)^{2/3} 2\pi G M n^{2/3} = 2.6031 G M n^{2/3} \tag{113}$$

and express $|\boldsymbol{F}|$ in terms of this unit:

$$|\boldsymbol{F}| = \beta Q_H = \beta a^{2/3}\,. \tag{114}$$

Equation (112) now takes the form

$$W(|\boldsymbol{F}|) = \frac{1}{Q_H} H(\beta)\,, \tag{115}$$

where we have written

$$H(\beta) = \frac{2}{\pi\beta}\int_0^\infty e^{-(x/\beta)^{3/2}} x \sin x\,dx\,. \tag{116}$$

Similarly, equation (110) becomes

$$W(\boldsymbol{F}) = \frac{1}{4\pi a^2}\frac{H(\beta)}{\beta^2}\,. \tag{117}$$

Finally, we may note the following asymptotic expressions for $H(\beta)$:

$$H(\beta) = \frac{4}{3\pi}\beta^2 - \frac{2}{9\pi}\Gamma\left(\frac{10}{3}\right)\beta^4 + O(\beta^6) \qquad (\beta \to 0) \tag{118}$$

and

$$H(\beta) = \frac{15}{8}\sqrt{\frac{2}{\pi}}\beta^{-5/2} + \frac{24}{\pi}\beta^{-4} + O(\beta^{-11/2}) \qquad (\beta \to \infty)\,. \tag{119}$$[10]

8. *The moments* $\overline{f_\xi^2}$, $\overline{f_\eta^2}$, *and* $\overline{f_\zeta^2}$.—Let us choose a system of axes (ξ, η, ζ) such that the ξ-axis is in the direction of $\boldsymbol{F}$. Then, according to equation (18),

$$\int_{|\boldsymbol{f}|=0}^{\infty} W(\boldsymbol{F}, \boldsymbol{f})\, f_\xi^2 d\boldsymbol{f} = \frac{1}{64\pi^6}\int_{|\boldsymbol{f}|=0}^{\infty}\int_{|\boldsymbol{\rho}|=0}^{\infty}\int_{|\boldsymbol{\sigma}|=0}^{\infty} e^{-i(\boldsymbol{\rho}\cdot\boldsymbol{F}+\boldsymbol{\sigma}\cdot\boldsymbol{f})} A(\boldsymbol{\rho}, \boldsymbol{\sigma})\, f_\xi^2 d\boldsymbol{\rho} d\boldsymbol{\sigma} d\boldsymbol{f}\,. \tag{120}$$

[9] Cf. Chandrasekhar, *op. cit.*, (eq. [12]).

[10] The coefficients of the higher-order terms in the two series (36 of the first and 20 of the second) have been tabulated by S. Verweij, *Pub. Ap. Inst. Amsterdam*, No. 5, Table 3, 1936.

But

$$\frac{1}{8\pi^3}\int_{|f|=0}^{\infty} e^{-i\boldsymbol{\sigma}\cdot f} f_\xi^2 df = -\delta''(\sigma_\xi)\,\delta(\sigma_\eta)\,\delta(\sigma_\zeta)\,, \tag{121}$$

where the δ denotes Dirac's δ-function and δ'' its second derivative. Remembering that

$$\int_{-\infty}^{+\infty} f(x)\,\delta''(x)\,dx = f''(0)\,, \tag{122}$$

equation (120) reduces to

$$\int_{|f|=0}^{\infty} W(\boldsymbol{F}, f)\, f_\xi^2 df = -\frac{1}{8\pi^3}\int_{|\boldsymbol{\rho}|=0}^{\infty} e^{-i\boldsymbol{\rho}\cdot\boldsymbol{F}}\left[\frac{\partial^2}{\partial\sigma_\xi^2}A(\boldsymbol{\rho},\boldsymbol{\sigma})\right]_{|\boldsymbol{\sigma}|=0} d\boldsymbol{\rho}\,. \tag{123}$$

Similarly,

$$\int_{|f|=0}^{\infty} W(\boldsymbol{F}, f)\, f_\eta^2 df = -\frac{1}{8\pi^3}\int_{|\boldsymbol{\rho}|=0}^{\infty} e^{-i\boldsymbol{\rho}\cdot\boldsymbol{F}}\left[\frac{\partial^2}{\partial\sigma_\eta^2}A(\boldsymbol{\rho},\boldsymbol{\sigma})\right]_{|\boldsymbol{\sigma}|=0} d\boldsymbol{\rho}\,, \tag{124}$$

and

$$\int_{|f|=0}^{\infty} W(\boldsymbol{F}, f)\, f_\zeta^2 df = -\frac{1}{8\pi^3}\int_{|\boldsymbol{\rho}|=0}^{\infty} e^{-i\boldsymbol{\rho}\cdot\boldsymbol{F}}\left[\frac{\partial^2}{\partial\sigma_\zeta^2}A(\boldsymbol{\rho},\boldsymbol{\sigma})\right]_{|\boldsymbol{\sigma}|=0} d\boldsymbol{\rho}\,. \tag{125}$$

According to equation (78) for $A(\rho, \sigma)$, we clearly have

$$\left[\frac{\partial^2}{\partial\sigma_\xi^2}A(\boldsymbol{\rho},\boldsymbol{\sigma})\right]_{|\boldsymbol{\sigma}|=0} = -b\,e^{-a|\boldsymbol{\rho}|^{3/2}}|\boldsymbol{\rho}|^{-3/2}\frac{\partial^2}{\partial\sigma_\xi^2}|\boldsymbol{\sigma}|^2\sin^2\gamma\,, \tag{126}$$

where it will be recalled that γ is the angle between $\boldsymbol{\rho}$ and $\boldsymbol{\sigma}$. Hence,

$$\left.\begin{aligned}\frac{\partial^2}{\partial\sigma_\xi^2}|\boldsymbol{\sigma}|^2\sin^2\gamma &= \frac{\partial^2}{\partial\sigma_\xi^2}\left(|\boldsymbol{\sigma}|^2 - \frac{1}{|\boldsymbol{\rho}|^2}[\boldsymbol{\rho}\cdot\boldsymbol{\sigma}]^2\right)\\ &= \frac{\partial^2}{\partial\sigma_\xi^2}\left(\sigma_\xi^2+\sigma_\eta^2+\sigma_\zeta^2 - \frac{1}{|\boldsymbol{\rho}|^2}[\rho_\xi\sigma_\xi+\rho_\eta\sigma_\eta+\rho_\zeta\sigma_\zeta]^2\right)\\ &= 2\left(1-\frac{\rho_\xi^2}{|\boldsymbol{\rho}|^2}\right).\end{aligned}\right\} \tag{127}$$

Combining equations (126) and (127), we have

$$\left[\frac{\partial^2}{\partial\sigma_\xi^2}A(\boldsymbol{\rho},\boldsymbol{\sigma})\right]_{|\boldsymbol{\sigma}|=0} = -2b\,e^{-a|\boldsymbol{\rho}|^{3/2}}|\boldsymbol{\rho}|^{-3/2}\left(1-\frac{\rho_\xi^2}{|\boldsymbol{\rho}|^2}\right). \tag{128}$$

Substituting the foregoing equation in equation (123), we obtain

$$\int_{|f|=0}^{\infty} W(\boldsymbol{F}, f)\, f_\xi^2 df = \frac{b}{4\pi^3}\int_{|\boldsymbol{\rho}|=0}^{\infty} e^{-i\boldsymbol{\rho}\cdot\boldsymbol{F}-a|\boldsymbol{\rho}|^{3/2}}\left(1-\frac{\rho_\xi^2}{|\boldsymbol{\rho}|^2}\right)|\boldsymbol{\rho}|^{-3/2}d\boldsymbol{\rho}\,. \tag{129}$$

Using polar co-ordinates, equation (129) becomes

$$\int_{|f|=0}^{\infty} W(\boldsymbol{F},f)\, f_\xi^2 df = \frac{b}{4\pi^3}\int_0^\infty\int_0^\pi\int_0^{2\pi} e^{-i|\boldsymbol{\rho}||\boldsymbol{F}|\cos\vartheta - a|\boldsymbol{\rho}|^{3/2}}(1-\cos^2\vartheta)\,|\boldsymbol{\rho}|^{1/2}\sin\vartheta\, d\omega d\vartheta d|\boldsymbol{\rho}|\,. \quad (130)$$

Similarly, equations (124) and (125) can be reduced to the forms

$$\left.\begin{aligned}\int_{|f|=0}^{\infty} W(\boldsymbol{F},f)\, f_\eta^2 df &= \frac{b}{4\pi^3}\int_0^\infty\int_0^\pi\int_0^{2\pi} e^{-i|\boldsymbol{\rho}||\boldsymbol{F}|\cos\vartheta - a|\boldsymbol{\rho}|^{3/2}} \\ &\qquad \times(1-\sin^2\vartheta\sin^2\omega)\,|\boldsymbol{\rho}|^{1/2}\sin\vartheta\, d\omega d\vartheta d|\boldsymbol{\rho}|\,, \\ \int_{|f|=0}^{\infty} W(\boldsymbol{F},f)\, f_\zeta^2 df &= \frac{b}{4\pi^3}\int_0^\infty\int_0^\pi\int_0^{2\pi} e^{-i|\boldsymbol{\rho}||\boldsymbol{F}|\cos\vartheta - a|\boldsymbol{\rho}|^{3/2}} \\ &\qquad \times(1-\sin^2\vartheta\cos^2\omega)\,|\boldsymbol{\rho}|^{1/2}\sin\vartheta\, d\omega d\vartheta d|\boldsymbol{\rho}|\,.\end{aligned}\right\} \quad (131)$$

After performing the integrations with respect to ω in the foregoing equations and some further reductions, they are seen to take the forms

$$\int_{|f|=0}^{\infty} W(\boldsymbol{F},f)\, f_\xi^2 df = \frac{b}{\pi^2}\int_{|\boldsymbol{\rho}|=0}^{\infty}\int_{y=0}^{1} e^{-a|\boldsymbol{\rho}|^{3/2}}\cos(|\boldsymbol{\rho}||\boldsymbol{F}|y)(1-y^2)\,|\boldsymbol{\rho}|^{1/2} dy d|\boldsymbol{\rho}| \quad (132)$$

and

$$\left.\begin{aligned}\int_{|f|=0}^{\infty} W(\boldsymbol{F},f)\, f_\eta^2 df &= \int_{|f|=0}^{\infty} W(\boldsymbol{F},f)\, f_\xi^2 df \\ &= \frac{b}{2\pi^2}\int_{|\boldsymbol{\rho}|=0}^{\infty}\int_{y=0}^{1} e^{-a|\boldsymbol{\rho}|^{3/2}}\cos(|\boldsymbol{\rho}||\boldsymbol{F}|y)(1+y^2)\,|\boldsymbol{\rho}|^{1/2} dy d|\boldsymbol{\rho}|\,.\end{aligned}\right\} \quad (133)$$

Putting

$$|\boldsymbol{\rho}||\boldsymbol{F}| = x\,; \qquad |\boldsymbol{F}| = a^{2/3}\beta = Q_H\beta\,, \quad (134)$$

equations (132) and (133) can be expressed in the alternative forms

$$\int_{|f|=0}^{\infty} W(\boldsymbol{F},f)\, f_{||}^2 df = \frac{b}{\pi^2 a}\frac{1}{\beta^{3/2}}\int_0^\infty\int_0^1 e^{-(x/\beta)^{3/2}}x^{1/2}(1-y^2)\cos xy\, dy dx\,, \quad (135)$$

and

$$\int_{|f|=0}^{\infty} W(\boldsymbol{F},f)\, f_{\perp}^2 df = \frac{b}{2\pi^2 a}\frac{1}{\beta^{3/2}}\int_0^\infty\int_0^1 e^{-(x/\beta)^{3/2}}x^{1/2}(1+y^2)\cos xy\, dy dx\,, \quad (136)$$

where we have further used $f_{||}$ and $f_{\perp}$ to denote the components of $\boldsymbol{f}$ in the direction of, and in a direction perpendicular to, $\boldsymbol{F}$.

Again, equations (135) and (136) can be further reduced by performing the integrations over y. Since

$$\left.\begin{aligned}\int_0^1 \cos xy\, dy &= \frac{1}{x}\sin x\,, \\ \int_0^1 y^2\cos xy\, dy &= \frac{1}{x^3}(2x\cos x + x^2\sin x - 2\sin x)\,,\end{aligned}\right\} \quad (137)$$

we readily obtain

$$\int_{|f|=0}^{\infty} W(\boldsymbol{F},f)\, f_{||}^2 df = \frac{2b}{\pi^2 a}\frac{1}{\beta^{3/2}}\int_0^{\infty} e^{-(x/\beta)^{3/2}}(\sin x - x\cos x)\, x^{-5/2}dx \tag{138}$$

and

$$\int_{|f|=0}^{\infty} W(\boldsymbol{F},f)\, f_{\perp}^2 df = \frac{b}{\pi^2 a}\frac{1}{\beta^{3/2}}\int_0^{\infty} e^{-(x/\beta)^{3/2}}(x^2\sin x + x\cos x - \sin x)\, x^{-5/2}dx\,. \tag{139}$$

From these equations we obtain the important formula

$$\int_{|f|=0}^{\infty} W(\boldsymbol{F},f)\, |f|^2 df = \frac{2b}{\pi^2 a}\frac{1}{\beta^{3/2}}\int_0^{\infty} e^{-(x/\beta)^{3/2}} x^{-1/2}\sin x dx\,. \tag{140}$$

Finally, to obtain the corresponding moments, we should divide the foregoing equations by $W(\boldsymbol{F})$ (eq. [117]). Hence,

$$\left.\begin{aligned} \overline{f_{||}^2} &= \frac{8ab}{\pi}\frac{\beta^{1/2}}{H(\beta)}\int_0^{\infty} e^{-(x/\beta)^{3/2}}(\sin x - x\cos x)^{-5/2}dx\,, \\ \overline{f_{\perp}^2} &= \frac{4ab}{\pi}\frac{\beta^{1/2}}{H(\beta)}\int_0^{\infty} e^{-(x/\beta)^{3/2}}(x^2\sin x + x\cos x - \sin x)\, x^{-5/2}dx\,, \end{aligned}\right\} \tag{141}$$

and

$$\overline{|f_{||}|^2}^{\boldsymbol{F}} = \frac{8ab}{\pi}\frac{\beta^{1/2}}{H(\beta)}\int_0^{\infty} e^{-(x/\beta)^{3/2}} x^{-1/2}\sin x dx\,. \tag{142}$$

There are some simple relations between $\overline{f_{||}^2}$ and $\overline{f_{\perp}^2}$ for the cases of weak and strong fields. To establish these relations it would clearly be sufficient to examine the behavior of the integrals

$$\int_0^{\infty} e^{-(x/\beta)^{3/2}}(\sin x - x\cos x)\, x^{-5/2}dx \tag{143}$$

and

$$\int_0^{\infty} e^{-(x/\beta)^{3/2}} x^{-1/2}\sin x dx \tag{144}$$

for $\beta \to 0$ and $\beta \to \infty$. Consider first the behavior as $\beta \to 0$. Setting

$$x = \beta y\,, \tag{145}$$

the integrals become

$$\beta^{-3/2}\int_0^{\infty} e^{-y^{3/2}}(\sin\beta y - \beta y\cos\beta y)\, y^{-5/2}dy \tag{146}$$

and

$$\beta^{1/2}\int_0^{\infty} e^{-y^{3/2}} y^{-1/2}\sin\beta y dy\,. \tag{147}$$

For $\beta \to 0$ these reduce, respectively, to

$$\frac{1}{3}\beta^{3/2}\int_0^{\infty} e^{-y^{3/2}} y^{1/2}dy \quad \text{and} \quad \beta^{3/2}\int_0^{\infty} e^{-y^{3/2}} y^{1/2}dy\,, \tag{148}$$

i.e., to the values

$$\frac{2}{9}\beta^{3/2} \quad \text{and} \quad \frac{2}{3}\beta^{3/2}\,. \tag{149}$$

For $\beta \to \infty$ the integrals tend respectively to

$$\int_0^\infty (\sin x - x \cos x)\, x^{-5/2} dx \quad \text{and} \quad \int_0^\infty x^{-1/2} \sin x dx\,; \tag{150}$$

in other words, to the values

$$\frac{2}{3}\sqrt{\frac{\pi}{2}} \quad \text{and} \quad \sqrt{\frac{\pi}{2}}. \tag{151}$$

On the other hand, according to equations (118) and (119), we have

$$H(\beta) \to \frac{4}{3\pi}\beta^2 \qquad (\beta \to 0) \tag{152}$$

and

$$H(\beta) \to \frac{15}{8}\sqrt{\frac{2}{\pi}}\beta^{-5/2} \qquad (\beta \to \infty)\,. \tag{153}$$

Combining these various relations, we find

$$\overline{f_{||}^2} = \frac{4}{3}ab\,; \qquad \overline{f_{\perp}^2} = \frac{4}{3}ab\,; \qquad \overline{|f|^2}_{|F|} = 4ab \qquad (\beta \to 0) \tag{154}$$

and

$$\overline{f_{||}^2} = \frac{64}{45}ab\beta^3\,; \qquad \overline{f_{\perp}^2} = \frac{16}{45}ab\beta^3\,; \qquad \overline{|f|^2}_{|F|} = \frac{32}{15}ab\beta^3 \qquad (\beta \to \infty)\,. \tag{155}$$

According to these relations,

$$\overline{f_{||}^2} = \overline{f_{\perp}^2} \qquad (\beta \to 0)\,, \tag{156}$$

and

$$\overline{f_{||}^2} = \overline{4}\,\overline{f_{\perp}^2} \qquad (\beta \to \infty)\,. \tag{157}$$

Hence, *for weak fields the probability of a change's occurring in the field acting at a given instant of time is independent of the direction and magnitude of the initial field, while for strong fields the probability of a change's occurring in the direction of the initial field is twice as great as in a direction at right angles to it.* The physical interpretation of this result is clear. A weak field results from a fluctuation of a symmetrical configuration of stars about the point considered. We should therefore expect the changes to follow, to be equally likely in all directions. On the other hand, a strong field acting at a point implies a highly asymmetrical configuration of stars about the point, and consequently changes are more likely to occur in the direction of the initial field than in other directions.

Of the three quantities $\overline{f_{||}^2}$, $\overline{f_{\perp}^2}$, and $\overline{|f|^2}$, the last is clearly of the greatest importance. We shall therefore consider this quantity a little more closely. We shall first re-write equation (142), giving this quantity in the form

$$\overline{|f|^2}_{|F|} = 4ab\frac{\beta^{1/2}G(\beta)}{H(\beta)}\,, \tag{158}$$

where

$$G(\beta) = \frac{2}{\pi}\int_0^\infty e^{-(x/\beta)^{3/2}} x^{-1/2} \sin x dx\,. \tag{159}$$

We shall now show how $G(\beta)$ can be expressed in terms of $H(\beta)$. Differentiating equation (159) with respect to β, we obtain

$$\frac{dG}{d\beta} = \frac{3}{\pi}\frac{1}{\beta^{5/2}}\int_0^\infty e^{-(x/\beta)^{3/2}} x \sin x\, dx \tag{160}$$

or

$$\frac{dG}{d\beta} = \frac{3}{2} H(\beta)\, \beta^{-3/2}. \tag{161}$$

Hence

$$G(\beta) = \frac{3}{2}\int_0^\beta \beta^{-3/2} H(\beta)\, d\beta. \tag{162}$$

We have already determined the behavior of the integral occurring on the right-hand side of equation (159) (cf. eqs. [149] and [151]). Accordingly, we now have

$$G(\beta) \to \frac{4}{3\pi}\beta^{3/2} \qquad (\beta \to 0) \tag{163}$$

and

$$G(\beta) \to \sqrt{\frac{2}{\pi}} = 0.79788 \qquad (\beta \to \infty). \tag{164}$$

The functions $G(\beta)$ and $H(\beta)$ are tabulated in Table 1.

TABLE 1*

THE HOLTSMARK FUNCTION $H(\beta)$, $G(\beta)$, AND THE MEAN LIFE $\tau(\beta)$ FOR A GIVEN FIELD STRENGTH

β	$H(\beta)$	$G(\beta)$	$\tau(\beta)$	β	$H(\beta)$	$G(\beta)$	$\tau(\beta)$
0.0	0.000000	0.00000	0.00000	2.7	0.219	0.7339	1.151
0.1	.004225	.01340	0.09987	2.8	.201	.7408	1.128
0.2	.01667	.03766	0.1989	2.9	.183	.7468	1.100
0.3	.03664	.06852	0.2964	3.0	.166	.7520	1.071
0.4	.06308	.1041	0.3915	3.25	.139	.7628	1.033
0.5	.09460	.1429	0.4837	3.75	.095	.7770	0.942
0.6	.1296	.1840	0.5722	4.0	.080	.7815	0.905
0.7	.1664	.2263	0.6562	5.0	.041	.7905	0.762
0.8	.2033	.2690	0.7353	6.0	.02417	.7943	0.669
0.9	.2387	.3113	0.8091	7.0	.01524	.7958	0.596
1.0	.2713	.3527	0.8770	8.0	.01038	.7965	0.543
1.1	.3000	.3926	0.9390	9.0	.007449	.7973	0.502
1.2	.324	.4305	0.9947	10.0	.005562	0.7979	0.469
1.3	.343	.4663	1.044	15.0	.001875	.....	0.369
1.4	.356	.4997	1.086	20.0	.000885	.....	0.315
1.5	.364	.5307	1.122	25.0	.000498	.....	0.279
1.6	.367	.5591	1.153	30.0	.000313	.....	0.254
1.7	.365	.5851	1.176	35.0	.000212	.....	0.234
1.8	.360	.6086	1.195	40.0	.000151	.....	0.219
1.9	.351	.6299	1.208	45.0	.000112	.....	0.206
2.0	.339	.6489	1.216	50.0	.000086	.....	0.195
2.1	.325	.6659	1.219	60.0	.000054	.....	0.178
2.2	.310	.6811	1.219	70.0	.000037	.....	0.165
2.3	.293	.6945	1.213	80.0	.000026	.....	0.154
2.4	.275	.7064	1.203	90.0	.000020	.....	0.145
2.5	.257	.7168	1.190	100.0	0.000015	.....	0.137
2.6	0.238	0.7259	1.173				

* β measures the field in the unit $2.603\, G[M^{3/2}]^{2/3} n^{2/3}$, and τ is measured in the unit $0.3201\, [M^{3/2}]^{1/6}/[M^{1/2}|\mathbf{v}|^2]^{1/2} n^{1/3}$. The values of $H(\beta)$ for $\beta \leq 1.1$ and for $\beta \geq 6$ have been recomputed. The intermediate values were taken from a table of Verweij (*Pub. Ap. Inst. Amsterdam*, No. 5, Table 3, 1936).

9. *The mean life of the state* F.—The physical ideas underlying the notion of the mean life of a *state* F can be described as follows.

First, we may remark that by a state $\boldsymbol{F}_0$ we mean that at some fixed point P a force per unit mass of intensity $\boldsymbol{F}_0$ is acting at a given instant of time ($t = 0$, say). Owing to

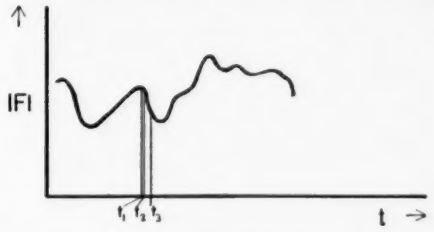

FIG. 3

the motions of the stars, the force acting at P will gradually change with time (see Fig. 3). If we denote by $\chi(\boldsymbol{F}_0; \boldsymbol{F}, t)$ the probability that a force of intensity $\boldsymbol{F}$ will act at P after a time t, it is clear on general grounds that

$$\chi(\boldsymbol{F}_0; \boldsymbol{F}, t) \to W(\boldsymbol{F}) \qquad (t \to \infty) \tag{165}$$

where $W(\boldsymbol{F})$ is given by equation (110). In other words, after a sufficient length of time the force acting at P will be totally uncorrelated with that acting at time $t = 0$. On the other hand, the force acting only after a very short interval of time will be strongly correlated with $\boldsymbol{F}_0$ acting at $t = 0$. But the phrases "after a sufficient length of time" and "after a very short interval of time" need to be made more precise, and the notion of the "*mean life*" is introduced just for this purpose.

If the process by which $\boldsymbol{F}$, acting at a given point, changes with time, could be included in the general class of stochastic processes of the Markoff type,[11] then we may expect the correlation between the forces $\boldsymbol{F}(t_1)$ and $\boldsymbol{F}(t_2)$, acting at two different instants and at the same point, to decrease exponentially with time according to a formula of the form

$$e^{-t/T}. \tag{166}$$

Under these circumstances, T can properly be called the mean life of the state $\boldsymbol{F}$. While the exact specification of T will depend on a deeper analysis of the nature of the stochastic phenomenon underlying the change of $\boldsymbol{F}$ with time at a given point, it is clear that with sufficient accuracy we may define the mean life by the formula

$$T = \frac{|\boldsymbol{F}|}{\sqrt{\overline{|f|^2_{\boldsymbol{F}}}}}, \tag{167}$$

where $\overline{|f|^2}$ has the same meaning as in § 8. According to equations (114) and (158), we therefore have

$$T = \sqrt{\frac{a^{1/3}}{4b}\frac{\beta^{3/2}H(\beta)}{G(\beta)}}. \tag{168}$$

The foregoing equation suggests that we measure T in terms of the following unit t_0, which appears natural to this problem:

$$t_0 = \sqrt{\frac{a^{1/3}}{4b}}. \tag{169}$$

Substituting for a and b from equation (79), we find that

$$t_0 = \frac{2^{1/3}}{3^{2/3}5^{1/6}\pi^{1/2}}\frac{j}{n^{1/3}}. \tag{170}$$

[11] See J. L. Doob, "The Brownian Movement and Stochastic Equations," *Ann. Math.* (in press).

For the Maxwellian distribution of velocities explicitly assumed in our present calculations

$$\overline{|v|^2} = \frac{3}{2j^2}. \tag{171}$$

Using this relation we can express t_0 alternatively in the form

$$t_0 = \frac{1}{(30)^{1/6}\pi^{1/2}} \frac{1}{n^{1/3}\sqrt{\overline{|v|^2}}} = \frac{0.32007}{n^{1/3}\sqrt{\overline{|v|^2}}}. \tag{172}$$

And, finally, if we denote by τ the mean life expressed in this unit, we have

$$\tau = \sqrt{\frac{\beta^{3/2}H(\beta)}{G(\beta)}}. \tag{173}$$[12]

According to equations (152), (153), (163), and (164), we have

$$\tau \to \beta, \qquad (\beta \to 0), \tag{174}$$

and

$$\tau \to \sqrt{\frac{15}{8}}\beta^{-1/2} = 1.3693\beta^{-1/2}, \qquad (\beta \to \infty). \tag{175}$$

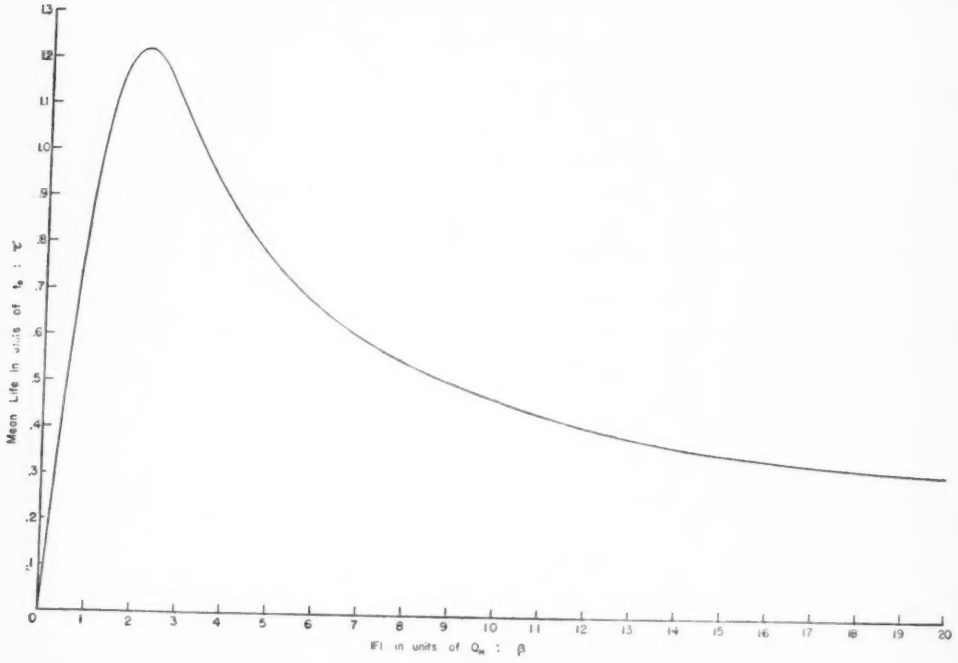

FIG. 4

The function $\tau(\beta)$ has been evaluated numerically and is tabulated in Table 1. Also, the dependence of τ on β is illustrated graphically in Figure 4. The very short lives for weak fields is to be particularly noted.

[12] As we shall see later (§ 12) in the forms (172) and (173), the equations are valid for general spherical distribution of the velocities and not only for distributions of the Maxwellian type.

We may also note that the asymptotic behaviors (174) and (175) for the mean life agree with that predicted by a formula suggested recently by one of us[13] on the basis of certain "intuitive" considerations.

Arguing in terms of the first-neighbor approximation for the probable fields[14] and using a formula due to Smoluchowski[15] on the mean life of a state in which n-particles are found in a given element of volume, it was suggested that

$$T \simeq \sqrt{\frac{2\pi GM}{3\bar{v}^2}} \frac{|F|}{Q_H^{3/2} + |F|^{3/2}}. \tag{176}$$

Equation (176) is equivalent to Smoluchowski's formula for the case in which a particular star continues to exist as the sole occupant of a sphere of radius r, where r is related to $|F|$ according to

$$r = \sqrt{\frac{GM}{|F|}}. \tag{177}$$

Equation (176) can be re-written in the form

$$T = \sqrt{\frac{2\pi GM}{3\bar{v}^2 Q_H}} \frac{\beta}{1+\beta^{3/2}} \tag{178}$$

or, after some minor transformations,

$$T = \sqrt{\frac{2\pi}{3\times 2.603}} \frac{\beta}{1+\beta^{3/2}} \frac{1}{n^{1/3}\sqrt{|v|^2}} = 0.896 \frac{\beta}{1+\beta^{3/2}} \frac{1}{n^{1/3}\sqrt{|v|^2}}. \tag{179}$$

It is seen, as already stated, that equation (179) predicts asymptotic behaviors for T which are the same as those derived from equation (168). However, it is also seen that equation (179) overestimates T by a factor of the order of 2 in the entire range.

The usefulness of our present more exact formula for the mean life to problems of stellar dynamics will be considered in a later paper.

10. *The distribution of f.*—Following a procedure similar to that adopted in § 7 for deriving the Holtsmark distribution, we find that

$$W(f) = \frac{1}{8\pi^3} \int_{|\sigma|=0}^{\infty} e^{-i\sigma\cdot f} [\, A(\rho, \sigma)\,]_{|\rho|=0} d\sigma \tag{180}$$

or, according to equation (101),

$$W(f) = \frac{1}{8\pi^3} \int_{|\sigma|=0}^{\infty} e^{-i\sigma\cdot f - c|\sigma|} d\sigma. \tag{181}$$

The foregoing equation is readily reduced to

$$W(f) = \frac{1}{2\pi^2 |f|} \int_0^{\infty} e^{-c|\sigma|} \sin(|\sigma|\,|f|)\, |\sigma|\, d|\sigma|. \tag{182}$$

[13] Chandrasekhar, *op. cit.*, see particularly § 6.

[14] See §§ 4 and 5 in the reference quoted in n. 13.

[15] *Op. cit.*, p. 557; see §§ 5, 6, and 7 and particularly eq. (30).

The integration over $|\sigma|$ can also be effected, and we obtain the closed expression

$$W(f) = \frac{1}{\pi^2} \frac{c}{(c^2 + |f|^2)^2}. \tag{183}$$

This formula suggests that we express $|f|$ in units of c. Let

$$|f| = ca\,. \tag{184}$$

Then

$$W(f) = \frac{1}{\pi^2} \frac{1}{c^3(1+a^2)^2}. \tag{185}$$

The distribution of $W(|f|)$ can also be written down. Since

$$W(|f|) = 4\pi |f|^2 W(f)\,, \tag{186}$$

we have

$$W(|f|) = \frac{4}{\pi} \frac{c|f|^2}{(c^2 + |f|^2)^2} \tag{187}$$

or, alternatively,

$$W(|f|) = \frac{4}{\pi} \frac{a^2}{c(1+a^2)^2}. \tag{188}$$

We may note that, according to equations (89) and (102),

$$c = \tfrac{2}{3}\pi^{3/2}(1.38017)GMnj^{-1} \tag{189}$$

or, expressing j in terms of $\overline{|v|}$,

$$c = \frac{\pi^2}{3}(1.38017)GMn\overline{|v|} = 4.5406\,GMn\overline{|v|}\,. \tag{190}$$

Finally, we remark on the formal identity between our present law of distribution of f and the law of distribution of the *field strengths* F to be expected from a random distribution of point dipoles.[16] However, a little consideration shows that we should, in fact, have this formal equivalence between the two problems.

11. *The probable field to be expected for an assigned rate of change.*—Let us choose a system of axes (ξ, η, ζ) such that the ξ-axis is in the direction of f. By a procedure analogous to that adopted in § 8 for deriving the moments $\overline{f_\xi^2}$, etc., we readily find that

$$\int_{|F|=0}^{\infty} W(F, f) F_\xi^2 dF = -\frac{1}{8\pi^3} \int_{|\sigma|=0}^{\infty} e^{-i\sigma\cdot f} \left[\frac{\partial^2}{\partial \rho_\xi^2} A(\rho, \sigma)\right]_{|\rho|=0} d\sigma\,. \tag{191}$$

There are, of course, similar expressions for the corresponding integrals involving F_η^2 and F_ζ^2. Adding these three equations, we obtain

$$\int_{|F|=0}^{\infty} W(F, f)\,|F|^2 dF = -\frac{1}{8\pi^3} \int_{|\sigma|=0}^{\infty} e^{-i\sigma\cdot f} \left[\nabla_\rho^2 A(\rho, \sigma)\right]_{|\rho|=0} d\sigma\,. \tag{192}$$

But, according to equation (101),

$$[\nabla_\rho^2 A(\rho, \sigma)]_{|\rho|=0} = -2d(\lambda + 3\mu)\, e^{-c|\sigma|}\,|\sigma|^{-1/3}\,. \tag{193}$$

[16] J. Holtsmark, *Ann. d. Phys.*, **58**, 577, 1919 (eqs. [66] and [69]).

Hence,

$$\int_{|F|=0}^{\infty} W(F,f)\,|F|^2 dF = \frac{d(\lambda+3\mu)}{4\pi^3}\int_{|\sigma|=0}^{\infty} e^{-i\sigma\cdot f-c|\sigma|}\,|\sigma|^{-1/3}d\sigma\,. \qquad (194)$$

Using polar co-ordinates and after some further minor reductions, we find that

$$\int_{|F|=0}^{\infty} W(F,f)\,|F|^2 dF = \frac{d(\lambda+3\mu)}{\pi^2|f|}\int_0^{\infty} e^{-c|\sigma|}\,|\sigma|^{2/3}\sin(|\sigma|\,|f|)\,d|\sigma|\,. \qquad (195)$$

Again the integration over $|\sigma|$ can be effected, and we obtain

$$\int_{|F|=0}^{\infty} W(F,f)\,|F|^2 dF = \frac{d(\lambda+3\mu)}{\pi^2}\Gamma\left(\frac{5}{3}\right)\frac{1}{|f|\,(c^2+|f|^2)^{5/6}}\sin\left(\frac{5}{3}\tan^{-1}\frac{|f|}{c}\right). \qquad (196)$$

The moment of $|F|_f^2$ is obtained by dividing the foregoing equation by $W(f)$. Accordingly, combining equations (183) and (196), we thus obtain

$$\overline{|F|_f^2} = \frac{d}{c}(\lambda+3\mu)\,\Gamma\left(\frac{5}{3}\right)\frac{(c^2+|f|^2)^{7/6}}{|f|}\sin\left(\frac{5}{3}\tan^{-1}\frac{|f|}{c}\right), \qquad (197)$$

or, expressing $|f|$ in units of c, we have

$$\overline{|F|_f^2} = d\,c^{1/3}(\lambda+3\mu)\,\Gamma\left(\frac{5}{3}\right)\frac{1}{\alpha}(1+\alpha^2)^{7/6}\sin\left(\frac{5}{3}\tan^{-1}\alpha\right). \qquad (198)$$

Substituting for c and d from equation (102), we find that

$$d\,c^{1/3} = (\tfrac{2}{3}\pi^{3/2}Q_0)^{1/3}G^2M^2n^{4/3} = 1.7239\,G^2M^2n^{4/3}\,. \qquad (199)$$

Further, according to equations (96),

$$\lambda+3\mu = \frac{2^{1/3}\Gamma(\frac{1}{6})\,\pi}{3}\int_0^1\frac{dt}{(1+3t^2)^{1/6}} = 7.3441\int_0^1\frac{dt}{(1+3t^2)^{1/6}}\,. \qquad (200)$$

A numerical evaluation of the integral occurring on the right-hand side of equation (200) gave

$$\int_0^1\frac{dt}{(1+3t^2)^{1/6}} = 0.90795\,. \qquad (201)$$

Combining the foregoing equations, we obtain

$$\overline{|F|_f^2} = 10.377\,G^2M^2n^{4/3}\frac{1}{\alpha}(1+\alpha^2)^{7/6}\sin\left(\frac{5}{3}\tan^{-1}\alpha\right); \qquad (202)$$

or, expressing $|F|$ in units of Q_H, we have

$$\frac{\sqrt{\overline{|F|_f^2}}}{Q_H} = 1.2375\,\Phi(\alpha)\,, \qquad (203)$$

where

$$\Phi(\alpha) = \alpha^{-1/2}(1+\alpha^2)^{7/12}\sin^{1/2}\left(\frac{5}{3}\tan^{-1}\alpha\right) \qquad (204)$$

The asymptotic behavior of $\Phi(a)$ may be noted:

$$\left.\begin{aligned} \Phi(a) &\to \sqrt{\frac{5}{3}} \qquad (a \to 0)\,, \\ \Phi(a) &\to \frac{1}{\sqrt{2}} a^{2/3} \quad (a \to \infty)\,. \end{aligned}\right\} \tag{205}$$

The function $\Phi(a)$ is tabulated in Table 2.

TABLE 2

$\Phi(a)$

a	$\Phi(a)$	a	$\Phi(a)$	a	$\Phi(a)$
0.0	1.29	0.9	1.44	4.0	2.34
.1	1.29	1.0	1.47	5.0	2.60
.2	1.30	1.2	1.53	6.0	2.84
.3	1.31	1.4	1.59	7.0	3.07
.4	1.33	1.6	1.65	8.0	3.30
.5	1.35	1.8	1.71	9.0	3.51
.6	1.37	2.0	1.77	10.0	3.72
.7	1.39	2.5	1.92	20.0	5.57
0.8	1.42	3.0	2.07	40.0	8.56

According to equations (203) and (205),

$$\sqrt{|\boldsymbol{F}|^2_f} \propto |\boldsymbol{f}|^{2/3} \qquad (|\boldsymbol{f}| \to \infty)\,. \tag{206}$$

It is of interest to compare the foregoing proportionality with a similar one, which results from equation (155), namely,

$$\sqrt{|\boldsymbol{f}|^2_F} \propto |\boldsymbol{F}|^{3/2} \qquad (|\boldsymbol{F}| \to \infty)\,. \tag{207}$$

12. *Generalizations to include arbitrary spherical distribution of the velocities.*—So far, we have assumed that the distribution of the velocities conforms to Maxwell's law. We shall now indicate how we can generalize our results to include an arbitrary spherical distribution of the velocities and to remove the restriction to a Maxwellian distribution. As a preliminary to this discussion, we shall first consider the case when all the stars have the same *absolute value* for $\boldsymbol{v}$ but with random orientations, in other words,

$$|\boldsymbol{v}| = v_0 = \text{constant}\,, \tag{208}$$

but is arbitrary otherwise. Under these circumstances we can still formally speak of a distribution of the velocities; but the function describing this distribution has the singular form

$$\tau = \frac{1}{4\pi v_0^3} \delta(|\boldsymbol{v}|^2 - v_0^2)\,, \tag{209}$$

where δ stands for Dirac's δ-function. The use of the δ-function at this stage is clearly only a formal device and can be avoided if one so wishes. On the other hand, the trans-

formations required in the subsequent analysis are more naturally suggested by its use, and we shall therefore not attempt to avoid it. Substituting then, the foregoing expression for τ in equation (29) and using equation (27), we obtain

$$\left.\begin{aligned} A(\boldsymbol{\rho}, \boldsymbol{\sigma}) = \lim_{\epsilon \to 0} \Bigg[\frac{3(GM)^{3/2}}{64\pi^2 v_0^3} \epsilon^{3/2} \int_{|\boldsymbol{\phi}|>\epsilon} \int_{|\boldsymbol{\psi}|<\infty} e^{i(\boldsymbol{\rho}\cdot\boldsymbol{\phi}+\boldsymbol{\sigma}\cdot\boldsymbol{\psi})} \\ \times \delta\{GM|\boldsymbol{\phi}|^{-3}\Big[|\boldsymbol{\psi}|^2 - \frac{3}{4}|\boldsymbol{\phi}|^{-2}(\boldsymbol{\phi}\cdot\boldsymbol{\psi})^2\Big] - v_0^2\}\, |\boldsymbol{\phi}|^{-9} d\boldsymbol{\phi} d\boldsymbol{\psi} \Bigg]^{\frac{4\pi}{3}\left(\frac{GM}{\epsilon}\right)^{3/2}n} . \end{aligned}\right\} \quad (210)$$

Consider the integral with respect to $\boldsymbol{\psi}$, which occurs in equation (210). We have

$$\int_{|\boldsymbol{\psi}|<\infty} e^{i\boldsymbol{\sigma}\cdot\boldsymbol{\psi}} \delta\{GM|\boldsymbol{\phi}|^{-3}[|\boldsymbol{\psi}|^2 - \frac{3}{4}(\boldsymbol{\phi}\cdot\boldsymbol{\psi})^2] - v_0^2\}\, d\boldsymbol{\psi} . \quad (211)$$

Put

$$\boldsymbol{\psi}_1 = \frac{(GM)^{1/2}}{v_0}\boldsymbol{\psi}; \qquad \boldsymbol{\sigma}_1 = \frac{v_0}{(GM)^{1/2}}\boldsymbol{\sigma} . \quad (212)$$

The integral (211) becomes

$$\frac{v_0^3}{(GM)^{3/2}} \int_{|\boldsymbol{\psi}_1|<\infty} e^{i\boldsymbol{\sigma}_1\cdot\boldsymbol{\psi}_1} \delta\{|\boldsymbol{\phi}|^{-3}\Big[|\boldsymbol{\psi}_1|^2 - \frac{3}{4}|\boldsymbol{\phi}|^{-2}(\boldsymbol{\phi}\cdot\boldsymbol{\psi}_1)^2\Big] - 1\}\, d\boldsymbol{\psi}_1 . \quad (213)$$

Now, choose a system of axes (ξ, η, ζ) such that the ξ-axis is along the $\boldsymbol{\phi}$-direction. The integral (213) becomes

$$\frac{v_0^3}{(GM)^{3/2}} \int_0^\infty\int_0^\infty\int_0^\infty e^{i(\sigma_{1\xi}\psi_{1\xi}+\sigma_{1\eta}\psi_{1\eta}+\sigma_{1\zeta}\psi_{1\zeta})} \delta\Big\{|\boldsymbol{\phi}|^{-3}\Big[\frac{1}{4}\psi_{1\xi}^2 + \psi_{1\eta}^2 + \psi_{1\zeta}^2\Big] - 1\Big\} d\psi_{1\xi} d\psi_{1\eta} d\psi_{1\zeta} . \quad (214)$$

Introduce two vectors $\boldsymbol{s}$ and $\boldsymbol{\chi}$ defined as follows:

$$\boldsymbol{s} = (2\sigma_{1\xi}, \sigma_{1\eta}, \sigma_{1\zeta}); \qquad \boldsymbol{\chi} = |\boldsymbol{\phi}|^{-3/2}\Big(\frac{1}{2}\psi_{1\xi}, \psi_{1\eta}, \psi_{1\zeta}\Big) . \quad (215)$$

In terms of these vectors the integral (214) is seen to reduce to

$$\left.\begin{aligned} \frac{2v_0^3}{(GM)^{3/2}}|\boldsymbol{\phi}|^{9/2} \int_{|\boldsymbol{\chi}|<\infty} e^{i|\boldsymbol{\phi}|^{3/2}(\boldsymbol{s}\cdot\boldsymbol{\chi})} \delta(|\boldsymbol{\chi}|^2 - 1)\, \delta\boldsymbol{\chi} \\ = \frac{8\pi v_0^3}{(GM)^{3/2}}|\boldsymbol{\phi}|^{9/2} \frac{\sin|\boldsymbol{s}|\,|\boldsymbol{\phi}|^{3/2}}{|\boldsymbol{s}|\,|\boldsymbol{\phi}|^{3/2}} . \end{aligned}\right\} \quad (216)$$

But, according to our definition of $\boldsymbol{s}$, we clearly have

$$|\boldsymbol{s}| = |\boldsymbol{\sigma}_1|\sqrt{1+3\cos^2\beta} , \quad (217)$$

where, as in equation (38), β is the angle between the vectors $\boldsymbol{\phi}$ and $\boldsymbol{\sigma}_1$ (or $\boldsymbol{\sigma}$). Thus our expression for $A(\boldsymbol{\rho}, \boldsymbol{\sigma})$ becomes

$$A(\boldsymbol{\rho}, \boldsymbol{\sigma}) = \lim_{\epsilon \to 0} \Bigg[\frac{3}{8\pi}\epsilon^{3/2} \int_{|\boldsymbol{\phi}|>\epsilon} e^{i\boldsymbol{\rho}\cdot\boldsymbol{\phi}} \frac{\sin\sqrt{|\boldsymbol{\sigma}_1|^2|\boldsymbol{\phi}|^3(1+3\cos^2\beta)}}{\sqrt{|\boldsymbol{\sigma}_1|^2|\boldsymbol{\phi}|^3(1+3\cos^2\beta)}} |\boldsymbol{\phi}|^{-9/2} d\boldsymbol{\phi} \Bigg]^{\frac{4\pi}{3}\left(\frac{GM}{\epsilon}\right)^{3/2}n} . \quad (218)$$

The foregoing expression for $A(\boldsymbol{\rho}, \boldsymbol{\sigma})$ has been derived on the assumption that only one value for $|\boldsymbol{v}|$ occurs. Let us now suppose that there is distribution of $|\boldsymbol{v}|$ and that the frequency function describing it can be written in the form

$$\Psi(|\boldsymbol{v}|^2)\,. \tag{219}$$[17]

Under these circumstances, equation (218) clearly generalizes to

$$\left.\begin{aligned} A(\boldsymbol{\rho}, \boldsymbol{\sigma}) = \operatorname*{limit}_{\epsilon \to 0} \Bigg[& \frac{3}{8\pi}\epsilon^{3/2}\int_0^\infty d|\boldsymbol{v}|\Psi(|\boldsymbol{v}|^2) \\ & \times \int_{|\boldsymbol{\phi}|>\epsilon} e^{i\boldsymbol{\rho}\cdot\boldsymbol{\phi}} \frac{\sin\sqrt{|\boldsymbol{\sigma}_1|^2|\boldsymbol{\phi}|^3(1+3\cos^2\beta)}}{\sqrt{|\boldsymbol{\sigma}_1|^2|\boldsymbol{\phi}|^3(1+3\cos^2\beta)}} \frac{d\boldsymbol{\phi}}{|\boldsymbol{\phi}|^{9/2}} \Bigg]^{\frac{4\pi}{3}\left(\frac{GM}{\epsilon}\right)^{3/2}n}, \end{aligned}\right\} \tag{220}$$

where, now,

$$\boldsymbol{\sigma}_1 = \frac{|\boldsymbol{v}|}{(GM)^{1/2}}\boldsymbol{\sigma}\,. \tag{221}$$

Since

$$\frac{3}{8\pi}\epsilon^{3/2}\int_0^\infty d|\boldsymbol{v}|\Psi(|\boldsymbol{v}|^2)\int_{|\boldsymbol{\phi}|>\epsilon}\frac{d\boldsymbol{\phi}}{|\boldsymbol{\phi}|^{9/2}} = 1\,, \tag{222}$$

equation (220) can be re-written as

$$\left.\begin{aligned} A(\boldsymbol{\rho}, \boldsymbol{\sigma}) = \operatorname*{limit}_{\epsilon \to 0} \Bigg[& 1 - \frac{3}{8\pi}\epsilon^{3/2}\int_0^\infty d|\boldsymbol{v}|\Psi(|\boldsymbol{v}|^2) \\ & \times \int_0^\infty \left\{1 - e^{i\boldsymbol{\rho}\cdot\boldsymbol{\phi}} \frac{\sin\sqrt{|\boldsymbol{\sigma}_1|^2|\boldsymbol{\phi}|^3(1+3\cos^2\beta)}}{\sqrt{|\boldsymbol{\sigma}_1|^2|\boldsymbol{\phi}|^3(1+3\cos^2\beta)}}\right\} \frac{d\boldsymbol{\phi}}{|\boldsymbol{\phi}|^{9/2}} \Bigg]^{\frac{4\pi}{3}\left(\frac{GM}{\epsilon}\right)^{3/2}n} \end{aligned}\right\} \tag{223}$$

or

$$A(\boldsymbol{\rho}, \boldsymbol{\sigma}) = e^{-\frac{1}{2}n(GM)^{3/2}C(\boldsymbol{\rho}, \boldsymbol{\sigma})}\,. \tag{224}$$

where we have written

$$\left.\begin{aligned} C(\boldsymbol{\rho}, \boldsymbol{\sigma}) = & \int_0^\infty d|\boldsymbol{v}|\Psi(|\boldsymbol{v}|^2) \\ & \times \int_0^\infty \left\{1 - \cos(\boldsymbol{\rho}\cdot\boldsymbol{\phi})\frac{\sin\sqrt{|\boldsymbol{\sigma}_1|^2|\boldsymbol{\phi}|^3(1+3\cos^2\beta)}}{\sqrt{|\boldsymbol{\sigma}_1|^2|\boldsymbol{\phi}|^3(1+3\cos^2\beta)}}\right\} \frac{d\boldsymbol{\phi}}{|\boldsymbol{\phi}|^{9/2}}. \end{aligned}\right\} \tag{225}$$

It is readily verified that, when Ψ has the form corresponding to a Maxwellian distribution of the velocities, equation (225) reduces identically to equation (45).

[17] It may be remarked in this connection that for a Maxwellian distribution of the velocities

$$\Psi = \frac{4j^3}{\pi^{1/2}}e^{-j^2|\boldsymbol{v}|^2}|\boldsymbol{v}|^2\,, \tag{219'}$$

i.e., the *radial* Gaussian function and *not* the Gaussian function itself.

After a series of transformations similar to that followed in § 4 we find that equation (225) can be expressed as

$$C(\boldsymbol{\rho}, \boldsymbol{\sigma}) = |\boldsymbol{\rho}|^{3/2} \int_0^\infty \Psi(|\boldsymbol{v}|^2)\, D\left(\frac{|\boldsymbol{\sigma}|^2 |\boldsymbol{v}|^2}{GM|\boldsymbol{\rho}|^3}\right) d|\boldsymbol{v}|\,, \tag{226}$$

where $D(p)$ has the following two alternative but equivalent forms (cf. eqs. [52] and [53]):

$$D(p) = \int_0^\infty \int_{-1}^{+1} \int_0^{2\pi} \left\{ 1 - \cos(zt) \frac{\sin \sqrt{p z^3 (1 + 3[t\cos\gamma + \sqrt{1-t^2}\sin\gamma\cos\omega]^2)}}{\sqrt{p z^3 (1 + 3[t\cos\gamma + \sqrt{1-t^2}\sin\gamma\cos\omega]^2)}} \right\} \times z^{-5/2} d\omega dt dz \tag{227}$$

and

$$D(p) = \int_0^\infty \int_{-1}^{+1} \int_0^{2\pi} \left\{ 1 - \cos\left(z[t\cos\gamma + \sqrt{1-t^2}\sin\gamma\cos\omega]\right) \frac{\sin \sqrt{p z^3 (1+3t^2)}}{\sqrt{p z^3 (1+3t^2)}} \right\} \times z^{-5/2} d\omega dt dz\,. \tag{228}$$

For our purposes it is necessary only to discuss the behavior of $D(p)$ for $p \to 0$ and $p \to \infty$. We shall consider first the case $p \to 0$.

i) *Behavior of* D(p) *for* p → 0.—As in § 5, we express $D(p)$ in the form

$$D(p) = D(0) + F(p)\,, \tag{229}$$

where (using eq. [227] for $D(p)$)

$$D(0) = \int_0^\infty \int_{-1}^{1} \int_0^{2\pi} (1 - \cos[zt])\, z^{-5/2} d\omega dt dz \tag{230}$$

and

$$F(p) = \int_0^\infty \int_{-1}^{1} \int_0^{2\pi} \cos(zt) \left\{ 1 - \frac{\sin \sqrt{p z^3 (1 + 3[t\cos\gamma + \sqrt{1-t^2}\sin\gamma\cos\omega]^2)}}{\sqrt{p z^3 (1 + 3[t\cos\gamma + \sqrt{1-t^2}\sin\gamma\cos\omega]^2)}} \right\} \times z^{-5/2} d\omega dt dz\,. \tag{231}$$

The integral on the right-hand side of equation (230) is the same as that which occurs in equation (55). Hence (cf. eq. [58])

$$D(0) = \frac{8}{15}(2\pi)^{3/2}\,. \tag{232}$$

Again, since $F(0) = 0$, we discuss the behavior of $F'(p)$ at $p = 0$. This problem is essentially the same as that considered in § 5 (pp. 497–98) and in the appendix; and, as in that discussion, we write

$$F'(p) = -\Re \int_0^\infty \int_{-1}^{1} \int_0^{2\pi} e^{izt} \frac{\partial}{\partial p} \frac{\sin \sqrt{p z^3 (1 + 3[t\cos\gamma + \sqrt{1-t^2}\sin\gamma\cos\omega]^2)}}{\sqrt{p z^3 (1 + 3[t\cos\gamma + \sqrt{1-t^2}\sin\gamma\cos\omega]^2)}} \times z^{-5/2} d\omega dt dz\,. \tag{233}$$

and, regarding z and t as complex variables, we finally obtain

$$F'(0) = \mathcal{R}\frac{1}{6}\int_0^{\infty}\int_{-1}^{1}\int_0^{2\pi} e^{izt}(1+3[t\cos\gamma+\sqrt{1-t^2}\sin\gamma\cos\omega]^2)\, z^{1/2}d\omega dt dz\,, \quad (234)$$

where the integrations over z and t are also to be carried out along suitable contours. Apart from a factor $\frac{3}{8}$, the integral on the right-hand side of equation (234) is the same as that which occurs in equation (65). Hence (cf. eq. [74])

$$F'(0) = \frac{1}{2}(2\pi)^{3/2}\sin^2\gamma\,. \quad (235)$$

Thus we have

$$D(p) = \frac{8}{15}(2\pi)^{3/2} + \frac{1}{2}(2\pi)^{3/2}p\sin^2\gamma + O(p^2)\,. \quad (236)$$

Substituting for D from the foregoing equation, in equation (226) we readily deduce that

$$C(\boldsymbol{\rho},\boldsymbol{\sigma}) = \frac{8}{15}(2\pi)^{3/2}|\boldsymbol{\rho}|^{3/2} + \frac{1}{2}(2\pi)^{3/2}\frac{\overline{|\boldsymbol{v}|^2}}{GM}\frac{|\boldsymbol{\sigma}|^2}{|\boldsymbol{\rho}|^{3/2}}\sin^2\gamma + O(|\boldsymbol{\sigma}|^4)\,, \quad (237)$$

where we have denoted by $\overline{|\boldsymbol{v}|^2}$ the average defined according to

$$\overline{|\boldsymbol{v}|^2} = \int_0^{\infty}\Psi(|\boldsymbol{v}|^2)\,|\boldsymbol{v}|^2 d|\boldsymbol{v}|\,. \quad (238)$$

From equations (224) and (237) we now obtain

$$A(\boldsymbol{\rho},\boldsymbol{\sigma}) = e^{-a|\boldsymbol{\rho}|^{3/2} - b|\boldsymbol{\sigma}|^2|\boldsymbol{\rho}|^{-3/2}\sin^2\gamma + O(|\boldsymbol{\sigma}|^4)}\,, \quad (239)$$

where we have written

$$a = \frac{4}{15}(2\pi GM)^{3/2}n\,; \qquad b = \frac{1}{4}(2\pi)^{3/2}(GM)^{1/2}\overline{|\boldsymbol{v}|^2}n\,. \quad (240)$$

It is now seen that equation (239) is of exactly the same form as our earlier formula (78). Hence, all the results of §§ 7 and 8 remain unaffected, except for the slightly modified definition of b, which we have now to adopt.[18] Similarly, the expressions for the mean life in § 9 also continue to be valid under our present more general assumptions, provided we measure T in units of t_0 defined according to equation (172) and remembering that the root mean square velocity $\sqrt{\overline{|\boldsymbol{v}|^2}}$, which occurs in the definition of t_0, has to be evaluated according to equation (238).

ii) *Behavior of* D(p) *for* p $\rightarrow \infty$.—Setting

$$z = p^{-1/3}y \quad (241)$$

in equation (228), we find that we can express $D(p)$ in the form

$$D(p) = p^{1/2}J(p)\,, \quad (242)$$

[18] A comparison of the two definitions of b in equations (79) and (240) shows that our present definition agrees with the earlier one, if we substitute for $\overline{|\boldsymbol{v}|^2}$ in equation (240) its value for a Maxwellian distribution of the velocities, namely, $3/2j^2$.

where

$$J(p)=\int_0^\infty\int_{-1}^{1}\int_0^{2\pi}\left\{1-\cos\left(p^{-1/3}[t\cos\gamma+\sqrt{1-t^2}\sin\gamma\cos\omega]\,y\right)\frac{\sin\sqrt{y^3(1+3t^2)}}{\sqrt{y^3(1+3t^2)}}\right\}\times y^{-5/2}d\omega dt dy\,. \tag{243}$$

To determine the behavior of $J(p)$ for $p\to\infty$, we re-write it in the form

$$J(p)=J(\infty)+K(p)\,, \tag{244}$$

where

$$J(\infty)=\int_0^\infty\int_{-1}^{1}\int_0^{2\pi}\left\{1-\frac{\sin\sqrt{y^3(1+3t^2)}}{\sqrt{y^3(1+3t^2)}}\right\}y^{-5/2}d\omega dt dy \tag{245}$$

and

$$K(p)=\int_0^\infty\int_{-1}^{1}\int_0^{2\pi}\frac{\sin\sqrt{y^3(1+3t^2)}}{\sqrt{y^3(1+3t^2)}}\{1-\cos\left(p^{-1/3}[t\cos\gamma+\sqrt{1-t^2}\sin\gamma\cos\omega]\,y\right)\}\times y^{-5/2}d\omega dt dy\,. \tag{246}$$

$J(\infty)$ is readily evaluated. After performing the integration with respect to ω and introducing the new variable

$$x=\sqrt{y^3(1+3t^2)}\,, \tag{247}$$

we obtain

$$J(\infty)=\frac{8\pi}{3}\int_0^1 dt\sqrt{1+3t^2}\int_0^\infty\frac{dx}{x^2}\left(1-\frac{\sin x}{x}\right)=\frac{2}{3}\pi^2Q_0\,, \tag{248}$$

where Q_0 is defined as in equation (89).

Returning to the evaluation of $K(p)$, it is clear that, since we are interested only in its behavior as $p\to\infty$, we can expand the term $\{1-\cos(\ldots.)\}$ occurring in the integrand in equation (246) in a power series. Retaining only the dominant term, we have

$$K(p)=\frac{1}{2}p^{-2/3}\int_0^\infty\int_{-1}^{1}\int_0^{2\pi}\frac{\sin\sqrt{y^3(1+3t^2)}}{\sqrt{y^3(1+3t^2)}}[t\cos\gamma+\sqrt{1-t^2}\sin\gamma\cos\omega]^2\times y^{-1/2}d\omega dt dy+O(p^{-4/3})\,. \tag{249}$$

After performing the integration over ω and introducing the variable x defined as in equation (247), we obtain

$$K(p)=\frac{4}{3}\pi p^{-2/3}\int_0^1\frac{t^2\cos^2\gamma+\frac{1}{2}(1-t^2)\sin^2\gamma}{(1+3t^2)^{1/6}}dt\int_0^\infty\frac{\sin x}{x^{5/3}}dx+O(p^{-4/3})\,. \tag{250}$$

But

$$\int_0^\infty\frac{\sin x}{x^{5/3}}dx=\frac{\pi}{2\Gamma(5/3)}\operatorname{cosec}\left(\frac{5\pi}{6}\right)=\frac{\pi}{\Gamma(5/3)}\,. \tag{251}$$

Hence

$$K(p)=\frac{2\pi^2}{3\Gamma(5/3)}p^{-2/3}\int_0^1\frac{(3t^2-1)\cos^2\gamma+(1-t^2)}{(1+3t^2)^{1/6}}dt\,. \tag{252}$$

Let

$$\left.\begin{aligned}2\lambda&=\frac{2\pi^2}{3\Gamma(5/3)}\int_0^1\frac{3t^2-1}{(1+3t^2)^{1/6}}dt\,,\\ 2\mu&=\frac{2\pi^2}{3\Gamma(5/3)}\int_0^1\frac{1-t^2}{(1+3t^2)^{1/6}}\,.\end{aligned}\right\} \tag{253}$$

Then

$$K(p) = 2(\lambda \cos^2 \gamma + \mu) p^{-2/3} + O(p^{-4/3}). \tag{254}$$

Combining equations (244), (248), and (254), we now have

$$J(p) = \frac{2}{3}\pi^2 Q_0 + 2(\lambda \cos^2 \gamma + \mu) p^{-2/3} + O(p^{-4/3}) \tag{255}$$

or

$$D(p) = \frac{2}{3}\pi^2 Q_0 p^{1/2} + 2(\lambda \cos^2 \gamma + \mu) p^{-1/6} + O(p^{-5/6}) . \tag{256}$$

Introducing the foregoing form for $D(p)$ in equation (226), we find

$$\left.\begin{aligned} C(\boldsymbol{\rho}, \boldsymbol{\sigma}) = \frac{2}{3}\pi^2 Q_0 \frac{\overline{|\boldsymbol{v}|}}{(GM)^{1/2}}|\boldsymbol{\sigma}| + 2(\lambda \cos^2 \gamma + \mu)(GM)^{1/6}\overline{|\boldsymbol{v}|^{-1/3}}\frac{|\boldsymbol{\rho}|^2}{|\boldsymbol{\sigma}|^{1/3}} \\ + O(|\boldsymbol{\rho}|^4) , \end{aligned}\right\} \tag{257}$$

where the bars denote that the averages of the corresponding quantities are to be understood. Finally, according to equations (224) and (257), we have

$$A(\boldsymbol{\rho}, \boldsymbol{\sigma}) = e^{-c|\boldsymbol{\sigma}| - d(\lambda \cos^2\gamma + \mu)|\boldsymbol{\rho}|^2 |\boldsymbol{\sigma}|^{-1/3} + O(|\rho|^4)} , \tag{258}$$

where

$$\left.\begin{aligned} c &= \frac{1}{3}\pi^2 Q_0 GM \overline{|\boldsymbol{v}|}\, n , \\ d &= (GM)^{5/3}\overline{|\boldsymbol{v}|^{-1/3}} n . \end{aligned}\right\} \tag{259}$$

Thus, it is again seen that equation (258) is of exactly the same form as the corresponding equation (101) derived on the basis of an assumed Maxwellian distribution of the velocities. Hence all the results of §§ 10 and 11 remain unaffected except for the modified definitions of c, d, λ, and μ, which we have now to adopt.[19] In particular, with c defined as in equation (190), the distribution of f and $|f|$ remains identically the same. Similarly, in § 11 the analysis up to and including equation (198) continues to be valid with the new definitions of c, d, λ, and μ. However, the numerical factors in the equations following equation (198) (namely, [199]–[203]) are slightly modified. But we need only note that equation (203) now takes the form

$$\frac{\sqrt{\overline{|\boldsymbol{F}|_f^2}}}{Q_H} = 1.2083\,(\overline{|\boldsymbol{v}|}^{1/3}\overline{|\boldsymbol{v}|^{-1/3}})^{1/2}\Phi(a) . \tag{260}$$

13. *Further generalizations to include a distribution over the masses.*—So far, we have assumed that all the stars have the same mass M. We shall now remove this restriction and allow a distribution over different values of the masses. But if we allow M to have

[19] A comparison of our present definitions of c, d, λ, and μ with the earlier definitions (eqs. [96] and [102]) shows that with our present definitions c, $d\lambda$, and $d\mu$ agree respectively with the corresponding quantities of § 6, if we substitute for $\overline{|v|}$ and $\overline{|v|^{-1/3}}$ their values for a Maxwellian distribution, namely, $2/\pi^{1/2}j$ and $2j^{1/3}\Gamma(4/3)/\pi^{1/2}$. It may be noted that the proof of this identity depends on the use of the relation

$$\Gamma(\tfrac{1}{6})\Gamma(\tfrac{5}{6}) = 2^{2/3}\pi^{1/2}\Gamma(\tfrac{1}{3}) .$$

different values we should not naturally suppose that the parameter in the function describing the spherical distribution of the velocities is independent of M. In other words, under the circumstances contemplated, we should strictly introduce a bivariate distribution

$$\Psi(|v|^2; M) \tag{261}$$

to describe the situation adequately.

Now, if the stars of different masses move independently of one another, it is clear that the formula (18) for $W(\boldsymbol{F}, f)$ continues to be valid with $A(\boldsymbol{\rho}, \boldsymbol{\sigma})$ given by

$$A(\boldsymbol{\rho}, \boldsymbol{\sigma}) = \lim_{\substack{N\to\infty \\ R\to\infty}} \left[\frac{3}{4\pi R^3} \int_{0<M<\infty} \int_{|r|<R} \int_{|v|<\infty} e^{i(\boldsymbol{\rho}\cdot\boldsymbol{\phi}+\boldsymbol{\sigma}\cdot\boldsymbol{\psi})} \tau \, dv \, dr \, dM \right]^N, \tag{262}$$

where τ is now a function not only of r and v but also of M. Substituting for τ the bivariate distribution (261) and transforming to the variables $\boldsymbol{\phi}$ and $\boldsymbol{\psi}$ (instead of r and v) we obtain (cf. eqs. [27], [29], and [210])

$$\left.\begin{aligned} A(\boldsymbol{\rho}, \boldsymbol{\sigma}) = {} & \lim_{\epsilon\to 0} \left[\frac{3}{4\pi} \left(\frac{\epsilon}{G}\right)^{3/2} \int\int d|v| \, dM \frac{G^3 M^3}{16\pi |v|^3} \Psi(|v|^2; M) \right. \\ & \times \int_{|\boldsymbol{\phi}|>\epsilon M} \int_{|\boldsymbol{\psi}|<\infty} e^{i(\boldsymbol{\rho}\cdot\boldsymbol{\phi}+\boldsymbol{\sigma}\cdot\boldsymbol{\psi})} \delta \left\{ GM |\boldsymbol{\phi}|^{-3} \left[|\boldsymbol{\psi}|^2 - \frac{3}{4} |\boldsymbol{\phi}|^{-2} (\boldsymbol{\phi}\cdot\boldsymbol{\psi})^2 \right] - |v|^2 \right\} \\ & \left. \times |\boldsymbol{\phi}|^{-9} d\boldsymbol{\phi} \, d\boldsymbol{\psi} \right]^{\frac{4\pi}{3}\left(\frac{G}{\epsilon}\right)^{3/2} n}. \end{aligned}\right\} \tag{263}$$

Put

$$\boldsymbol{\phi} = M\boldsymbol{\phi}_1; \qquad \boldsymbol{\rho} = \frac{1}{M}\boldsymbol{\rho}_1, \tag{264}$$

and

$$\boldsymbol{\psi} = \frac{M|v|}{G^{1/2}}\boldsymbol{\psi}_1; \qquad \boldsymbol{\sigma} = \frac{G^{1/2}}{M|v|}\boldsymbol{\sigma}_1. \tag{265}$$

Equation (263) becomes

$$\left.\begin{aligned} A(\boldsymbol{\rho}, \boldsymbol{\sigma}) = {} & \lim_{\epsilon\to 0} \left[\frac{3}{64\pi^2} \epsilon^{3/2} \int\int d|v| \, dM \Psi(|v|^2; M) \right. \\ & \times \int_{|\boldsymbol{\phi}_1|>\epsilon} \int_{|\boldsymbol{\psi}_1|<\infty} e^{i(\boldsymbol{\rho}_1\cdot\boldsymbol{\phi}_1+\boldsymbol{\sigma}_1\cdot\boldsymbol{\psi}_1)} \delta \left\{ |\boldsymbol{\phi}_1|^{-3} \left[|\boldsymbol{\psi}_1|^2 - \frac{3}{4} |\boldsymbol{\phi}_1|^{-2} (\boldsymbol{\phi}_1\cdot\boldsymbol{\psi}_1)^2 \right] - 1 \right\} \\ & \left. \times |\boldsymbol{\phi}_1|^{-9} d\boldsymbol{\phi}_1 \, d\boldsymbol{\psi}_1 \right]^{\frac{4\pi}{3}\left(\frac{G}{\epsilon}\right)^{3/2} n}. \end{aligned}\right\} \tag{266}$$

But, according to equations (213), (216), and (217),

$$\left.\begin{aligned} & \int_{|\boldsymbol{\psi}_1|<\infty} e^{i\boldsymbol{\sigma}_1\cdot\boldsymbol{\psi}_1} \delta \left\{ |\boldsymbol{\phi}_1|^{-3} \left[|\boldsymbol{\psi}_1|^2 - \frac{3}{4} |\boldsymbol{\phi}_1|^{-2} (\boldsymbol{\phi}_1\cdot\boldsymbol{\psi}_1)^2 \right] - 1 \right\} d\boldsymbol{\psi}_1 \\ & \qquad = 8\pi |\boldsymbol{\phi}|^{9/2} \frac{\sin \sqrt{|\boldsymbol{\sigma}_1|^2 |\boldsymbol{\phi}_1|^3 (1+3\cos^2\beta)}}{\sqrt{|\boldsymbol{\sigma}_1|^2 |\boldsymbol{\phi}_1|^3 (1+3\cos^2\beta)}}, \end{aligned}\right\} \tag{267}$$

where

$$\beta = \sphericalangle(\boldsymbol{\sigma}_1, \boldsymbol{\phi}_1) = \sphericalangle(\boldsymbol{\sigma}, \boldsymbol{\phi}). \tag{268}$$

Equation (266) now reduces to

$$A(\boldsymbol{\rho}, \boldsymbol{\sigma}) = \lim_{\epsilon \to 0} \left[\frac{3}{8\pi} \epsilon^{3/2} \iint d|\boldsymbol{v}|\, dM \Psi(|\boldsymbol{v}|^2; M) \right. \\ \left. \times \int_{|\boldsymbol{\phi}_1|>\epsilon} e^{i\boldsymbol{\rho}_1 \cdot \boldsymbol{\phi}_1} \frac{\sin \sqrt{|\boldsymbol{\sigma}_1|^2 |\boldsymbol{\phi}_1|^3 (1 + 3\cos^2\beta)}}{\sqrt{|\boldsymbol{\sigma}_1|^2 |\boldsymbol{\phi}_1|^3 (1 + 3\cos^2\beta)}} \frac{d\boldsymbol{\phi}_1}{|\boldsymbol{\phi}_1|^{9/2}} \right]^{\frac{4\pi}{3}\left(\frac{G}{\epsilon}\right)^{\frac{3}{2}n}}. \tag{269}$$

As in §§ 3 and 12 (see particularly pp. 494–96), we derive from the foregoing equation the formula

$$A(\boldsymbol{\rho}, \boldsymbol{\sigma}) = e^{-\frac{1}{3}nG^{3/2}C(\boldsymbol{\rho}, \boldsymbol{\sigma})}, \tag{270}$$

where

$$C(\boldsymbol{\rho}, \boldsymbol{\sigma}) = \iint d|\boldsymbol{v}|\, dM \Psi(|\boldsymbol{v}|^2; M) \\ \times \int \left\{ 1 - \cos(\boldsymbol{\rho}_1 \cdot \boldsymbol{\phi}_1) \frac{\sin \sqrt{|\boldsymbol{\sigma}_1|^2 |\boldsymbol{\phi}_1|^3 (1 + 3\cos^2\beta)}}{\sqrt{|\boldsymbol{\sigma}_1|^2 |\boldsymbol{\phi}_1|^3 (1 + 3\cos^2\beta)}} \right\} \frac{d\boldsymbol{\phi}_1}{|\boldsymbol{\phi}_1|^{9/2}}. \tag{271}$$

The second integral in equation (271) is seen to be of the same form as that which occurs in equation (225). Hence we can write it as

$$|\boldsymbol{\rho}_1|^{3/2} D\left(\frac{|\boldsymbol{\sigma}_1|^2}{|\boldsymbol{\rho}_1|^3}\right), \tag{272}$$

where $D(p)$ can be expressed in either of the two forms (227) or (228). Reverting to our original variables $\boldsymbol{\rho}$ and $\boldsymbol{\sigma}$, we can write

$$M^{3/2} |\boldsymbol{\rho}|^{3/2} D\left(\frac{|\boldsymbol{v}|^2 |\boldsymbol{\sigma}|^2}{GM|\boldsymbol{\rho}|^3}\right), \tag{273}$$

instead of (272). Thus $C(\boldsymbol{\rho}, \boldsymbol{\sigma})$ can be written in the form

$$C(\boldsymbol{\rho}, \boldsymbol{\sigma}) = |\boldsymbol{\rho}|^{3/2} \iint M^{3/2} \Psi(|\boldsymbol{v}|^2; M)\, D\left(\frac{|\boldsymbol{v}|^2 |\boldsymbol{\sigma}|^2}{GM|\boldsymbol{\rho}|^3}\right) d|\boldsymbol{v}|\, dM. \tag{274}$$

Now, we have already discussed the behavior of $D(p)$ for $p \to 0$ and $p \to \infty$ and have shown that (cf. eqs. [236] and [256]),

$$D(p) = \frac{8}{15}(2\pi)^{3/2} + \frac{1}{2}(2\pi)^{3/2} p \sin^2\gamma + O(p^2) \qquad (p \to 0) \tag{275}$$

and

$$D(p) = \frac{2}{3}\pi^2 Q_0 p^{1/2} + 2(\lambda \cos^2\gamma + \mu) p^{-1/6} + O(p^{-5/6}) \qquad (p \to \infty), \tag{276}$$

where λ and μ are defined as in equation (253). Corresponding to these two forms for $D(p)$, we obtain from equation (274) the two formulae

$$C(\rho, \sigma) = \frac{8}{15}(2\pi)^{3/2}\overline{M^{3/2}}|\rho|^{3/2} + \frac{1}{2}(2\pi)^{3/2}\frac{\overline{M^{1/2}|v|^2}}{G}\frac{|\sigma|^2}{|\rho|^{3/2}} + O(|\sigma|^4) \quad (|\sigma| \to 0) \tag{277}$$

and

$$C(\rho, \sigma) = \frac{2}{3}\pi^2 Q_0 G^{-1/2}\overline{M|v|}\,|\sigma| + 2(\lambda\cos^2\gamma + \mu)G^{1/6}\overline{M^{5/3}|v|^{-1/3}}\frac{|\rho|^2}{|\sigma|^{1/3}} + O(|\rho|^4) \quad (|\rho| \to 0), \tag{278}$$

where the bars indicate that the averages of the corresponding quantities are understood.

Thus we again have for $A(\rho, \sigma)$ the formulae

$$A(\rho, \sigma) = e^{-a|\rho|^{3/2} - b|\sigma|^2|\rho|^{-3/2}\sin^2\gamma + O(|\sigma|)^4} \quad (|\sigma| \to 0), \tag{279}$$

and

$$A(\rho, \sigma) = e^{-c|\sigma| - d(\lambda\cos^2\gamma + \mu)|\rho|^2|\sigma|^{-1/3} + O(|\rho|^4)} \quad (|\rho| \to 0), \tag{280}$$

where we have now written

$$\left.\begin{aligned} a &= \frac{4}{15}(2\pi)^{3/2}G^{3/2}\overline{M^{3/2}}n, \\ b &= \frac{1}{4}(2\pi)^{3/2}G^{1/2}\overline{M^{1/2}|v|^2}n, \\ c &= \frac{2}{3}\pi^2 Q_0 G\overline{M|v|}\,n, \\ d &= G^{5/3}\overline{M^{5/3}|v|^{-1/3}}n. \end{aligned}\right\} \tag{281}$$

With these new definitions of a, b, c, and d all the results of §§ 7–11 continue to be valid. We may, however, note explicitly that the normal field Q_H is now computed with an average mass $(\overline{M^{3/2}})^{2/3}$:

$$Q_H = 2.603\,G(\overline{M^{3/2}})^{2/3}n^{2/3}. \tag{282}$$

Similarly, the unit of time t_0 in which τ, defined according to equation (173), measures the mean life of the state $|F|/Q_H$ is given by

$$t_0 = \frac{0.32007}{n^{1/3}}\left(\frac{[\overline{M^{3/2}}]^{1/3}}{\overline{M^{1/2}|v|^2}}\right)^{1/2}. \tag{283}$$

Finally, we may note that equation (260) is now generalized to

$$\frac{\sqrt{|F|_f^2}}{Q_H} = 1.2083\frac{([\overline{M|v|}]^{1/3}[\overline{M^{5/3}|v|^{-1/3}}])^{1/2}}{[\overline{M^{3/2}}]^{2/3}}\Phi(a), \tag{284}$$

where $\Phi(a)$ has the same meaning as hitherto.

14. *The distribution in the accelerations in* $\boldsymbol{F}$ *acting at a given point.*—In § 10 we have already considered the problem of the distribution of the rate of change of $\boldsymbol{F}$ acting at some fixed point. We shall now consider, very briefly, the analogous problem of the distribution of the rate of change of $\dot{\boldsymbol{F}}$ acting at a point.

Differentiating equation (3) again with respect to the time, we obtain

$$\boldsymbol{g} = \frac{d^2\boldsymbol{F}}{dt^2} = 3G\Sigma M_i \left\{ 2\frac{\boldsymbol{v}_i(\boldsymbol{r}_i \cdot \boldsymbol{v}_i)}{|\boldsymbol{r}_i|^5} + \frac{\boldsymbol{r}_i |\boldsymbol{v}_i|^2}{|\boldsymbol{r}_i|^5} - 5\frac{\boldsymbol{r}_i(\boldsymbol{r}_i \cdot \boldsymbol{v}_i)^2}{|\boldsymbol{r}_i|^7} \right\}. \tag{285}$$

To determine the probability distribution $W(\boldsymbol{g})$ of $\boldsymbol{g}$, we follow the general method of §§ 2 and 3 and readily obtain the formulae

$$W(\boldsymbol{g}) = \frac{1}{2\pi^2 |\boldsymbol{g}|} \int_0^\infty A(|\boldsymbol{\rho}|)\, |\boldsymbol{\rho}| \sin(|\boldsymbol{g}|\,|\boldsymbol{\rho}|)\, d|\boldsymbol{\rho}|\,, \tag{286}$$

where

$$A(|\boldsymbol{\rho}|) = \lim_{R\to\infty} \left[\frac{3}{4\pi R^3} \int_{|\boldsymbol{r}|<R} \int_{|\boldsymbol{v}|<\infty} \int_0^\infty e^{i\boldsymbol{\rho}\cdot\boldsymbol{\chi}\tau}\, dM\, d\boldsymbol{v}\, d\boldsymbol{r} \right]^{4\pi R^3 n/3}. \tag{287}$$

In equation (287) we have written $\boldsymbol{\chi}$ to denote

$$\boldsymbol{\chi} = 3GM \left\{ 2\frac{\boldsymbol{v}(\boldsymbol{r}\cdot\boldsymbol{v})}{|\boldsymbol{r}|^5} + \frac{\boldsymbol{r}|\boldsymbol{v}|^2}{|\boldsymbol{r}|^5} - 5\frac{\boldsymbol{r}(\boldsymbol{r}\cdot\boldsymbol{v})^2}{|\boldsymbol{r}|^7} \right\}. \tag{288}$$

The evaluation of $A(|\boldsymbol{\rho}|)$ for a spherical distribution of the velocities is straightforward, and we shall not give the details of the analysis particularly as it follows rather closely certain calculations of Holtsmark and Gans[20] on the probability distribution of $\boldsymbol{F}$ arising from a random distribution of point quadrupoles. We find that

$$A(|\boldsymbol{\rho}|) = e^{-q|\boldsymbol{\rho}|^{3/4}}, \tag{289}$$

where

$$q = \frac{64\pi}{3^{1/4}7}\Gamma(1.25)\, \sin\frac{\pi}{8} \left\{ \int_0^1 (1 - 2t^2 + 5t^4)^{3/8} dt \right\} G^{3/4}\overline{M^{3/4}\,|\boldsymbol{v}|^{3/2}}\, n \tag{290}$$

or, numerically,

$$q = 8.1833\, G^{3/4}\overline{M^{3/4}\,|\boldsymbol{v}|^{3/2}}\, n\,. \tag{291}$$

Substituting for $A(|\boldsymbol{\rho}|)$ from equation (289) in equation (286), we obtain

$$W(\boldsymbol{g}) = \frac{1}{2\pi^2 |\boldsymbol{g}|} \int_0^\infty e^{-q|\boldsymbol{\rho}|^{3/4}} |\boldsymbol{\rho}| \sin(|\boldsymbol{\rho}|\,|\boldsymbol{g}|)\, d|\boldsymbol{\rho}|\,. \tag{292}$$

This formula for $W(\boldsymbol{g})$ can be expressed more conveniently if we measure $|\boldsymbol{g}|$ in units of $q^{4/3}$ and put

$$x = |\boldsymbol{\rho}|\,|\boldsymbol{g}|\,. \tag{293}$$

In this manner we find that equation (292) becomes

$$W(\boldsymbol{g}) = \frac{1}{2\pi^2 q^4 \gamma^3} \int_0^\infty e^{-(x/\gamma)^{3/4}} x \sin x\, dx\,, \tag{294}$$

where we have written

$$|\boldsymbol{g}| = q^{4/3}\gamma\,. \tag{295}$$

[20] See the references given in n. 2.

From equation (291) we find that the unit in which it now appears natural to measure $|\boldsymbol{g}|$ has the value

$$q^{4/3} = 16.491\, G[\overline{M^{3/4}|\boldsymbol{v}|^{3/2}}]^{4/3} n^{4/3}\,. \tag{296}$$

Finally, we may note that equation (294) implies for the distribution of $|\boldsymbol{g}|$ the expression

$$W(|\boldsymbol{g}|) = \frac{1}{q^{4/3}} \frac{2}{\pi\gamma} \int_0^\infty e^{-(x/\gamma)^{3/4}} x \sin x\, dx\,. \tag{297}$$

In the forms (296) and (297) we notice the formal identity of our present laws of distribution of $\boldsymbol{g}$ and $|\boldsymbol{g}|$ with the corresponding Holtsmark-Gans formulae giving the distribution of $\boldsymbol{F}$ and $|\boldsymbol{F}|$ arising from a random distribution of point quadrupoles.

We shall return to the applications of the results contained in this paper to problems of stellar dynamics after we have completed the discussion of the related problems of the correlations in the field acting simultaneously at two different points and also the speed of fluctuations of the field acting on a moving star.

We are indebted to Mrs. T. Belland for her assistance in the numerical work involved in the preparation of Tables 1 and 2.

One of us (S. Chandrasekhar) further wishes to record his indebtedness to the Institute for Advanced Study and the University of Princeton for having enabled him to stay at Princeton during the fall quarter of 1941, and which made the present collaboration possible.

YERKES OBSERVATORY
WILLIAMS BAY, WISCONSIN
INSTITUTE FOR ADVANCED STUDY
PRINCETON, NEW JERSEY
February 16, 1942

APPENDIX

1′. We wish to evaluate the integral

$$\left.\begin{aligned} F'(p) = \mathcal{R} \int_0^\infty \int_{-1}^{1} \int_0^{2\pi} & e^{izt - \frac{1}{2}pz^2(1+3[t\cos\gamma + \sqrt{1-t^2}\sin\gamma\cos\omega]^2)} \\ \times \frac{1}{4}(1+3[t\cos\gamma + \sqrt{1-t^2}\sin\gamma\cos\omega]^2)\, & z^{1/2}\, dz\, dt\, d\omega\,, \end{aligned}\right\} \tag{1′}$$

and in particular its asymptotic behavior for $p \gtrsim 0$ (cf. the discussion in § 5). This is a real integral, all integration paths are real, and in it

$$z^{1/2} \quad \text{and} \quad \sqrt{1-t^2} \quad \text{are real and} \geq 0\,. \tag{2′}$$

We shall now modify the integration paths in the

$$\int_0^\infty \int_{-1}^{1} \int_0^{2\pi} \ldots \quad dz\, dt\, d\omega$$

of equation (1′) for z and t by going into the complex plane. But we shall keep the integrand, i.e., the expressions in equation (2′), analytical by staying inside the domains

$$\mathcal{R}\, z \geqq 0 \quad \text{and} \quad \mathcal{I}t \geqq 0, \qquad |t| \leqq 1, \tag{3′}$$

and by choosing those branches in equation (2′) which are real and $\geqq 0$ for z, t real.

These being understood, the integration paths are modified as follows:

I. The real interval $\tau_0: -1 \leqq t \leqq 1$ is replaced by a curve τ running from -1 to 1, but so that it lies (except for its end points -1 and 1) entirely in the interior of the domain (3′). The exponent in the integral contains the factor

$$1 + 3\,[t\cos\gamma + \sqrt{1-t^2}\sin\gamma\cos\omega\,]^2\,.$$

This is real and $\geqq 1$ on τ_0. We choose τ so near to τ_0 that that factor has still an arcus $\leqq \pi/16$, $\geqq -\pi/16$ and an absolute value $\geqq \frac{1}{2}$ on τ.

II. The integrations on z and on t are interchanged so that the one on z is carried out first, for a fixed t. It will therefore be possible to choose the (complex) integration paths for z dependent on t.

If the arcus of z is $\leqq \pi/16$, $\geqq -\pi/16$, then the arcus of the expression

$$\tfrac{1}{4}pz^3(1 + 3\,[t\cos\gamma + \sqrt{1-t^2}\sin\gamma\cos\omega\,]^2) \tag{4′}$$

in the exponent of the integral is $\leqq \pi/4$, $\geqq -\pi/4$ (cf. sec. I concerning t). Hence its real part is positive and at least $\cos(\pi/4)$ times its absolute value. Besides, the absolute value of $(1 + 3\,[\ldots]^2)$ is $\geqq \frac{1}{2}$ (cf. sec. I)—so the absolute convergence of the integral is undisturbed. Consequently, we may use any integration path with such an arcus for z.

III. The positive real axis ζ_0: $0 < z < +\infty$ is replaced by the line ζ_{ω_t}, forming the angle ω_t with it. ω_t depends on t (cf. sec. I) and is $\leqq \pi/16$, $\geqq -\pi/16$ (cf. sec. II).

As t moves along τ for -1 to 1 (inside [3′]), its arcus varies from π to 0. We choose $\omega_t = ([\pi/2] - \text{arcus } t)/8$, which fulfils the above requirements. Now the arcus of izt is equal to

$$\frac{\pi}{2} + \omega_t + \text{arcus } t = \pi - \frac{7}{8}\left(\frac{\pi}{2} - \text{arcus } t\right),$$

and so it is never farther from π than by $7\pi/16$. Hence the real part of izt is negative and at most $\cos(7\pi/16)$ $(=\sin[\pi/16] > 0)$ times its absolute value; i.e.,

$$|\,e^{izt}\,| \leqq e^{-|z||t|\sin(\pi/16)}\,.$$

Now t moving along τ has a positive minimum distance from the origin (cf. sec. I). Let a be $\sin(\pi/16)$ times that distance. Then we have

$$|\,e^{izt}\,| \leqq e^{-a|z|} \qquad (a \text{ fixed and } > 0) \tag{5′}$$

all along our new integration paths.

2′. We need the evaluation

$$\left.\begin{aligned} e^w &= \sum_{n=0}^{m-1}\frac{1}{n!}w^n + \frac{\varphi_m(w)}{m!}w^m\,, \\ |\,\varphi_m(w)\,| &\leqq 1 \quad \text{for} \quad \Re w \leqq 0\,. \end{aligned}\right\} \tag{6′}$$

$\varphi_m(w)$ is everywhere analytic, and clearly

$$\varphi_m(w) \to 0 \quad \text{for} \quad w \to \infty \quad \text{in} \quad \Re w \leqq 0\,.$$

Hence $|\varphi_m(w)|$ assumes its maximum in $\Re w \leqq 0$ on the boundary, at $\Re w = 0$. So it suffices to prove equation (6′) for $\Re w = 0$, i.e., for $w = iu$, u real. Replacing u by $-u$

replaces w, $\varphi_m(w)$ by their complex conjugates, so we may even assume that $u \geqq 0$. Thus equation (6′) becomes

$$\left| e^{iu} - \sum_{n=0}^{m-1} \frac{1}{n!}(iu)^n \right| \leqq \frac{1}{m!}u^m \tag{7′}$$

for u real and $\geqq 0$. However, $e^{iu} - \sum_{n=0}^{m-1} (iu)^n/n!$ vanishes at $u = 0$, together with its $m - 1$ first derivatives, and its mth derivative is $i^m e^{iu}$. Hence it is equal to

$$\frac{1}{(m-1)!}\int_0^u (u-v)^{m-1} i^m e^{iv} dv\,,$$

and so its absolute value is majorized by

$$\frac{1}{(m-1)!}\int_0^u (u-v)^{m-1} dv = \frac{1}{(m-1)!}\frac{u^m}{m} = \frac{1}{m!}u^m\,,$$

proving equation (7′)—and consequently equation (6′).

3′. By section II the real part of equation (4′) is positive, hence we can use equation (6′):

$$\left.\begin{aligned} e^{-pz^3(1+3[\ldots.]^2)/4} = \sum_{n=0}^{m-1} \frac{1}{n!}\left(-\frac{1}{4}pz^3[\![1+3[\ldots.]^2]\!]\right)^n \\ + \frac{\psi_m(z,t,\omega)}{m!}\left(-\frac{1}{4}pz^3[\![1+3[\ldots.]^2]\!]\right)^m, \\ |\psi_m(z,t,\omega)| \leqq 1\,. \end{aligned}\right\} \tag{8′}$$

Combining this with equation (5′) in section III, we conclude that with our new integration paths the integral is uniformly and absolutely convergent for *all* $p > 0$, and we can even use for the

$$e^{-pz^3(1+3[\ldots.]^2)/4}$$

part of its exponential, the power-series expression with remainder term (8′).

Consequently, equation (1′) now gives

$$F'(p) = \sum_{n=0}^{m-1} \Re I_n + J_m\,, \tag{9′}$$

where

$$\left.\begin{aligned} I_n = (-1)^n \frac{p^n}{n!}\iiint e^{izt}\left(\frac{1}{4}z^3[\![1+3[t\cos\gamma + \sqrt{1-t^2}\sin\gamma\cos\omega]\!]^{n+1}\right) \\ \times z^{-5/2}\,dz\,dt\,d\omega \end{aligned}\right\} \tag{10′}$$

and (using eq. [5′] in sec. III)

$$|J_m| \leqq \frac{p^m}{m!}\iiint e^{-\alpha|z|}(C|z|^3)^{m+1} z^{-5/2}\,dz\,dt\,d\omega\,, \tag{11′}$$

with the fixed $\alpha > 0$ and a fixed C.

The right-hand side of equation (11′) is equal to

$$2\pi\frac{p^m}{m!}C^{m+1}\int_0^\infty e^{-\alpha|z|}\,|z|^{(6m+1)/2}\,dz$$

(l is the length of the curve τ in sec. I), i.e., to

$$2\pi\frac{p}{m!}C^{m+1}l\alpha^{-(6m+3)/2}\Gamma\left(3m+\frac{3}{2}\right).$$

Thus equation (11′) becomes

$$|J_m| \leqq \frac{\Gamma(3m+\frac{3}{2})\,p^m}{m!}AB^m, \tag{12′}$$

with two fixed A, B.

4′. Let us now evaluate I_n in equation (10′). Clearly,

$$I_n = (-1)^n\frac{p^n}{n!}\frac{1}{4^{n+1}}\sum_{l=0}^{n+1}\binom{n+1}{l}3^l\iiint e^{izt}(t\cos\gamma+\sqrt{1-t^2}\sin\gamma\cos\omega)^{2l} \times z^{(6n+1)/2}dz\,dt\,d\omega.$$

The last integral again is equal to

$$\sum_{h=0}^{2l}\binom{2l}{h}\cos^{2l-h}\gamma\sin^h\gamma\iiint e^{izt}t^{2l-h}(1-t^2)^{h/2}\cos^h\omega\, z^{(6n+1)/2}dz\,dt\,d\omega.$$

We can carry out the ω-integration. It gives

$$\int_0^{2\pi}\cos^h\omega d\omega = \frac{1}{2^h}\int_0^{2\pi}(e^{i\omega}+e^{-i\omega})^h d\omega = \frac{1}{2^h}\sum_{k=0}^{h}\binom{h}{k}\int_0^{2\pi}e^{i(2k-h)\omega}d\omega$$

$$\left\{\begin{array}{ll} = \dfrac{1}{2^h}\binom{h}{\frac{h}{2}}2\pi & \text{for } h \text{ even,} \\ = 0 & \text{for } h \text{ odd.}\end{array}\right\}$$

So we may put in the above $\sum_{h=0}^{2l}$ sum $h = 2j$, and the expression for that integral becomes

$$\sum_{j=0}^{l}\binom{2l}{2j}\cos^{2(l-j)}\gamma\sin^{2j}\gamma\frac{1}{4^j}\binom{2j}{j}2\pi\iint e^{izt}t^{2(l-j)}(1-t^2)^j z^{(6n+1)/2}dz\,dt.$$

Hence we have for I_n

$$I_n = (-1)^n\frac{p^n}{n!}\frac{2\pi}{4^{n+1}}\sum_{l=0}^{n+1}\sum_{j=0}^{l}\binom{n+1}{l}\binom{2l}{2j}\binom{2j}{j}\frac{3^l}{4^j}\cos^{2(l-j)}\gamma\sin^{2j}\gamma\iint e^{izt}t^{2(l-j)} \times (1-t^2)^j z^{(6n+1)/2}dz\,dt.$$

In this integral we are still bound to the old integration paths—so we have for z the line ζ_{ω_t} of section III, along which arcus $z = \omega_t = ([\pi/2] - \text{arcus } t)/8$. Now the integral is absolutely convergent along any line on which the real part of izt is negative, i.e., its arcus $< 3\pi/2$, $> \pi/2$, i.e., arcus $z < \pi -$ arcus t, $> -$ arcus t. (Remember that $0 <$ arcus $t < \pi$, cf. sec. III.) Our line ζ_{ω_t} is in this domain, and so is the line arcus $z = \pi/2 -$ arcus t. (Also the line arcus $z = 0$, i.e., the positive real axis. This determines the branch of $z^{(6n+1)/2}$, since that must be real and $\geqq 0$ there.) We can therefore replace the integration path ζ_{ω_t} by ζ_{ψ_t}: arcus $z = \pi/2 -$ arcus t.

On the new integration path $y = -izt$ is real and $\geqq 0$. Owing to what we said above concerning the branch of $z^{(6n+1)/2}$, the arcus of $z^{(6n+1)/2}dz$ is now equal to $(6n+3)([\pi/2] - \text{arcus } t)/2$. So we can carry out the z-integration, which is

$$\int e^{izt} z^{(6n+1)/2} dz ,$$

and it gives

$$e^{i\pi(6n+3)/4} t^{-(6n+3)/2} \int e^{-y} y^{(6n+1)/2} dy ,$$

with the arcus t we always had and y real and $\geqq 0$. The expression is therefore

$$e^{i3\pi(2n+1)/4} \Gamma\left(3n+\tfrac{3}{2}\right) t^{-(6n+3)/2} .$$

Thus the entire integral is equal to

$$e^{i3\pi(2n+1)/4} \Gamma\left(3n+\frac{3}{2}\right) \int t^{(4[l-j]-6n-3)/2} (1-t^2)^j dt .$$

Put (for any two $\alpha, \beta = 0, 1, 2, \ldots$.)

$$I(\alpha, \beta) = \int t^{-(2\alpha-1)/2} (1-t^2)^\beta dt . \tag{13'}$$

Remembering that

$$(-1)^n e^{i3\pi(2n+1)/4} = e^{-i\pi n + i3\pi(2n+1)/4} = e^{i\pi(2n+3)/4} ,$$

we obtain for I_n the expression

$$\left.\begin{aligned} I_n = e^{i\pi(2n+3)/4} \frac{\Gamma\left(3n+\frac{3}{2}\right) p^n}{n!} \frac{2\pi}{4^{n+1}} \sum_{l=0}^{n+1} \sum_{j=0}^{l} \binom{n+1}{l} \binom{2l}{2j} \binom{2j}{j} \frac{3^l}{4^j} \\ \times \cos^{2(l-j)} \gamma \sin^{2j} \gamma I(3n+2-2[l-j], j) . \end{aligned}\right\} \tag{14'}$$

5'. The determination of the $I(\alpha, \beta)$ of equation (13'), for

$$\alpha = 3n+2-2(l-j) \qquad (\beta = j),$$

remains.

The above imply

$$\alpha - 2\beta = 3n+2-2l$$

and, as

$$n = 0, 1, 2, \ldots .; \qquad l = 0\ \ 1, \ldots . n+1; \qquad j = 0, 1, \ldots ., l$$

therefore

$$\alpha, \beta, \alpha - 2\beta = 0, 1, 2, \ldots . \tag{15'}$$

In evaluating equation (13'), we put $t^2 = u$. Then

$$I(\alpha, \beta) = \frac{1}{2} \int u^{-(2\alpha+1)/4} (1-u)^\beta du , \tag{16'}$$

the integration path being the $t^2 = u$ image of τ in section I—i.e., a closed curve (from 1 to 1), circling the origin in the negative direction. Along this curve arcus t varies from π to 0 (cf. sec. III), so arcus u varies from 2π to 0. Further properties of this curve are immaterial, since any two such curves will give the same integral (16').

Equation (16') is the B-integral, except for the integration path.

Consider a $\beta \neq 0$, i.e., $\beta = 1, 2, \ldots .$ The factors $u^{-(2\alpha+1)/4}$ and $(1-u)^\beta$ in the integrand of equation (16') have the primitive function $-4u^{-(2\alpha-3)/4}/(2\alpha-3)$ and the

derivative $-\beta(1-u)^{\beta-1}$, and the factor $(1-u)^{\beta}$ vanishes at both ends of the integration path ($u=1$). So partial integration gives

$$I(\alpha,\beta) = -\frac{\beta}{\frac{1}{2}\alpha-\frac{3}{4}} I(\alpha-2,\beta-1)\,.$$

Hence (for any $\beta = 0, 1, 2, \ldots$.) by iteration

$$I(\alpha,\beta) = (-1)^{\beta}\frac{\beta(\beta-1)\ldots.1}{(\frac{1}{2}\alpha-\frac{3}{4})(\frac{1}{2}\alpha-\frac{7}{4})\ldots.(\frac{1}{2}\alpha-\beta+\frac{1}{4})} I(\alpha-2\beta,0)\,.$$

Again

$$\left.\begin{aligned} I(\alpha-2\beta,0) &= \frac{1}{2}\int u^{-(2\alpha-4\beta+1)/4}du \\ &= \frac{1}{2}\frac{1}{-\frac{1}{2}\alpha+\beta+\frac{3}{4}}\left[u^{-(2\alpha-4\beta-3)/4}\right]_{u=1}^{u=1}, \end{aligned}\right\}$$

the arcus at the beginning and end (i.e., lower and upper $u=1$) being 2π and 0 (cf. above). So this is equal to

$$\left.\begin{aligned} \frac{1}{2}\frac{1}{-\frac{1}{2}\alpha+\beta+\frac{3}{4}}(1-e^{-i\pi[2\alpha-4\beta-3]/2}) &= -\frac{1}{2}\frac{1}{\frac{1}{2}\alpha-\beta-\frac{3}{4}}(1-[-1]^{\alpha}e^{-i\pi/2}) \\ &= -\frac{1}{2}\frac{1}{\frac{1}{2}\alpha-\beta-\frac{3}{4}}(1+[-1]^{\alpha}i)\,. \end{aligned}\right\}$$

Consequently,

$$\left.\begin{aligned} I(\alpha,\beta) &= (-1)^{\beta+1}\frac{1}{2}(1+[-1]^{\alpha}i)\frac{\beta(\beta-1)\ldots.1}{(\frac{1}{2}\alpha-\frac{3}{4})(\frac{1}{2}\alpha-\frac{7}{4})\ldots.(\frac{1}{2}\alpha-\beta+\frac{1}{4})(\frac{1}{2}\alpha-\beta-\frac{3}{4})} \\ &= (-1)^{\beta+1}\frac{1}{2}(1+[-1]^{\alpha}i)\,\beta!\frac{\Gamma(\frac{1}{2}\alpha-\beta-\frac{3}{4})}{\Gamma(\frac{1}{2}\alpha+\frac{1}{4})}\,. \end{aligned}\right\}$$

And, finally,

$$I(3n+2-2[l-i],\,j) = (-1)^{j+1}\frac{1}{2}(1+[-1]^{n}i)\,j!\frac{\Gamma\left(\frac{3n}{2}+\frac{1}{4}-l\right)}{\Gamma\left(\frac{3n}{2}+\frac{5}{4}-l+j\right)}\,. \quad (17')$$

6′. Equations (14′) and (17′) give together I_n. But equation (9′) contains only $\Re I_n$, so we must compute this quantity. The complex factors in equations (14′), (17′) are $e^{i\pi(2n+3)/4}$ and $1+(-1)^n i$, so we need

$$-a_n = \Re\{e^{i\pi(2n+3)/4}(1+[-1]^n i)\}\,.$$

For $n = 0, 1, 2, 3 \pmod 4$ this $-a_n$ is in turn

$$\left.\begin{aligned} &\Re\left\{\left(-\frac{1-i}{\sqrt{2}}\right)(1+i)\right\}, \qquad \Re\left\{\left(-\frac{1+i}{\sqrt{2}}\right)(1-i)\right\}, \\ &\Re\left\{\left(\frac{1-i}{\sqrt{2}}\right)(1+i)\right\}, \qquad \Re\left\{\left(-\frac{1+i}{\sqrt{2}}\right)(1+i)\right\}, \end{aligned}\right\}$$

i.e.,

$$a_n = \sqrt{2},\ \sqrt{2},\ -\sqrt{2},\ -\sqrt{2} \quad \text{for} \quad n = 0,\ 1,\ 2,\ 3, \quad (\mathrm{mod}\ 4). \tag{18'}$$

And now equations (14'), (17') give

$$\left.\begin{aligned} \mathfrak{R} I_n = \frac{\Gamma(3n+\frac{3}{2})\, p^n}{n!} \frac{\pi a_n}{4^{n+1}} \sum_{l=0}^{n+1} \sum_{j=0}^{l} \binom{n+1}{l} \binom{2l}{2j} \binom{2j}{j} j! \\ \times (-1)^j \frac{\Gamma(\frac{3}{2}n+\frac{1}{4}-l)}{\Gamma(\frac{3}{2}n+\frac{5}{4}-l+j)} \frac{3^l}{4^j} \cos^{2(l-j)} \gamma \sin^{2j} \gamma . \end{aligned}\right\} \tag{19'}$$

We re-write equation (9'), using equations (12') and (17'). In doing this, we split off the factors $[\Gamma([6n+3]/2)p^n]/n!$ and $[\Gamma([6m+3]/2)p^m]/m!$ from $\mathfrak{R}I_n$ and J_m and rearrange the $\sum_{l=0}^{n+1}\sum_{j=0}^{l}$ in $\mathfrak{R}I_n$ by using $h = l - j$ instead of l. This gives

$$F'(p) = \sum_{n=0}^{m-1} \frac{\Gamma(3n+\frac{3}{2})\, p^n}{n!} \phi_n(\gamma) + \frac{\Gamma(3m+\frac{3}{2})\, p^m}{m!} \psi_m(p, \gamma) , \tag{20'}$$

where

$$\phi_n(\gamma) = \sum_{\substack{h,\, j = 0,\, 1,\, 2,\, \ldots \\ h+j \leqq n+1}} c_n^{h,\, j} \cos^{2h} \gamma \sin^{2j} \gamma , \tag{21'}$$

$$c_n^{h,\, j} = (-1)^j \frac{\pi a_n}{4^{n+1}} \binom{n+1}{h+j} \binom{2[h+j]}{2j} \binom{2j}{j} j! \frac{\Gamma(\frac{3}{2}n+\frac{1}{4}-h-j)}{\Gamma(\frac{3}{2}n+\frac{5}{4}-h)} \frac{3^{h+j}}{4^j}, \tag{22'}$$

and

$$|\psi_m(p, \gamma)| \leqq AB^m \tag{23'}$$

with two fixed A and B.

7'. Equations (18') and (20')–(23') contain the complete result. It is a semiconvergent asymptotic expansion for $F'(p)$ for $p \geq 0$. The emergence of the typical factor $\Gamma[(6n+3)/2]p^n/n!$ shows that convergence cannot be expected for any p—but the asymptotic behavior is described with any desired degree of precision.

The formulae used in § 5 correspond to the special case $m = 1$.

TERM ANALYSIS OF THE THIRD SPECTRUM OF IRON (*Fe* III)*

B. EDLÉN[1] AND P. SWINGS[2]

ABSTRACT

The *Fe* III spectrum has been measured in the region from approximately 500 A to 6500 A, and its analysis has been carried as far as the observational data permit. Of the 34 theoretically possible terms of the $3d^6$ configuration, 32 have been found, the 2 high ^1S and ^1D terms being the only missing ones. Of the 74 theoretical levels for $3d^5\,4s$, only 10 high-lying levels ^{1}, ^{3}(SPD) have not been found. Of the configuration $3d^5\,4p$, practically all theoretically possible levels corresponding to those found of $3d^6\,4s$ have been established. The final tables contain 320 levels and approximately 1500 classified lines.

The permitted and forbidden transitions of *Fe* III play an important role in a wide variety of stellar and nebular spectra.

INTRODUCTION

This analysis of the third spectrum of iron was originally started with the limited aim of securing the metastable levels for astrophysical needs but was gradually extended far beyond this scope. The final result presented here comprises the classification of more than 1500 lines by which some 320 energy levels are established, and it is a practically complete analysis of the available observational data.

The investigation was started in 1937 and was performed at the Astrophysical Institute of the University of Liége and the Physics Laboratory of the University of Uppsala. Some spectrograms of vital importance for the analysis were also secured at the Spectroscopy Laboratory of Massachusetts Institute of Technology. The greatest part of the measurements and wave-length computations were made at Liége. In connection with astrophysical applications some of the results obtained up to August, 1939, have been published.[3] The analysis was afterward carried on and completed at Uppsala.

When the present analysis began, Bowen[4] had identified 3 important multiplets of *Fe* III, namely $3d^5D-4s^5P$, $4s^5S-4p^5P$, and $4s^7S-4p^7P$. Later, Green[5] found the additional multiplets a^5G-z^5H, a^5G-z^5G, part of a^5G-z^5F, and other fragmentary quintets, in all some 30 new lines. They were also independently found during the present work.

THE SPECTROGRAMS

The spectrograms used in this description of *Fe* III cover the region from approximately 500 A to 6500 A. With a grazing incidence spectrograph[6] at Uppsala, spectra of a vacuum spark between pure iron rods were taken on Schumann plates from the short-wave-length end up to 2300 A. They were evaluated from about 1300 A down and furnished the only observations below 1017 A. The dispersion varied from 3.6 A/mm at 700 A to 4.3 A/mm at 1100 A. In this region no *Fe* II lines appear in the spark, but considerable difficulty is caused by the overlapping of lines of higher ionization stages in the same or higher grating orders. Spectra taken with various amounts of self-inductance permitted, however, the *Fe* III lines to be rather unambiguously picked out.

* *Contributions from the McDonald Observatory, University of Texas*, No. 49.

[1] Physics Laboratory of the University of Uppsala (Sweden).

[2] Now at the McDonald Observatory of the University of Texas and the Yerkes Observatory of the University of Chicago.

[3] Edlén and Swings, *Ap. J.*, **88**, 618, 1938; **90**, 378, 1939; *Observatory*, **62**, 234, 1939.

[4] *Phys. Rev.*, **52**, 1153, 1937.

[5] *Phys. Rev.*, **55**, 1209, 1939.

[6] Described by G. Arvidsson, *Ann. d. Phys.*, **12**, 787, 1932.

The best spectra for the long-wave-length part of the vacuum region were obtained with the normal-incidence vacuum spectrograph[7] of the Carnegie Institution of Washington, located in the Spectroscopy Laboratory of the Massachusetts Institute of Technology. With the grating normal falling at about 1850 A, it gives an almost constant dispersion of 4.2 A/mm and an excellent definition. A spark in nitrogen at 1/2 atm. pressure and Ilford Q-plates were used. For most of the exposures the slit was covered by a lithium fluorite window, in order to keep high vacuum in the spectrograph and to prevent the slit from being clogged by dust particles from the spark. This limited the spectra at about 1300 A. A few exposures taken without a window showed lines down to 1017 A; but the nitrogen, which was not specially purified, exerted a strong discontinuous absorption, as is clearly shown in Table 1 by the intensities in the region 1017–1143 A. The spark gap was 3–5 mm in length and was placed parallel to the slit at such a distance that different heights of the spark were stigmatically reproduced in the spectral lines. The *Fe* I and the *Fe* II lines were strongest in the middle of the spark, *Fe* III was somewhat strengthened at the poles and *Fe* IV appeared only near the poles; hence the different intensity distribution in the spectral lines provided a sharp distinction of the *Fe* III lines from the neighboring stages of ionization.

From 2023 A up through the visible region, spectra of the vacuum spark were taken with a Hilger E1 quartz-prism spectrograph,[8] supplemented with a small glass-prism spectrograph in the red. The main difficulty here is caused by the overlapping of the very rich spectra of *Fe* I and particularly *Fe* II. Though not contained in Dobbie's *Fe* II table,[9] many of the observed lines are probably high-excitation *Fe* II lines. As the experimental distinction between *Fe* III and the neighboring ionization stages is somewhat uncertain in these spectrograms, only the identified *Fe* III lines are included in Table 1. In the visible region of the prism spectra the measurements are rather uncertain, owing to low dispersion and overlapping of lines. A reobservation of this region with high dispersion is desirable. A few identified *Fe* III lines in the red end of the spectrum are evidently contained in King's measurements[10] of the spark in air; his wave lengths are given in Table 1.

Computed standard wave lengths of *Fe* II were used in the reduction of the measurements down to 1350 A. Further down the *Fe* III lines have been tied together step by step on the combination principle to form a system of working standards. It is connected to the system of computed *Fe* II standards through some lines measured on the M.I.T. plates, partly in the second order.

ANALYSIS

The deepest electron configuration of *Fe* III is $3d^6$. The next higher is $3d^5\,4s$, of which the main part lies well above the $3d^6$ terms. The transitions to $3d^6$ from the lowest odd configuration $3d^5\,4p$ form the group of short wave lengths in Table 1, extending from 679 A to 1143 A. About 450 combinations of this type are included in Table 1, though many as parts of unresolved blends. This table contains also in the same region 9 unidentified faint lines, which probably belong to the same transition. The largest number of observed *Fe* III lines is due to the transition $3d^5\,4s - 3d^5\,4p$, of which Table 1 contains nearly 1000 identified combinations. Except for a few sporadic identifications, they are comprised between 1700 A and 4000 A, and the main part of the strong lines is concentrated in the region 1800–2200 A.

No terms of higher electron configurations have been identified, except for such arising from the basic term $3d^5(^6S)$ of *Fe* IV. Among the various terms of the same con-

[7] K. T. Compton and J. C. Boyce, *Rev. Sci. Inst.*, **5**, 218, 1934.

[8] Cf. *Ap. J.*, **90**, 378, 1939.

[9] *Ann. Solar Phys. Obs.*, **5**, Part I, 1938.

[10] *Ap. J.*, **87**, 399, 1938.

figuration, those arising from ^6S are very predominant, especially for high n and l quantum numbers. Thus, $4p^7P-4d^7D$, $4p^5P-4d^5D$ and $4p^7P-5s^7S$ form outstanding multiplets in the region 1400–1600 A. Within approximately the same limits a very large number of partly unresolved *Fe* III lines are observed, doubtless due to the same type of transition, which should give very numerous lines. These lines are clearly distinguished from the sharp lines of 4s–4p by their nebulous appearance in the nitrogen spark. An attempt to identify terms of the 4d and 5s configurations other than those built on ^6S proved fruitless. As in the case of the transition 4p–4d, the septet and the quintet multiplets of the (^6S) system of 4d–4f and 4f–5g mark the limits on the short- and long-wave-lengths sides, respectively, of dense-line groups of corresponding transitions. In the case of 4f–5g this group is reduced to a strong continuum from 4370 to 4315 A.

The prominent character of the (^6S) system made it possible to trace three members of the (^6S)ns series. In good agreement with a nearly hydrogen-like value for $5g^7G^5G$, this locates the series limit at 247200 cm^{-1}, or 30.50 volts above the ground level.

The main result of the present analysis consists of the very complete location of the terms of the configurations $3d^6$, $3d^5$ 4s and $3d^5$ 4p. Of 34 theoretically possible levels of $3d^6$, only the two high ^1D and ^1S are not found. They are expected at 75,000 and 100,000 cm^{-1}, respectively, and may not cause any observed lines. The configuration $3d^5$ 4s gives theoretically 74 levels, of which the 10 forming the high terms ^{1,3}(SPD) are still missing. The $^{1,3}S$ terms should fall around 100,000 cm^{-1}, and ^3S ought to give observable lines with w^3P. The very high ^{1,3}(PD) may be approximately located around 130,000 cm^{-1}. Of $3d^5$ 4p practically all terms are found, except those corresponding to the above-mentioned high ^{1,3}(PD). Altogether, 189 levels are identified, a few, however, marked as questionable in the term table.

In the main region for 4s–4p transitions practically no lines remain unidentified. It is remarkable that no terms of the configurations $3d^4\,4s^2$ or $3d^4\,4s4p$ are found.

THE TABLE OF LINES

In Table 1, which contains some 1500 identified lines, are also included all unidentified lines observed with the grating spectrographs and experimentally classified as *Fe* III, except the diffuse group of 4p–4d, 5s at 1400–1600 A. The first column gives the wave length, above 2023 A in air and below in vacuum. The 7 lines above 5833 A from King's list[11] are marked with a *K*. King's intensities for these lines are given in brackets in the second column.

The second column gives estimates of the line intensity. The scale is fairly homogenous only for the grating plates. The various remarks following or replacing the intensity figure have the following meaning:

n = nebulous,

b = broad, double, or more complex,

unr = unresolved

m I or *m* II = masked by *Fe* I or *Fe* II,

bl I or *bl* II = blended by *Fe* I or *Fe* II.

blg = blended by grating ghost

A vertical arrow indicates that the line is winged or shaded. In the third column a wave number followed by a *c* is computed from the level values.

[11] *Loc. cit.*

THE TERM TABLE

Tables 2 and 3 contain the even and odd terms, respectively. The first column gives the electron configuration. In cases where two terms of the same kind of the configuration $3d^5$ appear as basic terms, the higher one is distinguished by a mark ′ (prime) attached to the term symbol. Thus the configuration of a^1F is given as $3d^5(^2F)4s$ and that of b^1F as $3d^5(^2F')4s$. The second column gives the term symbol according to the same system that was used by Curtis for the isoelectronic spectrum *Mn* II. This system is particularly suited to the present analysis of *Fe* III in separating the group of $3d^6$ terms from those of $3d^5$ 4s and pointing out the special character of the (^6S) system. When, however, the analysis revealed also the high ^3F, ^3P, and ^1G of the $3d^6$ configuration, it became necessary to make a distinction from the low terms of the same kind, and the prefix 3d′ instead of 3d was attached to the high terms.

The level values in the third column were computed in the following way. Since the main body of the level system, consisting of terms of $3d^5$ 4s and $3d^5$ 4p is well tied together by numerous combinations in a favorable wave-length region, it was first treated to form a central system, to which the $3d^6$ levels and the (^6S) system could afterward be attached. For the calculation of this central system, use was made of all the observed combinations with wave numbers between 60,000 and 25,000 cm^{-1}, which were judged to be unaffected by blends, close lines, or extreme faintness. These selected combinations amounted to about 400 and were all given equal weight. The levels were then obtained through successive approximations. Starting with a set of approximate odd-level values, each even level was computed from all its selected combinations, and the mean value was taken. Using these new values of the even levels, the odd levels were now computed in the same way, giving an improved set of odd-level values. The process was then repeated until no further change in the values took place. The (^6S) system was separately treated in a similar way and tied to the central system through the multiplet a^5P-4p^5P. The $3d^6$ levels were individually tied up with the odd terms of the central system.

Term perturbations are frequent, especially among the odd terms. Some of the most striking cases may be pointed out. The group $z^5F^5S^5D$ is mixed up in the same way as Curtis found for *Mn* II. The multiplet intensities are very anomalous, the z^5S, for instance, combining with a^5G. The most astonishing example is, perhaps, the absence of $3d^5D_4-z^5D_4$ in the otherwise strong multiplet. Multiplets involving z^3D, y^5D, and y^5P also show strange intensities, indicating strong mutual perturbations. The levels $z^3I_{7,6}$ and $z^3K_{7,6}$ are indistinguishable, as well as z^1D_2 and x^3F_2. The latter case combined with some exchange between a^5F and b^3D causes one of the few quintet-singlet combinations, $a^5F_1-z^1D_2$. Two others are caused by the closeness of z^1I_6 and y^5G_6. Another exchange takes place between a^3F_2 and a^1D_2. The designation of term symbols as well as limits for the odd terms are ambiguous in several cases.

THE ASTRONOMICAL APPLICATIONS

A. *Permitted lines.*—Many lines that were previously unidentified in the early B stars (absorption) or in the shell stars of early type (absorption and emission) are due to *Fe* III. More than 100 such identifications, including some strong stellar lines, have been mentioned in our earlier notes[12] and in several subsequent papers.[13] These may be supplemented on the basis of the present paper. For example, the 3 emission lines with violet

[12] *Ap. J.*, **88**, 618, 1938; **90**, 378, 1939.

[13] Struve and Roach, *Ap. J.*, **90**, 727, 1939 (P Cygni); Baldwin, *Ap. J.*, **93**, 421, 1941 (ζ Tauri); Struve and Elvey, *Pub. A.S.P.*, **52**, 140, 1940 (γ Cassiopeiae); Swings and Struve, *Ap. J.*, **91**, 589, 1940 (γ Cas), and *Pub. A.S.P.*, **52**, 392, 1940 (region $\lambda < 3300$ of P Cygni, which consists of one line of *He* I, four of *Si* III, and nineteen of *Fe* III).

absorption, observed in P Cygni[14] at λλ 4004.62, 4022.12, and 4038.74, are the leading lines of the $c^3F-z^3F^\circ$ multiplet of *Fe* III. Similarly, the following other lines are due to *Fe* III: λ 3747.40 observed in P Cygni,[15] γ Cassiopeiae,[16] and ζ Tauri;[17] λλ 3954.38, 3969.43, and 4005.04, observed in absorption in B stars.[18]

No attempt will be made here to revise or complete the identifications of the numerous lists of stellar wave lengths in which *Fe* III plays a role. The *Fe* III lines may help in discussing the ionization conditions in stellar atmospheres of early type.[19] In certain stars, like P Cygni or γ Cassiopeiae (at the sharp-line stage of 1939), the *Fe* III lines constituted the most conspicuous features of the entire spectrum, except *H* and *He* I.

Two types of strong permitted *Fe* III lines appear in the astronomical region. In the first group the lower levels are even terms of the configuration $3d^5\,4s$ situated between 65,000 and 100,000 cm^{-1}; these terms are all metastable or quasi-metastable. In the second group the lower levels are the high terms $4d^{5,7}D$, $4f^{5,7}F^\circ$, $5s^{5,7}S$, $5p^{5,7}P^\circ$, which are not metastable. In an extended atmosphere, excited by diluted radiation, the first group becomes considerably enhanced relative to the second. This is observed in P Cygni, γ Cassiopeiae, and ζ Tauri. The enhancement gives an estimate of the dilution factor; in various early-type shells this is the easiest way to ascertain the presence of dilution. For example, λ 4165 and λ 4372 (second group) are much stronger than λ 4419 (first group) in ordinary absorption B stars, whereas the opposite is true in P Cygni or γ Cassiopeiae.

In P Cygni the emission spectrum of *Fe* III is not of the recombination type; it is presumably emitted by fluorescence excited by the underlying radiation.

B. *Forbidden lines.*—Since our first announcement[20] of the assignment of the unidentified lines λλ 4658.1, 4701.5, 4733.6, 4755.0, and 4770 observed by Merrill in RY Scuti, to the $^5D-{}^3F$ transition of [*Fe* III], this multiplet has been extended and the $^5D-{}^3P$ transition has also been observed. The $^5D-{}^3H$ multiplet gives only very faint lines. As for $^5D-{}^3D$ and $^5D-{}^7S$, whose wave lengths are in the region λλ 3200–3400, they have not yet been observed; no trace of them appears on McDonald Observatory spectrograms of the Orion nebula taken for this purpose. Some of the observations of [*Fe* III] are summarized in Table 4. Besides the objects mentioned in this table, the [*Fe* III] lines were also strong and characteristic features in various novae; for example, DO Aquilae[21] (in 1925) and Nova RT Serpentis 1909.[22] All slow novae, after the η Carinae stage, pass through stages showing [*Fe* III], the relative intensities of [*Fe* II] and [*Fe* III] giving an indication of the ionization conditions. Typical stellar comparison spectra are η Carinae ([*Fe* II] only), MWC 17 ([*Fe* II] and [*Fe* III] present simultaneously), DO Aquilae in 1931 ([*Fe* III] stronger than in MWC 17), and RY Scuti ([*Fe* III] only).

Merrill has recently found[23] that the [*Fe* III] lines reached considerable intensity in the variable star BF Cygni, but no detailed description of this spectrum has been published.

[14] O. Struve, *Ap. J.*, **81**, 73, 1935.

[15] Struve and Roach, *loc. cit.*

[16] Baldwin, *Ap. J.*, **87**, 573, 1938.

[17] Baldwin, *Ap. J.*, **93**, 421, 1941.

[18] Kühlborn, *Veröff. Univ. Stern. Berlin-Babelsberg*, **12**, Heft I, 1938; λ 3954.38 is also present in P Cygni.

[19] See, e.g., J. L. Greenstein, *Ap. J.*, **91**, 438, 1940 (υ Sagittarii).

[20] *Observatory*, **62**, 234, 1939.

[21] Vorontsov-Velyaminov, *Ap. J.*, **92**, 283, 1940.

[22] In 1931 Joy observed strong bright lines at λλ 4658, 4701, and 4733 in RT Serpentis; these [*Fe* III] lines had become very faint in 1940 and were replaced by [*Fe* V] and [*Fe* VI].

[23] *Pub. A.A.S.*, **10**, 168, 1942.

The observation of [*Fe* III] lines—for which the transition probabilities have not yet been computed—helped considerably in predicting which of all the predicted [*Fe* V] lines should be the strongest. AX Persei showed recently these strongest [*Fe* V] transitions.[24]

Most objects in which [*Fe* III] has been observed are distant stars or binaries having a late-type companion. Of the two most characteristic forbidden lines—λ 4658 ($^5D_4-{}^3F_4$), and λ 5270 ($^5D_3-{}^3P_2$)—the former is intrinsically stronger and is observed as such when the star is not heavily reddened, as in BF Cygni.[25] Interstellar reddening reduces λ 4658 relative to λ 5270, and it may happen that λ 5270 becomes appreciably stronger than λ 4658. This is the case for the star MWC 349,[26] which is located in a dark region of the Milky Way and is reddened to a considerable extent; in this star λ 5270 and even λ 5010 are stronger than λ 4658.

For placing at our disposal the facilities of the laboratories where various parts of this investigation were performed, our thanks are due the directors: Professor A. Lindh of the Physics Laboratory of the University of Uppsala, Professor M. Dehalu of the Astrophysical Institute of the University of Liége, Professor G. R. Harrison of the Spectroscopy Laboratory of the Massachusetts Institute of Technology, Cambridge, Massachusetts. One of the authors (B. Edlén) wants to express his deep gratitude to Professor J. C. Boyce for his kind hospitality and encouraging help during the author's stay at the Spectroscopy Laboratory of the Massachusetts Institute of Technology. The same author gratefully acknowledges that his visit to the United States was made possible through a stipend from the Swedish-American Foundation.

Finally, our cordial thanks are extended to Mr. J. Grandjean for the important part which he has taken in the measurements and reductions.

[24] Struve and Swings, in preparation; *Ap. J.*, **91**, 613, 1940.

[25] Private communication of Dr. P. W. Merrill.

[26] Swings and Struve, *Ap. J.*, **95**, 159, 1942.

TABLE 1

THE SPECTRUM OF *Fe* III

λ_{air} A	Int.	ν_{vac} cm^{-1}	Combination
K 6032.30	7 (8n)	16572.8	$5s^5S_2 - 5p^5P_3$
K 5999.30	5 (4n)	16664.0	$5s^5S_2 - 5p^5P_2$
K 5978.90	5 n(2n)	16720.9	$5s^5S_2 - 5p^5P_1$
K 5953.65	6 (3n)	16791.8	$4d^5D_4 - 5p^5P_3$
5929.5	5	16860.2	$5s^7S_3 - 5p^7P_2$
K 5920.0	7 b(4N)	16887.2	$4d^5D_{32} - 5p^5P_2$
5901.0	3	16941.6	$4d^5D_{210} - 5p^5P_1$
K 5891.5	6 (10N)	16968.9	$5s^7S_3 - 5p^7P_3$
K 5833.65	10 (10N)	17137.2	$5s^7S_3 - 5p^7P_4$
5573.3	4	17937.7	$c^3G_5 - y^3H_6$
5485.6	3	18224.5	$c^3G_4 - y^3H_5$
5460.8	3	18307.3	$c^3G_3 - y^3H_4$
5306.6	4	18839.2	$4d^7D_3 - 5p^7P_2$
5302.5	6	18853.8	$4d^7D_2 - 5p^7P_2$
5299.9	5	18863.0	$4d^7D_1 - 5p^7P_2$
5282.1	7	18926.6	$4d^7D_4 - 5p^7P_3$
5276.2	7 bl II	18947.8	$4d^7D_3 - 5p^7P_3$
5272.0	3	18962.9	$4d^7D_2 - 5p^7P_3$
5243.3	10	19066.7	$4d^7D_4 - 5p^7P_4$
5235.3	5 bl II	19095.8	$4d^7D_4 - 5p^7P_4$
5156.0	4	19389.5	$a^5D_4 - 4p^5P_3$
4927.56	2	20288.4	$c^3F_4 - z^5G_5$
4570.34	4	21874.1	$b^1D_2 - z^1D_2$
4569.82	4	21876.6	$b^1G_4 - y^1G_4$
4430.95	7	22562.2	$a^5P_2 - 4p^5P_3$
4419.59	10	22620.2	$a^5P_3 - 4p^5P_3$
4395.78	6	22742.7	$a^5P_1 - 4p^5P_2$
4372.4	20 bn	22864	$4f^5F - 5g^5G$
Strong continuous radiation from λ 4372 to λ 4315			
4310.37	12 n	23193.4	$4f^7F_6 - 5g^7G_7$
4304.81	10 n	23223.3	$4f^7F_5 - 5g^7G_6$
4296.86	10 n	23266.3	$4f^7F_4 - 5g^7G_5$
4286.13	10 n	23324.5	$4f^7F_3 - 5g^7G_4$
4273.42	7 n	23393.9	$4f^7F_2 - 5g^7G$
4205.92	2	23769.3	$b^3G_5 - z^5G_5$
4184.09	4	23893.4	$b^3G_4 - z^5G_5$
4168.41	4	23983.2	$5p^7P_4 - 5d^7D_3$
4166.86	9	23992.1	$5p^7P_4 - 5d^7D_4$
4164.79	20	24004.1	$5p^7P_4 - 5d^7D_5$
4140.51	6	24144.8	$5p^7P_3 - 5d^7D_2$
4139.37	8	24151.5	$5p^7P_3 - 5d^7D_3$
4137.93	10	24159.9	$5p^7P_3 - 5d^7D_4$
4122.98	8	24247.5	$5p^7P_2 - 5d^7D_1$
4122.06	8	24252.9	$5p^7P_2 - 5d^7D_2$
4120.97	8	24259.3	$5p^7P_2 - 5d^7D_2$
4081.19	7	24495.8	$5p^7P_4 - 6s^7S_3$
4053.28	5	24664.4	$5p^7P_3 - 6s^7S_3$
4039.12	3	24750.9	$c^3F_2 - z^3F_2$
4035.54	4	24772.9	$5p^7P_2 - 6s^7S_3$
4025.07	3	24837.3	$a^1G_4 - z^3F_4$
4022.36	4	24854.0	$c^3F_3 - z^3F_3$
	m I	24961.5 c	$c^3F_4 - z^3F_4$
4003.41	4	24971.7	$(a^3H_4 - z^5G_4)$
3980.14	3	25117.7	$5p^5P_1 - 5d^5D_0$
3979.42	5	25122.2	$5p^5P_1 - 5d^5D_1$
3978.43	4	25128.5	$5p^5P_1 - 5d^5D_2$
3976.88	4	25138.25	$c^3G_5 - w^3G_5$
	m I	25185.4 c	$5p^5P_2 - 5d^5D_2$
3968.78	8	25189.6	$5p^5P_2 - 5d^5D_3$
3954.38	12	25281.3	$5p^5P_3 - 5d^5D_{4(3)}$
		25285.2 c	$c^3G_4 - w^3G_4$
3947.10	4	25327.91	$b^3G_4 - z^5H_4$, $c^3G_2 - w^3G_2$
3945.08	3	25340.88	$c^3G_4 - w^3G_3$
3828.44	2	26112.92	$c^3G_4 - y^1F_3$
3793.52	3	26353.29	$c^3G_4 - v^3F_3$
3786.94	4	26399.07	$c^3G_3 - v^3F_2$
3753.18	3	26636.53	$b^1G_4 - y^1H_5$
	m II	26677.6 c	$c^3G_5 - v^3F_4$
3700.14	2	27018.34	$b^1G_4 - x^1G_4$
3690.60	4	27088.18	$b^1G_4 - x^1F_3$
3620.27	3	27614.40	$b^3G_5 - z^5D_4$
3611.72	3	27679.77	$b^3F_3 - z^3F_2$
3603.88	9	27739.99	$b^3F_2 - z^3F_2$
3600.93	10	27762.71	$b^3F_3 - z^3F_3$
3599.49	3	27773.82	$b^3F_4 - z^3F_3$
3593.15	4	27822.82	$b^3F_2 - z^3F_3$
3587.53	3	27866.41	$b^3F_3 - z^3F_4$
3586.12	9	27877.36	$b^3F_4 - z^3F_4$
3525.17	3	28359.35	$c^5D_2 - x^3P_2$
3515.57	4	28436.79	$a^1G_4 - z^3G_5$
3514.87	2	28442.45	$b^3G_5 - z^3F_4$
3506.93	5	28506.84	$c^3F_2 - z^3G_3$
3504.40	2	28527.42	$c^3F_3 - z^3G_3$
3501.75	8	28549.01	$b^3G_3 - z^3F_2$, $c^3F_3 - z^3G_4$
3500.29	7	28560.92	$c^3F_4 - z^3G_5$
3499.57	7	28566.80	$b^3G_4 - z^3F_4$
3496.29	4	28593.59	$y^5D_4 - 4d^5D_4$
3488.92	3	28653.99	$c^3D_1 - x^3P_1$
3454.35	2	28940.75	$b^1G_4 - u^3G_3$
	m I	28957.9 c	$c^3F_4 - z^3D_3$
3432.97	3	29120.98	$b^1D_2 - z^1P_1$
3421.97	3	29214.58	$a^3F_2 - z^5G_2$
3419.49	3	29235.77	$a^3F_2 - z^5G_3$, $c^3F_3 - z^3D_2$
3410.74	3	29310.77	$c^3D_2 - y^5G_4$, $c^3D_2 - x^3D_1$
3406.18	2	29350.01	$c^3D_3 - x^3D_2$
3403.51	2	29373.03	$c^3D_2 - x^3D_2$
3396.71	8	29431.84	$a^3H_6 - z^5H_6$
3382.19	6	29558.18	$c^3G_5 - v^3G_5$
3373.51	2	29634.23	$a^3H_6 - z^5H_5$
3367.54	3	29686.77	$a^3H_4 - z^5H_4$
3360.84	6	29745.95	$c^3G_4 - v^3G_4$
3359.18	3	29760.65	$c^3G_5 - v^3G_4$
3358.74	4	29764.55	$c^3G_3 - v^3G_3$
3357.40	4	29776.43	$c^3D_3 - w^3D_2$, $c^3G_4 - v^3G_3$
3354.79	2	29799.59	$c^3D_2 - w^3D_3$
3347.70	8	29862.70	$a^3H_5 - z^5H_5$
3339.36	10	29937.28	$a^5F_1 - z^5G_2$
3333.27	3	29991.98	$a^3H_5 - z^5H_4$, $c^3G_4 - t^3F_4$
3331.62	5	30006.83	$c^3G_5 - t^3F_4$
3329.89	7	30022.42	$a^3H_4 - z^5H_4$
3324.72	3	30069.1	$y^5F_5 - 4d^5D_4$
3315.80	3	30149.99	$c^3G_3 - t^3F_2$
3307.53	5	30225.37	$a^5F_2 - z^5G_2$
3306.94	4	30230.76	$c^3G_4 - t^3F_3$
3305.22	10	30246.49	$a^5F_2 - z^5G_3$
3300.20	4	30292.50	$y^5F_4 - 4d^5D_3$
3294.50	4	30344.91	$a^1F_3 - z^3F_2$
3292.04	8 bl I	30367.6	$a^5F_3 - z^5G_3$
3288.81	15	30397.41	$a^5F_3 - z^5G_4$
3283.75	2	30444.25	$a^5F_4 - z^5G_3$
3283.30	2	30448.42	$a^1F_3 - z^3F_4$
3280.58	6	30473.66	$a^5F_4 - z^5G_4$
3276.08	15	30515.52	$a^5F_4 - z^5G_5$
3274.95	3	30526.05	$y^5F_3 - 4d^5D_2$
3273.53	6 bl II	30539.3	$a^5F_5 - z^5G_5$
3270.23	2 n	30570.1	$c^3D_1 - w^3D_1$

TABLE 1—*Continued*

λ_{air} A	Int.	ν_{vac} cm^{-1}	Combination
3266.88	20	30601.45	$a^5F_5 - z^5G_6$
3264.22	2	30626.39	$c^3D_3 - w^3F_2$
3263.04	1	30637.46	$c^3D_1 - w^3F_2$
3262.44	6	30643.10	$c^3G_5 - x^1G_4$
3256.54	2	30698.62	$c^3G_4 - x^1F_3$
3255.49	2	30708.52	$y^5F_2 - 4d^5D_2$
3239.04	2 bl I	30864.5	$c^3D_3 - w^3D_2$
3238.74	2	30867.3	$c^3D_3 - w^3F_3$
3218.34	6	31062.98	$b^1G_4 - w^1G_4$
3215.60	8	31089.45	$b^3D_1 - z^5G_2$
3206.98	4	31173.01	$b^3D_2 - z^5G_2$
3204.76	6	31194.60	$b^3D_2 - z^5G_3$
3201.90	1	31222.5	$b^3D_3 - z^5G_3$
3198.81	5	31252.62	$b^3D_3 - z^5G_4$
3189.74	3	31341.49	$a^1G_4 - y^3D_3$
3178.03	10	31456.97	$b^3F_3 - z^3G_4$
3176.00	10	31477.07	$b^3F_4 - z^3G_5$
3174.09	10	31496.01	$b^3F_2 - z^3G_3$
3164.67	3	31589.76	$a^5F_2 - z^5H_3$
3143.36	2	31803.91	$a^3F_3 - z^5D_3$
3136.43	10	31874.18	$b^3F_4 - z^3D_2$
3120.84	2	32033.40	$b^3G_5 - z^3G_4$
3120.03	3 bl II	32041.7	$b^3G_5 - z^3G_5$
3118.75	5 bl II	32054.9	$c^3F_4 - y^3F_4$
3111.609	8	32128.42	$a^5F_4 - z^5H_5$
3110.85	3	32136.26	$b^3G_4 - z^3G_3$
3110.052	8	32144.51	$b^3F_3 - z^3D_2$
3108.85	3	32156.94	$a^3F_4 - z^5F_5$
3107.950	6	32166.25	$b^3G_4 - z^3G_5$
3099.05	2	32258.62	$c^3D_3 - x^3G_3$
3096.86	2	32281.43	$c^3D_2 - x^3G_2$
3084.09	6	32415.1	$b^3F_3 - y^5D_2$
	m I	32419.3	$b^3F_2 - z^3D_1$
3070.072	5	32563.10	$b^3G_4 - z^3D_2$
3055.55	5	32717.8	$a^5F_1 - z^5D_0$
3054.134	6	32733.02	$a^5F_1 - z^5D_1$
3050.463	5	32772.41	$a^5F_1 - z^5D_2$
3045.877	3	32821.75	$c^3G_4 - u^3G_4$
3035.802	3	32930.67	$b^3G_3 - z^3D_3$
3027.46	3	33021.4	$a^5F_2 - z^5D_1$
3026.985	6	33026.59	$a^3H_6 - z^3G_5$
3023.85	8	33060.9	$a^5F_2 - z^5D_2$
3022.00	3	33081.0	$c^3G_5 - u^3G_5$
3018.744	6	33116.75	$a^5F_3 - z^5D_3$
3015.230	7	33155.33	$a^3F_4 - z^5F_5$
3013.125	20	33178.50	$a^5F_5 - z^5F_5$
3008.506	5	33229.44	$a^5F_3 - z^5F_4$
3007.802	6	33237.21	$a^5F_3 - z^5D_2$
3007.2	20 bn	33244	$4d^5D - 4f^5F$
		33246.6 c	$a^3H_5 - z^3G_4$
3006.122	4	33255.79	$a^3H_4 - z^3G_3$
3002.99	5	33290.5	$a^5F_1 - z^5F_1$
3001.589	12	33306.01	$a^5F_4 - z^5F_4$
2977.572	5	33574.65	$a^3F_3 - z^3F_3$
2977.222	6	33578.59	$a^5F_2 - z^5F_1$
2973.896	5	33616.15	$a^5F_2 - z^5F_2$
2963.230	8	33737.13	$a^5F_3 - z^5F_2$
2958.286	6	33793.51	$a^3F_2 - z^3F_2$
2955.060	4	33830.40	$a^5F_3 - z^5F_3$
2951.639	3	33869.61	$b^3D_1 - z^5D_0$
2950.295	4	33885.04	$b^3D_1 - z^5D_1$
2948.388	8	33906.96	$a^5F_4 - z^5F_3$
2946.864	3	33924.49	$b^3D_1 - z^5D_2$
2942.989	4	33969.15	$b^3D_2 - z^5D_1$
2939.55	7 bl II	34008.9	$b^3D_2 - z^5D_2$
2939.066	2	34014.50	$a^3F_3 - z^3H_4$
2934.779	3	34064.18	$b^3D_2 - z^5D_3$
2932.337	5	34092.55	$b^3D_3 - z^5D_3$
2923.902	8	34190.90	$a^3F_4 - z^3F_4$
2915.980	2	34283.78	$a^3F_4 - z^5P_3$
			$a^5F_3 - z^5D_4$
2908.651	5	34370.17	$b^3F_3 - y^3D_2$
2907.701	12	34831.39	$b^3F_4 - y^3D_3$
2907.497	10	34383.80	$a^5F_5 - z^5D_4$
2905.80	8 bl II	34403.9	$b^3D_1 - z^5S_2$
			$b^1F_3 - z^1D_2$
2904.431	12	34420.10	$b^3F_3 - y^3D_2$
2902.47	9 bl II	34443.3	$b^3D_1 - z^5F_1$
2899.386	4	34479.99	$b^3D_1 - z^5F_2$
			$b^3F_3 - y^3D_3$
2898.77	3 bl II	34487.4	$b^3D_2 - z^5S_2$
2895.464	3	34526.69	$b^3D_2 - z^5F_1$
			$a^3F_4 - z^3H_4$
2895.076	8 bl II	34531.32	$b^3F_2 - y^3D_1$
2893.792	5	34546.63	$c^3D_2 - y^1F_3$
2892.318	3	34564.23	$b^3D_2 - z^5F_2$
2890.000	3	34591.96	$b^3D_3 - z^5F_3$
2875.711	2	34763.83	$c^3D_3 - v^3F_3$
2873.795	4	34787.01	$c^3D_2 - v^3F_2$
2868.136	5	34855.64	$c^3D_1 - v^3F_2$
2865.54	3	34887.2	$a^5F_2 - z^3F_3$
2858.664	7 bl II	34971.14	$b^3F_4 - y^3F_4$
2854.190	4	35025.95	$a^3F_3 - z^3P_2$
2851.130	4	35063.53	$b^1F_3 - x^3F_2$
2850.834	3	35067.18	$z^5F_4 - 4d^5D_3$
2850.581	3	35070.29	$z^5F_4 - 4d^5D_4$
			$b^3G_4 - y^3D_3$
2850.288	7	35073.90	$c^3D_3 - v^3F_4$
2843.779	4	35154.17	$b^3F_3 - y^3F_3$
2842.869	2	35165.43	$b^3F_4 - y^3F_3$
2838.924	2	35214.28	$b^3F_2 - y^3F_3$
2838.38	5	35221.0	$z^5F_5 - 4d^5D_4$
2836.107	4 bl II	35249.26	$b^3F_2 - y^3F_2$
2821.665	2	35429.67	$a^3I_8 - z^5H_5$
2818.624	6	35467.88	$b^1D_2 - x^1F_3$
2816.600	3	35493.38	$(c^3D_2 - v^3D_2)$
2813.241	10 bl I	35535.74	$b^3G_5 - y^3F_4$
2813.17	3	35536.6	$c^3D_3 - v^3D_3$
2803.441	6 bl II	35659.97	$b^3G_4 - y^3F_4$
2792.29	2	35802.4	$a^3I_7 - z^5H_7$
2789.698	5	35835.63	$b^3D_2 - z^3F_3$
2788.258	6	35854.13	$b^3G_4 - y^3F_3$
2778.868	5	35975.29	$b^3G_3 - y^3F_2$
2773.306	8	36047.43	$b^1D_2 - x^1D_2$
2772.344	3	36059.93	$b^3D_3 - z^3P_3$
2767.92	2	36117.6	$c^3D_3 - u^3F_4$
2745.935	2	36406.73	$c^3D_2 - u^3F_3$
2741.952	2	36459.61	$a^5F_3 - z^3P_2$
2728.473	3	36639.71	$c^3D_1 - u^3F_2$
2720.381	5	36748.70	$a^3H_5 - y^3F_4$
2706.17	2 n	36941.6	$4d^7D_3 - 4f^7F_2$
2705.10	7 n	36956.2	$4d^7D_2 - 4f^7F_2$
2704.43	3 n	36965.4	$4d^7D_1 - 4f^7F_2$
2701.13	8 n	37010.6	$4d^7D_3 - 4f^7F_3$
2700.02	8 n	37025.8	$4d^7D_2 - 4f^7F_3$
2698.41	7 n	37047.9	$4d^7D_4 - 4f^7F_4$
	bl II	37062.2 c	$4d^7D_3 - 4f^7F_3$
2696.89	7 n	37068.8	$4d^7D_3 - 4f^7F_4$
2695.929	3	37081.99	$a^3F_4 - y^5F_4$
2695.34	9 n	37090.1	$4d^7D_4 - 4f^7F_5$
2695.13	10 n	37093.0	$4d^7D_5 - 4f^7F_6$
	m I	37314.8 c	$b^3D_3 - z^3P_2$
2678.810	6	37318.95	$b^1F_3 - z^1G_4$
2677.417	3	37338.36	$a^5F_2 - y^5F_1$
2662.331	4	37549.91	$a^3F_2 - z^3G_3$
2660.815	4	37571.32	$b^3D_3 - z^3P_1$
2659.614	4	37588.28	$a^5F_3 - y^5F_2$
2646.751	6	37770.94	$a^5F_3 - y^5F_3$
2645.39	9 bl II	37790.4	$a^3F_4 - z^3G_5$
2641.408	5	37847.33	$a^5F_4 - y^5F_3$

TABLE 1—*Continued*

λ_{air} A	Int.	ν_{vac}cm^{-1}	Combination	λ_{air} A	Int.	ν_{vac}cm^{-1}	Combination
2633.819...	4	37956.38	$a^3F_3-z^3D_2$	2329.905...	9	42907.02	$a^3D_1-z^3P_1$
2630.527...	2	38003.88	$a^3F_3-y^3F_4$	2329.730...	2	42910.24	$a^3G_5-z^3G_4$
2625.268...	3	38080.01	$a^3F_4-y^3F_4$	2327.668...	4	42948.26	$a^3G_4-z^3G_5$
2617.92....	2	38186.9	$a^3F_4-z^3D_3$	2326.948...	10	42961.55	$b^3G_3-y^3H_4$
2617.149...	8	38198.13	$a^1G_4-z^1H_5$	2324.359...	8 bl II	43009.38	$c^3D_2-w^3P_1$
2616.888...	2	38201.94	$b^3D_1-y^5F_1$	2323.786...	4	43019.98	$c^3D_1-w^3P_1$
2608.682...	5	38322.10	$c^3F_4-z^1H_5$	2321.71....	10 bl II	43058.5	$a^1H_5-z^1I_6$
2608.112...	7	38330.48	$a^5F_5-y^5F_5$	2319.466...	8 (1)	43100.10	$a^1G_4-w^3F_4$
2603.186...	3	38403.00	$c^3D_3-t^3F_4$	2319.220...	10 (2)	43104.65	$a^3D_1-z^3P_0$
2602.35....	2	38415.3	$b^3D_2-y^5F_2$	2318.102...	5	43125.46	$a^3P_1-z^5F_2$
2595.622...	8	38514.91	$a^3I_7-z^3H_6$	2315.70....	10 bl II	43170.2	$\cdot{}^3P_2-z^5S_2$
2594.67....	4 bl II	38529.0	$a^3F_2-y^5D_2$	2315.30....	5 bl II	43177.7	$b^3D_1-y^3F_2$
2592.533...	2	38560.80	$a^5F_2-z^3G_3$	2311.580...	4	43247.13	$a^3P_2-z^5F_2$
2590.043...	3	38597.86	$b^3D_2-y^5F_3$	2310.806...	3	43261.61	$b^3D_2-y^3F_2$
2584.038...	6	38687.55	$c^3F_3-x^3F_3$	2309.578...	4	43284.60	$a^1G_4-w^3F_3$
2583.739...	3	38692.04	$c^3F_2-x^3F_2$	2306.571...	5	43341.04	$a^3P_2-z^5F_3$
2582.37....	8 bl II	38712.5	$a^3I_6-z^3H_5$	2303.203...	3	43404.41	$c^3F_3-w^3F_3$
2575.798...	2	38811.30	$a^5F_5-z^3G_5$	2303.012...	7	43408.01	$c^3F_4-w^3F_3$
2574.838...	7	38825.78	$a^3I_5-z^3H_4$	2302.808...	8	43411.86	$b^1F_3-y^1F_3$
2558.172...	2	39078.70	$a^3F_3-y^5P_2$	2295.859...	15 (3)	43543.23	$a^1F_3-z^1D_2$
2556.207...	5	39108.74	$a^3F_2-z^3D_2$	2293.056...	10	43596.46	$c^3D_2-w^3P_2$
2552.937...	5	39158.84	$b^1F_3-z^1F_3$	2291.850...	6	43619.40	$c^3D_2-w^3P_2$
2551.098...	6	39187.06	$a^1H_5-z^1H_5$	2290.126...	5	43652.22	$b^1F_3-v^3F_3$
2545.750...	3	39269.37	$a^5F_2-z^3D_2$	2284.979...	5 n	43750.56	$a^3D_1-y^5F_2$
2537.934...	2	39390.30	$a^5F_3-z^3D_2$	2278.432...	6	43876.26	$b^3F_3-z^1G_4$
2537.537...	4	39396.46	$c^3F_4-x^3F_4$	2277.820...	8	43888.04	$b^3F_4-z^1G_4$
2531.890...	5	39484.33	$a^5F_2-z^3D_1$	2277.159...	4	43900.78	$a^3H_4-y^3H_5$
2520.162...	5	39668.06	$a^5F_4-y^5D_3$	2276.870...	8	43906.35	$a^3D_2-y^5F_3$
2512.902...	2	39782.66	$a^5F_4-y^5D_4$	2274.00....	8 bl II	43961.8	$b^1F_3-v^3F_4$
2511.418...	6 bl II	39806.16	$a^5F_5-y^5D_4$	2267.42....	10 (1)	44089.3	$a^1H_5-w^3F_4$
2507.244...	2	39872.42	$a^3D_2-z^5F_2$	2265.54....	4 bl II	44125.9	$b^3F_2-y^3G_3$
2502.903...	3	39941.57	$a^3D_3-z^5S_2$	2262.888...	3	44177.61	$a^1F_3-x^3F_3$
2501.526...	4	39963.55	$b^3D_3-z^3D_3$	2261.592...	12 (2)	44202.92	$a^1F_3-x^3F_2$
2496.696...	3	40040.86	$a^1H_5-y^3H_5$	2260.547...	7	44223.37	$a^3G_3-z^5H_3$
2487.922...	3	40182.07	$(a^3F_3-y^3D_3)$	2259.406...	2	44245.69	$a^3F_3-y^3P_2$
2487.191...	4	40193.87	$a^5F_2-y^5P_1$	2259.140...	2	44250.90	$a^1G_4-x^3H_5$
2485.741...	3	40217.32	$b^3D_2-z^3D_2$	2257.406...	8	44284.88	$a^3D_3-y^5F_4$
2484.820...	2	40232.22	$a^3F_3-y^3D_2$	2253.712...	3	44357.46	$b^1F_3-v^3D_2$
2469.126...	3	40487.93	$b^3D_2-y^5D_2$	2252.463...	4	44382.05	$a^3G_4-z^5H_4$
2462.978...	3	40588.98	$a^5F_4-y^5P_3$	2252.268...	5	44385.89	$a^3G_3-z^5H_4$
2456.571...	2	40694.82	$a^3F_4-y^3D_3$	2245.776...	4	44514.20	$b^3F_2-y^5G_2$
2447.374...	7 bl II	40847.74	$a^1G_4-z^1G_4$	2243.845...	4	44552.50	$b^3F_2-x^3D_3$
2439.963...	3	40971.80	$c^3F_4-z^1G_4$	2243.405...	8 (1)	44561.23	$a^3G_4-z^5H_5$
2438.174...	8	41001.86	$4s^5S_2-4p^7P_2$	2241.54....	12 (3) bl II	44598.3	$a^1D_2-z^1D_2$
2431.325...	5	41117.36	$a^3H_6-z^3I_7$	2238.155...	10 (2)	44665.75	$c^3F_4-x^3G_5$
.....	m II	41160.1	$a^3H_5-z^3I_5$	2235.908...	10 (1)	44710.64	$c^3F_3-x^3G_4$
2421.514...	5	41283.93	$a^3F_4-y^3F_4$	2235.699...	6	44714.82	$\begin{cases} c^3F_4-x^3G_4 \\ a^3P_2-z^5P_3 \end{cases}$
2421.376...	2	41286.28	$b^3D_2-y^5P_2$	2233.654...	6	44755.75	$b^3F_3-y^3G_4$
2420.405...	3	41302.84	$a^3F_2-y^3F_2$	2233.172...	4	44765.40	$b^3G_4-y^3G_3$
2419.742...	2	41314.17	$b^3D_3-y^5P_2$	2232.690...	10 (1)	44775.06	$c^3F_2-x^3G_3$
2418.568...	7	41334.22	$4s^5S_2-4p^7P_3$	2232.548...	8	44757.87	$(a^1F_3-y^3H_4)$
2406.409...	3	41543.05	$b^1G_4-v^1F_3$	2232.430...	10	44780.28	$a^3G_5-z^5H_6$
2403.551...	6	41592.44	$a^3H_4-z^3I_5$	2231.670...	4	44795.54	$c^3F_3-x^3G_3$
2389.533...	8	41836.42	$a^1H_5-z^1G_4$	2229.267...	10	44843.81	$b^3F_4-y^5G_5$
2376.725...	5	42061.85	$a^3H_5-z^3K_6$	2228.881...	4	44851.58	$b^3G_3-y^3G_3$
2373.904...	5	42111.84	$a^3H_6-z^3K_7$	2227.848...	7	44872.37	$a^3P_1-z^5P_2$
2363.51....	7 bl II	42297.0	$b^3G_4-x^3F_3$	2221.830...	10 (1)	44993.91	$a^3P_2-z^5P_2$
2362.401...	3	42316.86	$c^3F_4-w^3D_3$	2221.337...	2	45003.89	$a^1H_6-x^3H_4$
.....	m II	42354.81	$b^3G_5-y^3H_6$	2220.611...	3	45018.60	$a^3P_1-z^5P_1$
2353.820...	4	42471.12	$b^3D_3-y^3D_3$	2217.485...	5	45082.07	$b^3F_4-y^3G_4$
2352.616...	3	42492.85	$b^3D_2-y^3D_2$	2214.616...	4	45140.45	$a^3P_2-z^5P_1$
2346.961...	3 bl II	42595.22	$a^3D_2-z^3P_2$	2210.073...	6	45233.23	$\begin{cases} a^1D_2-x^3F_2 \\ b^3F_4-w^3D_3 \end{cases}$
2339.913...	5	42723.52	$b^1F_3-y^1D_2$	2209.739...	5 bl II	45240.07	$\begin{cases} a^1H_5-x^3H_5 \\ b^3G_3-y^5G_2 \end{cases}$
From here to λ 2023 intensities in parentheses refer to the M.I.T. grating spectrograms				2208.85....	10 (3) bl II	45258.3	$a^1D_2-x^3F_2$
2338.961...	10 (3)	42740.91	$a^3D_3-z^3P_2$	2207.847...	2	45278.84	$\begin{cases} b^3G_3-x^3D_3 \\ c^3F_2-z^1P_1 \end{cases}$
2338.59 ...	4	42747.7	$a^3P_2-z^5D_2$				
2336.768...	10 bl II	42781.02	$b^3G_4-y^3H_5$				
2331.539...	3	42876.95	$a^3G_4-z^5G_3$				
.....	bl II	42879.8 c	$a^3D_2-z^3P_1$				

TABLE 1—*Continued*

λ_{air} A	Int.	ν_{vac} cm^{-1}	Combination
2202.458...	8	45389.60	$a^3D_3-z^3D_3$
2196.240...	2	45518.10	$b^3F_4-x^5F_4$
2195.866...	5	45525.86	$a^3D_2-z^3D_2$
2195.532...	6	45532.78	$b^3G_4-y^5G_5$
2195.081...	5	45542.13	$b^3G_3-y^5G_4$
2193.294...	5	45579.23	$a^1H_5-x^3G_4$
2192.875...	4	45587.95	$a^3G_4-z^5F_5$
2191.215...	8	45622.48	$a^3G_5-z^5F_5$
2190.075...	3	45646.22	$b^3G_5-y^3G_4$
2189.154...	2	45665.42	$a^3H_5-z^1G_4$
2188.732...	4	45674.22	$b^3G_5-z^1I_6$
2187.667...	5 bl II	45696.47	$a^3H_4-z^1G_4$
2186.876...	6 n bl II	45712.99	$b^3F_4-x^5F_5$
2186.207...	2	45726.97	$a^3D_3-y^5D_3$
2185.654...	5	45738.54	$a^3G_4-z^5F_4$
2185.54....	3	45740.9	$a^1H_5-x^3H_6$ $a^3D_2-z^3D_1$
2185.264...	5	45746.70	$a^3G_4-z^5D_3$
2185.080...	3	45750.55	$a^3G_3-z^5D_3$
2184.114...	4	45770.78	$b^3G_4-y^3G_4$
2183.980...	6	45773.59	$a^3G_5-z^5F_4$
2182.889...	4	45796.48	$a^3D_2-y^5D_2$
2182.040...	4	45814.29	$b^1F_3-w^3H_4$
2181.407...	4	45827.58	$b^3G_5-y^3G_5$
2181.210...	2	45831.71	$b^3G_5-y^5G_6$
2180.410...	12 (4)	45848.53	$a^3P_1-z^3P_2$
2179.258...	6	45872.76	$a^3D_3-y^5D_3$
2179.071...	3	45876.69	$b^3D_1-y^3P_0$
2178.677...	5	45884.99	$a^3H_4-y^3G_3$
2175.972...	2	45942.03	$a^3D_3-y^5D_2$
2174.658...	15 (7)	45969.78	$a^3P_2-z^3P_2$
2173.829...	7 (1)	45987.31	$a^3D_3-y^5D_4$
2171.293...	2	46041.02	$b^3F_2-w^3D_1$
2171.045...	12 (4)	46046.28	$a^3P_0-z^3P_1$
2169.709...	5	46074.63	$c^3F_4-w^3G_5$
2168.106...	3	46108.68	$b^3F_2-w^3F_2$
2166.952...	12 (4)	46133.25	$a^3P_1-z^3P_1$
2166.604...	5	46140.65	$b^3F_4-w^3F_4$
2165.327...	4	46167.86	$a^1G_4-w^3G_3$
2165.071...	4	46173.32	$a^3G_3-z^5S_2$
2164.059...	4	46194.90	$b^3D_2-y^3P_1$
2163.475...	2	46207.37	$b^3G_4-x^5F_4$
2162.283...	5	46232.85	$c^3F_3-w^3G_4$
2161.478...	3	46250.07	$a^3G_3-z^3F_2$
2161.270...	10 (4)	46254.52	$a^3P_2-z^3P_1$
2160.655...	6	46267.68	$c^3F_2-w^3G_3$
2158.690...	3	46309.79	$b^3F_3-w^3D_2$
2158.472...	12 (4)	46314.46	$a^1G_4-y^1G_4$
2158.006...	3	46324.46	$b^3F_4-w^3F_3$
2157.710...	12 (4)	46330.83	$a^3P_1-z^3P_0$
2157.287...	3	46339.91	$a^3G_4-z^5F_3$
2157.109...	2	46343.73	$a^3G_3-z^5F_3$
2156.750...	2	46351.45	$c^3F_2-y^1D_2$
2156.183...	5	46363.63	$a^1F_3-x^3P_2$
2155.870...	5 bl II	46370.35	$b^3F_2-w^3D_2$
2154.420...	2	46401.56	$b^3G_4-x^5F_5$
2153.320	3	46425.26	$a^1I_6-z^3I_6$
2152.706...	6 (1)	46438.51	$c^3F_4-y^1G_4$
2151.776...	15 (8)	46458.58	$a^1F_3-z^1G_4$
2149.558...	2	46506.50	$b^3D_2-y^3P_2$
2148.254...	5	46534.72	$b^3D_3-y^3P_2$
2147.904...	7 (1)	46542.32	$a^5D_2-z^5D_1$
2146.339...	6 (1b)	46576.25	$a^3H_4-y^5G_4$ $a^5D_1-z^5D_0$
2146.062...	8 (4b)	46582.26	$a^5D_{32}-z^5D_2$
2145.616...	6 (0)	46591.94	$a^5D_1-z^5D_1$
2144.743...	7 (3)	46610.90	$a^1I_6-z^3I_7$
2144,282...	8 (5)	46620.92	$a^5D_4-z^5F_5$
2143.827...	7 (2)	46630.81	$a^5D_2-z^5F_4$ $a^5D_1-z^5D_2$
2143.76....	3	46632.3	$a^5D_0-z^5D_1$
2143.470...	8 (5)	46638.57	$a^5D_{3(2)}-z^5D_3$
2143.045...	7 (2)	46647.82	$a^3D_2-y^5P_3$
2142.533...	3	46658.98	$a^3H_6-z^1I_6$
2140.427...	4 (1n)	46704.88	$b^3G_5-w^3F_4$
2139.461...	2	46725.96	$b^3F_3-x^5D_4$
2137.365...	8 (5)	46771.79	$a^5D_4-z^5F_4$
2137.009...	5	46779.58	$a^5D_4-z^5D_3$
2136.360...	5 (1)	46793.78	$a^3D_3-y^5P_2$
2135.523...	4	46812.12	$a^3H_6-y^3G_5$
2134.861...	9 (5)	46826.63	$a^1I_6-z^3I_5$
2133.358...	2	46859.61	$a^3H_5-y^3G_4$
2132.089...	1	46887.50	$a^3H_5-z^1I_6$
2131.951...	3	46890.55	$a^3H_4-y^3G_4$
2130.829...	3	46915.23	$b^3G_3-w^3F_4$
2129.683...	5	46940.47	$a^1G_4-y^1F_3$
2129.238...	2	46950.27	$b^3F_4-x^5D_3$
2127.634...	2	46985.66	$a^1H_5-y^3I_5$
2125.170...	4	47040.14	$c^3F_2-y^1F_3$
2124.976 ..	3	47044.43	$b^3F_3-x^3H_4$ $b^1F_3-v^3G_4$ $a^3H_5-y^5G_6$
2124.225...	4	47061.06	$c^3F_3-y^1F_3$ $b^3F_3-x^5D_2$ $a^5D_{32}-z^5S_2$
2124.075...	2	47064.38	$c^3F_4-y^1F_3$
2123.590...	8 (1)	47075.13	$a^3F_2-z^1D_2$
2122.021...	5 (0)	47109.92	$a^5D_1-z^5S_2$
2120.767...	4 (0)	47137.79	$b^3F_2-x^5D_1$ $a^5D_{3,2}-z^5F_2$
2120.239...	5 (1)	47149.53	$a^5D_1-z^5F_1$
2118.567...	6 (3)	47186.73	$a^5D_1-z^5F_2$
2118.415...	5 (2)	47190.11	$a^5D_0-z^5F_1$
2116.588...	7 (5)	47230.85	$a^5D_2-z^5F_3$
2114.339...	3	47281.08	$c^3F_2-v^3F_3$ $a^3P_2-y^5F_3$
2113.891...	6 (4b)	47291.10	$b^1F_3-t^3F_4$ $b^3F_4-x^3H_5$
2113.344...	5 (2)	47303.33	$a^1H_5-y^1G_4$
2112.496...	4	47322.31	$a^1H_5-y^3I_6$
2112.282...	2	47327.11	$a^1I_6-z^3K_6$
2111.795...	4 (1)	47338.04	$c^3F_2-v^3F_2$
2108.676...	5	47408.04	$a^3F_3-x^3F_3$
2108.217...	2	47418.35	$a^1D_2-x^3P_2$
2107.324...	10 (10)	47438.44	$a^3G_3-z^3F_3$
2106.360...	3 (1)	47460.17	$b^1F_3-t^3F_3$
2105.020...	5 (2)	47490.37	$a^1G_4-v^3F_4$
2103.799...	12 (12)	47517.92	$a^3G_4-z^3F_3$
2103.647...	5 (3)	47521.36	$a^3G_3-z^3F_3$
2100.961...	8 (4)	47582.11	$b^3F_4-x^3G_5$
2099.718...	1	47610.27	$c^3F_3-v^3F_4$
2099.531...	2	47614.51	$c^3F_4-v^3F_4$
2099.332...	6 (4)	47619.02	$b^3F_3-x^3G_4$
2099.231...	5 (3)	47621.32	$a^3G_4-z^3F_4$
2098.816...	3	47630.73	$b^3F_4-x^3G_4$
2097.692...	12 (12)	47656.24	$a^3G_5-z^3F_4$
2097.480...	15 (15)	47661.06	$a^3G_5-z^3H_6$
2096.430...	6 (4)	47684.92	$a^5D_3-z^5D_4$
2095.688...	4 (1)	47701.82	$a^1D_2-y^3G_3$
2095.593...	2	47703.98	$b^3F_3-x^3G_3$
2095.327...	3 (1)	47710.04	$a^3F_2-x^3F_3$
2095.143...	3 (1)	47714.23	$a^3G_4-z^5P_3$
2093.504...	4 (1)	47751.57	$a^3D_2-y^3D_3$
2092.945...	6 (5)	47764.32	$b^3F_2-x^3G_3$

TABLE 1—*Continued*

λ_{air} A	Int.	ν_{vac} cm^{-1}	Combination
2091.488...	2	47797.58	$a^5F_1-z^1D_2$
2091.312...	7 (7)	47801.60	$a^3D_2-y^3D_2$
2090.240...	6 (6)	47826.12	$a^5D_4-z^5D_4$
2090.139...	12 (13)	47828.45	$a^3G_4-z^3H_5$
		47828.6 c	$a^3D_1-y^3D_2$
2090.053...	7 (6)	47830.40	$b^3G_3-x^3H_4$
2089.089...	6 (3)	47852.48	$a^3D_2-y^3D_1$
2088.625...	5 (2)	47863.10	$a^3G_5-z^3H_5$
2087.907...	7 (6)	47879.56	$a^3D_1-y^3D_1$
2087.132...	8 (9)	47897.33	$a^3D_3-y^3D_3$
2086.128...	4 (1)	47920.38	$a^3F_4-x^3F_3$
2085.839...	5 (3)	47927.01	$b^1F_3-x^1G_4$
2084.968...	5 (4)	47947.05	$a^3D_3-y^3D_2$
2084.515...	3 (2)	47957.47	$a^3G_4-z^3H_4$
2084.349...	10 (12)	47961.29	$a^3G_3-z^3H_4$
2083.530...	6 (5)	47980.13	$b^3G_4-x^3H_5$
2082.788...	1	47997.22	$b^1F_3-x^1F_3$
2082.377...	3 (1)	48006.69	$c^3F_3-v^3D_2$
2079.307...	3	48077.57	$c^3F_4-v^3D_3$
2078.989...	14 (18)	48084.92	$4s^5S_2-4p^5P_3$
2077.755...	4 (2)	48113.47	$a^3F_3-x^3F_4$
2077.089...	1	48128.89	$a^1D_2-x^3D_3$
2076.916...	1	48132.90	$a^3H_4-w^3F_3$
2076.316...	3 (1)	48146.81	$b^3G_5-x^3G_5$
2074.240...	3	48194.99	$b^3G_5-x^3G_4$
2071.889...	2	48249.67	$a^1D_2-y^5G_3$
2070.976...	2 (0)	48270.94	$b^3G_4-x^3G_5$
2070.539...	8 (9)	48281.12	$a^1I_6-z^1H_5$
2069.808...	2 (1)	48298.17	$a^1F_3-z^1F_3$
2068.243...	12 (17)	48334.72	$4s^3S_2-4p^3P_2$
2067.302...	6 (7)	48356.72	$b^3G_5-x^3H_6$
2065.268...	3 (2)	48404.33	$b^3G_4-x^3G_3$
2062.983...	3 (2)	48457.95	$a^5F_1-x^3F_2$
2062.083...	3 (3)	48479.09	$a^1H_5-v^3F_4$
2061.751...	9 (12)	48486.89	$a^3D_3-y^3F_4$
2061.552...	10 (15)	48491.57	$4s^4S_2-4p^5P_1$
2059.677...	7 (9)	48535.70	$a^3D_2-y^3F_3$
2058.560...	8 (11)	48562.05	$a^1I_6-z^1K_7$
2058.201...	3 (3)	48570.52	$a^3D_2-y^3F_2$
2057.921...	4 (4)	48577.13	$b^1F_3-x^1D_2$
2057.058...	6 (7)	48597.50	$a^3D_1-y^3F_2$
2056.145...	7 (9)	48619.07	$a^3P_2-z^3D_3$
2055.855...	6 (6)	48625.93	$a^3F_4-x^3F_4$
2054.480...	4 (3)	48658.46	$c^3F_4-u^3F_4$
2053.521...	3 (2)	48681.18	$a^3D_3-y^3F_3$
2052.269...	3 (2)	48710.89	$a^1F_3-w^3F_4$
2051.847...	2	48720.90	$a^5F_2-x^3F_2$
2050.739...	7 (7)	48747.22	$a^5D_4-z^5P_3$
2049.384...	7 (7)	48779.44	$a^3P_1-z^3D_2$
2047.126...	2 (1)	48833.25	$a^1I_6-y^3H_6$
			$a^3H_5-x^3H_4$
2046.784...	2 (1b)	48841.40	$a^5F_3-x^3F_3$
2046.043...	1 (1)	48859.04	$a^1D_2-w^3D_3$
2045.830...	5 (5)	48864.18	$a^3H_4-x^3H_4$
2044.970...	4 (4b)	48884.72	$a^5D_3-z^5P_2$
2044.541...	1 (1)	48894.97	$a^1F_3-w^3F_3$
2044.302...	4 (4)	48900.69	$a^3P_2-z^3D_2$
2044.034...	3 (3)	48907.10	$a^3P_0-z^3D_1$
2043.478...	3 (2)	48920.40	$c^3F_3-u^3F_3$
2042.236...	2 (2)	48950.14	$b^3D_1-z^1D_2$
2040.760...	2 (3)	48985.55	$a^3P_0-y^5D_1$
2040.538...	4 (5)	48990.89	$b^3F_4-w^3G_5$
2040.407...	3 (3)	48994.03	$a^3P_1-z^3D_1$
2039.507...	6 (8)	49015.64	$a^1H_5-y^1I_6$
2038.908...	2 (3)	49030.04	$a^5D_2-z^5P_1$
2038.742...	2 (2)	49034.03	$b^3D_2-z^1D_2$
2038.621...	1 (1)	49036.93	$b^3F_4-y^3I_5$
2038.092...	3 (3)	49049.66	$a^3P_1-y^5D_2$
2037.578...	1 (2)	49062.03	$b^3D_3-z^1D_2$
2037.292...	4 (6)	49068.92	$a^3H_5-x^3H_5$
2037.145...	2 (3)	49072.43	$a^3P_1-y^5D_1$
2036.845...	2 (2)	49079.71	$a^5D_1-z^5P_1$
2036.006...	2 (2)	49099.92	$a^3H_4-x^3H_5$
2035.939...	2 (3)	49101.54	$a^3P_2-y^5D_3$
2035.103...	2 (2b)	49121.70	$c^3F_2-u^3F_2$
2034.695...	4 (5)	49131.55	$a^3H_6-x^3G_5$
2034.537...	1 (1)	49135.36	$a^1I_6-y^3H_5$
2034.296...	3 (4)	49141.18	$b^3F_3-w^3G_4$
2030.767...	2 (2)	49226.57	.....
2029.522...	2 (3)	49256.76	$b^3F_2-w^3G_3$
2026.038...	4 (7)	49341.44	$a^3H_6-x^3H_6$
2025.557...	3 (5)	49353.15	$a^1D_2-z^1F_3$
2025.292...	.. (1)	49359.63	$a^3H_5-x^3G_5$
2023.289...	1 (4)	49408.48	$a^3H_5-x^3G_4$

From here to λ 1382 wave lengths and intensities are obtained from M.I.T. grating spectrograms only. Wave lengths in vacuum

2022.685...	1	49439.24	$a^3H_4-x^3G_4$
2019.225...	3	49523.95	$a^3H_4-x^3G_3$
2017.946...	4	49555.34	$b^3G_5-w^3G_5$
2017.363...	3	49569.66	$a^3H_5-x^3H_6$
2015.720...	3	49610.06	$b^3D_1-x^3F_2$
2015.453...	1	49616.63	$a^3P_0-y^5P_1$
2013.330...	4	49668.96	$b^3D_3-x^3F_3$
2012.539...	3	49688.48	$a^3F_3-z^1G_4$
2012.310...	1	49694.13	$b^3D_2-x^3F_2$
2012.192...	4	49697.05	$b^3D_3-x^3F_3$
2011.031...	3	49725.74	$b^3G_4-y^3I_5$
2009.118...	4	49773.08	$a^5P_1-z^5D_0$
2008.494...	6	49788.55	$a^5P_1-z^5D_1$
2006.914...	3	49827.75	$a^5P_1-z^5D_2$
2006.360...	4	49841.50	$b^3G_4-w^3G_4$
2006.095...	1	49848.09	$a^3P_1-y^5P_2$
2005.731...	4	49857.13	$a^5P_2-z^5D_1$
2005.613...	1	49860.07	$a^5D_2-z^5P_3$
2004.143...	8	49896.64	$a^5P_2-z^5D_2$
		49896.9 c	$b^3G_4-w^3G_3$
2003.233...	2	49919.31	$b^3G_5-y^1G_4$
2003.124...	3	49922.02	$b^1D_2-v^1F_3$
2002.473...	5	49938.25	$b^3G_5-y^3I_6$
2002.009...	1	49949.8	$a^1D_2-w^3F_3$
2001.909...	4	49952.32	$a^5P_2-z^5D_3$
2001.814...	3	49954.69	$a^5P_3-z^5D_2$
2000.688...	4	49982.81	$b^3G_3-w^3G_3$
2000.228...	9	49994.30	$a^3I_5-z^3I_6$
1999.893...	3	50002.68	$a^5P_3-z^5F_4$
1999.588...	9	50010.30	$a^3I_6-z^3I_6$
			$a^5P_3-z^5D_3$
1999.100...	1	50022.5	$a^3P_2-y^5P_3$
1996.420...	12	50089.66	$a^5G_{2(3)}-z^5G_2$
1995.563...	12	50111.17	$a^5G_3-z^5G_3$
1995.266...	7	50118.63	$a^5G_4-z^5G_3$
1994.366...	1	50141.2	$a^5G_3-z^5G_4$
1994.073...	13	50148.62	$a^5G_4-z^5G_4$
1993.262...	7	50169.02	$a^5G_5-z^5G_4$
1992.858...	6	50179.19	$a^3F_2-y^3G_3$
1992.427...	1	50190.04	$a^5G_4-z^5G_5$
1992.196...	9	50195.86	$a^3I_6-z^3I_7$
1992.017...	9	50200.37	$a^3I_7-z^3I_7$
		50200.8 c	$a^3F_4-z^1G_4$
1991.613...	14	50210.56	$a^5G_3-z^5G_5$
1989.975...	7	50251.89	$a^5G_6-z^5G_5$
1987.810...	3	50306.62	$a^5P_1-z^5S_2$
1987.503...	15	50314.39	$a^5G_6-z^5G_6$
1987.006...	1	50326.97	$b^3F_2-v^3F_2$

TABLE 1—*Continued*

λ_{vac} A	Int.	ν_{vac}cm^{-1}	Combination	λ_{vac} A	Int.	ν_{vac}cm^{-1}	Combination
1985.105	3	50375.17	$a^5P_2-z^5S_2$	1941.633	3	51503.04	$a^3D_2-y^3P_1$
1984.288	9	50395.91	$a^3I_5-z^3I_5$	1940.769	4	51525.97	$a^1G_4-x^1F_3$
1984.027	7	50402.54	$b^3D_3-x^3F_4$	1940.631	2	51529.6	$a^3D_1-y^3P_1$
1983.676	2	50411.46	$a^3I_6-z^3I_5$	1940.018	8	51545.91	$a^5D_4-y^5F_4$, $a^3F_4-w^3D_3$
1983.123	0	50425.5	$a^3F_3-y^5G_3$	1939.107	1	51570.12	$a^5F_1-x^3D_1$
1982.805	8	50433.60	$a^5P_3-z^5S_2$				
1982.076	6	50452.15	$a^5P_2-z^5F_2$			(51574.5 c	$b^3F_4-u^3F_4$
1980.392	2	50495.05	$c^3F_4-v^3G_5$	1938.901	10 ↑	51575.61	$a^3F_4-y^5G_5$
1979.002	1	50530.52	$b^3F_4-v^3F_4$	1938.775	4	(51578.96	$a^5F_2-y^5G_2$
1978.626	2	50540.12	$a^3H_6-w^3G_5$			51579.8 c	$c^3F_4-x^1G_4$
				1937.996	4	51599.69	$c^3G_4-v^3H_5$
1978.417	4	50545.46	$a^5P_2-z^5F_3$	1937.345	14	51617.03	$a^5G_3-z^5H_4$
1976.126	8	50604.06	$a^5P_3-z^5F_3$	1937.077	3	51624.17	$a^5G_4-z^5H_4$
1973.578	0	50669.39	$b^3G_4-y^1F_3$				
1972.638	2	50693.54	$c^3F_3-v^3G_4$	1936.806	4 bl II	51631.4	$b^3G_5-y^1I_6$
1972.245	2	50703.64	$c^3F_2-v^3G_3$	1932.818	5	(51737.92	$a^5F_2-y^5G_2$
						51738.4 c	$a^5F_3-x^3D_3$
1968.625	2	50796.88	$a^1H_5-w^1H_5$	1931.507	14	51773.05	$a^5D_4-y^5F_5$
1967.352	4	50829.74	$b^1G_4-w^1H_5$	1931.309	1	51778.35	$c^3D_2-s^3F_2$, $a^1F_3-w^3G_3$
1966.740	8	50845.56	$a^3H_4-y^3I_5$				
1966.201	2 bl II	50859.5	$a^5D_2-y^5F_1$	1930.917	2 bl II	51788.9	$c^3D_1-s^3F_2$, $a^3H_4-y^1F_3$
1966.074	3	50862.78	.....				
1965.309	8	50882.58	$a^3F_2-y^3G_4$	1930.387	15	51803.08	$a^4G_4-z^5H_5$
1964.776	8	50896.39	$a^3I_5-z^3K_6$	1930.184	2 b	51808.5	$a^1H_5-t^3F_4$
1964.260	7	50909.76	$a^5D_1-y^5F_1$, $b^4G_4-v^3F_3$	1929.941	2	51815.06	$a^3D_2-y^3P_2$
				1929.632	1	51823.35	$a^5G_5-z^5H_5$
1964.169	8	50912.12	$a^3I_6-z^3K_6$	1929.413	4 b	51829.2	$b^3F_2-u^3F_2$, $a^3F_2-z^1F_3$
1964.019	5 b	50916.0	$b^3F_2-v^3D_2$, $a^3I_7-z^3K_6$				
				1928.991	1	51840.57	$b^3F_4-u^3F_3$
1963.461	1	50930.47	$a^3H_5-w^3G_4$	1928.837	4	51844.71	$a^1D_2-z^1P_1$
1963.209	1	50937.01	$a^3F_4-y^5G_3$	1928.642	4	51849.95	$a^1I_5-z^1H_5$
1962.958	4	50943.53	$c^3F_4-t^3F_4$	1928.265	5 b	51860.1	$a^5F_3-y^5G_3$, $a^3F_3-w^3F_3$
1962.717	5	50949.78	$a^5D_0-y^5F_1$				
1961.724	1	50975.57	$b^3F_2-v^3D_2$	1928.178	4	51862.43	$a^1F_3-y^1D_2$
1961.456	1	50982.53	$b^3F_3-v^3D_3$	1927.679	2	51875.85	.....
1961.230	6	50988.41	$a^5D_2-y^5F_2$	1927.436	5	51882.39	$c^3G_4-r^3F_4$, $b^3D_3-x^3P_2$
1961.010	5	50994.13	$b^3F_4-v^3D_3$				
1960.318	13	51012.13	$a^3I_7-z^3K_8$	1926.898	3	51896.88	$c^3G_5-r^3F_4$
1959.324	8	51038.01	$a^5D_1-y^5F_2$	1926.304	18	51912.89	$4s^7P_3-4p^7P_2$
				1926.013	10 bl II	51920.7	$a^5P_2-z^5P_3$, $a^5F_2-x^3D_2$
1959.026	3	51045.77	$b^3F_2-v^3D_1$				
1958.732	4	51053.44	$b^4G_3-v^3F_2$				
1958.583	11	51057.32	$a^5P_3-z^5D_4$	1925.855	3	51924.99	$a^1F_3-y^1G_4$
1957.938	6	51074.14	$a^1G_4-y^1H_5$	1925.271	4	51940.74	$a^3F_3-w^3F_4$
1957.375	2	51088.83	$c^3F_2-t^3F_2$	1924.532	6	51960.68	$a^3D_3-y^3P_2$
				1924.119	4	51971.84	$b^1F_3-w^1G_4$
1957.137	3	51095.04	$b^3G_5-v^3F_4$	1923.877	7	51978.37	$a^5P_3-z^5P_3$
1955.943	0	51126.23	$a^3P_2-y^3D_3$				
1954.975	8	51151.55	$a^3H_5-y^3I_6$	1923.003	7	52002.00	$a^5F_2-y^5G_4$
1954.769	4	51156.94	$a^3F_4-y^5G_5$	1922.789	15	52007.79	$a^5G_5-z^5H_6$
1954.223	10 b	51171.2	$a^5D_{23}-y^5F_3$	1922.132	1	52025.56	$a^3F_4-x^5F_5$
				1921.990	1	52029.41	$a^3H_4-v^3F_3$
1953.968	4	51177.91	$c^3F_3-t^3F_3$	1921.132	2	52052.64	$c^3D_3-s^3F_3$
1953.821	1	51181.76	$c^3F_4-t^3F_3$				
1953.488	10	(51190.49	$a^3I_6-z^3K_7$	1920.752	2	52062.94	$a^1H_5-y^1H_5$
		51191.0 c	$a^3G_4-z^3G_3$	1920.260	2	52076.28	$c^3D_2-s^3F_3$
1953.322	13	51194.84	$a^3G_3-z^3G_3$, $a^3I_7-z^3K_7$	1920.186	4	52078.29	$a^5F_4-y^5G_4$
				1919.572	4	52094.94	$a^3F_2-w^3D_1$
1953.202	4	51197.98	$c^3F_4-y^1H_5$	1918.966	3	52111.40	$b^3F_2-u^3F_2$
1952.648	11	51212.51	$a^3G_4-z^3G_4$	.....	.....	(52121.9 c	$a^3F_2-w^3D_2$
1952.514	3	51216.0	$a^3G_3-z^3G_4$	1918.480	7 ↑	52124.59	$a^3F_3-w^3F_3$
1952.362	2 b	51220.0	$b^4G_4-v^3F_4$, $a^3G_4-z^3G_5$	1918.284	7	52129.92	$a^5P_1-z^5P_2$
				1917.960	6	52138.73	$b^3D_2-x^3P_1$, $b^3G_5-u^3F_4$
1951.318	3	51247.41	$a^3G_5-z^3G_4$				
1951.007	12	51255.58	$a^3G_5-z^3G_5$	1917.665	2	52146.75	$a^3I_6-z^1K_7$
1950.334	10	51273.27	$a^3H_6-y^3I_7$	1917.453	9	52152.52	$a^1I_6-z^1I_6$
1949.666	3	51290.83	$a^5F_1-y^5G_2$	1917.351	8	52155.29	$a^5F_4-y^5G_5$
1949.462	2	51296.20	$a^3D_1-y^3P_0$	1917.26	4	52157.8	$c^3G_4-r^3F_3$
1948.280	3	51327.32	$b^1G_4-v^1G_4$?	1917.087	2	52162.47	$a^3F_2-w^3F_2$
1946.769	3	51367.16	$c^3G_3-v^3H_4$	1916.507	5	52178.26	$a^5F_5-y^5G_6$
1946.321	0	51378.98	$c^3G_4-v^3H_4$	1915.750	2	52198.88	$a^5P_2-z^5P_2$
1945.724	2	51394.75	$a^3F_4-y^3G_4$	1915.083	15	52217.06	$a^5G_6-z^5H_7$
1945.342	12	51404.84	$a^5D_3-y^5F_4$	1914.056	19	52245.08	$4s^7S_3-4p^7P_3$
1943.715	2	51447.87	.....	1913.622	4	52256.92	$a^5P_3-z^5P_2$
1943.481	14 ↓	(51454.07	$a^5G_{5(3)}-z^5H_3$	1913.386	1	52263.37	$b^3G_4-u^3F_4$
		51455.9 c	$a^1G_4-x^1G_4$				

TABLE 1—*Continued*

λ_{vac} A	Int.	ν_{vac} cm^{-1}	Combination
1912.920...	4	52276.10	$a^5P_1-z^5P_1$
1911.703...	2 b	52309.4	$a^3H_5-v^3F_4$ $a^1I_6-y^3G_6$
1911.338...	7	52319.37	$a^1H_5-x^1H_5$
1910.401...	6	52345.03	$a^5P_2-z^5P_1$
1910.172...	1	52351.31	$c^3D_2-t^3D_1$
1909.846...	2	52360.24	$b^1G_4-u^1F_3$?
1909.782...	2	52361.99	$c^3D_1-t^3D_1$
1907.741...	4	52418.02	$a^3I_6-y^3H_6$
1907.577...	10 ↓	52422.52	$a^3I_7-y^3H_6$
		52423.9 c	$a^3F_2-w^3D_2$
1906.814...	6	52443.50	$b^3D_1-y^5G_2$ $a^5F_5-z^1I_6$
		52444.6 c	$a^1H_5-x^1G_4$
1906.457...	6	52453.32	$a^3F_4-w^3F_4$
1905.818...	2	52470.91	$a^5F_1-x^5F_2$
1905.214...	1	52487.5	$c^3D_3-t^3D_2$
1904.402...	4	52509.92	$a^5D_3-z^3D_3$
		52510.6c	$c^3D_2-t^3D_2$
1904.257...	2	52513.92	$b^1D_2-w^1D_2$?
1903.983...	1	52521.47	$c^3D_1-t^3D_2$
1903.706...	1	52529.12	$b^3G_4-u^3F_3$
1903.257...	3	52541.51	$a^3P_1-z^3S_1$
1903.18....	1	52543.6	$a^5F_4-w^3D_3$
1902.902...	5	52551.31	$a^1F_3-y^1F_3$
1902.402...	6	52565.13	$b^3D_2-x^3D_3$
1902.076...	5	52574.13	$a^5F_4-y^3G_5$
1901.540...	3	52588.95	$a^5F_1-x^5F_1$
1901.379...	5	52593.41	$b_2D_1-x^3P_0$ $b_2D_3-x^3D_3$
1901.096...	9	52601.24	$a^5F_5-y^5G_6$
1900.575...	1	52615.66	$b^3G_3-u^3F_3$
1899.931...	5	52633.49	$c^3D_3-s^3F_4$
1899.318...	5 b	52650.5	$a^5F_3-x^5F_3$ $a^5D_4-z^3D_3$ $c^3G_3-r^3F_2$
1898.870...	6	52662.89	$a^3P_2-z^3S_1$
1897.379...	3	52704.28	$a^3I_5-y^3H_5$
1897.028...	4	52714.03	$b^3D_3-y^5G_3$
1896.803...	9	52720.29	$a^3I_6-y^3H_5$
1896.73....	4	52722.3	$b^3D_1-x^3D_1$
1896.333...	4 n blg	52733.3	$c^3G_3-t^3G_3$
1895.912...	1	52745.06	$c^3G_4-t^3G_3$
1895.63....	?	52752.9	$a^5F_3-x^5F_4$
1895.456...	20	52757.75	$4s^7S_3-4p^7P_4$
		52759.1 c	$a^5F_3-x^5F_2$
1894.983...	4	52770.92	$a^5F_3-x^5F_3$
1894.52....	3 blg	52783.8	$b^3D_1-x^3D_2$
1894.252...	5	52791.29	$a^5D_{32}-z^3D_2$ $a^1F_3-v^3F_3$
1893.981...	11	52798.84	$a^3I_5-y^3H_4$
1893.113...	3	52823.04	$c^3D_2-t^3D_3$
1892.890...	5	52829.27	$a^5F_4-x^5F_4$
1892.598...	1	52837.42	$b^3G_3-u^3F_2$
1892.488...	1	52840.49	$a^5D_1-z^3D_2$
1892.339...	1	52844.65	$a^3H_5-y^1I_6$
1892.247...	5	52847.22	$a^5F_4-x^5F_3$
1892.140...	5	52850.21	$a^5G_5-z^5F_5$
1892.073...	5	52852.08	$a^5F_4-x^5F_4$
1891.909...	3	52856.66	$b^3D_3-y^5G_4$
1891.516...	5 b	52867.6	$c^3G_4-t^3G_4$ $b^3D_2-x^3D_2$
1891.339...	1	52872.59	$a^3F_2-x^5D_2$
1891.186...	3	52876.87	$a^5F_2-x^5F_1$
1891.070...	4	52880.12	$a^5F_3-x^5F_2$
1890.893...	2	52885.07	$a^5F_1-w^3F_2$ $a^3G_3-z^5D_1$
1890.669...	13	52891.33	$a^5G_6-z^5F_5$
1889.735...	4	52917.47	$a^1D_2-y^1D_2$
1889.451...	5	52925.43	$a^5D_{32}-z^5D_2$
1888.260...	2	52958.80	$c^3G_4-t^3G_5$
1887.734...	4	52973.57	$c^3G_5-t^3G_5$
1887.471...	8	52980.95	$a^5G_4-z^5F_4$ $a^5G_3-z^5D_3$
1887.197...	8	52988.64	$a^5G_4-z^5D_3$
1887.09....	1	52991.6	$a^5D_2-y^5D_3$
1886.757...	12	53001.00	$a^5G_5-z^5F_4$
1886.607...	5	53005.21	$a^5D_2-z^3D_1$
1885.947...	5	53023.76	$a^5F_4-x^5F_5$
1885.125...	9	53046.88	$a^5F_5-x^5F_5$
1884.596...	8	53061.77	$a^5D_{32}-y^5D_2$
1884.253...	2 b	53071.4	$b^3G_4-w^3H_4$
1883.816...	3	53083.74	$a^5D_2-y^5D_1$
1883.394...	1	53095.63	$a^5D_0-z^3D_1$
1883.185...	2	53101.53	$a^1F_3-v^3F_4$
1882.979...	4	53107.34	$a^5D_3-y^5D_4$
1882.357...	5	53124.89	$b^3G_4-w^3H_5$
1882,047...	10	53133.64	$a^5D_1-y^5D_1$ $a^5D_4-y^5D_3$
1881.578...	3	53146.87	$a^5F_1-w^3D_2$
1881.178...	5	53158.18	$b^3G_3-w^3H_4$
1880.704...	4	53171.58	$b^3D_3-y^3G_4$
1880.620...	3	53173.95	$a^5F_2-w^3F_2$ $a^5D_0-y^5D_1$
1878.550...	2	53232.55	$a^5P_3-z^3P_2$
1877.989...	12	53248.45	$a^5D_4-y^5D_4$
1873.534...	2	53375.07	$a^5F_3-w^3F_4$
1872.515...	4	53404.11	$a^5G_{22}-z^5S_2$
		53411.2 c	$b^3F_4-v^3G_5$
1872.214...	6 ↑	53412.70	$b^3G_5-w^3H_6$
1871.44....	0	53434.8	$a^5F_2-w^3D_2$
1871.319...	2	53438.24	$a^5F_2-w^3F_3$
1871.152...	9	53443.01	$a^5G_2-z^5F_1$
1869.91....	4	53478.5	$c^3F_2-u^3G_3$
1869.828...	10	53480.85	$a^5G_{22}-z^5F_2$
1866.900...	2	53564.73	$a^1F_3-v^3D_2$
1866.554...	5	53574.66	$a^5G_3-z^5F_3$
1866.305...	9	53581.81	$a^5G_4-z^5F_3$
1865.606...	2	53601.88	$b^3F_3-v^3G_4$
1865.445...	2	53606.51	$a^1D_2-y^1F_3$ $b^3D_3-x^5F_4$
1865.202...	7	53613.50	$b^1F_3-w^1F_3$
1864.53....	1	53632.8	$b^3F_3-v^3G_3$
1863.317...	4	53667.73	$a^5D_1-y^5D_0$
1862.446...	2	53692.83	$b^3F_3-v^3G_3$
1861.665...	3	53715.36	$a^5D_2-y^5P_1$
1859.955...	3	53764.74	$a^5D_1-y^5P_1$
1859.813...	5	53768.85	$c^3F_3-u^3G_4$
1858.542...	5	53805.62	$a^5D_0-y^5P_1$
1856.690...	7	53859.29	$a^5D_2-y^5P_2$
		53859.7 c	$b^3F_4-t^3F_4$
1855.510...	3	53893.54	$a^1G_4-u^3G_5$
1854.975...	5	53909.08	$a^5D_1-y^5P_2$
1854.826...	9 b	53913.4	$a^5D_{32}-y^5P_2$
		53914.1 c	$a^5F_1-x^5D_1$
1854.384...	3	53926.26	$a^5F_1-x^5D_0$
1852.812...	2	53972.02	$a^5F_3-x^5D_4$
1852.677...	6	53975.95	$b^3G_5-v^3G_5$
1852.366...	1	53985.0	$a^3H_6-w^3H_5$
1851.261...	6	54017.23	$c^3F_4-u^3G_5$
1850.650...	1	54035.1	$a^5G_4-z^5D_4$
1850.200...	5	54048.21	$a^5F_4-x^5D_4$
1849.960...	5	54055.22	$a^5D_4-y^5P_3$ $a^5G_5-z^5D_4$
1849.648...	1	54064.34	$a^5F_2-x^5D_2$
1849.407...	7	54071.39	$a^5F_5-x^5D_4$
1849.172...	1	54078.26	$b^3F_2-t^3F_2$
1848.883...	1	54086.71	$b^3F_3-t^3F_3$
1848.492...	1	54098.15	$b^3F_4-t^3F_3$
1848.428...	0	54100.0	$b^3G_4-v^3G_5$

TABLE 1—*Continued*

λ_{vac}A	Int.	ν_{vac}m^{-1}	Combination
1848.130...	2	54108.74	$c^3D_3-v^3P_2$
1847.637...	2	54123.19	$a^1G_4-u^3D_3$
1847.348...	1	54131.65	$c^3D_2-v^3P_2$
1846.943...	3	54143.52	$c^3F_2-u^3D_1$
1845.749...	1 b	54178.5	$b^3G_5-v^3G_4$ $a^3G_3-y^3D_2$
1845.521...	7	54185.24	$a^5F_3-x^5D_3$ $a^5F_2-x^5D_2$
1845.304...	5	54191.61	$a^3H_4-w^3H_4$
1844.942...	3	54202.25	$c^3F_2-u^3D_2$ $a^5F_2-x^5D_1$
1844.547...	6	54213.85	$a^3H_5-w^3H_5$
1844.263...	5	54222.20	$c^3F_3-u^3D_2$
1843.999...	3	54229.96	$b^3D_3-w^3F_4$
1843.502...	2	54244.58	$a^3H_4-w^3H_5$
1843.409...	4	54247.32	$c^3F_4-u^3D_3$
1842.927...	5	54261.51	$a^5F_4-x^5D_3$
1841.536...	5	54302.50	$b^3G_4-v^3G_4$
1841.387...	3	54306.89	$a^5F_3-x^5D_2$
1838.698...	1	54386.3	$b^3D_2-w^3F_3$
1838.621...	1	54388.6	$b^3G_3-v^3G_4$
1838.309...	7	54397.82	$a^3H_6-w^3H_6$
1837.588...	4	54419.16	$b^3G_3-v^3G_3$
1837.422...	1	54424.1	$b^3G_5-t^3F_4$
1834.096...	1	54522.77	$a^3P_1-y^3P_0$
1830.623...	3	54626.21	$a^3H_5-w^3H_6$
1829.172...	2	54669.54	$a^5G_3-z^3F_2$ $a^3P_0-y^3P_1$
1828.857...	1 bl H	54679.0	$b^3G_5-y^1H_5$
1826.267...	0	54756.5	$a^3P_1-y^3P_1$
1826.156...	1	54759.83	$a^5G_4-z^3F_3$
1824.659...	1	54804.76	$(b^3G_3-t^3F_3)$
1822.183...	1	54879.23	
1821.865...	0	54888.8	$a^5G_5-z^3H_6$
1820.496...	1	54930.08	$a^5G_6-z^3H_6$
1819.718...	1	54953.56	$a^3F_3-w^3G_4$ $a^1F_3-w^1H_4$
1819.480...	2	54960.76	$a^3H_6-v^3G_5$
1812.974...	2	55157.99	$a^5D_4-y^3D_3$
1811.924...	3	55189.95	$a^3P_2-y^3P_2$
1808.203...	0	55303.5	$a^3F_4-w^3G_5$
1805.337...	2	55391.32	$a^3H_5-v^3G_4$
1803.330...	1	55452.97	$a^3H_4-v^3G_3$
1801.766...	3	55501.10	$a^1G_4-w^1G_4$
1797.769...	0	55624.5	$c^3F_4-w^1G_4$
1793.785...	1	55748.04	$a^5D_4-y^3F_4$
1791.345...	0	55823.98	$a^5P_2-z^3D_3$
1777.737...	1	56251.29	$a^5P_1-z^3D_1$
1775.983...	6	56306.85	$a^5P_2-y^5D_3$ $a^5P_1-y^5D_2$
1775.590...	0	56319.3	$a^5P_2-z^3D_1$
1775.267...	1	56329.55	$a^5P_1-y^5D_1$
1773.098...	1	56398.46	$a^5P_2-y^5D_1$
1771.976...	2	56434.20	$a^5P_3-y^5D_2$
1770.554...	6	56479.50	$a^5P_3-y^5D_4$
1770.247...	3	56489.29	$a^1H_5-w^1G_4$
1753.455...	0	57030.26	$a^5P_2-y^5P_1$
1749.052...	1	57173.83	$a^5P_2-y^5P_2$
1748.177...	2	57202.45	$a^5G_2-y^5F_1$
1747.260...	1	57232.47	$a^5P_3-y^5P_2$
1745.638...	4	57285.65	$a^5P_3-y^5P_3$
1744.233...	3	57331.79	$a^5G_{32}-y^5F_2$
1739.201...	0	57497.7	$b^3G_5-u^3G_5$
1738.468...	3	57521.91	$a^5G_4-y^5F_3$
1730.842...	4	57775.35	$a^5G_5-y^5F_4$
1722.837...	4	58043.80	$a^5G_6-y^5F_5$
1717.414...	2	58227.08	$a^3H_4-u^3G_3$
1710.374...	3	58466.74	$a^3H_5-u^3G_4$
1709.892...	4	58483.23	$a^3H_6-u^3G_5$
1695.036...	2	58995.79	$4s^7S_3-4p^5P_3$
1656.831...	2	60356.2	$a^3I_7-y^3I_7$

λ_{vac}A	Int.	ν_{vac}m^{-1}	Combination
1628.304...	3	61413.59	$a^1I_6-x^1H_5$
1624.206...	2	61568.54	$a^3G_5-y^3H_6$
1617.171...	1	61836.4	$a^3G_4-y^3H_5$
1614.611...	1	61934.4	$a^3G_3-y_3H_4$
1611.763...	7 n	62043.9	$4p^5P_1-4d^5D_2$
1611.723...	7 n unr.	62045.4	$4p^5P_1-4d^5D_{10}$
1607.723...	9 n	62199.8	$4p^5P_2-4d^5D_{32}$
1606.014...	3 n	62266.0	$4p^5P_1-5s^5S_2$
1602.000...	5 n	62422.0	$4p^5P_2-5s^5S_2$
1601.289...	6 n	62449.7	$4p^5P_3-4d^5D_{32}$
1601.211...	10 n	62452.8	$4p^5P_3-4d^5D_4$
1595.597...	6 n	62672.5	$4p^5P_3-5s^5S_2$
1551.377...	4 n	64458.9	$4p^7P_4-4d^7D_3$
1550.862...	8 n	64480.3	$4p^7P_4-4d^7D_4$
1550.196...	12 n	64508.0	$4p^7P_4-4d^7D_5$
1539.480...	5 n	64957.0	$4p^7P_3-4d^7D_2$
1539.128...	8 n	64971.9	$4p^7P_3-4d^7D_3$
1538.632...	10 n	64992.8	$4p^7P_3-4d^7D_4$
1531.864...	7 n	65279.9	$4p^7P_2-4d^7D_1$
1531.644...	8 n	65289.3	$4p^7P_2-4d^7D_2$
1531.293...	6 n	65304.3	$4p^7P_2-4d^7D_3$
1505.166...	10 n	66437.9	$4p^7P_4-5s^7S_3$
1504.002...	2	66489.3	$a^5D_4-x^5F_5$
1493.640...	9 n	66950.5	$4p^7P_3-5s^7S_3$
1486.265...	7 n	67282.8	$4p^7P_2-5s^7S_3$
1484.546...	1	67360.7	$a^3G_3-x^3G_4$
1484.241...	0	67374.5	$a^3G_4-x^3G_4$
1481.169...	2	67514.2	$a^5D_4-x^5D_4$
1471.638...	1	67951.5	$3d'^3F_2-z^3F_2$
1471.051...	0	67978.6	$3d'^3F_2-z^3F_2$
1468.986...	2	68074.2	$3d'^3F_4-z^3F_4$
1395.750...	2	71646.1	$3d'^3F_3-z^3G_4$
1395.382...	0	71665.0	$3d'^3F_4-z^3G_4$
1395.213...	3	71673.6	$3d'^3F_4-z^3G_5$
1394.024...	1	71734.8	$3d'^3F_2-z^3G_3$
1382.857...	1	72314.1	$a^5G_6-y^5G_6$

From here to λ 1017 intensities in parentheses refer to M.I.T. plates

1143.67....	3 (3 bl)	87437.8	$3d^3D_1-z^3F_2$
1143.54....	1 (2 bl)	87447.7	$3d^3D_2-z^3F_2$
1142.955...	5 (5)	87492.5	$3d^3D_3-z^3F_4$
1142.464...	4 (4)	87530.1	$3d^3D_2-z^3F_3$
1141.272...	3 (3)	87621.5	$3d'^1G_4-x^1H_5$
1131.914...	3 (3)	88345.9	$3d^3D_2-4p^5P_3$
1131.194...	7 (5)	88402.2	$3d^3D_1-4p^5P_2$
1130.404...	5 (3)	88463.9	$3d^3D_0-4p^5P_1$
1129.19....	7	88559.1	$3d^3D_1-4p^5P_1$
1128.72....	7	88595.9	$3d^3D_2-4p^5P_2$
1128.02....	8	88650.9	$3d^3D_3-4p^5P_3$
1126.72....	6 (0)	88753.2	$3d^3D_3-4p^5P_1$
1124.883...	9 (5)	88898.1	$3d^3D_3-4p^5P_2$
1122.526...	9 (2)	89084.8	$3d^3D_4-4p^5P_3$
1099.05....	2	90987.7	$3d'^3P_2-v^3D_2$
1098.24....	5 (0)	91054.8	$3d'^3P_2-v^3D_3$
1097.65....	m (1)	91103.7	$3d'^3F_3-v^3D_2$
1096.61....	bl (3)	91190.1	$3d'^3F_4-v^3D_4$
1095.47....	5 (1)	91285.0	$3d'^3F_2-v^3D_1$
1093.32....	2	91464.5	$3d^1F_3-z^1G_4$
1089.671...	4	91770.8	$3d'^3F_4-u^3F_4$
1089.416...	4	91792.3	$3d'^1G_4-w^1G_4$
1089.061...	3	91822.2	$3d'^3P_1-v^3D_2$
1088.224...	1	91892.8	$3d'^3P_1-v^3D_1$
1086.748...	5 (3)	92017.6	$3d'^3F_3-u^3F_3$
1083.176...	2	92321.1	$3d'^3P_0-v^3D_1$
1082.838...	4 (1)	92349.9	$3d'^3F_2-u^3F_2$
1075.024...	4	93021.2	$3d^3G_3-z^3F_2$

TABLE 1—*Continued*

λ_{vac}A	Int.	ν_{vac}cm^{-1}	Combination
1072.061	1	93104.6	$3d^3G_3-z^3F_3$
1072.217	4 (1)	93264.7	.....
		93303.2 c	$3d^1F_3-z^1F_3$
1071.746	5 (4)	93305.7	$3d^3G_4-z^3F_3$
1070.556	3 (0)	93409.4	$3d^3G_4-z^3F_4$
1070.284	4 (1)	93433.1	$3d'^1G_4-w^1F_3$
1069.019	5 (3)	93543.7	$3d^3G_3-z^3H_4$
1068.299	3 (1)	93606.8	$?d'^3F_4-v^3G_5$
1068.190	5 (4)	93616.3	$3d^3G_4-z^3H_5$
		93790.8 c	$3d'^3F_3-v^3G_4$
1066.181	10 b (3)	93792.7	$3d^3G_5-z^3F_4$
1066.143	(4)	93796.0	$3d^3G_5-z^3H_6$
1064.611	1	93931.0	$3d'^3F_2-v^3G_2$
1063.872	8 (5)	93996.3	$3d^3D_3-y^3D_3$
1063.309	3 (1)	94046.0	$3d^3D_3-y^3D_2$
1063.188	4	94056.7	$3d'^3F_4-t^3F_4$
1062.272	3	94137.8	$3d^3D_2-y^3D_3$
1061.827	4	94177.3	$3d^3D_1-y^3D_2$
1061.708	6 (3)	94187.9	$3d^3D_2-y^3D_2$
1061.245	5 (2)	94228.9	$3d^3D_1-y^3D_1$
1061.127	4 (0)	94239.4	$3d^3D_2-y^3D_1$
1060.723	4 (0)	94275.3	$3d'^3F_3-t^3F_3$
1060.258	4 (0)	94316.7	$3d'^3F_2-t^3F_2$
1038.355	6 (2)	96306.2	$3d^3F_2-z^3F_2$
1037.462	1	96389.1	$3d^3F_2-z^3F_3$
1036.659	2	96463.7	$3d^3F_3-z^3F_2$
1035.768	6 (5)	96546.7	$3d^3F_3-z^3F_3$
1034.654	2	96650.7	$3d^3F_3-z^3F_4$
1034.054	2	96706.7	$3d'^3F_2-u^3G_3$
1033.298	5 (4)	96777.5	$3d^3G_3-z^3G_3$
1033.24	2	96782.9	$3d^3F_4-z^3F_3$
1033.079	1	96798.0	$3d^3G_3-z^3G_4$
1032.342	4 (1)	96867.1	$3d'^3F_3-u^3G_4$
			$3d^1F_3-y^1D_2$
1032.123	8 (5)	96887.7	$3^3F_4-z^3F_4$
1030.924	6 (3)	97000.4	$3d^3G_4-z^3G_4$
1030.844	2	97007.9	$3d^3G_4-z^3G_5$
1029.551	2	97129.7	$3d'^3F_4-u^3G_5$
1026.790	6	97390.9	$3d^3G_5-z^3G_5$
1024.108	3	97646.0	$3d^3D_1-y^3P_0$
1021.561	4	97889.4	$3d^3D_2-y^3P_1$
1020.022	2	98037.1	$3d'^3P_1-u^3D_2$
1019.789	6 (1)	98059.5	$3d^3D_3-y^3P_2$
		98201.3 c	$3d^3D_3-y^3P_2$
1018.286	8 (1)	98204.2	$3d^3H_4-z^3H_4$
1017.745	8 (2)	98256.4	$3d^3H_5-z^3H_5$
1017.254	9 (1)	98303.9	$3d^3H_6-z^3H_6$
1012.411	3	98774.1	$3d^3P_0-z^3P_1$
1010.005	4	99009.4	$3d^3P_1-z^3P_2$
1007.113	3	99293.7	$3d^3P_1-z^3P_1$
1006.341	2	99369.9	$3d^1G_4-z^1I_5$
1005.106	2	99492.0	$3d^3P_1-z^3P_0$
999.376	5	100062.4	$3d^3F_2-z^3G_2$
997.794	1	100221.1	$3d^3F_3-z^3G_3$
997.599	6 bl	100240.7	$3d^3F_3-z^3G_4$
997.081	7	100292.8	$3d^3P_2-z^3P_2$
995.223	2	100480.0	$3d^3F_4-z^3G_4$
995.150	6	100487.4	$3d^3F_4-z^3G_5$
994.724	6	100530.4	$3d^3G_3-y^3F_2$
994.257	3	100577.6	$3d^3P_2-z^3P_1$
993.080	7	100696.8	$3d^3G_4-y^3F_3$
992.337	2 bl	100772.2	$3d^3F_3-z^3D_2$
991.829	6	100823.8	$3d^1G_4-z^1H_5$
991.232	9	100881.6	$3d^3F_4-z^3D_3$
			$3d^3G_5-y^3F_4$
990.800	6	100928.5	$3d^3F_3-z^3D_2$
990.235	4	100986.1	$3d^3F_2-z^3D_1$
989.467	4	101064.5	$3d^3F_2-y^3D_1$
988.148	2	101199.4	$3d^3F_3-y^3D_2$
986.637	5	101354.4	$3d^1I_6-z^1H_5$
986.514	4	101367.0	$3d^3F_4-y^3D_3$
985.824	8	101438.0	$3d^3H_4-z^3G_3$
983.877	10 b	101638.7	$3d^1I_6-z^1K_7$
			$3d^3H_5-z^3G_4$
983.510	2	101676.6	$3d^1F_3-t^3F_3$
			$3d^1G_4-y^3H_5$
981.373	10	101898.1	$3d^3H_6-z^3G_5$
981.084	1	101928.1	$3d^3D_3-x^3F_4$
980.416	1	101997.5	$3d^3F_2-y^3P_2$
979.704	2	102071.6	$3d^1F_3-x^1G_4$
979.032	5	102141.7	$3d^1F_3-x^1F_3$
977.790	2	102271.4	$3d'^1G_4-v^1F_3$
973.505	4	102721.6	$3d^1F_3-x^1D_2$
971.929	3	102888.2	$3d^1D_2-z^1P_1$
970.435	2	103046.6	$3d^3F_2-y^3D_2$
970.381	2	103052.3	.....
969.954	3	103097.7	$3d^3F_2-y^3D_1$
969.423	2	103154.1	$3d^3F_3-y^3D_3$
968.955	4	103204.0	$3d^3F_3-y^3D_2$
967.197	6	103391.6	$3d^3F_4-y^3D_3$
965.717	1	103550.0	$3d^3D_2-x^3P_2$
963.880	3 bl	103747.4	$3d^3P_0-y^3D_1$
963.197	2 b	103820.9	$3d^3F_2-y^3F_2$
			$3d^3D_1-x^3P_1$
962.655	5	103879.4	$3d^1S_0-z^1P_1$
962.108	1	103938.0	$3d^3F_3-y^3F_3$
961.901	7	103960.8	$3d^1D_2-y^1D_2$
961.709	2	103981.6	$3d^3F_4-y^3F_4$
960.454	1	104117.4	$3d^3D_3-x^3D_3$
959.552	4	104215.3	$3d^3P_1-y^3D_2$
959.329	1	104239.5	$3d^3D_3-y^3G_3$
959.070	1	104267.7	$3d^3P_1-y^3D_1$
956.355	1	104563.7	$3d^3D_2-x^3D_2$
955.572	5	104649.4	$3d^1D_2-y^1F_3$
955.141	2	104696.6	$3d^3D_3-y^3G_4$
953.383	3	104889.6	$3d^1D_2-v^3F_2$
950.722	3	105183.2	$3d^3P_0-z^3S_1$
950.663	4	105189.7	.....
950.334	10	105226.2	$3d^1I_6-z^1I_6$
948.918	4	105383.2	$3d^1I_6-y^3G_5$
948.322	5	105449.4	$3d^3P_2-y^3D_3$
946.056	6	105702.0	$3d^3P_1-z^3S_1$
942.363	2	106116.2	$3d^1F_3-w^1G_4$
934.703	7	106985.9	$3d^3P_2-z^3S_1$
931.124	1	107397.1	$3d^3P_0-y^3P_1$
930.086	4	107516.9	$3d^3G_3-y^3H_4$
929.163	5	107623.7	$3d^3G_4-y^3H_5$
928.474	5	107703.6	$3d^3G_5-y^3H_6$
928.004	4	107758.2	$3d^1F_3-w^1F_3$
923.215	1	108317.1	$3d'^3P_2-t^3D_3$
918.800	1	108838	$3d'^3P_1-t^3D_2$
917.932	4	108940.5	$3d^1G_4-y^1G_4$
917.684	2	108970.0	$3d^3D_3-y^1G_4$
915.455	3	109235.3	$3d^1D_2-x^1F_3$
913.919	2	109418.9	$3d^3G_4-z^1G_4$
913.324	1	109490.2	$3d^1I_6-y^3I_6$
913.132	1	109513.2	$3d^3P_2-y^3P_2$
912.794	3	109553.7	$3d^3H_5-z^3I_6$
912.683	5	109567.1	$3d^1G_4-y^1F_3$
912.197	2	109625.4	$3d'^3P_2-v^3P_2$
911.265	2	109737.6	$3d^3D_2-y^1F_3$
911.205	1	109744.8	$3d^3F_3-z^1D_2$
910.961	6	109774.2	$3d^3H_4-z^3I_5$
910.693	4	109806.5	$3d^3H_6-z^3I_6$
			$3d^1G_4-v^3F_3$
910.639	3	109813.0	$3d^1D_2-x^1D_2$
909.279	2	109977.2	$3d^3D_3-v^3F_3$
909.178	4	109989.5	$3d^3H_6-z^3I_7$
908.885	2	110024.9	$3d^3D_1-v^3F_2$

TABLE 1—*Continued*

λ_{vac}A	Int.	ν_{vac}cm^{-1}	Combination
908.800...	1	110035.2	$3d^3D_2-v^3F_2$
908.131...	5	110116.3	$3d^1G_4-v^3F_4$
907.891...	4	110145.4	$3d^3D_3-v^3F_4$
907.041...	1	110248.6	$3d^3F_2-x^3F_2$
905.964...	1	110379.7	$3d^3F_3-x^3F_3$
905.338...	7	110456.0	$3d^3H_5-z^3K_6$
904.320...	3	110580.3	$3d^1G_4-v^3D_3$
902.869...	3	110758.0	$3d^3G_5-y^5G_5$
901.034...	5	110983.6	$3d^3H_6-z^3K_7$
900.940...	3	110995.2	$3d^3G_5-y^3G_4$
900.432...	2	111057.8	$3d^3G_3-z^1F_3$
899.417...	8	111176.5 c	$3d^3G_5-y^3G_5$
		111180.7 c	$3d^3G_5-y^5G_6$
		111183.1	$3d^1I_6-y^1I_6$
		111189.2 c	$3d^3D_3-u^3F_4$
899.052...	1	111228.3	$3d^3H_4-z^1H_5$
898.805...	1	111258.8	$3d^3G_4-z^1F_3$
897.747...	2	111390.0	$3d^3G_3-w^3F_2$
897.580...	1	111410.7	$3d^3H_5-z^1H_5$
896.380...	1	111559.8	$3d'^1G_4-w^1H_5$
896.072...	1	111598.2	$3d^3D_2-u^3F_3$
894.008...	4	111855.8	$3d^3G_4-w^3F_3$
892.417...	6	112055.2	$3d^3G_5-w^3F_4$
			$3d'^1G_4-v^1G_4$
891.442...	8	112177.8	$3d^3H_4-y^3H_4$
891.172...	10	112211.8	$3d^3H_6-y^3H_6$
890.755...	9	112264.3	$3d^3H_5-y^3H_5$
890.008...	2	112358.5	$3d^3H_5-y^3H_4$
888.777...	2	112514.2	$3d^3H_6-y^3H_5$
887.372...	3	112692.3	$3d^3F_2-y^3G_3$
886.138...	1	112849.2	$3d^3F_3-y^3G_3$
884.600...	5	113045.4	$3d^3G_3-x^3G_3$
884.263...	4	113088.5	$3d'^1G_4-u^1F_3$
883.688...	6	113162.1	$3d^3G_4-x^3G_4$
883.090...	3	113238.7	$3d^3F_2-y^5G_2$
			$3d^3F_2-y^5G_3$
882.295...	1	113340.8	$3d^3P_0-x^3P_1$
882.147...	4	113359.8	$3d^3F_2-x^3D_1$
881.477...	3	113446.0	$3d^1G_4-t^3F_4$
881.088...	7	113496.0	$3d^3G_5-x^3G_5$
880.949...	6	113513.9	$3d^3F_4-x^3D_2$
880.447...	6	113578.7	$3d^3F_2-x^3D_2$
880.008...	5	113635.3	$3d^3F_4-y^5G_2$
879.505...	4	113700.3	$3d^1G_4-y^1H_5$
878.287...	4 b	113858.0	$3d^3F_4-y^5G_5$
			$3d^3F_3-y^3G_4$
			$3d^3P_1-x^3P_1$
876.679...	3	114066.8	$3d^3H_4-y^3G_3$
876.564...	3	114081.8	$3d^1G_4-x^1G_4$
876.483...	3	114092.3	$3d^3F_4-y^3G_4$
876.021...	5	114152.5	$3d^1G_4-x^1F_3$
875.423...	5	114230.5	$3d^1I_6-y^1H_5$
875.090...	2	114274.0	$3d^3F_4-y^3G_5$
874.560...	1	114343.2	$3d^3F_2-z^1F_3$
874.129...	2	114399.6	$3d^3P_1-x^3P_0$
873.988...	1	114418.0	$3d^3F_3-x^5F_2$
873.462...	8	114486.9	$3d^1I_6-x^1H_5$
873.130...	2	114530.5	$3d^3F_4-x^5F_4$
			$3d^3P_1-x^3D_1$
873.080...	3	114537.0	$3d^3G_3-w^3G_3$
872.027...	4	114675.3	$3d^3F_2-w^3F_2$
871.968...	4	114683.1	$3d^3G_4-w^3G_4$
871.552...	2	114737.8	$3d^3F_4-z^1F_3$
870.621...	5	114860.5	$3d^3P_2-x^3P_2$
870.274...	2 unr.	114906.3	$3d^3G_5-w^3G_5$
870.235...	2 unr.	114911.5	$3d^3F_3-w^3F_4$
870.041...	3	114937.1	$3d^3F_2-w^3D_2$
			$3d^3H_5-y^5G_4$
868.836...	5	115096.5	$3d^3F_3-w^3D_2$
			$3d^3F_2-w^3F_3$
868.450...	4 b	115147.7	$3d^3P_2-x^3P_1$
			$3d^3F_4-w^3F_4$
867.639...	5	115255.3	$3d^3H_5-y^3G_4$
			$3d^3P_0-w^3D_1$
866.905...	1	115352.9	$3d^5D_0-z^5D_1$
865.896...	4	115487.3	$3d^5D_1-z^5D_2$
865.267...	1	115571.3	$3d^3P_2-x^3D_3$
864.425...	4	115683.8	$3d^5D_2-z^5D_2$
			$3d^3H_6-y^3G_5$
864.375...	2 unr.	115690.5	$3d^3H_6-y^5G_6$
			$3d^3P_2-y^5G_3$
864.034...	6	115736.2	$3d^5D_2-z^5D_3$
863.730...	1	115776.9	$3d^3P_1-w^3D_1$
863.302...	4	115834.3	$3d^1D_2-y^1P_1?$
863.232...	4	115843.7	$3d^3P_1-w^3F_2$
863.004...	1	115874.3	$3d^3P_2-x^3D_2$
862.735...	5	115910.4	$3d^5D_0-z^5F_1$
862.468...	3	115946.3	$3d'^3F_4-r^3F_4$
862.326...	2	115965.4	$3d^5D_1-z^5S_2$
862.191...	2	115983.6	$3d^5D_3-z^5D_2$
862.028...	5	116005.5	$3d^5D_1-z^5F_1$
861.832...	10 unr.	116031.8	$3d^5D_3-z^5F_4$
861.761...	8 unr.	116041.5	$3d^5D_3-z^5D_3$
			$3d^5D_1-z^5F_2$
861.284...	4	116105.7	$3d^3P_1-w^3D_2$
861.087...	2	116132.3	$3d^3H_4-w^3F_4$
			$3d^3H_6-x^5F_5$
860.889...	2	116159.0	$3d^5D_2-z^5S_2$
860.565...	2 bl	116202.7	$3d'^3F_3-s^3F_2$
860.315...	5	116236.5	$3d^5D_2-z^5F_2$
859.838...	6	116301.0	$3d^3P_2-w^3D_3$
859.721...	8	116316.8	$3d^5D_4-z^5F_5$
859.626...	6	116329.7	$3d^5D_2-z^5F_3$
			$3d^3F_2-x^3G_3$
859.086...	3	116402.8	$3d^3F_3-x^3G_4$
858.602...	6 unr.	116468.4	$3d^5D_4-z^5F_4$
858.565...	4 unr.	116473.4	$3d^5D_4-z^5D_3$
857.690...	5	116592.2	$3d^3F_4-x^3G_5$
857.392...	5	116632.8	$3d^5D_3-z^5F_3$
856.480...	1	116757.0	$3d^3D_3-u^3D_2$
856.325...	5	116778.1	$3d^3D_3-u^3D_3$
856.244...	1	116789.1	$3d'^3F_3-t^3G_3$
856.039...	2	116817.1	$3d'^3F_2-r^3F_2$
855.935...	2	116831.3	$3d^3D_1-u^3D_1$
855.879...	2	116838.1	$3d^3D_2-u^3D_1$
855.441...	3	116898.8	$3d^3D_2-u^3D_2$
855.336...	1	116913.1	$3d'^3F_3-t^3G_4$
854.532...	2	117023.1	$3d'^3F_4-t^3G_5$
854.367...	6 bl	117045.7	$3d^3H_4-x^3H_4$
854.205...	1	117067.9	$3d^3D_4-z^5F_3$
854.073...	5	117086.0	$3d^3D_3-z^5D_4$
853.456...	1	117170.7	$3d^3G_3-u^3F_3$
853.045...	1	117227.1	$3d^3H_5-x^3H_4$
852.644...	2	117282.2	$3d^3H_4-x^3H_5$
851.992...	6	117372.0	$3d^3G_4-u^3F_3$
851.842...	6	117392.7	$3d^3G_3-u^3F_2$
851.332...	7	117463.0	$3d^3H_5-x^3H_5$
851.150...	7	117488.1	$3d^3G_5-u^3F_4$
849.569...	4 unr.	117706.7	$3d^5D_2-z^5P_3$
849.524...	5 unr.	117713.0	$3d^3G_3-w^3H_4$
848.977...	3	117788.8	$3d^5D_1-z^5D_2$
848.729...	4	117823.2	$3d^3F_2-w^3G_3$
848.601...	4	117841.0	$3d^5D_0-z^5P_1$
848.07....	1	117915	$3d^3G_4-w^3H_4$
847.984...	5	117926.8	$3d^3F_3-w^3G_4$
847.924...	6	117935.1	$3d^5D_1-z^5P_1$
847.700...	6	117963.7 c	$3d^3H_5-x^3H_6$
		117966.3	$3d^3G_4-w^3H_5$

TABLE 1—*Continued*

λvacA	Int.	ν_{vac}cm^{-1}	Combination	λvacA	Int.	ν_{vac}cm^{-1}	Combination
847.578...	7	117983.2	$3d^5D_2-z^5P_2$	815.52....	1 bl	122621	$3d^5D_1-y^5P_1$
847.425...	8 b	118004.5	$3d^3FI_4-w^3G_5$ $3d^5D_3-z^5P_3$	815.363...	3	122644.8	$3d^3F_2-t^3F_2$
				814.565...	5	122764.9	$3d^5D_1-y^5P_2$
		118127.0 c	$3d^1G_4-w^1G_4$	814.242...	6	122813.6	$3d^5D\ -y^5P_1$
846.534...	6	118128.7	$3d^5D_2-z^5P_1$	814.148...	1	122827.8	$3d^5D_4-y^5D_3$
846.089...	2	118190.9	$3d^3D_1-w^3P_1$				
846.035...	3	118198.4	$3d^3D_2-w^3P_1$	813.862...	5	122871.0	$3d^3F_4-t^3F_4$ $3d^3F_3-t^3F_3$
845.925...	7	118213.8	$3d^3H_6-x^3H_6$	813.382...	10	122943.4	$3d^5D_4-y^5D_4$
845.686...	1	118247.2	$3d^5D_4-z^5F_3$	813.288...	4	122957.7	$3d^5D_2-y^5P_2$
845.408...	9	118286.1	$3d^5D_3-z^5P_2$	812.931...	5	123011.7	$3d^5D_2-y^5P_3$
844.954...	2	118349.6	$3d^3G_5-w^3H_5$ $3d^5D_4-z^3F_4$	811.284...	8 unr.	123261.4	$3d^5D_2-y^5P_2$
				811.246...	4 unr.	123267.2	$3d^3H_5-w^3H_6$
844.838...	4	118365.9	$3d^3F_4-y^1G_4$				
				810.940...	7	123313.7	$3d^5D_3-y^5P_3$
844.284...	10	118443.6	$3d^5D_4-z^5P_3$	809.675...	3	123506.3	$3d^3F_4-x^1G_4$
842.686...	5	118668.2	$3d^3D_3-w^3P_2$	808.840...	8	123633.8	$3d^3H_4-v^3G_5$
842.09....	5 bl	118752	$3d^3F_3-y^1F_3$	808.079...	5	123750.3	$3d^5D_4-y^5P_3$
842.020...	6	118762.0	$3d^3G_5-w^3H_6$	807.855...	8	123784.6	$3d^3H_5-v^3G_4$
841.688...	2	118808.9	$3d^3D_2-w^3P_2$				
				807.547...	9	123831.8	$3d^3H_6-v^3G_5$
841.088...	5	118893.6	$3d^3F_2-v^3F_2$	801.32....	1	124794	$3d^3H_6-x^1H_5$
840.741...	2	118942.7	$3d^3G_4-v^3G_5$ $3d^3G_3-v^3G_4$	797.16....	2	125445	$3d^5D_4-y^5F_4$
				797.055...	2	125461.9	$3d^3F_3-u^3G_4$
840.629...	3	118958.5	$3d^5D_3-z^5P_2$	795.550...	2	125699.2	$3d^3F_2-u^3D_1$
840.518...	4	118974.3	$3d^3G_3-v^3G_3$				
840.381...	5	118993.6	$3d^3F_3-v^3F_3$	794.19....	2	125914	$3d^3F_3-u^3D_2$
				794.01....	1	125943	$3d^3F_4-u^3G_5$
840.141...	4	119027.6	$3d^3H_4-y^3I_5$	792.559...	3	126173.5	$3d^3F_4-u^3D_3$
839.981...	3	119050.3	$3d^5D_1-z^5P_1$	788.469...	2	126828.1	.....
839.319...	5	119144.2	$3d^3H_4-w^3G_4$ $3d^3G_4-v^3G_4$	788.082...	4	126890.3	.....
839.195...	2	119161.8	$3d^3H_5-w^3G_5$	785.76....	1	127265	$3d^3D_2-s^3F_2$
839.092...	2	119176.4	$3d^3G_4-v^3G_3$	783.069...	3	127702.6	$3d^3D_2-t^3D_2$ $3d^3D_3-s^3F_4$
838.997...	4	119189.9	$3d^1F_3-w^1D_2$?	782.035...	3	127871.5	$3d^3D_3-t^3D_3$
838.936...	5	119198.6	$3d^3H_4-w^3G_3$	776.097...	2	128849.9	.....
838.869...	2	119208.1	$3d^3H_5-y^3I_5$	757.279...	2	132051.7	.....
838.498...	2	119260.9	$3d^5D_3-z^5P_2$				
838.048...	8	119324.9	$3d^3H_5-w^3G_4$ $3d^3G_5-v^3G_5$	757.167...	2	132071.3	.....
				754.478...	2	132542.0	$3d^3G_3-s^3F_2$
				751.648...	2	133041.0	$3d^3G_4-s^3F_3$
837.803...	3	119359.8	$3d^3G_3-t^3F_2$	751.427...	2	133080.1	.....
837.439...	7	119411.7	$3d^3H_6-w^3G_5$	746.247...	3	134003.9	$3d^3G_5-s^3F_4$
836.628...	3	119527.4	$3d^3G_5-v^3G_4$				
836.521...	7	119542.7	$3d^3F_4-v^3F_4$ $3d^3H_5-y^3I_6$	739.724...	4	135185.6	$3d^5D_1-x^5F_2$
				739.594...	2	135209.3	$3d^5D_0-x^5F_1$
835.917...	2	119629.1	$3d^3G_4-t^3F_3$	739.264...	5	135269.7	$3d^5D\ -x^5F_3$
				738.742...	1	135365.3	$3d^5D_3-r^3F_4$
835.627...	2	119670.6	$3d^5D_0-y^5F_1$	737.708...	5	135555.0	$3d^5D_3-x^5F_4$
834.944...	6	119764.7 c	$3d^5D_1-y^5F_1$				
		119768.5	$3d^1G_4-w^1F_3$	736.47....	0	135783	$3d^3D_2-r^3F_3$
		119773.4 c	$3d^3G_5-t^3F_4$	735.338...	1	135991.9	$3d^5D_4-x^5F_4$
.....	m	119795.1 c	$3d^3H_6-y^3I_6$	734.296...	4	136184.9	$3d^5D_4-x^5F_5$
834.067...	4	119894.4	$3d^5D_1-y^5F_2$	733.13....	1	136401	$3d^3F_2-t^3D_1$
833.532...	2	119971.4	$3d^3H_4-y^1F_3$	732.425...	2	136532.8	$3d^5D_0-x^5D_1$
.....	m 0 II	120087.3 c	$3d^5D_2-y^5F_3$	732.004...	3	136611.3	$3d^5D_1-x^5D_2$
832.328...	5	120144.9	$3d^3H_6-y^3I_7$	731.90....	1	136631	$3d^5D_1-x^5D_1$
831.464...	5	120269.8	$3d^5D_2-y^5F_3$	731.846...	2	136640.8	$3d^5D_1-x^5D_0$
830.500...	1	120409.4	$3d^3G_5-x^1G_4$	731.612...	2	136684.5	$3d^5D_2-x^5D_2$
829.375...	4	120572.7	$3d^5D_3-y^5F_3$	731.443...	1	136716.1	$3d^3F_3-t^3D_2$
827.777...	6	120805.5	$3d^5D_3-y^5F_4$	731.130...	1	136774.6	$3d^5D_3-x^5D_4$
824.800...	3	121241.5	$3d^5D_4-y^5F_4$	730.96....	2	136806	$3d^5D_2-x^5D_2$
823.257...	6	121468.8	$3d^5D_4-y^5F_5$	.....	m	136822.2 c	$3d^5D_2-x^5D_1$
822.314...	3	121608.0	$3d^5D_2-z^5D_3$	729.996...	5	136987.1	$3d^5D_3-x^5D_3$
821.723...	3	121695.5	$3d^5D_1-z^5D_2$	729.349...	3	137108.6	$3d^5D_3-x^5D_2$
820.915...	3	121815.3	$3d^5D_0-z^5D_1$	728.810...	6	137210.0	$3d^5D_4-x^5D_4$
820.409...	3 bl	121890.4	$3d^5D_2-z^5D_2$ $3d^5D_0-y^5D_1$	728.52....	1	137265	$3d^3F_4-t^3D_3$
				727.681...	3	137422.9	$3d^5D_4-x^5D_3$
820.271...	3	121910.9	$3d^5D_3-z^5D_3$ $3d^5D_1-z^5D_1$	722.419...	4	138423.8	$3d^1\ I_6-w^1H_5$
				707.444...	1	141353.9	$3d^3G_3-r^3F_2$
819.898...	3	121966.4	$3d^5D_1-y^5D_2$				
819.742...	1	121989.6	$3d^5D_1-y^5D_1$	705.892...	2 bl	141664.7	$3d^3G_5-r^3F_4$
				704.923...	1	141859.5	$3d^3G_3-r^3F_2$
819.066...	4	122090.3	$3d^5D_2-y^5D_3$	703.506...	1	142145.2	$3d^3G_4-t^3G_3$
818.981...	1	122103.0	$3d^5D_2-z^5D_1$	700.575...	1	142739.9	$3d^3G_5-t^3G_5$
818.598...	4	122160.1	$3d^5D_2-y^5D_2$	688.53....	0	145237	$3d^3H_4-v^3H_4$
818.383...	3	122192.2	$3d^5D_3-z^5D_2$				
817.348...	3	122346.9	$3d^5D_4-z^5D_3$	686.63....	1	145639	$3d^3H_5-v^3H_5$
				684.858...	1	146015.7	$3d^3H_4-r^3F_3$
817.166...	3	122374.2	$3d^3H_4-w^3H_4$	684.28....	1	146139	$3d^3H_6-v^3H_6$
817.038...	7	122393.3	$3d^5D_3-y^5D_3$	682.10....	2 bl	146606	$3d^3H_4-t^3G_3$
816.273...	6	122508.0	$3d^5D_2-y^5D_4$	680.700...	2	146907.6	$3d^3H_5-t^3G_4$
816.163...	6	122524.5	$3d_5D_1-y^5D_0$ $3d^5D_0-y^5P_1$	679.129...	3	147247.4	$3d^3H_6-t^3G_5$
815.612...	3	122607.3	$3d^3H_4-w^3H_5$				

TABLE 2

EVEN TERMS OF THE *Fe* III SPECTRUM

Configuration	Symbol	Level Value	Separation	Configuration	Symbol	Level Value	Separation
$3d^6$	$3d^5D_4$	− 0.8		$3d^6$	$^3P_1$	49576.1	
			− 436.2				+ 429
	$^5D_3$	+435.4			$^3P_0$	49147	
			− 302.7	$3d^6$	$3d'^1G_4$	57220.9	
	$^5D_2$	738.1					
			− 193.5	$3d^5(^4G)4s$	a^5G_6	63424.37	
	$^5D_1$	931.6					− 41.22
			− 94.9		$^5G_5$	63465.59	
	$^5D_0$	1026.5					− 20.39
$3d^6$	$3d^3P_2$	19404.0			$^5G_4$	63485.98	
			−1283.6				− 7.22
	$^3P_1$	20687.6			$^5G_3$	63493.20	
			− 520.1				− 0.56
	$^3P_0$	21207.7			$^5G_2$	63493.76	
$3d^6$	$3d^3H_6$	20050.3		$3d^5(^4P)4s$	a^5P_3	66463.84	
			− 249.7				− 58.31
	$^3H_5$	20300.0			$^5P_2$	66522.15	
			− 181.1				− 68.73
	$^3H_4$	20481.1			$^5P_1$	66590.88	
$3d^6$	$3d^3F_4$	21461.4		$3d^5(^4D)4s$	a^5D_4	69694.93	
			− 237.7				− 141.10
	$^3F_3$	21699.1			$^5D_3$	69836.03	
			− 157.3				− 0.93
	$^3F_2$	21856.4			$^5D_2$	69836.96	
							+ 49.57
$3d^6$	$3d^3G_5$	24558.0			$^5D_1$	69787.39	
			− 382.1				+ 40.79
	$^3G_4$	24940.1			$^5D_0$	69746.60	
			− 201.5	$3d^5(^4G)4s$	a^3G_5	70693.23	
	$^3G_3$	25141.6					− 34.72
$3d^5(^6S)4s$	$4s'^7S_3$	30088.04			$^3G_4$	70727.95	
							+ 3.74
$3d^6$	$3d'^1I_6$	30355.4			$^3G_3$	70724.21	
$3d^6$	$3d'^3D_3$	30857.0		$3d^5(^4P)4s$	a^3P_2	73726.84	
			+ 141.6				− 121.46
	$^3D_2$	30715.4			$^3P_1$	73848.30	
			− 9.6				− 86.86
	$^3D_1$	30725.0			$^3P_0$	73935.16	
$3d^6$	$3d'^1G_4$	30885.6		$3d^5(^4D)4s$	a^3D_3	76955.99	
							− 145.64
$3d^6$	$3d'^1S_0$	34811.6			$^3D_2$	77101.63	
							+ 27.13
$3d^6$	$3d'^1D_2$	35802.9			$^3D_1$	77074.50	
$3d^5(^6S)4s$	$4s'^5S_2$	40999.07		$3d^5(^2I)4s$	a^3I_7	79839.32	
							− 4.62
$3d^6$	$3d'^1F_3$	42896.1			$^3I_6$	79843.94	
							− 15.68
$3d^6$	$3d'^3F_4$	50275.3			$^3I_5$	79859.62	
			− 19.1	$3d^5(^2D)4s$	b^3D_3	82382.07	
	$^3F_3$	50294.4					− 28.07
			+ 110.3		$^3D_2$	82410.14	
	$^3F_2$	50184.1					− 83.94
					$^3D_1$	82494.08	
$3d^6$	$3d'^3P_2$	50411.5					
			+ 835.4				

TABLE 2—*Continued*

Configuration	Symbol	Level Value	Separation	Configuration	Symbol	Level Value	Separation
$3d^5(^4F)4s$....	a^5F_5	83137.43		$3d^5(^2D')4s$...	b^1D_2	109570.04	
			− 23.25				
	$^5F_4$	83160.68		$3d^5(^2G')4s$...	c^3G_5	114324.55	
			− 76.38				− 14.60
	$^5F_3$	83237.06			$^3G_4$	114339.15	
			− 121.02				− 11.97
	$^5F_2$	83358.08			$^3G_3$	114351.12	
			− 288.10				
	$^5F_1$	83646.18		$3d^5(^2G')4s$...	b^1G_4	117949.52	
$3d^5(^2I)4s$....	a^1I_6	83428.81		$3d^5(^6S)4d$....	$4d^7D_5$	147353.9	
							+ 27.9
$3d^5(^2F)4s$....	a^3F_4	84158.75			$^7D_4$	147326.0	
			− 512.32				+ 21.0
	$^3F_3$	84671.07			$^7D_3$	147305.0	
			+ 301.95				+ 14.8
	$^3F_2$	84369.12			$^7D_2$	147290.2	
							+ 9.2
$3d^5(^2D)4s$....	a^1D_2	86846.31			$^7D_1$	147281.0	
$3d^5(^2F)4s$....	a^1F_3	87901.07		$3d^5(^6S)5s$....	$5s^7S_3$	149283.6	
$3d^5(^2H)4s$....	a^3H_6	88922.27		$3d^5(^6S)4d$....	$4d^5D_4$	151536.9	
			+ 228.40				+ 3.6
	$^3H_5$	88693.87			$^5D_3$	151533.3	
			+ 30.80				− 0.5
	$^3H_4$	88663.07			$^5D_2$	151533.8	
							− 2.3
$3d^5(^2G)4s$....	b^3G_5	89907.05			$^5D_1$	151536.1	
			+ 124.26				
	$^3G_4$	89782.79			$^5D_0$	.....	
			+ 86.07				
	$^3G_3$	89696.72		$3d^5(^6S)5s$....	$5s^5S_2$	151755.9	
$3d^5(^4F)4s$....	b^3F_4	90471.73		$3d^5(^6S)5d$....	$5d^7D_5$	190424.9	
			− 11.41				+ 12.2
	$^3F_3$	90483.14			$^7D_4$	190412.7	
			+ 60.26				+ 8.7
	$^3F_2$	90422.88			$^7D_3$	190404.0	
							+ 6.8
$3d^5(^2H)4s$....	a^1H_5	92523.11			$^7D_2$	190397.2	
							+ 5.5
$3d^5(^2F')4s$...	c^3F_4	93387.95			$^7D_1$	190391.7	
			− 3.70				
	$^3F_3$	93391.65		$3d^5(^6S)6s$....	$6s^7S_3$	190916.9	
			− 20.48				
	$^3F_2$	93412.13		$3d^5(^6S)5d$....	$5d^5D_4$	193610.0	
							+ 0.5
$3d^5(^2G)4s$....	a^1G_4	93511.84			$^5D_3$	193609.5	
							+ 4.2
$3d^5(^2F')4s$...	b^1F_3	97040.58			$^5D_2$	193605.3	
							+ 6.3
$3d^5(^2S)4s$....	a^3S_1	.....			$^5D_1$	193599.0	
							+ 4.5
	a^1S_0	.....			$^5D_0$	193594.5	
$3d^5(^2D')4s$...	c^3D_3	105928.36		$3d^5(^6S)5g$....	$5g^7G$	207640	
			+ 22.93		$5g^5G$	207642±	
	$^3D_2$	105905.43					
			+ 10.88				
	$^3D_1$	105894.55					

TABLE 3

ODD TERMS OF THE *Fe* III SPECTRUM

Configuration	Symbol	Level Value	Separation	Configuration	Symbol	Level Value	Separation
$3d^5(^6S)4p$....	$4p\,^7P_4$	82845.79		$3d^5(^4G)4p$...	$z\,^3H_6$	118354.21	
			+ 512.67				− 202.24
	$^7P_3$	82333.12			$z\,^3H_5$	118556.45	
			+ 332.19				− 129.00
	$^7P_2$	82000.93			$z\,^3H_4$	118685.45	
$3d^5(^6S)4p$....	$4p\,^5P_3$	89083.99		$3d^5(^4P)4p$....	$z\,^5P_3$	118442.12	
			− 249.80				− 278.68
	$^5P_2$	89333.79			$^5P_2$	118720.80	
			− 156.85				− 146.27
	$^5P_1$	89490.64			$^5P_1$	118867.07	
$3d^5(^4G)4p$...	$z\,^5G_6$	113738.82		$3d^5(^4P)4p$....	$z\,^3P_2$	119696.84	
			+ 62.61				− 284.62
	$^5G_5$	113676.21			$^3P_1$	119981.46	
			+ 41.67				− 197.69
	$^5G_4$	113634.54			$^3P_0$	120179.15	
			+ 29.97	$3d^5(^4D)4p$...	$y\,^5F_5$	121468.02	
	$^5G_3$	113604.57					+ 227.15
			+ 21.17		$^5F_4$	121240.87	
	$^5G_2$	113583.40					+ 232.89
$3d^5(^4G)4p$...	$z\,^5H_7$	115641.43			$^5F_3$	121007.98	
			+ 167.98				+ 182.61
	$^5H_6$	115473.45			$^5F_2$	120825.37	
			+ 184.34				+ 129.07
	$^5H_5$	115289.11			$^5F_1$	120696.30	
			+ 178.99	$3d^5(^4G)4p$...	$z\,^3G_5$	121948.82	
	$^5H_4$	115110.12					+ 8.33
			+ 162,37		$^3G_4$	121940.49	
	$^5H_3$	114947.75					+ 21.55
$3d^5(^4G)4p$...	$z\,^5F_5$	116315.83			$^3G_3$	121918.94	
			− 150.78	$3d^5(^4P)4p$....	$z\,^3D_3$	122345.81	
	$^5F_4$	116466.61					− 281.73
			− 601.15		$^3D_2$	122627.54	
	$^5F_3$	117067.76					− 214.69
			+ 93.51		$^3D_1$	122842.23	
	$^5F_2$	116974.25		$3d^5(^4D)4p$...	$y\,^5D_4$	122943.35	
			+ 37.48				+ 114.60
	$^5F_1$	116936.77			$^5D_3$	122828.75	
$3d^5(^4P)4p$....	$z\,^5S_2$	116897.42					− 69.29
					$^5D_2$	122898.04	
$3d^5(^4P)4p$....	$z\,^5D_4$	117521.11					− 22.53
			+1046.47		$^5D_1$	122920.57	
	$^5D_3$	116474.64					− 534.55
			+ 56.05		$^5D_0$	123455.12	
	$^5D_2$	116418.59		$3d^5(^4D)4p$...	$y\,^5P_3$	123749.59	
			+ 39.32				+ 53.21
	$^5D_1$	116379.27			$^5P_2$	123696.38	
			+ 15.31				+ 144.23
	$^5D_0$	116363.96			$^5P_1$	123552.15	
$3d^5(^4G)4p$...	$z\,^3F_4$	118349.44		$3d^5(^4D)4p$...	$y\,^3D_3$	124853.24	
			+ 103.72				− 49.88
	$^3F_3$	118245.72			$^3D_2$	124903.12	
			+ 82.96				− 50.96
	$^3F_2$	118162.76					

TABLE 3—*Continued*

Configuration	Symbol	Level Value	Separation	Configuration	Symbol	Level Value	Separation
$3d^5(^4D)4p\ldots$	$^3D_1$	124954.08		$3d^5(^2D)4p\ldots$	x^3D_3	134975.42	
							− 302.8
$3d^5(^4D)4p\ldots$	y^3F_4	125442.78			$^3D_2$	135278.2	
			− 194.40				+ 61.9
	$^3F_3$	125637.18			$^3D_1$	135216.3	
			− 34.85				
	$^3F_2$	125672.03		$3d^5(^2I)4p\ldots$	z^1I_6	135581.28	
$3d^5(^4P)4p\ldots$	z^3S_1	126389.77		$3d^5(^2F)4p\ldots$	w^3D_3	135704.9	
							−1088.1
$3d^5(^4D)4p\ldots$	y^3P_2	128916.71			$^3D_2$	136793.0	
			+ 311.86				+ 328.9
	$^3P_1$	128604.85			$^3D_1$	136464.1	
			+ 234.12				
	$^3P_0$	128370.73		$3d^5(^2F)4p\ldots$	y^3G_5	135734.51	
							+ 180.9
$3d^5(^2I)4p\ldots$	z^3I_7	130039.76			$^3G_4$	135553.61	
			+ 185.76				+1005.41
	$^3I_6$	129854.00			$^3G_3$	134548.20	
			− 401.47				
	$^3I_5$	130255.47		$3d^5(^4F)4p\ldots$	y^5G_6	135738.67	
							+ 423.05
$3d^5(^2I)4p\ldots$	z^3K_8	130851.45			$^5G_5$	135315.62	
			− 182.82				+ 76.68
	$^3K_7$	131034.27			$^5G_4$	135238.94	
			+ 278.23				+ 142.90
	$^3K_6$	130756.04			$^5G_3$	135096.04	
							+ 159.00
$3d^5(^2D)4p\ldots$	z^1D_2	131444.23			$^5G_2$	134937.04	
$3d^5(^2I)4p\ldots$	z^1H_5	131709.99		$3d^5(^4F)4p\ldots$	x^5F_5	136184.37	
							+ 194.55
$3d^5(^2I)4p\ldots$	z^1K_7	131990.78			$^5F_4$	135989.82	
							− 18.12
$3d^5(^2I)4p\ldots$	y^3H_6	132261.86			$^5F_3$	136007.94	
			− 302.05				− 109.20
	$^3H_5$	132563.91			$^5F_2$	136117.14	
			− 94.46				− 117.90
	$^3H_4$	132658.37			$^5F_1$	136235.04	
$3d^5(^2D)4p\ldots$	x^3F_4	132784.56		$3d^5(^2D)4p\ldots$	z^1F_3	136199.33	
			+ 705.45	$3d^5(^2F)4p\ldots$	w^3F_4	136611.98	
	$^3F_3$	132079.11					− 184.27
			− 25.03		$^3F_3$	136796.25	
	$^3F_2$	132104.14					+ 264.6
$3d^5(^2D)4p\ldots$	x^3P_2	134264.62			$^3F_2$	136531.65	
			− 284.0	$3d^5(^4F)4p\ldots$	x^5D_4	137208.93	
	$^3P_1$	134548.6					− 213.27
			− 538.7		$^5D_3$	137422.20	
	$^3P_0$	135087.3					− 121.60
$3d^5(^2F)4p\ldots$	z^1G_4	134359.60			$^5D_2$	137543.80	
							− 16.5
					$^5D_1$	137560.3	
							− 12.1

TABLE 3—*Continued*

Configuration	Symbol	Level Value	Separation	Configuration	Symbol	Level Value	Separation
$3d^5(^4F)4p\ldots$	$^5D_0$	137572.4		$3d^5(^2G)4p\ldots$	v^3G_5	143882.94	
							− 202.23
$3d^5(^2H)4p\ldots$	x^5G_5	138053.79			$^3G_4$	144085.17	
			− 48.53				− 30.67
	$^3G_4$	138102.32			$^3G_3$	144115.84	
			− 84.81				
	$^3G_3$	138187.13		$3d^5(^2F')4p\ldots$	t^3F_4	144331.41	
							− 238.32
$3d^5(^2G)4p\ldots$	x^3H_6	138263.67			$^3F_3$	144569.73	
			+ 500.77				+ 68.79
	$^3H_5$	137762.90			$^3F_2$	144500.94	
			+ 235.78				
	$^3H_4$	137527.12		$3d^5(^2G)4p\ldots$	y^1H_5	144586.03	
$3d^5(^2D)4p\ldots$	z^1P_1	138691.01		$3d^5(^2H)4p\ldots$	x^1H_5	144842.44	
$3d^5(^4F)4p\ldots$	w^5G_5	139462.56		$3d^5(^2H)4p\ldots$	x^1G_4	144967.70	
			− 161.81				
	$^3G_4$	139624.37		$3d^5(^2G)4p\ldots$	x^1F_3	145037.81	
			− 55.30				
	$^3G_3$	139679.67		$3d^5(^2F')4p\ldots$	x^1D_2	145617.59	
$3d^5(^2F)4p\ldots$	y^1D_2	139763.68		$3d^5(^2F')4p\ldots$	u^3G_5	147405.34	
							+ 244.78
$3d^5(^2G)4p\ldots$	y^1G_4	139826.37			$^3G_4$	147160.56	
							+ 270.4
$3d^5(^2H)4p\ldots$	y^3I_7	140195.53			$^3G_3$	146890.2	
			+ 350.15				
	$^3I_6$	139845.38		$3d^5(^2F')4p\ldots$	u^3D_3	147635.15	
			+ 336.74				+ 21.30
	$^3I_5$	139508.64			$^3D_2$	147613.85	
							+ 58.20
$3d^5(^2F)4p\ldots$	y^1F_3	140452.30			$^3D_1$	147555.65	
$3d^5(^2G)4p\ldots$	v^3F_4	141002.19		$3d^5(^2F')4p\ldots$	w^1G_4	149012.56	
			+ 309.63				
	$^3F_3$	140692.56		$3d^5(^2S)4p\ldots$	w^3P_2	149524.83	
			− 57.62				+ 610.3
	$^3F_2$	140750.18			$^3P_1$	148914.5	
							+ 260.5
$3d^5(^4F)4p\ldots$	v^3D_3	141465.73			$^3P_0$	148654	
			+ 67.49				
	$^3D_2$	141398.24		$3d^5(^2F')4p\ldots$	w^1F_3	150654.1	
			− 70.41				
	$^3D_1$	141468.65		$3d^5(^2S)4p\ldots$	y^1P_1	151636.5 ?	
$3d^5(^2H)4p\ldots$	y^1I_6	141538.75		$3d^5(^2D')4p\ldots$	s^3F_4	158561.9	
							+ 580.7
$3d^5(^4F)4p\ldots$	u^3F_4	142046.2			$^3F_3$	157981.2	
			− 265.9				+ 297.7
	$^3F_3$	142312.10			$^3F_2$	157683.5	
			− 222.17				
	$^3F_2$	142534.27		$3d^5(^2D')4p\ldots$	t^3D_3	158728.5	
							+ 312.5
$3d^5(^2H)4p\ldots$	w^3H_6	143320.05			$^3D_2$	158416.0	
			+ 412.37				+ 159.5
	$^3H_5$	142907.68			$^3D_1$	158256.5	
			+ 52.89				
	$^3H_4$	142854.79		$3d^5(^2D')4p\ldots$	v^1F_3	159492.2	

TABLE 3—*Continued*

Configuration	Symbol	Level Value	Separation	Configuration	Symbol	Level Value	Separation
$3d^5(^2D')4p\ldots$	v^3P_2	160037.1			$^3G_3$	167084.2	
	$^3P_1$	.....		$3d^5(^6S)5p\ldots.$	$5p^5P_3$	168328.7	
	$^3P_0$	.....					− 91.2
					$^5P_2$	168419.9	
$3d^5(^2D')4p\ldots$	w^1D_2	162084.0 ?					− 56.9
					$^5P_1$	168476.8	
$3d^5(^2G')4p\ldots$	v^3H_6	166186 ?		$3d^5(^2G')4p\ldots$	w^1H_5	168779.3	
			+ 247				
	$^3H_5$	165938.8		$3d^5(^2G')4p\ldots$	v^1G_4	169276.8 ?	
			+ 220.5				
	$^3H_4$	165718.3		$3d^5(^2G')4p\ldots$	u^1F_3	170309.8 ?	
$3d^5(^2G')4p\ldots$	r^3F_4	166221.4		$3d^5(^6S)4f\ldots.$	$4f^7F_6$	184446.9	
			− 276				+ 30.8
	$^3F_3$	166497			$^7F_5$	184416.1	
			− 504				+ 42.2
	$^3F_2$	167001			$^7F_4$	184373.9	
							+ 58.1
$3d^5(^6S)5p\ldots.$	$5p^7P_4$	166420.8			$^7F_3$	184315.8	
			+ 168.3				+ 69.3
	$^7P_3$	166252.5			$^7F_2$	184246.5	
			+ 108.3				
	$^7P_2$	166144.2			$^7F_1$	.....	
$3d^5(^2G')4p\ldots$	t^3G_5	167298.1			$^7F_0$	.....	
			+ 91.6				
	$^3G_4$	167206.5		$3d^5(^6S)4f\ldots.$	$4f^5F_{5-1}$	184780±	
			+ 122.3				

TABLE 4

[*Fe* III] LINES IN STELLAR OR NEBULAR SPECTRA

	Transition	λ Predicted	RY Scuti*		RY Scuti†		MWC 349‡		MWC 17§		R Aqr§		Orion Neb.‖	
			λ_{Obs}	Int.	λ_{Obs}	Int.	λ_{Obs}	Int.	λ_{Obs}	Int.	λ_{Obs}	Int.	λ_{Obs}	Int.
$^5D-^3F\ldots.$	4–4	4658.05	58.1	4	58.2	5	58.	1	57.36	2	58.	2	58.3	1.5
	4–3	4607.03	.....	.....	06.4	0	.....	.....	.....	.....	.....	.....	07.2	0.5
	3–4	4754.69	55.0	1	56.3	1	.....	.....	55.4	1	55.	0	54.1	0.9
	3–3	4701.54	01.5	2	01.5	3	01.	0	01.8	1–2	02.	1	01.9	0.8
	3–2	4667.01	.....	.....	70.	0	.....	.....	.....	.....	.....	.....	63.9	0.6
	2–3	4769.43	70.	1	69.3	1	.....	.....	69.0	0	.....	.....	67.8	0.8
	2–2	4733.91	33.6	1+	33.8	1	.....	.....	32.1	1 bl	.....	.....	37.3	0.8
	1–2	4777.69	.....	.....	77.6	0	.....	.....	.....	.....	.....	.....	77.	0.7?
$^5D-^3P\ldots.$	3–2	5270.41	.....	.....	70.2	5	70.	3	70.3	2	.....	.....	71.4	1.0 bl
	2–1	5011.26	.....	.....	10.5	1	10.	2	10.1	1	.....	.....	.....	bl
	1–1	5060.35	.....	.....	58.	0	.....	.....	.....	.....	.....	.....	56.9	0.8 bl

* Merrill, *Ap. J.*, **67,** 179, 1928.

† Swings and Struve, *Ap. J.*, **91,** 581, 1940.

‡ Merrill, Humason, and Burwell, *Ap. J.*, **76,** 156, 1932 (star MW 203); Swings and Struve, *Ap. J.*, **95,** 159, 1942.

§ Swings and Struve, *Ap. J.*, **93,** 349, 1941.

‖ Wyse, *Ap. J.*, **95,** 356, 1942.

ON THE CLUSTERING OF NEBULAE. I

F. ZWICKY

ABSTRACT

Three methods to analyze the nature of the statistical distribution of nebulae are discussed. Method A, which makes use of the subdivision of space into cells of arbitrary size, is carried out by Katz and Mulders for the nebulae of the *Shapley-Ames Catalogue* in a paper following this. Method B is concerned with the frequency in dependence of their population of suitably defined swarms or clusters of nebulae. This method is applied in the sections III(*a*) and III(*b*), where it is shown that bright nebulae and nebulae of the globular and elliptic types in the Virgo cluster show a greater tendency toward clustering than fainter nebulae and nebulae of the spiral types, respectively. Method C involves an analysis of the morphology of individual swarms and clusters of nebulae. It is particularly interesting to investigate the physical structure of spherically symmetrical clusters such as the clusters in Coma, Hydra, Perseus, etc. It is shown that the radial distribution-curve of the Coma cluster as determined with the 18-inch Schmidt telescope can, within the expected statistical fluctuations, be represented by Emden's distribution-curve for a bounded gravitational isothermal gas sphere. An application of the previously (see n. 6) derived relation between the central density of the cluster, its velocity dispersion, and its radius leads to the conclusion that the average mass $\overline{\mathfrak{M}}$ of the nebulae involved in our counts is of the order of $\overline{\mathfrak{M}} = 2 \times 10^{11}\, \mathfrak{M}_{\odot}$.

I. ANALYSIS OF THE CLUSTERING OF NEBULAE

Newton's law of the gravitational interactions of celestial bodies was originally derived from observations of the motions of the moon and of the planets. Subsequently it was applied to the relative motions of the components in double stars, which it successfully describes. Cosmological theories generally assume that Newton's law as a good first approximation may be used to describe the gravitational interactions between celestial bodies whose mutual separations are far greater than the distances between the components of a double star. Qualitatively, it would seem obvious that the agglomeration of stars in nebulae and the formation of clusters of nebulae are due to forces identical with the gravitational forces operating between the various components of the solar system. However, little or nothing has been done to prove the strict validity of this assertion when the distances between the interacting objects become so great that they can be measured only in thousands or even millions of light-years.

In view of the considerable discrepancy between the claims of practically all cosmologies concerning the universality of Newton's law of interaction and the meagerness of the direct data available, it seems desirable to analyze as many as possible of the observations available, in order to lessen or even to close the gap now existing between hypothesis and actual knowledge.

The ordinary methods of proving the validity of Newton's law are based either on the direct measurements of forces or on the observations of orbits, velocities, and accelerations of the bodies involved. Also, such effects as the gravitational red shift and the deflection of light-rays might in principle be used. None of these methods would seem to be applicable to the problem of deriving the law of force between celestial objects, such as the nebulae, which are separated by vast distances. We therefore must inquire whether any additional and practically effective methods are available in this case. There are obviously two types of observations which we can make on nebulae and which might be useful for the problem in question. In the first place, we may observe the instantaneous spatial distribution of nebulae. In the second place, with the help of the Doppler effect, we may determine the distribution of the nebulae in radial velocities. It was shown previously[1] that from this velocity distribution the law of force may be

[1] F. Zwicky, *Ap. J.*, **86**, 217, 1937, and *Helvetica physica acta*, **6**, 110, 1933.

derived with the help of the virial theorem, provided that the masses of the individual interacting objects are known. Unfortunately, at the present time there still exists a serious uncertainty regarding the masses of nebulae, and the virial theorem cannot be effectively applied because both the masses and the law of interaction enter as unknowns. In this investigation we shall therefore discuss the possibility of making use of observations of the spatial distribution of nebulae. Three modes of attack suggest themselves, which we proceed to describe.

Method A.—The spatial distribution of the nebulae is analyzed by the subdivision of space into cells of arbitrary size. It is often convenient to make the cells all of the same volume V and to investigate the distribution function of the nebulae in dependence of V. If a total number of N nebulae is known to occupy n cells, the distribution function gives the average number $z(\nu)$ of cells in which ν nebulae are found. It is

$$\sum_{\nu=1}^{N} z(\nu) = n \tag{1}$$

and

$$\sum_{\nu=1}^{N} \nu z(\nu) = N . \tag{2}$$

For a random distribution of noninteracting nebulae the function $z(\nu)$ is easily calculated. If the observed distribution function $z_0(\nu)$ is definitely different from $z(\nu)$, we may conclude that the interactions between the nebulae cannot be neglected.[2]

In the following paper by Katz and Mulders in this issue the method here described is applied to the distribution of the nebulae brighter than about $m_p = 13$, and it is shown that the observed function $z_0(\nu)$ substantially differs from the theoretical $z(\nu)$. To demonstrate, however, that the interactions between the nebulae can be described by Newton's law is more difficult and cannot at the present time be accomplished on the basis of method A. This method may, nevertheless, prove useful to obtain data on the average size V_c of clusters of nebulae. If the volumes V of the cells of our artificial subdivision of space are so chosen that either $V \ll V_c$ or $V \gg V_c$, the observed function $z_0(\nu)$ will practically always approach the theoretical function $z(\nu)$, regardless of what the distribution of the nebulae looks like. For the choice $V \cong V_c$, the difference between $z(\nu)$ and $z_0(\nu)$ will be the most conspicuous. On the other hand, if for a choice $V = V_c$ the functions $z(\nu)$ and $z_0(\nu)$ show a maximum difference, we may conclude that V_c is closely related to the average volume of the clusters involved in the counts.

Method B.—This method is concerned with the distribution function $\zeta(\nu)$ of swarms and clusters which contain ν nebulae. Taking the ith nebula in an assembly of N nebulae, we may ask how many nebulae $\nu - 1$ are located within a given distance d of the ith nebula, thus constituting a swarm of ν nebulae. This method will be discussed in another place in more detail. A partial application will be given in section III, where we shall investigate the segregation of nebulae of different brightness in the Virgo cluster.

Method C.—This method considers the structure of individual swarms of nebulae. If a swarm has reached a statistically stationary state, it will possess approximate spherical symmetry, and the radial distribution of nebulae will be determined by the law of interaction between them. If this law is Newton's law of gravitation, the radial distribution-curve will be identical with Emden's curve for a bounded isothermal gravitational "gas sphere." From counts of nebulae with the 18-inch Schmidt telescope one may deduce

[2] Another alternative would be that deviations from $z(\nu)$ are due to real deviations from the stationary state such as might, for instance, occur in an expanding universe. Which alternative is the correct one must be decided through a co-ordination of all the statistical analyses.

that the clusters in Coma,[1] Hydra,[3] Pegasus,[3] Cancer, Perseus, Fornax, etc., possess spherical symmetry and that their radial distribution-curves can all be reduced to Emden's standard curve for the isothermal gas sphere—a fact which proves the universality of Newton's law, extending its validity to the interaction of objects whose mutual distances must be measured in millions of light-years. As an illustration of this method we shall discuss in section II, a few features of the Coma cluster of nebulae.

II. SOME PHYSICAL CHARACTERISTICS OF THE COMA CLUSTER OF NEBULAE

Some time ago the nebulae brighter than the apparent photographic magnitude $m_p = 16.6$ were counted in the Coma cluster, and the results were communicated in this journal.[1] If from the data there given we subtract the nebulae which belong to the general background (7.4 nebulae per sq. deg.), we obtain for the average number of nebulae N_r per square degree and brighter than $m_p = 16.6$ the list given in Table 1.

In the third column are listed the dimensionless radial increments of the standard Emden curve[4] as defined through the equation (3) given below. The fourth column gives the values of the density D (multiplied by 1000) of the projected standard infinite isothermal gas sphere.[5,6] The best agreement with the observations is reached if a bounded gas sphere is considered, the projected densities of which are approximately[6] given by $1000\,D - 37$. The apparent radius of this sphere is 170′ of arc, which, at the distance of 13.8 million parsecs of the Coma cluster, corresponds to $R = 2\times10^{24}$ cm $= 2\times10^{6}$ light-years. The Coma cluster as considered here, therefore, possesses a diameter of about 4,000,000 light-years. Counts of the fainter nebulae will no doubt lead to a further increase in this diameter. In Figure 1 the drawn-out curve represents the density $1000\,D - 37$ of the projected bounded Emden sphere multiplied by a factor 1000, while the crosses indicate the observational values. The remarkable agreement between the observations and the theoretical curve encourages us to draw from the results obtained some quantitative conclusions concerning the masses of the nebulae involved. If, according to Emden, we write[4,5]

$$r = a\,r_1, \qquad \rho(r) = \rho_0 \rho_1(r_1), \tag{3}$$

where ρ_0 is the average central density of the cluster and a is an appropriate length, the Emden differential equation for the isothermal gas sphere becomes dimensionless. As was shown previously,[4] the reduction factor a, which is a *structural index* or structural length of the cluster is given by

$$a = \frac{(\overline{w^2})^{1/2}}{(12\pi\Gamma\rho_0)^{1/2}}, \tag{4}$$

where $(\overline{w^2})^{1/2}$ is the dispersion of the peculiar velocities in the cluster and $\Gamma = 6.68\times10^{-8}$ a.u. is the universal gravitational constant. According to Table 1, the reduction factor a for the Coma cluster is a length corresponding to 2′ of arc at the distance of 13.8×10^{6} parsecs. Therefore

$$a = 2.48\times10^{22}\ \text{cm}. \tag{5}$$

The central surface density σ_0 for the projected Emden sphere is

$$\sigma_0 = 2\int_0^{+\infty} \rho(r)\,dr = 2\rho_0 a \int_0^{+\infty} \rho_1(r_1)\,dr_1. \tag{6}$$

[3] F. Zwicky, *Proc. Nat. Acad. Sci.*, **27**, 264 and 366, 1941.

[4] F. Zwicky, *Th. von Kármán Anniversary Volume*, May, 1941.

[5] R. Emden, *Gaskugeln*, Leipzig: Teubner, 1907. [6] E. Hubble, *Ap. J.*, **71**, 231, 1930.

TABLE 1

RADIAL DISTRIBUTION OF NEBULAE IN THE COMA CLUSTER

r	N_r	r_1	$1000D$	$1000D-37$	r	N_r	r_1	$1000D$	$1000D-37$
2.5′	2777	1.25	2729	2692	70	62	35	.....	.....
5	1431	2.5	1800	1763	75	24	37.5	.....	.....
10	643	5	832	795	80	15	40	70	33
15	485	7.5	480	443	85	17	42.5	.....	.....
20	285	10	318	281	90	13	45	.....	.....
25	193	12.5	245	208	95	13	41.5	.....	.....
30	193	15	195	158	100	23	50	56.5	19.5
35	81	17.5	162	125	110	6	55	.....	.....
40	120	20	140	103	120	12	60	.....	.....
45	77	22.5	125	88	130	8	65	.....	.....
50	95	25	111	74	140	1	70	41.5	4.5
55	75	27.5	100	63	150	6	75	.....	.....
60	66	30	92	55	160	2	80	38	1
65	47	32.5	.....	.....					

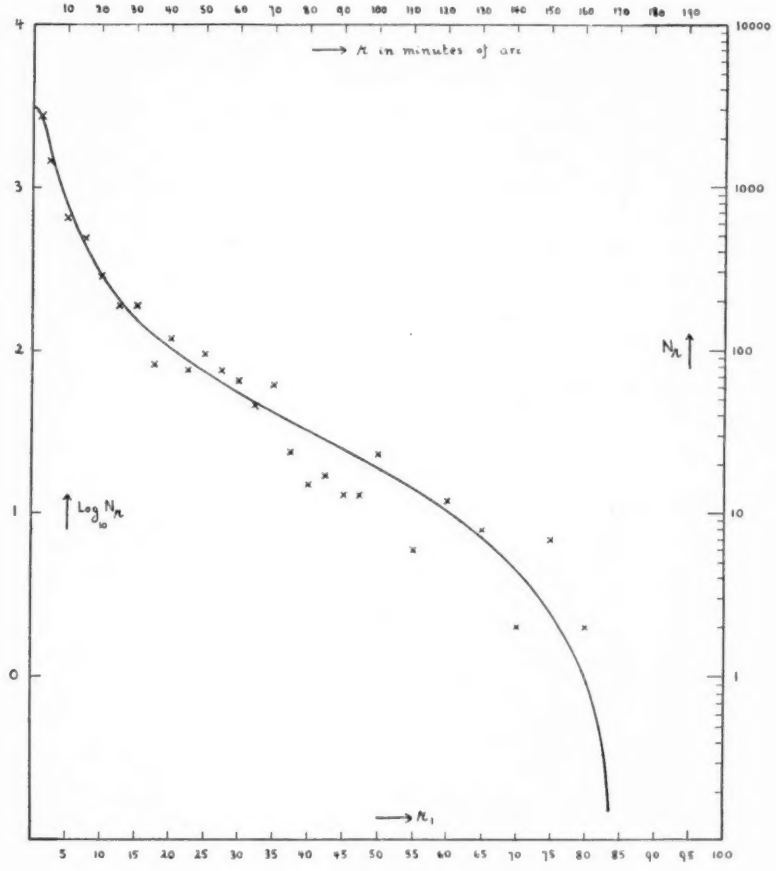

FIG. 1

The integral can be evaluated numerically with the help of Emden's Table 14 for ρ_1.[5] One obtains

$$\rho_0 = \frac{\sigma_0}{3.03a}. \tag{6a}$$

At the distance of the Coma cluster 1′ of arc corresponds to 1.24×10^{22} cm. From the observations plotted in Figure 1 we have $\sigma_0 \cong 3000$ nebulae per square degree or $\sigma_0 = 5/6$ nebulae per square minute of arc. Therefore,

$$\left.\begin{aligned} \rho_0 &= \frac{5\overline{\mathcal{M}}}{6}\times(1.24\times10^{22})^2\times 2.48\times10^{22}, \\ \overline{\mathcal{M}} &= 1.4\times10^{67}\rho_0, \end{aligned}\right\} \tag{7}$$

where $\overline{\mathcal{M}}$ is the average mass of a nebula included in our observational counts.

According to information kindly furnished me by Dr. Hubble and Mr. Humason, the dispersion in the radial velocities w_r in the Coma cluster is of the order of $(\overline{w_r^2})^{1/2} = 1200$ km/sec, and, correspondingly, the dispersion in the peculiar velocities is given by

$$(\overline{w^2})^{1/2} = (\overline{3w_r^2})^{1/2} \cong 2100 \text{ km/sec}. \tag{8}$$

Substituting the observational values of a and $(\overline{w^2})^{1/2}$ in equation (4), we obtain for the central density in the Coma cluster

$$\rho_0 = 2.8\times10^{-23} \text{ gm/cm}^3 \tag{9}$$

and consequently

$$\overline{\mathcal{M}} = 3.92\times10^{44} \text{ gm} \cong 2\times10^{11}\,\mathcal{M}_\odot, \tag{10}$$

where $\mathcal{M}_\odot = 2\times10^{33}$ gm is the mass of the sun. These values for ρ_0 and the average mass $\mathcal{M}$ of the nebulae brighter than about the absolute magnitude -14.5 in the Coma cluster agree in order of magnitude with the values previously derived from the virial

TABLE 2

$(\overline{w^2})^{1/2}$ (Km/Sec)	ρ_0 (Gm/Cm^3)	$\overline{\mathcal{M}}/\mathcal{M}_\odot$	$(\overline{w^2})^{1/2}$ (Km/Sec)	ρ_0 (Gm/Cm^3)	$\overline{\mathcal{M}}/\mathcal{M}_\odot$
250	4.0×10^{-25}	2.8×10^{9}	1250	1.0×10^{-23}	7.0×10^{10}
500	1.6×10^{-24}	1.1×10^{10}	1500	1.4×10^{-23}	1.0×10^{11}
750	3.6×10^{-24}	2.5×10^{10}	2000	2.6×10^{-23}	1.8×10^{11}
1000	6.4×10^{-24}	4.5×10^{10}	2500	4.0×10^{-23}	2.8×10^{11}

theorem.[1] The values (9) and (10) are exorbitantly large as compared with all other types of estimates previously made. The method here applied, however, would seem to be as trustworthy as any other method offered thus far for the practical determination of the masses of nebulae, particularly so because the Coma cluster is not by any means an isolated case. Other clusters, such as those in Hydra, Perseus, Pegasus, and Fornax, can be reduced to the same standard distribution-curve as the Coma cluster. The discrepancies met within the different determinations of the masses of nebulae, therefore, present a real problem.

Since observations of the velocity dispersion are naturally difficult because of the possible selection of foreground and background nebulae which do not belong to the Coma cluster, we list in Table 2 the calculated values for ρ_0 and $\mathcal{M}$ for a range in veloci-

ties outside of which the real velocity dispersion can hardly fall. The lowest possible value for $(\overline{w^2})^{1/2}$ is 250 km/sec, since this is the velocity dispersion for the field nebulae.

The fact that the observed radial distribution in spherically symmetrical clusters of nebulae agrees so well with the Emden distribution, in spite of the presence of nebulae of different mass, raises some interesting problems. Two explanations which immediately suggest themselves are, first, that, because of segregation effects the total mass of the cluster is largely accounted for by the brighter nebulae and, second, that, as we go to smaller individual masses, the velocity dispersion $(\overline{w^2})^{1/2}$ rather than the average kinetic energy tends to be a constant (Smoluchowski distribution in velocities).

III. SEGREGATION OF NEBULAE IN THE VIRGO CLUSTER

If the globular clusters of nebulae are statistically stationary objects, according to Boltzmann's principle a partial segregation of nebulae of different mass should be expected. Qualitatively, the lighter nebulae in dependence of the distance from the center of the cluster should follow a flatter distribution-curve than the heavier nebulae. Unfortunately, with the 18-inch Schmidt telescope we can reach only the brighter nebulae in the globular clusters in Coma, Hydra, Perseus, etc., and a speedy test for the segregation of nebulae of different mass will be possible only when the 48-inch Schmidt telescope is available. However, we may get some preliminary data through an investigation of the Virgo cluster which, although spatially not of spherical symmetry, is characterized by a constant velocity dispersion throughout.[7] In the following we shall confine ourselves to a discussion of the distribution of nebulae given in the *Shapley-Ames Catalogue*. The brightness of all nebulae brighter than the photographic magnitude $m_p = 15$ is now being measured from films taken with the 18-inch Schmidt telescope. These data when complete will be used to extend the analysis presented here.

TABLE 3

NUMBERS OF BRIGHT AND FAINT NEBULAE IN STRIPS OF 1° WIDTH PARALLEL TO THE AXIS OF THE VIRGO CLUSTER

	d (In Degrees)	1	2	3	4	5	6	7	8	9	10	11
$m_p \leq 12.3$	east	18	10	6	10	5	4	1	1	0	0	0
	west	18	7	7	6	2	0	1	1	0	0	0
$m_p > 12.3$	east	16	7	9	9	4	3	0	1	0	0	0
	west	11	12	11	8	4	6	0	1	2	1	1

a) Distribution of Shapley-Ames nebulae normal to the axis of symmetry in the Virgo cluster.—A straight line connecting the points $\alpha\ 13^h0^m$, $\delta\ -18°$, and $\alpha\ 12^h10^m$, $\delta + 26°$, epoch 1950, is a symmetry axis for the projected spatial distribution of the Shapley-Ames nebulae in the Virgo cluster. We divide these nebulae into two approximately equal groups comprising the objects of photographic magnitude $m_p \leq 12.3$ and $m_p > 12.3$, respectively. Although it is not at present possible to correlate the absolute brightness of a stellar system with its mass, we may, nevertheless, expect that on the average a nebula of a given type is the more massive, the brighter it is. In fact, if, as we shall find to be the case, a segregation of nebulae takes place in the sense of an increasing tendency toward clustering for increasing brightness, not only shall we conclude that the realm of the nebulae is in a stationary state, but we shall also have produced indirect evidence that the mass and the luminosity of nebulae increase simultaneously.

[7] S. Smith, *Ap. J.*, **83**, 499, 1936.

In a first test for segregation effects we have counted the population of Shapley-Ames nebulae in strips of 1° width parallel to the axis of symmetry. The results obtained east and west of this axis are given in Table 3. Altogether, there are 97 nebulae in the brighter class and 106 nebulae in the fainter class. Reducing these numbers to 100 in each class and adding the numbers in symmetrical strips of equal d east and west of the axis, we obtain the dependence on d listed in Table 4.

In Figure 2, *a*, *b*, a graphical representation of these results is given. As we had expected, the distribution function of the nebulae in the range $13.3 \geq m_p > 12.3$ is considerably flatter than that for the nebulae $m_p \leq 12.3$. Unfortunately, in the case of an

TABLE 4

NEBULAR DISTRIBUTION IN THE VIRGO CLUSTER IN DEPENDENCE OF THE DISTANCE d FROM THE AXIS OF SYMMETRY

d (In Degrees)	1	2	3	4	5	6	7	8	9	10	11
$m_p \leq 12.3$	37.1	17.5	13.4	16.5	7.2	4.1	2.05	2.05	0	0	0
$m_p > 12.3$	25.5	17.9	18.9	16.1	7.55	8.5	0	1.89	1.89	0.94	0.94

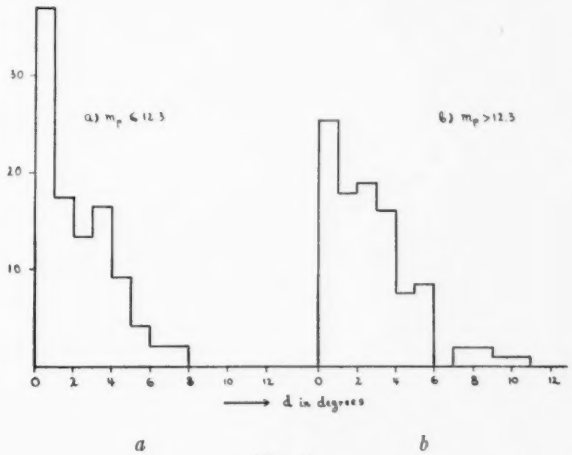

a *b*

FIG. 2

irregular cluster like the Virgo cluster there is no practical way of deriving the spatial distribution from the projected distribution actually observed, but it is to be anticipated that the spatial distribution will exhibit still more pronounced segregation effects than the projected distribution. Once sufficient observations on the segregation in the projected images of stationary globular clusters are available, it should be possible to carry out the reduction to the true spatial distributions and to determine the relative masses of various types of nebulae.

b) On the degree of compactness of the Virgo cluster with respect to nebulae of different brightness.—The degree of compactness of a spherically symmetrical cluster is measured through the determination of its radial distribution-curve. The degree of compactness or of the swarm formation in an irregular cluster may be measured through an analysis patterned schematically after the procedure applied to spherically symmetrical clusters. This procedure consists in counting successively the total number n_r of nebulae in rings

between the radii $r = (g - 1)r_1$ and $r = gr_1$, respectively, and deriving the average number N_r per unit area in these rings by writing $N_r = n_r/(2g - 1)\pi r_1^2$. Schematically speaking, equal areas of the size πr_1^2 containing essentially decreasing numbers of nebulae are bunched together in groups of one, three, five, etc., and averages are taken inside of these groups. In the case of an irregular cluster we therefore may proceed as follows.

If the cluster contains a total of N nebulae and occupies a projected area A, we choose an elementary area equal to or somewhat smaller than A/N. We then place a circle or a square of this area on the projected image of the cluster in a location such that it contains the highest possible number of nebulae, say n_1, and we associate the density $N_1 = n_1$ with

TABLE 5

$m_p \leq 12.3$

Fictitious r	Numbers of Nebulae per Elementary Area of 6 Square Degrees											N_r = Average Number per 6 Square Degrees
1	12											12
2	11	5	5									7
3	4	4	4	4	4							4
4	3	3	3	3	3	3	2					2.86
5	2	2	2	2	2	2	2	1	1			1.78
6	1	1	1	1	1	1	1	1	0	0	0	0.73
7	0	0										0

TABLE 6

$m_p > 12.3$

Fictitious r	Numbers of Nebulae per Elementary Area of 6 Square Degrees											N_r = Average Number per 6 Square Degrees
1	9											9
2	8	7	6									7
3	5	5	4	4	4							4.4
4	3	3	3	3	3	3	3					3
5	2	2	2	2	2	2	2	2	2			2
6	1	1	1	1	1	1	1	1	1	1	1	1
7	1	1	1	1	0	0						0.3

a fictitious radius $r = 1$. Then, avoiding overlapping with the first square, we place the next three squares on the three next densest spots so that they contain n_2', n_2'', n_2''' nebulae, respectively, and we associate the density $N_2 = (n_2' + n_2'' + n_2''')/3$ with the fictitious radius $r = 2$, and so on. Since the Virgo cluster covers about 800 square degrees and contains about 100 nebulae each in the two classes $m_p \leq 12.3$ and $13.3 \geq m_p > 12.3$, an elementary square of 6 square degrees was chosen, and the sequences listed in the Tables 5 and 6 were found.

The ratios γ between the numbers N_r for the fainter and the brighter nebulae are listed in Table 7. These data clearly demonstrate the considerably greater tendency toward clustering for the brighter nebulae. The results obtained here are of importance for the determination of the luminosity function of nebulae. Because of the segregation of nebulae of different brightness, selective effects will tend to falsify the luminosity func-

tion unless regions of space are thoroughly canvassed which are large compared with one cluster of nebulae.

The statistical considerations presented in the sections III (*a*) and III (*b*) were repeated for a subdivision of the Shapley-Ames nebulae into two classes: $m_p \leq 12$ and $m_p > 12$. As should be expected, the segregation effects become more pronounced than for the subdivision into the classes $m_p \leq 12.3$ and $m_p > 12.3$.

A preliminary test was also made to apply the analysis given in the preceding to the faint nebulae listed in the NGC and IC catalogues but not contained in the *Shapley-Ames Catalogue*. Qualitatively, it is at once obvious that these fainter nebulae are more dispersed than the Shapley-Ames nebulae considered in this paper. The catalogues mentioned, however, do not satisfy the necessary requirements of uniformity with respect to the selection of the faintest nebulae. It is therefore advisable not to carry out the

TABLE 7

RATIOS γ OF THE NUMBERS OF FAINTER NEBULAE TO BRIGHTER NEBULAE IN DEPENDENCE OF THE FICTITIOUS RADIUS r

r	1	2	3	4	5	6	7
γ.....	0.75	1.00	1.10	1.05	1.12	1.37	∞

TABLE 8

DISTRIBUTION OF SPIRALS AND OF ELLIPTICAL NEBULAE IN THE VIRGO CLUSTER IN DEPENDENCE OF THE DISTANCE d FROM THE AXIS OF SYMMETRY

d (In Degrees)		1	2	3	4	5	6	7	8	9	10	11
Spirals	east.....	20	13	10	12	9	4	1	1	0	0	0
	west.....	19	15	13	10	5	3	0	2	1	1	0
Elliptical nebulae	east.....	8	4	2	5	0	1	0	0	0	0	0
	west.....	11	0	3	3	1	0	1	0	0	0	0

analysis of the distribution of the fainter nebulae ($13 < m_p \leq 15.5$) until uniformity of selection has been secured through the photometric work now in progress at this Institute.

c) On the degree of compactness of the Virgo cluster with respect to nebulae of different structural types.—In the compact clusters of nebulae, according to Hubble,[8] nebulae of the globular and elliptical types predominate, whereas in the general field the spirals are relatively more numerous. It is therefore of interest to apply to the distributions of nebulae of the spiral and the elliptical types the tests described in sections III(*a*) and III(*b*).

Among the 205 nebulae in the *Shapley-Ames-Catalogue* which belong to the Virgo cluster, 137 are spirals and 39 are elliptical nebulae, according to information kindly supplied me by Dr. Hubble. In addition there are a few irregular nebulae, while the types of the remaining nebulae have not been identified. It must be kept in mind that in the following statistical discussion we deal with two groups of nebulae containing rather unequal numbers. In addition to segregation effects, our results will include the dispersions due to random effects in the distributions of the two types of nebulae. Fortu-

[8] E. Hubble, *The Realm of the Nebulae*, p. 79, Yale University Press, 1936.

nately, these dispersions are such that they tend to obliterate rather than enhance the segregation effects actually found, and we therefore may consider the results arrived at as qualitatively trustworthy. Counting the numbers of spirals and of elliptical nebulae in strips 1° wide east and west of the symmetry axis of the Virgo cluster, we obtain the results listed in Table 8.

Reducing elliptical and spiral nebulae to 100 each and adding the numbers in the two halves of the cluster, we obtain the distributions shown in Figure 3, *a*, *b*. Although the number of the elliptical nebulae is so small that large fluctuations might falsify the corresponding distribution, it may, nevertheless, be stated with all reserve that, as far as our test goes, the results are in accord with Hubble's remarks[8] on the segregation of nebular types in clusters.

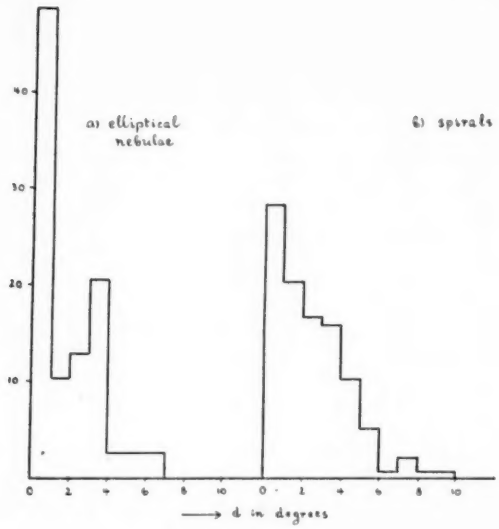

a *b*

FIG. 3

The test for compactness described in section III(*b*) was also applied to the two distributions of elliptical and spiral nebulae, respectively. Again it is found that elliptical nebulae exhibit a much more pronounced tendency toward clustering than the spiral nebulae of the same average brightness. A possible interpretation of this fact is that the elliptical nebulae are, on the average, more massive than the spirals of the same brightness, as was suggested in a previous communication.[1] Before drawing any quantitative conclusions it will be necessary to analyze the segregation of nebulae of different structural types in spherically symmetrical clusters of nebulae.

It should be mentioned that, in order to be on the safe side, we have grouped nebulae of Hubble's type S_0 with the spirals. Should it be found that type S_0 must be considered as being more closely related to the elliptical nebulae than to the spirals, the relatively larger tendency toward clustering becomes still more pronounced.

CALIFORNIA INSTITUTE OF TECHNOLOGY
PASADENA, CALIFORNIA
February 1942

ON THE CLUSTERING OF NEBULAE.[1] II

L. KATZ and GERARD F. W. MULDERS

ABSTRACT

Counts of nebulae brighter than magnitude 12.7 (from the *Shapley-Ames Catalogue*) show the probability that the observed distribution is a random one to be 1:420,000,000.

The distribution over the sky of extragalactic nebulae brighter than the thirteenth magnitude is conspicuously irregular. As investigations are pushed to fainter limits, the irregularities may tend to smooth out; but this tendency, if it exists, has not been formulated in a quantitative manner. This paper presents a simple statistical procedure by which the irregularities of distribution may be described by the numerical probability that the observed distribution can be interpreted as a random distribution of noninteracting objects. As an example, this probability will be calculated for nebulae brighter than magnitude 12.7.

I. SOURCE OF DATA

The material was obtained from the *Shapley-Ames Catalogue*,[2] which lists all external galaxies brighter than the thirteenth magnitude. It was decided to choose 12.9 as the faintest magnitude. On account of the heavy obscuration near the plane of the Galaxy, the belt bounded by $\pm 30°$ galactic latitude was omitted. For the remaining region of the sky the magnitudes given in the *Catalogue* were corrected for absorption, according to the formula[3]

$$\Delta m = 0.25 \ (\text{cosec } b\text{-}1) \ .$$

TABLE 1

NUMBER OF NEBULAE IN STRIPS OF GALACTIC LONGITUDE 10° IN WIDTH

l	ν_i	l	ν_i	l	ν_i
0°*	7	120°	20	240°	32
10	3	130	15	250	49
20	2	140	16	260	40
30	4	150	16	270	41
40	6	160	24	280	23
50	14	170	19	290	9
60	16	180	24	300	18
70	11	190	17	310	45
80	10	200	43	320	32
90	15	210	17	330	9
100	54	220	13	340	7
110	29	230	21	350	3

* 0°–9°, 10°–19°, 20°–29°, etc.

[1] This investigation was suggested to the authors by Dr. Fritz Zwicky in a seminar on the morphology of nebulae, conducted by him at the California Institute of Technology.

[2] "A Survey of External Galaxies Brighter than the Thirteenth Magnitude," *Harvard Ann.*, **88**, No. 2, 1932.

[3] Edwin Hubble, *The Realm of the Nebulae*, p. 65. New Haven: Yale University Press, 1932.

This correction amounts to

$$0.2 \text{ mag. for } 30° < b < 39°,$$
$$0.1 \text{ mag. for } 39° \leqq b < 57°,$$
$$0.0 \text{ mag. for } 57° \leqq b \leqq 90°.$$

If the faintest magnitude is 12.9 for the first zone, it should be 12.8 for the second and 12.7 for the third, to make the material homogeneous.

When the nebulae are counted in this way, the *Shapley-Ames Catalogue* yields 724 objects to and including magnitude 12.7 corrected to the galactic pole. Table 1 shows the distribution of these nebulae in galactic longitude. Table 2 gives the numbers of nebulae to various limiting magnitudes in the northern and southern galactic hemispheres. To

TABLE 2

NUMBER OF NEBULAE IN THE NORTHERN AND SOUTHERN GALACTIC HEMISPHERES TO VARIOUS LIMITING MAGNITUDES

Limiting magnitude	10.0	10.5	11.5	12.7
Northern galactic hemisphere	11	26	108	485
Southern galactic hemisphere	8	24	37	239
Total	19	50	145	724

magnitude 10.5, approximately equal numbers occur in the two hemispheres, but fainter nebulae predominate in the northern hemisphere.

II. STATISTICAL CONSIDERATIONS

It will be found convenient to divide the space containing the nebulae into n cells of equal size. In this system two groups, V_s and V_s', consisting of s and of $n-s$ adjacent cells, respectively, can be chosen in n different ways. The distribution of N nebulae among these n pairs of cell-groups is now considered. The ith pair has, say, ν_i nebulae in V_s and $N-\nu_i$ in V_s'. The dispersion for the n spaces V_s is defined by

$$\sigma_s' = \sqrt{\frac{\sum_{i=1}^{n} (\nu_i - \bar{\nu})^2}{n}}.$$

where $\nu = (s/n)N$, the average number of nebulae per space V_s. If the distribution were random and n large, the dispersion could be computed by the Gaussian distribution function, which gives

$$\sigma_s = \sqrt{p_s(1-p_s)N},$$

where $p_s = s/n$.

The ratio $\sigma_s'/\sigma_s = k$ may be taken as a measure of the deviation of the actual distribution from a purely random one. In other words, we can calculate the probability of a dispersion $\sigma_s' = k\sigma_s$. A few values of this probability[4] are given in Table 3 for various values of k.

[4] R. Pearl, *Medical Biometry and Statistics*, 2d ed., p. 439, Table B. Philadelphia: W. B. Sanders Co., 1930.

III. RESULTS OF THE ANALYSIS

In this investigation the nebulae are projected upon the celestial sphere, thus reducing the problem to a two-dimensional one. The n cells become thirty-six *areas*, chosen as strips of galactic longitude 10° in width. Table 1 shows the number of nebulae in each cell. The cells might be further subdivided into northern and southern sections, making n equal to 72.

TABLE 3

PROBABILITY OF A DISPERSION k TIMES THE STANDARD DISPERSION

k	Probability	k	Probability
0.6745	1:1	4	1:15,770
1	1:2	5	1:1,744,000
2	1:21	6	1:500,000,000
3	1:370		

TABLE 4

DISPERSION OF THE DISTRIBUTION OF NEBULAE FOR VARIOUS VALUES OF s AND THE PROBABILITY OF SUCH A DISPERSION

s	σ_s'	σ_s	k	Probability	s	σ_s'	σ_s	k	Probability
1	13.6	4.4	3.1	1:516	22	77.2	13.2	5.9	1:290,000,000
2	23.8	6.2	3.8	1:6,900	26	70.1	12.0	5.8	1:150,000,000
4	38.1	8.5	4.5	1:150,000	28	61.9	11.2	5.5	1:28,000,000
6	50.4	10.0	5.0	1:1,750,000	30	50.4	10.0	5.0	1:1,750,000
8	61.9	11.2	5.5	1:28,000,000	32	38.1	8.5	4.5	1:150,000
10	70.1	12.0	5.8	1:150,000,000	34	23.8	6.2	3.8	1:6,900
14	77.2	13.2	5.9	1:290,000,000	35	13.6	4.4	3.1	1:516
18	80.2	13.4	5.97	1:420,000,000					

TABLE 5

PROBABILITY OF RANDOM DISTRIBUTION FOR VARIOUS LIMITING MAGNITUDES

Limiting Magnitude	σ_s'	σ_s	k	Probability	Limiting Magnitude	σ_s'	σ_s	k	Probability
10.0	1.8	2.2	0.8	1:1.4	11.5	25.1	6.0	4.2	1:38,000
10.5	5.8	3.2	1.8	1:13	12.7	80.2	13.4	5.97	1:420,000,000
11.0	13.2	4.2	3.1	1:516					

As outlined in the previous section, the strips are now grouped together to form larger areas containing s strips each. The smallest value s can have is 1, the largest 35. For every value of s a series of thirty-six portions of the celestial sphere is obtained, and the distribution of the nebulae among these is analyzed. In Table 4 the values of σ_s', σ_s, k and the probability of such a distribution are given for each value of s.

It is interesting that for $s=18$, k is 5.1 (prob. 1:1,758,000) for the northern galactic hemisphere and 3.6 (prob. 1:3,140) for the southern.

The region of space under consideration is effectively limited by the maximum magnitude included in the analysis, the boundary being pushed out farther as fainter and

fainter nebulae are included. For this reason calculations were carried through for various limiting magnitudes. The results are shown in Table 5. Here s was taken equal to 18, since, according to Table 4, this gives the maximum value of k.

IV. CONCLUSION

Tables 2 and 5 show that nebulae brighter than magnitude 10.5 are distributed in a fairly random fashion over the whole sky. This indicates that the nearer nebulae have little tendency to form clusters, although they may be members of a fairly homogeneous local cluster with our own Galaxy near its center. On the other hand, as fainter and fainter magnitudes are included, the value of k increases, showing that random distribution of these nebulae is extremely improbable. The physical interpretation is well known: the region of space under consideration has been extended to include clusters. The maximum dispersion occurs when the number of "cluster" nebulae is greatest relative to the number of "field" nebulae. If the analysis were extended to magnitudes fainter than 12.7, one would expect the value of k to pass through a maximum and to decrease as more field nebulae are counted. Of course, if the analysis were extended far enough, k might pass through secondary maxima as other clusters are included but should eventually approach unity for a very large region of space containing many clusters.

One more conclusion can be drawn from Table 4: when clustering does occur, one would expect k to become especially large when V_s is equal to the area of a cluster. The results of the analysis for various values of s show this to be true.

The enormous deviation from a Gaussian distribution indicates either that the nebulae are not in a stationary state or, more probably, that they are controlled by organized forces.

California Institute of Technology
Pasadena, California
February 1942

NOTES

THE CENTRAL DENSITY OF THE STARS[1]

In a recent note entitled "The Central Density of the Stars"[2] W. J. Luyten criticized my investigation on "The Structure of Main-Sequence Stars."[3] His note opened with a sweeping statement that ". . . . the observational material, if properly discussed, gives no evidence whatsoever to support Kopal's assertion." The writer regrets that Luyten did not hesitate to advance this claim, which all his subsequent objections—even if sound—fail to justify. Moreover, none of Luyten's objections can be maintained in the light of the following facts:

1. The quantity k, given in column 3 of Table II in *Harvard Circular*, No. 443, is defined by

$$2k = \frac{2\psi_2(\xi_1) - \xi_1\psi_2(\xi_1)}{3\psi_2(\xi_1) + \xi_1\psi_2'(\xi_1)},$$

where ξ_1 is the first zero of the Emden equation, $\psi_2(\xi)$ an associated Emden function of second order, and ψ_2' its derivative with respect to ξ. For the polytropic index $n = 3.5$ we have[4] $\psi_2(\xi_1) = 20.1390$, $\psi_2'(\xi_1) = 4.0706$, and $\xi_1 = 9.5358$. Inserting these values in the formula, we obtain $k = 0.0073$, as is correctly given in *Harvard Circular*, No. 443.

2. The uncertainty of apsidal motion in V 380 Cygni depends almost entirely upon the uncertainty of photometric observations on the ascending and descending branches of the displaced secondary minimum. Luyten[5] had based his estimate on Kron's[6] value of the probable error of his single normal as ± 0.006 mag. My rediscussion[7] has shown that about one-half of the residuals interpreted by Kron as accidental errors were due to the neglect of photometric ellipticity (which in systems exhibiting eccentric orbits varies inversely proportionally to the cube of the radius-vector). Allowance for the ellipticity reduces the probable error of a single normal to ± 0.003 mag., and the uncertainty of the apsidal advance to about 25 per cent—which justly ranks V 380 Cygni among stars considered to be of first-class quality.

As to MR Cygni, my investigation was completed several months before Miss Swope's results[8] became known. A final decision on the apsidal motion in this system should be postponed until the Victoria results (claiming a large eccentricity, not confirmed by Swope), known thus far only in abstract,[9] are published in full.

3. My derivation of the absolute dimensions of V 380 Cygni[7] involves no assumptions. There is no distinct gap in the Russell diagram between supergiants and main-sequence stars for stars of spectral type as early as B2 and hence no a priori reason why V 380

[1] Reply to a note by W. J. Luyten.

[2] *Ap. J.*, **95**, 327, 1942.

[3] *Harvard Circ.*, No. 443, 1940.

[4] *M.N.*, **93**, 539 (cf. 574), 1933; cf. also *British Association Tables*, Vol. **2**.

[5] *B.A.N.*, **8**, 271, 1938.

[6] *Ap. J.*, **82**, 225, 1935.

[7] *Harvard Circ.*, No. 441, 1940.

[8] *Harvard Bull.*, No. 914, 1940.

[9] Pearce, *J.R.A.S. Canada*, **29**, 411, 1935.

Cygni should not be built up according to the same family of models as the "normal" main-sequence stars of the same spectral class.

4. The writer must protest against Luyten's unspecified allegations of "numerous errors" in *Harvard Circular*, No. 443. To my present knowledge there is none. Three misprints have been detected since its publication—all in Table III[10]—but they all concern auxiliary quantities, and their character is so evident that they are not likely to create any misunderstanding.

5. According to Bethe and his associates[11] the logarithm of the central density of the sun, expressed in terms of its mean density, is 1.90. This figure may not yet represent the last word; but, when plotted in the diagram on page 8 of *Harvard Circular*, No. 443, the sun does not fit exactly upon the straight line expressing the statistical relation between the logarithms of mass and central density of main-sequence stars, but neither does it deviate from it more than an average second-class star.

A linear relation between the logarithms of mass and central density has been derived on the basis of material including stars with masses ranging from (approximately) 1 to 50 solar masses. Whether or not it continues to be linear for stars with masses considerably less than that of the sun remains conjectural; a distinct deviation of the sun may, indeed, indicate that this is not the case. If Luyten, in order to arrive at a central density as high as 17,000, extrapolates the linear relation to masses as small as $0.1\odot$, he does it at his own risk; and his assertion that I "failed to realize" these facts belongs in the same category of unsubstantiated claims as all his previous allegations.

Luyten's note contains also some obvious distortions. Thus, in its first paragraph he writes (concerning the relation between mass and central density): "This relation is made the basis of claims concerning the structure of main-sequence stars and the origin of binary stars"—while, in reality, the relation was based on observed facts (which Luyten now attacks), and it was not until after it had been derived that certain conclusions concerning the structure of main-sequence stars were drawn. Luyten also writes that "Kopal adds the data for the seven massive stars of Trumpler . . . . but does not mention the main-sequence stars for which Chandrasekhar has similarly derived central densities and which do not agree with Kopal's curve." The truth is, however, that Chandrasekhar could not have derived the central densities of main-sequence stars (again unspecified by Luyten) "similarly" as for the Trumpler stars but must have done it in a quite different way—by assuming either their model or their chemical composition. Whether or not such stars agree with my relation is then irrelevant.[12]

ZDENĚK KOPAL

HARVARD COLLEGE OBSERVATORY
March 1942

[10] β Sco (col. 13): *for* 0.96 *read* 0.096; MR Cyg (col. 12): *for* 0.18 *read* 0.28; HV 7498 (col. 11): *for* 0.56 *read* 0.36.

[11] *Ap. J.*, **94**, 37, 1941.

[12] [The following information pertinent to Dr. Kopal's discussion has been furnished by Dr. S. Chandrasekhar:

"In view of the discussion between Drs. Luyten and Kopal, I wish to point out that, unfortunately, my integrations for $n = 3.5$ were not carried out with the precision needed to determine $k_2 (= [\Delta_2 - 1]/2$, in my notation) to the accuracy needed in practice. However, the integrations for $n = 1$, 1.5, 2, 3, and 4 have the necessary accuracy and, interpolating between them, I find for Δ_2 the value 1.011 for $n = 3.5$ instead of the published value 1.015 (*M.N.*, **93**, 567, 1933). The corresponding value for k_2 would be 0.0055 ± 0.0002."

Dr. Kopal has read this note and has stated that this "would change somewhat a few of my calculated central densities, but would require no appreciable modifications of any of the results of my statistical investigation."

Since all relevant points have now been brought out in Dr. Luyten's and Dr. Kopal's notes, the discussion is closed herewith.—EDITOR.]

REVIEWS

Earth, Moon, and Planets. By FRED L. WHIPPLE. ("Harvard Books on Astronomy.") Philadelphia: Blakiston Co., 1941. Pp. 293. $2.50.

The "Harvard Books on Astronomy," edited by Dr. Shapley and Dr. Bok, have set such a high standard of quality that it is hardly surprising to find after a few moments of reading that Whipple's new book is by far the most thorough and most readable account of the planets written in recent years. As the title shows, the subject matter does not cover the entire solar system: the problems of comets and meteors have already been described by Dr. Watson, and the physics of the sun will soon (it is hoped) appear from the pen of Dr. Menzel. By thus restricting the subject matter, Dr. Whipple was able to deal adequately with what is unquestionably the most fascinating, yet often neglected, branch of astronomy.

Perhaps the most distinctive feature of the book consists of the large number of judiciously chosen illustrations, more than half of which are actual photographs from Lowell, Mount Wilson, Lick, and other observatories. Many of these photographs have not previously been published, and they alone constitute a veritable treasure-store of information. Astronomy, in common with the other exact sciences, has permitted a certain amount of artificiality to influence its progress. Those properties of the physical universe which are easily described in terms of numbers are adequately dealt with, while those which are not susceptible to this type of description are sometimes lost sight of. In stellar spectroscopy, for example, the displacement of spectral lines became the subject of many elaborate studies some thirty years before the microphotometer opened the way for a numerical description of the shapes of the lines. Yet the early spectroscopists must have been struck by the fact that the shapes of the lines are intrinsically a much more conspicuous attribute of a stellar spectrogram than are the relatively small Doppler displacements. Planetary research has undoubtedly suffered in a similar manner. Perhaps it may be appropriate in this connection to suggest that an atlas of planetary photographs, preferably consisting of photographic reproductions rather than of halftones, would constitute the best way to eliminate this artificiality. The great success of Professor Ross's *Atlas of the Milky Way* shows that there is a real need and appreciation of the direct photographic presentation of features which cannot be adequately expressed in tabular form.

Dr. Whipple has approached his task with thorough knowledge and clear understanding. He himself has contributed to various phases of research on the solar system; and the careful reader will find not only that his book is a critical summary of published work but that it contains, here and there, a number of new ideas and suggestions. Aside from questions of taste in the selection of material, the reviewer finds very little that he can criticize. On page 162 he would have stressed the great contribution by Wildt to the problem of identifying the absorption features of the giant planets. On page 177 he would have given prominence to the results of photometric research of the rings of Saturn and would have recommended that the radial velocities of the ring be again investigated with the highest possible dispersion. (In fact, stimulated by Dr. Chandrasekhar, the reviewer intended to undertake such a study with the large Coudé spectrograph of the McDonald Observatory.) Since the book is written for amateurs rather than for professional astronomers and explains many of the simple terms used in astronomy, the reviewer is not sure that the reference to a curve in Figure 26 at the bottom of page 31 will be understood. There is no curve in that figure.

It is of interest to compare Whipple's book with that of Gamow, *The Biography of the Earth*, since both cover, at least in part, the same ground. Whipple's book lacks the glamour and the intuition which make Gamow's book particularly pleasant reading. But it contains more substantial and accurate information. Taken together, they provide a balanced diet of fact and fancy.

O. STRUVE

INDEX TO VOLUME 95

INDEX TO SUBJECTS

PAGE

Abundances of the Elements and Their Isotopes, An Attempt To Interpret the Relative. *S. Chandrasekhar and Louis R. Henrich* 288

"Barred Spirals," The Equilibrium and Stability of Ring-shaped. *Gunnar Randers* . . 88

Be Spectra, Special Problems of. *Paul W. Merrill* 268

42 Capricorni, The Spectrographic Orbit of. *Roscoe F. Sanford* 425

α Carinae, The Spectrum of. *Jesse L. Greenstein* 161

VV Cephei, Atmospheric Velocities in. *Victor Goedicke* 319

α Cygni, Intensity Anomalies in. *Lawrence H. Aller* 73

α Cygni and α Lyrae in the Region λλ 3000–3300, The Spectra of. *J. H. Rush* . . . 213

Distribution of Mass and Luminosity in Messier 33, A Note on the. *Lawrence H. Aller* . 48

Eros, A Composite Light-Curve of. *F. E. Roach* 310

Fe I, Absolute *f*-Values for Lines of. *Robert B. King* 78

(*Fe* III), Term Analysis of the Third Spectrum of Iron. *B. Edlén and P. Swings* . . . 532

Globular Cluster Messier 3, Note on the Periods of the Variable Stars in the. *W. C. Martin* 314

Interstellar Medium. III. Galactic Distribution, The Dynamics of the. *Lyman Spitzer, Jr.* 329

Isotopes, An Attempt To Interpret the Relative Abundances of the Elements and Their. *S. Chandrasekhar and Louis R. Henrich* 288

17 Leporis, Spectrographic Observations of. *Burke Smith and Otto Struve* 468

α Lyrae in the Region λλ 3000–3300, The Spectra of α Cygni and. *J. H. Rush* . . . 213

Meteors, A Remark on. *Theodore E. Sterne* 437

Molecules, Considerations regarding Cometary and Interstellar. *P. Swings* 270

Nebula Messier 33, The Rotation of the Spiral. *N. U. Mayall and L. H. Aller* . . . 5

Nebulae. I. On the Clustering of. *F. Zwicky* 555

Nebulae. II. On the Clustering of. *L. Katz and Gerard F. W. Mulders* 565

Nebulae, The Spectra of Ten Gaseous. *A. B. Wyse* 356

PAGE

Nebulae Messier 31 and Messier 33, Distribution of Mass in the Spiral. *A. B. Wyse and N. U. Mayall* 24

Nebulosities in Messier 33, The Spectra of the Emission. *Lawrence H. Aller* 52

Negative Hydrogen Ion, The Absorption Coefficient of the Free-Free Transitions of the. *John A. Wheeler and Rupert Wildt* 281

Notice. *Dean B. McLaughlin* 219

Novae, Spectral Stages of. *Dean B. McLaughlin* 428

Peculiar Stars. III. Spectrographic Observations of. *P. Swings and O. Struve* . . . 152

Photographic Plates, The Curvature of. *Leigh Page* 1

Planetary Nebulae of Low Surface Brightness, Spectra of. *R. Minkowski* 243

Radial Velocities of Proper-Motion Stars. *Daniel M. Popper* 307

Reviews:

Bok, Bart J., and Priscilla F. Bok. *The Milky Way* (Jesse L. Greenstein) 220

Campbell, Leon, and Luigi Jacchia. *The Story of Variable Stars* (Dean B. McLaughlin) 223

Maurolico, Francesco. *The "Photismi de Lumine" of Maurolycus.* Translated by Henry Crew (Philip Fox) 220

Seabrook, William. *Doctor Wood: Modern Wizard of the Laboratory* 223

Watson, Fletcher G. *Beyond the Planets* (N. T. Bobrovnikoff) 328

Whipple, Fred L. *Earth, Moon and Planets* (Otto Struve) 571

Rigel, The Spectrographic Orbit of the Companion to. *Roscoe F. Sanford* 421

Rotation, On Stellar. *Martin Schwarzschild* 441

Rotation of Stars with Convective Core, On the. *Gunnar Randers* 454

δ Sagittae, Note on the Spectrum of. *J. A. Hynek* 324

Solar Observations in Hydrogen and Helium Light, Recent. *Helen W. Dodson and Suzanne E. A. van Dijke* 325

Spectra of Comets 1941*c* (Paraskevopoulos–de Kock) and 1941*d* (van Gent) Remarks on the. *C. T. Elvey, P. Swings, and H. W. Babcock* 218

Spectra of α Cygni and α Lyrae in the Region $\lambda\lambda$ 3000–3300, The. *J. H. Rush* . . . 213

Spectra of the Emission Nebulosities in Messier 33, The. *Lawrence H. Aller* 52

Spectra of Planetary Nebulae of Low Surface Brightness. *R. Minkowski* 243

Spectra of Wolf-Rayet Stars and Related Objects, The. *P. Swings* 112

Spectral Stages of Novae. *Dean B. McLaughlin* 428

Spectrographic Observations of 17 Leporis. *Burke Smith and Otto Struve* 468

Spectrographic Observations of Peculiar Stars. III. *P. Swings and O. Struve* 152

Spectrographic Orbit of 42 Capricorni, The. *Roscoe F. Sanford* 425

PAGE

Spectrographic Orbit of the Companion to Rigel, The. *Roscoe F. Sanford* 421

Spectrophotometry of 67 Bright Stars with a Photoelectric Cell: Discussion. *John S. Hall* 231

Spectrum of BD+11°4673 during the Years 1937–1941, The. *Paul W. Merrill* . . . 386

Spectrum of α Carinae, The. *Jesse L. Greenstein* 161

Spectrum of Iron (*Fe* III), Term Analysis of the Third. *B. Edlén and P. Swings* . . . 532

Spectrum of δ Sagittae, Note on the. *J. A. Hynek* 324

Spectrum of Vega, A Determination of the Energy Distribution in the Near Infrared. *John S. Hall and Robley C. Williams* 225

Stars, The Central Density of the. *Zdeněk Kopal* 569

Stars, The Central Density of the. *W. J. Luyten* 327

Stars, The Nearest. *Gerard P. Kuiper* 201

Statistics of the Gravitational Field Arising from a Random Distribution of Stars. I. The Speed of Fluctuations, The. *S. Chandrasekhar and J. von Neumann* 489

Stellar Atmospheres, The Opacity in the Early-Type. *Jesse L. Greenstein* 299

Stellar Atmospheres: A Review of the Problems of Gaseous Shells, Extended. *Otto Struve* 134

Sun, Abundance of Iron in the. *Robert B. King* 82

Sun, The Excitation Temperature of the. *Ervin J. Prouse* 322

Sun, On the Limb Darkening of the. *Julius Ashkin, John E. Nafe, and Jerome Rothstein* . 76

Variable Stars, Mean Absolute Magnitudes and Space Motions of the Long-Period. *Ralph E. Wilson and Paul W. Merrill* 248

Variable Stars in the Globular Cluster Messier 3, Note on the Periods of the. *W. C. Martin* 314

Variables, Notes on Eclipsing. *Henry Norris Russell* 345

Variables, The Pulsation Theory of Long-Period. *R. M. Scott* 58

Variables of Small Range, Luminosities of the M-Type. *Philip C. Keenan* 461

Vega, A Determination of the Energy Distribution in the Near Infrared Spectrum of. *John S. Hall and Robley C. Williams* 225

Wolf-Rayet Star and the Expanding-Envelope Hypothesis, Absolute Dimensions of a. *O. C. Wilson* 402

Wolf-Rayet Stars and Related Objects, The Spectra of. *P. Swings* 112

INDEX OF AUTHORS

PAGE

ALLER, LAWRENCE H. Intensity Anomalies in α Cygni 73

ALLER, LAWRENCE H. A Note on the Distribution of Mass and Luminosity in Messier 33 48

ALLER, LAWRENCE H. The Spectra of the Emission Nebulosities in Messier 33 . . . 52

ALLER, L. H., and N. U. MAYALL. The Rotation of the Spiral Nebulae Messier 33 . . 5

ASHKIN, JULIUS, JOHN E. NAFE, and JEROME ROTHSTEIN. On the Limb Darkening of the Sun 76

BABCOCK, H. W., C. T. ELVEY, and P. SWINGS. Remarks on the Spectra of Comets 1941*c* (Paraskevopoulos–de Kock) and 1941*d* (van Gent) 218

BOBROVNIKOFF, N. T. Review of: *Beyond the Planets*, Fletcher G. Watson 328

CHANDRASEKHAR, S., and LOUIS R. HENRICH. An Attempt To Interpret the Relative Abundances of the Elements and Their Isotopes 288

CHANDRASEKHAR, S., and J. VON NEUMANN. The Statistics of the Gravitational Field Arising from a Random Distribution of Stars. I. The Speed of Fluctuations . . . 489

DIJKE, SUZANNE E. A. VAN, and HELEN W. DODSON. Recent Solar Observations in Hydrogen and Helium Light 325

DODSON, HELEN W., and SUZANNE E. A. VAN DIJKE. Recent Solar Observations in Hydrogen and Helium Light 325

EDLÉN, B., and P. SWINGS. Term Analysis of the Third Spectrum of Iron (*Fe* III) . . . 532

ELVEY, C. T., P. SWINGS, and H. W. BABCOCK. Remarks on the Spectra of Comets 1941*c* (Paraskevopoulos–de Kock) and 1941*d* (van Gent) 218

FOX, PHILIP. Review of: *The "Photismi de Lumine" of Maurolycus*, Francesco Maurolico. Translated by Henry Crew 220

GOEDICKE, VICTOR. Atmospheric Velocities in VV Cephei 319

GREENSTEIN, JESSE L. The Opacity in Early-Type Stellar Atmospheres 299

GREENSTEIN, JESSE L. Review of: *The Milky Way*, Bart J. Bok and Priscilla F. Bok . 220

GREENSTEIN, JESSE L. The Spectrum of α Carinae 161

HALL, JOHN S. Spectrophotometry of 67 Bright Stars with a Photoelectric Cell: Discussion 231

HALL, JOHN S., and ROBLEY C. WILLIAMS. A Determination of the Energy Distribution in the Near Infrared Spectrum of Vega 225

HENRICH, LOUIS R., and S. CHANDRASEKHAR. An Attempt To Interpret the Relative Abundances of the Elements and Their Isotopes 288

HYNEK, J. A. Note on the Spectrum of δ Sagittae 324

PAGE

KATZ, L., and GERARD F. W. MULDERS. On the Clustering of Nebulae. II. 565

KEENAN, PHILIP C. Luminosities of the M-Type Variables of Small Range 461

KING, ROBERT B. Absolute *f*-Values for Lines of *Fe* I 78

KING, ROBERT B. Abundance of Iron in the Sun 82

KOPAL, ZDENĚK. The Central Density of the Stars 569

KUIPER, GERARD P. The Nearest Stars 201

LUYTEN, W. J. The Central Density of the Stars 327

MCLAUGHLIN, DEAN B. Notice 219

MCLAUGHLIN, DEAN B. Review of: *The Story of Variable Stars*, Leon Campbell and Luigi Jacchia 223

MCLAUGHLIN, DEAN B. Spectral Stages of Novae 428

MARTIN, W. C. Note on the Periods of the Variable Stars in the Globular Cluster Messier 3 314

MAYALL, N. U., and L. H. ALLER. The Rotation of the Spiral Nebula Messier 33 . . . 5

MAYALL, N. U., and A. B. WYSE. Distribution of Mass in the Spiral Nebulae Messier 31 and Messier 33 24

MERRILL, PAUL W. Special Problems of Be Spectra 268

MERRILL, PAUL W. The Spectrum of BD+11°4673 during the Years 1937–1941 . . . 386

MERRILL, PAUL W., and RALPH E. WILSON. Mean Absolute Magnitudes and Space Motions of the Long-Period Variable Stars 248

MINKOWSKI, R. Spectra of Planetary Nebulae of Low Surface Brightness 243

MULDERS, GERARD F. W., and L. KATZ. On the Clustering of Nebulae. II. 565

NAFE, JOHN E., JEROME ROTHSTEIN, and JULIUS ASHKIN. On the Limb Darkening of the Sun 76

NEUMANN, J. VON, and S. CHANDRASEKHAR. The Statistics of the Gravitational Field Arising from a Random Distribution of Stars. I. The Speed of Fluctuations 489

PAGE, LEIGH. The Curvature of Photographic Plates 1

POPPER, DANIEL M. Radial Velocities of Proper-Motion Stars 307

PROUSE, ERVIN J. The Excitation Temperature of the Sun 322

RANDERS, GUNNAR. The Equilibrium and Stability of Ring-shaped "Barred Spirals" . 88

RANDERS, GUNNAR. On the Rotation of Stars with Convective Core 454

ROACH, F. E. A Composite Light-Curve of Eros 310

ROTHSTEIN, JEROME, JULIUS ASHKIN, and JOHN E. NAFE. On the Limb Darkening of the Sun 76

PAGE

RUSH, J. H. The Spectra of α Cygni and α Lyrae in the Region λλ 3000–3300 213

RUSSELL, HENRY NORRIS. Notes on Eclipsing Variables 345

SANFORD, ROSCOE F. The Spectrographic Orbit of 42 Capricorni 425

SANFORD, ROSCOE F. The Spectrographic Orbit of the Companion to Rigel 421

SCHWARZSCHILD, MARTIN. On Stellar Rotation 441

SCOTT, R. M. The Pulsation Theory of Long-Period Variables 58

SMITH, BURKE, and OTTO STRUVE. Spectrographic Observations of 17 Leporis . . . 468

SPITZER, LYMAN, JR. The Dynamics of the Interstellar Medium. III. Galactic Distribution 329

STERNE, THEODORE E. A Remark on Meteors 437

STRUVE, OTTO. Extended Stellar Atmospheres: A Review of the Problems of Gaseous Shells 134

STRUVE, OTTO. Review of: *Earth, Moon and Planets*, Fred L. Whipple 571

STRUVE, OTTO, and BURKE SMITH. Spectrographic Observations of 17 Leporis . . . 468

STRUVE, O., and P. SWINGS. Spectrographic Observations of Peculiar Stars. III. . . . 152

SWINGS, P. Considerations regarding Cometary and Interstellar Molecules 270

SWINGS, P. The Spectra of Wolf-Rayet Stars and Related Objects 112

SWINGS, P., H. W. BABCOCK, and C. T. ELVEY. Remarks on the Spectra of Comets 1941*c* (Paraskevopoulos–de Kock) and 1941*d* (van Gent) 218

SWINGS, P., and B. EDLÉN. Term Analysis of the Third Spectrum of Iron (*Fe* III) . . . 532

SWINGS, P., and O. STRUVE. Spectrographic Observations of Peculiar Stars. III . . . 152

WHEELER, JOHN A., and RUPERT WILDT. The Absorption Coefficient of the Free-Free Transitions of the Negative Hydrogen Ion 281

WILDT, RUPERT, and JOHN A. WHEELER. The Absorption Coefficient of the Free-Free Transitions of the Negative Hydrogen Ion 281

WILLIAMS, ROBLEY C., and JOHN S. HALL. A Determination of the Energy Distribution in the Near Infrared Spectrum of Vega 225

WILSON, O. C. Absolute Dimensions of a Wolf-Rayet Star and the Expanding-Envelope Hypothesis 402

WILSON, RALPH E., and PAUL W. MERRILL. Mean Absolute Magnitudes and Space Motions of the Long-Period Variable Stars 248

WYSE, A. B. The Spectra of Ten Gaseous Nebulae 356

WYSE, A. B., and N. U. MAYALL. Distribution of Mass in the Spiral Nebulae Messier 31 and Messier 33 24

ZWICKY, F. On the Clustering of Nebulae. I. 555

An important contribution to astronomical literature

PRINCIPLES OF STELLAR DYNAMICS

By S. CHANDRASEKHAR, *Yerkes Observatory*

In this monograph the dynamical methods of interpreting the motions in the galaxy, spiral nebulae, and star clusters are developed from a coherent point of view. An introductory chapter deals with the essential kinematical aspects of stellar motions and the later chapters include discussions of stellar encounters, star streaming and the rotation of the galaxy, spiral structure in nebulae, and the disintegration of star clusters. It is intended that the monograph should provide a concise and authoritative account of current investigations in this rapidly advancing field of astronomy.

Contents: I. Kinematics. II. The Time of Relaxation of Stellar Systems. III. Galactic Dynamics: The Dynamics of Differential Motions. IV. General Dynamics of Stellar Systems: Spiral Structure. V. The Dynamics of Star Clusters.

(In the *Astrophysical Monographs Series*)

Just published, $5.00

THE UNIVERSITY OF CHICAGO PRESS

Astronomical

LANTERN SLIDES

Since 1903, the Yerkes Observatory of the University of Chicago has been reproducing in lantern slides, transparencies, and prints the original astronomical photographs made at Williams Bay.

The lantern slides are uniformly 4×3¼ inches in size. The frequent call for small sets of slides for school and lecture purposes has led to the preparation of a list of 100 representative slides (price $62.50), a catalogue of which may be obtained upon request to the University of Chicago Press, 5750 Ellis Avenue, Chicago.

Prints as well as slides can be furnished, and for many subjects window transparencies are also supplied.

For catalogue and further information write

The University of Chicago Press

5750 Ellis Avenue, Chicago, Ill.

POPULAR ASTRONOMY

A magazine now in its fiftieth year, devoted to the elementary aspects of Astronomy and allied sciences.

Published monthly, except July and September.

Yearly subscription rates: Domestic $4.00; Canadian $4.25; Foreign $4.75 (including war tax).

Address

POPULAR ASTRONOMY

CARLETON COLLEGE

NORTHFIELD, MINNESOTA, U.S.A.

ASTROPHYSICAL MONOGRAPHS

Sponsored by the Editors of the Astrophysical Journal

A series designed to provide a growing library of precise, up-to-date, authoritative material of modern astronomy and astrophysics for astronomers, physicists, mathematicians, and chemists. By combining the advantages of an advanced textbook with the interest of a research narrative, the monographs will serve as reference volumes for astronomers and as manuals for teachers.

Ready June

PRINCIPLES OF STELLAR DYNAMICS

By S. CHANDRASEKHAR — $5.00

Published

SPECTRA OF LONG-PERIOD VARIABLE STARS

By PAUL W. MERRILL

This monograph is devoted largely to the observational side of the subject, but some discussion of the physical significance of various spectral features is included. A brief introduction and a historical chapter are inserted for the benefit of the reader who is not a specialist in stellar spectra. The spectra at maximum light and their chief periodic variations are then described. Following chapters are concerned with certain technical problems and with individual variables of special interest. The monograph concludes with a brief discussion of a few general problems of long-period variables. $2.50

THE MASSES OF THE STARS, WITH A GENERAL CATALOGUE OF DYNAMICAL PARALLAXES

By HENRY NORRIS RUSSELL *and* CHARLOTTE E. MOORE

"Astrophysicists will be grateful to the authors for so thorough an examination of available knowledge. . . . . We may be permitted to congratulate the senior author on this magnificent outgrowth from an idea which germinated in his mind thirty years ago."—PROFESSOR A. S. EDDINGTON, *The Observatory* (England). *236 pages, 53 tables, paper, $3.50*

AN INTRODUCTION TO THE STUDY OF STELLAR STRUCTURE. By S. CHANDRASEKHAR

Treats in a deductive manner the subject of stellar interiors. The necessary physical theories and mathematical methods are fully explained. Includes accounts of the foundations of thermodynamics, the theory of radiation, the quantum theory of a perfect gas, and a discussion of the elements of nuclear physics. "The material is throughout presented with enviable crispness and clarity of expression. The work will undoubtedly become an indispensable handbook for future researchers in this field."—*Nature* (England). *502 pages, 22 pages of engravings, $10.00*

THE DISTRIBUTION OF THE STARS IN SPACE

By BART J. BOK

". . . . an extremely important contribution to the field of galactic structure, invaluable alike to both students and research workers in the field."—*Science*. The large number and variety of researches carried out in this field during the past fifteen years are discussed critically in this study with clarity and dispatch. *124 pages, paper, $2.50*

In preparation

AN ATLAS OF STELLAR SPECTRA WITH AN OUTLINE OF SPECTRAL CLASSIFICATION. By W. W. MORGAN

THE UNIVERSITY OF CHICAGO PRESS